

istituto nazionale di fisica nucleare  
laboratori nazionali di Frascati

2010

ANNUAL REPORT



*Scientific Editor*  
F. Cerutti

*Technical Editor*  
L. Invidia

*Editorial Office*  
D. Bifaretti  
A. Cupellini

*Cover: Spring at Laboratory*  
*Cover artwork: Claudio Federici*

istituto nazionale di fisica nucleare  
laboratori nazionali di Frascati

2010

# ANNUAL REPORT

**LNF-11/06 (IR)**  
May, 2011

*Published by  
SIDS-Publications & Library  
P.O. Box 13 – I-00044 Frascati (Italia)*

Available at [www.lnf.infn.it/rapatt](http://www.lnf.infn.it/rapatt)

Mario Calvetti  
*LNF Director*

Vitaliano Chiarella  
*Head, Research Division*

Pantaleo Raimondi  
*Head, Accelerator Division*

Claudio Sanelli  
*Head, Technical Division*

*LNF Scientific Coordinators*

Riccardo de Sangro  
*Particle Physics*

Francesco Terranova  
*Astroparticle Physics*

Pasquale Di Nezza  
*Nuclear Physics*

Gino Isidori  
*Theory and Phenomenology*

Roberto Cimino  
*Technological and Interdisciplinary Research*

# 2010 ANNUAL REPORT

## CONTENTS

### *Research Division*

#### *1 – Particle Physics*

ATLAS .....	3
BaBar .....	17
BESIII .....	21
CDF .....	27
CMS .....	35
KLOE .....	42
LHCb .....	62
NA62 .....	70
P-SuperB .....	77

#### *2 – Astroparticle Physics*

BENE_DTZ .....	85
NEMO .....	86
OPERA .....	87
ROG .....	97
WIZARD/PAMELA .....	100

#### *3 – Nuclear Physics*

ALICE .....	107
JLAB12 .....	117
KAONNIS .....	125
PANDA .....	134
VIP .....	138

#### *4 – Theory and Phenomenology*

FA-51 .....	147
LF-21 .....	149
LF-61 .....	153
MI-12 .....	157
PG-21 .....	161

## ***5 – Technological and Interdisciplinary Research***

ALTCRISS .....	165
FAST .....	167
FLUKA2 .....	171
HCPAF .....	172
IMCA .....	179
MoonLIGHT-ILN .....	182
MUEXC .....	192
N@BTF .....	198
ODRI .....	204
TERASPARC .....	206
TPS .....	201
CATHERINE .....	214
Occupational Exposure to Nanomaterials .....	218

## ***6 – Accelerator Physics***

DAΦNE .....	223
DAΦNE-BTF .....	239
DAΦNE-L .....	245
GILDA .....	254
NTA CLIC .....	258
NTA ILC .....	260
NTA PLASMONX .....	262
SPARC .....	281
SuperB .....	291

## ***General Informations***

<i>Communication and Outreach</i> .....	301
<i>Conferences</i> .....	308
<i>Publications</i> .....	309
<i>Seminaries</i> .....	315
<i>Technical Division</i> .....	318
<i>Glossary</i> .....	325

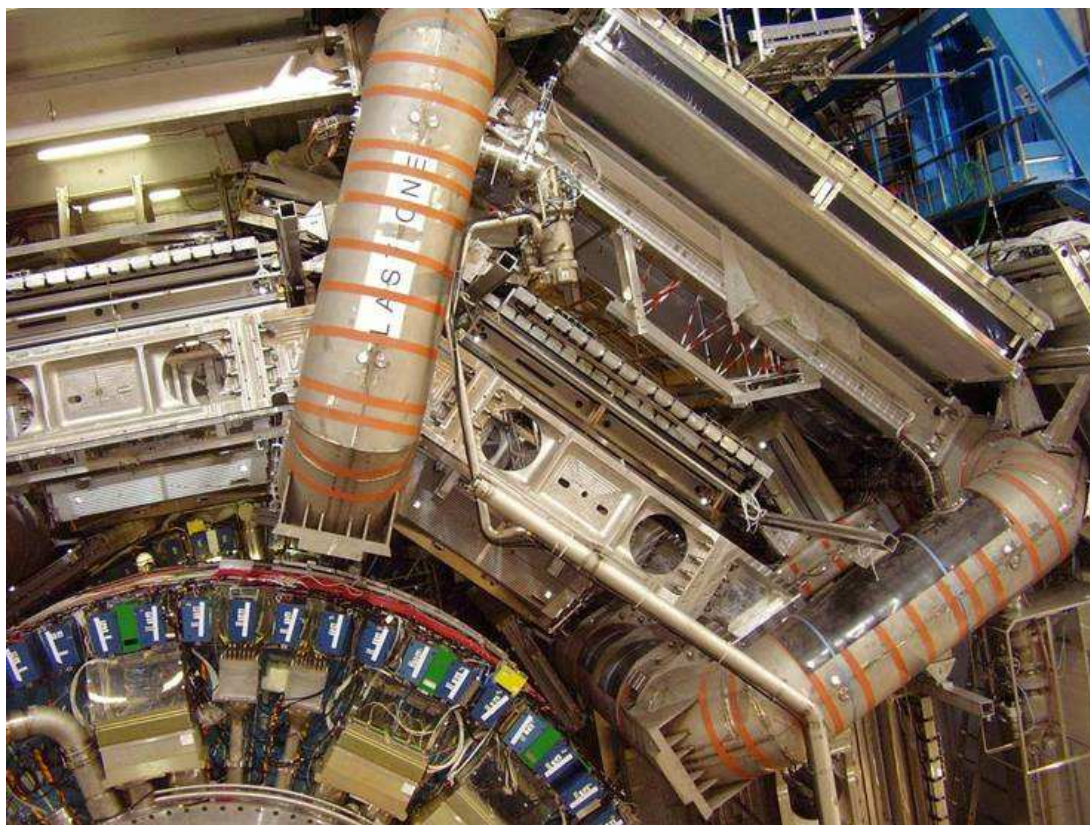
## *1 – Particle Physics*



## ATLAS

A. Annovi, M. Antonelli (Resp.), M.M. Beretta, H. Bilokon, E. Capitolo (Tech.),  
F. Cerutti, V. Chiarella, M. Curatolo, M. Dreucci, B. Esposito (Resp.), M.L. Ferrer,  
M. Gatta (Tech.), C. Gatti, P.F. Laurelli, G. Maccarrone, A. Martini, G. Nicoletti,  
G. Pileggi (Tech.), B. Ponzio(Tech.), V. Russo (Tech.), A. Salvucci (Laur.),  
A. Sansoni, M. Testa (Ass. Ric.), T. Vassilieva (Tech.), E. Vilucchi, G. Volpi

In collaboration with:  
Centro di Calcolo:  
M. Pistoni, C. Soprano



### 1 Introduction

After more than 20 years of continuous work and several months of commissioning with cosmic muon data, the ATLAS experiment started data taking at the Large Hadron Collider (CERN). From November 2009 to October 2010, ATLAS collected data proton-proton collisions at 900 GeV, 2.36 GeV, and 7 TeV center of mass energy corresponding to an integrated luminosity of about  $40 \text{ pb}^{-1}$ . November has been dedicated to lead-lead collisions at 2.67 nucleon-nucleon centre of mass energy. An integrated luminosity of about  $6.7 \mu\text{b}^{-1}$  has been collected in this last run.

These data samples have been used to study the detector performance in detail and are currently being used also for the first physics studies.

The Frascati group is involved in the study of the performances and the optimization of the muons, of the  $\cancel{E}_T$  reconstruction and on the analysis on the following channels:  $Z \rightarrow \mu\mu$ ,  $W \rightarrow \mu\nu$ ,  $Z' \rightarrow \mu\mu$ , the inclusive muon cross section, and the study of the  $J/\Psi$  and  $Z$  production in Pb-Pb collisions.

The activity of our group is also focused on the operation of the computing resources of the Frascati Proto-Tier2 and the development of the Fast Track (FTK) proposal for the upgrade of the trigger system. In the following sections a brief description of these activities is reported.

## 2 Measurement of the muon momentum resolution with 2010 collision data

The physics program of the ATLAS experiment at the LHC includes investigations of many processes with final state muons. The ATLAS detector is equipped with a Muon Spectrometer (MS) optimized to provide a momentum measurement with a relative resolution designed to be better than 3% over a wide  $p_T$  range and 10% at  $p_T = 1$  TeV, where  $p_T$  is the muon momentum component in the plane transverse to the beam axis. The momentum in the MS is measured from the deflection of the muon trajectory in the magnetic field generated by a system of air-core toroid coils. The MS track is reconstructed using three layers of precision drift tube (MDT) chambers in the pseudorapidity range  $|\eta| < 2.0$  and two layers of MDT chambers behind one layer of cathode strip chambers (CSC) for  $2.0 < |\eta| < 2.7$ . Large and small MDT and CSC chambers alternate to cover the full angle in the transverse plane,  $\phi$ , following the azimuthal segmentation of the toroid magnet system. Three layers of resistive plate chambers (RPC) in the barrel region ( $|\eta| < 1.05$ ) and three layers of thin gap chambers (TGC) in the end-caps ( $1.0 < |\eta| < 2.4$ ) provide fast response to select events with muons in the final state in real-time, forming the ATLAS level-1 muon trigger. The trigger chambers also measure the muon trajectory in the non-bending (longitudinal) plane of the spectrometer magnets. An additional determination of the muon momentum is provided by the Inner Detector (ID) for  $|\eta| < 2.5$ . The ID is composed of three detectors providing coordinate measurements for track reconstruction inside a solenoidal magnetic field of 2 T. A silicon pixel detector is mounted close to the interaction point and is surrounded by a silicon strip detector (SCT). The outermost part is a transition radiation straw tube tracker (TRT) whose full coverage is given up to  $|\eta| = 1.9$  in pseudorapidity. Muons considered for this analysis are reconstructed as combined muons. The underlying muon identification relies on the principle that first separate tracks are measured in ID and MS before the two tracks are reconstructed as a single trajectory with higher momentum resolution than each of the individual tracks could achieve.

We briefly describe here the measurement of the muon momentum resolution in the first pass reconstruction<sup>1)</sup>, done, within the ATLAS muon performance group, with the first data collected in 2010, corresponding to an integrated luminosity of  $40 \text{ pb}^{-1}$ . First pass reconstruction uses preliminary calibration and alignment and is expected to provide a poorer resolution. The resolution is measured from the width of the di-muon invariant mass distribution in  $Z \rightarrow \mu\mu$  decays and from the comparison of the individual ID and MS momentum determination for muons from  $Z \rightarrow \mu\mu$  and  $W \rightarrow \mu\nu$  decays.

The relative resolution on the momentum measurement,  $\sigma(p)/p$ , is dictated by different effects related to the amount of material that the muon traverses, the accuracy of the magnetic field description, the spatial resolution of the individual track points and the degree of internal alignment of the two subsystems. The MS is designed to provide a uniform momentum resolution as a function of the pseudorapidity. For a given value of  $\eta$ , the resolution can be parametrized in the following

way as a function of the transverse component  $p_T$ :

$$\frac{\sigma(p)}{p} = \frac{p_0^{MS}}{p_T} \oplus p_1^{MS} \oplus p_2^{MS} \times p_T \quad (1)$$

where  $p_0^{MS}$ ,  $p_1^{MS}$  and  $p_2^{MS}$  are the energy loss in the calorimeter material, multiple scattering and intrinsic resolution terms, respectively. For the ID a similar parametrization can be found. In this case the curvature measurement depends on the track length of the muon in the active material, which is reduced close to the edge of the TRT fiducial volume. This translates into a uniform response in the central part and a rapidly worsening resolution beyond this region. The following approximate parametrization of the resolution is used:

$$\frac{\sigma(p)}{p} = p_1^{ID} \oplus p_2^{ID} \times p_T \quad (2)$$

for  $\eta < 1.9$ . For  $\eta > 1.9$

$$\frac{\sigma(p)}{p} = p_1^{ID} \oplus p_2^{ID} \times p_T \times \frac{1}{\tan^2(\theta)} \quad (3)$$

where  $\eta = -\log(\tan(\theta/2))$  and  $\theta$  the muon polar angle.

Four regions of pseudorapidity are distinguished for which we expect to have different resolutions in the ID and MS:

- *barrel* – covering  $0 < |\eta| < 1.05$ ,
- *transition region* – covering  $1.05 < |\eta| < 1.7$ ,
- *end-caps* – covering  $1.7 < |\eta| < 2.0$  and
- *CSC/no TRT*: – covering  $2.0 < |\eta| < 2.5$ .

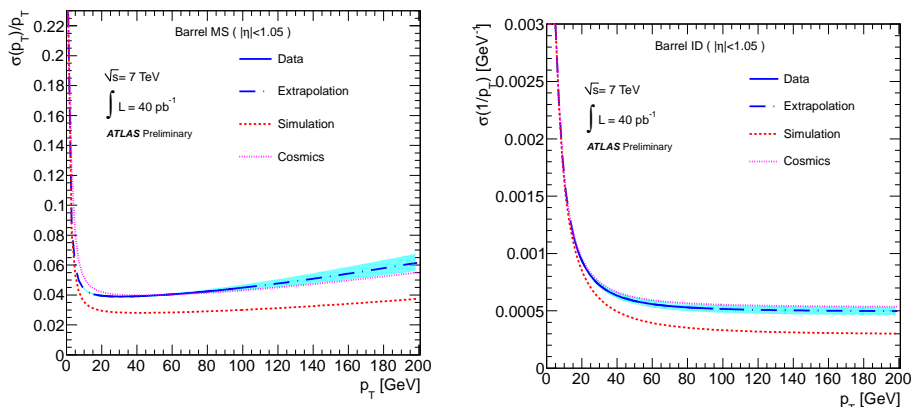


Figure 1: *Muon momentum resolution in the MS (left) and ID (right) barrel: (blue line) collision data; (red dashed line) Monte Carlo; (pink dot-dashed line) Cosmic-ray data.*

The measurement of the MS and ID momentum resolution are obtained using a Monte Carlo template technique: additional momentum smearing is added to the Monte Carlo momenta to reproduce the data distributions. External information coming from alignment with straight tracks and from the estimation of amount of material in the ID are used to constrain the fit result. The resolution parameters in Eq. 2 and 3 are determined for the four  $\eta$  regions. Fig. 1 shows the measured resolution for the MS and ID barrel (blue band) together with the MC expectation (red dashed line) and results from cosmic-ray data (pink dot-dashed line).

The additional momentum smearing measured in this way is added at analysis level. The good data-MC agreement obtained after this correction for the Z invariant mass distribution is shown in Fig. 5.

### 3 Measurement of the muon reconstruction efficiency with 2010 collision data

A study of the combined reconstruction efficiency for prompt muons in the range of  $p_T$  from 4 to 50 GeV/c has been performed using data muons from  $B$ -meson decays.

The process  $pp \rightarrow b\bar{b}X \rightarrow \mu X$  has a cross section  $\sim 7.78\mu\text{b}$  @ 7 TeV, and represents the largest source of low  $p_T$  muons at LHC. Therefore, special procedure to extract muons from  $B$ -meson decays to test the muon spectrometer efficiency has been developed. A pure sample of muons has been selected using only information from the inner detector(ID), and the muon identification capabilities of the calorimeter.

All tracks reconstructed with the Inner Detector(ID) with transverse momentum larger than 4 GeV and the absolute value of the pseudorapidity  $\eta$  smaller than 2.5 are considered as good tracks. Each track is then extrapolated to the calorimeter surface to associate it to the nearby cluster. The distance  $\Delta R$  between the intersection point and the cluster centroid position is required to be smaller than 0.05. Energy distribution and position along the shower axis of all cells associated to the cluster allow for  $\mu$  particle identification exploiting the longitudinal granularity of the calorimeter: muons behave like minimum ionizing particles while electrons and charged hadrons shower and deposit their energy mainly in the first planes of the calorimeters.

An upper and a lower cut on each energy deposition in the calorimeter layer has been set at values  $E_{\text{max}}$  and  $E_{\text{min}}$ . The values of  $E_{\text{max}}$  and  $E_{\text{min}}$  are calculated according:

$$\int_{E_{\text{min}}}^{E_{\text{max}}} f(E)dE = 0.9 \times \int_{-\infty}^{+\infty} f(E)dE, \quad |E_{\text{max}} - E_{\text{min}}| \rightarrow \text{min},$$

where  $f(E)$  is the probability density to measure energy  $E$  from a muon deposition. The values of  $E_{\text{max}}$  and  $E_{\text{min}}$  are calculated as function of  $\eta$  to account for the  $\eta$  dependence calorimeter geometry. After this selection the purity of the sample in Minimum Bias events is about 58%.

The purity can be improved selecting processes naturally enriched of leptons in final state. The process  $pp \rightarrow b\bar{b}X \rightarrow \mu X$  has a cross section  $\sim 7.78\mu\text{b}$ , and represents the largest source of low  $p_T$  muons at LHC.

Jets from  $b$  quark are tagged by using the impact parameter significance  $d_{PV}/\sigma_d$ : we select tracks associated to muon candidate with  $|d_{PV}/\sigma_d| > 3$ . To improve the rejection only tracks with an impact parameter resolution  $\sigma_d$  smaller than  $0.043 + 0.02\eta^2 + 0.009\eta^4$  mm.

Additional rejection can be made by the use of the relatively high mass of the  $b$  quark. Therefore its decay products tend to have relatively high momentum.

We use the momentum of the muon candidate in the  $b$  centre of mass,  $E_{\mu}^{CM}$ . To this purpose we search over all jets for a muon candidate within a cone of  $\Delta R=0.4$  from the jet axis.  $E_{\mu}^{CM}$  is calculated from the track parameters and the reconstructed jet momentum. The Jet energy is calculated according:  $E_{\text{Jet}}^2 = P_{\text{Jet}}^2 + m_B^2$ , where  $P_{\text{Jet}}$  is jet momentum from JetCone4H1TP algorithm,  $m_B = 5.279$  GeV is the average  $B$ -meson mass. Using this definition of the jet energy we perform a Lorentz transformation of the muon momentum in the jet rest frame. The value of  $E_{\mu}^{CM}$  is required to be larger than 1.4 GeV.

The expected number of the selected events is about 17500 per  $\text{pb}^{-1}$  depending slightly on the trigger type. The purity of the sample is larger than 99% for  $p_T > 4$  GeV and about 100% for  $p_T > 4$  GeV.

The efficiencies for the combined muon reconstruction are shown in Fig. 2 as a function of  $p_T$  for the L1Calo(left) and for the MuonswBeam(right) streams.

The results from the two streams are consistent and indicate that the MC efficiency is about 2% larger with respect to that obtained in data. For  $p_T > 5$  GeV, we obtain  $\epsilon_{DATA}/\epsilon_{MC} =$

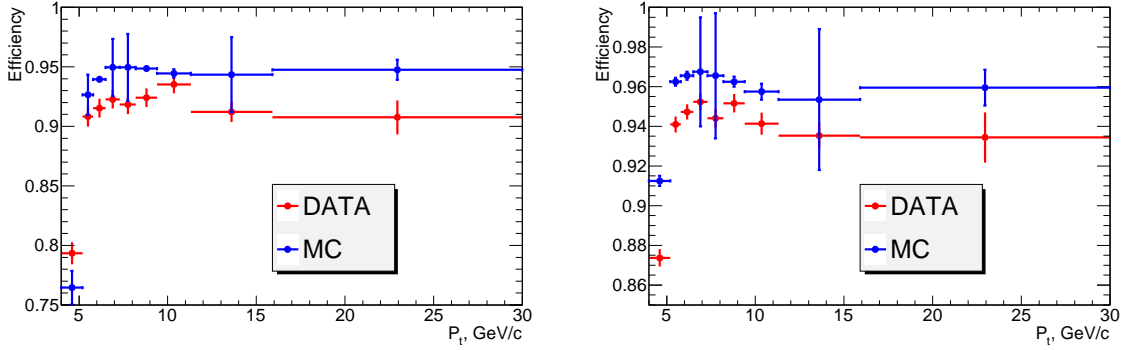


Figure 2: Efficiency as a function of the transverse momentum for MC and data: L1Calo stream on the left, MuonswBeam stream on the right.

$0.980 \pm 0.005$ , and  $\epsilon_{DATA}/\epsilon_{MC} = 0.983 \pm 0.003$  for the L1Calo(left) and for the MuonswBeam(right) respectively.

Most of the events probed in the MuonswBeam stream (with the exception of events with two semileptonic b decays) are triggered by the muon itself. The consistency of the results indicates that the reconstruction efficiency is independent on the trigger efficiency. This hypothesis is supported from the observation of the consistency of the efficiency evaluated on a pure muon trigger unbiased sample, the JetTauEtmiss sample, with that obtained in the MuonswBeam stream.

#### 4 Reconstruction of the missing transverse energy

The reconstruction and calibration of the missing transverse energy ( $\cancel{E}_T$ ) developed in ATLAS makes use of the full event reconstruction and of a calibration based on reconstructed physics objects (refined calibration).

Calorimeter cells are associated with a parent reconstructed and identified high- $p_T$  object in a chosen order: electrons, photons, hadronically decaying  $\tau$ -leptons, jets and muons.

Cells belonging to topologically formed clusters (topoclusters) not associated with any such objects are also taken into account in the  $\cancel{E}_T$  calculation.

Once the cells are associated with a category of object as described above and calibrated accordingly,  $\cancel{E}_T$  is calculated as follows:

$$E_{x(y)}^{\text{miss,calo}} = E_{x(y)}^{\text{miss,e}} + E_{x(y)}^{\text{miss,\gamma}} + E_{x(y)}^{\text{miss,\tau}} + E_{x(y)}^{\text{miss,jets}} + E_{x(y)}^{\text{miss,softjets}} + E_{x(y)}^{\text{miss,calo,\mu}} + E_{x(y)}^{\text{miss,CellOut}} \quad (4)$$

where each term is calculated from the negative sum of calibrated cell energies inside the corresponding objects:

- $E_{x(y)}^{\text{miss,e}}$ ,  $E_{x(y)}^{\text{miss,\gamma}}$ ,  $E_{x(y)}^{\text{miss,\tau}}$  are reconstructed from cells in electrons, photons and taus, respectively
- $E_{x(y)}^{\text{miss,jets}}$  is reconstructed from cells in jets with  $p_T > 20$  GeV
- $E_{x(y)}^{\text{miss,softjets}}$  is reconstructed from cells in jets with  $7 \text{ GeV} < p_T < 20$  GeV
- $E_{x(y)}^{\text{miss,calo,\mu}}$  is the contribution to  $\cancel{E}_T$  originating from the energy lost by muons in the calorimeter

- the  $E_{x(y)}^{\text{miss,CellOut}}$  term is calculated from the cells in topoclusters which are not included in the reconstructed objects. For the calculation of this term an energy flow algorithm is used.

The final  $E_{x(y)}^{\text{miss}}$  is then calculated adding the  $E_{x(y)}^{\text{miss},\mu}$  term.

The  $\cancel{E}_T$  muon term is calculated from the momenta of muon tracks reconstructed with  $|\eta| < 2.7$ :

$$E_{x(y)}^{\text{miss},\mu} = - \sum_{\text{selected muons}} p_{x(y)}^\mu \quad (5)$$

In the region  $|\eta| < 2.5$ , only well reconstructed muons in the muon spectrometer with a matched track in the inner detector are considered.

In order to deal appropriately with the energy deposited by the muon in calorimeters, the muon term is calculated differently for isolated and non-isolated muons.

This algorithm, allowing to calibrate cells separately and independently according to the object to which they belong, has the best performances in terms of linearity and resolution of the  $\cancel{E}_T$  for events containing electrons, photons, taus and muons.

In events with  $W$  and  $Z$  boson production, the calibration of the  $E_T^{\text{miss,CellOut}}$  term is of particular importance this  $\cancel{E}_T$  contribution balances the  $W/Z$  boson  $p_T$  to a large extent.

The purpose of the energy-flow algorithm is to improve the calculation of the low- $p_T$  contribution to  $\cancel{E}_T$  ( $E_T^{\text{miss,CellOut}}$ ) by adding tracks to recover the contribution from low- $p_T$  particles which do not reach the calorimeter or do not seed a topocluster. It thus exploits the better calibration and resolution of tracks at low momentum with respect to topoclusters.

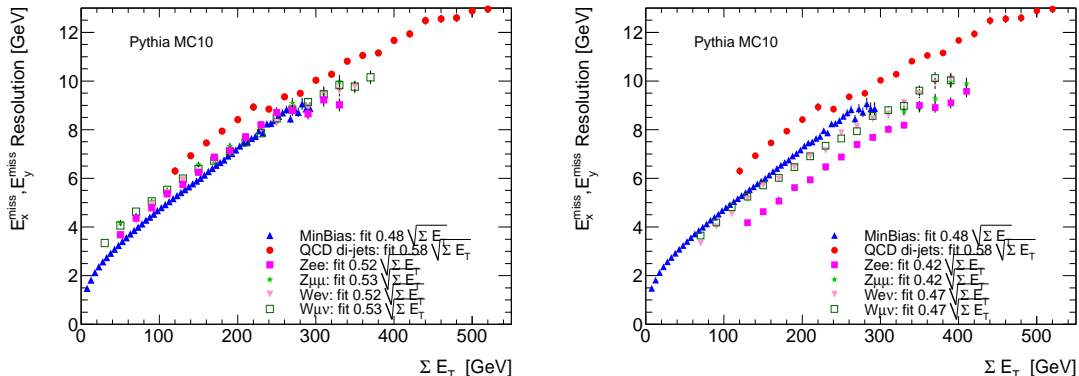


Figure 3:  $E_x^{\text{miss}}$  and  $E_y^{\text{miss}}$  resolution as a function of the total transverse hadronic energy in calorimeters (left) and the total transverse energy in the event (right). The resolution in  $W\nu\nu$  and  $W\mu\mu$  MC events is compared with the resolution in MC events for Zee,  $Z\mu\mu$ , minimum bias and QCD di-jet events.

Reconstructed tracks with  $p_T > 400$  MeV, passing track quality selection criteria such as number of hits and  $\chi^2$ , are used for the calculation of the  $E_T^{\text{miss,CellOut}}$  term. If a track is neither associated to a topocluster nor a reconstructed object, its transverse momentum is added to the calculation of  $E_T^{\text{miss,CellOut}}$ . In the case where the track is associated to a topocluster, its transverse momentum is also used but the topocluster energy is discarded. For this purpose, all selected tracks are extrapolated to the second sampling of the electromagnetic calorimeter and very conservative criteria are used for association.

To avoid double-counting, tracks associated to any high- $p_T$  objects used in the  $\cancel{E}_T$  reconstruction are vetoed. Tracks associated to muons and within the cone size of the jet reconstruction algorithm are not used.

In addition tracks connected to topoclusters entering the reconstructed objects are vetoed.

The clusters which enter the  $E_T^{\text{miss,CellOut}}$  term associated to the selected tracks must also be vetoed. For this purpose the selected tracks are extrapolated to the second sampling of the electromagnetic calorimeter and the topocluster with the largest energy associated to the track is excluded from the  $\cancel{E}_T$  calculation. The remaining topoclusters not associated to tracks are finally added for the  $\cancel{E}_T$  calculation.

Figure 3 shows the  $\cancel{E}_T$  resolution as a function of total transverse hadronic energy in calorimeters (left) and the total transverse energy in the event (right) for different processes.

## 5 Measurement of the cross section for the processes $pp \rightarrow Z/\gamma^* \rightarrow \mu\mu$ and $pp \rightarrow W \rightarrow \mu\nu$

Within the ATLAS Standard Model group, we have contributed to the cross section measurement of  $W$  and  $Z$  production in p-p collisions, in particular in the muon decay channels<sup>3)</sup>. The measurement is based on an integrated luminosity of  $35 \text{ pb}^{-1}$  collected in 2010. A total of 84103  $W^+$ , 55163  $W^-$  and 11669  $Z$  candidates are selected in the muon channels. The transverse and invariant mass distributions are shown in Fig. 4 and Fig. 5 for  $W$  and  $Z$ , respectively.

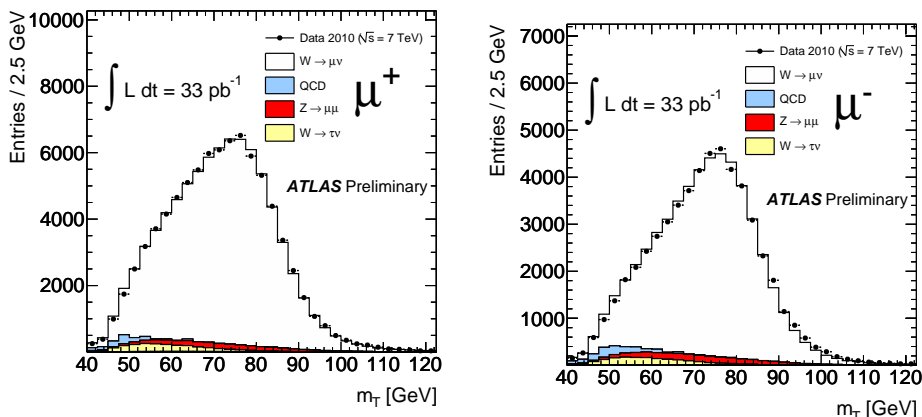


Figure 4: *Transverse mass of candidate  $W^+$  (left) and  $W^-$  (right) events.*

The luminosity contribution to the final error is 3.4%. Beside this error, the  $W \rightarrow \mu\nu$  cross section is measured with an uncertainty of 2.4%, dominated by the contribution of uncertainty on missing transverse energy and scale. The  $Z \rightarrow \mu\mu$  cross section is measured with an uncertainty of 1.1%, dominated by the uncertainty on the reconstruction efficiency.

In Fig. 6 we show the result for the ratio of  $W$  and  $Z$  cross sections after combining the results obtained for the muon and electron channels. In this ratio the uncertainty on the luminosity and part of the uncertainty due to the parton distributions cancel out. The experimental result is compared with the prediction obtained from four different sets of NNLO parton distributions. The final uncertainty on this ratio is about 2.7%.

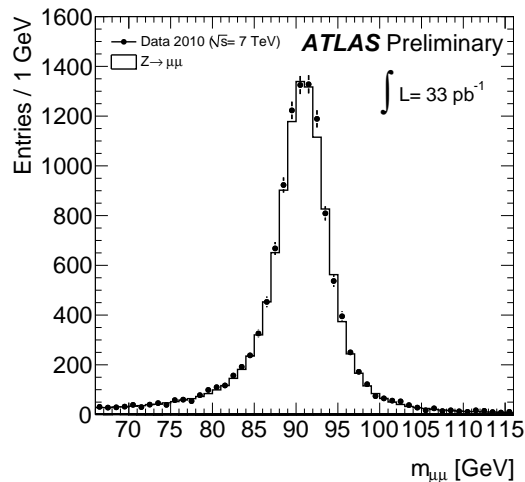


Figure 5: *Invariant mass distribution for candidate  $Z \rightarrow \mu\mu$  events.*

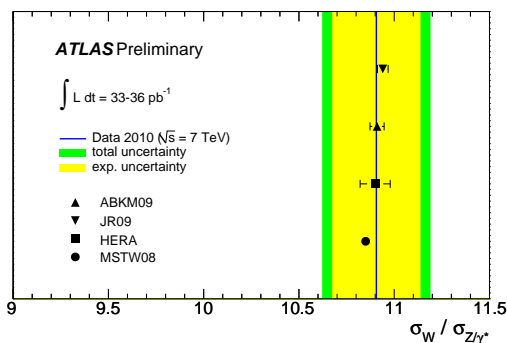


Figure 6: *Measured and predicted cross section ratio,  $(\sigma_W/\sigma_Z)$ .*

## 6 Measurement of the muon inclusive cross section

High transverse momentum muons are a key signature of interesting processes in hadronic interactions. At low transverse momenta the muon spectrum is dominated by light hadron decays, while at intermediate momenta it is dominated by heavy flavour decays before the onset of the W/Z Jacobian peak. In the range  $4 < p_T < 100$  GeV the muon inclusive spectrum is most sensitive to heavy flavour production.

A measurement in this region is useful to optimize theoretical models and effective Monte Carlo generators to improve the evaluation of the heavy flavour production mechanism.

At high  $p_T$  the NLO + NLL prediction becomes in fact more accurate due to the reduction of the scale uncertainty and the deviation between the NLO computation and the NLO + NLL becomes larger. Here we present first probe of the Next to Leading Log resummation at high  $p_T$  directly in the perturbative part of the QCD calculation in heavy flavour production at hadron

The muon inclusive cross section is given by:

$$\frac{d\sigma(pp \rightarrow \mu X)}{dp_T} = \frac{1}{L} \frac{dN_\mu}{dp_T} \quad (6)$$

where  $L$  is the integrated luminosity of the data sample and  $N_\mu$  is the number of muons in a  $p_T$  bin corrected for the fraction of background and for all trigger, selection and reconstruction efficiency and after the unfolding of the detector resolution. The measurement is done in the interval  $|\eta| < 2.5$  and  $4 < p_T < 100$  GeV. The data were collected in 2010 in the periods A,B,C,D, E corresponding to an integrated luminosity of  $1.4 \text{ pb}^{-1}$ .

In fig. 7 we show the cross section measurement with its total error (statistical plus systematic added in quadrature) as a function of  $p_T$ . The systematic error includes the 3.4% error on the luminosity measurement. The theoretical predictions for the cross section are shown.

In particular MC@NLO with CTEQ6.6 pdfs has been used for the W and Z shapes normalized to the measured  $W^\pm, Z$  cross section to muons measured by ATLAS<sup>3)</sup> ( $\sigma_{W^+}^\mu = 6.21 \pm 0.02_{\text{stat.}} \pm 0.25_{\text{syst.}}$ ,  $\sigma_{W^-}^\mu = 4.107 \pm 0.02_{\text{stat.}} \pm 0.19_{\text{syst.}}$ ,  $\sigma_Z^\mu = 0.941 \pm 0.008_{\text{stat.}} \pm 0.038_{\text{syst.}}$ ) where the systematic error has been computed summing in quadrature the acceptance and the measurement systematic error, the error on the luminosity has not been included being fully correlated with the present measurement. The heavy flavour contribution is taken from the FONLL central prediction while the the Drell Yan processes with  $m_{\mu\mu} < 60$  GeV are evaluated using Pythia. The data show very good agreement with the theoretical expectation over six order of magnitude.

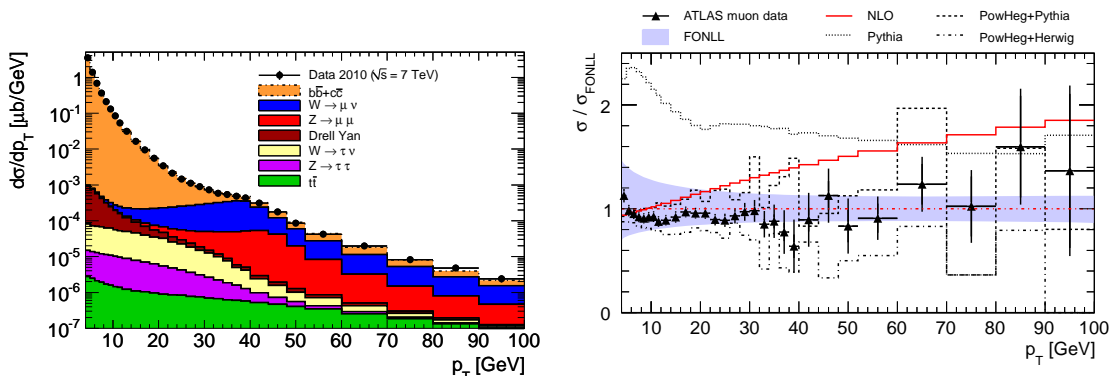


Figure 7: Muon inclusive differential cross section: (left)total, (right) ratio with FONLL theoretical prediction for heavy flavours component. The prediction from Pythia and PowHeg are also shown.

In order to compare with theoretical predictions of inclusive muons from heavy flavours, we subtract from the measured cross section the electro-weak contribution and show the results in Fig. 7(right). The prediction is compared with the FONLL calculation with CTEQ6.6 pdfs, whose uncertainty band is shown. The total uncertainty, dominated by renormalization and factorization, is around 20%, rising above 30% at low  $p_T$ .

## 7 Measurement of the centrality dependence of $J/\Psi$ yields and observation of Z production in lead-lead collisions

The measurement of quarkonia production in ultra-relativistic heavy ion collisions provides a potentially powerful tool for studying the properties of hot and dense matter created in these collisions. If deconfined matter is indeed formed, then colour screening is expected to prevent the formation of quarkonium states when the screening length becomes shorter than the quarkonium size. Since this length is directly related to the temperature, a measurement of a suppressed quarkonium yield

may provide direct experimental sensitivity to the temperature of the medium created in high energy nuclear collisions.

The interpretation of  $J/\psi$  suppression in terms of colour screening is generally complicated by the quantitative agreement between the overall levels of  $J/\psi$  suppression measured by the NA50 experiment at the CERN SPS ( $\sqrt{s_{NN}} = 17.3$  GeV) and the PHENIX experiment at RHIC ( $\sqrt{s_{NN}} = 200$  GeV). Data from proton-nucleus and deuteron-gold collisions also show decreased rates of  $J/\psi$  production, indicating that other mechanisms may come into play. Finally, there exist proposals for  $J/\psi$  enhancement at high energies from charm quark recombination. Measurements at higher energies, with concomitantly higher temperatures and heavy quark production rates, are clearly needed to address these debates with new experimental input. The production of  $Z$  bosons, only available in heavy ion collisions at LHC energies, can serve as a reference process for  $J/\psi$  production, since  $Z$ 's are not expected to be affected by the hot, dense medium, although modifications to the nuclear parton distribution functions must be considered.

The data sample consists of approximately  $6.7 \mu\text{b}^{-1}$  from the 2010 LHC heavy ion run. In order to determine the  $J/\psi \rightarrow \mu^+\mu^-$  reconstruction efficiency, Monte Carlo (MC) samples have been produced superimposing  $J/\psi$  and  $Z$  events from PYTHIA into simulated Pb-Pb events generated with the HIJING event generator. HIJING was run in a mode with effects from jet quenching turned off, since they have not been adjusted to agree with existing experimental data. Elliptic flow was imposed on the events subsequent to generation, with a magnitude and  $p_T$  dependence derived from RHIC data.

Lead-lead collision centrality percentiles are defined from the total transverse energy,  $\Sigma E_T^{\text{FCal}}$ , measured in the forward calorimeter (FCal), which covers  $3.2 < |\eta| < 4.9$ .

The full data sample is divided into four bins of collision centrality, 40-80%, 20-40%, 10-20%, and 0-10%. The most peripheral 20% of collisions are excluded from this analysis due to larger systematic uncertainties in estimating the number of binary nucleon-nucleon collisions in these events. The  $J/\psi \rightarrow \mu^+\mu^-$  reconstruction efficiency is obtained from the MC samples as a function of the event centrality. The inefficiency gradually increases from peripheral to central collisions, due primarily to an occupancy-induced inefficiency in the ID tracking.

The oppositely-charged di-muon invariant mass spectra in the  $J/\psi$  region after the selection are shown in Figure 8(left). The number of  $J/\psi \rightarrow \mu^+\mu^-$  decays is then found by a simple counting technique. The signal mass window is defined by the range 2.95–3.25 GeV. The background is derived from two mass sidebands, 2.4–2.8 GeV and 3.4–3.8 GeV, with a linear extrapolation.

The “relative yield” is defined by normalizing to the yield found in the most peripheral 40-80% centrality bin after correcting for the reconstruction efficiency:  $R_c = N_c^{\text{corr}}/N_{40-80\%}^{\text{corr}}$ .

The ratio of these two values,  $R_{cp}$ , is shown as a function of centrality in the right panel of Figure 8. The data points are not consistent with their average, giving a  $P(\chi^2, N_{\text{DOF}})$  value of 0.11% with three degrees of freedom, computed conservatively ignoring any correlations among the systematic uncertainties. Instead, a significant decrease of  $R_{cp}$  as a function of centrality is observed as a function of centrality indicating a deviation from the simplest expectation based on QCD factorization.

The  $R_{cp}$  variable for the  $Z$  candidates is computed in the same way as for the  $J/\psi$  sample.

The measured  $Z$  yields are, within the large statistical uncertainty, consistent with a linear scaling with the number of binary collisions, the low statistics preclude drawing any definitive conclusion.

## 8 LNF Tier-2 activity

The LNF Tier-2 computing farm is considered a proto-Tier-2 by INFN and is in the process of getting officially approved. However, during 2010 it has worked at full efficiency providing

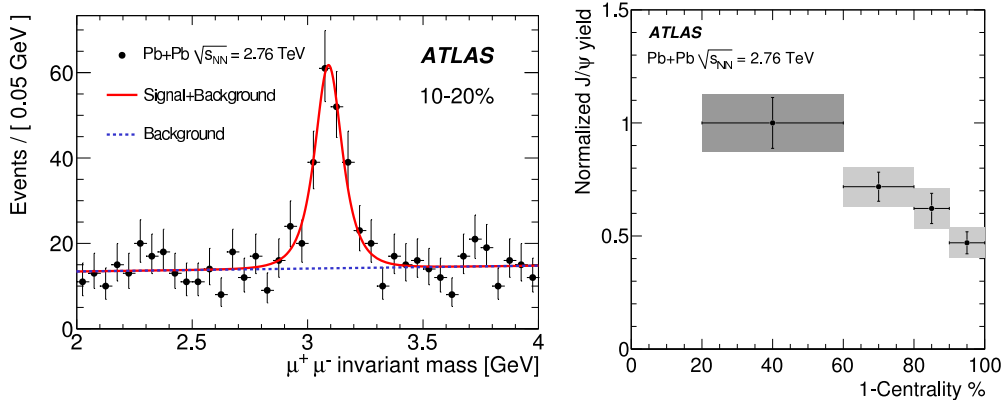


Figure 8: (left) invariant mass distribution of the  $\mu^+ \mu^-$  candidates for a 10-20% centrality. (right) Value of  $R_{cp}$ , as described in the text, as a function of centrality. The statistical errors are shown as vertical bars while the grey boxes also include the combined systematic errors. The darker box indicates that the 40-80% bin is used to set the scale for all bins, but the uncertainties in this bin are not propagated into the more central ones.

computing power and data storage for official and private ATLAS simulation and production campaigns. Fig. 9 shows in red the available KSI2k per day and in bordeaux the CPU used by the experiment. In 2010 the storage dedicated to data increased to about 100TB sufficient to satisfy ATLAS policies for data replication.

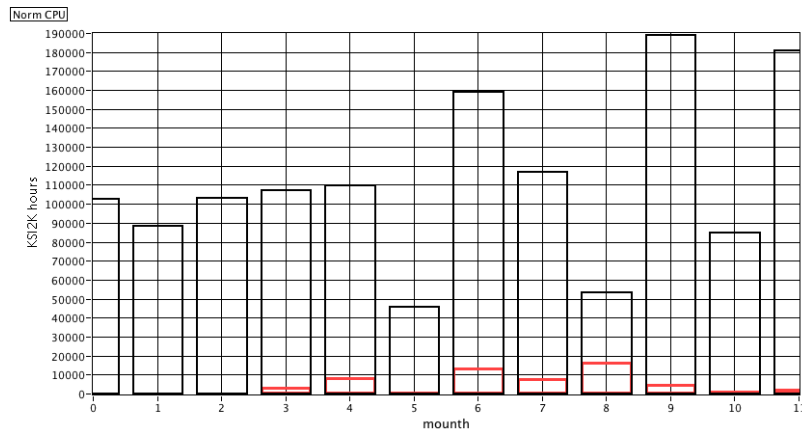


Figure 9: CPU usage by month during year 2010.

The financial support received, both from central and local resources, made possible to expand the configuration and to buy some resources dedicated to the local group. The farm currently has three racks dedicated to servers, computing nodes and storage, with a fourth one to be installed in 2011. Tier-2 resources were bought in conjunction with the other three Italian ATLAS Tier-2s. In this way the site has begun to standardize its hardware to those of the other Italian Tier-2s. Furthermore, with the increased number of nodes in 2010, we installed two 10Gbs switches connected to each other and to the disk servers. In this way critical communications have a

maximum bandwidth of 10Gbs. The connection with the LNF network is at 1 Gbs.

The current configuration of the Tier-2 and local farm are:

- The Tier-2 computing power increased by 3 twin worker nodes, for a total number of 168 computing slots<sup>1</sup>
- Two new servers replaced the old Computing Element and Storage Element, an additional server is the CREAM Computing Element;
- The Tier-2 storage capability is currently of 145TB usable;
- The local computing power corresponds to three 8-core servers;
- The local storage capability is 36TB raw.

At present the Tier-2 has a dedicated man-power equivalent to 1.5 FTE: 0.2 FTE from the Computing Service, responsible of maintenance and software installations, and 1.3 FTE (three people) from the ATLAS group, responsible of all ATLAS related interventions and users support. The local group is involved in periodic activities such as:

- Participation to the ATLAS Italian shifts for cloud monitoring;
- Participation to phone conferences like SA1, accounting, Tier-2 Federation, analysis activities;

The LNF Tier-2 personnel, in collaboration with the Federation of ATLAS Italian Tier-2s, has contributed to improve the efficiency of Tier-2s computing activities, to be ready for the next data taking; see works in <sup>5, 6</sup>) and Hammer Cloud analysis tests listed in <http://hammercloud.cern.ch/atlas/all/test/>.

## 9 Fast Track

The trigger is a fundamental part of any experiment at hadron colliders. It is needed to select on-line the low cross-section physics from the huge QCD background.

Experience at high luminosity hadron collider experiments shows that controlling trigger rates at high instantaneous luminosity can be extremely challenging. As the luminosity increases, physics goals change in response to new discoveries, and detector aging. It is thus essential that the trigger system be flexible and robust, and have redundancy and significant operating margin. Providing high quality track reconstruction over the full ATLAS Inner Detector by the start of processing in the level-2 computer farm can be an important element in achieving these goals.

With the goal to improve and make more robust the ATLAS trigger, during summer 2007 the group joined the Fast-Track (FTK) proposal for “A hardware track finder for the ATLAS trigger”. This is a proposal to build a hardware track finder as an upgrade to the ATLAS trigger. It will provide global reconstruction of tracks above 1 GeV/c in the silicon detectors, with high quality helix parameters, by the beginning of level-2 trigger processing. FTK can be particularly important for the selection of 3rd-generation fermions (b and  $\tau$ ). These have enormous background from QCD jets, which can be quickly rejected in level-2 if reconstructed tracks are available early. This R&D proposal was completed with the submission of the FTK Technical Proposal that was approved by ATLAS in April 2010. The Fast-Tracker project is continuing the approval process by the ATLAS collaboration. It was presented for the initial review in December 2010 and it was approved by the ATLAS EB. We are continuing the design and prototyping R&D aiming to prepare the FastTrack Technical Design Report in 2 years.

---

<sup>1</sup>All nodes installed after 2009 use hyper-threading to optimize the use of resources and have two slots for each CPU core.

The simulation work in 2010 generated new ideas and important changes that are a major improvement in the Fast-Tracker pattern-recognition technology. The goal was to design the FTK architecture for online tracking at the LHC design luminosity of  $10^{34} \text{ cm}^{-2} \text{ s}^{-1}$  and  $3 \cdot 10^{34} \text{ cm}^{-2} \text{ s}^{-1}$ , corresponding to up to 75 pile-up events per bunch-crossing.

The FTK processor performs pattern recognition with a custom device called the Associative Memory (AM). It is an array of VLSI chips that stores pre-calculated trajectories for a ultra-fast comparison with data. The first way to reduce the combinatorial at high luminosity is to work with better resolution in the AM. In order to do that, we will need a new AM chip with a high density of patterns, so that all possible tracks with a thinner resolution can be stored in the AM. Even with better resolution the number of candidate tracks that the AM will find at these high instantaneous luminosities will be very large. For this reason we redesigned the FTK architecture to increase the internal parallelism and data-flow to accommodate a larger flux of data. Beyond increasing the computing power and parallelism we designed and simulated 3 different pattern matching strategies. The 11 layer architecture that uses the AM to find tracks segment in all 11 layers (3 pixel layers and 4 double SCT layers). The 8 layer architecture that uses the AM to find tracks segment in the 4 double SCT layers and then extends the found track in the pixels using a second AM system. The 7 layer architecture that uses the AM to find tracks segment in the 3 pixel layers and the 4 r-phi SCT layers. The 7 layer segments are then extended extrapolating and searching for the 4 extra hits in the 4 SCT stereo layers. For all architectures the final fit is a 11 layer fit with full resolution. This is currently being extended to a 12 layer fit including the new Insertable B-Layer. This work was a joint effort between Frascati, Pisa, Chicago and Illinois that resulted in the FTK Technical Proposal (2010). Later on studies continued and the last architecture option was chosen as a valid candidate that reduces combinatorial in the first step to a manageable level. For this purpose it was essential a new ideas. The efficiency curves for patterns is slowly increasing for efficiencies above 70%. This is due to the fact that many low probability patterns are needed to gain the missing efficiency. This is a consequence of the fact that the AM performs pattern recognition with a fixed resolution. We developed the idea of variable resolution patterns. This can be implemented in the AM if the lowest significant bits of the hit positions can be ignored (don't care option) on a pattern by pattern and layer by layer basis. In this way the effective shape of a pattern can be optimized in each layer to provide a larger coverage (meaning less patterns) for a lower fake rate. The implementation of this feature required major modifications to the FTK simulation. After these were implemented with found that using 1 don't care bit per layer, allowing for a factor of 2 flexibility in resolution, we could gain the equivalent of a factor of 3 extra patterns. We also studied the case of 2 don't care bits per layer, allowing for a factor of 4 flexibility in resolution. In this case the gain is of an equivalent factor of 5 in patterns. It is a very important result. Indeed, while the hardware size is proportional to number of patterns, each don't care bits correspond to an increase of approximately 8% in the AMchip area. Such a good result was possible and was the motivation of this study, but it was not possible to foresee that the variable resolution was so effective.

In 2010 we continued the R&D of the new AM chip in collaboration with Pisa, Milano and Fermilab. This is a very challenging task because we need to increase the pattern per chip with respect to the current AM chip designed for the SVT upgrade at CDF by a factor 30 with similar power consumption running at 100 MHz clock speed instead of 40 MHz. In order to achieve these goals we need several separate improvements: better technology 65 nm instead of 180 nm, design full custom cell that implements the core AM logic, a specific optimization of the global logic, and possibly implement a 3D silicon device to increase the available area. Frascati and Milano worked on the design of the full custom AM cell. This work is the critical element of this project because advanced techniques are required to meet the density and power consumption goals. This element will require intensive simulation to verify functionality under all conditions. The originally

planned mini-asic chip with 90nm technology became very expensive after Europractice increased by a factor 3 prices because European Community financial support for these prototypes was reduced. For this reason it became convenient to prepare a larger area (12mm<sup>2</sup>) MPW run with 65nm technology. While taking advantage of the experienced gained with the 90nm design, we started a new design with 65nm technology. Based on FTK simulation results, the 65nm AM cell was designed to work with up to 3 don't care bits per layer. At the end of 2010 a preliminary associative memory cell was designed. We expect the AM chip prototype to be fully designed and submitted for MPW run in 2011.

The Frascati group studied a hardware-implementable clustering algorithm for the pixel detector. Clustering in the pixel detector is a non trivial computational problem because of the 2D nature of the pixel detectors and of the huge amount of data involved. The pixel detector's RODs deliver data over 132 S-Link fibers each with a 1.2 Gbs bandwidth. The clustering algorithm must identify and cluster hits as well as calculate the center of the cluster.

These ideas have been studied and resulted in a first implementation of the algorithm that solves the clustering problem with a sensible amount of hardware that is one FPGA (XC6SLX150T) for each S-Link fiber. We have a FPGA implementation of the algorithm core. It is a proof of feasibility in the FPGA simulation framework.

## References

1. ATLAS Coll., "ATLAS muon momentum resolution in the first pass reconstruction of the 2010 pp collision data at  $\sqrt{s} = 7$  TeV", ATL-CONF-2011-046.
2. ATLAS Coll., "Performance of the Missing Transverse Energy Reconstruction and Calibration in Proton-Proton Collisions at a Center-of-Mass Energy of 7 TeV with the ATLAS Detector", ATL-CONF-2011-057; ATLAS Coll., "Performance of the missing transverse energy reconstruction in minimum bias events at s of 900 GeV and 2.36 TeV with the ATLAS detector", ATL-CONF-2011-008.
3. ATLAS Coll., "A measurement of the total  $W^\pm$  and  $Z/\gamma^*$  cross sections in the  $e$  and  $\mu$  decay channels and of their ratios in  $pp$  collisions at  $\sqrt{s} = 7$  TeV with the ATLAS detector", ATL-CONF-2011-041.
4. ATLAS Coll., "Measurement of the centrality dependence of  $J/\psi$  yields and observation of  $Z$  production in lead-lead collisions with the ATLAS detector at the LHC," Phys. Lett. B **697**, 294 (2011). [arXiv:1012.5419 [hep-ex]].
5. A. Doria *et al.*, "Deployment of job priority mechanisms in the Italian cloud of the ATLAS experiment", Journal of physics. Conference series. - ISSN 1742-6588. - ISSN 1742-6596. - 219:7(2010), pp. 072001.1-072001.10. (Presented at the 17th Inter. Conference on computing in high energy and nuclear physics, Praga, 2009.
6. A. Andreatza *et al.* "Computing infrastructure for ATLAS data analysis in the Italian Grid cloud", (Presented at the 18th Inter. Conference on computing in high energy and nuclear physics, Taiwan, 2010.
7. A. Andreani *et al.*, "The FastTracker Real Time Processor and Its Impact on Muon Isolation, Tau and b-Jet Online Selections at ATLAS", Conf. Record 17th IEEE NPSS Real Time Conference Record of the 17th Real Time Conference, Lisbon, Portugal, 24 - 28 May 2010.
8. A. Annovi *et al.*, "Associative Memory Design for the FastTrack Processor (FTK) at ATLAS", Conference Record 17th IEEE NPSS Real Time Conference Record of the 17th Real Time Conference, Lisbon, Portugal, 24 - 28 May 2010.

## **BABAR**

A. Calcaterra, R. de Sangro, G. Finocchiaro, S. Pacetti,  
P. Patteri, I. Peruzzi (Resp.), M. Piccolo, M. Rama, A. Zallo

### **1 Introduction**

The *BABAR* experiment has been running at the PEP-II asymmetric *B* factory of the SLAC National Laboratory (Stanford, USA) from 1999 to 2008, collecting a data sample corresponding to approximately  $0.5 \text{ ab}^{-1}$ . The data were collected mostly at the CM energy corresponding to the  $\Upsilon(4S)$  mass; large data sample were also obtained at the CM energy corresponding to the  $\Upsilon(2S)$  and  $\Upsilon(3S)$  resonances. The experiment has produced a wealth of important physics results, ranging from the measurement of the three angles of the Unitarity triangle to the discovery of the  $D - \bar{D}$  mixing, the  $\eta_b$  and several interesting charm and charmonium states. To date the *BABAR* analysis effort has resulted in about 450 publications in *Phys. Rev. Lett.* or *Phys. Rev. D*. After the end of data taking the complete data set was reprocessed, and large amount of Monte Carlo events were generated and fully reconstructed; 2010 was supposed to be the last year of the intense analysis period but this activity is not yet slowing down. The preparation of a "Physics of the *B*-factories" book to illustrate the analysis strategies and the physics results of the *B*-factories is near completion, in collaboration with the Belle group. In 2010 the main activity at LNF has been the analysis of  $B \rightarrow D^{*+}D^{*-}$  selected with a partial reconstruction technique described in the next section.

### **2 Measurement of Time-dependent *CP* violation in $B \rightarrow D^{*+}D^{*-}$ decays with partial reconstruction**

In this analysis the selection of  $B \rightarrow D^{*+}D^{*-}$  candidates is made using the concept of a "partially reconstructed decay": one of the  $D^*$  mesons is reconstructed with the  $D^{*\pm}$  decaying to  $D^0\pi^+$  (or  $\bar{D}^0\pi^-$ ), and the  $D^0$  decaying into one of the 4 modes  $K\pi$ ,  $K\pi\pi^0$ ,  $K3\pi$ ,  $K_s^0\pi^+\pi^-$ , but for the other  $D^*$  only a slow pion is required. A candidate is selected if the kinematics is compatible with the assumption that the slow pion originates from the decay  $D^* \rightarrow D^0\pi$  with a missing  $D^0$ : candidates having a missing mass  $m_{D^0} \geq 1.836 \text{ GeV}/c^2$ , and having been tagged as  $B^0$  or  $\bar{B}^0$  are accepted and passed on to the fit of the *CP* parameters  $C$  and  $S$ . In the  $\Delta t$  fit the ordered decay times of the *CP* and *tag* vertices are simultaneously fit for the signal component and possible combinatorial and peaking backgrounds mainly coming from  $B\bar{B}$  and  $c\bar{c}$  decays.

The number of signal events in the final sample is substantially higher with this technique than in full reconstruction analyses, clearly at the price of higher backgrounds. The main challenge of the analysis is in fact controlling the background sources, which is performed with an accurate description of their kinematical and  $\Delta t$  properties.

In 2010 this analysis has been finalized for publication, and it is presently under review by an internal review panel. The major advancements have been:

- a full review of the various part of the analysis, including tagging, vertexing etc.;
- finalization of the  $S, C$  *CP* violating parameters fitting procedure, including toy Monte Carlo validation studies of the fit;
- inclusion of the full data set collected until the end of BaBar data taking, corresponding to runs 1 through 6, using the latest reconstruction software developments;

- completion of the study of the systematic errors;

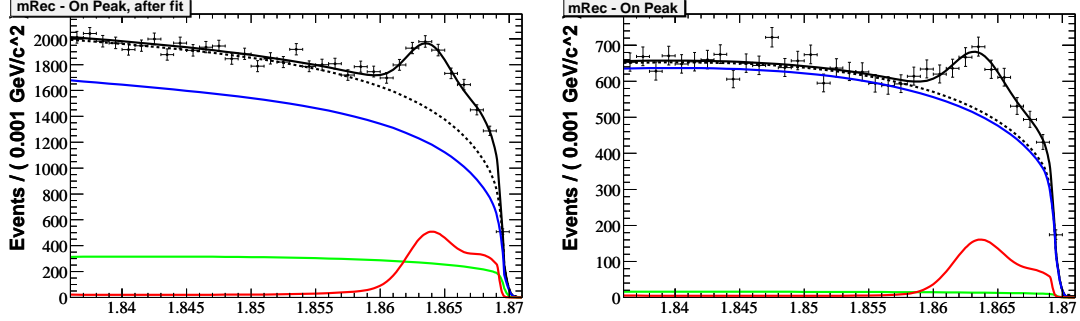


Figure 1: *Missing mass for  $B \rightarrow D^{*\pm} \pi^\mp (X)$  for kaon (left) and lepton (right) tagged events. The curves represent the probability distribution functions (p.d.f.) for signal (red), continuum background (green),  $B\bar{B}$  background (blue) and their sum (black).*

In fig. 1 we show the recoil mass distribution of real data from RUN 1 through 6 (black crosses), corresponding to  $\approx 435 \text{ fb}^{-1}$  of integrated luminosity. The presence of an excess of events in the signal region is evident. We fit the data with a PDF (black curve), made of a signal component (red) plus a continuum (green) and  $B\bar{B}$  (blue) combinatorial background component. We find a total of 4170 (1117) events in the kaon (lepton) sample. We fit the time distribution in the data,

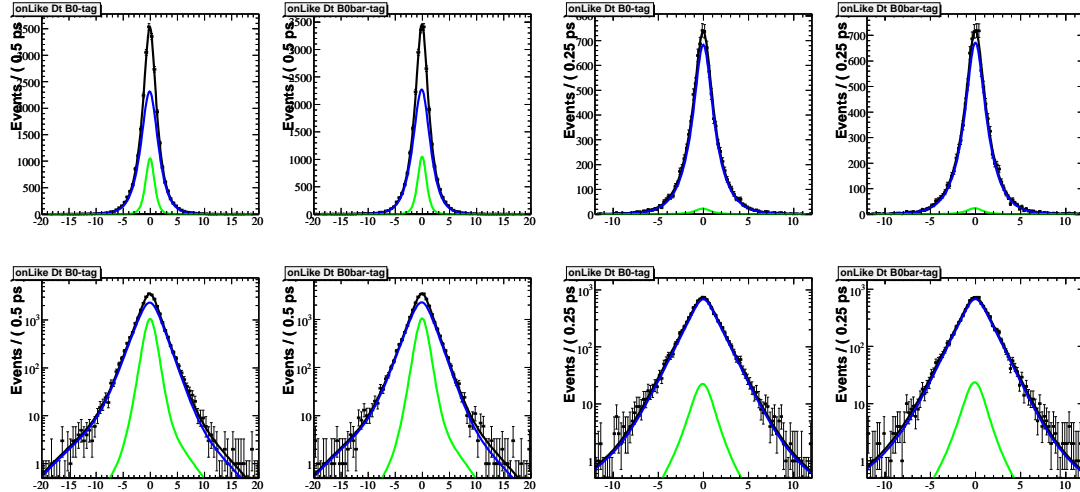


Figure 2:  *$\Delta t$  fit to RUN 1-6 data. The curves represent the total pdf (black) with the continuum (green) and  $B\bar{B}$  background (blue). We do not show the signal component pdf, as the result is blinded at this time.*

whose result we show in fig. 2 where we plot the time difference distribution of all data events for the full RUN 1-6 statistics.

At present the results are still blind, pending the end of the internal review process. However, we can summarize here the errors obtained from the fit and their corresponding systematic. We find, for kaon tagged events:

$$\delta C = 0.11 \pm 0.02 \quad (1)$$

$$\delta S = 0.16 \pm 0.05, \quad (2)$$

and lepton tagged ones:

$$\delta C = 0.15 \pm 0.04 \quad (3)$$

$$\delta S = 0.20 \pm 0.07. \quad (4)$$

The combined statistical error is:

$$\delta C = \pm 0.09 \quad (5)$$

$$\delta S = \pm 0.12, \quad (6)$$

This measurement reduces the error of the previous BaBar measurement performed with fully reconstructed  $D^{*+} D^{*-}$  final states by  $\approx 25\%$ .

## References

1. P. del Amo Sanchez *et al.*, *BABAR* Coll., *Phys. Rev. D* **82**, 111101 (2010) [arXiv:1009.2076 [hep-ex]].
2. P. del Amo Sanchez *et al.*, *BABAR* Coll., *Phys. Rev. D* **82**, 112002 (2010) [arXiv:1009.1529 [hep-ex]].
3. P. del Amo Sanchez *et al.*, *BaBar* Coll., *Phys. Rev. D* **82**, 091103 (2010) [arXiv:1008.4080 [hep-ex]].
4. P. del Amo Sanchez *et al.*, *BABAR* Coll., *Phys. Rev. D* **82**, 052004 (2010) [arXiv:1008.0338 [hep-ex]].
5. P. del Amo Sanchez *et al.*, *BABAR* Coll., *Phys. Rev. Lett.* **105**, 172001 (2010) [arXiv:1007.3526 [hep-ex]].
6. B. Aubert *et al.*, *BABAR* Coll., *Phys. Rev. D* **82**, 031102 (2010) [arXiv:1007.1370 [hep-ex]].
7. P. del Amo Sanchez *et al.*, *BABAR* Coll., *Phys. Rev. D* **82**, 072004 (2010) [arXiv:1007.0504 [hep-ex]].
8. P. del Amo Sanchez *et al.*, *Babar* Coll., *Phys. Rev. D* **82**, 072006 (2010) [arXiv:1006.4241 [hep-ex]].
9. B. Aubert *et al.*, *BABAR* Coll., *Phys. Rev. D* **82**, 091102 (2010) [arXiv:1006.2216 [hep-ex]].
10. P. del Amo Sanchez *et al.*, *BABAR* Coll., *Phys. Rev. D* **82**, 011101 (2010) [arXiv:1005.5190 [hep-ex]].
11. P. del Amo Sanchez *et al.*, *BABAR* Coll., *Phys. Rev. D* **82**, 051101 (2010) [arXiv:1005.4087 [hep-ex]].
12. P. del Amo Sanchez *et al.*, *BABAR* Coll., *Phys. Rev. Lett.* **105**, 121801 (2010) [arXiv:1005.1096 [hep-ex]].

13. P. del Amo Sanchez *et al.*, *BABAR* Coll., Phys. Rev. D **82**, 092006 (2010) [arXiv:1005.0068 [hep-ex]].
14. P. del Amo Sanchez *et al.*, *BABAR* Coll., Phys. Rev. Lett. **105**, 081803 (2010) [arXiv:1004.5053 [hep-ex]].
15. P. del Amo Sanchez *et al.*, BaBar Coll., Phys. Rev. D **82**, 011502 (2010) [arXiv:1004.0240 [hep-ex]].
16. P. del Amo Sanchez *et al.*, *BABAR* Coll., Phys. Rev. D **82**, 111102 (2010) [arXiv:1004.0175 [hep-ex]].
17. P. del Amo Sanchez *et al.*, *BABAR* Coll., Phys. Rev. D **81**, 111103 (2010) [arXiv:1003.3397 [hep-ex]].
18. P. del Amo Sanchez *et al.*, *BABAR* Coll., Phys. Rev. D **82**, 031101 (2010) [arXiv:1003.0640 [hep-ex]].
19. J. P. Lees *et al.*, BaBar Coll., Phys. Rev. D **81**, 111101 (2010) [arXiv:1002.4550 [hep-ex]].
20. P. del Amo Sanchez *et al.*, *BABAR* Coll., Phys. Rev. Lett. **104**, 191801 (2010) [arXiv:1002.4358 [hep-ex]].
21. J. P. Lees *et al.*, *BABAR* Coll., Phys. Rev. D **81**, 052010 (2010) [arXiv:1002.3000 [hep-ex]].
22. B. Aubert *et al.*, *BABAR* Coll., Phys. Rev. D **81**, 092003 (2010) [arXiv:1002.0281 [hep-ex]].
23. J. P. Lees *et al.*, *BABAR* Coll., Phys. Rev. Lett. **104**, 151802 (2010) [arXiv:1001.1883 [hep-ex]].
24. B. Aubert *et al.*, *BABAR* Coll., Phys. Rev. Lett. **105**, 051602 (2010) [arXiv:0912.0242 [hep-ex]].
25. B. Aubert *et al.*, BaBar Coll., Phys. Rev. D **81**, 011102 (2010) [arXiv:0911.2024 [hep-ex]].
26. B. Aubert *et al.*, *BABAR* Coll., Phys. Rev. D **81**, 052009 (2010) [arXiv:0909.2171 [hep-ex]].
27. B. Aubert *et al.*, *BABAR* Coll., Phys. Rev. Lett. **104**, 021802 (2010) [arXiv:0908.2381 [hep-ex]].
28. B. Aubert *et al.*, *BABAR* Coll., Phys. Rev. D **81**, 032003 (2010) [arXiv:0908.0415 [hep-ex]].
29. B. Aubert *et al.*, *BABAR* Coll., Phys. Rev. Lett. **104**, 011802 (2010) [arXiv:0904.4063 [hep-ex]].
30. B. Aubert *et al.*, *BABAR* Coll., Phys. Rev. D **81**, 051101 (2010) [arXiv:0809.4027 [hep-ex]].

## BESIII

M. Anelli (Tech.), R. Baldini Ferroli, M. Bertani (Resp.), A. Calcaterra, S. Pacetti, A. Zallo

### 1 The BESIII experiment

The BESIII experiment is running at the Beijing Electron Positron Collider BEPC-II, a major upgrade of the previous BEPC, at the Beijing Institute of High Energy Physics, IHEP.

The BESIII detector, a scheme is shown in Fig. 1, is designed to study the  $\tau$ -charm physics, it consists of the following components:

- a Helium-gas based drift chamber with a single wire resolution  $< 120 \mu\text{m}$  and a  $dE/dx < 6\%$ . The momentum resolution in the 1 Tesla magnetic field is  $< 0.5\%$  for charged tracks with a momentum of 1 GeV/c;
- a CsI(Tl) crystal calorimeter with an energy resolution that is  $< 2.5\%$  and position resolution  $< 6 \text{ mm}$  for 1 GeV electrons and gammas;
- a Time-of-Flight system with an intrinsic timing resolution  $< 90 \text{ ps}$ ;
- a super-conducting solenoid magnet with a central field of 1 Tesla;
- a 9-layer RPC-based muon chamber system with a spatial resolution  $< 2 \text{ cm}$ .

On July 19, 2008, the first physics event was observed. In November 2008, about  $20 \text{ pb}^{-1}$  were accumulated at the  $\psi(2S)$  to check the performance of both detector and software. The detector worked properly and stably, and the performance has reached the design requirements. On March 14, 2009, BESIII finished accumulating the world's largest  $\psi(2S)$  data set, with more than  $10^8$  events. The  $J/\psi$  data taking, from June 12 to July 28, collected about  $2 \times 10^8 J/\psi$  events. At present, BESIII is taking data at  $\psi(3770)$ .

At the end of 2009 the LNF group has started an activity within the BESIII Collaboration, which is mainly focused on initial state radiation (ISR) studies. In particular our interest is twofold:

- physics analyses of processes with light (non-charm) hadrons;
- design, construction and installation of a new detector for zero-degree photons tagging.

In 2010 the CSN1 (Commissione Scientifica Nazionale 1) officially approved the BESIII activity within INFN and financed the proposed detector. Together with LNF, the Torino University and INFN section are involved in the project.

### 2 Initial State Radiation technique at BESIII

Processes of annihilation to hadrons can be studied in a wide center of mass (CoM) energy range at a high luminosity machine using the ISR in the reaction

$$e^+e^- \rightarrow H\gamma, \tag{1}$$

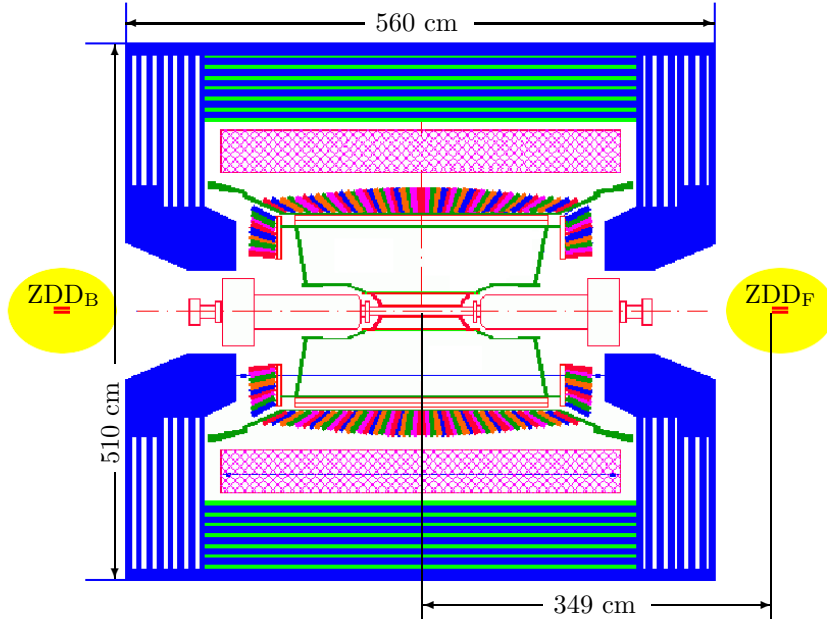


Figure 1: Overview of BESIII with ZDD detector installed. The ZDD stations are shown in red, highlighted by yellow ovals. All components are reported in scale.

where  $H$  could be a generic hadronic final state and the recoiling photon is emitted by one of the initial leptons. The cross section for this process is related to the direct  $e^+e^- \rightarrow H$  cross section  $\sigma_H(s)$  by

$$\frac{d^2\sigma}{dx d\cos\theta}(s_M, x) = W(x, \theta) \sigma_H(s_M(1-x)), \quad (2)$$

where  $\sqrt{s_M}$  is the initial  $e^+e^-$  CoM energy,  $x = 2E_\gamma/\sqrt{s_M}$  is the fractional energy of the ISR photon and  $\sqrt{s_M(1-x)} \equiv \sqrt{s}$  is the effective CoM energy at which the final state  $H$  is produced. The function  $W$  which multiplies  $\sigma_H$  in eq. (2) is the radiator function, it gives the probability for ISR photon to be emitted with scattering angle  $\theta$  and energy  $E_\gamma$ .

An important feature of the ISR technique is that a wide range of energies is scanned simultaneously in one experiment, so that no structure is missed and the relative normalization uncertainties in data from different experiments or accelerator parameters are avoided. Furthermore, for large values of  $x$  the hadronic system is collimated, reducing efficiency issues and allowing measurements at energies down to **production threshold**.

### 3 Zero-degree detector

Usually, ISR measurements are performed by requiring the detection of the initial photon in the main detector. Such a constraint, being the ISR angular distribution peaked at small angles, reduces the statistics by a factor of about five.

At the BEPC-II facility there is the unique possibility to install two small calorimeters ( $\sim 50 \text{ cm}^2$

of cross-section each) along the beam line, just outside BESIII detector, that can cover the very-forward and very-backward region (few milliradians around  $\theta = 0$  and  $\theta = \pi$ ). Such a detection device, called zero-degree detector, ZDD, can be used to tag the forward-backward initial-state-photons, increasing by at least a factor of two the main detector acceptance.

### 3.1 Design

The ZDD is made of two identical stations, ZDD<sub>F</sub> and ZDD<sub>B</sub> in the forward and backward direction, located along the ideal  $z$ -axis, i.e. the beam direction in the  $e^+e^-$  CoM, see Fig. 1. We are interested in ISR processes, where the initial state photon,  $\gamma_{\text{IS}}$ , is emitted by one of the colliding leptons. The angular distribution of the ISR, see Fig. 2, is peaked at small values of the scattering angle  $\theta_{\gamma_{\text{IS}}}$ , this makes the ISR acceptance of the ZDD compatible with the wide angle acceptance in the whole BESIII volume ( $20^\circ \leq \theta_{\gamma_{\text{IS}}} \leq 160^\circ$ ).

However, besides the ISR events, the small angle region is dominated by Bremsstrahlung photons produced in the process  $e^+e^- \rightarrow e^+e^-\gamma$ , which represent a severe background.

In fact, the ZDD design is dictated by the need to suppress such a Bremsstrahlung background. The almost totality of photons produced in  $e^+e^- \rightarrow e^+e^-\gamma$  are emitted at very small angles. The corresponding angular distribution, shown in Fig. 2 as a black histogram, is more peaked than the ISR one, red histogram.

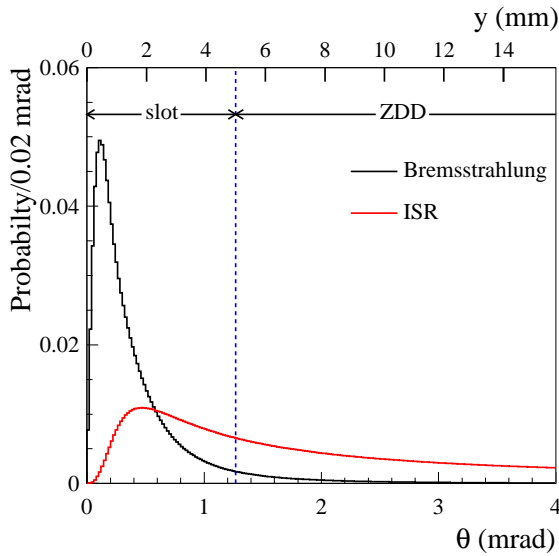


Figure 2: Angular distributions for emitted photons in Bremsstrahlung (black) and ISR (red) processes. The vertical dashed line indicates the slot (see text). The curves are not in scale.

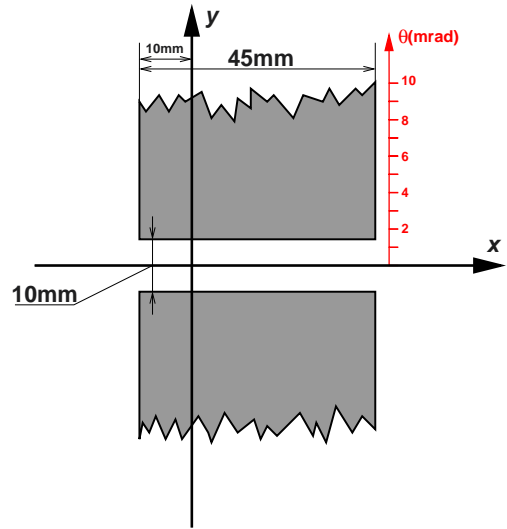


Figure 3: Front view of the ZDD detector. The central 10 mm-wide region represents the Bremsstrahlung slot.

This fact makes possible a geometrical separation of the two effects. A 10 mm wide slot in the detector, along the  $x$  axis, between  $y = -5$  mm and  $y = +5$  mm (blue dashed line in Fig. 2) would drastically reduce the Bremsstrahlung contamination in ISR events.

Figure 3 shows the front view,  $x$ - $y$  cross section, of the ZDD. It is split in two identical pieces with an empty horizontal region, that we call “slot”. Such a region collects more than the 97% of the Bremsstrahlung photons, i.e. the Bremsstrahlung contamination over the active surface of the

ZDD is reduced by a factor of  $\sim 35$ .

Thanks to a mild angular behavior, see Fig. 2, the ISR cross section is affected by a smaller reduction as a consequence of the slot. More in detail, the ISR contributions of ZDD and slot are

$$\frac{\sigma_{\text{ISR}}(\text{ZDD})}{\sigma_{\text{ISR}}(4\pi)} = 13.7\% \qquad \frac{\sigma_{\text{ISR}}(\text{slot})}{\sigma_{\text{ISR}}(4\pi)} = 19.6\%. \quad (3)$$

**This ISR luminosity for the ZDD is similar to that of *BABAR* at wide angle.** We considered also other possible positions of the ZDD. Table 3.1 reports results for ratios and Bremsstrahlung cross sections obtained with three possible values of  $x_{\text{min}}$ , i.e. the left side coordinate of the ZDD. By shifting the ZDD on the right, see Fig. 3, the geometrical acceptance and corresponding cross sections decrease for both Bremsstrahlung and ISR events.

$x_{\text{min}}$ (mm)	$\frac{\sigma_{\text{B}}(\text{ZDD})}{\sigma_{\text{B}}(\text{ZDD} + \text{slot})}$	$\frac{\sigma_{\text{B}}(\text{ZDD})}{\sigma_{\text{B}}(4\pi)}$	$\sigma_{\text{B}}(\text{ZDD})$ (mb)	$\frac{\sigma_{\text{ISR}}(\text{ZDD})}{\sigma_{\text{ISR}}(\text{ZDD} + \text{slot})}$	$\frac{\sigma_{\text{ISR}}(\text{ZDD})}{\sigma_{\text{ISR}}(4\pi)}$
-10	2.8%	2.8%	9.7	41.2%	13.7%
-5	2.5%	2.5%	8.8	40.0%	12.0%
0	2.9%	1.5%	5.2	46.8%	9.3%

The physical occupancy of the ZDD is primarily determined and constrained by the available space which is 180 mm long with a front width of 56 mm and rear width of 69 mm. Concerning the height, apparently there are no stringent limitations. As a consequence of the narrowness of the available region, the design of the detector must be very compact.

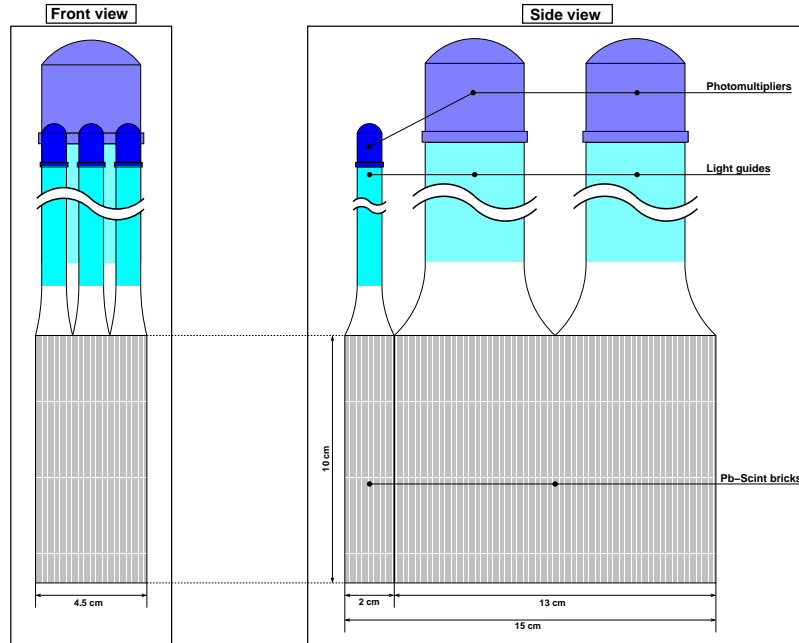


Figure 4: *Front and side view of an upper-half ZDD station.*

For the upper half of a ZDD station we propose the scheme shown in Fig. 4. The lower half

has the same structure but for the read-out system, which is connected to the lower face of the calorimeter. This structure fits well into a volume of  $45(w) \times 70(h) \times 160(l)$  mm<sup>3</sup>, leaving room for the mechanical support shown in fig 5.

We studied a lead-scintillating fiber (Pb-Scint) calorimeter (à la KLOE) instrumented with photomultipliers, that are connected through bundles of white scintillating fibers which work as light-guides.

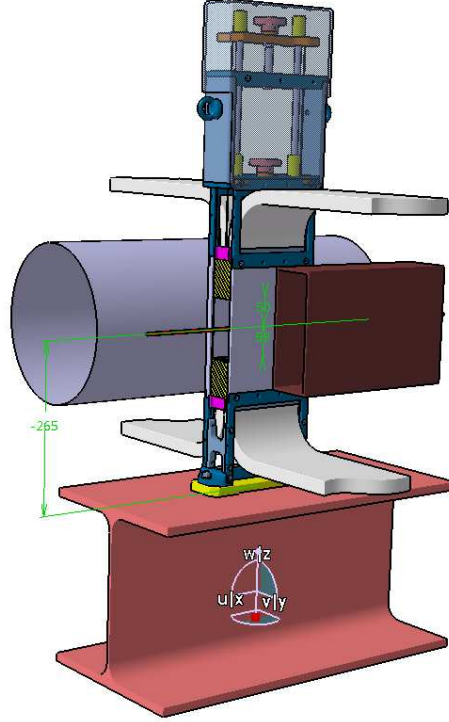


Figure 5: *Mechanical support. The brown parallelepiped and the gray cylinder are the beam pipes. The frame is in blue and the ZDD stations are the yellow bricks connected to the fiber bundles, in gray, through pink supports.*

#### 4 Physics: $e^+e^- \rightarrow n\bar{n}\gamma_{\text{IS}}$

We are interested in using the ISR technique in BESIII to measure baryon-antibaryon hadronic cross sections, i.e. cross sections of processes like  $e^+e^- \rightarrow \mathcal{B}\bar{\mathcal{B}}\gamma_{\text{IS}}$ , where  $\mathcal{B}$  stands for a generic baryon. Thanks to its time-of-flight system and hence its capability of neutral particles detection, BESIII offers a unique opportunity to measure the  $n\bar{n}$  cross section. There are two main sources of background:  $e^+e^- \rightarrow n\bar{n}\pi^0$  and  $e^+e^- \rightarrow n\bar{n}\pi^0\gamma_{\text{IS}}$ . The  $n\bar{n}\pi^0$  background, once the ISR photon is tagged in the ZDD, is suppressed by a factor (ZDD-solid angle)/ $4\pi \sim 4 \times 10^{-5}$ .

The ISR process  $e^+e^- \rightarrow n\bar{n}\pi^0\gamma_{\text{IS}}$ , when the  $\pi^0$  remains undetected, has the same signature of the signal. To reduce such a background we rely first in the BESIII efficiency in detecting  $\pi^0$ 's and second, for those events where  $\pi^0$  photons escape detection, we use the kinematic fit procedure which reduces to only few % the ratio  $[n\bar{n}\pi^0\gamma_{\text{IS}} \text{ background events}]/[n\bar{n}\gamma_{\text{IS}} \text{ signal events}]$ .

## 5 Publications and presentations

- M. Ablikim *et al.*, Phys. Rev. Lett. **105**, 261801 (2010) [arXiv:1011.0885 [hep-ex]].
- Presentation: “A proposal to tag ISR events at BESIII” given at the “BESIII 2010 Spring Collaboration Meeting”, June 3-7, 2010, Liaoning University, Liaoning China.

## CDF

A. Annovi, M. Cordelli (Resp.), P. Giromini, F. Happacher

### 1 Introduction

The Tevatron, with a  $p\bar{p}$  collision energy of 1.96 TeV in the center of mass system, is running with a record instantaneous luminosity,  $L$ , delivered to the experiments of  $350 \times 10^{30} \text{ cm}^{-2}\text{s}^{-1}$  (*vs.*  $\sim 10^{31}$  of Run I). At the end of year 2010, the Tevatron has delivered to the experiments more than  $\sim 10 \text{ fb}^{-1}$ ; CDF experiment has collected on tape  $\sim 8 \text{ fb}^{-1}$ , during the whole Run I we collected  $\sim 109 \text{ pb}^{-1}$ . The CDF data taking is expected to end during the year 2011.

The CDF group of Frascati has built the central hadronic calorimeter (the iron-scintillator based calorimeter in the central and end-wall region, CHA and WHA) and is responsible for the hardware maintenance and for the energy scale calibration.

The analysis interest of the Frascati group focuses on the measurements of  $b$  quark production cross sections and vector Bosons production.

Indeed, the bottom quark production at the Fermilab Tevatron has been called one of the few instances in which experimental results appear to challenge the ability of perturbative QCD to accurately predict absolute rates in hadronic collisions. We are repeating the most significant  $b$  quark cross section measurements from Run I in order to clarify the current situation.

Analysis searching for SM production of heavy boson pair in the lepton neutrino jet jet channel, that is sensitive to the WW and WZ processes together, is interesting since these events have the same signature of low mass SM Higgs events. This analysis is a very interesting results since it shows a discrepancy between data and prediction in the distribution of the invariant mass of the two jets associated to a  $W$  boson in the region  $145 \text{ GeV}/c^2$  with a statistical significance of  $3.5 \sigma$ .

### 2 Calibration of the central hadron calorimeter

The Frascati group plays a leading role in the calibration of the central hadron calorimeters, CHA/WHA.

For the WHA calorimeter the original Run I  $^{137}\text{Cs}$  Sources system is fully working and therefore it can be used to set the absolute energy scale for all the towers; we have taken two  $^{137}\text{Cs}$  Source runs during 2007 and we have accordingly computed a set of Linear Energy Response:

$$LER = \frac{{}^{137}\text{Cs}(\text{test} - \text{beam})e^{-\Delta t/\tau}}{{}^{137}\text{Cs}(\text{today})}$$

that have been downloaded in the front end electronics to correct the raw ADMEM counts. This system effectively probes the behavior of the calorimeter since the source runs in front of the inner scintillator plane of the wedges thus irradiating few of the scintillator/absorber layers of the calorimeter. In this way we monitor aging phenomena of the scintillator together with PM gain variations. We calibrate the CHA calorimeter looking at the energy deposition of Minimum Ionizing Particles (i.e. muons from  $J/\Psi$  decays).

We briefly recall the procedure to set the absolute calorimeter energy scale using Mip's. Looking at  $\mu$ 's from the  $\sim 81 \text{ pb}^{-1}$  dimuon trigger sample collected in Run Ib, we determined the necessary statistics to determine the peaks of  $\mu$ 's hadronic energy, HadE, distributions with

enough precision per every CHA tower. With a statistics of  $\sim 40 \text{ pb}^{-1}$  we find that the tower by tower peak is determined with a precision of  $\sim 1.5\%$ . The LER's correction factors are derived comparing tower by tower the HadE deposition for Run I and Run II mips every 30-40  $\text{pb}^{-1}$  of data; the LER at a given time  $t$  are defined as the previous set of LER ( $t-1$ ) multiplied by the observed ratio of the Mip's at a time  $t$  and in Run I:

$$LER(t) = LER^{t-1} \times \frac{MIP(\text{RunI})}{MIP(t)}$$

We look at Mip's peaks response every  $\sim 100 \text{ pb}^{-1}$  and the typical response shows a tiny 1.5% gain variations on average and few channels that drift more than 5%.

The laser system represents a quick tool to follow the trend of the PM's gains. We have continuously acquired laser runs since year 2003 to monitor the gain variations of each photomultiplier; the CHA is stable within  $\sim 2\%$ .

## 2.1 ONLINE-OFFLINE energy scale calibration

At CDF with the current luminosity the data are being processed through the OFFLINE reconstruction every couple of months. Before producing the fully reconstructed events from the raw information of the detector we first produce small dedicated calibration samples to derive the calibrations constants for all the sub detectors. Every 6-8 weeks we run an executable called CalibExe which produces all the data ntuples for different data sets, including the dimuon trigger data sample where we reconstruct  $J/\Psi$  events; then the various calibrators use these samples to derive the calibrations. We made all this procedure automatic during the year 2006.

Usually for the Hadron calorimeters we produce two set of calibrations: ONLINE calibrations are directly downloaded in the ADMEM electronics and are intended to correct the energy response for data that have to be acquired afterward; the OFFLINE calibrations attempts to propagate back to the data already acquired the needed corrections. The calibration constants are then filled in appropriate ORACLE data base tables called CHALINERESPONSE and CHAOFFLER. To validate the OFFLINE calibrations, the same data sets are reconstructed again picking the right calibration tables for every run range they have been produced for and the calibrators have to repeat their analysis to check that the calibrations are correct.

With this procedure the calorimeter response is kept constant at  $\sim 2\%$  level over the running period.

## 3 Measurement of the average time-integrated mixing probability of $b$ -flavored hadrons produced at the Tevatron

The time-integrated mixing probability is defined as  $\bar{\chi} = \frac{\Gamma(B^0 \rightarrow \bar{B}^0 \rightarrow \ell^+ X)}{\Gamma(B \rightarrow \ell^\pm X)}$ , where the numerator includes  $B_d^0$  and  $B_s^0$  mesons and the denominator includes all  $B$  hadrons. The average probability is then  $\bar{\chi} = f_d \cdot \chi_d + f_s \cdot \chi_s$ , where  $\chi_d$  and  $f_d$ , and  $\chi_s$  and  $f_s$  are the time-integrated mixing probability and the fraction of produced  $B_d^0$  and  $B_s^0$  mesons, respectively. Using the world averages  $\chi_d = 0.1873 \pm 0.0024$  and  $\chi_s = 0.49927 \pm 0.00003$ ,  $\bar{\chi}$  measurements help improve the determination of the fractions  $f_d$  and  $f_s$  in an unbiased sample of weekly decaying  $b$  hadrons produced in high-energy collisions. The value of  $\bar{\chi}$  is inferred from the ratio,  $R$ , of  $LS$  to  $OS$  dileptons due to  $b\bar{b}$  production and decay. The average of the  $\bar{\chi}$  value measured at LEP,  $0.1259 \pm 0.0042$ , and at the Tevatron,  $0.147 \pm 0.011$ , differ by a  $1.8 \sigma$  deviation.

The CDF collaboration makes use of the precision tracking provided by the CDF silicon microvertex (SVX) detector to evaluate the fractions of leptons due to long-lived  $b$ - and  $c$ -hadron decays, and to the other background contributions. For leptons originating from the decay of long

lived particles, the impact parameter is  $d = |\beta\gamma ct \sin(\delta)|$ , where  $t$  is the proper decay time of the parent particle from which the lepton track originates,  $\delta$  is the decay angle of the lepton track with respect to the direction of the parent particle, and  $\beta\gamma$  is a Lorentz boost factor. The impact parameter of the lepton is proportional to the lifetime of the parent particle. The markedly different impact parameter distributions for leptons from  $b$  decays,  $c$  decays, and prompt sources allow the determination of the parent fractions. The procedure is to fit the observed impact parameter distribution of the lepton pairs with those expected for the various sources.

The study in Ref. <sup>1)</sup> has identified a previously ignored contribution to the dimuon sample (referred to as ghost contribution) in which candidate muons are produced by the decay of objects with a lifetime longer than that of  $b$  quarks. Misidentified muons from ordinary sources such as in-flight-decays of pions and kaons and hyperons decays account for  $(81.6 \pm 4.7)\%$  of the ghost events, and the rest is yet unexplained. Ghost muons are almost equally split into  $LS$  and  $OS$  pairs. The relative size of the overall contribution depends upon the type of SVX requirement applied to the trigger muons. As the SVX requirements select trigger muons produced closer to the beamline, the size of the ghost contribution is reduced in comparison to that of the P+HF components that are not strongly affected by this requirement. The CDF study in Ref. <sup>2)</sup> selects events in which both muons are produced within a distance of  $\simeq 1.5$  cm from the beam line and measure a correlated  $b\bar{b}$  cross section whose ratio to the NLO prediction is  $1.2 \pm 0.1$  without including the theoretical uncertainty.

In this study, we show that the  $\bar{\chi}$  discrepancy is indeed produced by ghost events by measuring  $R$  with a data sample in which each muon is produced within 1.5 cm distance from the beamline, and with events in which we allow a decay distance as large as 10.6 cm, first neglecting and then removing the ghost contribution as determined with data.

This analysis follows and complements a recent study <sup>2)</sup> by the CDF collaboration which has used a dimuon data sample to re-measure the correlated  $\sigma_{b \rightarrow \mu, \bar{b} \rightarrow \mu}$  cross section. We use the same data and Monte Carlo simulated samples, and a quite similar analysis method.

The data sample is defined by events containing two central ( $|\eta| < 0.7$ ) muons, each with transverse momentum  $p_T \geq 3$  GeV/ $c$ , and with invariant mass larger than 5 and smaller than 80 GeV/ $c^2$ . It consists of 743006 events corresponding to an integrated luminosity of 742 pb $^{-1}$ .

The value of the  $b\bar{b}$  contribution is determined by fitting the impact parameter distribution of these primary muons with the expected shapes from all sources believed to be significant.

We utilize these same heavy flavor and prompt impact-parameter templates constructed in Ref. <sup>2)</sup>, and a similar fit procedure, this time applied to  $OS$  and  $LS$  pairs separately.

The new templates are compared in Fig. 1 to that used in Ref. <sup>2)</sup>.

### 3.1 Determination of $R$ for events due to $b\bar{b}$ production

We determine the  $b\bar{b}$  content of the data by fitting the observed impact parameter distribution of the  $OS$ ,  $++$ , and  $--$  muon pairs with the expected impact parameter distributions from various sources.

We use a binned maximum log likelihood method to fit the dimuon impact parameter distribution. The likelihood function  $L$  is defined as

$$L = \prod_i \prod_j [l_{ij}^{n(i,j)} e^{-l_{ij}} / n(i,j)!] \quad (1)$$

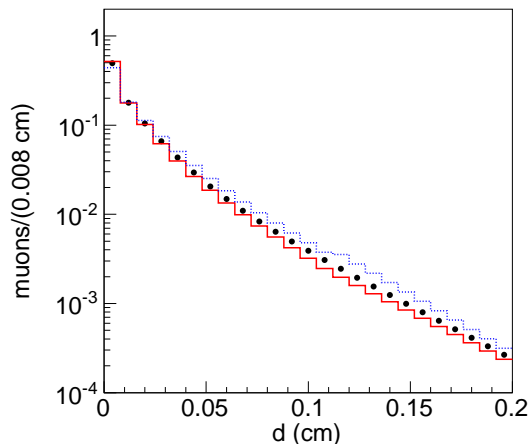


Figure 1: Impact parameter distribution,  $S_b$ , of muons produced by semileptonic  $b$  decays for all simulated events ( $\bullet$ ). The distributions  $S_b^{OS}$  (histogram) and  $S_b^{LS}$  (dotted histogram) are constructed from  $b\bar{b}$  events containing  $OS$  pairs and  $LS$  pairs, respectively. Distributions are normalized to unit area.

where  $n(i, j)$  is the number of events in the  $(i, j)$ -th bin. The function  $l_{ij}$  is defined as

$$\begin{aligned}
 l_{ij} = & BB^{XS} \cdot S_b^{XS}(i) \cdot S_b^{XS}(j) + BB_{FK}^{XS} \cdot S_b(i) \cdot S_b(j) + \\
 & (CC + CC_{FK}^{XS}) \cdot S_c(i) \cdot S_c(j) + PP^{XS} \cdot S_p(i) \cdot S_p(j) + \\
 & 0.5 \cdot [(BP^{XS} \cdot (S_b(i) \cdot S_p(j) + S_p(i) \cdot S_b(j))) + CP^{XS} \cdot (S_c(i) \cdot S_p(j) + S_p(i) \cdot S_c(j)) + \\
 & BC^{XS} \cdot (S_b(i) \cdot S_c(j) + S_c(i) \cdot S_b(j))],
 \end{aligned} \tag{2}$$

where  $XS$  indicates the fit function used for  $OS$ , and  $LS = ++$  or  $LS = --$  pairs, respectively. The impact parameter templates  $S_b$ ,  $S_c$ , and  $S_p$  are the same as those used in Ref. <sup>2)</sup>. The templates  $S_b^{OS}$  and  $S_b^{LS}$  are shown in Fig. 1.

The fit parameters  $BB^{XS}$ ,  $CC$ , and  $PP^{XS}$  represent the  $b\bar{b}$ ,  $c\bar{c}$ , and prompt dimuon contributions, respectively.

The fit parameter  $BP = BP^{OS} + BP^{++} + BP^{--}$  ( $CP = CP^{OS} + CP^{++} + CP^{--}$ ) estimates the number of events in which one muon arise from the semileptonic decays of a  $b$  ( $c$ ) quarks and the second one is a misidentified prompt pion or kaon.

### 3.2 Result of the fits to the muon impact parameters

We fit the the two-dimensional distributions of dimuons with impact parameter  $d \leq 0.2$  cm using the likelihood function defined in Eqn. (1).

We cannot construct simulated templates for ghost events since we cannot even account for the size of their contribution with ordinary sources. We model the ghost contribution using the data. Following the pioneering work of Ref. <sup>1)</sup>, we evaluate the distribution of muons in  $P + HF$  events selected with standard SVX requirements as  $IP^{P+HF} = IP^{\text{tight}} \epsilon_{SVX}^{\text{st}} / \epsilon_{SVX}^{\text{tight}}$ , where  $IP^{\text{tight}}$  is the two-dimensional impact parameter distribution of dimuons selected with tight SVX cuts, and  $\epsilon_{SVX}^{\text{tight}} = 0.244 \pm 0.002$  and  $\epsilon_{SVX}^{\text{st}} = 0.88 \pm 0.01$  are the efficiencies of the tight and standard SVX selection measured in Ref. <sup>1)</sup>. The ghost distribution is derived as  $IP^T - IP^{P+HF}$ , where  $IP^T$  is the two-dimensional distribution of the data passing the standard SVX selection.

Table 1: Number of events attributed to the different dimuon sources by the fit to the impact parameter distribution. The errors correspond to a 0.5 change of  $-\ln L$ .

Component	OS	++	--
<i>BB</i>	$114113 \pm 1225$	$26641 \pm 386$	$26520 \pm 382$
<i>CC</i>	$41817 \pm 1799$	0	0
<i>PP</i>	$119865 \pm 940$	$17411 \pm 554$	$12963 \pm 518$
<i>BP</i>	$17743 \pm 832$	$9880 \pm 502$	$8905 \pm 473$
<i>CP</i>	$22836 \pm 1341$	$13974 \pm 834$	$12142 \pm 786$
<i>BC</i>	$5460 \pm 882$	$2743 \pm 444$	$2744 \pm 444$

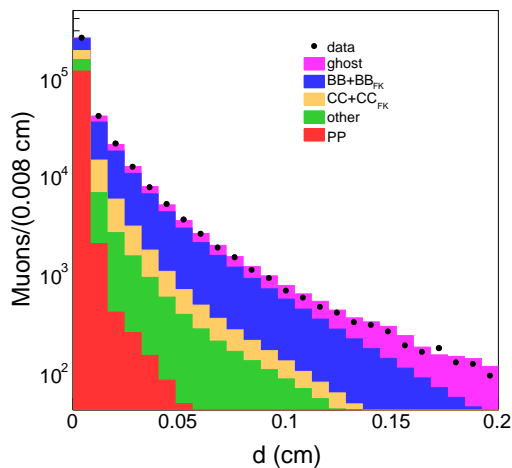


Figure 2: The projection of the two-dimensional impact parameter distribution of OS dimuons onto one of the two axes is compared to the fit result (histogram). Muons are selected with standard SVX requirements. The  $BB + BB_{FK}$ ,  $CC + CC_{FK}$ ,  $PP$ , and ghost components are also shown separately on top of the remaining contributions.

The ghost impact parameter distribution is normalized to unity and, multiplied by the number of ghost events expected in our sample, is added bin-by-bin to the  $l_{ij}$  function in Eqn. (2).

The result of the fit is shown in Table 1. The projection of the two-dimensional impact parameter distribution is compared to the fit result in Fig. 2.

### 3.3 Determination of $\bar{\chi}$

The  $R$  value determined with the fit to dimuons selected with tight SVX requirement ( $R = 0.472 \pm 0.011$ ) is consistent with that obtained using the standard SVX requirement and accounting for the ghost contribution determined with data ( $R = 0.466 \pm 0.018$ ). Events selected with tight SVX requirements are a subsample (24%) of the events selected with standard SVX requirements. Since the uncertainty of the first result is statistical and that of the second is dominated by the systematic uncertainty of the ghost contribution, their error-weighted average ( $R = 0.470 \pm 0.009$ ) could be used to derive the  $\bar{\chi}$  value. The agreement of the two results proves that the contribution of ghost events to the sample selected with tight SVX requirements is indeed negligible.

In absence of mixing, the double semileptonic decay of a  $B\bar{B}$  pair results in an  $OS$  lepton pair; when one of the mesons undergoes mixing a  $LS$  lepton pair is produced. The mixing probability  $\bar{\chi}$  can be inferred from  $R$ , the ratio of  $LS$  to  $OS$  dileptons due to  $b\bar{b}$  production. Sequential decays of  $b$ -hadrons also contribute to  $R$ . Therefore, in the assumption that mixing and sequential decays are the dominant sources of  $LS$  dimuon, the ratio  $R$  relates to the time-integrated mixing probability as:

$$R = \frac{f[\bar{\chi}^2 + (1 - \bar{\chi})^2] + 2\bar{\chi}(1 - \bar{\chi})(1 - f)}{(1 - f)[\bar{\chi}^2 + (1 - \bar{\chi})^2] + 2\bar{\chi}(1 - \bar{\chi})f} \quad (3)$$

with  $f = 2f_\mu(1 - f_\mu) = 0.2157 \pm 0.011$  (syst.).

From the measured value  $R = 0.467 \pm 0.011$ , Eqn. (3) yields  $\bar{\chi} = 0.126 \pm 0.008$ . The uncertainty is obtained adding in quadrature the 0.005 systematic uncertainty due to  $R$  and the 0.006 systematic uncertainty due to  $f^{\text{eff}}$ .

The main scope of this study was to correct a number of oversights in previous measurements, and understand the cause of the discrepancy between the hadron-collider and LEP results. Reference <sup>1)</sup> has suggested a plausible explanation in terms of events in which muons are produced by objects with a lifetime longer than that of  $b$  quarks. This type of event is not yet completely accounted for with ordinary sources such as pion and kaons in-flight-decays or hyperon decays. However, by suppressing or by accounting properly for this contribution, this study reports  $\bar{\chi} = 0.126 \pm 0.008$  in agreement with the LEP average  $0.1259 \pm 0.0042$ .

#### 4 Measurement of Heavy Boson pair production

As CDF has collected more data, the search for the Higgs is becoming more and more interesting with limits getting close to SM expectations. We started in 2009 an analysis searching for SM pair production of heavy boson pair in the lepton neutrino jet jet channel, that is sensitive to the  $WW$  and  $WZ$  processes together, that was published in Ref. <sup>3)</sup>. We then further studied this data sample to investigate the properties of an excess of events at a dijet invariant mass of about 150 GeV as seen in Fig. 3. This work was done in collaboration with Viviana Cavaliere (University of Siena and INFN Pisa, and now with University of Illinois at Urbana-Champaign) and Pierluigi Catastini (Fermilab, and now with University of Harvard).

In this new analysis, we increase the jet  $E_T$  threshold to 30 GeV motivated by the interest in a higher invariant mass range. After this selection, which improves the experimental accuracy for jet measurement and reduces the theoretical uncertainties, the excess at 150 GeV becomes more significant. We investigate the modeling of each background component and found that all backgrounds appear well modeled in the control samples. After considering systematics for non- $W$  event modeling, Jet Energy Scale and renormalization/factorization scale for the main  $W$ +jets background, we still observe a significant excess in the 120-160 GeV/ $c^2$  region, see Fig. 4.

We try to model the excess with an additional Gaussian peak and perform a  $\Delta\chi^2$  test of this hypothesis. The Gaussian is chosen as the simplest hypothesis compatible with the assumption of a two jet decay of a narrow resonance with definite mass. The width of the Gaussian is fixed to the expected dijet mass resolution by scaling the width of the  $W$  peak in the same spectrum:  $\sigma_{\text{resolution}} = \sigma_W \sqrt{\frac{M_{jj}}{M_W}} = 14.3 \text{ GeV}/c^2$ , where  $\sigma_W$  and  $M_W$  are the resolution and the average dijet invariant mass for the hadronic  $W$  in the  $WW$  simulations respectively, and  $M_{jj}$  is the dijet mass where the Gaussian template is centered. We take the difference between the  $\chi^2$  of the two fits ( $\Delta\chi^2$ ), with and without the additional Gaussian structure to assess the significance of the excess. Assuming only background contributions, and systematic errors, the probability to observe an excess larger than in the data is  $7.6 \times 10^{-4}$  corresponding to a significance of 3.2 standard deviations for a Gaussian distribution. A full description of this analysis is available in Ref. <sup>4)</sup>.

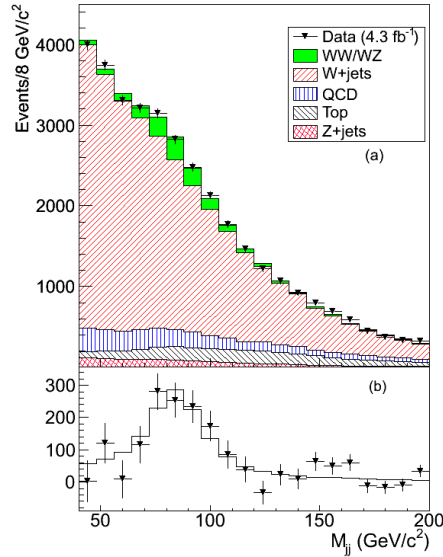


Figure 3: Sum of the electron and muon fit along with background subtracted plot.

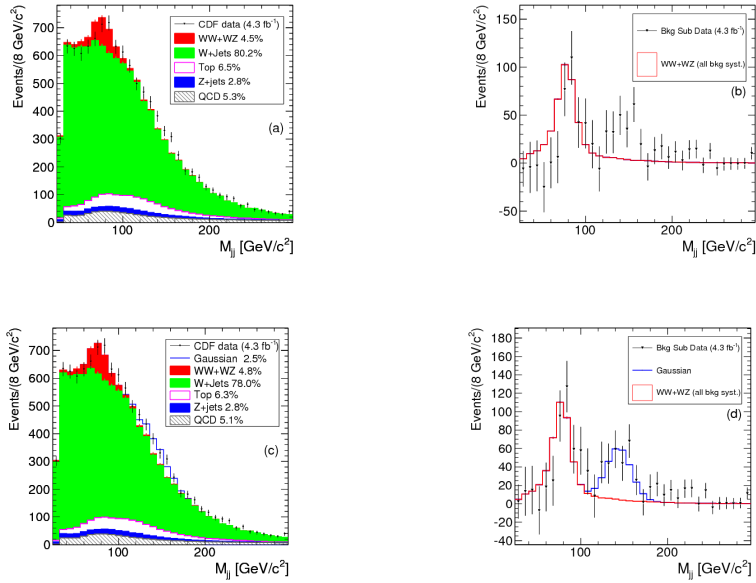


Figure 4: The dijet invariant mass distribution. The sum of electron and muon events is plotted. In the left plots we show the fits for known processes only (a) and with the addition of a hypothetical Gaussian component (c). On the right plots we show, by subtraction, only the resonant contribution to  $M_{jj}$  including WW and WZ production (b) and the hypothesized narrow Gaussian contribution (d). In plot (b) and (d) data points differ because the normalization of the background changes between the two fits. The band in the subtracted plots represents the sum of all background shape systematic uncertainties described in the text. The distributions are shown with a  $8 \text{ GeV}/c^2$  binning while the actual fit is performed using a  $4 \text{ GeV}/c^2$  bin size.

## Publications

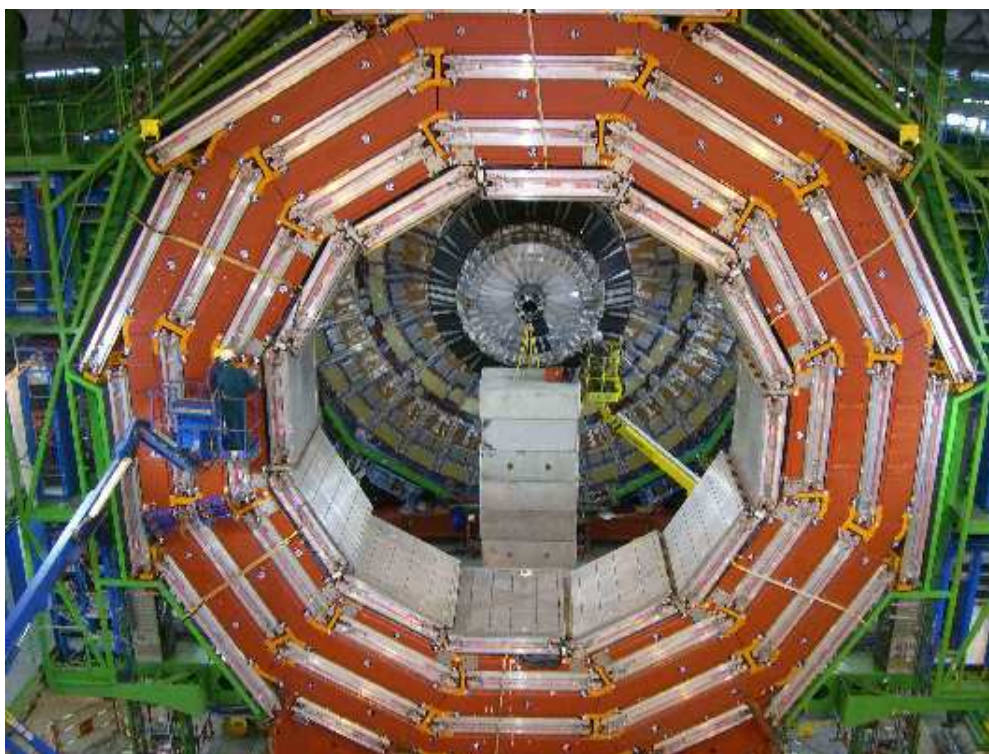
1. T. Aaltonen *et al.*, arXiv:0810.5357, Eur. Phys. J. C **68**,109 (2010).
2. T. Aaltonen *et al.*, Phys. Rev. D **77**, 072004 (2008).
3. T. Aaltonen *et al.* (CDF Coll.), “Measurement of the WW+WZ Production Cross Section using Lepton+Jets Final State at CDF II”, Phys. Rev. Lett. **104**, 101801 (2010). arXiv:0911.4449.
4. T. Aaltonen *et al.* (CDF Coll.), arXiv:1104.0699 [hep-ex].

## CMS

R. Aurilio (Laur.), E. Basile (Dott.), L. Benussi, S. Bianco (Resp.), M.A. Caponero (Ass.)  
S. Colafranceschi (Dott.), F.L. Fabbri (Ass.), F. Felli (Ass.), M. Ferrini (Ass.)  
M. Giardoni (Ass.), T. Greci (Laur.), M. Pallotta (Ass.), M. Parvis (Ass.), L. Passamonti (Tecn.),  
D. Piccolo, D. Pierluigi (Tecn.), A. Russo (Tecn.), G. Saviano (Ass.)

In collaboration with:

B.Dulach (SPECAS), D.Orecchini (SPECAS), B.Ortenzi (Tecn.), B. Ponzio (Tecn.)



The Compact Muon Solenoid (CMS) experiment <sup>1)</sup> will search for the missing block of Nature - the Higgs boson - and for new exotic elementary particles that are predicted by theory and by cosmological observations. The CMS detector uses Resistive Plate Chambers (RPC) as muon detectors, coupled to Drift Tubes in the barrel region, and to Cathode Strip Chambers in the endcaps. Resistive Plate Chambers (RPC) detectors are widely used in HEP experiments for muon detection and triggering at high-energy, high-luminosity hadron colliders, in astroparticle physics experiments for the detection of extended air showers, as well as in medical and imaging applications. While gain and efficiency stability are always a must, in the case of RPC detectors in high-rate experiments which use freon-based gas mixtures, utmost care has to be paid also for the possible presence of gas contaminants. RPC counters <sup>3)</sup> are fast, efficient and economical charged particles detectors, well-suited for operation in high magnetic field. The elementary component is

a gap, a gas volume enclosed between two resistive plates. Resistive plates are made of bakelite, coated with linseed oil for surface uniformity. Gas mixture used is 95.2%  $C_2H_2F_4$  / 4.5% Iso- $C_4H_{10}$  / 0.3%  $SF_6$ , with a 45% relative humidity. Signal pulses are picked up by readout strips. In CMS, RPC counters are operated in avalanche mode to sustain high-rate operation, with the streamer suppressed by the addition of  $SF_6$  gas in the mixture.

## 1 Status of the CMS experiment and the RPC muon detector

The CMS experiment has started data taking in December 2009 and continued successfully over 2010. LHC delivered  $47 \text{ pb}^{-1}$  useful for reliable operations and CMS recorded  $43 \text{ pb}^{-1}$ , with an overall data taking efficiency larger than 92%, and more than 85% recorded with all subdetectors in perfect conditions. All subdetectors have at least 98% of all channels operational.

CMS published a lot of physics results which are available at

<https://twiki.cern.ch/twiki/bin/view/CMSPublic/PhysicsResults>

Topics covered so far are heavy ions, jet production, HQ production, vector boson production, Higgs searches, searches for supersymmetry, exotic signatures. For a total of 83 physics analyses approved so far based on 2010 data, 45 papers completed (published, submitted, or close to submission), 23 papers in preparation, 24 analyses to be approved soon.

The excellent performance of the muon system is shown by the dimuon spectrum (Fig.1) which contains very clean signals from all known resonances.

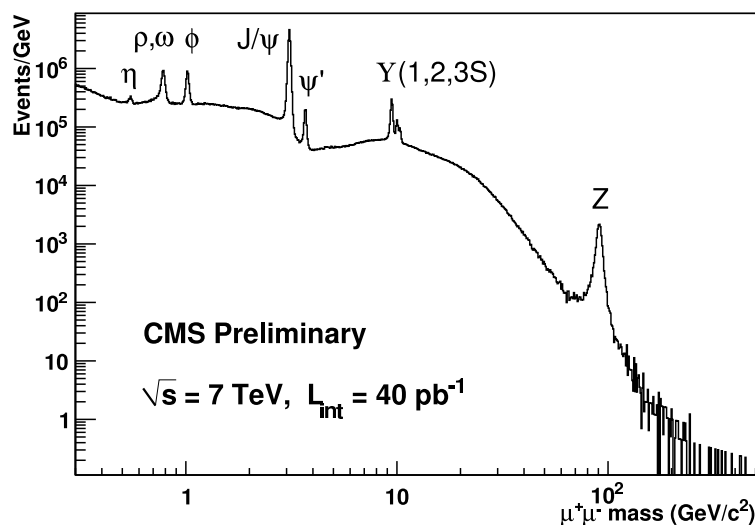


Figure 1: *Dimuon spectrum from CMS for a  $40 \text{ pb}^{-1}$  integrated luminosity.*

The RPC barrel and endcap systems, which were fully characterized during year 2009 by participating at the CMS global cosmic ray events runs, performed up to specifications in 2010. The detector efficiency was measured for each chamber with a resolution of about  $100 \text{ cm}^2$ , showing a very uniform distribution and an average value above 95% in both the barrel and endcaps region.

The RPC system successfully participated to the November and December 2009 LHC data taking contributing in the detection and trigger of muon events, and continued over the year 2010

data taking. The beam splash events have been used to synchronize the endcap electronic channels and to check all the data taking procedures. The colliding beam muon events have been used to measure the overall detection and trigger efficiency showing results comparable to that obtained with cosmics. Data taken in December 2009 have been promptly analyzed and the first CMS paper was submitted to journal in March 2010. The stability of the RPC system, already shown in the 2008 and 2009 cosmic runs, has been confirmed at the initial low luminosity, showing a very low current and noise rate even in the endcap region.

During p-p and heavy-ion runs, the overall behaviour of the RPC system was up to specifications both in terms of detector and trigger performance. This result was achieved through fine-tuned analysis procedures. The study the chamber performance, efficiency, cluster size and noise have been done in greater details using the full 2010 data. The Barrel efficiency was stable at about 94% at constant working voltage. For the Forward, a high voltage scan was performed. An average efficiency of about 93% was achieved. Noise rate studies were performed: with optimization procedures more than 98 % of chambers presented a rate less than 1 Hz/cm<sup>2</sup>, with 1.2% of dead and masked strips in the full system.

During the last months of year 2010, the "RPC monitor stream", which uses a reduced event content in order to collect a very high rate of muons satisfying L1 trigger criteria, has been validated. It will allow to spot rapidly possible problems and make efficiency studies.

Since beginning of data taking the synchronization parameters were update five times and were applied to fine-tune the RPC hits timing. After those corrections the number of the muon hits assigned to incorrect BX dropped to 0.07%. Here only the chamber hits consistent with the reconstructed muon trajectory are taken. Virtually all RPC PAC trigger muon candidates corresponding to the collision muons are assigned to the correct bunch crossing.

Major effort was made to understand the components of the RPC PAC trigger inefficiencies. The trigger efficiency was determined to be 83% (85.9% in barrel and 75,4% in the endcap region), slightly below specifications but acceptable anyway. It was found that the PAC algorithm is responsible for about 1-2% efficiency loss, while the rest is the result of the geometrical coverage of the RPC detector and the chamber inefficiencies.

Extensive improvements were implemented as far as the operation is concerned. Control room procedures and documentations were consolidated; communication between RPC crew and central shifters were fine-tuned, allowing prompt reactions in order to prevent major problems. At CMS centre the prompt feedback about quality of data and the run certification were improved by a better organization of tasks and by prioritizing the operation.

The organizational improvement were possible thanks to the several changes on the control and monitoring software which provide prompt diagnostics on the status of the entire system. The Detector Control System (DCS) which controls and monitors the on-detector electronics and environmental conditions have been further improved in order to provide early warnings about abnormal conditions, issue alarms, execute control actions to protect the detector and its electronics from severe damage. The DCS automation matrix, based on the LHC machine and beam mode have been defined in order to automatic put the RPC system in safe or ON states for any possible machine- beam mode combinations (DCS-LHC handshake mechanism). Efforts have been put also on finalizing the Detector Safety System (DSS) which provide hard-wired detector protection, executing "actions" in response to the detection of "alarms". The full "alarm-action matrix" have been configured, tested during LHC technical access time and monitored during all the data-taking period. The high functionality of both systems, DCS and DSS, under central control operation allowed to operate the system with only the on-call RPC shifter in PT5 already in June, after only two months of beam operation. The monitoring software kept evolving for all 2010 with the aim of providing a fast summary of the status of the system not only to be able detect efficiently any problems, but also focusing in providing longer term summaries. Consequently, a lot of effort

have been put on Data Quality Monitoring (DQM) and in the Web Based Monitoring (WBM) tools. The RPC DQM system has been extensively used during the 2010 data taking both by CMS central shifters and by RPC experts to study the detector and trigger performance. The central shifters have been used only the so called "summary plots" to understand the quality of the data taken by the RPC while the RPC experts have been used all the plots and histograms produced by the DQM to quantify the RPC performances and to make the run validation. During last months also more effort were put in developing WBM tool, which is a set of web applications which will allow to check, also remotely, detector (voltage currents, gas flow, noise) and environmental parameters during a run or for a time window. WBM will be a powerful tool for the run validation and long term studies. Tools to monitor the noise in the detector have been developed and the procedure to optimize the threshold level wrt noise rate, by keeping the fake trigger rate and muon reconstruction under control, were established.

The RPC Cosmic Trigger (RBC/TTU) algorithms were enabled for collision runs and were extensively for calibration and commissioning purpose by the tracker and RPC systems.

The hardware was quite stable: both gas and power systems did not present significant problems during the data-taking period, confirming the high reliability achieved. Only few interventions on some HV or LV channels were necessary during the periodical technical accesses. The overall result is given by the stable percentage of active channels at about 98.5% and by no CMS downtime due to RPC hardware failure. These powerful monitoring tools and general stability of the system are also confirmed by the very low percentage of RPC contribution to CMS dead time: less than 1 due to any RPC hardware failure, but due to a bug in the readout firmware, which was found and corrected.

The monitoring of gas system, the gas gain monitoring system and purifier studies are responsibilities of the Frascati group. The CMS RPC muon detector uses a huge volume of expensive gas mixture. This has demanded the need for a gas recirculation system (Closed Loop) with filters for gas purification. The CL system has been in operation since years with performance meeting specifications. All modules of the gas system (primary supply, mixer, purifier module I e II, humidifier, pump, pre-distribution and distribution) have been operational in closed loop mode since mid 2008. The clean mix fraction is about 10%. The system is integrated in DCS PVSS. Both IR analyzer for isobutane and  $O_2 + H_2O$  analyzer have been installed and are operational. The gas quality monitoring system (gas chromatograph and electrodes) are operational and routinely used to check the mix composition and presence of major pollutants. The gas system is stable and no currents increase have been observed due to closed loop mode. During year 2010 the activity at the scaled-down closed loop system in the ISR test area has continued for full characterization of purifiers. The CL system ran smoothly during the collision runs over the entire 2010.

## 2 Activity

The Frascati group has joined CMS in the RPC muon detectors at the end of year 2005. The Frascati group contributes to the electroweak studies, namely in the measurement of the Z cross section in the dimuon channel. Frascati is responsible for the Gas Gain Monitoring system, RPC materials studies, and the test of the Closed Loop recirculation system for characterization of gas purifiers.

Frascati has rapidly harmonized with the RPC group, and the quality of work provided was rapidly recognized by the RPC collaboration which, during 2010, decided to ask members of the Frascati group to cover L2 responsibilities such as DPG coordinator and Run coordinator.

## 2.1 Physics analysis

The Frascati group is working in the CMS Electroweak Analysis group and is involved in the study of the measurement of inclusive  $Z \rightarrow \mu^+\mu^-$  cross section. This process is characterized by a clear signature in an almost free background environment and has been studied since the arrival of the first colliding beams.

The work has been focused on the development of methods to select events and measure reconstruction and trigger efficiencies directly from data. An original method has been proposed which consists in five different categories of Z candidates according to the way the muons have been reconstructed (tracker track, standalone muon detector system, combined track+standalone muon) and trigger topologies.

A fit of Z production yield, reconstruction and trigger efficiency is then performed simultaneously on the five categories, thus allowing to extract all the needed information in a single step. This method has been showed to be very robust in handling also a low statistical sample as could be expected in case of few  $\text{pb}^{-1}$  of integrated luminosity collected.

## 2.2 The CMS Closed Loop Gas System

Because of high costs and huge volumes of the freon-based gas mix used, CMS RPC uses a recirculation (Closed Loop) gas system developed by the CERN gas group. The Closed Loop is a critical component of RPC. CMS has accumulated experience on its use and performances during the test at the Gamma Irradiation Facility at CERN in 2001 <sup>4)</sup>, and currently at the ISR where chambers are tested in CL prior to installation. At the GIF facility we observed substantial production of HF, linearly correlated with the signal current.

In the Closed Loop (CL) system, purifiers are the crucial component. Purifiers were determined after tests at the GIF in order to minimize the unknown contaminants which showed as spurious peaks besides the known gas mix components. Three filters were selected: 5A molecular sieve, Cu/Cu-Zn, Ni/Al<sub>2</sub>O<sub>3</sub>. A small scale CL system is currently in use with cosmic rays in the ISR test area.

A measurement campaign <sup>5)</sup> on purifiers is in progress, using chemical, SEM/EDS (Scanning Electron Microscopy/Energy Dispersive Spectroscopy), XRD (x-ray Diffraction) analyses. During year 2010 the activity at the scaled-down closed loop system in the ISR test area has continued for full characterization of purifiers, with new sampling points for detection of gas pollutants produced in the system in correlation with RPC currents increase. The release of contaminants in gas was observed with correlation to the increase of currents. A simple model for the current increase followed the studies and results have been presented at the RPC10 conference (Darmstadt, Germany).

## 2.3 Gas Gain Monitoring System

The Gas Gain Monitoring (GGM) system of RPC detectors in CMS monitors the changes in working point due to gas variations, by means of monitoring of anodic charge in small RPC gaps in a cosmic ray telescope. The system is composed of three subsystem of RPC single gaps, readout by 45cm x 45cm pads in a cosmic ray telescope located in the SGX5 gas building. Each subsystem is flushed with a different gas. The Reference subsystem is flushed with fresh open loop gas mixture. The MonitorOut subsystem is flushed with CL gas downstream of CMS RPCs. The MonitorIn subsystem is flushed with CL gas upstream of CMS RPCs. Each subsystem is composed of three gaps, whose high voltage is set to the standard working point voltage at the efficiency knee, and to 200 V above and below the knee respectively. Each cosmic ray track therefore provides completely correlated pulses in the three subsystems, allowing one to study the differential response of gaps

and by disentangling any effect due to changes in the gas mixture. In case a working point change is detected, an alarm condition is released and the gas quality monitoring system will verify what the change of work point is due to.

The system was located in the SGX5 gas room of CMS in December 2008 and operated before the January 2009 shutdown. During 2008 the GGM was operated at the scaled down closed loop gas system in the ISR test area. The large experience allowed one to determine both sensitivity to working point changes and cancellation algorithms for changes due to environmental variables. Results have been presented at RPC07 and IEEE08. At the end of 2008 the integration of GGM with the CMS DCS-based monitoring has started, with data exchange with PVSS and data save to the OMDS online database. A beta-release control panel was released in December 2008. The system has been integrated during 2009 in the CMS DCS system. Data on operational experience in 2009 have been published. A novel model based on neural networks for the modellization of RPC response was developed on data from the GGM.

The GGM performed up to specifications over the entire 2010, with limited down times due mainly to technical software interventions while finalizing the full integration with the CMS CDS framework. At the end of 2010 one out of twelve chambers showed reduced efficiency, and, while still operated at higher voltage, it was planned to be replaced at the beginning of 2011.

A proposal for PRIN was submitted and approved at the end of 2009. The PRIN will study optical fiber sensors for gas contaminants detection, in collaboration with Politecnico Torino and Sapienza Università di Roma.

### 3 Activity planned for 2011

The main activity in 2011 will be the physics analysis, participation to data taking shifts and operation of the RPC detector. The test at the scaled down Closed Loop system will continue in at high-radiation environment at the GIF facility. At the GIF, optical sensors for contaminants detection will be developed in the framework of the PRIN project approved and funded.

The measurement of inclusive  $Z \rightarrow \mu^+ \mu^-$  cross section work will be completed with a study of systematic effects and geometrical acceptance. The analysis will be performed running the software through the GRID on the Tier2 where the data will be saved, and the development of the tools is essential in order to be able to run in a fast and efficient way as soon as the data are ready.

Studies for medium and long-term upgrades of the RPC detector have been finalized in collaboration with the SPECAS service of Frascati. A simulation study was performed to verify the possibility of doubling the gaps in the inner layer of the barrel RPC, in order to add an orthogonal coordinate. Work on the option of installing a GEM detector in the forward region was started. Finally, the Frascati group will contribute to the construction and installation of a fifth endcap disk, so far missing (upscope), by installing FBG sensors for temperature, humidity and gas contaminants, participation to design of and testing link boards trigger electronics, upscope of distributors in gas system.

### 4 Conference Talks

1. L. Benussi, “New QCD results from CMS”, presented at LC10, November 30th, 2010, Frascati (Italy).
2. D. Piccolo, “CMS muon detector and trigger performances”, presented at the 12th Vienna Conference on Instrumentation (VCI2010), Vienna (Austria).
3. S. Colafranceschi for the CMS Coll., “A new approach in modeling the response of RPC detectors”, presented at the RPC10 Conference, February 2010, Darmstadt (Germany).

4. G. Saviano for the CMS Coll., “Study of gas purifiers for the CMS RPC detector”, presented at the RPC10 Conference, February 2010, Darmstadt (Germany).

## 5 Preprints

1. D. Abbaneo *et al.*, “Characterization of GEM Detectors for Application in the CMS Muon Detection System,” arXiv:1012.3675 [physics.ins-det].

## 6 CMS Notes

1. L. Benussi *et al.*, “A new approach in modeling the response of rpc detectors”, CMS NOTE-2010/009.
2. S. Bianco *et al.*, “Chemical analyses of materials used in the cms rpc muon detector”, CMS NOTE-2010/006.

## 7 Papers

1. For the listing of CMS papers in 2010 see /www.slac.stanford.edu/spires/
2. L. Benussi *et al.*, “Study of gas purifiers for the CMS RPC detector,” arXiv:1012.5511 [physics.ins-det]. To appear on Nucl. Instr. & Meth.
3. L. Benussi *et al.*, “A new approach in modeling the response of RPC detectors,” arXiv:1012.5508 [physics.ins-det]. To appear on Nucl. Instr. & Meth.
4. D. Piccolo *et al.*, “Resistive plate chambers performance with cosmic rays in the CMS experiment,” Nucl. Instr. & Meth. A **617**, 180 (2010).
5. S. Colafranceschi *et al.*, “Operational experience of the gas gain monitoring system of the CMS RPC muon detectors,” Nucl. Instr. & Meth. A **617**, 146 (2010).
6. N. Dardanov *et al.* [CMS Collaboration], “The CMS RPC system overview,” AIP Conf. Proc. **1203**, 43 (2010).

## References

1. CMS Collaboration home page is /cms.cern.ch/.
2. R. Adolphi *et al.* [CMS Collaboration], “The CMS experiment at the CERN LHC,” JINST **3**, S08004 (2008).
3. M. Abbrescia *et al.*, Nucl. Instr. & Meth. A**533**, 102( 1994); M. Abbrescia *et al.*, Nucl. Instr. & Meth. A**515**, 342 (1993).
4. M. Abbrescia *et al.*, “HF production in CMS Resistive Plate Chambers”, submitted to Nucl. Instr. & Meth., presented by R. Guida at the RPC Conference, Seoul (Korea) 2005.
5. M. Abbrescia *et al.*, Frascati preprint LNF-06/26(IR) (2006).
6. M. Abbrescia *et al.*, “Gas analysis and monitoring systems for the RPC detector of CMS at LHC”, presented by S. Bianco at the IEEE 2006, San Diego (USA), arXiv:physics/0701014.

# KLOE

The KLOE Collaboration at the LNF

D. Babusci, G. Bencivenni, C. Bloise(Resp.), F. Bossi, P. Campana, G. Capon, P. Ciambrone, E. Dane' (Art. 23), E. De Lucia, P. de Simone, D. Domenici (Art. 23), M. Dreucci (Ass.), G. Felici, C. Gatti, S. Giovannella, F. Happacher, E. Iarocci (Ass.)\*, M. Jacewicz (Bors. PD), J. Lee-Franzini (Ass), M. Martini (Ass)\*, S. Miscetti, M. Moulson, M. Palutan, V. Patera (Ass.)\*, P. Santangelo, B. Sciascia, T. Spadaro, G. Venanzoni, R. Versaci (Ass)\*

*\*Also Dipartimento di Energetica, "La Sapienza" University, Rome*

The KLOE-LNF Technical Staff

M. Anelli, G. Fortugno, M. Iannarelli, M. Pistilli (Art. 15), R. Rosellini, F. Sborzacchi, E. Turri

## 1 Outline

The roll-in of the KLOE detector, following all the maintenance work to fully operate the drift chamber and the calorimeters, was successfully completed on January, 29. The DAΦNE renovation went on much longer than planned. The machine commissioning was started by mid of November.

The crucial operations for the insertion of the DAΦNE focusing section inside the KLOE apparatus finished by the beginning of June. Besides the beam pipe and the final focusing magnets, i) the LET calorimeters and ii) a lead screen of 7 X<sub>0</sub>, 90 cm long, for machine background shielding, have been installed.

The LET calorimeters of the tagger system for  $\gamma\gamma$  physics have been assembled, installed and integrated in the KLOE DAQ system for data taking. The Roman pot for the insertion of the other station of the tagger system, the HET, has been realized, equipped with step-motors for the positioning inside the beam pipe, and used for housing test-scintillators to measure the background levels, and the radiative-Bhabha scattering as soon as beam collisions are delivered at DAΦNE.

The upgrades of the KLOE apparatus, i) the inner tracker, ii) the calorimeters for low-angle particles (CCALT) and iii) the sampling tile-calorimeter (QCALT) designed for the instrumentation of the final focusing section, have been worked on to test and fix all of the construction details. We aim to install them in early 2012.

The KLOE results on the measurements of the hadronic cross section have been presented at CERN, on March, 29. A summary on the analyses is reported in Sec.4.

A paper on the KLOE-2 physics program has been published on EPJ C <sup>1</sup>). It includes contributions from theoreticians and phenomenologists of the worldwide community interested to different aspects of the experimentation with KLOE-2.

New students and postdoc are involved in the experiment, from i) the Jagiellonian University of Krakow, ii) Messina University, iii) Rome University of Tor Vergata, iv) the University of Warsaw, v) the University of Uppsala, and vi) the European Network MCPAD. They are trained in all of the activities of the experiment, i.e. on the R&D, realization and test of the particle detectors as well as on data-analysis.

## 2 Results on kaons

From 2000 to 2006, the KLOE experiment collected 2.5 fb<sup>-1</sup> of  $e^+e^-$  collisions at the  $\phi$  peak and about 240 pb<sup>-1</sup> below the  $\phi$  resonance ( $\sqrt{s} = 1$  GeV). With data taking at the  $\phi$  peak,

KLOE has obtained precision measurements in the kaon sector, such as masses <sup>2)</sup>, decay branching fractions <sup>3, 4, 5, 6, 7)</sup>, and lifetimes <sup>8, 9)</sup>. The  $K_S$  lifetime, known from the world average to 0.6 per mil relative accuracy, was recently determined on a sample of about 20 million  $K_S \rightarrow \pi^+ \pi^-$  decays, corresponding to an  $e^+e^-$  integrated luminosity of  $0.4 \text{ fb}^{-1}$ . A pure  $K_S \rightarrow \pi^+ \pi^-$  sample was selected imposing cuts on the invariant mass of the pions and on the position of the  $K_S \rightarrow \pi^+ \pi^-$  vertex. The proper time distribution of the  $K_S$  sample is obtained from i) the kaon production point P, ii) the  $K_S$ -meson vector momentum  $\mathbf{p}_K$ , and iii) the decay point D. The average position of the interaction point P and the centre-of-mass (CM) energy is measured from Bhabha scattering events, on the basis of 2-hours runs. The reconstruction of the  $K_S \rightarrow \pi^+ \pi^-$  decays provides the  $K_S$  momentum and the decay point D. From a fit to the proper time distribution  $\tau(K_S) = (89.562 \pm 0.029_{\text{stat}} \pm 0.043_{\text{syst}}) \text{ ps}$  is obtained, in good agreement with the world average. KLOE data rules out any lifetime dependence from the  $K_S$  direction, excluding in particular any asymmetry in the direction parallel/antiparallel to the dipole anisotropy of the cosmic microwave background to the per mil precision level <sup>10)</sup>.

The best limit on the CP-violating decay  $K_S \rightarrow \pi^0 \pi^0 \pi^0$  comes from KLOE <sup>11)</sup> with the analysis of  $450 \text{ pb}^{-1}$  taken during 2001-2002. We tagged the  $K_S$  by means of a  $K_L$  interaction in the calorimeter,  $K_L$ -crash, and searched in the sample with six photons coming from the region close to the IP. Discriminating variables based on kinematic fit and photon pairing were used to eliminate the obvious background from  $K_S \rightarrow 2\pi^0 + 2$  unwanted clusters (either by splitting or accidental overlap with machine background clusters). In the signal box we got 2 candidates out of an expected background of  $3.13 \pm 0.82$ , with a signal efficiency of 24.4 %. The normalization was provided by the counting of the  $K_S \rightarrow 2\pi^0$  events in the same tagged sample of 38 million events. We set an upper limit on the branching fraction of  $1.2 \times 10^{-7}$  at 90 % C.L. The composition of the estimated background in the old MC generated files (equivalent to  $\sim 1.8 \text{ fb}^{-1}$ ) shows that, out of 19 surviving events, the dominant source is related to splitting (17) while smaller contributions are due to accidentals (1) and “ $K_L$  fakes” (1) (events such as  $K_S \rightarrow \pi^+ \pi^-$ ,  $K_L \rightarrow 3\pi^0$  where the  $K_L$  crash is created by delayed clusters from pion interaction on the quadrupoles). We have therefore started an analysis campaign on a larger sample ( $1.7 \text{ fb}^{-1}$  data,  $3.4 \text{ fb}^{-1}$  MC) aiming to obtain a much stronger background reduction. Driven by MC studies of signal and background, we add two cuts: (i) splitting rejection, by rejecting events with minimal distance among clusters closer than 65 cm,  $R_{\text{min}} < 65 \text{ cm}$ , and (ii) rejection of fakes, by hardening the  $K_L$ -crash selection ( $E > 150 \text{ MeV}$  and  $0.200 < \beta_K < 0.225$ ). At the end of the streaming, we got 108 (236) million tags in data (MC) and about 65000 events with six photons on data. A reasonable data/MC agreement has been found with the study of the discriminating variables. In particular, the simulated distribution of the  $\chi^2$  of the kinematic fit for the six photon sample closely reproduces the distribution of real data. At the end of a preliminary cut optimization, we find 0 candidates in the simulated sample while keeping an overall efficiency of  $\sim 22 \%$ . We are still completing the optimization of the cuts and the calibration of the background components. We expect to reach a limit on the branching fraction which is not anymore background limited and therefore scale with the luminosity increase to values of  $\sim 2\text{-}4 \times 10^{-8}$ .

### 3 Results on $\eta$ meson decays

The KLOE data sample includes  $10^8$   $\eta$ 's and  $5 \times 10^5$   $\eta'$ 's produced through the radiative decays  $\phi \rightarrow \eta\gamma/\eta'\gamma$  and tagged by means of the monochromatic recoil photon.

The isospin-violating decay  $\eta \rightarrow \pi\pi\pi$  is sensitive to the  $u$ - $d$  quark mass difference, one of the fundamental parameters of the Standard Model (SM). A precision measurement of  $Q^2 = (m_s^2 - \hat{m}^2)/(m_d^2 - m_u^2)$  can be obtained from the analysis of the Dalitz plot of this decay.

At KLOE, the background for both charged and neutral final states is at the level of few per mil (12, 13) allowing precision measurements of the kinematical distributions. The conventional Dalitz plot variables for the  $\pi^+\pi^-\pi^0$  final state are  $X \propto T_+ - T_-$  and  $Y \propto T_0$ , where  $T$  is the kinetic energy of the pions. The measured distribution is parametrized as:  $|A(X, Y)|^2 = 1 + aY + bY^2 + cX + dX^2 + eXY + fY^3$ . As expected from  $C$  parity conservation, the odd powers of  $X$  have been found to be consistent with zero. The other parameters are measured with an accuracy between 5 per mil and 10%.  $C$  parity conservation has been tested also by measuring the left-right-, quadrants- and sextants- charge asymmetries: all of them are consistent with zero at  $10^{-3}$  level, thus improving previous evaluations obtained combining different experiments. In the  $\eta \rightarrow \pi^0\pi^0\pi^0$  decay, the Dalitz plot density is described by a single parameter  $\alpha$ :  $|A(z)|^2 \propto 1 + 2\alpha z$ , where  $z$  is related to the distance from the center of the Dalitz plot. Photons are paired to obtain  $\pi^0$ 's momenta, after kinematically constraining the total four-momentum to the  $\phi$  momentum to improve energy resolution. Three samples, with different cuts imposed on the photon pairing criteria, have been analyzed. The result, recently published by PLB, is:  $\alpha = -0.0301 \pm 0.0035_{\text{stat}}^{+0.0022} - 0.0035_{\text{syst}}$ . A new dispersive analysis of  $\eta \rightarrow 3\pi$  is being worked on by Colangelo and coworkers<sup>14)</sup>, at the University of Bern. The preliminary results obtained are very promising for a more accurate determination of the quark mass double ratio that makes a new analysis worthwhile.

The  $\eta/\eta' \rightarrow \pi^+\pi^-\gamma$  is a probe of box anomaly<sup>15)</sup>. The corresponding terms in the Wess-Zumino-Witten (WZW) Lagrangian have been evaluated in the chiral limit for processes such as  $\eta \rightarrow \pi^+\pi^-\gamma$  and  $\eta' \rightarrow \pi^+\pi^-\gamma$ . Effective Lagrangians are studied in the framework of Chiral Perturbation Theory ( $\chi$ PT) using vector dominance to extend the range of validity above the chiral limit, in the  $\rho$  region of interest for the  $\eta - \eta'$  decays. The effective theory<sup>15)</sup> points out that i) since  $\rho$  contribution is not completely dominant in the case of  $\eta \rightarrow \pi^+\pi^-\gamma$ , the partial width is sensitive to the direct term, ii)  $\eta' \rightarrow \pi^+\pi^-\gamma$  decays whose partial width is completely dominated by the resonance, present a dipion invariant mass distribution affected by anomaly. Experimental data on  $\eta$  decay have been obtained by<sup>16, 17)</sup>; more recent results from the CLEO collaboration, based on 900 events<sup>18)</sup>, on  $\Gamma(\eta \rightarrow \pi^+\pi^-\gamma)/\Gamma(\eta \rightarrow \pi^+\pi^-\pi^0)$ , are  $3\sigma$  below the world average. The analysis of the  $\eta$  channel at KLOE is well advanced and the preliminary measurement of the ratio  $\Gamma(\eta \rightarrow \pi^+\pi^-\gamma)/\Gamma(\eta \rightarrow \pi^+\pi^-\pi^0)$  has been presented, among other international conferences, to the PrimeNet Workshop in Lisbon<sup>19)</sup>; also the study of the  $\eta'$  decays is in progress. The KLOE analysis is based on  $\simeq 5 \times 10^6$   $\eta \rightarrow \pi^+\pi^-\gamma$  selected events. The analysis on the  $\eta$  channel starts with the selection of samples of  $\eta \rightarrow \pi^+\pi^-\gamma$  and  $\eta \rightarrow \pi^+\pi^-\pi^0$ . The main background is given by  $\phi \rightarrow \pi^+\pi^-\pi^0$ . The kinematical constraints from the two-body  $\phi \rightarrow \eta\gamma$  decay are exploited to extract  $\gamma_\phi$  energy from  $\gamma_\phi$  polar angle  $\vartheta$ . In order to reject  $\phi \rightarrow \pi^+\pi^-\pi^0$  background, the angle between the two photons in the  $\pi^0$  rest frame is computed using the  $\phi$  and  $\pi^+\pi^-$  momenta. In the background case, the two photons are flying back to back. Other background has been rejected with: i) TOF requirements, identifying pions and electrons, rejecting Bhabha background and other processes with electrons in the final state and ii) angle cuts on the minimal angle between neutral cluster and the closest track, to reject background from  $e^+e^- \rightarrow e^+e^-(\gamma)$  with photon conversions on the beam-pipe and drift chamber walls. The process  $\phi \rightarrow \eta\gamma$  with  $\eta \rightarrow \pi^+\pi^-\pi^0$  represents a good control sample for  $\eta \rightarrow \pi^+\pi^-\gamma$ . We perform same preselection on both, the  $\eta \rightarrow \pi^+\pi^-\gamma$  signal, and the  $\eta \rightarrow \pi^+\pi^-\pi^0$  used also as normalization for the width measurement because the ratio of branching fractions is free from several systematics. The  $\eta \rightarrow \pi^+\pi^-\pi^0$  events are identified on the basis of the missing mass,  $\vec{p}^{\text{miss}} = \vec{p}_\phi - \vec{p}_{\pi^+} - \vec{p}_{\pi^-} - \vec{p}_\gamma^\phi$ , requiring  $|M_{\text{miss}} - m_{\pi^0}| < 15$  MeV. The rest of the background is efficiently rejected by applying an angular cut on photon momenta,  $\theta_{\gamma\gamma}^{\pi^0} > 165^\circ$ , that leads to a background-to-signal ratio (B/S) at 6 per mil level. From the comparison on control samples of  $\phi \rightarrow \pi^+\pi^-\pi^0$  selected with the

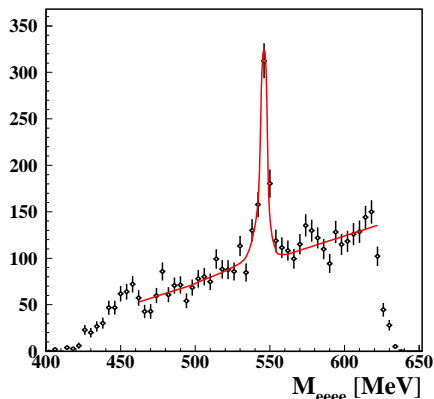


Figure 1: *Fit to the four-electrons invariant mass for events  $\eta \rightarrow e^+e^-e^+e^-$ .*

same procedure but the cut on  $\theta_{\gamma\gamma}$  ( $\theta_{\gamma\gamma}^{\pi^0} < 165^\circ$  was used instead), the correction terms to account for data–Monte Carlo discrepancies on tracking resolution have been obtained. The preliminary measurement of  $\Gamma(\eta \rightarrow \pi^+\pi^-\gamma)/\Gamma(\eta \rightarrow \pi^+\pi^-\pi^0)$  based on  $1.2 \text{ fb}^{-1}$  of integrated luminosity, gives:  $\Gamma(\eta \rightarrow \pi^+\pi^-\gamma)/\Gamma(\eta \rightarrow \pi^+\pi^-\pi^0) = 0.2014 \pm 0.0004_{\text{stat}} \pm 0.0060_{\text{syst}}$ . Work on systematics is in progress aiming to reach 1% in the relative accuracy. The result, that is in agreement with other previous analyses, significantly differs from the most recent CLEO measurement.

KLOE has obtained first observation of the  $\eta \rightarrow e^+e^-e^+e^-$  decay, based on the same sample used for the analysis of the  $\eta \rightarrow \pi^+\pi^-e^+e^-$  channel, published in <sup>20)</sup>. Events with four electrons are selected using time of flight information provided by the calorimeter. The number of signal events is obtained by fitting the distribution of four electron invariant mass,  $M_{eeee}$ , with signal and background shapes (Fig.3). From the fit we extract  $N_{\eta \rightarrow e^+e^-e^+e^-} = 413 \pm 31$ . The studies of the efficiency and systematics are progressing to obtain the measurement of the branching fraction.

Pseudoscalar production at the  $\phi$  factory associated to internal conversion of the photon into a lepton pair allows the measurement of the form factor  $\mathcal{F}_P(q_1^2 = M_\phi^2, q_2^2 > 0)$  of pseudoscalar mesons  $P$  in the kinematical region of interest for the VMD model. The only existing data on  $\phi \rightarrow \eta e^+e^-$  come from the SND experiment at Novosibirsk which has measured the  $M_{ee}$  invariant mass distribution on the basis of 213 events <sup>21)</sup>. At KLOE, the preliminary analysis of the  $\eta \rightarrow \pi^+\pi^-\pi^0$  final state has been performed on  $739 \text{ pb}^{-1}$ , corresponding to 40% of the total sample. Preselection cuts require: (i) four tracks in a cylinder around the interaction point (IP) plus two photon candidates; (ii) the best  $\pi^+\pi^-\gamma\gamma$  match to the  $\eta$  mass using the pion hypothesis for tracks; (iii) other two tracks assigned to  $e^+e^-$ ; (iv) loose cuts on  $\eta$  and  $\pi^0$  invariant masses. These simple cuts allow to clearly see the peak due to  $\phi \rightarrow \eta e^+e^-$  events in the distribution of the missing mass of the  $e^+e^-$  pair,  $M_{\text{miss}}(ee)$  (Fig. 2-left). A cut  $535 < M_{\text{miss}}(ee) < 560$  MeV is then applied. A residual background contamination, due to  $\phi \rightarrow \eta\gamma$  events with photon conversion on beam pipe (BP) or drift chamber walls (DCW), is rejected by tracking back to BP/DCW surfaces the  $e^+$ ,  $e^-$  candidates and reconstructing the electron-positron invariant mass ( $M_{ee}$ ) and the distance between the two particles ( $D_{ee}$ ). Both quantities are small for photon conversions.  $\phi \rightarrow K\bar{K}$  and  $\phi \rightarrow \pi^+\pi^-\pi^0$  events surviving analysis cuts have more than two pions in the final state. They are rejected using time-of-flight to the calorimeter. When an EMC cluster is connected to a track, the arrival time to the calorimeter is evaluated both with the calorimeter ( $T_{\text{cluster}}$ ) and the drift chamber ( $T_{\text{track}}$ ). Events with an  $e^+$ ,  $e^-$  candidate outside a  $3\sigma$ 's window on the  $DT = T_{\text{track}} - T_{\text{cluster}}$  variable are rejected. In Fig. 2-right the  $M_{ee}$  distribution evaluated at IP for data at different steps of the analysis is shown. In Fig. 3 the comparison between data and Monte Carlo (MC) events for  $M_{ee}$  and  $\cos\psi_{ee}$  is shown. The latter is the angle between  $e^+$  and  $e^-$ .

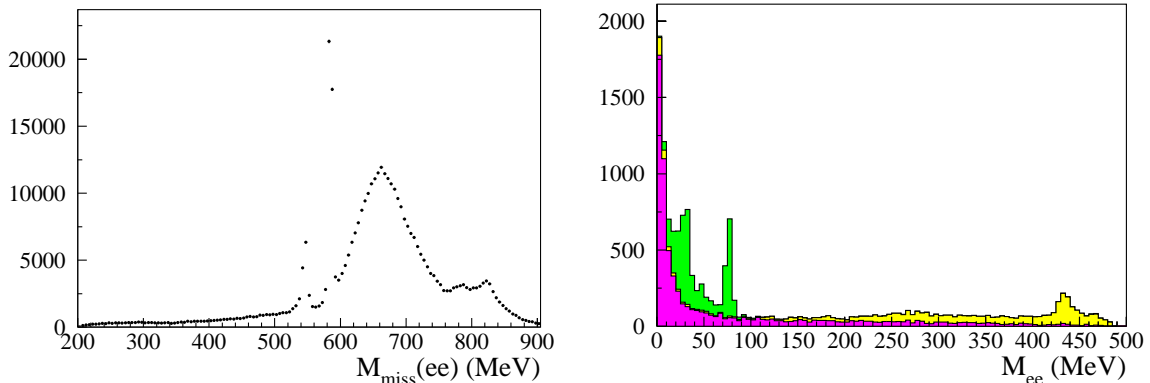


Figure 2: *Left: missing mass of the  $e^+e^-$  pair for data sample after preselection cuts. The  $\phi \rightarrow \eta e^+e^-$  signal is clearly visible in the peak corresponding to  $\eta$  mass. The second peak at  $\sim 590$  MeV is due to  $K_S \rightarrow \pi^+\pi^-$  events with wrong mass assignment. Right:  $M_{ee}$  distribution for data at different analysis steps: preselection (green), conversion (yellow) and ToF (purple) cuts.*

About 7000  $\phi \rightarrow \eta e^+e^-$ ,  $\eta \rightarrow \pi^+\pi^-\pi^0$  candidates are found, with a negligible residual background contamination. The MC simulation is based on the Vector Meson Dominance model and the poorly-known form factor slope parameter from the measurement of the SND experiment <sup>21</sup>). We have recently obtained the form factor slope parameter from our data to improve on the accuracy of the  $\phi \rightarrow \eta e^+e^-$  contribution to the  $\phi \rightarrow \eta U$  search, as reported in Sec.5. The decay distribution is parametrized as in Ref. <sup>22</sup>):

$$\frac{d}{dq^2} \frac{\Gamma(\phi \rightarrow \eta e^+e^-)}{\Gamma(\phi \rightarrow \eta\gamma)} = \frac{\alpha}{3\pi} \frac{|F_{\phi\eta}(q^2)|^2}{q^2} \sqrt{1 - \frac{4m^2}{q^2}} \left(1 + \frac{2m^2}{q^2}\right) \left[ \left(1 + \frac{q^2}{m_\phi^2 - m_\eta^2}\right)^2 - \frac{4m_\phi^2 q^2}{(m_\phi^2 - m_\eta^2)^2} \right]^{3/2} \quad (1)$$

where  $F_{\phi\eta}(q^2)$  is given by <sup>23</sup>):

$$F_{\phi\eta}(q^2) = \frac{1}{1 - q^2/\Lambda_{\phi\eta}^2}. \quad (2)$$

The preliminary result of the fit to the  $M_{ee}$  shape is shown in Fig.4: a relative accuracy on the form factor slope,  $b = \Lambda_{\phi\eta}^{-2}$ , of 4.6% is obtained with  $\chi^2/\text{ndf} = 1.4$ .

#### 4 The hadronic cross section

KLOE has already published two measurements of the dipion cross section for  $M_{\pi\pi}^2$  between 0.35 and 0.95  $\text{GeV}^2$  using  $e^+e^- \rightarrow \pi^+\pi^-\gamma$  <sup>24, 25</sup>), both at a collision energy  $W=M_\phi$ , selecting events with ISR photons at low angle, and normalizing the sample to the luminosity obtained with the study of Bhabha scattering events at large angle. In year 2010 we progressed on the measurement of the dipion cross section normalized to the  $e^+e^- \rightarrow \mu^+\mu^-\gamma$  sample and finalized a new analysis <sup>26</sup>), based on data taken at  $W = 1$  GeV, about 20 MeV below the  $\phi$ -meson mass. The latter requires ISR photons detected in the electromagnetic calorimeter, at large polar angles, allowing the extension of the  $M_{\pi\pi}^2$  region down to the threshold for dipion production. However, compared to the measurements with photons at small angle, the statistics is reduced by a factor of 5 and the background from  $\phi \rightarrow \pi^+\pi^-\pi^0$  as well as the irreducible background from events with final state radiation and from  $\phi$  radiative decays, are higher. The off-peak data sample, with the reduction

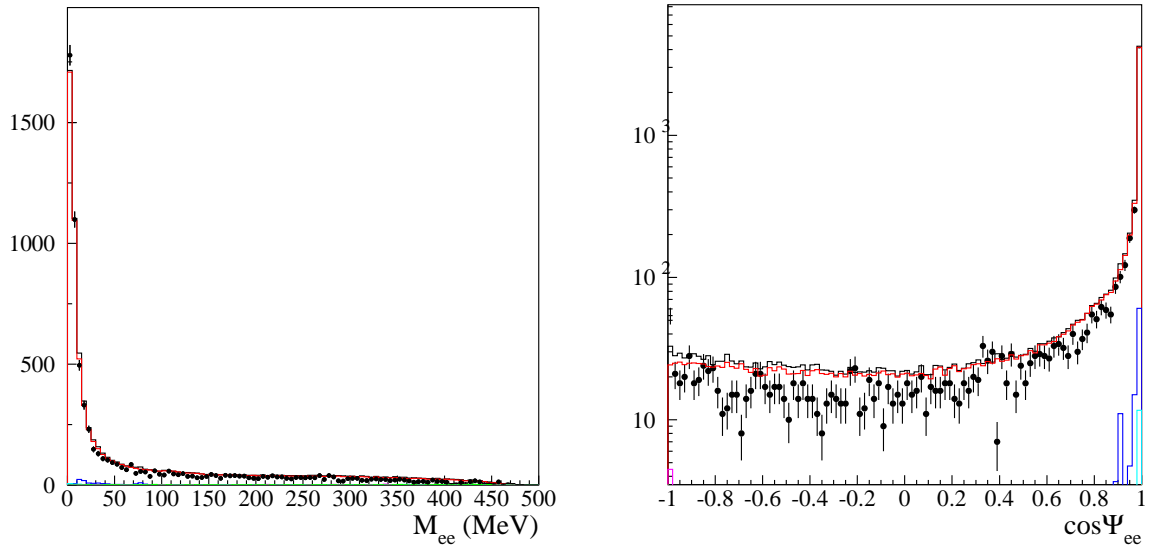


Figure 3: *Invariant mass (left) and opening angle (right) of the  $e^+e^-$  pair for  $\phi \rightarrow \eta e^+e^-$ ,  $\eta \rightarrow \pi^+\pi^-\pi^0$  events. Dots are data, the red line represents the expected MC shape for signal while the residual background contamination from  $\phi$  decays is shown in blue. The black solid line is the sum of all MC contributions.*

by a factor of 80 of the  $\phi$  meson contribution, has been chosen in order to improve on the S/B ratio keeping within a few percent the hadronic uncertainties associated with the production of  $f_0(980)$  and  $f_0(600)$  scalars and from  $\phi \rightarrow \rho\pi \rightarrow (\pi\gamma)\pi$  decays. The differential radiative cross section  $d\sigma(e^+e^- \rightarrow \pi^+\pi^-\gamma)/dM_{\pi\pi}^2$  in the interval  $0.1 < M_{\pi\pi}^2 < 0.85$  GeV<sup>2</sup> that has been obtained is affected by a systematic uncertainty of 1% above 0.4 GeV<sup>2</sup>, rising up to 7.5% when approaching 0.1 GeV<sup>2</sup>. The increase is mainly due to the uncertainty in the production mechanism of  $\phi$  radiative decays. From this measurement, we have extracted the squared modulus of the pion form factor in the time-like region,  $|F_\pi|^2$ , and the bare cross section for the process  $e^+e^- \rightarrow \pi^+\pi^-$ ,  $\sigma_{\pi\pi}^{\text{bare}}$ , in intervals of 0.01 GeV<sup>2</sup> of  $(M_{\pi\pi}^0)^2$ , the squared mass of the virtual photon produced in the  $e^+e^-$ -collision after radiation of a hard photon in the initial state. The measurement is in agreement with previous KLOE results, with the Novosibirsk experiments CMD-2 (27, 28) and SND (29), especially at low values of  $(M_{\pi\pi}^0)^2$ , and with the Babar analysis (30) below 0.4 GeV<sup>2</sup>, while above the BaBar measurement is higher by 2-3%.

Evaluating the dispersion integral for the dipion contribution to the muon magnetic moment anomaly,  $\Delta a_\mu^{\pi\pi}$ , and combining all of the KLOE results, we obtain:

$$\Delta a_\mu^{\pi\pi}(0.1 - 0.95 \text{ GeV}^2) = (488.6 \pm 5.0) \times 10^{-10},$$

that confirms the  $3\sigma$  discrepancy between the SM evaluation for  $a_\mu$  and the experimental value measured by the Muon g-2 collaboration at BNL (31).

## 5 Searches for U-bosons

The existence of a secluded gauge sector could explain several puzzling astrophysical observations. Such hypothesis can be tested at low energy  $e^+e^-$  colliders such as DAΦNE. Preliminary results obtained with KLOE data and perspectives for the KLOE-2 run, are reported. In recent years,

several astrophysical observations have failed to find easy interpretations in terms of standard astrophysical and/or particle physics sources. A non exhaustive list of these observations includes the 511 keV gamma-ray signal from the galactic center observed by the INTEGRAL satellite <sup>32)</sup>, the excess in the cosmic ray positrons reported by PAMELA <sup>33)</sup>, the total electron and positron flux measured by ATIC <sup>34)</sup>, Fermi <sup>35)</sup>, and HESS <sup>36, 37)</sup>, and the annual modulation of the DAMA/LIBRA signal <sup>38, 39)</sup>. An intriguing feature of these observations is that they suggest the existence of a WIMP dark matter particle belonging to a secluded gauge sector under which the Standard Model (SM) particles are uncharged <sup>40, 41, 42, 43, 44, 45, 46, 47, 48, 49)</sup>. An abelian gauge field, the  $U$  boson with mass at the GeV scale, couples the secluded sector to the SM through kinetic mixing with the SM hypercharge gauge field. The kinetic mixing parameter,  $\epsilon$ , can naturally be of the order  $10^{-4}$ – $10^{-2}$ . In a very minimal scenario, in addition to the  $U$ , it is natural to have a secluded Higgs boson, the  $h'$ , which spontaneously breaks the secluded gauge symmetry. A consequence of the above hypotheses is that observable effects can be induced in  $\mathcal{O}(\text{GeV})$ –energy  $e^+e^-$  colliders <sup>50, 51, 52, 53, 54, 55)</sup> and fixed target experiments <sup>56, 57, 58, 59)</sup>. The  $U$  boson can be produced at DAΦNE through radiative decays of neutral mesons, such as  $\phi \rightarrow \eta U$ . With the statistics already collected at KLOE, this decay can probe couplings down to  $\epsilon \sim 10^{-3}$  <sup>52)</sup>, covering most of the parameter range of interest for the theory. The  $U$  boson can be observed by its decay into a lepton pair, while the  $\eta$  can be identified by the reconstruction of one of the dominant decay modes. Assuming also the existence of the  $h'$ , both the  $U$  and the  $h'$  can be produced at DAΦNE if their masses are smaller than  $M_\phi$ . The mass of the  $U$  and  $h'$  are both free parameters, and the possible decay channels can be very different depending on which particle is heavier. In both cases, an interesting production channel is the  $h'$ -strahlung,  $e^+e^- \rightarrow U h'$  <sup>50)</sup>. Assuming the  $h'$  to be lighter than the  $U$  boson, it turns out to be very long-lived, so that the signature process will be a lepton pair, generated by the  $U$  boson decay, plus missing energy. In the case  $m_{h'} > m_U$ , the dark higgs frequently decays to a pair of real or virtual  $U$ 's. In this case one can observe events with 6 leptons in the final state, due to the  $h'$ -strahlung process, or 4 leptons and one photon, from the  $e^+e^- \rightarrow h' \gamma$  reaction. Another possible channel to look for is the  $e^+e^- \rightarrow U \gamma$  <sup>50)</sup>. The expected cross section can be as high as  $\mathcal{O}(\text{pb})$  at DAΦNE energies. The on-shell boson can decay into a lepton pair, giving an  $e^+e^- \gamma$  signal.

As discussed above, the search of the  $U$  boson can be performed at KLOE using the decay chain  $\phi \rightarrow \eta U$ ,  $U \rightarrow e^+e^-$ . An irreducible background is the Dalitz decay of the  $\phi$  meson,  $\phi \rightarrow \eta e^+e^-$ . It has been studied by SND and CMD-2 experiments obtaining  $BR(\phi \rightarrow \eta e^+e^-) = (1.19 \pm 0.19 \pm 0.07) \times 10^{-4}$  and  $BR(\phi \rightarrow \eta e^+e^-) = (1.14 \pm 0.10 \pm 0.06) \times 10^{-4}$  respectively <sup>21, 60)</sup>. This corresponds to a cross section of  $\sigma(\phi \rightarrow \eta l^+l^-) \sim 0.7$  nb, while for the signal

$$\sigma(\phi \rightarrow \eta U) = \epsilon^2 |F_{\phi\eta}(m_U^2)|^2 \frac{\lambda^{3/2}(m_\phi^2, m_\eta^2, m_U^2)}{\lambda^{3/2}(m_\phi^2, m_\eta^2, 0)} \sigma(\phi \rightarrow \eta\gamma) \sim 40 \text{ fb}, \quad (3)$$

assuming  $\epsilon = 10^{-3}$ ,  $|F_{\phi\eta}(m_U^2)|^2 = 1$ . The resonant shape of the  $e^+e^-$  invariant mass distribution for the  $U$ -boson signal allows however the opportunity to probe  $\epsilon$  parameters down to  $10^{-3}$  with the KLOE data sample <sup>52)</sup>. In Eq. (3),  $|F_{\phi\eta}(m_U^2)|^2$  is the form factor of the  $\phi \rightarrow \eta\gamma$  decay evaluated at the  $U$  mass while the other term is the ratio of the kinematic functions of the decays. The best channel to search for is the  $U \rightarrow e^+e^-$ , for two reasons: (i) a wider range of  $U$  boson mass can be tested; (ii)  $e^\pm$  are easily identified using the time-of-flight (ToF) measurement. The  $\eta$  can be identified by the three-pion or two-photon final states which represent  $\sim 85\%$  of the total decay rate. We have performed a preliminary analysis using the  $\eta \rightarrow \pi^+\pi^-\pi^0$  channel, which provides a clean signal with four charged tracks and two photons in the final state. Studies are under way also for the  $\eta \rightarrow \gamma\gamma$  sample. The preliminary analysis of the  $\eta \rightarrow \pi^+\pi^-\pi^0$  final state has been performed

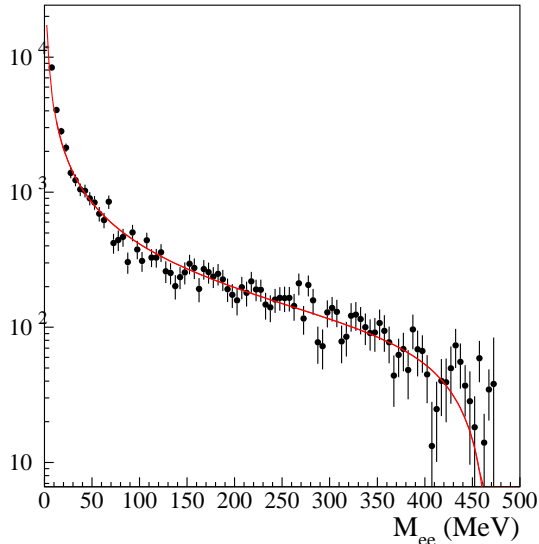


Figure 4: *Fit to the  $M_{ee}$  spectrum for the Dalitz decays  $\phi \rightarrow \eta e^+e^-$ , using the  $\eta \rightarrow \pi^+\pi^-\pi^0$  final state.*

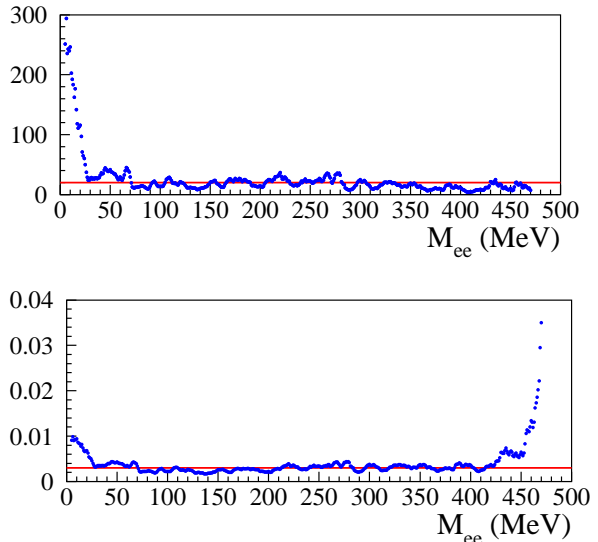


Figure 5: *Top: exclusion plots on number of events for the decay chain  $\phi \rightarrow \eta U$ ,  $\eta \rightarrow \pi^+\pi^-\pi^0$ ,  $U \rightarrow e^+e^-$ . Bottom: exclusion plot on  $\epsilon$  parameter, obtained from the previous one in the hypothesis that the  $U$  boson decays only to lepton pairs.*

on 739/pb, corresponding to 40% of the total sample. The shape of the  $\phi \rightarrow \eta e^+e^-$  irreducible background was extracted directly from our data, as discussed in Sec.3. The  $\phi \rightarrow \eta U$  MC signal has been produced according to Ref. <sup>52)</sup>. Events are then divided in sub-samples of 1 MeV width. For each  $M_{ee}$  value, signal hypothesis has been excluded at 95% C.L. using two different methods, CLS technique <sup>61)</sup> and Bayesian approach, obtaining consistent results. The expected shape for the irreducible background  $\phi \rightarrow \eta e^+e^-$  is taken from our fit to the  $M_{ee}$  distribution. In Fig. 5-top, the preliminary exclusion plot on the number of events obtained with CLS technique is shown. In the region  $25 < M_{ee} < 425$  MeV, an upper limit of  $\sim 20$  events is obtained. Systematics are not yet included. The exclusion plot for the  $\epsilon$  parameter is obtained using Eq.(3), taking into account of the analysis efficiency and opening of the  $U \rightarrow \mu^+\mu^-$  channel. Results are reported in Fig. 5-bottom. The search for  $\phi \rightarrow \eta U$  with  $\eta \rightarrow \pi^+\pi^-\pi^0$  using 739 pb<sup>-1</sup> of KLOE data, gives a preliminary upper limit on the  $\epsilon$  parameter,  $\epsilon < 3 \times 10^{-3}$  @ 95% C.L., in the  $25 < M_{ee} < 425$  MeV region. The limit can be improved to  $10^{-3}$  level with the KLOE-2 data taking.

A similar analysis strategy has been developed for the decay chain  $\phi \rightarrow \eta U$ ,  $U \rightarrow e^+e^-$ ,  $\eta \rightarrow \gamma\gamma$ . The preselection requires: (i) two tracks coming from a cylinder around IP, classified as  $e^\pm$  using ToF information; (ii) two photon candidates; (iii) the angle between photons in  $\eta$  rest frame to be  $\sim 1$ ; (iv) a loose cut on the total invariant mass of the system,  $950 < M_{tot} < 1150$  MeV. The most severe background is generated by double radiative Bhabha events and it is strongly reduced by cutting on the opening angle between the charged tracks and the photons. Residual non-Bhabha background is rejected by using electron identification based on the  $E/p$  ratio for the  $e^+e^-$  candidates. The  $M_{ee}$  spectrum obtained with 1.7 fb<sup>-1</sup> shows a clear evidence of  $\phi \rightarrow \eta e^+e^-$  Dalitz decays at low values and some residual background contamination at high  $M_{ee}$  due to Bhabha events. Work is in progress to further clean the sample. The feasibility study of the search

for  $e^+e^- \rightarrow Uh'$  has been performed considering the  $m_{h'} < m_U$  case. At DAΦNE energies, for  $\epsilon \sim 10^{-3}$ , a production cross section of  $\approx 20$  fb is expected. The lifetime,  $\tau_{h'} > 10 \mu\text{s}$ , is such that  $h'$ 's escape detection. The signature is therefore one lepton pair from the  $U$  boson plus missing energy. The  $U \rightarrow e^+e^-$  events are not selected by any official KLOE event classification (ECL) algorithm; on the contrary, ECL is fully efficient for  $U \rightarrow \mu^+\mu^-$  events, when  $h'$  mass does not exceed 300 MeV,  $m_{h'} < 300$  MeV. We therefore are considering the  $\mu^-\mu^-$  final state only. The search for higgs'-strahlung events,  $e^+e^- \rightarrow Uh'$ , with  $U \rightarrow \mu^+\mu^-$  plus missing energy, is limited by the  $\phi \rightarrow K^+K^-$  background in a wide region of the  $M_{\mu^+\mu^-}$ ,  $M_{\text{recoil}}$  plane. Work is in progress to reduce such contamination. At KLOE-2, the higher accuracy on vertex resolution, achievable with the help of the inner tracker, can provide a higher rejection factor. We are also discussing the feasibility of a high statistics off-peak run, e.g. at 1 GeV, to suppress  $\phi \rightarrow K^+K^-$  background contribution.

## 6 The tagger system for $\gamma\gamma$ physics

The process  $e^+e^- \rightarrow e^+e^-\gamma^*\gamma^* \rightarrow e^+e^-X$ , where  $X$  is some scalar or  $\pi\pi$  final state, can give access to  $J^{PC} = 0^{\pm+}; 2^{\pm+}$  states, not directly coupled to one photon ( $J^{PC} = 1^{--}$ ). KLOE is progressing on the analysis of  $e^+e^- \rightarrow e^+e^-\eta$  and  $e^+e^- \rightarrow e^+e^-\pi^0\pi^0$ . The study is based on 240/pb of integrated luminosity at  $\sqrt{s} = 1$  GeV, 20 MeV below the  $\phi$  peak to suppress background contributions from  $\phi$  decays. For the  $e^+e^- \rightarrow e^+e^-\eta$  channel, the reconstruction of  $\eta \rightarrow \pi^+\pi^-\pi^0$  is required leading to the selection of more than 600 signal events. The irreducible background is constituted of  $e^+e^- \rightarrow \eta\gamma \rightarrow \pi^+\pi^-\pi^0\gamma$  events with missing photon from the primary process. The background subtraction requires the knowledge of the cross section at 1 GeV of  $e^+e^- \rightarrow \eta\gamma \rightarrow \pi^+\pi^-\pi^0\gamma$  that has been obtained at KLOE from the analysis of the sample with three photons in the final state, yielding to  $\sigma(e^+e^- \rightarrow \eta\gamma \rightarrow \pi^+\pi^-\pi^0\gamma, 1 \text{ GeV}) = (198 \pm 2_{\text{stat}})$  pb. For the  $e^+e^- \rightarrow e^+e^-\pi^0\pi^0$  channel, of interest for the study of the  $f_0(600)$  scalar, KLOE has found evidence at low  $M_{4\gamma}$  of an excess consistent with expectations from  $e^+e^- \rightarrow e^+e^-\pi^0\pi^0$ . Systematic study of the cross section and understanding of the  $\sigma \rightarrow \pi^0\pi^0$  contribution are in progress. The analyses represent also a feasibility test for the study of  $\gamma\gamma$  processes with KLOE-2, that has a tagging system for the detection of electron/positron in the final state and thus can perform the measurements on the on-peak sample.

The tagger system for  $\gamma\gamma$  physics<sup>1)</sup> is composed by two stations (on the electron and positron machines) of LYSO calorimeters (LET), inside the KLOE apparatus, and two stations of position detectors (HET) with 32 scintillator pixels of  $5 \times 6 \times 3 \text{ mm}^3$ . In year 2010 the detectors have been realized and the LET calorimeters have been installed on the final focusing region of DAΦNE.

The HET optical system is ready, including shaped optical guides, scintillators and optical guide glued and wrapped with aluminized mylar. The three main components of the HET mechanics are the insertion and vacuum systems, the structural support for the phototubes and the external support. The insertion and vacuum systems have been installed inside the beam pipe. The structural support for the phototubes and the external support have been designed and under construction. Two out of four boards for the acquisition chain, the Front End Buffer board (FEBb), and the Fast Discriminator Shaper board (FDSb), are being tested, while the others, the Acquisition V5 board (ACQ-V5b) and the Slow Environment Control System board (SECSb), are being constructed. The characterization of the two HET detectors with final electronics is planned by May at the Frascati Beam Test Facility (BTF).

## 7 The KLOE-2 inner tracker

The Inner Tracker <sup>62)</sup> (IT) for the upgrade of the KLOE apparatus is composed by 4 cylindrical layers of triple-GEM (CGEM) at radii from 13-23 cm, installed between the spherical beam pipe (external radius of 10 cm) and the drift chamber (internal radius of 25 cm). The large radius of the beryllium beam pipe at the interaction region retaining the quantum-interference pattern of  $K_S$ - $K_L$  beams in vacuum was chosen to perform the most sensitive tests of quantum mechanics and CPT conservation with correlated kaon pairs. The total active length for all layers is 70 cm. The anode readout of each CGEM is segmented with 650- $\mu$ m pitch, XV-patterned strips at a stereo angle of  $\sim 40^\circ$ , for a total of 30,000 FEE channels. The Front-End Electronics for the IT is based on GASTONE ASIC <sup>63)</sup>, a dedicated 64-channels chip developed for the KLOE-2 experiment. The construction and extensive test of a full-size CGEM prototype has demonstrated the feasibility of such a novel low-mass and dead-zone-free vertex detector. The final readout configuration has been successfully validated testing small planar prototypes operated in magnetic field. During 2010, to conclude the R&D phase, a large area planar GEM prototype 300x700 mm<sup>2</sup> has been built using foils realized with the new single-mask photolithographic technique <sup>64)</sup>, to test their quality and homogeneity. This detector, the largest GEM detector ever operated, has been equipped with the GASTONE 64-channels final release, readout by the Off Gastone Electronic (OGE) board <sup>62)</sup> and tested at CERN-PS T9 beam-line in October, 2010. The detector mechanics, assembly and quality control tools have been prepared and are now ready for the construction of the Inner Tracker. The Vertical Insertion System (VIS) has been built; this system will allow us to assemble each IT layer by inserting the cylindrical electrodes one inside the other with high precision.

### 7.1 Towards IT construction

In 2010 the activity has mainly focused on the design of the detector components and tools necessary for the construction of the Inner Tracker.

#### *Detector Components*

The design of the detector components and construction tools as well as the choice of the materials originates both from the experience of the construction of the GEM detectors <sup>65)</sup> of the LHCb Muon apparatus, and, more specifically, for the construction of the full scale prototype of the CGEM <sup>66)</sup>. In particular, the materials used for the CGEM were largely tested and validated for high-rate environments <sup>67)</sup> and for different gas mixtures (Ar, i-C4H10, CF4, CO2 ) <sup>68)</sup>. The CGEM has the typical triple-structure of such a kind of micro-pattern gas detector: the gaps among the different electrodes of the detector (cathode-G1, G1-G2, G2-G3 and G3-anode) define the various regions of the detector itself: drift (3 mm wide), transfers and induction (2 mm wide). The gas, supplied in open mode through the six gas inlets realized on the annular frame of the cathode, flows through the holes of the three GEM and then exits from the detector by the six outlets of the anode frame. Frames are realized in EPCG203 fiberglass, a composite material that allows precise machining: a crucial feature against spurious discharges. The frames, glued at the edge of the cylindrical electrodes outside their active area, define the various gaps of the detector. The most relevant modification with respect to the prototype design is represented by the embedded-anode, consisting of a very light honeycombed carbon fiber cylinder (CFC) on which the anode readout circuit is glued. The CFC acts as a rigid support for the whole detector layer. The simulation studies of the CFC deformation indicated that for an axial load of 600 kg applied to the CFC, the maximal radial displacement is about 150  $\mu$ m for a CGEM with the dimension of the first layer (up to 700 mm length). The load tests have shown that the break-down of the CFC

prototype occurs at about 8 tons, well above the expected load on the final IT structure. The 700 mm long GEMs are realized at CERN with the new single mask procedure that allows large area foils to be built <sup>64</sup>). In order to overcome the limit on the width of the raw material used for the GEM foils (600 mm), all the large electrodes of each layer are realized by splicing three smaller foils: the gluing technique is the same used for the construction of the prototype, exploiting the vacuum bag technique for epoxy glue polymerization. The GEM foils as well as the XV strip-pad patterned anode readout circuits and the cathode foils are realized on the basis of our design by the CERN EST-DEM Printed Circuit Board Workshop.

*Construction and tooling*

The construction strategy and the toolings of the CGEM layers are the same used for the prototype. The main construction steps can be summarized as follows: i) the three GEMs, as well as the anode and cathode foils are glued together in order to obtain a single large foil. For this operation we exploit a precise Alcoa plane and the vacuum bag technique. ii) the large foil is then rolled on a very precise aluminum cylindrical mould covered with a 0.4 mm machined Teflon film for easy and safe extraction of the cylindrical electrode (Fig.6-left). The mould is then enveloped with the vacuum bag, and vacuum is applied for the glue curing time (about 12 hours). iii) the final assembling of a CGEM layer is performed by means of the Vertical Insertion System (VIS), Fig.6-right, a quite complex device that allows a precise and safe insertion of the cylindrical electrodes one inside the other. The system is designed to permit a very precise alignment of the cylindrical electrodes ( $\sim 100\mu\text{m}$ ) along their vertical axis. The bottom electrode is fixed, while the top one is slowly moved downwards by a step-motor, coupled with a reduction gear system. The operation is performed with the help of three small web-cameras, placed at 120 degrees one to each other around the top cylindrical electrode, thus allowing the monitoring of the radial distance between the electrodes (2-3 mm). The up-down rotation of the assembly machine allows an easy sealing of the detector on both sides.

*Material preparation and Quality Controls*

Before the final assembly of the detector, each component follows a well defined preparation procedure that generally includes a global optical inspection, a cleaning and an HV test. In particular



Figure 6: *Left: The aluminum moulds used for the construction of the cylindrical electrodes of the inner tracker. Right: The assembly machine (Clessidra) used for the insertion of the cylindrical electrodes one into the other.*

for GEMs the HV test is repeated at each construction step, in order to avoid the assembly of damaged GEM and to minimize the losses of precious components.

#### *Final readout*

The IT will be inserted between the beam pipe and the Drift Chamber inner wall. Unfortunately the location has i) very poor heat-exchange capability, ii) inaccessibility after system installation and iii) small space for I/O cables. In addition, because of the GEM moderate gas gain, front-end electronics must be installed on the detector to maximize S/N ratio. Therefore low power consumption and low number of I/O connections are required together with high reliability of the entire system. To fulfill the requirements, a 64-channels ASIC named GASTONE (Gem Amplifier Shaper Tracking ON Events) has been developed. The chip, that is built with the 0.35 CMOS technology, implements a mixed analog-digital circuit with 64 channels. Each channel is made of 4 blocks: a charge preamplifier with a sensitivity of about 20 mV/fC, a shaper, a leading-edge discriminator with programmable threshold and a monostable circuit to stretch the discriminated signals then allowing their synchronization with the KLOE trigger. Up to 180 chips assembled on 90 boards are required to fully instrument the detector. Digital output signals are serially readout by means of dedicated boards (then minimizing I/O cables) located about 4 m from the detector. Readout boards provide also LV and L0 to the front-end boards and ECS connection.

## 8 The QCALT: a Quadrupole Calorimeter with Tiles

To increase the photon detection efficiency for  $K_L \rightarrow 3\pi^0$  events we are developing a new Quadrupole Calorimeter to cover the area where the inner focalizing quadrupoles (and correcting permanent dipoles) are located. There will be two detectors, one per side with respect to the IP, named QCALT, each one consisting of a dodecagonal structure,  $\sim 0.9$  m long, composed by a sampling of five layers of 5 mm thick scintillator plates alternated with 3.5 mm thick W/Cu (90/10) plates. The total absorption depth will be of 4.75 cm ( $5.5 X_0$ ). The active part of each plane is divided into sixteen tiles of  $\sim 5 \times 5$  cm<sup>2</sup> area with 1 mm diameter WLS fibers embedded in circular grooves. Each fiber is then optically connected to a silicon photomultiplier of 1 mm<sup>2</sup> area, SIPM, for 80 channels/module and 1920 channels in total. The “T” in QCALT stays for tile, since we intend to read-out each tile singularly improving, with respect to the previous version of these calorimeters, the resolution along z (from 8-10 cm down to 2 cm) and its capability of sustaining the rate thanks to the increased granularity. Relying to the new quality SIPM of Hamamatsu, we have reached a light yield of  $\sim 30$  p.e./MIP and a time resolution of  $\sim 1$  ns. This translates to an efficiency above 95% for photons down to 20 MeV as shown by a preliminary simulation study carried out with Geant4. During 2010, we have realized the first full size “module-0” (Fig.7) in order to understand the assembly techniques and the problems of integrating the readout in the small space available inside KLOE. Here are the lessons we have learnt during this construction.

#### *Survey of plastic scintillator and preparation of the grooves*

We acquire plastic scintillators in slabs of  $500 \times 200 \times 5$  mm<sup>3</sup> and then cut them to the desired tile dimensions. During survey of their thickness we found that  $\sim 30$  % of the received material exceeds the tolerance of 0.2 mm required for allowing a regular construction of the stack. We now follow a much more tight control of these slabs and a rigid acceptance criteria agreed upon with the producer. The grooves and the final milling is done with the automatic control milling machine of the Apparata Design and Construction Service at LNF (SPCM).

#### *W/Cu plates preparation*

The plates have been machined to the required shape by a Chinese firm which succeeded to build pieces as long as 250 mm while keeping the thickness tolerance below 0.1 mm.

#### *“Wrapping” of tiles*

Three different wrapping methods have been tried: i) with Tyveck manually arranged around the



Figure 7: *The full-scale prototype of one module of the QCALT calorimeter, with the tiles assembled and the fibers for the transport of the light to the readout end side.*

tile, ii) with adhesive Tyveck and iii) by spraying on the tile a reflective paint from St.Gobain. Light outputs of single tiles wrapped with different techniques have been compared. No differences larger than 10% have been found. We have built the module 0 as a mixture of the three different techniques, the two innermost layers with method i), the central one with method ii) and the two outermost ones with method iii). Easiness of construction and thickness uniformity indicates to select method iii) as the final one.

#### *Fiber-SIPM coupling*

We have realized a first set of single fiber-SIPM PVC connector to check the optical contact reproducibility. We discovered that the mechanical precision needed in positioning should be better than 0.1 mm in order not to deteriorate this coupling. The realized connector was not good enough for this purpose. We therefore readout the module 0 by means of a much simpler, even if larger, connector done in aluminum which allowed us to test it in groups of five channels at the time. The problems found during these tests suggested a more radical solution for this interface. The fibers will be “glued” to a PVC holder and then milled in order to assure good positioning and a flat and clean surface. In front of this there will be a PCB where “surface mounted” (SMD) SIPM’s will be bond in a matching position to the fibers with the required precision.

#### *Procedure of calibration after assembly*

After assembly, we have acquired cosmic rays in most of the columns (i.e. five planes at a time) by triggering with an external  $100 \times 200 \times 50 \text{ mm}^3$  scintillator above the module. In Fig.8, we show the pulse height and time resolution obtained for few channels. Most of the towers have shown similar behaviour. Few of them were giving lower light yield, this being related to a bad SIPM-fiber optical coupling which remains the *technical issue* to be solved with the Fiber-SIPM PCB interface.

#### *Test of FEE*

With module 0, we have also tested the prototype of the amplifiers that are going to be used in the final version. A set of twenty single channel amplifiers (dimension  $10 \times 20 \text{ mm}^2$ ) has been produced by the Electronics Service of the LNF (SELF), together with the HV driver done in NIM standard. All FEE prototypes were performing as expected.

In collaboration with Cosenza University group, we have also studied the long-term stability of the tiles by firing a reference tile with a UV LED, in a temperature controlled environment. We observed no hints of signal deterioration along an observation period of few months apart a slow

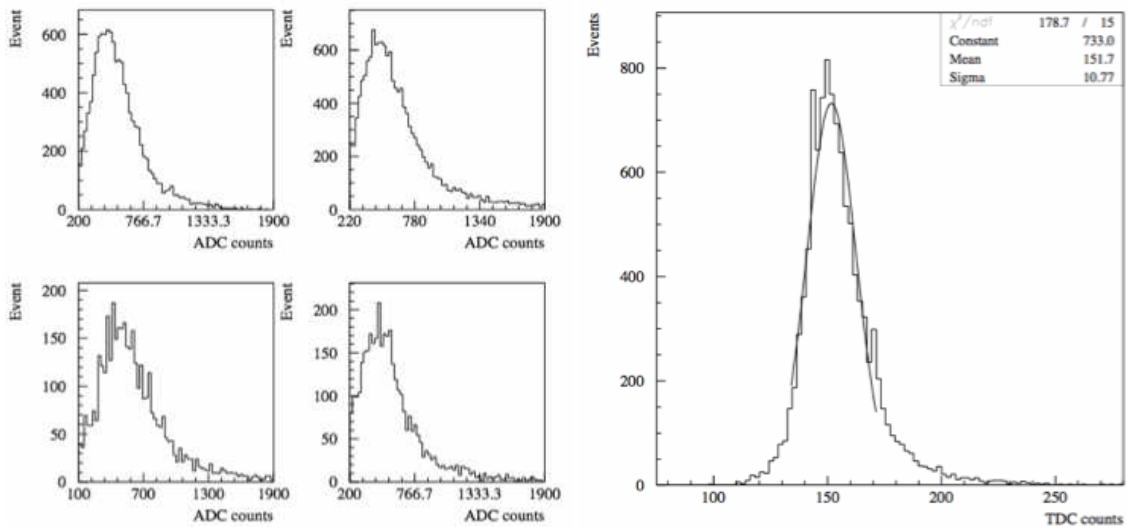


Figure 8: *Left: QCALT pulse height distribution Right: QCALT time resolution.*

increase in response attributed to LED pulse variation. When repeating this measurement for the largest tiles of the outermost plane we instead find out a fast deterioration along time such to reduce the signal of a factor three in a week. After a deep investigation, we realized that the grooves had a mechanical defect and were not as smooth as expected. By lapping the groove in the proper way, we see no further sign of signal deterioration in the new set of similar tiles under test. We have then carried out, in collaboration with the engineering department of SPCM, a complete study on how to safely handle the calorimeter both during assembly and during installation over the BPS. Each QCALT will be divided in two halves (SemiQCAL) of six modules. Each SemiQCAL will be assembled over a rotating frame to have the module under construction in horizontal position. During assembly, we will leave the fibers passing through the fiber holder and extending them outside of  $\sim 50$  cm for the connection to reference SIPM's by means of special aluminum connector. This will allow the construction control, for each plane, by firing with a UV LED along the tiles. We plan to assembly one plane/day, check the uniformity soon after and double-check the uniformity the following day, before starting the assembly of another plane. We expect to construct one module/week for each assembly station. We will then bring the module to the SPCM for final fiber milling over the PVC holder.

Due to the difficulty of positioning 80 SIPM's in the front calorimeter face, we are working to integrate them over a PCB. The SELF has already developed such a PCB, realized by an external firm. We have also contacted the IRST/FBK firm at Trento to construct 120 SMD SIPM's of  $1.2 \times 1.2$  mm<sup>2</sup> dimension (and a first set or circular ones of 2.6 mm diameter) in order to simplify the alignment with the fibers. The IRST will also bond the SIPM's on the PCB. We expect to have a final PCB ready for spring 2011. Some light yield reduction with respect to the Hamamatsu SIPM is expected (between 30% to 50%) since the PDE of the IRST SIPM's is lower than the Hamamatsu ones. However IRST SIPM's better match the light frequency emitted by the WLS fibers which is peaked on green. The FEE, on detector, will consists of four boards/module, of 20 channels each, where the preamplifiers and the HV regulator will be positioned. The OFF-detector electronics will consist of a 40 channel transition board that will do both the discrimination and the HV master. The general interface boards (GIB), in the readout crate, set the HV. The readout

is organized by a TDC multihit with a range of 0.6-0.8  $\mu\text{sec}$  and 1 ns resolution. We expect to use the leading-trailing edge measurement to have an approximate reconstruction of the charge, needed only to study the gain stability of the system. Design of the FEE is underway. We expect to have the first prototypes ready for spring 2011.

## 9 The CCALT: a Crystal Calorimeter with Timing

The CCALT is a crystal calorimeter which covers the solid angle between 10 and 18 degrees in order to extend our acceptance to low energy photons. The necessity of a calorimeter with high photon reconstruction efficiency ( $\epsilon_\gamma > 99\%$  for  $E_\gamma > 20$  MeV) and good time resolution ( $\sigma_t \simeq 200\text{--}500$  ps) in this angular region has been proposed with the double task of i) vetoing the presence of additional unwanted photons in rare  $\eta$  and  $K_S$  decay channels (such as  $K_S \rightarrow 2\gamma$  or  $\eta \rightarrow \pi^0\gamma\gamma$ ); ii) increasing the acceptance in very rare decay channels such as  $K_S \rightarrow 3\pi^0$ .

A good timing resolution and a fast response ( $\tau_{scint} < 50$  ns) are needed since the CCALT will be positioned in between the interaction point and the first inner quadrupole, QD0, where an intense flux of photons of O(MHz) per side, produced from Touschek particles, is expected. The detector is composed of two calorimeters (one per side with respect to the IP) each divided in twelve modules. Each module is constituted by four crystals of special shapes. Each crystal will be of 8-9 cm length with the transversal area of the larger face of about  $25 \times 25$  mm<sup>2</sup>. Given the reduced space available in this region, we need fast and high density crystals with a large light yield. The crystal matching these requirements is the LYSO which has a density of 7.5 g/cm<sup>3</sup>, a radiation length of 0.9 cm, a Moliere radius of 2 cm, a  $\tau$  of 40 ns and a light yield of 500 p.e./MeV, when readout with a high efficiency Bialcali PM.

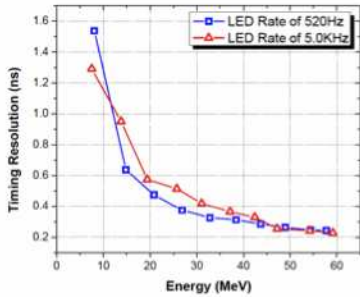


Figure 9: *Time resolution as a function of energy for a LYSO crystal of  $20 \times 20 \times 130$  mm<sup>3</sup> volume readout by a  $4 \times 4$  mm<sup>2</sup> SIPM. The signal is generated by illuminating the crystal with a UV LED.*

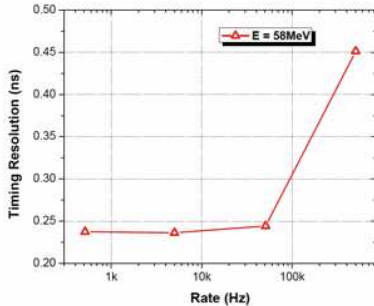


Figure 10: *Time resolution as a function of rate for a LYSO crystal of  $20 \times 20 \times 130$  mm<sup>3</sup> volume readout by a  $4 \times 4$  mm<sup>2</sup> SIPM when illuminated by a UV LED simulating a signal of 50 MeV.*

In 2009, we have built a first prototype done by an inner matrix of ten LYSO crystals, from

different producers, readout by means of  $5 \times 5 \text{ mm}^2$  APD's. We have tested this prototype with 100 to 500 MeV electrons at the Beam Test Facility at LNF (BTF) obtaining an energy resolution parametrized as  $\sigma_E/E = 1.2\%/(E/\text{GeV}) + 1.7\%/\sqrt{E/\text{GeV}} + 5\%$  and a timing resolution between 100 to 200 ps. The k/E energy resolution term resulted too large with respect to the measured noise term of 500 keV/channel. In order to understand that, we have constructed a new prototype with longer LYSO crystals readout by larger area APD's ( $10 \times 10 \text{ mm}^2$ ). These new crystals have been purchased from SICCAS (Shanghai) that furnished also all crystals for the LET detector and we have already achieved a noise term of 150 keV/channel during laboratory tests. We plan to study the components of the energy resolution at the tagged photon beam facility of Mainz Microtron (MAMI) in spring 2011. The integration with the other detectors, IT and QCALT, inside KLOE asks for tight requirements such as reducing as much as possible the thermal dissipation and respecting the severe space constraints. We have therefore investigated if we can readout successfully the CCALT by means of large area SIPM thus avoiding the usage of preamplifiers which have a typical power consumption of 100 mV/channel and a minimal transversal size of  $10 \times 20 \text{ mm}^2$ . Two crystals have been connected with optical grease to two different SIPM's, a  $4 \times 4$  ( $6 \times 6$ )  $\text{mm}^2$  from IRST/FBK (Hamamatsu) and their response to a UV LED has been tested both in charge and in time. In Fig.9, we report the timing resolution of the crystal readout by IRST SIPM's as a function of the rate for a 50 MeV equivalent signal and as a function of energy for low rate pulsing. We see no deterioration of the timing response up to 50 kHz and a worsening up to a factor of 2 for rate close to the MHz. The timing resolution remains between 200 to 450 ps also at low energies, for  $E_\gamma > 50$  MeV. The 96 signals from the crystals are transmitted to the Transition Board that transfer them to the standard SDS boards for splitting and discrimination. The GIB boards set and control the HV of each SIPM, in a way very similar to the LET calorimeter.

## Acknowledgements

We would like here to thank all the engineers and technicians belonging to the LNF services that provided a fundamental contribution to KLOE2 both to the apparatus maintenance and to the construction and development of the new detectors for the upgrade. For the SPCM service we acknowledge the work of M.Arpaia, G.Bisogni, A.Ceccarelli, A.de Paolis, G.Ferretti, E.Iacuessa, U.Martini, M.Meli, A.Olivieri. They were/are strong enough to support the construction of toolings and detector components for the upgrades. A special thank goes to A. Saputi that is designing much of the QCALT, CCALT and HET mechanics. For the SPAS service, we cannot forget S.Cerioni that remains one of the main contributor for the IT design and realization. For the SEA service we thank A. Balla, M.Beretta, G.Corradi, U.Denni, E.Frani, M.Gatta, C.Paglia, G.Papalino and D.Tagnani. This service is in charge of following the realization of mainly all ON-detector and OFF-detector electronics for the upgrades while maintaining KLOE main apparatus still alive. Finally, we would like to thank B.Ponzio and G.Pileggi for their help in the construction and test of QCALT module-0 and the CCALT prototype to be used at the tagged photon source of MaMi.

## Papers

1. F. Ambrosino *et al.* (KLOE), *Measurement of the  $\eta \rightarrow 3\pi^0$  slope parameter  $\alpha$  with the KLOE detector*, Phys. Lett. **B0694** (2010) 16
2. G. Amelino-Camelia *et al.* (KLOE-2 Collaboration), *Physics with the KLOE-2 experiment at the upgraded DAFNE*, Eur. Phys. J. **C68** (2010) 619

## Public notes and documents

1. F. Archilli *et al.* (KLOE-2), *Technical Design Report of the Inner Tracker for the KLOE-2 experiment*, LNF 10-3(P), February 2010, and arXiv:1002.2572
2. D. Babusci *et al.* (KLOE-2), *Proposal for taking data with the KLOE-2 detector at the DAFNE collider upgraded in energy*, LNF 10-17(P), July 2010, and arXiv:1007.5219
3. F. Ambrosino *et al.* (KLOE) *Measurement of  $\sigma(e^+e^- \rightarrow \pi^+\pi^-)$  from threshold to 0.85 GeV<sup>2</sup> using Initial State Radiation with the KLOE detector*, arXiv:1006.5313, Jun 2010.
4. A. Antonelli, M. Dreucci (KLOE) *Precision Measurement of  $K_S$  Meson Lifetime with the KLOE detector*, arXiv:1011.2668, November 2010
5. C. Redmer, T. Pena, B. Hoistad (PrimeNet) *Proceedings of the International PrimeNet Workshop*, arXiv:1102.4999, February 2011

## 10 Contributions to Conferences and Seminars

1. M. Cordelli *et al.*, *QCALT: a tile calorimeter for KLOE-2*, Nucl. Instrum. & Meth. **A617** (2010) 105; Proceedings of the Frontier detectors for frontier physics conference
2. M. Cordelli *et al.*, *Test of a LYSO matrix with an electron beam between 100 MeV and 500 MeV for KLOE-2*, Nucl. Instrum. & Meth. **A617** (2010) 109; Proceedings of the Frontier detectors for frontier physics conference
3. M. Alfonsi *et al.*, *Activity of CERN and LNF groups on large-area GEM detectors*, Nucl. Instrum. & Meth. **A617** (2010) 151; Proceedings of the Frontier detectors for frontier physics conference
4. E. De Lucia, *Status of the cylindrical-GEM project for the KLOE-2 inner tracker*, Nucl. Instrum. & Meth. **A628** (2011) 194; VCI2010 conference, Vienna, Austria, February 15-20, 2010
5. B. Sciascia, *Kaon physics with KLOE*, arXiv:1005.2873; Les Rencontres de physique de la Vallée d'Aoste, La Thuile, Italy, February 28–March 6, 2010
6. F. Happacher, *CCALT*, CALOR 2010, Beijing, China, May 10-14, 2010
7. G. Venanzoni, *Misura della sezione durto  $e^+e^-$  in coppie di pioni a KLOE con la radiazione di stato iniziale e loro contributo al  $g-2$  del muone* Seminar at the Department of Physics, Sapienza University, Rome, May 27, 2010
8. S. Giovannella, *Physics with KLOE and KLOE-2 experiments at DAFNE*, ME(son)NU(cleon) 2010, Williamsburg, Virginia, May 31-June 4, 2010
9. D. Domenici, *A new cylindrical-GEM inner tracker for the upgrade of the KLOE experiment*, 12th topical seminar on innovative particle and radiation detectors (IPRD10), Siena, Italy, June 7-10, 2010
10. F. Bossi, *KLOE-2, how to do fundamental physics at a low energy facility*, Seminar at the Department of Physics, Mainz University, Mainz, Germany, June 9, 2010
11. E. Czerwinski, *Hadron Physics with KLOE-2*, QCD 2010, Montpellier, France, June 28–July 3, 2010

12. F. Bossi, *Updates from KLOE and KLOE-2*, 3rd Int. Workshop on Theory, Phenomenology and Experiments in Heavy Flavor Physics, Capri, Italy, July 5-7, 2010
13. G. Bencivenni, *Status of KLOE-2 Inner Tracker*, 3rd JointGEM meeting at HIP, Helsinki, Finland, July 15, 2010
14. S. Miscetti, *Hadron Physics with KLOE and KLOE-2*, Quark Confinement and the Hadron Spectrum, Madrid, Spain, August 30-September 3, 2010
15. E. De Lucia, *Determination of  $V_{us}$  at the KLOE experiment: present results and future perspectives*, CKM 2010, Coventry, UK, September 6-10, 2010
16. G. Venanzoni, *KLOE measurement of  $\sigma(e+e\rightarrow \pi+\pi-(\gamma))$  with Initial State Radiation and the pion-pion contribution to the muon anomaly*, TAU 2010, Manchester, UK, September 13-17, 2010
17. S. Giovannella,  *$\eta$  and  $\eta'$  decays at KLOE*, PrimeNet Workshop, Lisbon, Portugal, September 16-18, 2010
18. C. Bloise, *The KLOE-2 project*, XCVI Congresso Nazionale della SIF, Bologna, Italy, September 20-24, 2010
19. B. Sciascia, *Status and prospects for the  $Ke_2/K\mu_2$  at KLOE and KLOE-2*, Heavy quarks and leptons, Frascati, Italy, October 11-15, 2010
20. C. Bloise,  *$V_{us}$  from precision measurements with Kaons*, Heavy quarks and leptons, Frascati, Italy, October 11-15, 2010
21. S. Giovannella,  *$U$  bosons searches at KLOE-2*, DISCRETE 2010, Rome, Italy, December 6-11, 2010
22. S. Miscetti, *Status and prospects for the KLOE-2 experiment*, DISCRETE 2010, Rome, Italy, December 6-11, 2010

## References

1. G. Amelino-Camelia *et al.*, EPJ **C68**, 619 (2010).
2. F. Ambrosino *et al.* (KLOE), JHEP **0712**, 073 (2007), 0710.5892.
3. F. Ambrosino *et al.* (KLOE), Phys. Lett. **B632**, 43 (2006), hep-ex/0508027.
4. F. Ambrosino *et al.* (KLOE), Phys. Lett. **B632**, 76 (2006), hep-ex/0509045.
5. F. Ambrosino *et al.* (KLOE), Eur. Phys. J. **C48**, 767 (2006), hep-ex/0601025.
6. F. Ambrosino *et al.* (KLOE), JHEP **02**, 098 (2008), 0712.3841.
7. F. Ambrosino *et al.* (KLOE), Phys.Lett. **B666**, 305 (2008), 0804.4577.
8. F. Ambrosino *et al.* (KLOE), Phys. Lett. **B626**, 15 (2005), hep-ex/0507088.
9. F. Ambrosino *et al.* (KLOE), JHEP **01**, 073 (2008), 0712.1112.
10. M. Antonelli, M. Dreucci (KLOE) (2010), 1011.2668.
11. F. Ambrosino *et al.* (KLOE), Phys. Lett. **B619**, 61 (2005), hep-ex/0505012.

12. F. Ambrosino *et al.* (KLOE), JHEP **0805**, 006 (2008), 0801.2642.
13. F. Ambrosino *et al.* (KLOE), Phys.Lett. **B694**, 16 (2010), 1004.1319.
14. G. Colangelo, S. Lanz, E. Passemar, PoS **CD09**, 047 (2009), 0910.0765.
15. M. Benayoun, P. David, L. DelBuono, P. Leruste, H.B. O'Connell, EPJ **C31**, 525 (2003).
16. M. Gormley, E. Hyman, W.Y. Lee, T. Nash, J. Peoples *et al.*, Phys.Rev. **D2**, 501 (1970).
17. J. Layter, J. Appel, A. Kotlewski, W.Y. Lee, S. Stein *et al.*, Phys.Rev. **D7**, 2565 (1973).
18. A. Lopez *et al.* (CLEO), Phys. Rev. Lett. **99**, 122001 (2007), 0707.1601.
19. C. Redmer, T. Pena, B. Hoistad (2011), 1102.4999.
20. F. Ambrosino *et al.* (KLOE), Phys.Lett. **B675**, 283 (2009), 0812.4830.
21. M.N. Achasov *et al.*, Phys. Lett. **B504**, 275 (2001).
22. L.G. Landsberg, Phys. Rept. **128**, 301 (1985).
23. N. Achasov, A. Kozhevnikov, Sov. J. Nucl.Phys. **55**, 449 (1992).
24. A. Aloisio *et al.* (KLOE), Phys. Lett. **B606**, 12 (2005), hep-ex/0407048.
25. F. Ambrosino *et al.* (KLOE), Phys. Lett. **B670**, 285 (2009), 0809.3950.
26. F. Ambrosino *et al.* (KLOE) (2010), 1006.5313.
27. R.R. Akhmetshin *et al.* (CMD-2), Phys. Lett. **B648**, 28 (2007), hep-ex/0610021.
28. V.M. Aulchenko *et al.* (CMD-2), JETP Lett. **82**, 743 (2005), hep-ex/0603021.
29. M.N. Achasov *et al.*, J. Exp. Theor. Phys. **103**, 380 (2006), hep-ex/0605013.
30. B. Aubert *et al.* (BABAR), Phys. Rev. Lett. **103**, 231801 (2009), 0908.3589.
31. G.W. Bennett *et al.* (Muon g-2), Phys. Rev. **D73**, 072003 (2006), hep-ex/0602035.
32. P. Jean *et al.*, Astron. Astrophys. **407**, L55 (2003), astro-ph/0309484.
33. O. Adriani *et al.* (PAMELA), Nature **458**, 607 (2009), 0810.4995.
34. J. Chang *et al.*, Nature **456**, 362 (2008).
35. A.A. Abdo *et al.* (Fermi LAT), Phys. Rev. Lett. **102**, 181101 (2009), 0905.0025.
36. F. Aharonian *et al.* (H.E.S.S.), Phys. Rev. Lett. **101**, 261104 (2008), 0811.3894.
37. F. Aharonian *et al.* (H.E.S.S.), Astron. Astrophys. **508**, 561 (2009), 0905.0105.
38. R. Bernabei *et al.*, Int. J. Mod. Phys. **D13**, 2127 (2004), astro-ph/0501412.
39. R. Bernabei *et al.* (DAMA), Eur. Phys. J. **C56**, 333 (2008), 0804.2741.
40. M. Pospelov, A. Ritz, M.B. Voloshin, Phys. Lett. **B662**, 53 (2008), 0711.4866.
41. N. Arkani-Hamed, D.P. Finkbeiner, T.R. Slatyer, N. Weiner, PR **D79**, 015014 (2009).

42. D.S.M. Alves, S.R. Behbahani, P. Schuster, J.G. Wacker (2009), 0903.3945.
43. M. Pospelov, A. Ritz, Phys. Lett. **B671**, 391 (2009), 0810.1502.
44. J. Hisano, S. Matsumoto, M.M. Nojiri, Phys. Rev. Lett. **92**, 031303 (2004), hep-ph/0307216.
45. M. Cirelli, M. Kadastik, M. Raidal, A. Strumia, Nucl. Phys. **B813**, 1 (2009), 0809.2409.
46. J. March-Russell, S.M. West, D. Cumberbatch, D. Hooper, JHEP **07**, 058 (2008), 0801.3440.
47. I. Cholis, G. Dobler, D.P. Finkbeiner, L. Goodenough, N. Weiner, PR **D80**, 123518 (2009).
48. I. Cholis, D.P. Finkbeiner, L. Goodenough, N. Weiner, JCAP **0912**, 007 (2009), 0810.5344.
49. N. Arkani-Hamed, N. Weiner, JHEP **12**, 104 (2008), 0810.0714.
50. B. Batell, M. Pospelov, A. Ritz, Phys. Rev. **D79**, 115008 (2009), 0903.0363.
51. R. Essig, P. Schuster, N. Toro, Phys. Rev. **D80**, 015003 (2009), 0903.3941.
52. M. Reece, L.T. Wang, JHEP **07**, 051 (2009), 0904.1743.
53. F. Bossi (2009), 0904.3815.
54. N. Borodatchenkova, D. Choudhury, M. Drees, Phys. Rev. Lett. **96**, 141802 (2006).
55. P.F. Yin, J. Liu, S.h. Zhu, Phys. Lett. **B679**, 362 (2009), 0904.4644.
56. J.D. Bjorken, R. Essig, P. Schuster, N. Toro, Phys. Rev. **D80**, 075018 (2009), 0906.0580.
57. B. Batell, M. Pospelov, A. Ritz (2009), 0906.5614.
58. R. Essig, P. Schuster, N. Toro, B. Wojtsekhowski (2010), 1001.2557.
59. M. Freytsis, G. Ovanesyan, J. Thaler, JHEP **01**, 111 (2010), 0909.2862.
60. R.R. Akhmetshin *et al.* (CMD-2), Phys. Lett. **B501**, 191 (2001), hep-ex/0012039.
61. T. Junk, Nucl. Instr. & Meth. **A434**, 435 (1999), hep-ex/9902006.
62. F. Archilli *et al.* (KLOE-2) (2010), 1002.2572.
63. A. Balla *et al.*, Nucl. Instr. & Meth. **A604**, 23 (2009).
64. M. Alfonsi *et al.*, Nucl. Instr. & Meth. **A617**, 151 (2010).
65. G. Bencivenni *et al.*, Nucl. Instr. & Meth. **A494**, 156 (2002).
66. G. Bencivenni, D. Domenici, Nucl. Instr. & Meth. **A581**, 221 (2007).
67. M. Alfonsi *et al.*, IEEE Trans. Nucl. Sci. **52**, 2872 (2005).
68. M. Alfonsi *et al.*, Nucl. Instr. & Meth. **A518**, 106 (2004).

## LHCb

M. Anelli (Tecn.), G. Bencivenni, P. Campana, G. Capon, M. Carletti (Tecn.),  
P. Ciambrone, P. de Simone, A. Di Virgilio (Tecn.), G. Lanfranchi, G. Mannocchi,  
F. Murtas, M. Palutan, M. Pistilli (Tecn.), R. Rosellini (Tecn.), M. Santoni (Tecn.),  
A. Saputi, A. Sarti (Art. 23), A. Sciubba (Resp. Ass.), A. Zossi (Tecn.)

In collaboration with:

“LNF-SSCR”

(M. Arpaia, G. Bisogni, A. Cassara, A. Ceccarelli, E. Iacuesa, U. Martini);

“LNF-SEA”

(A. Balla, G. Corradi, M. Gatta, D. Tagnani)

## 1 Introduction

The main goal of the LHCb experiment at the CERN Large Hadron Collider is to perform precision tests of the Standard Model (SM) in the flavour sector, namely the decays of the  $b$ -hadrons, with enough sensitivity to disentangle possible new physics effects. The detector is a single-arm spectrometer and covers a pseudo-rapidity range of  $2 < \eta < 6$ . It consists of a vertex locator, a warm dipole magnet with a bending power of  $\int Bdl = 4\text{Tm}$ , a tracking system, two ring-imaging Cherenkov detectors, a calorimeter system and a muon system. Between July and October 2010 the experiment collected  $\sim 37 \text{ pb}^{-1}$  of  $pp$  collisions at 7 TeV center of mass energy, with the detector fully operational.

From the beginning, the main focus of the LNF group activities has been on the muon detector and its applications in the data analysis. This is particularly relevant in the context of the LHCb experiment, since an efficient muon identification is of fundamental importance in many CP-sensitive B decays (such as the gold-plated decays  $B_{(s)}^0 \rightarrow J/\psi(\mu^+\mu^-)$ ), and in rare B decays such the flavour-changing neutral current  $B_s^0 \rightarrow \mu^+\mu^-$ , which may reveal new physics beyond the SM.

The LHCb muon sistem, which has the purpose of muon triggering and offline muon identification, is composed of five stations (M1-M5) of rectangular shape, placed perpendicular to the beam axis. The full system comprises 1380 chambers of MWPC type, except in the highest rate region of M1, where triple-GEM’s are used. The LNF group made a substantial effort during the past years to built the muon system: about 30% of the MWPC chambers and half of the GEM detectors have been assembled at the LNF production site, most of the mechanical structure (including services) and front-end electronics have been realized by the qualified manpower of this laboratory. Moreover, the LNF team contributed greatly in the installation and testing of the whole system, and in the preparation of the software needed to control its hardware configuration. This work is being pursued during 2010, with contribution to detector maintenance (spare chambers assembly and reparation), and to muon piquet shifts. Moreover, a software to monitor the muon chamber efficiency has been developed by the LNF team, and is now part of the official package to certify the quality of the collected collision data (sec.2).

During 2010, with the start of data taking, a considerable effort has been put on the validation and calibration of the offline muon identification algorithm (see sec.3), with contributions to many analyses, and particularly to the study of  $J/\psi$  production in  $pp$  collisions (with measurement of the contribution from  $b$ -decays) and to the search of  $B_s^0 \rightarrow \mu^+\mu^-$ . In this last case, the LNF team partecipated also in all of the other aspects of the analysis (sec.4), giving a strong contribution (G. Lanfranchi as a convener of the analysis group, too) to a prompt publication of a result which

is competitive with respect to the best world achievements, from Tevatron data.

The leading role of the LNF group and the qualities of the team leaders have been recognized at the end of 2010, when the collaboration board appointed Pierluigi Campana as the next LHCb spokesperson, for a three years period, starting in May 2011.

## 2 Monitoring of the muon chamber efficiency

A monitor of the muon chamber efficiency to be run on real collision data has been developed by the LNF group, and is now part of the official package to monitor the quality of the collected collision data.

This procedure select tracks reconstructed by the tracking detectors of LHCb. Each track is extrapolated through the muon stations and is selected within the geometrical acceptance of the detector. For each muon station we look for the closest hit to the impact point of the extrapolated tracks within a *search window* that takes into account of the extrapolation errors the multiple scattering. The tracks are selected as muon candidates if we find at least three hits over M2, M3, M4 and M5 stations. Fig. 1 shows the measured efficiency for each muon station for selected tracks with momentum above 12 GeV/c. The data points (blue) are compared with the MC results (red),

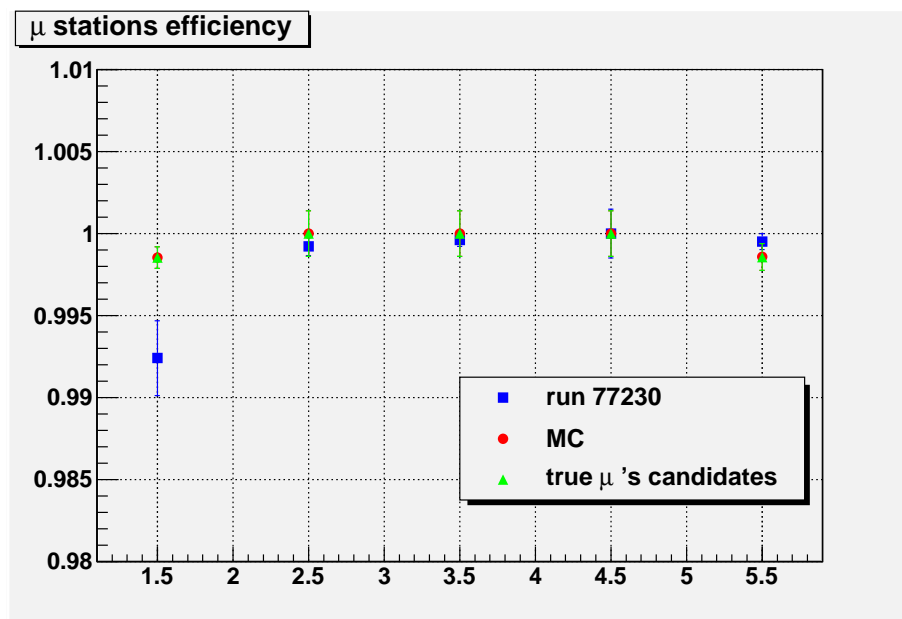


Figure 1: Muon hit reconstruction efficiency on each station for tracks with  $p > 12$  GeV/c for collision data (blue), and MC, evaluated with the same procedure as for data (red) and for true muons (green).

evaluated with the same method as in data (red). The green points represent instead the MC efficiencies evaluated when the selected tracks are true muons.

### 3 Offline muon identification

The muon identification (muonID) procedure is applied to tracks reconstructed in the spectrometer with momentum above 3 GeV/c, which is the threshold for being in the acceptance of the muon detector. It consists of two main steps: 1) 5)

1. IsMuon selector: hits in the muon stations are searched in some Field of Interest (FOI) around the track extrapolation. A Boolean decision (*IsMuon*) is applied to tracks which satisfy the requirement of having at least one hit in FOI in a number of stations which depends on the momentum of the track: two hits in M2 and M3 for  $3 < p < 6$  GeV/c, one hit more in M4 or M5 for  $6 < p < 10$  GeV/c, and four hits in stations M2 to M5 for  $p > 10$  GeV/c.
2. The hypothesis test: with tracks surviving the *IsMuon* requirement, an hypothesis test is performed by evaluating for each track the compatibility with the muon and non-muon hypothesis. The hypothesis test is based on how the hits in the muon chambers are aligned with respect to the extrapolation of the tracks from the tracking system. The muonID performance is then further improved by combining the muon chambers' information in a Global Likelihood (*combDLL*) together with that coming from all others subdetectors, mainly calorimeters and RICHs.

The muonID efficiency is defined as the probability for muons reconstructed as tracks to survive the *IsMuon* requirement, and does not include the efficiency for the muon likelihood selection, since it is strictly analysis dependent. A  $J/\psi \rightarrow \mu^+\mu^-$  inclusive sample is used to measure the muonID efficiency with the *tag-and-probe* method. <sup>4)</sup> The  $J/\psi \rightarrow \mu^+\mu^-$  decay is an abundant process with a very clean signature and therefore it can be used as a pure source of muons. For the *tag-and-probe* method, one of the two muons from  $J/\psi \rightarrow \mu^+\mu^-$  is requested to be identified by the muonID (*tag* muon) while the second muon is selected without using any information from the muon system (*probe* muon). This second muon is used to estimate the muonID efficiency.

The cross sections for the prompt  $J/\psi \rightarrow \mu^+\mu^-$  and for  $J/\psi \rightarrow \mu^+\mu^-$  from  $b$  decays have been measured by the LHCb experiment with the 2010 data at  $\sqrt{s} = 7$  TeV and are respectively  $\sigma(\text{prompt } J/\psi, p_T < 14\text{GeV}/c, 2 < y < 4.5) = (10.8 \pm 0.05 \pm 1.51_{-2.25}^{+1.69})\mu\text{b}$ , and  $\sigma(J/\psi \text{ from } b, p_T < 14\text{GeV}/c, 2 < y < 4.5) = (1.16 \pm 0.01 \pm 0.17)\mu\text{b}$ , <sup>3) 7)</sup> resulting in a  $\sim 100$   $J/\psi \rightarrow \mu^+\mu^-$  events per  $\text{nb}^{-1}$  triggered and reconstructed ( $\sim 10$  events per  $\text{nb}^{-1}$  of  $J/\psi \rightarrow \mu^+\mu^-$  from  $b$ ).

The data set considered in the first survey of muonID efficiency was made essentially of  $J/\psi$  from  $b$  decays, which was necessary to reduce the combinatorial background of the tracks coming from the primary vertex. This was obtained by cutting on the impact parameter of the two tracks, and on the decay vertex flight distance. To further clean up the sample, we required the *probe* muon to release in the electromagnetic and hadronic calorimeter a signal compatible with a minimum ionising particle. The  $J/\psi \rightarrow \mu^+\mu^-$  mass distribution after this selection is shown in Fig. 2. The average muonID efficiency obtained with background-subtracted events is  $(97.5 \pm 0.2)\%$  for data and  $(96.3 \pm 0.1)\%$  for MC, the residual discrepancy between data and MC being due mainly to a difference in the track and/or muon hits occupancy.

The muon misidentification (misID) probabilities have also been evaluated, using pure samples of  $\pi$ ,  $p$ , and  $K$  extracted from  $K_S \rightarrow \pi^+\pi^-$ ,  $\Lambda \rightarrow p\pi$ , and  $\phi \rightarrow KK$  decay channels. The  $\epsilon(p \rightarrow \mu)$  misID probability gives an estimate of the contribution of the punch-through and combinatorial hits to the total misID probability, while decays in flight are expected to dominate the  $\epsilon(\pi \rightarrow \mu)$  and  $\epsilon(K \rightarrow \mu)$  misID probabilities. This is confirmed by the results shown in Fig 3, where the  $\pi \rightarrow \mu$  and  $p \rightarrow \mu$  probabilities are shown as a function of particle momentum.

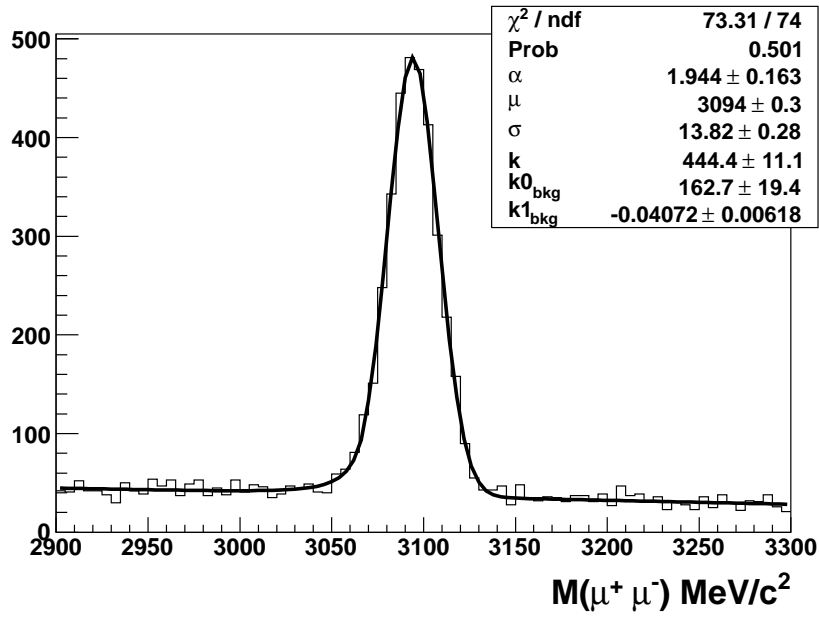


Figure 2: Clear  $J/\psi$  peak in the  $\mu^+\mu^-$  invariant mass distribution after tag-and-probe selection.

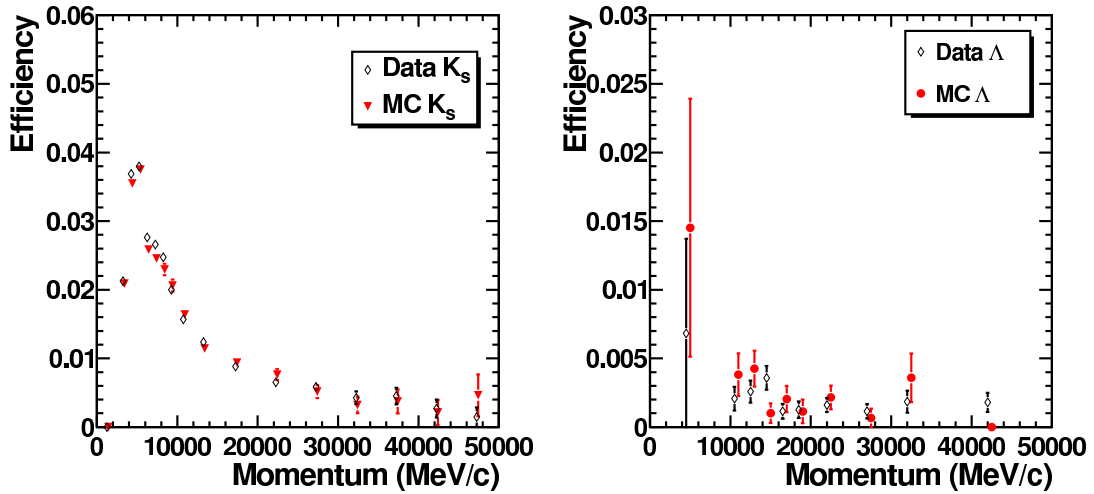


Figure 3: *MisID* probability as a function of the track momentum. Left:  $\epsilon(\pi \rightarrow \mu)$  from a  $K_S \rightarrow \pi^+\pi^-$  sample. Right:  $\epsilon(p \rightarrow \mu)$  from a  $\Lambda \rightarrow p\pi$  sample. Open markers are data, filled markers are MC simulation.

#### 4 Search for the rare decays $B_s^0 \rightarrow \mu^+\mu^-$ and $B^0 \rightarrow \mu^+\mu^-$

The results of the search for the very rare dimuon decays of the  $B^0$  and  $B_s^0$  mesons are expected with high interest by the high energy physics community, and it is certainly one of the most promising

results on the initial phase of the LHCb physics program. These decays can only happen through loop diagrams and are furthermore suppressed by helicity within the SM (see Fig. 4), but can have very different different branching ratios (BR) in new physics models, especially those with an extended Higgs sector. In particular, in supersymmetric models large enhancements are possible. The SM predictions have a relative precision of 10%:

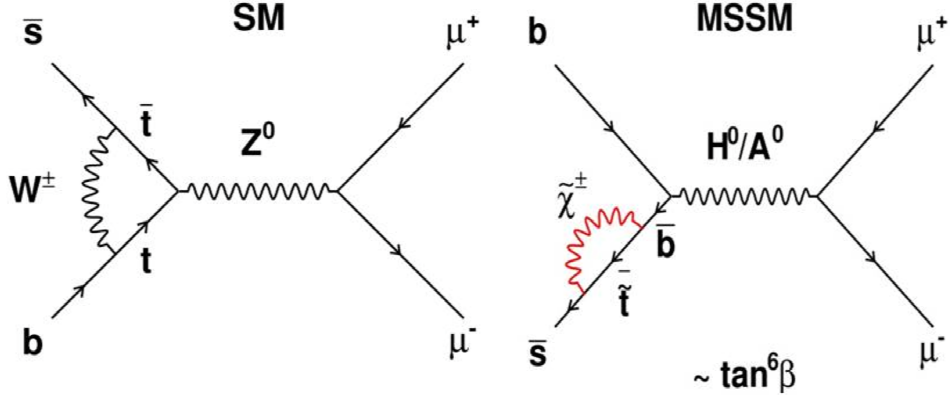


Figure 4: Dominant Feynman diagram contribution to the branching ratio within the SM (left) and within the MSSM with  $R$ -parity conservation (right).

$$\text{BR}(B_s^0 \rightarrow \mu^+ \mu^-)_{\text{SM}} = (3.2 \pm 0.2) \times 10^{-9} \quad (1)$$

$$\text{BR}(B^0 \rightarrow \mu^+ \mu^-)_{\text{SM}} = (1.0 \pm 0.1) \times 10^{-10}. \quad (2)$$

The search for  $B_q^0 \rightarrow \mu^+ \mu^-$  has been performed both at  $e^+e^-$  colliders and at the Tevatron. The highest sensitivity so far has been achieved at the Tevatron due to the very large  $b\bar{b}$  cross section at hadron colliders. Using  $3.7 \text{ pb}^{-1}$  of data, the CDF collaboration pushed the limits down to  $\text{BR}(B_s^0 \rightarrow \mu^+ \mu^-) < 43 \times 10^{-9}$  and  $\text{BR}(B^0 \rightarrow \mu^+ \mu^-) < 7.6 \times 10^{-9}$ , at 95% C.L.

The LHCb experiment is well suited for such searches due to its excellent invariant mass resolution, vertex resolution, muon identification and trigger acceptance. Moreover, among the LHC experiments, LHCb has a unique trigger capability of providing large samples of hadronic  $B_q^0 \rightarrow h^+ h^-$  decays. These are used as control samples in order to reduce the dependence of the results on the simulation. <sup>8)</sup> Assuming the SM branching ratio and using the  $b\bar{b}$  cross-section measured by LHCb, <sup>3)</sup>  $(284 \pm 53) \mu\text{b}$ , about 0.7 (0.08)  $B_s^0 \rightarrow \mu^+ \mu^-$  ( $B^0 \rightarrow \mu^+ \mu^-$ ) events are expected to be reconstructed in the LHCb acceptance. The first step of the analysis consists of a loose selection, which significantly reduces the size of the dataset by rejecting most of the background.

The second step consists of the study of three normalization channels:  $B^+ \rightarrow J/\psi(\mu^+ \mu^-)K^+$ ,  $B_s^0 \rightarrow J/\psi(\mu^+ \mu^-)\phi(K^+ K^-)$  and  $B^0 \rightarrow K^+ \pi^-$ . Using these normalization channels the branching ratios can be calculated as:

$$\text{BR}_{\text{sig}} = \text{BR}_{\text{norm}} \times \frac{\epsilon_{\text{norm}}^{\text{REC}} \epsilon_{\text{norm}}^{\text{SEL}} | \epsilon_{\text{norm}}^{\text{TRIG}} | \epsilon_{\text{norm}}^{\text{SEL}}}{\epsilon_{\text{sig}}^{\text{REC}} \epsilon_{\text{sig}}^{\text{SEL}} | \epsilon_{\text{sig}}^{\text{TRIG}} | \epsilon_{\text{sig}}^{\text{SEL}}} \times \frac{f_{\text{norm}}}{f_{B_q}} \times \frac{N_{\text{sig}}}{N_{\text{norm}}}, \quad (3)$$

where  $f_{B_q}$  and  $f_{\text{norm}}$  denote the probabilities that a  $b$ -quark fragments into a  $B_q^0$  and into the  $b$ -hadron relevant for the chosen normalization channel with branching fraction  $\text{BR}_{\text{norm}}$ . The

reconstruction efficiency ( $\epsilon^{\text{REC}}$ ) includes the acceptance and particle identification, while  $\epsilon^{\text{SEL|REC}}$  denotes the selection efficiency on reconstructed events. The trigger efficiency on selected events is denoted by  $\epsilon^{\text{TRIG|SEL}}$ .

This normalization ensures that the knowledge of the absolute luminosity and total cross-section is not needed, and that many systematic uncertainties cancel in the ratio of the efficiencies. The selection procedure for these channels is specifically designed to be as close as possible to the signal selection. The ratios of reconstruction and selection efficiencies are estimated from MC, while the ratio of trigger efficiencies on selected events is mainly data-driven.

In the third part of the analysis each event is given a probability to be signal or background in a two-dimensional space. This probability is defined by two variables: the  $\mu^+\mu^-$  invariant mass and the geometrical likelihood, GL. The GL is a mathematical combination of several variables mainly related to the geometry of the event. The optimization of the combination of variables that enters in the GL is performed using MC. However, the probability for a signal event to have a given value of GL is obtained from the data itself using trigger unbiased  $B_q^0 \rightarrow h^+h^-$  events. The parameters entering in the invariant mass line shape for the signal are extracted both from the fit to the invariant mass distribution of  $B_q^0 \rightarrow h^+h^-$  decays, and by interpolating the results obtained with dimuon resonances. The probability for a background event to have a given GL and invariant mass value is obtained by interpolating the events in the mass sidebands.

The definition of the GL variable is such that background events cluster around zero, and signal events will be uniformly distributed between zero and one. Therefore the *sensitive region* (i.e. the region from which most of the sensitivity to the  $B_s^0 \rightarrow \mu^+\mu^-$  and  $B^0 \rightarrow \mu^+\mu^-$  branching fractions comes from) is defined by the 2-dimensional region  $\text{GL} > 0.5$  and  $M_B - 60\text{MeV}/c^2 < M(\mu^+\mu^-) < M_B + 60\text{MeV}/c^2$ . The observed distribution of GL vs  $M(\mu^+\mu^-)$  for the selected dimuon events is shown in Fig. 5.

The 2-dimensional space formed by the invariant mass likelihood and GL is binned, and for each bin we compute how many events are observed in data, how many signal events are expected for a given BR hypothesis and luminosity, and how many background events are expected for a given luminosity. The compatibility of the observed distribution of events in all bins with the expected number for a given BR hypothesis is then computed using the modified frequentist approach method, also known as  $\text{CL}_s$  method, which allows to exclude a given hypothesis for a given confidence level. The observed distribution of  $\text{CL}_s$  vs BR can be seen in fig.6. The expected distributions of  $\text{CL}_s$  assuming the background only hypothesis are also shown in the same figure as a green area that covers the region of  $\pm 1\sigma$  of possible observations. The uncertainties in the signal and background likelihoods and normalization factors, including systematics, are propagated into the  $\text{CL}_s$  evaluation.

A slight deficit of events is observed in the most sensitive bins with respect to the background only hypothesis, though not statistically significant, which gives a small deviation between the observed and the expected  $\text{CL}_s$ . The upper limits are finally computed using the  $\text{CL}_s$  distributions of fig.6, with the results:

$$\text{BR}(B_s^0 \rightarrow \mu^+\mu^-) < 43 (56) \times 10^{-9} \text{ at } 90\% (95\%) \text{ C.L.}, \quad (4)$$

$$\text{BR}(B^0 \rightarrow \mu^+\mu^-) < 12 (15) \times 10^{-9} \text{ at } 90\% (95\%) \text{ C.L.}, \quad (5)$$

while the expected values of the limits are  $\text{BR}(B_s^0 \rightarrow \mu^+\mu^-) < 51(65) \times 10^{-9}$  and  $\text{BR}(B^0 \rightarrow \mu^+\mu^-) < 14(18) \times 10^{-9}$  at 90% (95%) C.L. The limits observed are similar to the best published limits proving, already with very limited statistics, the effectiveness of the LHCb design and performances.

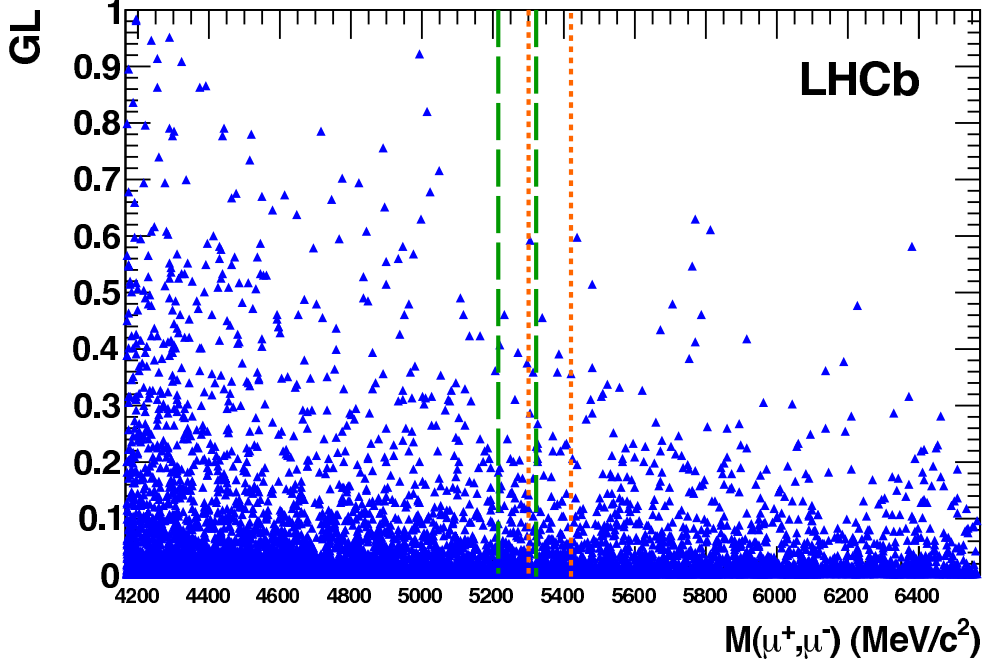


Figure 5: Observed distribution of selected dimuon events in the plane  $GL$  vs dimuon invariant mass. The green long-dashed (orange short-dashed) lines indicate the  $B^0 \pm 60\text{MeV}/c^2$  ( $B_s \pm 60\text{MeV}/c^2$ ) search windows.

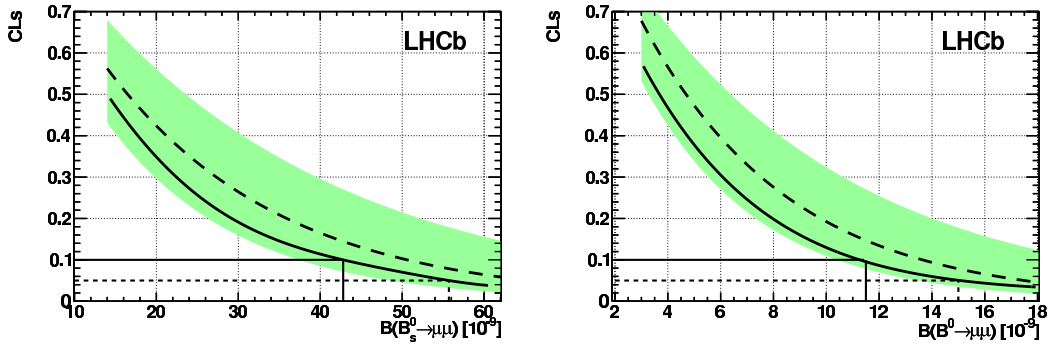


Figure 6: (a) Observed (solid curve) and expected (dashed curve)  $CL_s$  values as a function of  $BR(B_s \rightarrow \mu^+\mu^-)$ . The green band contains the  $\pm 1\sigma$  interval of possible results compatible with the expected value when only background is observed. The 90% (95%)  $CL$  observed value is identified by the solid (dotted) line. (b) the same for  $BR(B^0 \rightarrow \mu^+\mu^-)$ .

## 5 Conference Talks

1. A. Sarti, “Tevatron e LHCb: Risultati e prospettive”, Incontri di Fisica delle Alte Energie (IFAE 2010), Roma, Italy.
2. G. Lanfranchi, “Heavy Flavour Results and Prospects in LHC”, 30th Inter. Symp. on Physics in Collision, Karlsruhe, Germany.

## References

1. M. Anelli *et al.*, “Performance of the LHCb muon system with cosmic rays”, JINST 5:P10003,2010.
2. The LHCb Coll., Phys. Lett. **B 693**, 69 (2010).
3. The LHCb Coll., Phys. Lett. **B 694**, 209 (2010).
4. A. Sarti, S. Furcas, G. Lanfranchi, M. Palutan, “Calibration strategy and efficiency measurement of the muon identification procedure at LHCb”, CERN-LHCb-PUB-2010-002.
5. X. Cid Vidal *et al.*, “A muon Identification procedure for LHCb with Kalman filter, CERN-LHCb-INT-2010-052.
6. J. Albrecht *et al.*, Measurement of the  $J/\psi$  production cross-section in LHCb” (Summer Conferences 2010), CERN-LHCb-ANA-2010-004.
7. J. Albrecht *et al.*, “Updated measurement of the  $J/\psi$  production cross-section in LHCb, CERN-LHCb-ANA-2010-012.
8. C. Adrover *et al.*, “Search for the rare decays  $B_{(s)}^0 \rightarrow \mu^+ \mu^-$  with the LHCb experiment”, CERN-LHCb-ANA-2011-007.

## NA62

A. Antonelli (Resp.), G. Di Raddo (Bors.), M. Moulson, M. Raggi (Art. 23), T. Spadaro,

In collaboration with:

E. Capitolo, R. Lenci, B. Ponzio, V. Russo, M. Santoni, S. Valeri, T. Vassilieva

the Servizio di Progettazione Apparati Sperimentali (SPAS):

C. Capoccia, A. Cecchetti, B. Dulach

the Servizio di Sviluppo e Costruzione Rivelatori (SSCR):

G. Bisogni, A. Franceschi

the Divisione Acceleratori, Servizio di Vuoto:

R. Di Raddo, V. Lollo

and the Servizio di Elettronica:

G. Corradi, C. Paglia, D. Tagnani

### 1 The NA62 Experiment

The branching ratio (BR) for the decay  $K^+ \rightarrow \pi^+ \nu \bar{\nu}$  can be related to the value of the CKM matrix element  $V_{td}$  with minimal theoretical uncertainty, providing a sensitive probe of the flavor sector of the Standard Model. The measured value of the BR is  $1.73^{+1.15}_{-1.05} \times 10^{-10}$  on the basis of seven detected events [1]. NA62, an experiment at the CERN SPS, was originally proposed as P326 with the goal of detecting  $\sim 100$   $K^+ \rightarrow \pi^+ \nu \bar{\nu}$  decays with a S/B ratio of 10:1 [2]. The experimental layout is illustrated in Fig. 1.

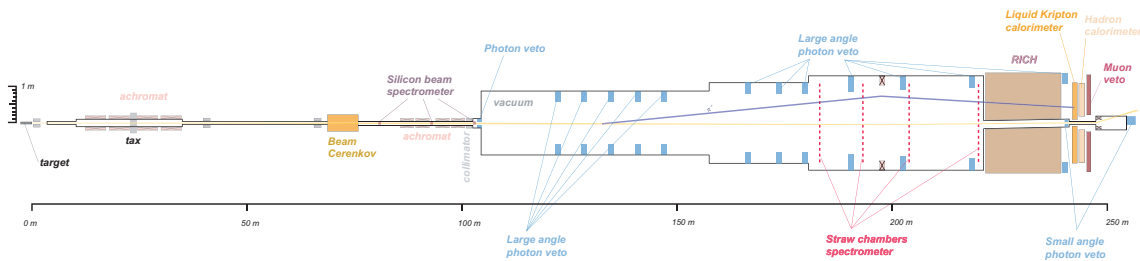


Figure 1: *The NA62 experimental layout.*

The experiment will make use of a 75 GeV unseparated positive secondary beam. The total beam rate is 800 MHz, providing  $\sim 50$  MHz of  $K^+$ 's. The decay volume begins 102 m downstream of the production target. 10 MHz of kaon decays are observed in the 120-m long vacuum decay region. Ring-shaped large-angle photon vetoes are placed at 12 stations along the decay region and provide full coverage for decay photons with  $8.5 \text{ mrad} < \theta < 50 \text{ mrad}$ . The last 35 m of the decay region hosts a dipole spectrometer with four straw-tracker stations operated in vacuum. The NA48 liquid krypton calorimeter [3] is used to veto high-energy photons at small angle. Additional detectors further downstream extend the coverage of the photon veto system (e.g. for particles traveling in the beam pipe).

The experiment must be able to reject background from, e.g.,  $K^+ \rightarrow \pi^+ \pi^0$  decays at the level of  $10^{12}$ . Kinematic cuts on the  $K^+$  and  $\pi^+$  tracks provide a factor of  $10^4$  and ensure 40 GeV of electromagnetic energy in the photon vetoes; this energy must then be detected with an inefficiency

of  $\leq 10^{-8}$ . For the large-angle photon vetoes, the maximum tolerable detection inefficiency for photons with energies as low as 200 MeV is  $10^{-4}$ . In addition, the large-angle vetoes (LAVs) must have good energy and time resolution and must be compatible with operation in vacuum.

The principal involvement of the LNF NA62 group is in the design and construction of the LAV system. In 2010, the main responsibilities of the LNF NA62 group were the following:

- continued development of tools and procedures for assembly of the ANTI station;
- production of final drawings for the downstream LAV stations;
- assembly of 4 LAV stations;
- vacuum testing and outgassing measurements for finished LAV stations;
- development and testing of the front-end electronics for the LAV system;
- continued in-beam testing of LAV station;
- coordination of the NA62 Photon Veto working group.

The group also contributed to the analysis of NA62 data on  $R_K \equiv \Gamma(K_{e2})/\Gamma(K_{\mu2})$ .

## 2 Large-Angle Photon Vetoes

The LAV design is based on the reuse of 3800 lead-glass blocks from the central part of the OPAL electromagnetic calorimeter barrel [4]. The blocks are made of SF57 lead glass and have an asymmetric, truncated square-pyramid shape. The front and rear faces of the blocks measure about  $10 \times 9 \text{ cm}^2$  and  $11 \times 10 \text{ cm}^2$ , respectively; the blocks are 37 cm long. The modules are read out at the back side by Hamamatsu R2238 76-mm PMTs, coupled via 4-cm cylindrical light guides of SF57.

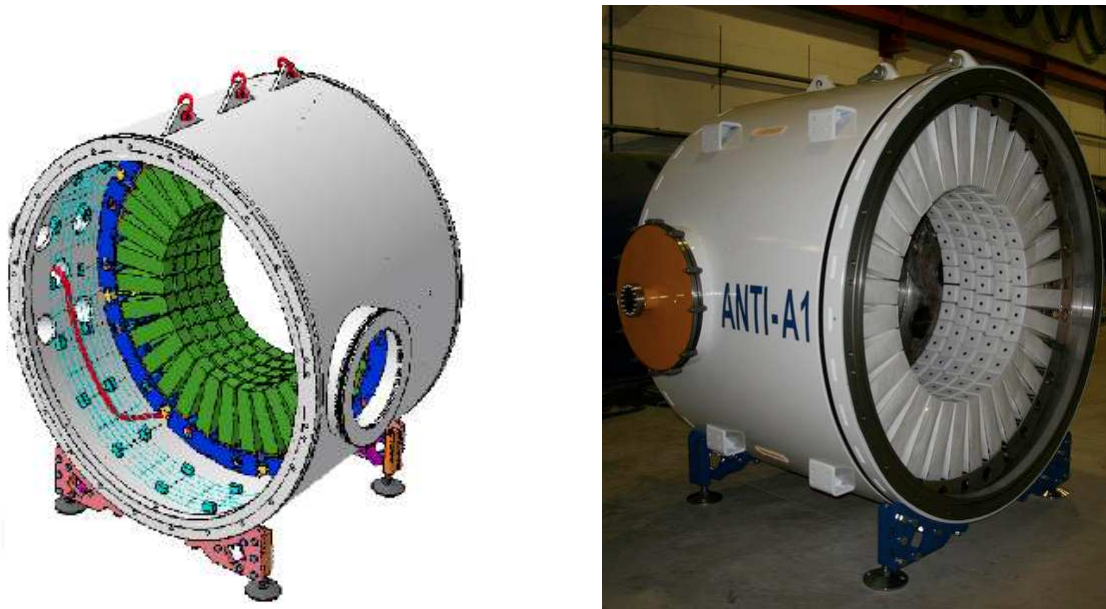


Figure 2: *Left: Design study for the upstream LAV stations. Right: Photograph of the prototype ANTI-A1.*

The LAV system consists of 12 stations. The diameter of the stations increases with distance from the target, as does the number of blocks in each, from 160 to 256, for a total of about 2500

blocks. Each station consists of four or five rings of blocks, with the blocks staggered in azimuth in successive rings. The total depth of a five-layer station is 27 radiation lengths. This structure guarantees high efficiency, hermeticity, and uniformity of response. The final design for the first five stations is illustrated in Fig. 2, left.

## 2.1 LAV construction

The first LAV station, ANTI-A1, one of the upstream (small-diameter) LAV stations, was constructed in 2009. (This station served as a prototype, but, with minor modifications, will be used in the experiment.) During 2010, three more of the upstream LAV stations, ANTI-A2, A3, and A4, were built at LNF. These three stations incorporate a new system to deliver light pulses to the blocks for the purposes of monitoring and calibration. The system makes use of a blue LED mounted on each block in an optical port next to the light guide. Care is taken in routing the signal and LED cables to avoid crosstalk. When construction is complete, each station is tested to verify the signal, HV, and LED connections. The station is also checked for vacuum leaks to the level of  $10^{-10}$  mbar  $\cdot$  l/s.

We have also made progress on the mechanical designs for the larger stations. The drawings for the vacuum vessels of intermediate (A6–A8) and large (A9–A11) diameter have been finalized and the construction contract has been assigned. Preparation for the construction of the A6 vessel was started at the Fantini SpA facility in Anagni (FR) at the end of 2010.

## 2.2 Front-end electronics

Monte Carlo simulations have shown that photons from  $K^+ \rightarrow \pi^+ \pi^0$  decay with a wide range of energies, from a few tens of MeV to several GeV, reach the veto stations. To allow photons from  $\pi^+ \pi^0$  events to be rejected with a maximum inefficiency of  $10^{-4}$ , the detectors must simultaneously furnish time and energy measurements. The time resolution is dominated by the intrinsic contribution from the detectors. For the energy measurement, the biggest challenge in the design of the readout electronics is the need to accept signals over an extended dynamic range, from a few millivolts to tens of volts, while providing charge measurements with a precision better than 10%.

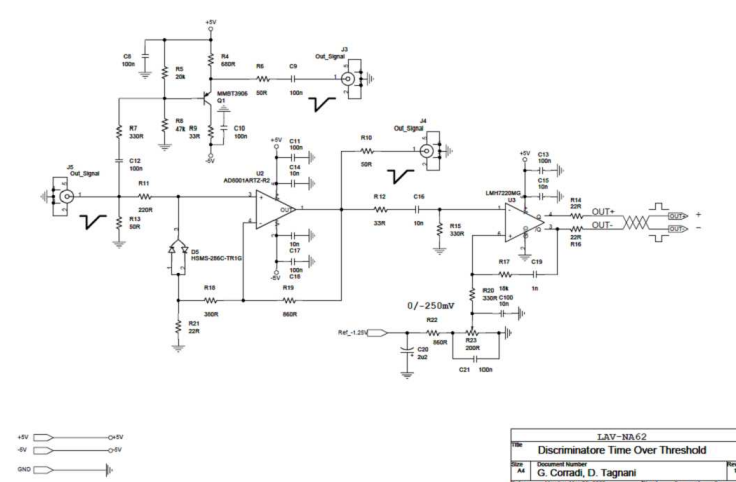


Figure 3: *Layout of a single channel of prototype time-over-threshold board.*

During 2010, the LNF group was responsible for the design and construction of prototypes of the front-end electronics for the large-angle veto system. The basic idea is to exploit the time-over-threshold technique to measure the signal charge over a broad interval. A new board designed by the LNF Servizio di Elettronica converts the analog signals from the PMTs into an LVDS logic signal of the same width. The width will be measured by a TDC and its value used to reconstruct the charge. The energy can thus be measured via TDC time measurements only.

A final prototype front-end electronic card was designed and tested during 2010. The system consists of three main stages, as shown in the single-channel layout of Fig. 3:

- **Clamping:** Protects the amplifier from PMT signals as high as 10V. The clamp stage preserves the time duration of the input analog signal to allow the measurement of time over threshold (ToT).
- **Amplifier:** Amplifies the input signal by  $5\times$  to reduce slewing in threshold crossing at the comparator stage.
- **Comparator and LVDS driver:** Compares the amplified signals with an adjustable threshold (0-50mV) and produces an LVDS output signal. The LVDS signal has a duration equal to the time during which the analog signal is above threshold.

### 2.3 A2 test beam

LAV station A2 was tested at the T9 area at the CERN PS during a three-week run in August 2010. The T9 beam is composed of electrons, pions, and muons with energies between 0.3 and 10 GeV. A pair of Cerenkov counters was used to select electron samples of different energy. Part of the test beam data was taken using the final prototype front-end board.

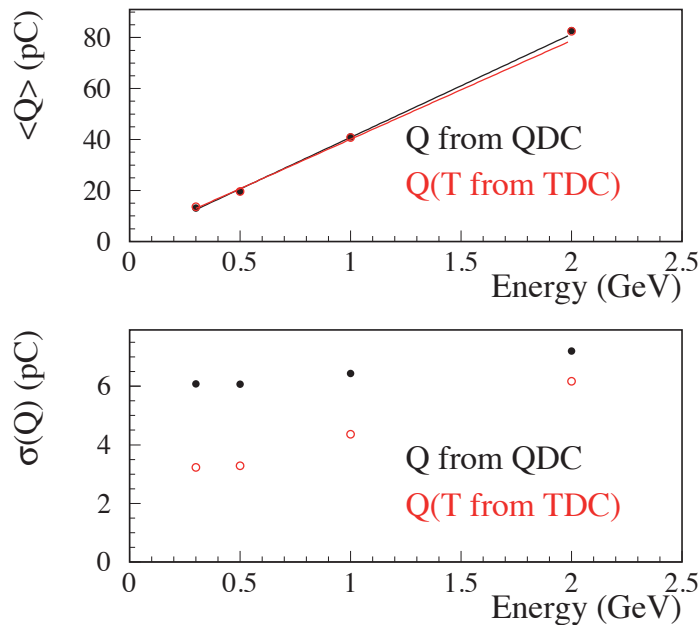


Figure 4: 2010 test beam data. Top panel: linearity of energy response, comparing measurement via TDC to those via QDC. Bottom: resolution of the energy response.

Given a measurement of the time over threshold via TDC, the energy  $E(T_{\text{over}})$  is computed from a non-linear relation. The  $Q$  vs.  $T_{\text{over}}$  parameterization is obtained from a polynomial fit of the  $Q$  vs.  $T_{\text{over}}$  distributions for all blocks. To test the linearity of  $E(T_{\text{over}})$ , this is compared to the direct charge measurement obtained from a QDC, as shown in the upper panel of Fig. 4. The energy resolution is shown the lower panel of Fig. 4. At small energies, the energy resolution from  $E(T_{\text{over}})$  is better than that from  $E(Q)$ . The fractional energy resolution is shown in Fig. 5. The energy measurement is used to correct for time slewing. The time resolution, after slewing corrections, is evaluated from the difference between the arrival times for the two most upstream blocks. The timing performance is excellent, as shown in Fig. 6. The resolution is  $\sim 200$  ps/ $\sqrt{E[\text{GeV}]}$  for a single block.

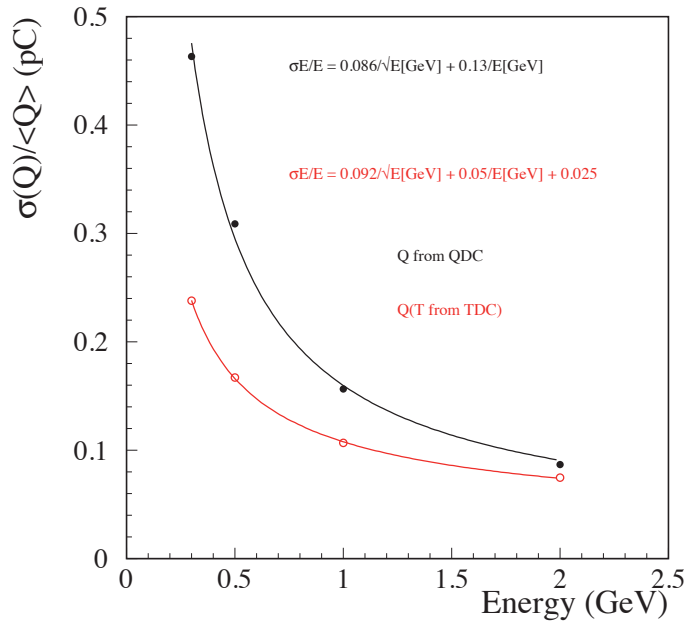


Figure 5: 2010 test beam data. Fractional resolution of the energy response from TDC and QDC measurements.

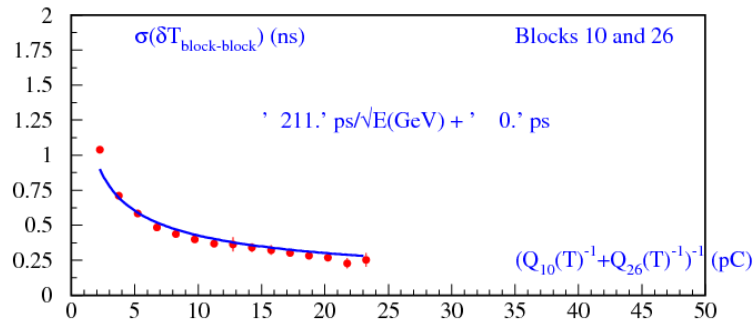


Figure 6: 2010 test beam data. Time resolution evaluated from the time difference of the two most upstream blocks, called 10 and 26.

After the test beam, the front-end electronics design was revised and finalized. Production will begin in early 2011.

## 2.4 LAV simulation

With the construction work on the LAV stations well underway, we are now focusing significant attention on the Monte Carlo simulation of detector system. The complete LAV geometry has now been incorporated into the official NA62 Monte Carlo. A detailed simulation of the Cerenkov light emission and transmission to the photocathode and of the resulting PMT signal includes all relevant time and amplitude fluctuations and provides good comparison with test beam data. The group is using this detailed simulation to develop a more efficient parameterization of the detector response to be incorporated in the Monte Carlo for production work.

## 3 NA62 and the Measurement of $R_K$

Despite poor knowledge of the meson decay constants, ratios of leptonic decay rates of pseudoscalar mesons such as  $R_K \equiv \Gamma(K_{e2})/\Gamma(K_{\mu2})$  can be predicted with high accuracy within a given model, and have been considered to be stringent tests of the  $V - A$  structure of the weak interaction and of lepton universality. By convention, the definition of  $R_K$  includes the contribution of inner bremsstrahlung (IB) to the radiative  $K_{l2\gamma}$  width, while the structure-dependent (DE) processes are considered as background. The Standard-Model prediction is [5]:

$$R_K^{\text{SM}} = \left(\frac{m_e}{m_\mu}\right)^2 \left(\frac{M_K^2 - m_e^2}{M_K^2 - m_\mu^2}\right)^2 (1 + \delta R_{\text{QED}}) = (2.477 \pm 0.001) \cdot 10^{-5} \quad (1)$$

where  $\delta R_{\text{QED}} = -3.6\%$  is a correction due to the contributions to the  $K_{l2\gamma}$  width from IB and virtual photon processes. Theoretical studies point out that lepton-flavor violating effects arising in supersymmetric extensions of the Standard Model can induce sizable violations of  $\mu$ - $e$  universality, shifting the value of  $R_K$  by as much as a few percent, without contradicting any other presently known experimental constraints [6]. The  $K_{e2}$  decay rate is particularly sensitive to new physics because the Standard Model contribution is helicity suppressed.

The 2006 world average [7] is determined by experiments performed in the 1970s; the relative error on this average is  $\delta R_K/R_K = 4.5\%$ . Inclusion in the average of the recent results from the KLOE collaboration (final result [8]) and from NA48/2 (preliminary result) leads to a new value of  $R_K^{2007} = (2.468 \pm 0.025) \cdot 10^{-5}$ , with a precision of  $\delta R_K/R_K = 1\%$ .

During a dedicated run in 2007, NA62 collected more than 110 000  $K_{e2}$  events, together with various smaller data samples to allow detailed systematic studies. LNF group members have played a central role in the analysis of this data, in helping to define the  $K_{e2}$  selection criteria and the treatment of radiative corrections. The issue of radiative corrections is particularly sensitive. Since the DE component is not suppressed by helicity, it constitutes an order-unity background to IB. Therefore, the criteria for vetoing additional photons detected by the liquid krypton calorimeter were chosen so as to retain as many  $K \rightarrow e\nu(\gamma)$  IB events as possible, while rejecting radiative  $K \rightarrow e\nu\gamma$  events from the DE process, as well as other backgrounds.  $K \rightarrow e\nu(\gamma)$  events from IB are selected by requiring the missing mass squared at the  $K$  decay vertex to be below  $\sim 0.001 \text{ GeV}^2$ . The efficiency for this condition increases inversely with the energy of the emitted photon, so that the implementation of an accurate simulation of the  $K \rightarrow e\nu\gamma$  IB component is crucial for an evaluation of the related acceptance with an accuracy better than the percent level. The LNF group provided a new simulation of the IB signal with an exponentiated photon energy spectrum and no photon energy cutoff. A result obtained using a large fraction of the data set was published in Physics Letters B at the beginning 2011. This result has a total error of about 0.5% [9]:

$$R_K = (2.487 \pm 0.011_{\text{stat}} \pm 0.007_{\text{syst}}) \cdot 10^{-5} = (2.487 \pm 0.013) \cdot 10^{-5}.$$

## References

1. E949 Collaboration, A. Artamonov *et al.*, Phys. Rev. Lett. **101**, 191802 (2008).
2. G. Anelli *et al.*, CERN, Geneva, Tech. Rep. CERN/SPSC 2005-013 (2005).
3. NA48 Collaboration, V. Fanti *et al.*, Nucl. Instr. & Meth. A **574**, 433 (2007).
4. OPAL Collaboration, K. Ahmet *et al.*, Nucl. Instr.& Meth. A **305**, 275 (1991).
5. V. Cirigliano, I. Rosell, Phys. Rev. Lett. **99**, 231801 (2007).
6. A. Masiero, P. Paradisi, R. Petronzio, Phys. Rev. D **74**, 011701 (2006).
7. Particle Data Group, W. M. Yao *et al.*, J. Phys. G **33**, 1 (2006).
8. KLOE Collaboration, F. Ambrosino *et al.*, Eur. Phys. J. C **64** (2009) 627
9. NA62 Collaboration, C. Lazzeroni *et al.*, Phys. Lett. B, in press, arXiv:1101.4805 [hep-ex].

## The Super*B* Project

A. Calcaterra, R. de Sangro, G. Felici, G. Finocchiaro (Resp.),  
P. Patteri, I. Peruzzi, M. Piccolo, M. Rama

### 1 Introduction

Motivated by the enormous impact shown by the *B* Factories on the physics of flavour and in several other areas, an Italian led, INFN hosted, collaboration of scientists from Canada, Italy, Israel, France, Norway, Spain, Poland, UK and USA have worked together to design and propose a high luminosity asymmetric *B*-Factory project. This project, called Super*B*, exploits a novel collision scheme based on very small beam dimensions and betatron function at the interaction point, on large crossing and Piwinsky angle and on the “crab waist” scheme <sup>o1)</sup>. This approach allows to reach the required luminosity of  $10^{36} \text{ cm}^{-2}\text{s}^{-1}$  and at the same time overcome the difficulties of early super  $e^+e^-$  collider designs, most notably very high beam currents and very short bunch lengths. The wall-plug power and the beam-related background rates in the detector are therefore kept within affordable levels. A conceptual design report of such a project had been published in 2007 <sup>o2)</sup>. Much more advanced progress reports have been published in 2010 discussing important advances in the physics motivations <sup>1)</sup>, detector <sup>2)</sup> and accelerator designs <sup>o3)</sup>.

The LNF group is involved in the design of the Super*B* Drift Chamber with important responsibilities. In particular, a member of the group is co-convening the general Super*B* DCH group, which includes also several Canadian Institutions, and another member is co-convening the FastSim and the Detector Geometry working groups (see secs. 4 and 5).

The baseline of the Super*B* tracking detector is the *BABAR* drift chamber, which was already optimized to perform measurements of *B*-physics events, and has been working quite well for the entire *BABAR* lifetime. The main differences, with respect to *BABAR*, concerning the tracking system to be designed for Super*B* detector are:

- reduced center-of-mass boost ( $\beta\gamma = 0.24$  compared to 0.56 in *BABAR*);
- demise, in the machine design, of the support tube holding the final focus quads (as in PEP-II);
- higher occupancy due to radiative Bhabha events scattered in the tracking devices by bending/focussing elements of the machine optics;
- possible presence in the backward region of an electromagnetic calorimeter.

The four items mentioned before require a device possibly lighter in terms of radiation length with respect to *BABAR*, faster and with lighter endplates too. The lower boost, envisaged for Super*B*, points also toward a detector more sensitive to multiple scattering.

## 2 R&D for the SuperB Drift Chamber

Various R&D programs are underway towards the definition of an optimal drift chamber design for SuperB, in particular to study the properties of different gas mixtures and cell layouts with small drift chamber prototypes and simulations, and verify the potential and feasibility of the *cluster counting* option. Finally, wire aging tests are also being conducted to quantify the lifetime of the detector in the potentially high background environment of SuperB.

A precision tracker made of 3 cm diameter, 400  $\mu\text{m}$  thick Aluminum tubes operating in limited streamer mode with a single tube spatial resolution of around 100  $\mu\text{m}$  has been set up at LNF. A small prototype with a cell structure resembling the one used in the BABAR DCH has also been built and commissioned. The tracker and prototype chamber have been collecting cosmic ray data during 2010.

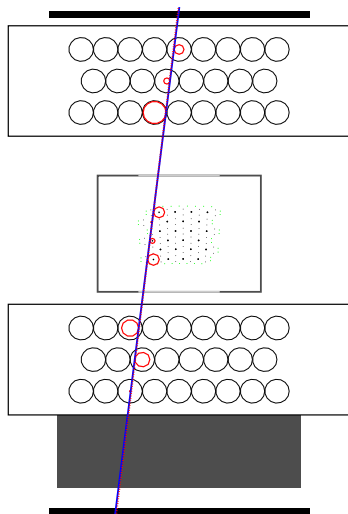


Figure 1: Schematic view of the experimental setup, showing also hits and fitted track in a sample event (see text).

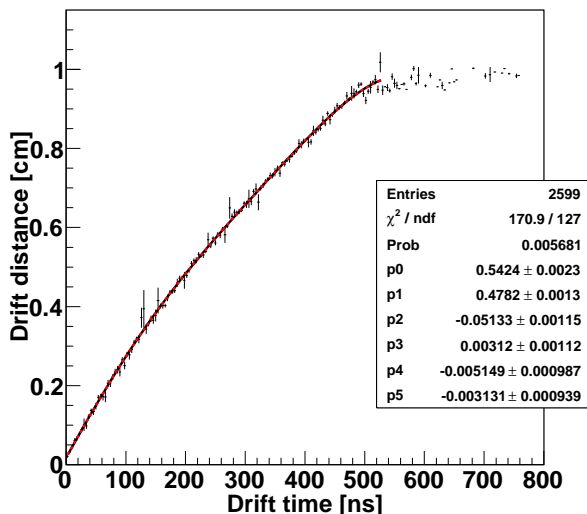


Figure 2: Track distance VS. drift time in a prototype cell. The line is the result of a 5<sup>th</sup>-order Chebyshev polynomial fit.

A schematic view of the experimental setup is shown in Fig. 1: tracks with a minimum momentum of about 150 MeV/c (a 10 cm thick lead block) are triggered by the coincidence of two scintillator counters; the prototype is sandwiched between the two halves of the tracking telescope. Fig. 1 also shows in a sample event the hits in both detectors, and the track fits using either the telescope (continuous blue line) or the prototype (dashed red line). Tracks are extrapolated in the DCH prototype with a precision of 80  $\mu\text{m}$  or better.

Different gas mixtures have been tried in the prototype: starting with the original BABAR mixture (80%He-20%iC<sub>4</sub>H<sub>10</sub>) used as a calibration point, both different quencher proportions and different quenchers have been tested in order to assess the viability of lighter and possibly faster

operating gases. As an example, the correlation between the extrapolated drift distance and the measured drift time is shown in Fig. 2 for a 75%He-25% $C_2H_6$  gas mixture. The result of a fit to a 5<sup>th</sup>-order Chebyshev polynomial is superimposed to the experimental points. Track-fit residuals

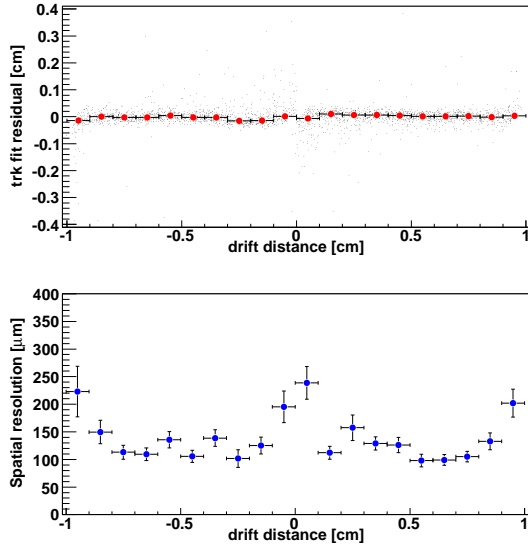


Figure 3: *Track fit residuals (top) and spatial resolution (bottom) as a function of the drift distance. The track is fitted with the tracking telescope.*

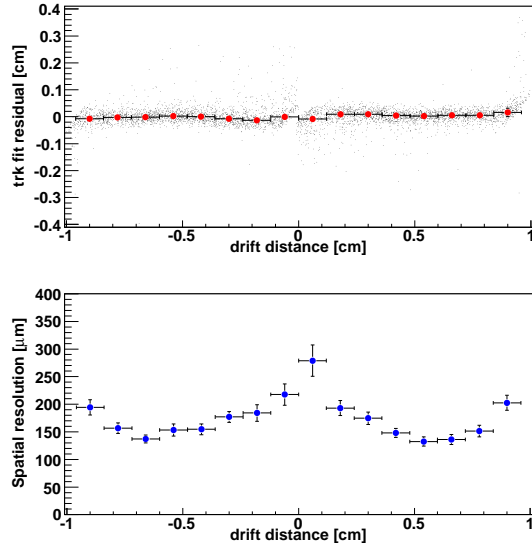


Figure 4: *Track fit residuals (top) and spatial resolution (bottom) as a function of the drift distance. The track is fitted with the drift chamber prototype.*

and spatial resolution as a function of the drift distance for the same gas mixture are shown in Fig. 3. Consistent results are obtained when the track is fitted using the drift chamber prototype itself. This is shown in Fig. 4, where the contribution due to the track-fit extrapolation error has not been subtracted.

A compilation of results for He-based mixtures with different proportions of isobutane, methane and ethane is in progress. Detailed studies of the Lorentz angle and possibly tests in a magnetic field will also have to be carried out in order to consider these mixtures as a viable alternatives.

To improve performances of the gas tracker a possible technique could be the use of the *cluster counting* method which in principle holds the promise of a better resolution both spatially and in the energy loss measurement. Detailed comparisons of the traditional methods to extract spatial position and energy losses and the *cluster counting* methods will be available in the near future.

### 3 Electronics

The year 2010 has been mainly devoted to the definition of the DCH readout architecture and to investigate the possibility of introducing cluster counting capability in the readout chain by means, as a first attempt, of a dedicated circuit counting individual spikes in the wire extracted signal.

In addition to the usual timing and amplitude information the front-end electronics has to provide also the primitives to trigger the detector. The actual design includes two main blocks, one located on the chamber end-plate, the second located at a small distance from the setup. The number of readout channels is about ten thousand.

On-detector electronics will include HV distribution, blocking capacitors for signal extraction, protection network and preamplifier boards. It will be located on the (backward) chamber end-plate to maximize the S/N ratio.

Off-detector electronics will be located on dedicated racks near the apparatus (to minimize power dissipation and electromagnetic interference due to the massive use of fast switching FPGAs in the data conversion and data acquisition stages) and will include TDCs (1 ns resolution), ADCs (6 bits dynamic range) and trigger primitives generation circuits. The stage could also include cluster counting circuits to improve both tracking and  $dE/dx$  measurements. Finally Readout Modules will collect digitized data and will send them to DAQ and Trigger Systems through dedicated optical links.

A possible cluster counting implementation circuit could be based on a fast analog differentiator. The block diagram is shown in Fig. 5 together with an example of input-output waveforms. Preliminary results looks encouraging, but work must be done to optimise both peak detection and noise rejection.

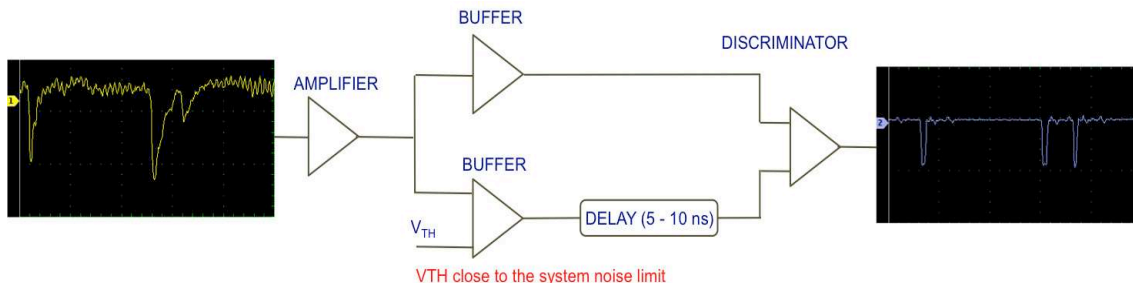


Figure 5: *Circuit block diagram for cluster counting.*

### 4 Development of Simulation Tools for Detector Design and Physics Studies

The design of the SuperB detector and the study of the physics reach of the experiment require specific simulation tools. A detailed simulation of the detector, with its various options, followed by the complete reconstruction of the events is beyond the capability of the current SuperB computing infrastructure. For this reason a fast simulation program, FastSim, has been developed. It relies on simplified models of the detector geometry, materials, response, and reconstruction to achieve an event generation rate a few orders of magnitude faster than is possible with a Geant4-based

detailed simulation, but with sufficient detail to allow realistic physics analyses. To produce more reliable results, FastSim incorporates to some extent the effects of expected machine and detector backgrounds. It is easily configurable, allowing different detector options to be selected at runtime, and is compatible with the *BABAR* analysis framework, allowing sophisticated analyses to be performed. In 2010 FastSim has been further developed becoming a mature tool for detector optimization and physics reach studies. Our group is contributing through the co-convenership of the FastSim working group and the development of those aspects of the simulation concerning the drift chamber, such as the geometry and material definition, the modeling and tuning of the  $dE/dx$  measurement, etc.. FastSim has also been used to quantify the drift chamber performance as a function of parameters such as the inner radius, the number of cells, the length in the forward and backward regions and many more.

## 5 The Detector Geometry Working Group

A Detector Geometry Working Group (DGWG) was setup at the end of 2008 to study the physics tradeoffs of the open Super $B$  detector options<sup>o2)</sup>, such as a) a forward PID detector compared to a longer drift chamber (DCH), b) a backward EM calorimeter vs. no backward EM calorimeter, c) the internal geometry of the Silicon Vertex Tracker (SVT), d) the SVT-DCH transition radius and e) the distribution and amount of absorber in the muon system. Several of the studies have been finalized in 2010, while others are close to completion. The performance of the design options has been studied either by determining the sensitivity reach in a number of benchmark rare  $B$  decays, or by quantifying the overall quality of tracks and photons reconstruction. For example, the impact of a possible forward PID device or backward EM calorimeter has been evaluated in terms of the improved sensitivity in the measurements of  $B \rightarrow K^{(*)}\nu\bar{\nu}$  and  $B \rightarrow \tau\nu$  using both FastSim and the full simulation. A member of our group is co-coordinating the DGWG and is a member of the Forward Geometry Selection Task Force whose goal is to broadly investigate all issues involved in the installation of a hadronic PID detector in the forward region and provide recommendations to the Super $B$  technical board.

## 6 List of Conference Talks

1. M. Rama, Fast Simulation of the Super $B$  detector, Nuclear Science Symposium 2010, Knoxville, USA.
2. M. Rama, Status of the Super $B$  project, BEACH 2010, Perugia
3. G. Finocchiaro, *The Super $B$  Project*, HQL 2010, Laboratori Nazionali di Frascati, 11-15 October 2010.

## Publications

- 1 . B. O’Leary *et al.*, “Super $B$  Progress Report - Physics”, arXiv:1008.1541v1 [hep-ex].
- 2 . E. Grauges *et al.*, “Super $B$  Progress Report - Detector”, arXiv:1007.4241v1 [hep-ex].

- 3 . M. Rama, “Fast Simulation of the Super*B* detector”, Conference Record of the Nuclear Science Symposium 2010.
- 4 . M. Rama, “Status of the Super*B* project”, proceedings of the BEACH 2010 conference (to be published in Nucl. Phys. B).
- 5 . G. Finocchiaro, “The Super*B* Project”, proceedings of the HQL2010 conference (Frascati, 11-15 October 2010), arXiv:1012.2449v1 [hep-ex].

#### Other References

- o1 . P. Raimondi, talk given at the 2<sup>nd</sup> Super *B*-Factory Workshop, <http://www.lnf.infn.it/conference/superb06/talks/raimondi1.ppt>; P. Raimondi, D. Shatilov, M. Zobov, arXiv:physics/0702033v1 [physics.acc-ph].
- o2 . Super*B* Conceptual Design Report, <http://www.pi.infn.it/SuperB/CDR> arXiv:0709.0451v2 [hep-ex]
- o3 . M. E. Biagini *et al.*, “Super*B* Progress Report - Accelerator”, arXiv:1009.6178 [physics.acc-ph].

## *2 – Astroparticle Physics*



## BENE\_DTZ

F. Ronga, F. Terranova (Resp.)

BENE-INFN is a study group closely related to the European initiative BENE (Beams for European Neutrino Experiments) and its follow-up in the 7th Framework Program of EU: EUROnu[1] and NEu2012[2]. It is aimed at developing novel sources for high intensity neutrino beams and is focused on the conceptual design of Superbeams, Beta Beams and Neutrino factories. LNF contributed particularly on future applications of OPERA-like detectors[3], i.e. hybrid emulsion cloud chambers with and without magnetic field, as a far detector to exploit the  $\nu_e \rightarrow \nu_\tau$  transitions (“silver channel”) at the Neutrino Factories. LNF is also involved in the search of more innovative source based on laser-accelerated protons to produce neutrinos in the GeV range. Further activities focused on the combination of accelerator data from Beta Beams with natural sources (atmospheric neutrinos) to improve the sensitivity to the neutrino mass hierarchy (sign of  $\Delta m_{32}^2$ ) [4], high-Q Beta Beams and the study of the upgrades of the CERN acceleration complex to host a European high intensity  $\nu$  source[5]. Finally, in 2010 a new approach based on tagged neutrino beams has been undertaken [6]: it is particularly suited for the study of short baseline appearance of  $\nu_e$  in connection with the Miniboone/LSND anomaly.

### Conference Talks

1. F. Terranova “Perspectives in experimental neutrino physics” Seminar at Univ. Roma La Sapienza, October 2010.

### References

1. EUROnu is a European Commission FP7 Design Study entitled: “A High Intensity Neutrino Oscillation Facility in Europe”. Info available at <http://www.euronu.org/>.
2. NEu2012 is a Networking Activity (WP3) in the Framework of the FP7 Integrating Activity EuCARD (European Coordinated Accelerator R&D). Info available at <http://bene.web.cern.ch/bene/NEU2012.htm>.
3. T. Abe *et al.* [ISS Detector Working Group], JINST **4** (2009) T05001.
4. P. Coloma, A. Donini, P. Migliozzi, L. S. Lavina, F. Terranova, arXiv:1004.3773 [hep-ph] (to appear in EPJC).
5. R. Battiston, M. Mezzetto, P. Migliozzi and F. Terranova, “European facilities for accelerator neutrino physics: perspectives for the decade to come,” Riv. Nuovo Cim. **033**, 313 (2010).
6. L. Ludovici, F. Terranova, Eur. Phys. J. **C69** , 331 (2010).

## NEMO

M. Cordelli, A. Martini, L. Trasatti (Resp.), R. Habel (Ass.)

### 1 Activity

The NEMO collaboration, in the framework of the KM3Net initiative, aims at building a 1 km<sup>3</sup> Cerenkov neutrino detector in the Mediterranean Sea. During the year 2010 the collaboration has concentrated on the construction of NEMO Phase II, an 8 floor tower to be deployed at the final site, 100 km SE of Capo Passero, in the fall of 2011, taking advantage of the electrooptical cable already deployed from the site to the counting room in Portopalo.

In 2011 the LNF group has developed a new addition to the project, PORFIDO, which is a method for acquiring oceanographic data from the optical modules without the use of connectors or penetrators, but using an RFID system that reads the data through the glass. The system has undergone a series of tests, pressure, independence of sea water, absence of electromagnetic disturbances to the experiment electronics, that have all been successful and have proven the feasibility of the systems.

We are now finalizing the design of the PORFIDO probes that are going to be installed in the NEMO Phase II apparatus.

### Publication

1. M. Cordelli, R. Habel, A. Martini, L. Trasatti, Frascati Report, LNF-10/02 (P) (2010).

## OPERA

V. Chiarella, B. Dulach, G. Felici, A. Franceschi, F. Grianti (Ass.),  
A. Gambarara (Tecn.), N. Intaglietta (Tecn.), A. Mengucci (Tecn.), T. Napolitano,  
M. Paniccia (Ass.Ric.), L. Pellegrino, N. Mauri (Ass.Ric.), A. Paoloni, C. Sanelli,  
M. Spinetti, F. Terranova (Resp.), T. Tonto (Tecn.), M. Ventura (Tecn.), L. Votano

in collaboration with

LNF-SEA (Div. Ric.): A. Balla, G. Corradi, U. Denni, A. Frani,  
M. Gatta, G. Paoluzzi, G. Papalino  
LNF-SPAS (Div. Ric.): A. Cecchetti, S. Cerioni, D. Orecchini  
LNF-SPCM (Div. Tec.): G. Catitti, A. Ceccarelli, A. Tiburzi  
LNF-SIE (Div. Tec.): C. Fusco, F. Iungo

### 1 The experiment

OPERA <sup>1)</sup> has been designed to provide a very straightforward evidence for  $\nu_\mu \rightarrow \nu_\tau$  oscillations in the parameter region indicated by Super-Kamiokande as the explanation of the zenith dependence of the atmospheric neutrino deficit. It is a long baseline experiment located at the Gran Sasso Laboratory (LNGS) and exploiting the CNGS neutrino beam from the CERN SPS. The detector <sup>2)</sup> is based on a massive lead/nuclear emulsion target. The target is made up of emulsion sheets interleaved with 1 mm lead plates and packed into removable “bricks” (56 plates per brick). Each brick is equipped with a detachable emulsion doublet (“Changeable Sheet”, CS), which is scanned before the full development of the brick emulsions. The bricks are located in a vertical support structure making up a “wall”. These bricks were produced in situ by a “brick assembly machine” (BAM) located near the OPERA experimental Hall; they are inserted into the wall support structure by a dedicated robot (BMS). Nuclear emulsions are used as high resolution tracking devices for the direct observation of the decay of the  $\tau$  leptons produced in  $\nu_\tau$  charged current interactions. Electronic detectors positioned after each wall locate the events in the emulsions. They are made up of extruded plastic scintillator strips read out by wavelength-shifting fibers coupled with photodetectors at both ends. Magnetized iron spectrometers measure charge and momentum of muons. Each spectrometer consists of a dipolar magnet made of two iron walls interleaved with pairs of precision trackers. The particle trajectories are measured by these trackers, consisting of vertical drift tube planes. Resistive Plate Chambers (RPC) with inclined strips, called XPC, are combined with the precision trackers to provide unambiguous track reconstruction in space. Moreover, planes of RPC are inserted between the magnet iron plates. They allow for a coarse tracking inside the magnet to identify muons and ease track matching between the precision trackers. They also provide a measurement of the tail of the hadronic energy leaking from the target and of the range of muons which stop in the iron. A block of 31 walls+scintillator planes, followed by one magnetic spectrometer constitutes a “super-module”. OPERA is made up of two supermodules (SM) located in the Hall C of LNGS (see Fig. 1). Since 2008 all bricks have been inserted: the OPERA target is made of 150036 bricks corresponding to a target mass of 1.25 kton. OPERA is able to observe the  $\nu_\tau$  signal with an impressively low background level. The direct and unambiguous observation of  $\nu_\mu \rightarrow \nu_\tau$  appearance will constitute a milestone in the study

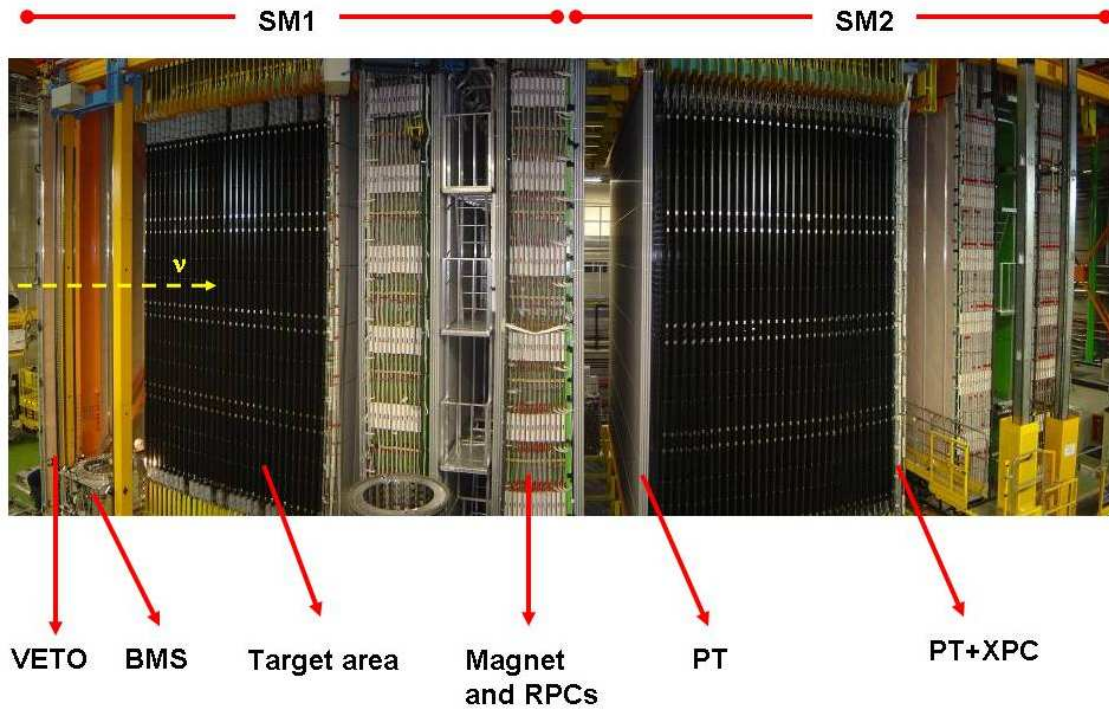


Figure 1: A fish-eye view of the OPERA experiment. The upper red horizontal lines indicate the position of the two identical supermodules (SM1 and SM2). The “target area” is made up of planes of walls filled with lead-emulsion bricks interleaved with planes of plastic scintillators (TT): the black covers visible in the photograph are the end-caps of the TT. Arrows show also the position of the VETO planes, the drift tubes (PT) followed by the XPC, the magnets and the RPC installed among the magnet slabs. The Brick Manipulator System (BMS) is also visible. The direction of incoming neutrinos from CERN is indicated by the yellow arrow.

of neutrino oscillations. Moreover, OPERA has some sensitivity to the sub-dominant  $\nu_\mu \rightarrow \nu_e$  oscillations in the region indicated by the atmospheric neutrino experiments. It has been shown<sup>3)</sup> that the CNGS beam optimized for  $\nu_\tau$  appearance, will improve significantly (about a factor of three) the current limit of CHOOZ. Further results, concerning sterile neutrinos and non-standard interactions have been considered in<sup>4, 5)</sup>.

Opera is an international collaboration (Belgium, Croatia, France, Germany, Israel, Italy, Japan, Russia, Switzerland, Tunis and Turkey) and the INFN groups involved are Bari, Bologna, LNF, LNGS (Gran Sasso), Naples, Padova, Rome and Salerno. The Technical Coordinator (M. Spinetti), the Coordinator for detector operation and maintenance (A. Paoloni) and the Deputy Spokesperson of the Collaboration (F. Terranova) are LNF researchers.

## 2 Overview of the OPERA activities in 2010

2010 has been a very special year for OPERA. In June, the first tau analysis - covering about 30% of the 2008-2009 statistics - was published together with the first tau candidate event <sup>6)</sup>. In addition, the 2010 run has been extremely successful. In terms of duration and accumulated statistics it has been the longest since the CNGS startup. In 2010, the CNGS facility accumulated  $4.03 \times 10^{19}$  proton-on-target, corresponding to about 4250 events in the bricks, with an overall duty-cycle for the accelerator complex of 82%. The run started on April 29 and finished on November 22: the OPERA subdetectors were, thus, active and in nominal conditions for about 7 months. On the data analysis side, the 2008 sample has been fully studied, together with a large fraction of the 2009 data; the analysis includes the extraction of the candidate bricks, the scanning of the CS, the vertex localization and the search for a decay topology. The analysis of 2009 data is well advanced and it will be completed by spring 2011. Before the publication of the tau candidate, very important milestones have been achieved. In particular, together with ancillary cosmic ray measurements <sup>7)</sup>, OPERA has published the first analysis of a high purity charm sample <sup>6)</sup>, which represents a crucial benchmark for the tau and demonstrates appropriate knowledge of the detector efficiencies. The charm sample studied in <sup>6)</sup> corresponds to the same integrated statistics as for the tau candidate. Here, 20 events were observed, to be compared with a MC expectation of 16 events. Significant improvements have also been achieved in the study of systematics from hadron rescattering and charm contamination in the tau sample. Such achievements were mainly boosted by the analysis of the tau candidate, interpreted as a  $\tau \rightarrow$  hadron (1-prong) event (see Fig. 2). In order to avoid post-processing biases, data have been analyzed using the same selection cuts as for the experiment Proposal <sup>1)</sup>. However, a complete reevaluation and tuning of the selection criteria are in progress: the new analysis will take advantage of the large statistics accumulated so far and allow for a data-driven evaluation of the detector efficiencies.

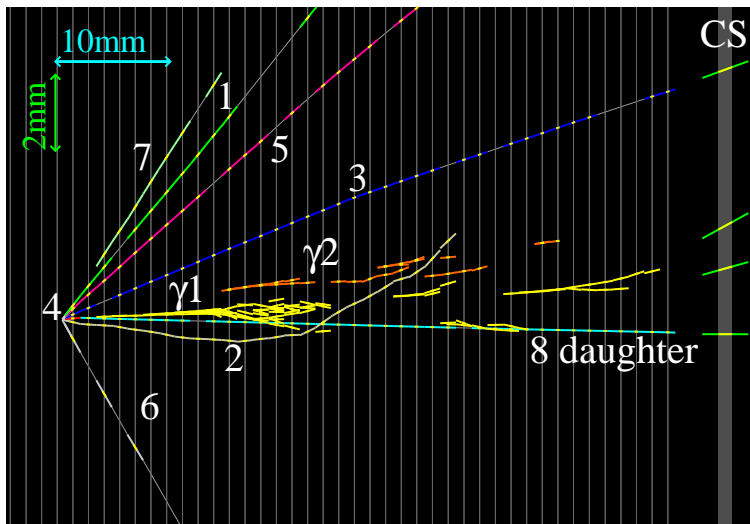


Figure 2: *The first OPERA tau candidate (see <sup>6)</sup> for details).*

### 3 Activities in Frascati

The Frascati group has been responsible for the design and construction of the dipolar magnets and the general support structure for the subdetectors. It shares responsibility with INFN Padova and LNGS for the construction and running of the bakelite RPC planes. Frascati and Naples also designed and prototyped the wall support structures housing the lead/emulsion bricks and LNF was responsible for their production and installation. The Frascati group is also involved, with the University of Hamburg, in the trigger of the drift tubes, performed by the Resistive Plate Chambers. Moreover, the group contributes to software development and to analyses. On the emulsion side, LNF was highly involved in the construction and operation of the Brick Assembly Machine (BAM) and, since 2008, contributes to the emulsion scanning with two dedicated microscopes located in Frascati. Finally, since 2007 LNF follows the brick handling of OPERA, i.e. the operation chain that goes from the extraction of the brick after an interaction has occurred up to the emulsion development.

#### 3.1 OPERA General layout

The OPERA general support structure is a project by LNF-SPAS and external firms and it has been mounted in parallel with the electronic subdetectors and the brick walls between 2003 and 2006<sup>8)</sup>. The project was completed in 2006 and, during 2007 and 2008, only auxiliary installations were added. The structure has been designed by LNF-SPAS; construction and mounting has been carried out by external firms under the supervision of LNF. LNF-SPAS has also been involved in the realignment and revision of the structure after the April 2009 earthquake and it takes care of the maintenance during the run of the BMS.

#### 3.2 Magnets

The OPERA magnets and their infrastructures have been commissioned in spring 2006 and were fully operative since the first CNGS run<sup>9)</sup>.

During the 2010 physics runs the magnets were operated continuously for about 200 days and the performance were well in specs. During the run, two short interruptions were experienced. The former was due to a leak in the chiller used for the closed-cycle cooling system of OPERA<sup>8)</sup>, the latter to a defective AC/DC converter in the power supply of the first magnet. In fact, during the repair of the chiller, the backup cooling system based on the water circuits of LNGS was employed. The backup system was commissioned in 2009 and it operated within specs during the whole period of the chiller failure. The LNGS input water temperature is, however, at the limit of tolerances for OPERA (11°C): such high temperature is mainly due to the operation of the ICARUS cryogenic plant. In the course of 2011, interventions are planned by the LNGS Technical Division to reduce the output temperature and decouple the cooling of Hall C from the rest of the experimental halls. As a consequence, OPERA plans to downgrade the chiller-based system as a backup system once the LNGS intervention will be completed, i.e. at the end of the 2011 CNGS run.

### 3.3 Resistive Plate Chambers

After major contributions in the construction of the RPC system, the LNF group is still highly involved in its running during the CNGS data taking. One of the duties of the group is the monitoring of the performances as a function of time (aging, efficiency fluctuations etc.). In OPERA, Resistive Plate Chamber with bakelite electrodes are arranged into layers, 22 in each spectrometer, inserted into 2 cm gaps inside the magnetized iron. Two additional layers are placed in each Super-Module between the Target Tracker and the spectrometer. The XPC layers and 7 out of 22 RPC layers in each spectrometer are instrumented with dedicated Timing Boards (TBs) for triggering the drift tubes. A complete description of the OPERA RPC system can be found on (2, 10, 11).

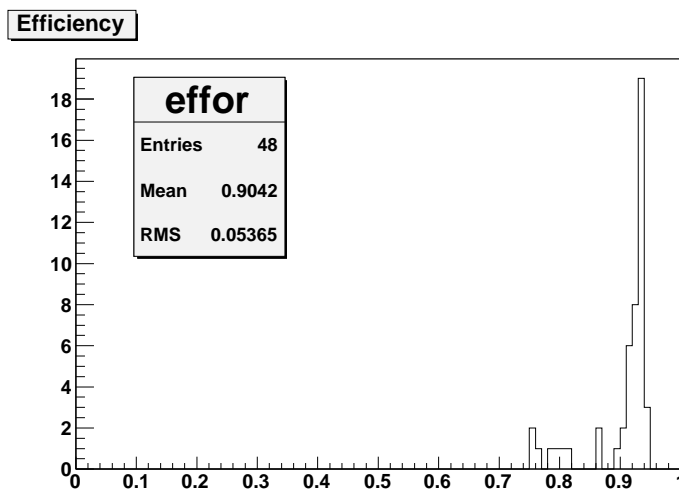


Figure 3: Efficiency measured for RPC and XPC layers during 2010 electronic detector run.

The detectors are operated in streamer mode at 5.7 kV with the gas mixture  $Ar/C_2H_2F_4/i - C_4H_{10}/SF_6 = 75.4/20.0/4.0/0.6$  (12). An automatic correction is applied for the pressure, according to (13); the temperature is quite stable, between 15 and 18°C, depending on the detectors position. Signals from the vertical strips, measuring the bending coordinate, are discriminated at 40 mV, while the threshold for the horizontal strips is 26 mV, in order to correct for the different impedance matching with the read-out twisted flat cables.

The full RPC system ran smoothly during the 2010 run, with almost no dead-time and with performances similar to those observed in previous years (8), matching the required specifications.

RPC layers showed typical efficiencies around 94%, mostly limited by their geometrical acceptance (dead areas between the chambers). The efficiencies measured during the run are displayed in Fig. 3; the tail at values lower than 90% is due to layers with problems in the high-voltage chain: such defects can be fixed only at the end of the run to avoid interference with the operation of the BMS. Average cluster size values were about 2.04 strips in the bending projection and 1.36 strips in the other projection, with tracking resolutions  $\sim 1$  cm. In Fig. 4 the measured cluster sizes in each RPC layer are shown. Counting rates as low as 20 Hz/m<sup>2</sup> have been observed with operating

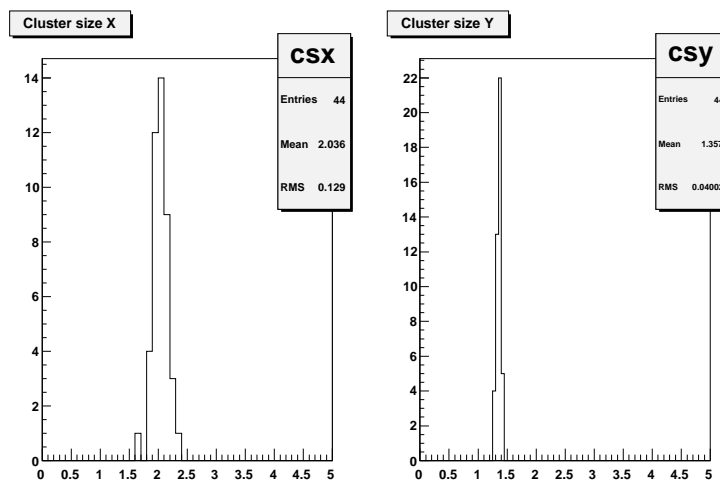


Figure 4: *Cluster sizes measured for RPC layers during 2010 electronic detector run.*

currents around 500 nA for each RPC row (3 chambers, corresponding to a sensitive area of  $9 \text{ m}^2$ ). The detector time resolution is  $\sim 4 \text{ ns}$ , ensuring  $300 \text{ }\mu\text{m}$  resolution of the drift tubes.

No major aging effect has been observed in terms of detector efficiency and performance, while  $\sim 6\%$  of the system is showing higher currents (above  $2 \text{ }\mu\text{A}$  for single RPC rows) and rates (as high as  $100 \text{ Hz/m}^2$ ). The effect is localized in the first spectrometer and it is probably due to the operation during the previous years at low gas flux in presence of leakages, which has now been fixed.

### 3.4 Wall support structure

The wall support structure (“wall”) is made of thin stainless steel vertical bands welded to light horizontal trays where the bricks are positioned with a precision of one millimeter. The structure is suspended through rods and joints from the general support structure and tensioned from the bottom through a spring system. The walls were installed in parallel with the plastic scintillators. This project has been under the responsibility of LNF-SSCR and was successfully completed in 2006<sup>8)</sup>. In 2010 only maintenance operations, fixing of damaged parts and alignment updates during the filling phase have been carried out. In addition, the LNF technical team contributes to the recovery of the 163 bricks blocked in the trays during the 2008-2010 extraction procedures. The recovery operations are in progress and will be completed in spring 2011.

### 3.5 Brick Assembly Machine

After the production of the bulk of the target in 2007-2008, the Brick Assembly Machine (BAM) has been reactivated in 2009 for a short time to build additional 3000 bricks. In fact, such production was originally scheduled in 2008, as well, but it was delayed by an accident occurred at the firm producing the lead for OPERA (JL Goslar, Germany). In February 2009 the BAM was finally put in standby mode. The whole facility was dismantled in winter 2010 by the LNF-SPAS and the

LNGS Technical Division; the anthropomorphic robots were reset and will be sold back to external firms in 2011; two of them have also been re-employed by INFN for the CUORE experiment and used by INFN workshops (Naples) to automatize soldering procedures.

### 3.6 The LNF scanning station

The OPERA brick is based on the Emulsion Cloud Chamber technique, fulfilling the requirements of high granularity and micrometric resolution necessary to distinguish the  $\tau$  decay vertex from the primary  $\nu_\tau$  interaction. The brick (see Sec.1) acts as a standalone detector, that can be selectively removed from the target, developed and analyzed after the interaction took place.

Each emulsion film is made of two active layers 44  $\mu\text{m}$  thick poured on a 210  $\mu\text{m}$  plastic base. The nuclear emulsions consist of AgBr crystals suspended in a gelatine binder. The passage of charged particles creates perturbations at atomic scale (latent image), amplified by a chemical-physical process called development: the resulting silver grains of about 0.6  $\mu\text{m}$  diameter are visible with an optical microscope. About 30 grains every 100  $\mu\text{m}$  are left by a minimum ionizing particle. The excellent emulsion space ( $\sim 1 \mu\text{m}$ ) and angular ( $\sim 2 \text{ mrad}$ ) resolutions are ideal for detection of short-lived particles. The three-dimensional tracks of charged particles crossing the brick are reconstructed from the optical tomography of each field of view obtained adjusting the focal plane of the objective lens through the emulsion thickness. A detailed description of the automatic microscopes developed for OPERA can be found in Ref. <sup>14)</sup>. The brick dimensions and length are optimized to contain the primary as well the decay vertex and to provide particle identification and kinematical reconstruction. The use of passive material, combined with high accuracy tracking devices, allows for momentum measurement of charged particles via multiple Coulomb scattering (MCS) and for electromagnetic shower identification <sup>15)</sup>.

The bricks selected by the electronic detectors as containing a neutrino interaction vertex are extracted from the OPERA target and equally shared between Japan and Europe for the scanning. For the events assigned to the European side the CS doublets are analyzed at the LNGS scanning station. The CS doublet acts as a confirmation of the trigger provided by the Target Tracker: the brick is developed only if the prediction is confirmed, otherwise the CS is replaced and the brick is put back in the target. In case of positive CS result, the brick is assigned to one of the European scanning laboratories dedicated to the neutrino vertex localization in Switzerland and Italy, one of which is at LNF. The scanning load at the LNGS scanning station is shared among the European members of the OPERA Collaboration. Since 2008 the LNF group contributes to the CS doublets scanning performing shifts at the LNGS station, in addition to the work load at the home scanning laboratory.

The LNF emulsion scanning station is equipped with two optical microscopes, one of them has been instrumented with a system for the emulsion plates loading on the microscope stage (Plate Changer), in order to scan in full automatic mode. The installation of the Plate Changer electronics and of its hardware interfaces to the microscope have been completed while the installation of the software needed to remotely operate the machine from the scanning software framework as well as the commissioning of the fully automatic system is in progress.

The activity of the LNF scanning station in 2010 has been focused on the OPERA event scanning and analysis. The whole chain for brick scanning at LNF, typical of each European

scanning laboratory, is fully operational since 2008: it consists of three phases: the brick scanning, the event reconstruction and the data publication on the central database.

The brick scanning procedure for vertex localization is carried on in different steps. When the brick is shipped from LNGS to the scanning laboratory, the information of the tracks found in the CS doublet are downloaded at LNF from the central database. The tracks are extrapolated into the brick and searched for with a prediction scan. Once the so-called connection between the CS and the brick is validated, the tracks are followed with a prediction scan from film to film (ScanBack). When tracks converge and stop, the stopping point gives a first indication of the neutrino interaction vertex. A general scan is performed around the stopping point to reveal all the particles that are involved in the interaction (TotalScan). The TotalScan is a wide area scan ( $1 \text{ cm}^2$ ) for 15 consecutive emulsion films, in which all the tracks are searched for, contrary to the ScanBack. The volume is large enough to reconstruct all primary and possible decay daughter particle tracks.

After the scanning phase, once the vertex is located, the reconstruction process links the tracks of the different films in 3-D tracks, evaluates the momentum of charged particles and analyzes the event kinematics. With the information of all particle trajectories, a dedicated decay search procedure is applied, to search for interesting decay topologies.

At the end of the brick analysis, the scanning laboratory publishes a feedback of the vertex localization and of the decay search results, as well as the complete set of emulsions scanning data in the central OPERA database, where they are made available to the whole Collaboration for global analysis.

Bricks from Physics Runs 2008, 2009 and 2010 were assigned to the Frascati laboratory. The scanning and analysis flow is smoothly running on-time with the brick assignation. Even if the event statistics is low, the LNF scanning lab shows good performances with a 75% location efficiency, in agreement with the expectations. In 2011, thanks to improvements in the manpower and in the expertise of the operators, we plan to further increase the number of located vertices; LNF will also be involved in the full kinematic analysis of a subsample of located events (“minimum bias sample”) done in a collaboration-wide framework (Bern, Naples, Salerno and Toho Univ.) to improve the kinematic selection for tau events (see Sec. 2) and study hadron interaction background.

### 3.7 Brick handling

During nominal CNGS operation, about 20 neutrino interactions per day occur in the OPERA target and several candidate bricks are tagged as containing the corresponding primary vertex. These predictions are validated scanning preliminarily a pair of detachable emulsions (“changeable sheets”, CS <sup>16</sup>). If confirmed, the corresponding brick is extracted, aligned using an X-ray machine and sent to the facilities located on surface for cosmic ray exposure (high precision alignment) and development. All the operations of CS and brick handling require dedicated tools and personnel running synchronously with the CNGS data taking. LNF is responsible of the coordination of these tasks and provides most of the tools for brick handling. In particular, during the 2010 run, the whole Brick Handling (BH) chain has been re-optimized and synchronized with the operation of the BMS. In particular, the shift duties have been redefined to speed up the procedure and provide support to the BMS operators, as well. Since 2010, OPERA is able to run simultaneously

the BMS and BH chain employing at most 4 operators (8h/shift). Moreover, it has been demonstrated that the extraction of the candidate bricks at nominal CNGS performance can be achieved running BMS+BH in 1 shift/day mode for the whole year and supplementing the running of the BMS with an additional 8h shift (2 shift mode) from September to November. In 2011, further optimization are under study, which also involve the facilities of emulsion development underground (CS development) and on surface.

#### 4 List of Conference

1. N. Mauri, “Measurement of the atmospheric muon charge ratio with the OPERA detector at Gran Sasso.” Poster at The XXIV International Conference on Neutrino Physics and Astrophysics (NEUTRINO 2010), Athens, June 14-19, 2010.
2. N. Mauri, “Measurement of the cosmic ray muon charge ratio with the OPERA detector”, Talk at the 96th Congresso Nazionale della Società italiana di Fisica, Bologna, September 20-24, 2010.
3. A. Paoloni “Performance and aging of the OPERA RPC’s”, Talk at the X Workshop on Resistive Plate Chambers and related Detectors, RPC-2010, GSI, Darmstadt, February 9-12, 2010.
4. F. Terranova, “From tau to electron neutrinos: the study of leptonic mixing in the precision era of neutrino physics”, Seminar at Univ. of Pisa, October 2010.

#### References

1. M. Guler *et al.*, OPERA proposal, CERN/SPSC 2000-028, SPSC/P318, LNGS P25/2000.
2. R. Acquafredda *et al.*, JINST **4**, P04018 (2009).
3. M. Komatsu, P. Migliozzi, F. Terranova, J. Phys. **G29**, 443 (2003); P. Migliozzi, F. Terranova, Phys. Lett. **B563**, 73 (2003).
4. A. Donini, M. Maltoni, D. Meloni, P. Migliozzi and F. Terranova, JHEP **0712**, 013 (2007).
5. M. Blennow, D. Meloni, T. Ohlsson, F. Terranova and M. Westerberg, Eur. Phys. J. **C56**, 529 (2008).
6. N. Agafonova *et al.* [OPERA Coll.], Phys. Lett. **B691**, 138 (2010).
7. N. Agafonova, *et al.* [OPERA Coll.], Eur. Phys. J. **C67**, 25 (2010).
8. See “LNF 2009 Annual Report”, D. Babusci ed., LNF-10/15 (IR), p.97, “LNF 2008 Annual Report”, D. Babusci ed., LNF-09/04 (IR), p.99, “LNF 2007 Annual Report”, M. Antonelli ed., LNF-08/20 (IR), p.103; “LNF 2006 Annual Report”, M. Antonelli ed., LNF-07/10 (IR), p.87; “LNF 2005 Annual report”, E. Nardi ed., LNF-06/10 (IR), p.78; “LNF 2004 Annual

Report”, E. Nardi ed., LNF-05/5 (IR), p.70; “LNF 2003 Annual Report”, S. Dell’Agnello ed., LNF-04/08 (IR), p.64.

9. A. Cazes *et al.*, JINST **2**, T03001 (2007).
10. S. Dusini *et al.*, Nucl. Instr. & Meth., **A602**, 631 (2009).
11. A. Paoloni *et al.*, Nucl. Instrum. Meth., **A602**, 635 (2009).
12. A. Mengucci, A. Paoloni, M. Spinetti, L. Votano, Nucl. Instr. & Meth., **A583**, 264 (2007);  
A. Paoloni *et al.*, LNF Technical Note **LNF-08/14(NT)** (2008).
13. M. Abbrescia *et al.*, Nucl. Instr. & Meth., **A359**, 603 (1995).
14. N. Armenise *et al.*, Nucl. Instr. & Meth. A **551**, 261 (2005).
15. L. Arrabito *et al.*, JINST **2**, P05004 (2007).
16. A. Anokhina *et al.* [OPERA Coll.], JINST **3**, P07005 (2008).

## ROG

G. Giordano (Resp.), M. Iannarelli (Tecn.), R. Lenci (Tecn.), A. Marini,  
G.P. Murtas (Ass.), G. Pizzella (Ass.), F. Ronga (Ass.), E. Turri (Tecn.)

ROG Collaboration includes groups at :  
University of Rome La Sapienza and INFN Roma 1,  
University of Rome Tor Vergata and INFN Roma 2

### 1 Introduction

The ROG group is currently operating the cryogenic gravitational wave (GW) bar detector NAUTILUS, hosted in Frascati National Laboratory. The other detector that was operated by the ROG group, EXPLORER at CERN, ceased its operation on June 2010, by decision of INFN. The main goal of this search is the direct detection of the GW's that could be emitted by astrophysical sources (such as Supernovae or Coalescent Binaries). Such detection would be of enormous interest for general relativity and astrophysics.

The NAUTILUS detector consists of an aluminum cylindrical bar having a mass of  $\simeq 2.3$  tons, with a capacitive resonant transducer mounted on one of the bar faces. It is contained in a vacuum cryostat, cooled at cryogenic temperatures (at present  $\simeq 3$  K, but a temperature as low as 0.1 K can be reached) to reduce thermal noise, and isolated from seismic and acoustic disturbances.

The capacitive transducer is coupled to a very low noise superconducting amplifier (d.c. SQUID) whose output is acquired by a VME ADC board, sampled at 5 kHz.

A GW signal would excite the mechanical resonant modes of the bar-transducer system. When searching for impulsive signals, the data are filtered with an adaptive filter matched to a delta-like signal. This search for bursts is suitable for any transient GW which shows a nearly flat Fourier spectrum at the two resonance frequencies of the detector.

Both EXPLORER and NAUTILUS have been kept in continuous observational mode since 2003, with a duty cycle between 80 and 90%, mainly limited by the necessary periodic cryogenic operations.

The LNF group has major responsibilities in the maintenance and running of NAUTILUS (including the production of liquid Helium), in the maintenance, upgrading and running of the cosmic ray detectors, in the data acquisition and in many items of data analysis.

### 2 NAUTILUS and EXPLORER

The ultra-cryogenic detector NAUTILUS is operating at the INFN Frascati National Laboratory since December 1995. It is equipped with a cosmic ray detector based on a streamer tube assembly.

The present data taking started in 2003, with a new bar tuned at 935 Hz, where a pulsar, remnant of the SN1987A, is supposed to emit GW's, with a more sensitive readout chain (the same as for EXPLORER), and a new suspension cable, to provide a more stable position setting. At present, the temperature of the bar is 3.5 K and the resulting strain noise (the minimum detectable spectral density) is  $\tilde{h} \simeq 1 \cdot 10^{-21} / \sqrt{Hz}$  around 935 Hz, and  $\tilde{h} \leq 10^{-20} / \sqrt{Hz}$  over about 50 Hz. At the beginning of 2009, we discovered that some wide-band noise was due to a malfunctioning of the UPS system. After changing the UPS and some adjustments in the SQUID electronic chain, the noise temperature decreased down to less than 1 mK, corresponding to an adimensional amplitude of GW bursts  $h \simeq 2.4 \cdot 10^{-19}$ .

The EXPLORER antenna was located at CERN and was very similar to NAUTILUS. Also its duty cycle was very high (of the order of 90%), its noise temperature was about 2 mK, with a strain sensitivity  $\tilde{h} \simeq 2 \div 3 \cdot 10^{-21} / \sqrt{\text{Hz}}$  around the two resonances at 904 Hz and 927 Hz, and  $\tilde{h} \leq 10^{-20} / \sqrt{\text{Hz}}$  over about 30 Hz. EXPLORER was equipped with a cosmic ray detector, based on a set of long plastic scintillators.

The read-out systems installed in 2001 on EXPLORER and in 2003 on NAUTILUS, obtained a larger bandwidth and consequently improved the time resolution (a few ms), as it is also been checked with the events due to cosmic ray showers.

In the last years a continuous effort has been paid in improving the data analysis system already present and in testing independent algorithms and new methods. As a result of these, still going, efforts we were able to improve the accuracy in the reconstruction of both the amplitude and time characteristic of the signals. At the same time, we performed detailed studies of the detectors response to other class of signals than the simple delta-like burst previously considered. All this was done also with a particular eye on the perspective of performing joint analyses with the interferometric type of GW detectors, which do have a much better sensitivity than the resonant bar detectors, but up to now have suffered from very long interruptions in their operation. This situation will persist in the next few years, when both the american interferometers (LIGO) and the french-italian one (VIRGO) will be down for major upgrades, leaving the INFN bar detectors (AURIGA and NAUTILUS) the only operational GW detectors.

## 2.1 Analysis of EXPLORER-NAUTILUS data

We continued to study all possible wide-band noises that can result in a candidate event and also, through simulations and software injections of signals, to find the event characteristics (e.g. length vs. amplitude) that an event due to a real excitation must have. All this was used to reduce the number of candidate events by putting vetos on periods or single events with understood instrumental noise excess, in addition to the usual vetos on events triggered by cosmic rays showers.

In 2010, up to the EXPLORER shutdown in June 10<sup>th</sup>, we had a total of  $\simeq 113$  days of good data periods in the overlap between EXPLORER and NAUTILUS.

We are in the process of analyzing the amount of data (about 3 years) of the two detectors covering from the end of the period considered in the last IGEC analysis (April 2007) up to the EXPLORER shutdown (June 2010).

## 2.2 Other types of analyses

- **Cosmic Rays** - The study of the response of our detectors to cosmic ray showers continues to demonstrate experimentally the actual capability to detect very small mechanical excitations of the bars. While the study of the timing characteristics of the larger events produced by the rare very high density showers allows us a real measure of the accuracy in the time reconstruction, the study of the much more numerous cases of low density showers, performed with a cumulative-type analysis, constitutes an independent cross-check of the amplitude response calibration.

- **Exotic particles** - We continued the studies for exotic particles impinging on Nautilus or Explorer. Such particles could be with a quark "s" (nuclearites) and particles with only gravitational interactions. Figure 1 shows the preliminary results on the limits for the nuclearites flux obtained with new data, compared to the old limits obtained with the Explorer data of 1992, published on Ph.Rev. D **47**,4770 (1993).

- **Astrowatch** - Since the large interferometric GW detectors (LIGO, Virgo) will soon suspend operations for major upgrades, in the next 3-4 years the only continuously operating GW detectors will be NAUTILUS and AURIGA, at Legnaro National Laboratory. The two groups have reached an agreement to be in a coordinated "astrowatch operation". The intent is to be ready for a

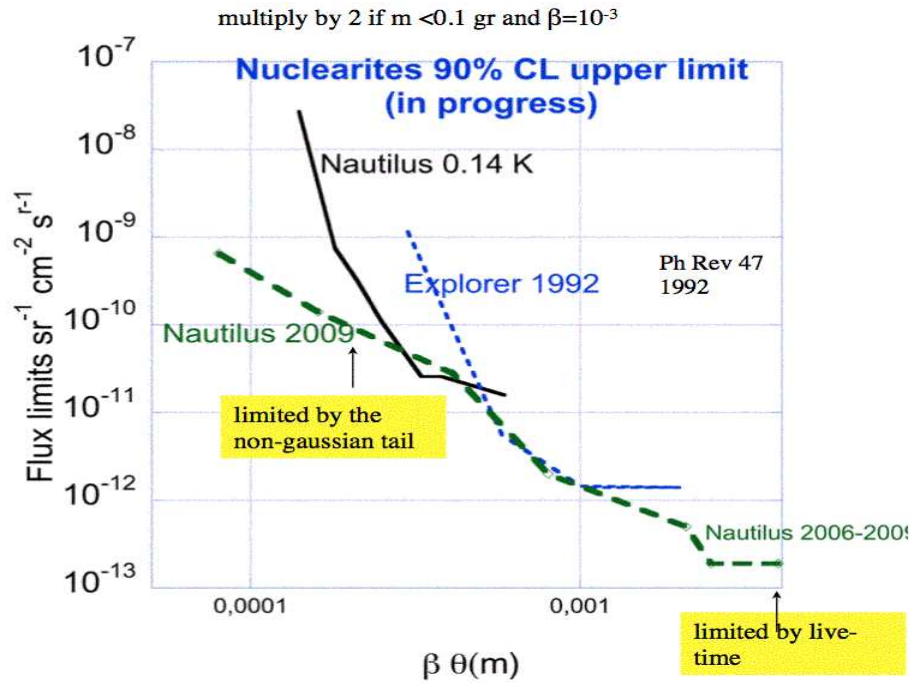


Figure 1: Limits on nuclearities flux.  $\beta$  is the speed (unit of  $c$ ) and  $\theta(m)$  is a function of the mass ( $\theta = 1$  if the mass less than 1.5 ng).

common data analysis in case an important astrophysical event (that is an event thought to be a source of GW radiation) would happen. This would lead to at least the establishment of an upper limit on the amount of GW delivered by the event, or, in the most optimistic case, if the data would show a clear behaviour above any reasonable possibility of a noise fluctuation and in agreement with the expectations for that event, to a claim for detection.

### 3 Conference Talks

1. F. Ronga, Frascati, “Acoustic detectors of gravitational waves as Dark Matter exotics particle detectors“. XIX Congresso della Sigrav, Pisa.

### References

1. P. Astone *et al.*, Phys. Rev. D **82**, 022003 (2010). arXiv:1002.3515 [gr-qc].
2. I. Leonor *et al.*, Class. Quant. Grav. **27**, 084019 (2010). arXiv:1002.1511 [astro-ph.IM]
3. M. Bassan *et al.*, Class. Quant. Grav. **27**, 025014 (2010).

## WIZARD/PAMELA

G.Basini, F.Bongiorno (Ass.),  
G.Mazzenga (Tecn.), G. Pizzella (ass.), M.Ricci (Resp.)

Participant Institutions:

ITALY: INFN Bari, LNF, Firenze, Napoli, Roma 2-Tor Vergata, Trieste;  
CNR Ist. Fisica Applicata “Nello Carrara” Firenze;  
ASI (Italian Space agency);  
Electronic Engineering Department, University of Roma 2 “Tor Vergata”;  
RUSSIA: MePhi Moscow;  
FIAN Lebedev Moscow;  
IOFFE St Petersburg;  
TsSKB-Progress Samara;  
SWEDEN: KTH Stockholm;  
GERMANY: Siegen University;

### 1 The satellite mission PAMELA

PAMELA, a part of the WIZARD international experimental program on balloon, satellite and Space Station activities, is a cosmic ray space experiment installed and running on board a Russian satellite (Resurs-DK1) which has been successfully launched on June 15th, 2006 from the cosmodrome of Baikonur, Kazakhstan, by a Soyuz TM2 rocket.

The satellite is flying in a low altitude, elliptic orbit (350-610 km) with an inclination of 70.0 degrees. The PAMELA telescope consists of a magnetic spectrometer composed of a permanent magnet coupled to a silicon tracker, an electromagnetic silicon-tungsten calorimeter, a time-of-flight system, an anticoincidence system, a shower tail catcher scintillator and a neutron detector 1, 2). A sketch of the PAMELA instrument is shown in fig.1 and a photo of the complete Flight Model is shown in fig.2.

The total height of PAMELA is  $\sim 130$  cm, the mass is 470 kg and the power consumption is 355 W.

The observational objectives of the PAMELA experiment are to measure the spectra of antiprotons, positrons and nuclei in the cosmic rays over an extended range of energies, to search for antimatter and for indirect signatures of dark matter and to study cosmic ray fluxes over a significant portion of the Solar cycle.

The main scientific goals can be schematically listed as follows:

- a) measurement of the antiproton spectrum in the energy range 80 MeV-190 GeV;
- b) measurement of the positron spectrum in the energy range 50 MeV-300 GeV;
- c) measurement of the electron spectrum up to 500 GeV;
- d) measurement of the proton spectrum up to 700 GeV;
- e) measurement of the electron+positron spectrum up to  $\sim 1$  TeV;
- f) measurement of light nuclei spectra (He/Be/C) up to 200 GeV/n;
- g) search for antinuclei with a sensitivity of  $3 \times 10^{-8}$  in the  $\overline{He}/He$  ratio.

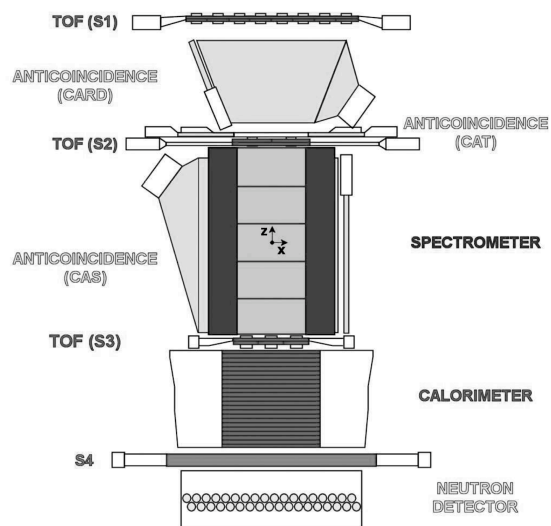


Figure 1: *Schematic overview of the PAMELA detectors.*

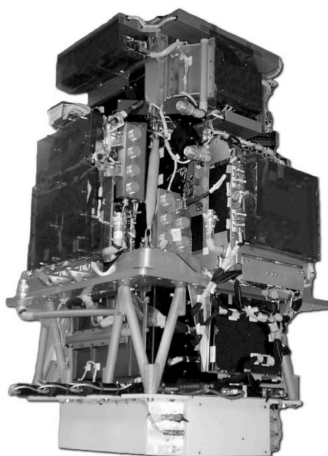


Figure 2: *The PAMELA Flight Model.*

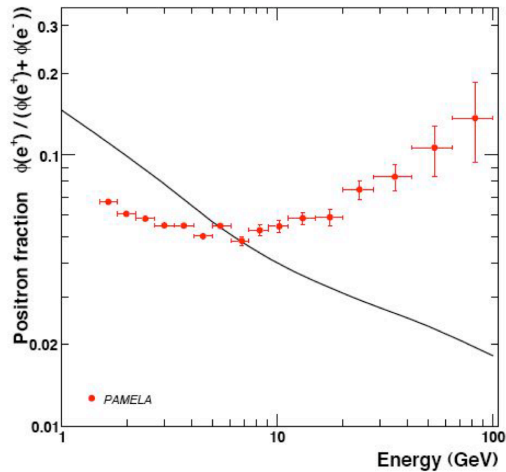


Figure 3: *The PAMELA positron fraction compared with theoretical model. The solid line shows a calculation by Moskalenko and Strong <sup>3)</sup> for pure secondary production of positrons during the propagation of cosmic-rays in the Galaxy. One standard deviation error bars are shown. If not visible, they lie inside the data points.*

Additional objectives achievable all over the duration of the mission are:

- Long-term monitoring of the solar modulation of cosmic rays;
- Measurements of Energetic Particles from the Sun;
- High-energy Particles in the Earth magnetosphere and Jovian electrons.

After more than four and half years of operation, both the satellite and the PAMELA instrument have shown to be properly functioning and the performance of the detectors to be fairly good. Every day, an average of 14 GBytes of data are transmitted to the main Receiving Station NTsOMZ located in Moscow where quick-look and first control of the performances of the instrument are performed. Then, all data are transferred through high-speed networks to CNAF, Bologna and to the participating institutions of the PAMELA International Collaboration for the full analysis of data. PAMELA, at present, has collected some 23 TBytes of data corresponding to about 2.5 billion events.

The year 2011 will be the last one of the operation of PAMELA and of the Satellite after benefitting of two more years of running in orbit (the mission was initially planned for three years) due to the overall good performance of both the satellite and the instruments on board.

Among the results so far obtained by the experiment, the most relevant are the anomalous spectrum of positrons, the antiproton to proton flux ratio studied up to the highest energies ever achieved so far (180 GeV) with the available statistics (see the list of publications for references), together with the electron flux and the proton-Helium spectra (publications in progress). In particular, the positron result (Fig. 3) shows a significant distortion in the spectrum differently from what was expected according to the most credited models of propagation and acceleration of cosmic rays in the Galaxy. This effect could be an indication of production by dark matter particles or could be explained by the presence of an astrophysical source like, e.g., young nearby pulsars. Many articles (more than 500), showing several possible interpretations and new models, have appeared after the first presentations at Conferences and publication of the PAMELA results. Work

is in progress to push - thanks to the increasing statistics - the spectrum to higher energies (beyond 100 GeV) and to study the electron spectrum up to the highest achievable energies, which is of most interest also due to the recent results obtained by the South Polar balloon experiment ATIC and the space mission FERMI-GLAST.

## 2 Activity of the LNF group during year 2010 and for 2011

The LNF PAMELA group has been fully involved in all the previous balloon and present satellite programs in the design, prototyping, test and instrumental R&D for space. During the year 2010 the LNF group has continued the activity in the analysis, running and quick-look control of the mission. The same activity is foreseen in 2011 which, as mentioned above, will be the last year of running. Final publications are expected from the analysis of the last data.

## 3 A selection of most recent and relevant publications

1. O. Adriani *et al.*, “New measurement of the Antiproton-to-Proton Flux Ratio up to 100 GeV in the Cosmic Radiation”, *Phys. Rev. Lett.* **102**, 051101-1 (2009).
2. O. Adriani *et al.*, “An anomalous positron abundance in cosmic rays with energies 1.5 – 100 GeV”, *Nature* **607**, (2009)
3. M. Casolino *et al.*, “PAMELA: a high-precision cosmic-ray observatory in space”, *Il Nuovo Saggiatore (Societa’ Italiana di Fisica)* vol. 25, n. 5-6, pp 5-18 (2009)
4. O. Adriani *et al.*, “A statistical procedure for the identification of positrons in the PAMELA experiment”, *Astrop.Phys.* **34**, 1 (2010).
5. O. Adriani *et al.*, “PAMELA results on the cosmic-ray antiproton flux from 60 MeV to 180 GeV in kinetic energy”, *Phys. Rev. Lett.* **34**, 121101 (2010).

## References

1. M. Casolino *et al.*, ”Launch of the space experiment PAMELA”, *Adv. Space Res.* **42**, 455 (2008)
2. P. Papini *et al.*, “In-flight performances of the Pamela satellite experiment”, *Nucl. Instr. and Meth. Phys. Res.* **A588**, 259 (2008).
3. I.V. Moskalenko, A.W. Strong, “Production and propagation of cosmic-ray positrons and electrons”, *Astrophys. J.* **493**, 694 (1998).



### *3 – Nuclear Physics*



## ALICE

N. Bianchi (Resp. Loc.), G.P. Capitani (Ass.), A. Casanova (Ass.), L. Cunqueiro (Ass.),  
P. Di Nezza, A. Fantoni, P. Gianotti, A. Moregula (Ass.), V. Muccifora,  
A. Orlandi (Tecn.), W. Quian (Ass.), F. Ronchetti (Ass.), A.R. Reolon, A. Viticchié (Tecn.)

### 1 Introduction

ALICE is an experiment at CERN which involves about 1000 physicists from more than 100 Institutions from several Countries. Italy participates with 12 groups and more than 150 physicists. The Frascati group is participating to the electromagnetic calorimeter project (EMCal). The EMCal enables ALICE to explore the physics of jet quenching, i.e. the interaction of energetic partons with the QCD hot and dense medium, over the large kinematic range provided by the LHC. The EMCal provides both fast triggers (level 0 and 1) for photons, electrons, and jets and a High Level Trigger (HLT) as well. The EMCal also measures the neutral energy component of jets, enabling full jet reconstruction in all collision systems, from proton-proton to Pb-Pb. The combination of the EMCal, the excellent ALICE charged tracking capabilities, and the modest ALICE magnetic field strength, is a preferred configuration for jet reconstruction in the high background environment of heavy ion collisions, allowing detailed optimization of background rejection while preserving the crucial jet quenching signals at moderate transverse momentum. The ALICE experiment was ready to take data at the start of LHC in November 2009 and with the first-day proton-proton collisions the first LHC physics papers has been published already in January 2010. During the 2010 run both p-p and Pb-Pb were collected and part of these data have been already published or are currently under analysis. A EMCal extension, called DCal, has been approved and funded.

### 2 EMCAL

In 2010 the EMCAL modules production, started at LNF in 2008, has been completed. 24 modules have been assembled in Frascati using two production lines composed by two stacking fixture and four kits of pressor sensors used to apply and measure the internal load of the modules, as already done in previous years. Four bundles of 36 polished, aluminized and glued wavelength shifting fibers, produced at LNF, have been inserted in each module longitudinally through the Pb/Scint stack providing light collection (Shashlick).

Two strip-modules have been assembled, with 12 aligned modules and with the corresponding optoelectronic chain of Light Guide (LG)-Avalanche PhotoDiode (APD)-Charge Sensitive Preamplifier (CSP) package each. These strip-modules have been delivered to Grenoble, with a safe and special aluminum structure, for testing the signals of APDs using a led system and eventually adjusting the APD gain. The strip-modules have been inserted in the super-module crate, the largest building block of EMCal, made by 24 strip-modules. With the assembly of these two strip-modules, the LNF contribution of one super-module (24 strip-modules, for a total number of 288 modules) to EMCAL has been completed.

The EMCAL is composed by 10 super-modules, which represent the basic structural unit of the detector. All EMCal modules production has been done from 2008 to 2010, with a overall number of 7 American and 3 European super-modules, of which one done in Frascati. From 10, only 4 super-modules were installed in ALICE, operational and taking data in 2010, for a corresponding angular coverage of  $\Delta\eta \cdot \Delta\phi=1.4 \cdot 1.05$ . The other 6 super-modules, assembled, tested and calibrated both in 2009 and 2010, have been re-tested again at the end of the year at CERN with LEDs because of the installation of the Trigger Units and of the DTC cards on all

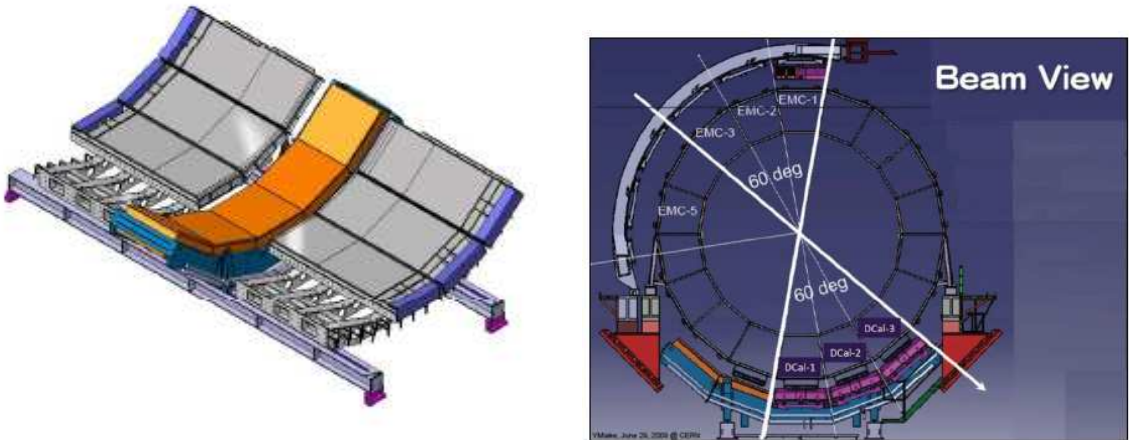


Figure 1: *Left panel: 6 DCAL super-modules (in gray) with the PHOS super-modules (in orange) in between. Right panel: beam view of EMCAL and DCAL.*

Front-End electronics. The temperature sensors, as well as the APD+CSP, have been checked and fixed when needed, confirming the full operability of all super-modules before the insertion in the experiment, scheduled in January 2011.

### 3 DCAL

Even though EMCAL was the last ALICE detector to be proposed, approved, assembled and also partially installed, the first upgrade approved by the ALICE collaboration was an extension of EMCAL, denominated DCAL (Di-jet Calorimeter). The DCAL expands the physics capabilities of the EMCAL by enabling back-to-back correlation measurements, which are impossible with the EMCAL alone, but are essential to obtain a complete picture of the physics addressed by the EMCAL. Together, the DCAL and EMCAL form a two-arm electromagnetic calorimeter. The EMCAL subtends  $100^\circ$  and the DCAL subtends  $60^\circ$  in the azimuthal angle  $\phi$ , with both detectors covering  $|\eta| < 0.7$ , thereby providing good acceptance for di-jets with radii  $R < 0.4$  up to transverse momenta  $p_T \sim 150\text{-}200$  GeV/c. Simulation studies of the DCAL have been carried out and have verified that the technology originally developed for and implemented in the EMCAL meets all the needs of the DCAL project. As a consequence, from a technical perspective, DCAL is an extension of EMCAL. DCAL super-modules are built exactly as they are in EMCAL, out of strip-modules, but with reduced length in  $\eta$ : in fact, each DCAL super-module contains 16 strip-modules instead of 24 present in EMCAL. DCAL will be situated immediately adjacent to PHOS on both the ALICE “A” and “C” sides. DCAL+PHOS can be considered as one integrated detector system for the study of jets, consequently all simulations done include PHOS as well as DCAL super-modules. On the left panel of Fig. 1 is shown a schematic view of the 6 DCAL super-modules with the PHOS super-modules in between and on the right panel the beam view of EMCAL and DCAL is illustrated.

The assembly of the DCAL modules started in summer 2010, after the completion of EMCAL. The DCAL Coll. is the EMCAL Coll. with the Tsukuba (Japan) and Wuhan (China) groups in addition. In Frascati DCAL modules will be not assembled but the Frascati group has the responsibility of coordinating the construction/assembly in the European-Asiatic zone.

The two full assembly station used in Frascati have been sent and delivered to Wuhan, where



Figure 2: *Left panel: 4 DCAL modules done at Wuhan for testing the assembly stations and starting the massive production. Right panel: Picture of Wuhan and LNF teams during one module assembly.*

around 200 modules will be assembled to prepare one DCAL super-module. A third assembly station has been sent also to Japan. The Frascati group tested the assembly stations in China and started the module production, teaching all procedures to the chinese colleagues. In Fig. 2 are reported two pictures done during the assembly. Moreover, the Frascati group in 2010 has cutted, ice-polished, aluminized (using a thin film deposition sputtering chamber built for this purpose) at one end all WLS fibers for 1.5 DCAL super-module. A total of about 45000 fibers, grouped in 1200 bundles, with 36 fibers each have been produced at LNF, in collaboration with the Wuhan group. As for EMCAL, each fiber bundle is built of two sub-bundles to match the different path lengths between central and peripheral fibers in the four towers of the single module. The goal is to have all 6 DCAL super-modules assembled, tested and ready to be installed in ALICE as soon as a long shutdown will be available.

#### 4 High Level Trigger

ALICE experimental setup yields a huge sample of data, read out via a few millions of channels from its different sub-detectors with an overall data rate of up to 25 GByte/s which casts a challenge to both storage facilities and offline data analysis. On-line data processing must be applied in order to reduce the data volume and selection of interesting events is implemented to increase the significant information in the recorded data. ALICE applies multi-level hardware scheme via the so-called Central Trigger Processor where fast detectors are used to feed a three-level deep hardware trigger chain. at the end of this trigger chain a fourth filtering stage is introduced: the High-Level Trigger (HLT) able to reduce the data stream to the permanent storage down to 1.25 GB/s. The HLT layer is designed to perform complex event selection functions via fast reconstruction algorithms in order to provide trigger decisions, Regions-of-Interest, and compressed data to the DAQ and to reduce the data rate to permanent storage. In addition to the event selection and triggering tasks, HLT produces online detector performance monitoring histograms (QA) and detector calibration information.

In order to exploit the functionality of the HLT system for the EMCal detector, software components have been developed to be run into the HLT software framework. These components are structured using the publisher/subscriber paradigm used by the HLT software architecture and are targeted on the online reconstruction of photons from the decay of the neutral mesons. At the

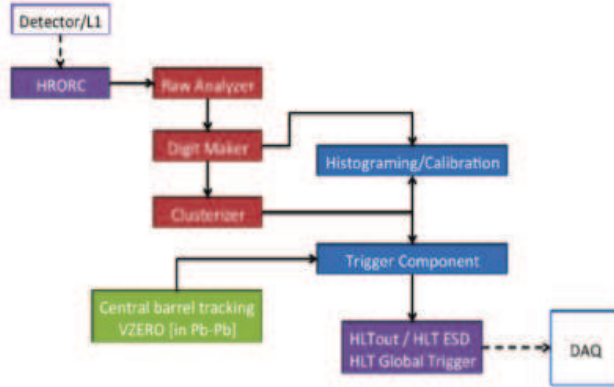


Figure 3: *Functional diagram of the EMCAL analysis chain running online on the ALICE High Lever Trigger (HLT) cluster.*

present stage of the work, the online EMCAL reconstruction chain mainly focus on photon clusters and produce event data both for the online event display and for the storage under the form of HLT ESDs. The chain logic scheme is shown if Fig. 3: the chain has access to a copy the raw data produced by the detector via a direct connection of the HLT readout-receiver cards to the Front End Electronics. During the during data taking, the tower signal extraction is performed by the so called RawAnalyzer component. The signal processing can be done according to different schemes: from a crude peak extraction by subtracting the max of the peak amplitude from the baseline noise to fast-non fitting algorithms. The signal is then digitized by the DigitMaker component which can access the OCDB (Offline Conditions Data Base) in a local copy kept by the HLT in order to perform the correct digit to energy conversion. The output of the DigitMaker is fed to the clusterizer algorithm which provides the reconstructed position and energy for photons in the calorimeter granularity space up to 6-7 GeV/c. The clustering efficiency is closely dependent on the algorithms used in the reconstruction especially for high-multiplicity environments. Different clustering algorithms have been implemented to optimize the reconstruction in the case of pb-pb collisions, where the background is much more present with respect to the p-p case, and further testing is underway. We expect that the more advanced clustering algorithm under development (which can perform cluster deconvolution) will allow us to reconstruct photos from  $\pi^0$  decay up to 12-15 GeV/c.

The chain provides also a basic triggering component which can access the central barrel tracking information (ITS, TRD, TPC). This component will be used in conjunction with the jet reconstruction component (which development is still underway) to access the information on the charged part of the jet . In addition, multiplicity (from V0) and centrality (from ZDC) sensitive components have been developed in HLT which can provide correlation information between the multiplicity and transverse energy deposition as shown in Fig. 4.

In addition to the work described above some technical issues have been solved during the past year to allow the HLT system to run the EMCAL reconstruction chain online. The most prominent one was the implementation of a procedure to handle the calibration triggers generated by the EMCAL within the HLT framework. In fact, in the ALICE L0 triggering scheme, calibration or "software" triggers are generated during the regular physics data taking so the HLT must be aware of the existence of this kind of triggers in order not to confuse them with a physics event.

As mentioned in the intro, besides triggering and event reduction, the HLT system can provide

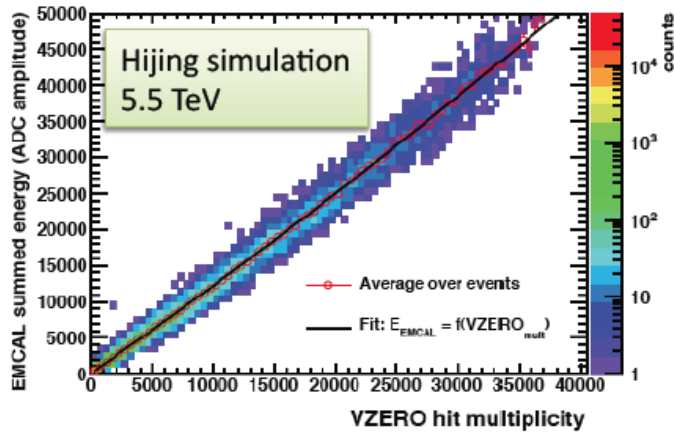


Figure 4: *Correlation of the transverse energy deposited in the EMCAL and multiplicity using the V0 information.*

both online calibration and monitoring. In this view, several histogramming components for the EMCAL have been developed in HLT such those for: cluster energy spectra, track matching,  $\pi^0$  invariant mass spectrum, and  $E_t$  correlations. Obviously the above list is not exhaustive and more work is underway to introduce new monitoring histograms (such as L0 trigger turn on curves) and to refine the one already existent.

Another important task carried on during year 2010 was the inclusion of the EMCAL into the HLT online event display as shown in Fig. 5. This was accomplished by developing and debugging the HLT components to handle the cluster and digit information in the EMCAL geometry. The HLT event display have been extensively used in november 2010 during the first LHC heavy ion run, since it was the only stable event display system at the moment and the only one one able to reconstruct/show the event practically in real time.

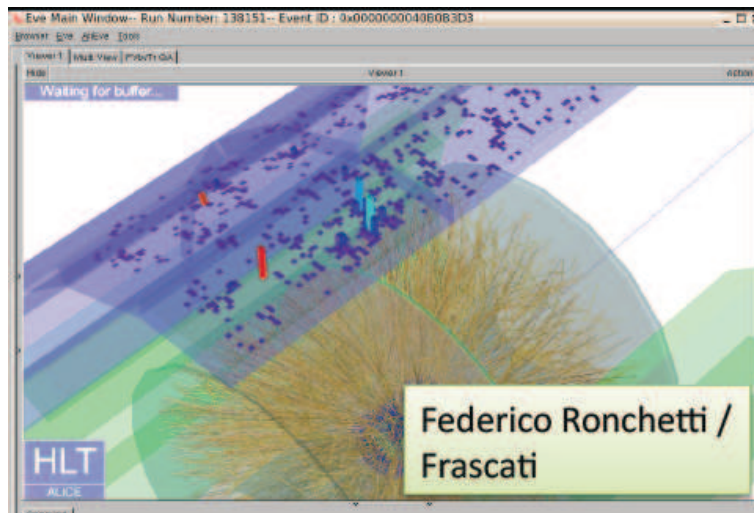


Figure 5: *EMCAL lead-lead hits as reconstructed by the HLT during the first LHC heavy ion run on November 2010.*

On January 2011 the remaining 6 EMCal supermodules have been successfully installed in ALICE and for this reason during the past year an upgrade of the computing power devoted to the EMCal was carried on thanks to a founding request to INFN made by the Frascati group in June 2010 in order to have 5 EMCal dedicated HLT Front End Processors (computing nodes which receive a copy of the event raw data) and 4 general purpose computing nodes (which can run several online tasks, for example, triggering and online calibration). The request was approved and the computing nodes have been installed at the end of 2010. In the same period the responsibility of the EMCal HLT coordination has been taken by the Frascati group.

## 5 Commissioning

During the past year, several tasks related to hardware and software commissioning on the four EMCal super-modules installed in the ALICE cavern have been carried on. More specifically, on the hardware side, firmware performance and debugging tests of the detector readout GTL bus Readout Control Units (RCU) have been carried on for several weeks. The goal was to lower and optimize the overall detector standalone dead time. For year 2010 the EMCal dead time was settled down to  $630 \mu\text{s}$  (1.5 kHz data rate for p-p). Further optimization of the readout dead time and busy handling are still possible using new and more efficient firmware releases which are periodically produced for the TPC readout (which being based on the ALTRO chip is in common with the EMCal). However, due to the industrial obsolescence of the GTL bus chip, a full R&D cycle has been carried on to replace the GTL bus based (serial) readout of the RCUs with a point to point framework, called SRU, Scalable Readout Unit. This approach is much more reliable (being based on more alive industry standards and commodity hardware such as ethernet) than the GTL bus which is also operated out-of-specs. It implements a parallel management of the electronic Front End Cards (FEC) which remain basically untouched. The new readout will be able to bring the EMCal readout rates (in standalone) up to 30 kHz in p-p. This work has been finalized at the end of 2010 with the mezzanine cards installed on each of the EMCal front end cards. A testing phase is foreseen where the two readouts scheme will coexist. We expect that the SRU will be in production by the end of 2011.

On the trigger side, the EMCal L0 trigger signal (0EMC) to the ALICE Central Trigger Processor is now operational. A high statistic run with roughly  $10 \times 10^6$  triggers generated by the detector L0 units has been successfully collected during October 2010. This run is equivalent to  $3 \times 10^9$  sampled MB events and is being used to perform a full tower by tower energy calibration at the level of 2% using the  $\pi^0$  invariant mass spectra.

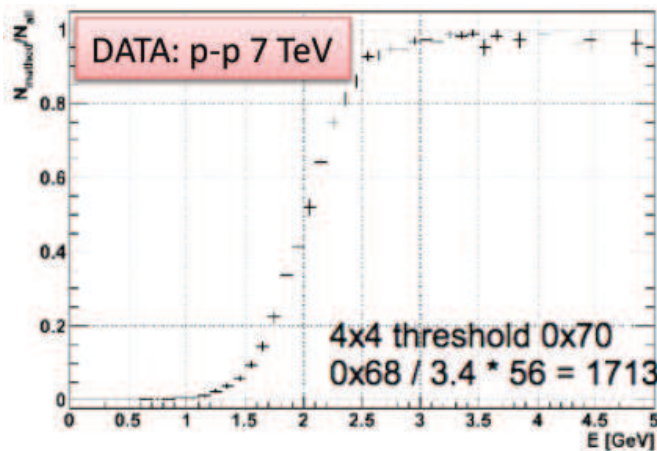


Figure 6: *EMCal L0 trigger turn on curve for p-p data.*

In addition extensive testing of the Heavy Ion (HI) data volumes generated by the installed EMCal supermodules have been carried on to prepare for the November 2010 lead-lead run. The relevant event size for the EMCal was found to be around 123 kB/event + the 7 kB/event generated by the Summary Trigger Unit (STU) which can be handled without particular problems by the ALICE data acquisition system. The STU is the L1 hardware jet trigger finder of the EMCal, and was also extensively debugged and several communication issues between the L0 (TRU) and the STU have been solved or identified.

During the November lead-lead run, the overall collected data was  $13.3 \times 10^6$  Pb+Pb min bias events and  $13.8 \times 10^6$  Pb+Pb high multiplicity accumulated events with the bunch content of the ion beam reaching 114 bunches in ALICE with a luminosity of  $2.5 \times 10^{25} \text{cm}^{-2} \text{s}^{-1}$  (being by design  $10 \times 27 \text{cm}^{-2} \text{s}^{-1}$ ) equivalent to 8kHz).

In addition to the hardware work carried on on the installed supermodules, several software parts have been debugged and commissioned such as the implementation of the EMCal geometry in AliRoot. Corrections to the existing data have been calculated by cleaning up the geometry code and minimizing the cluster-track residuals.

Extensive work have been done on the study of the response uniformity using the installed supermodules in ALICE and, more effectively, using the data specifically obtained during a full test beam period on an up-to-date prototype (conformal to the modules in the cavern) that has been performed at the PS T10 beam-line during the period August 2-16.

The beam-line setup was using a mixed beam with momenta from 0.5 GeV/c to 6 GeV/c. In addition to this beam, a second test beam at the SPS beam-line T2-H4 during the period for August 23-30 was carried on using a beam with momenta from 6 GeV/c to 250GeV/c.

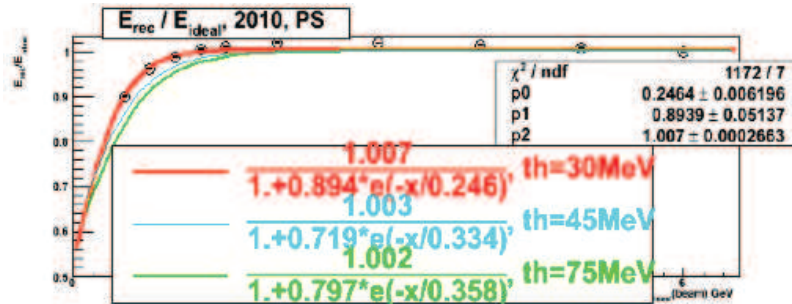


Figure 7: EMCal response for different Zero Suppression (ZS) thresholds as obtained from the PS test-beam data.

The working conditions for the APD gains were determined by the values taken from cosmic calibrations as for super-modules installed at P2 while the operating temperatures were monitored together with LED gains as a function of time. The goal of the test beam setup was to obtain a full characterization of electron and hadron response of the calorimeter as built and operated. Moreover relevant data that is being used to characterize the energy, position, timing resolutions, and for the uniformity of the response as shown in Fig. 7. and its dependency on the Zero Suppression (ZS) threshold (varying ZS=1,2,3,4) has been collected and is being analyzed.

## 6 Offline analysis

In heavy ion collisions jets are the one of the main probe to access the hot medium since the interaction of the scattered partons with the medium induces changes to the internal jet structures

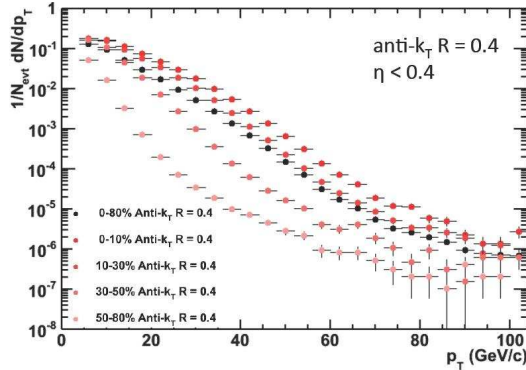


Figure 8: *Raw jet spectrum for PbPb collisions at 2.36 TeV for different centrality values.*

and may alter the jet size. The modification of these properties of the reconstructed jets are the observables for the jet quenching.

The LNF group is responsible for the jet reconstruction algorithms implementation and for the effects induced by the interplay between jet finding and limited acceptance. In 2010, with the first high luminosity pp data and the first PbPb collisions, the efforts were concentrated on the analysis of the inclusive jet cross section using charged particles and the implementation of the neutral signals from the calorimeters. The measurement of jets in high energy heavy ion collisions is more complex than in elementary collisions due to the large fluctuations in the underlying background. The first measurement required in such a program is, indeed, the inclusive jet cross section, which quantifies the degree to which unbiased jet reconstruction has been achieved in practice. The group has produced the first raw jet spectrum in PbPb collisions at 2.36 TeV (Fig. 8) where the background has been subtracted but no unfolding procedure has been applied yet.

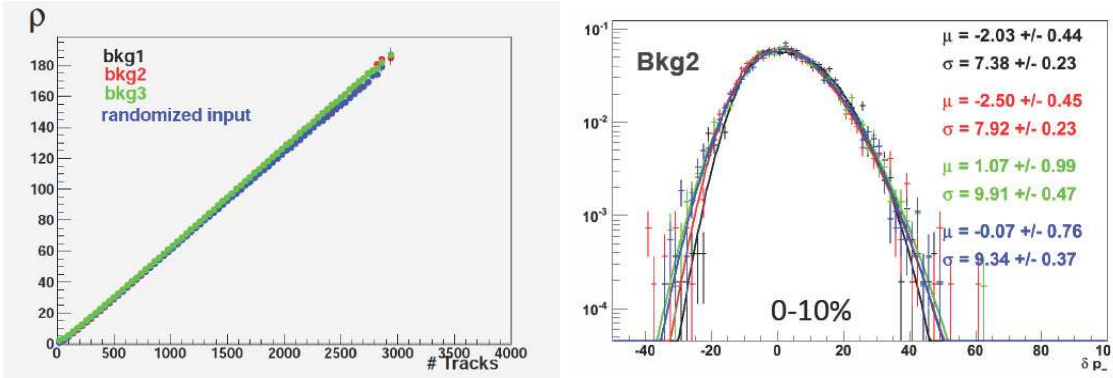


Figure 9: *Left panel: The median background energy density as a function of the number of charged track multiplicity and using three different adaptation of the area method for the systematic uncertainty evaluation.. Right panel: Deconvolution of the background fluctuations for a centrality 0-10% and for different  $p_T$  values (black 20-40 GeV, red 40-60 GeV, green 60-80 GeV, blue 80-100 GeV).*

The LNF group plays also another leading role, been responsible for the measurement of background and its subtraction for the jet signal. Underlying event fluctuations distort the inclusive jet distribution significantly, and the corresponding correction is by far the largest source

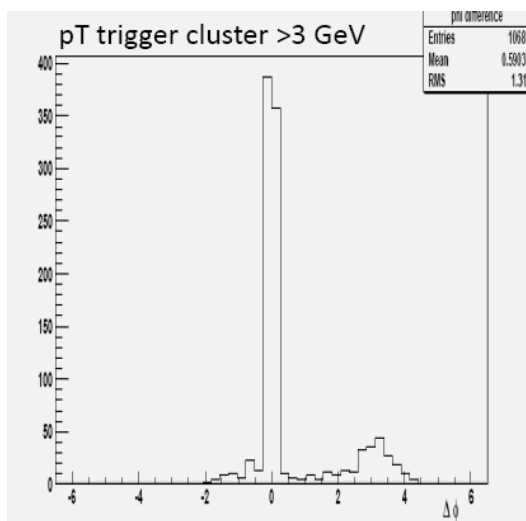


Figure 10: Azimuthal correlation of the EMCAL calorimeter clusters with charged jet reconstruction.

of systematic uncertainty in this measurement. The background correction to the inclusive cross section measurement proceeds in two steps:

1. Event-wise background estimate: reconstruct all jets in the experimental acceptance using the  $k_T$  algorithm with  $R = 0.4$  and determine the median energy density  $\rho$ . This accounts on average for the underlying event background, but not residual fluctuations.
2. Deconvolution of fluctuations: estimate inclusive spectrum distortion due to fluctuations, expressed in terms of bin migration and correct by regularized matrix inversion.

Following point 1, in 0-10% central collisions in ALICE at 2.76 GeV we measure an average level of background of 50 GeV in a jet of  $R = 0.4$ , Fig. 9 (left).

The residual fluctuations discussed at point 2 are currently been parametrized as gaussians of  $\sigma = 9$  GeV, Fig. 9 (right). The study of the sensitivity of the correction to the fragmentation pattern of the jet signal (background smearing should not depend on the fragmentation pattern which is unknown) and non-Gaussian residual tails towards positive fluctuations that can distort the spectrum over a wide  $p_T$  range are under study.

The implementation of the neutral signals, in particular from the large acceptance calorimeter EMCAL, to the jet reconstruction allowed to reconstruct, for the first time, full jets. Unfortunately the calorimeter acceptance was of 40% and only in the 2011 data taking will benefit of the the full installation of the calorimeter. In Fig. 10 is shown the azimuthal correlation of the EMCAL clusters and jet reconstructed by the TPC charged tracks only with  $p_T > 20$  GeV. The peak centered around zero represents the neutral particles inside the jet while the opposite peak is due to the back-to-back dijet events.

## 7 Conferences and Papers

### 7.1 Publications

1. The ALICE Coll., Phys. Rev. Lett. **105**, 252302 (2010).
2. The ALICE Coll., Phys. Rev. Lett. **105**, 252301 (2010).

3. The ALICE Coll., Phys. Lett. B **693**, 5368 (2010).
4. The ALICE Coll., Phys. Rev. D **82**, 052001 (2010).
5. The ALICE Coll., Phys. Rev. Lett. Vol. **105**, No.7, (2010).
6. The ALICE Coll., Eur. Phys. J. C **68**, 345354 (2010).
7. The ALICE Coll., Eur. Phys. J. C **65**, 111 (2010).

## 7.2 Conferences and Talks

1. V. Muccifora, “First Results from ALICE LC10 Workshop on New Physics, November 2010, Frascati.
2. V. Muccifora, “Di-JETCAL : A Di-Jet Electromagnetic Calorimeter for Jet Quenching Study and Electromagnetic Calorimeter for Jet Quenching Study Hadron Physics3 meeting”, September 2010 Parigi.
3. A. Fantoni, “The ALICE Electromagnetic Calorimeter (EMCAL)”, XIV CALOR 2010, May 2010, Beijing.
4. A. Fantoni, “The ALICE Electromagnetic Calorimeter EMCAL: its status and its physics capabilities”, Workshop on discovery Physics at the LHC, December 2010, Kruger Park.
5. L. Cunqueiro, “Progress in MC for quenching and jet hadronization”, Alice Physics Week, May 2010, Paris.
6. L. Cunqueiro, “ALICE First Physics Results”, Light Cone 2010, June 2010, Valencia.
7. L. Cunqueiro, “qPythia/qHERWIG”, Workshop on Jets in Proton-Proton and Heavy Ion Collisions, August 2010, Prague.
8. L. Cunqueiro, “Jet Quenching: probing the hot dense matter”, WISH2010, October 2010, Catania.
9. P. Di Nezza, “Hadron propagation in nuclei”, EIC workshop, April 2010, Argonne.

## JLAB12

M. Aghasyan (Ass.), R. Baldini Ferroli, E. De Sanctis, L. Hovsepyan (Post-doc),  
M. Mirazita, J. de Oliveira Echeimberg (Post-doc), A. Orlandi (Tech.), S. A. Pereira (Art. 23),  
W. Pesci (Tech.), E. Polli, P. Rossi (Resp. Naz.), A. Viticchié (Tech.).

### 1 Introduction

The JLAB12 group participates into the physics program carried on at the 6 GeV Continuous Electron Beam Accelerator Facility (CEBAF) at the Jefferson Laboratory (JLab). The program is focused on the precision study of the structure of the nucleon and the nature of the strong interaction. At present it counts 42 physicists ( $\sim 30$  FTE) plus 25 technicians and it includes groups from the INFN units at: (1) the University of Bari, (2) the University of Catania, (3) the Frascati National Lab and the associated Fermi Center, (4) the University of Genova, (5) the Istituto Superiore di Sanita' and Rome University La Sapienza, and (6) the University of Rome Tor Vergata.

The Frascati JLAB12 group participates into the physics program carried on by the CLAS collaboration in Hall B which counts about 250 physicists from 43 Institutions from 8 Countries.

CEBAF will increase its beam energy from currently 6 GeV to 12 GeV by 2014. This requires the upgrade of the CLAS detector, called CLAS12.

In the period covered by this report the Frascati JLAB12 group has continued to work in the 6 GeV program and in the preparation of the 12 GeV one. In both cases it is focused on the study of the 3D-structure of the nucleon and its internal dynamics. This is achieved through the determination of new parton distribution functions which include information not only on the longitudinal but also on the transverse distributions of partons in a fast moving hadron. This information is encoded in the Generalized Parton Distribution functions (GPDs) and Transverse Momentum Distribution functions (TMDs).

### 2 Transverse Momentum Dependent parton distribution functions (TMDs)

The exploration of the internal structure of the hadrons has undergone enormous progress in the last decades. The investigation both theoretical and experimental of their partonic structure has been extended beyond the universal parton distribution functions (PDFs) and fragmentation functions (FFs) by exploring the parton's motion in the direction perpendicular to the parent hadron's momentum. This study allows the extraction of new types of parton distributions depending on the parton transverse momentum (TMDs). The role of correlations between partonic transverse momentum and spin are crucial for our understanding of the spin structure of the nucleon in terms of the quark and gluon degrees of freedom of QCD. Such spin-orbit correlations give rise to interesting single-spin phenomena in semi-inclusive lepton- and hadron-induced processes. TMDs are probability densities for finding a polarized/unpolarized parton with a longitudinal momentum fraction  $x$  and transverse momentum  $\vec{k}_T$  in a polarized/unpolarized nucleon and they represents a generalization of the partonic momentum, longitudinal and transverse spin distribution functions,  $f_1$ ,  $g_1$ ,  $h_1$ . Two fundamental mechanisms have been identified leading to SSAs in hard processes: the Sivers mechanism <sup>1, 2, 3, 4, 5</sup>, which generates an asymmetry in the distribution of quarks due to orbital motion of partons, and the Collins mechanism <sup>4, 6</sup>, which generates an asymmetry during the hadronization of quarks. TMDs studies are one of the primary goal of experiments at

JLab 12 GeV but their investigation has already started with the 6 GeV beam using unpolarized, longitudinally and transversely polarized target.

## 2.1 The 6 GeV program

### 2.1.1 TMDs studies with a longitudinally polarized target

Data collected with longitudinally polarized  $NH_3$  and  $ND_3$  targets and a 6 GeV polarized electron beam (experiment E05-133) have been calibrated and prepared for the analysis. For a longitudinally polarized target the only azimuthal asymmetry, defined as the ratio of polarized and unpolarized cross-section, arising at leading order is the  $\sin 2\phi$  moment (6, 7, 8)

$$A_{UL}^{\sin(2\phi_h)} = \frac{\sigma_{UL}}{\sigma_{UU}} \quad (1)$$

In Eq. 1 the subscripts in  $\sigma_{UL}$  specify the beam and target polarizations, respectively ( $L$  stands for longitudinally polarized and  $U$  for unpolarized) and the azimuthal angle  $\phi_h$  is the angle between leptonic and hadronic plane. This asymmetry involves the Collins fragmentation function  $H_1^\perp$  and the Ralston-Soper-Mulders-Tangerman (RSMT) distribution function  $h_{1L}^\perp$  (6, 9) describing the transverse polarization of quarks in a longitudinally polarized proton (6, 7, 8, 10). The statistic accumulated in the experiment E05-133 is ten times that of the previous CLAS experiment (11) and will allow us for the first time a statistically significant measurement of the  $\sin 2\phi$  moment.

### 2.1.2 Beam Spin Asymmetry Measurement

During the year 2010 the paper of the beam-spin asymmetry measurement in single neutral semi-inclusive pion electroproduction  $\bar{e}p \rightarrow e'\pi^0 X$ , has been reviewed by the CLAS Collaboration. For this measurement 5.77 GeV polarized electrons with polarization between  $P = 76\%$  and  $83\%$  were scattered off a 2.5 cm long liquid unpolarized hydrogen target. The beam-spin asymmetry,  $A_{LU}^{\sin\phi}$ , in single-pion production off the unpolarized target are higher-twist by their nature (15, 16). The higher twist observables are important for understanding the long-range quark-gluon dynamics.

At fixed and moderate values of the four momentum transfer  $Q^2$  and at large values of  $x_B$  and  $z$  (where  $x_B$  is the fraction of the momentum of the nucleon carried by the struck quark and  $z$  is the fraction of the virtual photon energy carried by the detected  $\pi^0$ ), the contribution of multiparton correlations or higher twist effects increases, eventually leading to a breakdown of the partonic description. Kinematical dependences of observables, will thus provide tests of the applicability of partonic descriptions.

In CLAS the kinematic dependences of the  $\pi^0$  beam-spin asymmetry on  $x_B$ ,  $z$  and  $P_T$  (where  $P_T$  is the transverse momentum of the  $\pi^0$ ) have been measured. The  $\sin\phi$  amplitude, integrating over the  $z$ -range  $0.4 < z < 0.7$ , has been extracted as a function of  $x_B$  and  $P_T$ . The asymmetry shows no significant  $x_B$  - dependence for fixed  $P_T$  range as shown in Fig. 1 (left). The  $A_{UL}^{\sin\phi}$  moment as a function of  $P_T$  is shown in Fig. 1 (right). The  $A_{UL}^{\sin\phi}$  moment increases with increasing  $P_T$  and reaches a maximum at  $P_T$  values of about 0.4 GeV. There is an indication, within available statistics, that the expected decrease of  $A_{UL}^{\sin\phi}$  at larger  $P_T$  could start already at  $P_T$  values of about 0.7 GeV.

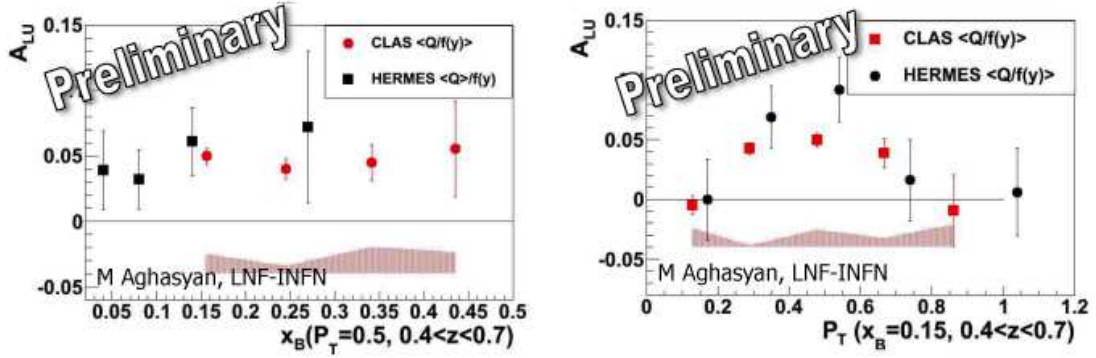


Figure 1: The measured  $\pi^0$  beam-spin asymmetry amplitude  $A_{LL}^{\sin\phi}$  for  $P_T=0.5$  as function of  $x_B$  (left) and for  $x_B=0.15$  as a function of  $P_T$  (right). Both amplitudes are integrated over  $0.4 < z < 0.7$ . Error bars present the statistical and the bands the systematic uncertainties. The CLAS data are compared with the HERMES ones <sup>17)</sup>.

### 2.1.3 Lambda Polarization in Semi-Inclusive Deep Inelastic Scattering

Measurements of  $\Lambda$  polarization in Semi-Inclusive Deep Inelastic Scattering (SIDIS) provide an important probe of the strange sea in the nucleon <sup>18, 19)</sup> and may shed light on the proton spin puzzle. The advantage of detecting  $\Lambda$  in the final state lies in the fact that the  $\Lambda$  is self-analyzing and that it can be used as a  $s$  quark polarimeter since the polarization of  $\Lambda$  is almost completely determined by polarization of its  $s$  quark. Measurements of  $\Lambda$  polarization have been made in deep-inelastic scattering experiments at CERN with  $\sim 44$  GeV  $\nu$  and  $\bar{\nu}$  <sup>20, 21, 22)</sup>, Fermilab with 470 GeV muons <sup>23)</sup> and HERMES with 27.5 GeV positrons <sup>12)</sup>. Non-negligible *positive* longitudinal polarization of  $\Lambda$ , measured with respect to the direction of the momentum transfer from the beam, has been observed in the so-called target fragmentation region,  $x_F = 2P_{\Lambda}^{\parallel}/W < 0$  (being  $W$  the total CM energy and  $P_{\Lambda}^{\parallel}$  is the CM  $\Lambda$  longitudinal momentum). Results in the current fragmentation region ( $x_F > 0$ ) show smaller polarization but have larger error bars. However, new, higher statistics, HERMES results <sup>24)</sup> of the analysis of all the data taken between 1996 and 2005 for  $x_F > 0$  showed nice agreement with NOMAD results for  $x_F < 0$ , thus suggesting that target fragmentation contributions might be relevant also in the current fragmentation region.

The data collected at CLAS with 5.5 GeV beam with longitudinal polarization  $P_B = 0.74 \pm 0.03$  off an unpolarized hydrogen target 5 cm long have been used to measure the  $\Lambda$  polarization transfer in the  $ep \rightarrow e\Lambda X$  semi-inclusive reaction. The invariant mass distribution of the detected  $p$  and  $\pi^-$  shows a clear peak due to the  $\Lambda$  production (see Fig. 2 left), with signal to background ratio between 2 and 5, depending on the cuts used to identify the final particles. Deep inelastic events are selected with the cuts  $Q^2 > 1$  GeV<sup>2</sup> and  $W^2 > 5$  GeV<sup>2</sup>. A cut on the missing mass of the  $ep \rightarrow e'\Lambda X$  reaction above 0.65 GeV (see Fig. 2 right) is applied to remove the dominating  $ep \rightarrow e'\Lambda K^+$  channel and to select inclusive events.

The longitudinal  $\Lambda$  polarization can be written as the sum of a contribution transferred by the incoming beam and an induced term, independent from the beam polarization, and it can be measured by looking at the angular distribution of the decay proton with respect to the virtual photon direction. An unbinned, log-likelihood fit is performed to extract the transferred component as a function of  $x_F$ . The preliminary results are shown in Fig. 3. The  $\Lambda$  polarization is

of the order of about 30% for negative  $x_F$ , while for positive  $x_F$  the data are consistent with zero, even if with large error bars.

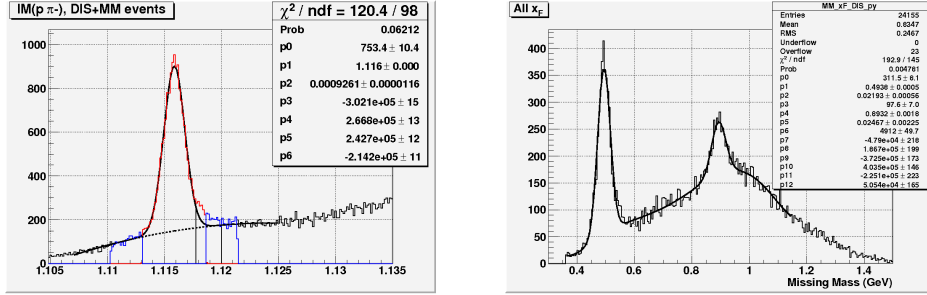


Figure 2: Invariant mass of the detected  $p$  and  $\pi^-$  (left); missing mass of the  $ep \rightarrow e'\Lambda X$  (right). Clearly visible are the  $K^+$  and  $K^{*+}$  peaks.

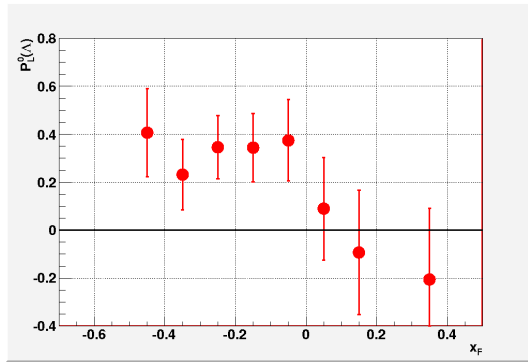


Figure 3: Preliminary results of the longitudinal  $\Lambda$  polarization transfer measured in CLAS as a function of  $x_F$ .

## 2.2 The 12 GeV program

To carry on the physics program at 12 GeV the CLAS detector in Hall B be will be upgraded. The new detector, called CLAS12 optimized for studying exclusive and semi-inclusive reactions, consists of a two-part detector: a Forward Spectrometer and a Central Detector.

The LNF-JLAB12 group has been working in the project of a RICH detector, to be placed in the Forward Spectrometer, to improve the actual CLAS12 Particle Identification (PID) and a neutron detector as a part of the Central Detector.

## 2.3 RICH detector for CLAS12

The RICH detector needs to carry on some measurements of high interests (25, 26, 27) that required a  $\pi/K$  rejection factor of 1:1000 i.e. a  $\pi/K$  separation of 4-5  $\sigma$  at 8 GeV/c. To support this project and discuss the role CLAS12 can play in addressing open questions in the strangeness physics field a workshop has been organized in October 2010 (28).

Several groups are working in the RICH project: from INFN (Bari, Ferrara, Genova, Roma I/ISS), from US (Argonne National Lab) and from UK (Glasgow University). The INFN has positively evaluated the project and in 2009 has started to fund its R&D.

To fit the CLAS12 geometry, the RICH should have a projective geometry with six sectors matching the torus bores and covering scattering angles from 5 to 30 degrees. Being downstream to the torus magnet at more than 5 m from the interaction point, the RICH has to cover a large surface, each sector having an area of the order of  $4 m^2$  in the front and  $8 m^2$  in the back. Being constrained between already existing detectors, the gap depth can not exceed 1 m. The proposed solution is a proximity focusing RICH. The preliminary results of ongoing Monte Carlo analysis show that RICH requirements can be matched by using aerogel as radiator and detecting light in the visible wavelength range. The RICH performances have been studied as a function of aerogel refractive index and thickness, and photon detector pad size (minimum spatial resolution) for several geometry configurations compatible with CLAS12. The study shows that, using a 3 cm thick aerogel with 1.03 refractive index, a pion-kaon separation greater than  $4\sigma$  at 8 GeV/c momentum can be achieved if the detector pad size is less than  $1 \times 1 cm^2$ . The corresponding average number of detected photo-electrons is expected to be around 10. To match a less than  $1 \times 1 cm^2$  photon-detector resolution multi-anode photomultipliers (MA-PMTs) have been considered. Among MA-PMTs, the H8500 MA-PMT by Hamamatsu, although it is not optimized for single-photon detection, is being considered as a suitable option thanks to its excellent packing factor (89 %). Several tests are ongoing on H8500 by various collaborations, with promising results. Another option under study is the R8900. This MA-PMT is optimized for single-photon detection, has a good packing factor (80%) but is quite sensitive to the magnetic field. In CLAS12 at the photon-detector surface a magnetic field of 20-40 gauss is expected so this option has to be considered carefully. The best solution could be the MA-PMT R11265. The R11265 matches all the requirements: it is optimized for single-photon detection, it has an excellent packing factor and it is quite insensitive to the magnetic field. However, although the 64 channels version ( $3 \times 3 mm^2$  pixel) is already available the 16 channels should be developed. The use of aerogel as radiator and the detection of light in the visible wavelength range is an expensive solution. Work is in progress to limit the area of the photon detector to about  $1-1.5 m^2$  per sector. The approach is to instrument a limited area around the beam line to have direct detection in the forward region at high momenta. At larger angles and lower momenta, where the requirements on RICH performances can be loosened, a system of focusing mirrors catch the light and reflect it toward the photon detector.

In 2010 we have order some samples of MA-PMTs by Hamamatsu and started to test the a H8500 MA-PMT held by the Glasgow group.

#### 2.4 Neutron detector for CLAS12

The physics motivation for having a neutron detector is to measure Deeply Virtual Compton Scattering (DVCS) on the neutron, with a deuterium target. The interest for this reaction is strong because it is the most sensitive to the Generalized Parton Distribution (GPD) E which allows, via the Ji's sum rule and with the knowledge of the GPDs H (accessible through DVCS on the proton) the extraction of the orbital angular momentum of the quarks.

This detector has stringent requirements for signal read-out due to the required time resolution ( $\sim 150 ps$ ) to discriminate neutrons from photons, the presence of a high magnetic field (1.5-2 Tesla) and the limited space. Silicon Photomultipliers (SiPM) are a possible solution to fulfill these requirements. This option has been investigated during the year 2010 when tests have been performed using Hamamatsu  $3 \times 3 mm^2$  ( $25 \mu m$  and  $100 \mu m$  pixel) and Hamamatsu  $2 \times 2$  and  $4 \times 4$  matrices ( $6 \times 6 mm^2$  and  $12 \times 12 mm^2$ ) SiPMs. Based on the Sr90 and cosmic ray measurement performed with the SiPM matrix the conclusions were the following:

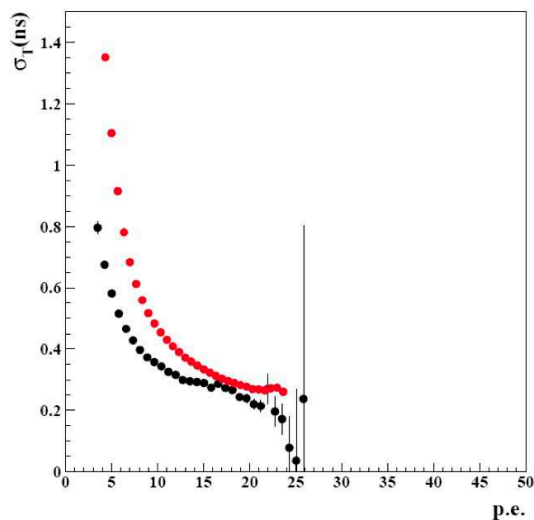


Figure 4: Time resolution as a function of the average charge for matrix channel. The black points show the time resolution obtained by combining the time measured by the 4 channels as a weighted average. The red points show the time resolution achieved by summing the 4 channel signals after the preamplifier and before going to the discriminator.

- the time resolution measured on a single channel of the matrix is completely consistent with what measured on single sensors.
- Combining at the software level the time measured by 4 channels of the matrix leads to an improvement of the time resolution of about a factor 2 as expected.
- Timing resolution of about 500 ps was obtained with 4 channels of this matrix in the cosmic ray setup (see Fig. 4). This was strongly limited by problems with the preamplifiers that we assume can be resolved with a dedicated design of the electronics. Based on the measurement we did with the single sensors we know that the light yield should be about 20 photoelectrons and the single sensor resolution about 600 ps. Using a 16 channel matrix should give us a factor 4 gain, resulting in about 150 ps resolution.

### 3 Publications

1. Baghdasaryan *et al.* and CLAS Coll., Tensor correlations measured in  $3\text{He}(e,e'ppn)$  Phys. Rev. Lett. **105**, 222501 (2010).
2. M. Wood *et al.*, Absorption of the  $\omega$  and  $\phi$  mesons in nuclei, Phys. Rev. Lett. **105**, 112301 (2010).
3. B. Dey *et al.*, Differential cross sections and recoil polarizations for the reaction  $\gamma p \rightarrow K^+\Sigma^0$ , Phys. Rev. C **82**, 025202 (2010).
4. H. Avakian *et al.*, Measurement of single and double spin asymmetries in deep inelastic pion electroproduction with a longitudinally polarized target, Phys. Rev. Lett. **105**, 26 (2010).

5. Y. Ilieva *et al.*, Evidence for a backward peak in the  $\gamma d \rightarrow \pi^0 d$  cross section near the  $\eta$  threshold, *Eur. Phys. Jour. A* **43**, 261 (2010).
6. M. Osipenko *et al.*, Measurement of the nucleon structure function  $F_2$  in the nuclear medium and evaluation of its moments, *Nucl. Phys. A* **845**, 1 (2010).
7. S. Anefalos Pereira *et al.*, Differential cross section of  $\gamma n \rightarrow K^+ \Sigma^-$  on bound neutrons with incident photons from 1.1 to 3.6 GeV, *Phys. Lett. B* **688**, 289 (2010).
8. M. McCracken *et al.*, Differential cross section and recoil polarization for the  $\gamma p \rightarrow K^+ \Lambda$  reaction using CLAS, *Phys. Rev. C* **81**, 025201 (2010).

#### 4 Presentation at Conferences, Workshops, Seminars

1. P. Rossi, *Transverse spin physics at Hall B*, “XVIII International Workshop on Deep Inelastic Scattering and Related Subjects” - Firenze (Italy), April 19-23, 2010. Invited talk.
2. P. Rossi, *Studies of TMDs with CLAS and CLAS12*, -“Exclusive Reactions at High Momentum Transfer IV” - Newport News (VA-USA), May 18-21, 2010. Invited talk.
3. P. Rossi, *Recent results on SIDIS from pion production at CLAS*, “MENU 2010” - Williamsburg (VA-USA), May 31-June 4, 2010. Invited talk.
4. S. A. Pereira, *Hyperon Production and Polarization with CLAS at Jefferson Lab*, - “SPIN-PRAHA-2010” - Prague (Czech Republic), July 18 - 24, 2010. Invited talk.
5. M. Mirazita, *Physics perspectives at JLab with 12 GeV beam*. “XCVI Congresso Nazionale di Fisica”, Bologna (Italy), September 20-24, 2010. Invited talk.
6. M. Aghasyan *Studies of Spin-Orbit Correlations at JLab*. “SPIN2010 19th International Spin Physics Symposium” - Jlich (Germany), September 27 October 2, 2010. Contributed talk.
7. M. Mirazita, *Lambda polarization measurements in SIDIS* “PSHP”, Frascati (Italy), October 18-21, 2010. Invited talk.
8. P. Rossi, *TMD flavor decomposition at CLAS12*. “BARYONS’10” - Osaka (Japan), December 7- 11, 2010. Invited talk.

#### References

1. D. W. Sivers, *Phys. Rev.* **D43**, 261 (1991).
2. M. Anselmino and F. Murgia, *Phys. Lett.* **B442**, 470 (1998), hep-ph/9808426.
3. S.J. Brodsky, D.S. Hwang and I. Schmidt, *Phys. Lett.* **B530**, 99 (2002), hep-ph/0201296.
4. J.C. Collins, *Phys. Lett.* **B536**, 43 (2002), hep-ph/0204004.
5. X.d. Ji and F. Yuan, *Phys. Lett.* **B543**, 66 (2002), hep-ph/0206057.
6. P.J. Mulders and R.D. Tangerman, *Nucl. Phys.* **B461**, 197 (1996), hep-ph/9510301.
7. A. Kotzinian, *Nucl. Phys.* **B441**, 234 (1995), hep-ph/9412283.
8. A. Kotzinian and P.J. Mulders, *Phys. Rev.* **D54**, 1229 (1996), hep-ph/9511420.

9. J.P. Ralston and D.E. Soper, Nucl. Phys. **B152**, 109 (1979).
10. E. Di Salvo, Int. J. Mod. Phys. **A22**, 2145 (2007), hep-ph/0603005.
11. H. Avakian *et al.*, and CLAS collaboration, Phys. Rev. Lett. **105**, 262002 (2010).
12. A. Airapetian *et al.* [HERMES Collaboration], Phys. Rev. **D64**, 112005 (2001) hep-ex/9911017; S. Belostotski, *IXth Workshop on High-Energy Spin Physics*, Dubna, Russia, Aug 2 - 7, 2001.
13. H. Avakian *et al.*, Phys. Rev. D **77**, 014023 (2008), arXiv:hep-ph/0709.3253
14. A. V. Efremov, K. Goeke, and P. Schweitzer, Phys. Rev. D **67**, 114014 (2003), arXiv:hep-ph/0208124.
15. A. Afanasev and C.E. Carlson, (2003), hep-ph/0308163.
16. F. Yuan, Phys. Lett. **B589**, 28 (2004), hep-ph/0310279.
17. HERMES, A. Airapetian *et al.*, (2006), hep-ex/0612059.
18. J. Ellis, D. E. Kharzeev and A. Kotzinian, Z. Phys. **C69**, 467 (1996).
19. W. Melnitchouk and A. W. Thomas, Z. Phys. **A353**, 311 (1996).
20. P. Astier *et al.*, [NOMAD Collaboration], Nucl. Phys. **B588**, 3 (2000); D. V. Naumov [NOMAD Collaboration], AIP Conf. Proc. **570**, 489 (2001), hep-ph/0101325.
21. S. Willocq *et al.*, (WA59 Collaboration), Z. Phys. **C53**, 207 (1992).
22. V. Ammosov *et al.*, Nucl. Phys. **B162**, 208 (1980).
23. M. R. Adams *et al.* [E665 Collaboration], Eur. Phys. J. **C17**, 263 (2000), hep-ex/9911004.
24. D. Veretennikov, DIS2010 Conference.
25. PR-09-008 “Studies of the Boer-Mulders Asymmetry in Kaon Electroproduction with Hydrogen and Deuterium Targets”;  
[http://www.jlab.org/exp\\_prog/PACpage/PAC34/agenda.pdf](http://www.jlab.org/exp_prog/PACpage/PAC34/agenda.pdf).
26. PR-09-009 “Studies of Spin-Orbit Correlations in Kaon Electroproduction in DIS with polarized hydrogen and deuterium Targets”;  
[http://www.jlab.org/exp\\_prog/PACpage/PAC34/agenda.pdf](http://www.jlab.org/exp_prog/PACpage/PAC34/agenda.pdf).
27. PR-09-007 “Studies of partonic distributions using semi-inclusive production of kaons”;  
[http://www.jlab.org/exp\\_prog/PACpage/PAC34/agenda.pdf](http://www.jlab.org/exp_prog/PACpage/PAC34/agenda.pdf).
28. <http://www.lnf.infn.it/conference/pshp2010/index.html>

## KAONNIS

M. Bazzi (Ass. Ric.), M. Bragadireanu (Bors. UE), A. Clozza,  
C. Curceanu Petrascu (Resp. Naz.), A. D'Uffizi (Ass. Ric.), C. Guaraldo (Art. 2222),  
M. Iliescu (Assoc.), P. Levi Sandri, F. Lucibello (Tecn.), S. Okada (Bors. PD),  
D. Pietreanu (Ass. Ric.), K. Piscicchia ( Bors.), M. Poli Lener (Art. 23), A. Rizzo (Bors.),  
A. Romero Vidal (Bors PD), E. Sbardella (Bors.), A. Scordo (Bors.), D. Sirghi (Art. 23),  
F. Sirghi (Bors. UE), O. Vazquez Doce (Art. 23)

### 1 The KAONNIS scientific program

KAONNIS represents an integrated activity in the field of low-energy kaon-nucleon/nuclei interaction studies. It, basically, contains the following scientific lines:

- the study of kaonic atoms by the SIDDHARTA experiment
- the study of kaon-nuclei interaction at low energies in the framework of AMADEUS.

We briefly present in what follows these scientific lines, together with 2010 activities and 2011 plans.

### 2 The SIDDHARTA experiment

The objective of the SIDDHARTA (Silicon Drift Detector for Hadronic Atom Research by Timing Application) experiment and of its successor, SIDDHARTA2, is to performing precision measurements of X-ray transitions in exotic (kaonic) atoms at DAΦNE.

The precise determination of the shift and width of the  $1s$  level with respect to the purely electromagnetic calculated values, in kaonic hydrogen and kaonic deuterium, generated by the presence of the strong interaction, through the measurement of the X-ray transitions to this level, will allow the first precise experimental determination of the isospin dependent antikaon-nucleon scattering lengths, fundamental quantities in understanding low-energy QCD in strangeness sector.

The shift  $\epsilon$  and the width  $\Gamma$  of the  $1s$  state of kaonic hydrogen are related to the real and imaginary part of the complex  $s$ -wave scattering length,  $a_{K^-p}$ , through the Deser formula (in the isospin limit):

$$\epsilon + i\Gamma/2 = 2\alpha^3 \mu^2 a_{K^-p} = (412 \text{ eV fm}^{-1}) \cdot a_{K^-p} \quad (1)$$

where  $\alpha$  is the fine structure constant and  $\mu$  the reduced mass of the  $K^-p$  system. In the isospin limit, i.e. in the absence of the electromagnetic interaction and at  $m_d = m_u$ ,  $a_{K^-p}$  can be expressed directly in terms of the scattering lengths for isospin  $I=0$  and  $I=1$ :

$$a_{K^-p} = \frac{1}{2}(a_0 + a_1) \quad (2)$$

A similar relation applies to the case of kaonic deuterium and to the corresponding scattering length  $a_{K^-d}$ :

$$\epsilon + i\Gamma/2 = 2\alpha^3 \mu^2 a_{K^-d} = (601 \text{ eV fm}^{-1}) \cdot a_{K^-d} \quad (3)$$

An accurate determination of the  $K^-N$  isospin dependent scattering lengths will place strong constraints on the low-energy  $K^-N$  dynamics, which, in turn, constraints the  $SU(3)$  description of chiral symmetry breaking in systems containing the strange quark.

The DEAR measurement on kaonic hydrogen, performed in 2002 (Phys. Rev. Lett 94 (2005), 212302):

$$\epsilon = -193 \pm 37(stat.) \pm 6(syst.) eV \quad (4)$$

$$\Gamma = 249 \pm 111(stat.) \pm 39(syst.) eV. \quad (5)$$

has already triggered an increased activity of the theoretical groups working in the low-energy kaon-nucleon interaction field, as well as in more general non-perturbative QCD.

The SIDDHARTA(2) experiment aims to improve the precision obtained by DEAR and to perform the first measurement ever of kaonic deuterium. SIDDHARTA has performed, as well, accurate measurements on kaonic helium transitions to the 2p level (L-series). The kaonic helium 3 was measured for the first time - see below,

## 2.1 The SIDDHARTA setup

SIDDHARTA represents a new phase in the study of kaonic atoms at DAΦNE. The DEAR precision was limited by a signal/background ratio of about 1/70. To significantly improve this ratio, a breakthrough is necessary. An accurate study of the background sources present at DAΦNE was redone. The background includes two main sources:

- synchronous background: coming together with the kaons – related to  $K^-$  interactions in the setup materials and also to the  $\phi$ -decay processes; it can be defined as hadronic background;
- asynchronous background: final products of electromagnetic showers in the machine pipe and in the setup materials originating from particles lost from primary circulating beams either due to the interaction of particles in the same bunch (Touschek effect) or due to the interaction with the residual gas.

Accurate studies performed by DEAR showed that the main background source in DAΦNE is of the second type, which shows the way to reduce it. A fast trigger correlated to a kaon entering into the target would cut the main part of the asynchronous background.

X rays were detected by DEAR using CCDs (Charge-Coupled Devices), which are excellent X-ray detectors, with very good energy resolution (about 140 eV FWHM at 6 keV), but having the drawback of being non-triggerable devices (since the read-out time per device is at the level of 10 s). A recently developed device, which preserves all good features of CCDs (energy resolution, stability and linearity), but additionally is triggerable - i.e. fast (at the level of  $1\mu s$ ), was implemented. This new detector is a large area Silicon Drift Detector (SDD), specially designed for spectroscopic application. The development of the new  $1\text{ cm}^2$  SDD device, together with readout electronics and very stable power supplies, was partially performed under the Joint Research Activity JRA10 of the I3 project “Study of strongly interacting matter (HadronPhysics)” within FP6 of the EU.

The trigger in SIDDHARTA was given by a system of scintillators which recognized a kaon entering the target making use of the back-to-back production mechanism of the charged kaons at DAΦNE from  $\phi$  decay: of the type:

$$\phi \rightarrow K^+ K^-. \quad (6)$$

The SIDDHARTA setup contains 144 SDD chips of  $1\text{ cm}^2$  each, placed around a cylindrical target, containing high density cryogenic gaseous hydrogen (deuterium or helium). The target was made of kapton,  $75\mu m$  thick, reinforced with aluminium grid.

The SIDDHARTA setup was installed on DAΦNE in late summer 2008, see Fig. 1 - and the period till the end of 2008 was used to debug and optimize the setup performances (degrader optimization included). The kaonic atoms (hydrogen, deuterium, helium4 and 3) measurements were done in 2009.

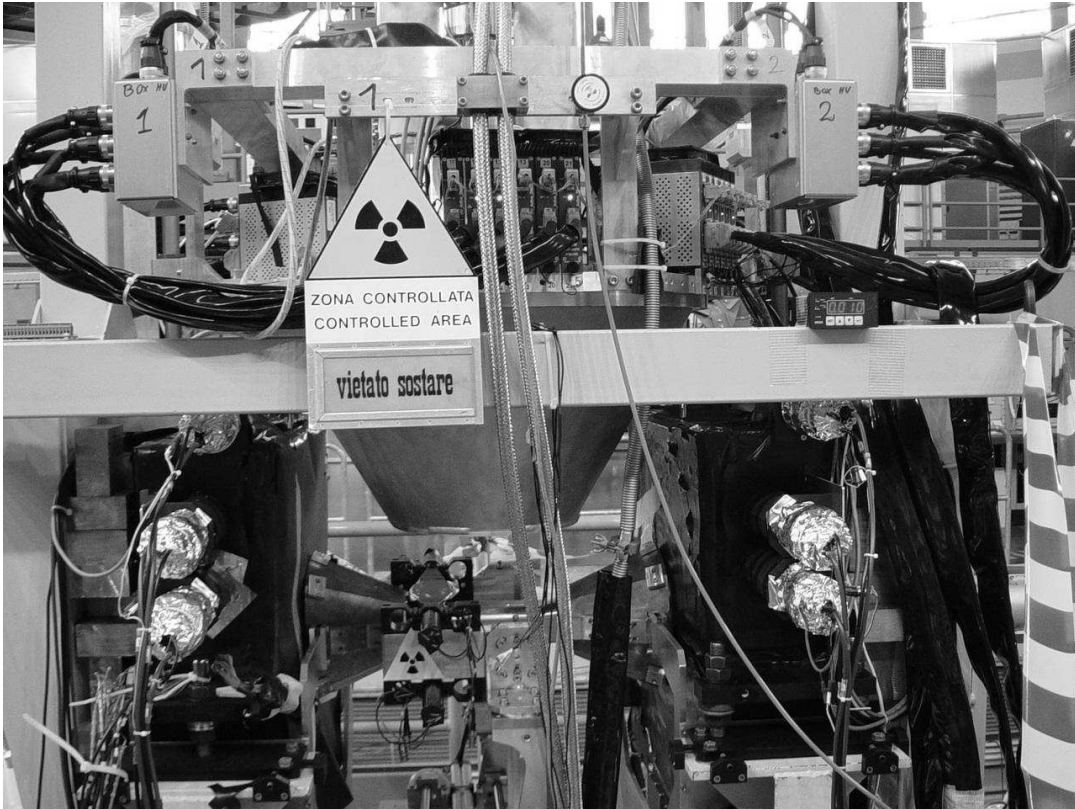


Figure 1: *The SIDDHARTA setup installed at DAΦNE.*

## 2.2 SIDDHARTA activities in 2010

SIDDHARTA was in data taking until 9 November 2009. In 2010 the group activity was dedicated to kaonic helium 3 and haonic hydrogen data analyses, and to the preparation of a proposal for the upgrade of the setup, SIDDHARTA2, to perform in the future the kaonic deuterium and other precision kaonic atoms measurements.

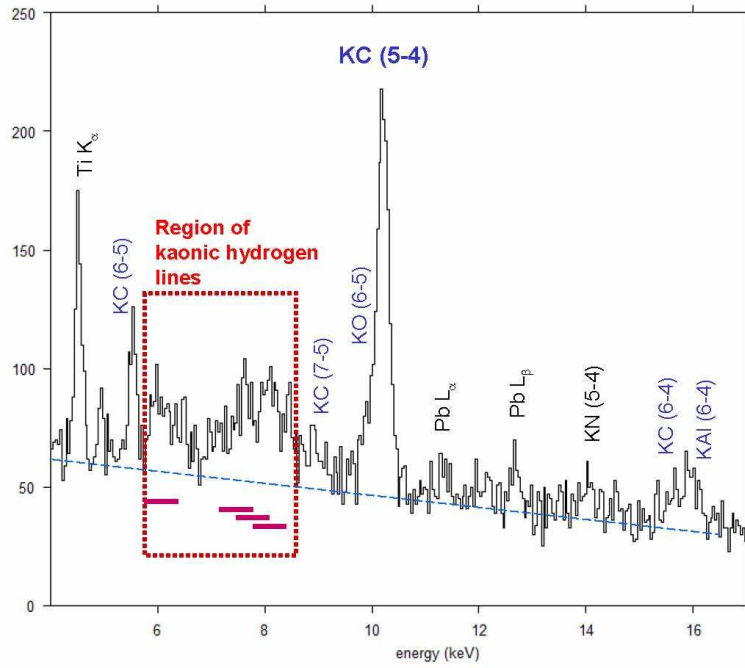
### 2.2.1 Kaonic hydrogen measurement

The kaonic hydrogen measurement was performed in the period 15 March - 31 July 2009 and during October 2009, for a total of about  $400 \text{ pb}^{-1}$  of integrated luminosity.

In Fig. 2 we present a preliminary triggered kaonic hydrogen spectrum, where kaonic hydrogen transitions to the 1s level (K-series) are clearly seen. Data analyses are presently over and a paper in preparation.

### 2.2.2 Kaonic helium 3 measurement

In the last days of data taking, early November 2009, we measured for the first time ever the kaonic helium3 L-transitions. The total integrated luminosity for this measurement was about  $10 \text{ pb}^{-1}$ . The data analysis is over, and produced the spectrum shown in Fig. 3. A paper was published in Phys. Lett. B697 (2011) 199.



2

Figure 2: The Kaonic Hydrogen triggered spectrum. The kaonic Hydrogen transitions are clearly visible. In red the e.m. position of the lines.

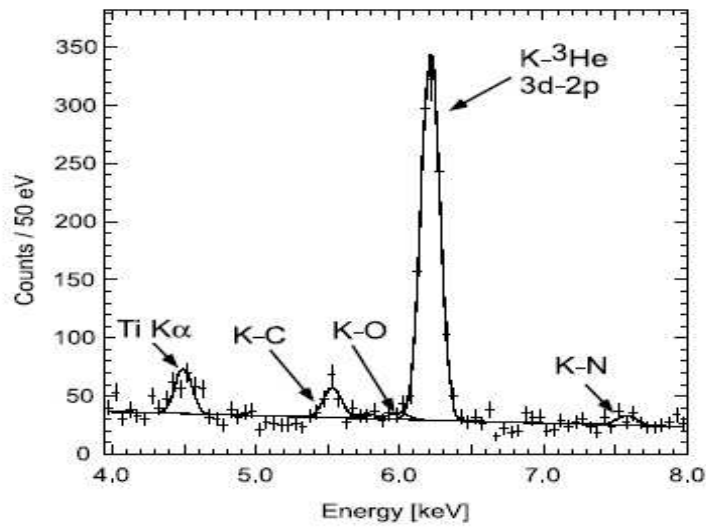


Figure 3: The Kaonic helium3 triggered spectrum where the 6.2 keV line of kaonic helium transitions is clearly visible.

### 2.2.3 ECT\* Workshop organization

In the period 4-8 October 2010 the Workshop entitled “Strangeness in Nuclei” was organized, having Catalina Curceanu as main Organizer, at the ECT\* in Trento. The Workshop was very successful. For more details see CERN Courier, Volume 51, January/February 2011.

### 2.2.4 SIDDHARTA2

In 2010 the proposal for the SIDDHARTA upgrade was put forward. The upgrade concerns mainly the cryogenic system, the target, the shielding and the trigger system, and is going to improve on the signal and signal/background ratio such as to allow the kaonic deuterium and other exotic atoms measurements in the near future.

More details can be found in the presentations to the LNF International Scientific Committee on the LNF-INFN web-site.

## 2.3 Activities in 2011

The LNF group main activities in SIDDHARTA for 2011 are the following ones:

- publication of the kaonic hydrogen data;
- finalize analyses of kaonic deuterium data and publish them;
- Monte Carlo simulations for the final definition of the SIDDHARTA2 setup;
- construction of the SIDDHARTA2 setup;
- definition of the strategy for SIDDHARTA2 measurements (including interaction region definition and construction).

To be mentioned that the SIDDHARTA scientific program is important part of the Network LEANNIS (WP9) in the framework of the EU FP7 HadronPhysics2 program.

## 3 The AMADEUS experiment

The AMADEUS experiment plans to perform a complete study of the interaction of low-energy charged kaons with nuclei, by using various cryogenic gaseous targets, as: deuterium, helium 3 and helium 4. In particular, AMADEUS plans to study, in formation and decay, the so-called “deeply bound kaonic nuclei”, if existent (the scientific case is strongly debated presently). The AMADEUS collaboration plans to implement inside the KLOE drift chamber a dedicated setup, containing a beam pipe, a target and a trigger system and, maybe, an inner additional tracker. The scientific case of AMADEUS, as well as R&D performed on various items were presented in various LNF Scientific Committees and can be found on the respective dedicated web pages.

### 3.1 AMADEUS activities in 2010

The main activities of AMADEUS in 2010 concerned:

- R&D for the cryogenic target;
- R&D for the trigger system: a prototype was built based on scintillating fibers read by Silicon PhotoMultipliers (see Fig. 4) and tested in the laboratory and PSI pion beam:

- R&D for the inner tracker - a small TPC-GEM prototype was built, Fig. 5, and is being presently tested:
- Monte Carlo simulations:
- KLOE data analyses for the data 2002-2005 to search for processes generated by stopped kaons in the Drift Chamber volume (which contains helium) - see paper list and LNF Scientific Committee presentations.

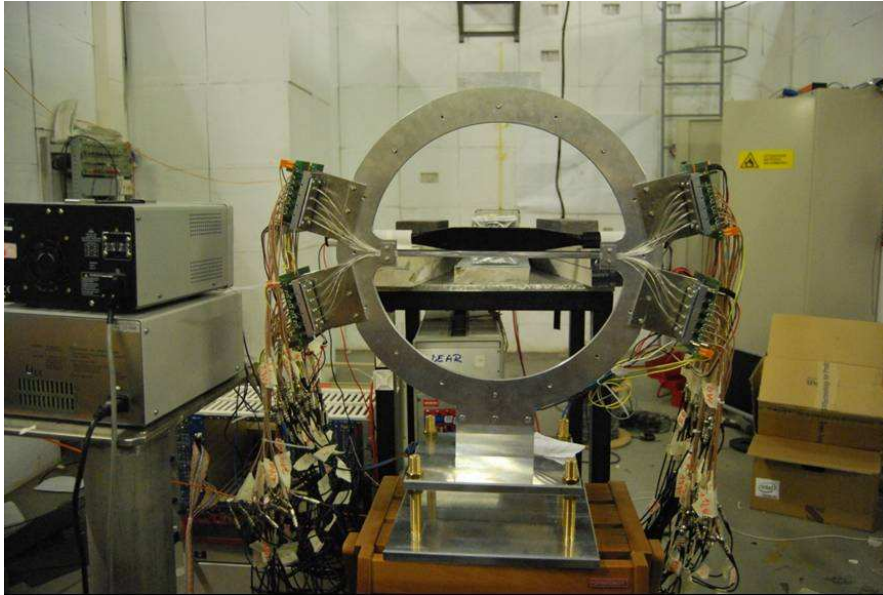


Figure 4: *The AMADEUS trigger prototype, based on scintillating fibers read at both ends by SiPM.*



Figure 5: *The TPC-GEM prototype.*

### 3.2 AMADEUS activities in 2011

The main activities of AMADEUS in 2011 will be

- continuation of the R&D for the cryogenic target:
- continuation of the R&D for the trigger system: tests of the prototype and readout electronics at BTF-LNF and PSI:
- continuation of the R&D for the inner tracker: tests of the prototype at BTF-LNF and PSI
- Monte Carlo simulations:
- finalization of the KLOE data analyses and publication
- definition of the experiment strategy

To be mentioned that the AMADEUS activities are supported is important in the framework of the EU FP7 HadronPhysics2 as WP24 (GEM), WP28 (SiPM) and WP9 (Network on kaon-nuclei interaction studies at low energies) program.

#### Acknowledgements

The support from HadronPhysics2 FP7 (227431) projects is acknowledged.

## 4 Publications

### 4.1 List of Conference Talks

1. K. Piscichia, “Kaon nuclei interaction studies at low energies (the AMADEUS experiment)” BEACH 2010, 21-26 June 2010, Perugia, Italy.
2. A. Scordo, “MPPC and Scintillating fibers: report from LNF-INFN group”, Hadron Physics 2 WP29 group meeting, 7 June 2010, Pisa, Italy.
3. A. Scordo, “First detection of kaons with MPPS and SciFi at DAΦNE collider”, XLVII International Winter Meeting on Nuclear Physics, 25-29 January 2010, Bormio, Italy.
4. S. Okada, “Experimental studies on kaonic atoms at DAΦNE”, BARYONS2010, 7-11 December 2010, Osaka, Japan.
5. S. Okada, “Kaonic hydrogen results from SIDDHARTA”, Strangeness in Nuclei, 4-8 October 2010, ECT\* Trento, Italy.
6. S. Okada, “Kaonic Atoms at DAΦNE”, The many facets of QCD, 1-5 November 2010, Gent, Belgium.
7. S. Okada, “X-ray spectroscopy of kaonic atoms at DAΦNE”, HSQCD, 5-9 July 2010, Gatchina, Russia. S. Okada, “X-ray spectroscopy of kaonic atoms at DAΦNE”, poster at INPC 2010, 4-9 July, TRIUMF, Canada.
8. O. Vazquez Doce, “Search for the kaonic clusters at DAΦNE: KLOE and AMADEUS”, BARYONS2010, 7-11 December 2010, Osaka, Japan.
9. O. Vazquez Doce, “Kaonic atoms/nuclei studies at DAΦNE: SIDDHARTA and AMADEUS experiments”, Quark Confinement and the Hadron Spectrum IX, September 2010, Madrid, Spain.

10. O. Vazquez Doce, "Analysis of the hadronic interactions of negative kaons in the KLOE experiment data", seminar at the SMI-Vienna, November 2010, Vienna, Austria.
11. O. Vazquez Doce, "Kaonic atoms/nuclei studies at DAΦNE: SIDDHARTA and AMADEUS experiments", Strangeness production in Hadron Collisions, FOPI Collaboration Meeting, TUM, Munchen, May 2010, Munchen, Germany.
12. O. Vazquez Doce, "Scintillating fibers coupled to MPPC detectors", MAPD2010, Second G-APD workshop WP28 of HadronPhysics2 FP7, February 2010, Prague, Czech Republic.
13. M. Ilescu, "Kaon-nucleon strong interaction in kaonic atoms (SIDDHARTA experiment)", QCD2010, 28 June-2 July 2010, Montpellier, France.
14. A. Romero Vidal, "X-ray spectroscopy of kaonic atoms at DAΦNE", MESON2010, 10-15 June 2010, Cracow, Poland.
15. D. Sirghi, "Kaonic helium measurements in SIDDHARTA experiment", MESON2010, 10-15 June 2010, Cracow, Poland.
16. D. Sirghi, "The SIDDHARTA experiment, general overview", Strangeness in Nuclei, 4-8 October 2010, ECT\* Trento, Italy.
17. C. Curceanu, "The SIDDHARTA2 experiment at DAΦNE", Strangeness in Nuclei, 4-8 October 2010, ECT\* Trento, Italy.
18. C. Curceanu, "Low energy kaon-nucleon/nuclei interaction studies at DAΦNE (SIDDHARTA and AMADEUS)", EFB21, 29 August - 3 September 2010, Salamanca, Spain.
19. A. Rizzo, "Kaonic atoms studies in the SIDDHARTA experiment at DAΦNE collider: present results and future perspectives", SIF - XCVI Congresso Nazionale Bologna, 20-24 September 2010, Bologna, Italy.
20. A. Clozza, "Kaon-nuclei interaction studies at low energies (the AMADEUS experiment)", SIF - XCVI Congresso Nazionale Bologna, 20-24 September 2010, Bologna, Italy.
21. M. Bazzi, "Experimental test for a trigger prototype for the AMADEUS experiment", SIF - XCVI Congresso Nazionale Bologna, 20-24 September 2010, Bologna, Italy.

#### 4.2 Papers and Proceedings

1. C. Curceanu *et al.*, "Nuclear strangeness comes to Trento", CERN Courier, Volume 51, January/February 2010, Number 1.
2. M. Ilescu *et al.*, "Kaon-nucleon strong interaction in kaonic atoms (SIDDHARTA experiment)", Nucl. Phys. B, vol. **207-208**, 208 (2010).
3. J. Zmeskal *et al.*, "The AMADEUS experiment - precision measurements of low-energy antikaon-nucleon/nucleus interactions", Nucl. Phys. **A 835**, 410 (2010).
4. M. Cargnelli *et al.*, "Kaonic atoms studies at DAΦNE by the SIDDHARTA experiment", Nucl. Phys. **A 835**, 27 (2010).
5. A. Bazzi *et al.*, "First measurement of kaonic helium-3 X-rays", Phys. Lett. **B697**, 199 (2011).

6. T. Ishiwatari *et al.*, “Precision spectroscopy of light kaonic atom X-rays in the SIDDHARTA experiment”, AIP Conf. Proc. **1322**, 468 (2010).
7. M. Bazzi *et al.*, “Kaonic atoms measurement at DAΦNE by SIDDHARTA”, PoS BORMIO2010:035 (2010).
8. T. Ishiwatari *et al.*, “Precision spectroscopy of kaonic helium-3 and helium-4 3d to 2p X-raus”, AIP Conf. Proc. **1257**, 765 (2010).
9. T. Hiraiwa *et al.*, “A search for deeply bound kaonic nuclear states at J-PARC”, AIP Conf. Proc. **1257**, 755 (2010).
10. M. Poli Lener, “Performances of a GEM-based TPC prototype for new high-rate particle experiment”, Nucl. Instr. & Meth. **A617**, 183 (2010).
11. O. Vazquez Doce, *et al.*, “Low energy kaon nuclei interaction studies at DAΦNE”, EPJ Web Conf 3, 03021 (2010).
12. M. Anelli *et al.*, “Measurement of the neutron detection efficiency of a 80calorimeter”, arXiv:1004.2241.
13. C. Curceanu and J. Marton, “Mini-Proceedings ECT\* Workshop Hadronic Atoms and Kaonic Nuclei: Solved puzzles, open problems and future challenges in theory and experiment”, arXiv:1003.2328.
14. A. Scordo *et al.*, “First detection of kaons with scintillating fibers read by MPPC at the DAΦNE collider”, PoS BORMIO2010:019 (2010).
15. O. Vazquez Doce “Study of the hadronic interactions of kaons in light nuclei at DAΦNE”, AIP Conf. Proc. **1257**, 741 (2010).

## $\bar{P}$ ANDA - $\bar{p}$ Annihilation at Darmstadt

A. M. Bragadireanu (Ass.), B. Dulach (Ass.), P. Gianotti (Resp. Naz.), M. Giardoni, C. Guaraldo (Ass.), M. A. Iliescu (Ass.), V. Lucherini, D. Orecchini (Tec.), E. Pace, L. Passamonti (Tec.), D. Pierluigi (Tec.), A. Russo (Tec.), D. L. Sirghi Diana (Ass.)

### 1 Introduction

$\bar{P}$ ANDA is one of the biggest future experiments in hadron and nuclear physics that will be carried out at the new Facility for Antiproton and Ion Research (FAIR) at Darmstadt, Germany. It is dedicated to the study of the annihilations of antiprotons on nucleons and nuclei up to a maximum center-of-mass energy in  $\bar{p}p$  of 5.5 GeV.

Presently, the  $\bar{P}$ ANDA collaboration consists of 400 physicists from 16 countries spread all over the world. The Italian groups involved are: Torino, University, Politecnico and INFN, Trieste, University and INFN, Genova INFN, Pavia, University and INFN, Ferrara, University and INFN, Frascati INFN laboratory, Catania, University and INFN. The LNF group is involved in the design and construction of the central tracker of the  $\bar{P}$ ANDA detector.

### 2 $\bar{P}$ ANDA experiment

A new facility for hadronic physics is under construction in Germany. It consists of a major upgrade of the presently running GSI accelerator complex of Darmstadt <sup>1)</sup>. An intense, high momentum

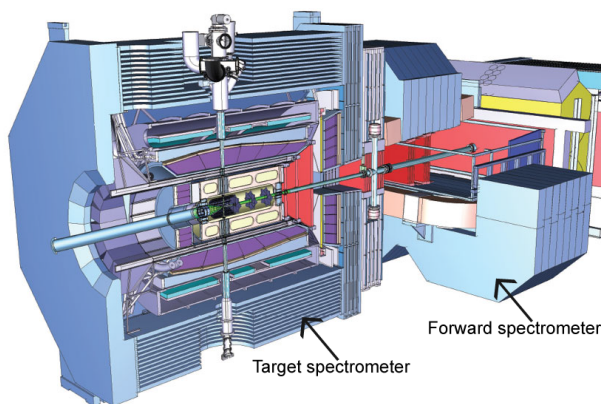


Figure 1: A schematic view of the  $\bar{P}$ ANDA apparatus consisting of two distinct detectors: the target spectrometer (left) and the forward spectrometer (right).

resolution antiproton beam, with momenta between 1.5 and 15 GeV/c, will be available at the High Energy Storage Ring (HESR), and the experimental activity will be carried out using a general purpose detector  $\bar{P}$ ANDA that will be build surrounding an internal target station installed in one of the two straight sections of the storage ring. Figure 1 shows a schematic drawing of the  $\bar{P}$ ANDA apparatus. It is designed as a large acceptance multi-purpose detector consisting of two distinct parts: a solenoidal spectrometer, surrounding the interaction target region, and a forward spectrometer to cover the solid angle between 5 and 22 degrees. It will allow the detection and the identification of either the neutral and the charged particles emitted following  $\bar{p}$  annihilation.

### 3 The $\bar{\text{P}}\text{ANDA}$ Central Tracker

The  $\bar{\text{P}}\text{ANDA}$  Central Tracker (CT) is a tracking device placed in the target spectrometer. It has to satisfy the following requirements:

- almost full solid angle coverage;
- momentum resolution  $\delta p/p \sim 1.5\%$ ;
- low material budget  $X/X_0 \sim \text{few } \%$ ;
- good spatial resolution  $\sigma_{r,\phi} = 150, \mu\text{m}$ ,  $\sigma_z = \text{few mm}$ .

This detector will be placed around the Micro Vertex Detector (MVD) at a radial distance from the interaction point between 15 and 42 cm. Along the beam axis the allowed space is 150 cm. Presently, for this detector, two options are under study: a Straw Tube Tracker (STT) and a Time Projection Chamber (TPC). The Technical Design Report (TDR) of the tracking system is in preparation and will be completed during 2011. This document will be evaluated by a review committee which will give the collaboration advice for choosing the most appropriate CT.

The LNF  $\bar{\text{P}}\text{ANDA}$  group, having experience in straw tubes, is involved in the realization of the STT.

#### 3.1 Layout of the straw tube detector

The  $\bar{\text{P}}\text{ANDA}$  CT volume will be divided in two halves by the beam-target cross-pipe, therefore the detector will consist of two identical semi-chambers. In the hypothesis of a straw tube tracker, each one will be made of aluminized mylar straw tubes, diameter 10 mm, length 1500 mm, thickness 30  $\mu\text{m}$ , arranged in planar double layers (see figure 2).

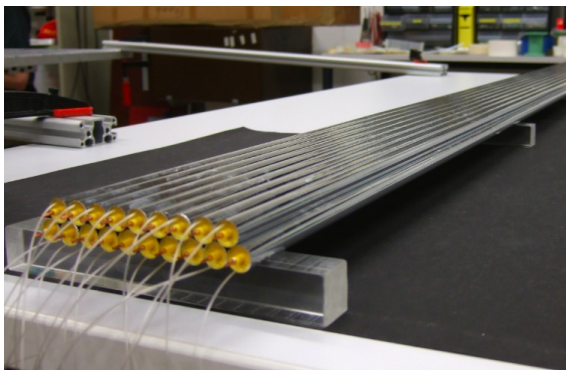


Figure 2: A *straw tube double layer*.

Inside a double layer the tubes are glued together and operated with an  $\text{Ar}+\text{CO}_2$  (90+10) gas mixture with an over-pressure of 1 bar. This solution will help to avoid strong support structures and will keep the detector design modular and simple. To measure also particle  $z$  coordinate, some layers will be mounted with a skew angle  $\pm 3^\circ$  with respect to the beam axis.

Figure 3 shows the layout for the STT. There are 4 internal double-layers parallel to the beam axis, then 4 double-layers mounted with opposite skew angles, and finally 2 other layers parallel to the beam axis. To fill up the cylindrical volume, the remaining region houses smaller tube layers.

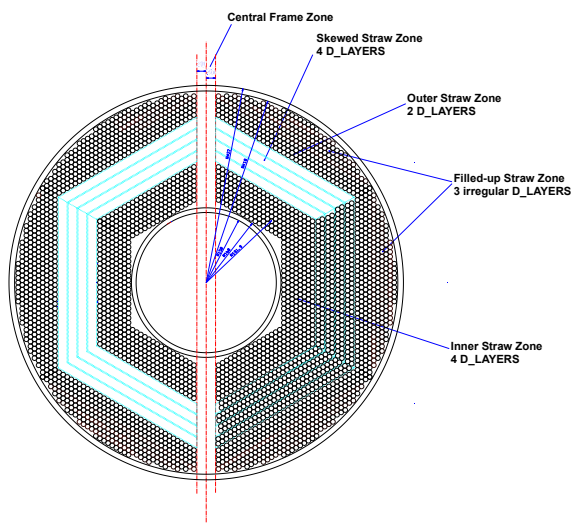


Figure 3: *The layout of the STT. In blue the axial tubes, in green the skewed layers (see text for more details).*

#### 4 Activity of the LNF $\bar{\text{PANDA}}$ group

The STT mechanical structure has to support also the beam-target cross-pipe and the MVD. This frame, has to be extremely light and has to allow the movement of the whole block of detectors during the installation procedure or the maintenance operations (see fig. 4). The activity of the LNF  $\bar{\text{PANDA}}$  group during 2010 has been devoted to two main tasks:

- the test of some straw tubes prototypes in order to determine the detector performances <sup>3)</sup>;
- the development, together with the Torino INFN group, of a prototype of the mechanical Central Frame (see fig. 5).

Concerning the first item, LNF  $\bar{\text{PANDA}}$  group has collected data with radioactive sources, cosmic rays, and test beams in order to check the performance of the straw tubes. These data are presently under analysis and will be included in the TDR that will be issued in June 2011.

#### 5 List of Conference Talks by LNF Authors in Year 2010

1. P. Gianotti, “Antiproton Physics with PANDA at FAIR”, invited talk at the International conference *Strong interaction in the 21st century*, Mumbai, India, February 10-12, 2010.
2. P. Gianotti, “Hadron Spectroscopy: An Experimental Overview”, invited talk at the 7th plenary session -Hadron Structure- at the *International Nuclear Physics Conference 2010*, Vancouver, Canada, July 4-9, 2010.
3. P. Gianotti, “Stato del progetto FAIR e prospettive per la fisica adronica”, invited talk at the *XCVI Congresso Nazionale della Società Italiana di Fisica*, Bologna, September 20-24, 2010.

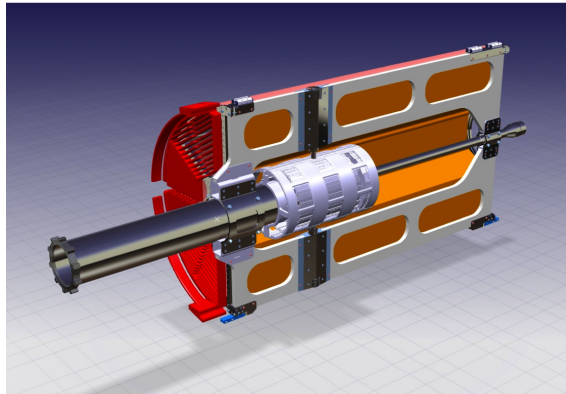


Figure 4: *Layout of one half of the STT mounted on the Central Frame that hold also the target-beam cross-pipe and the MVD.*



Figure 5: *The Central Frame prototype (see text for more details).*

## 6 Publications

1. S. Costanza *et al.*, “The straw tube tracker of the PANDA experiment”, Nucl. Instr. & Meth. **A617**, 148-150, 2010.
2. P. Gianotti, “The PANDA experiment at FAIR”, Nucl. Phys. **A835**, 96-101, 2010.

## References

1. <http://www.fair-center.com/>.
2. <http://www-panda.gsi.de/>.
3. S. Costanza *et al.*, Nucl. Instr. & Meth. **A617**, 148-150, 2010.

## VIP

S. Bartalucci, M. Bazzi (Ass. Ric.), C. Curceanu Petrascu (Resp. Naz.),  
C. Guaraldo, M. Iliescu (Assoc.), F. Lucibello (Tecn.),  
S. Okada (Bors. PD), D. Pietreanu (Bors. UE), A. Romero Vidal (Bors. PD),  
D. Sirghi (Art. 2222), F. Sirghi (Bors. UE), O. Vazquez Doce (Art. 23)

### 1 The VIP scientific case and the experimental method

The Pauli exclusion principle (PEP), which plays a fundamental role in our understanding of many physical and chemical phenomena, from the periodic table of elements, to the electric conductivity in metals, to the degeneracy pressure (which makes white dwarfs and neutron stars stable), is a consequence of the spin-statistics connection. Although the principle has been spectacularly confirmed by the number and accuracy of its predictions, its foundation lies deep in the structure of quantum field theory and has defied all attempts to produce a simple proof. Given its basic standing in quantum theory, it seems appropriate to carry out precise tests of the PEP validity and, indeed, mainly in the last 15-20 years, several experiments have been performed to search for possible small violations. The indistinguishability and the symmetrization (or antisymmetrization) of the wave-function should be then checked independently for each particle, and accurate tests were and are being done.

The VIP (VIolation of the Pauli Exclusion Principle) experiment, an international Collaboration among 6 Institutions of 4 countries, has the goal to improve the limit on the probability of the violation of the PEP for electrons, ( $P < 1.7 \times 10^{-26}$  established by E. Ramberg e G. A. Snow: *Experimental limit on a small violation of the Pauli principle*, Phys. Lett. **B 238** (1990) 438) by three-four orders of magnitude ( $P < 10^{-29 \div -30}$ ), exploring a region where new theories might allow for a possible PEP violation.

The experimental method consists in the introduction of electrons into a copper strip, by circulating a current, and in the search for X-rays resulting from the forbidden radiative transition that occurs if one of the new electrons is captured by a copper atom and cascades down to the 1s state already filled by two electrons with opposite spins. The energy of this transition would differ from the normal  $K_\alpha$  transition by about 300 eV (7.729 keV instead of 8.040 keV) providing an unambiguous signal of the PEP violation. The measurement alternates periods without current in the copper strip, in order to evaluate the X-ray background in conditions where no PEP violating transitions are expected to occur, with periods in which current flows in the conductor, thus providing “fresh” electrons, which might possibly violate PEP. The rather straightforward analysis consists on the evaluation of the statistical significance of the normalized subtraction of the two spectra in the region of interest.

The experiment is being performed at the LNGS underground Laboratories, where the X-ray background, generated by cosmic rays and natural radioactivity, is reduced.

### 2 The VIP experimental setup

The VIP setup was built in 2005, starting from the DEAR setup, reutilizing the CCD (Charge Coupled Devices) X-ray detectors, and consists of a copper cylinder, 4.5 cm in radius, 50  $\mu$ m thick, 8.8 cm high, Fig. 1, surrounded by 16 equally spaced CCDs of type 55.

The CCDs are at a distance of 2.3 cm from the copper cylinder, grouped in units of two chips vertically positioned. The setup is enclosed in a vacuum chamber, and the CCDs are cooled to



Figure 1: *The VIP copper target.*

about 165 K by the use of a cryogenic system. A schematic drawing of the VIP setup is shown in Fig. 2.

The DAQ alternates periods in which a 40 A current is circulated inside the copper target with periods without current, referred as background.

VIP was installed at the LNGS Laboratory in Spring 2006 and was taking data in this configuration until Summer 2010 (presently, see below, we are working on an improved version of the setup). The setup was surrounded by layers of copper and lead (as seen in the picture) to shield the setup against the residual background present inside the LNGS laboratory.

### 3 Activities in 2010

#### 3.1 VIP data taking and analyses results

Until summer 2010 the VIP experiment was in data taking, alternating periods of “signal” ( $I=40$  A) with periods without signal ( $I=0$  A). Data analyses were performed (energy calibration, sum of spectra, subtraction of background) and the probability of violation of PEP for electrons obtained (upper limit).

A preliminary result on the probability of violation of PEP by electrons was obtained:

$$\frac{\beta^2}{2} < 4 \times 10^{-29} \quad (1)$$

#### 3.2 Discussion of the results

We are attempting an interpretation of our results in the framework of quon-theory, which turned out to be a consistent theory of *small* violations of PEP. The basic idea of quon theory is that

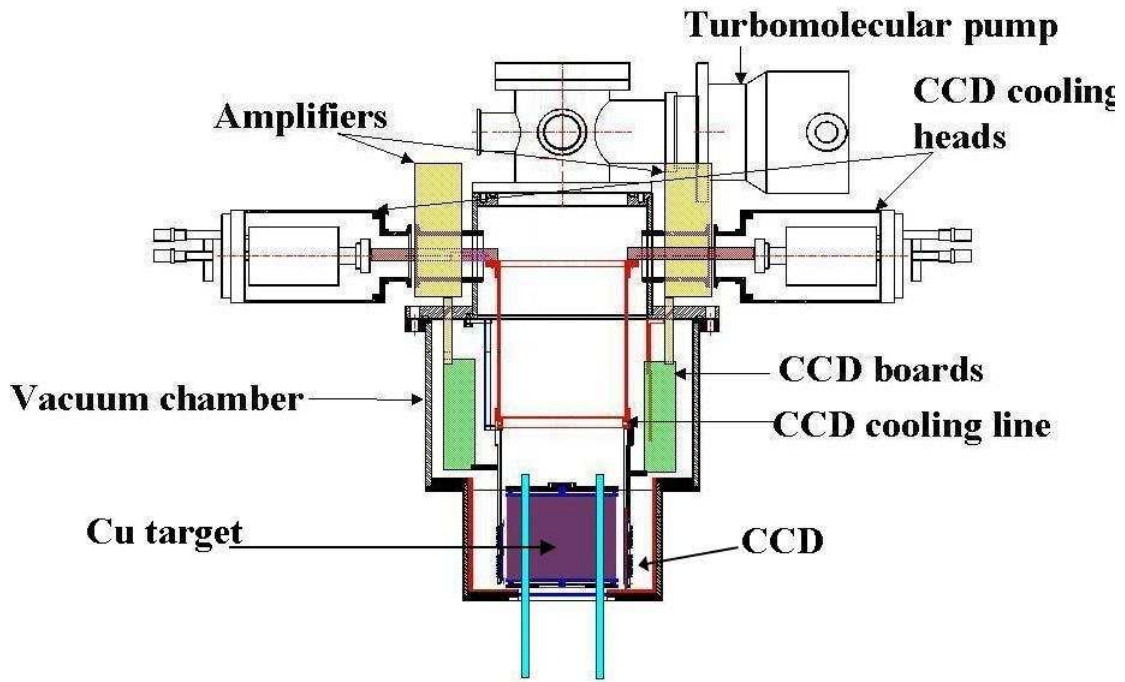


Figure 2: *The VIP setup. All elements of the setup are identified in the figure.*

(anti)commutators, are replaced by weighted sums

$$\frac{1-q}{2} [a_i, a_j^+]_+ + \frac{1+q}{2} [a_i, a_j^+]_- = a_i a_j^+ - q a_j^+ a_i = \delta_{i,j} \quad (2)$$

where  $q = -1$  ( $q = 1$ ) gives back the usual fermion (boson) commutators. The statistical mixture in equation (2) also shows that the PEP violation probability is just  $(1+q)/2$  and thus our best experimental bound on  $q$  is

$$\frac{1+q}{2} < 4 \times 10^{-29} \quad (3)$$

A consistent interpretation of the VIP results can thus be based on quon theory; however here we note that is not easy to devise tests of PEP, because of many conceptual difficulties, presented in our published papers (see list at the end).

Even if at the moment these are just speculations we do strongly feel that the test is meaningful and we are now planning an improved version.

### 3.3 The VIP upgrade

The present VIP setup uses CCD detectors which are excellent X-ray detectors (good energy resolution, background rejection based We plan to switch to a new type of detectors for precision X-rays measurements, the triggerable Silicon Drift Detectors (SSD) which have a fast readout time ( $\simeq 1\mu s$ ) and large collection area ( $100 \text{ mm}^2$ ). These detectors, see fig. 3, were successfully used in the SIDDHARTA experiment at LNF-INFN (see report on SIDDHARTA) for measurements of the kaonic atoms transitions at the DAΦNE accelerator of LNF-INFN; using a proper trigger system a background rejection factor of the order of  $10^{-4}$  was achieved in SIDDARTHA.

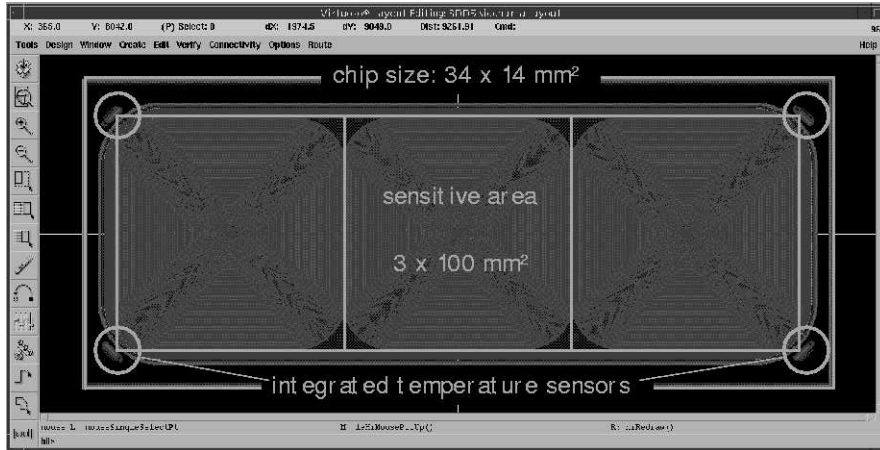


Figure 3: *SDD layout on the readout side: 3 SDD cells, independently read, each with an area of 100 mm<sup>2</sup>.*

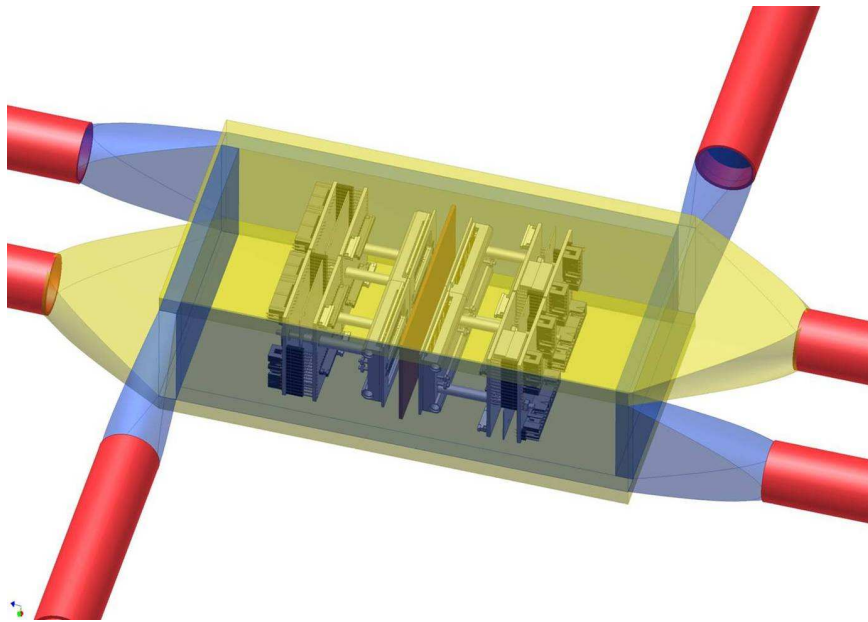


Figure 4: *The possible implementation of the upgrade of the VIP experiment using SDD detectors and an external veto-system.*

With these new setup is then possible, on one side, to increase the signal due to a higher acceptance and efficiency, and on the other to reduce the background by using an external veto-system which should allow to reduce that background produced by charged particles from the outside.

In 2010 we performed a series of tests at LNF and at LNGS with a test setup which showed that is possible to gain at least an order of magnitude in the probability of PEP violation. A schematic layout of the new setup is shown in fig. 4. Presently, based on the results of the tests performed and on Monte Carlo simulations we are designing the final upgraded VIP setup and prepare elements for its construction.

#### 4 Activities in 2011

In 2011 the data analyses of the VIP data will continue to arrive to the final value for the PEP violation probability for electrons. We plan, as well, to finalize the design of the upgraded setup and to proceed with its construction and installation at LNGS. We are, as well, considering to extend the scientific program towards a feasibility study of limits on parameters of the collapse model (as a solution of the measurement problem, put initially forward by Ghirardi, Rimini and Weber) by measurements of X rays spontaneously emitted in the continuous spontaneous localization (CSL) model.

#### Acknowledgements

The VIP Collaboration wishes to thank all the LNGS laboratory staff for the precious help and assistance during all phases of preparation, installation and data taking. The support from the HadronPhysics FP6 (506078), HadronPhysics2 FP7 (227431) and MIUR PRIN2008 2008LX2X28-004. projects are acknowledged.

#### 5 Publications

##### 5.1 Conference Talks

1. C. Curceanu, “Experimental tests of quantum mechanics: Pauli Exclusion Principle and spontaneous collapse models”, Quantum 2010, 23-29 May 2010, Torino, Italy.
2. C. Curceanu, “Stepping into Bertlmann’s socks: some experimental tests on quantum mechanics. Pauli Exclusion Principle and spontaneous collapse models”, Reinhold Bertlmann’s fest, June2010, Puchberg am Schneeberg, Austria.
3. C. Curceanu, “Experimental tests of quantum mechanics: Pauli Exclusion Principle and spontaneous collapse models”, DICE2010, 13-17 September 2010, Castiglioncello, Italy.
4. C. Curceanu, “Experimental tests of quantum mechanics: Pauli Exclusion Principle and spontaneous collapse models”, Physics of Fundamental Symmetries and Interactions, PSI2010, 11-14 October 2010, Villigen, Switzerland.
5. C. Curceanu, “Experimental tests of quantum mechanics: Pauli Exclusion Principle and spontaneous collapse models”, seminar at Pavia University, 6 December 2010, Pavia, Italy.
6. A. Rizzo, “Spontaneous emission by free electrons, search for experimental hints”, PRIN08 group meeting, 21 July 2010, Milano, Italy.

7. A. Rizzo, "Spontaneous emission by free electrons, search for experimental hints", mini-workshop at ICTP, 8-9 November 2010, Trieste, Italy.

## 5.2 Papers and Proceedings

1. C. Curceanu and E. Milotti Editors of a Special Issue of Foundation of Physics dedicated to Spin - Statistics, vol. 40, Number 7 (2010).
2. C. Curceanu, E. Milotti, S. Adler and M. Berry, "Special Issue on Spin Statistics", Foundation of Physics, vol. 40, n. 7 (2010), 681.
3. S. Bartalucci *et al.*, "The VIP Experimental Limit on the Pauli Exclusion Principle Violation by Electrons", Foundation of Physics, vol. 40, n. 7 (2010), 765
4. C. Curceanu *et al.*, "New experimental limits on the Pauli exclusion principle violation by electrons - the VIP experiment", Foundation of Physics, vol. 41, n. 3 (2011), 282
5. C. Curceanu *et al.*, "New experimental limits on the Pauli exclusion principle violation by electrons - the VIP experiment", AIP Conference Proceedings, Vol. 1232 (2010) 206.
6. J. Marton *et al.*, "Testing the Pauli Exclusion Principle for electrons", to appear in Proceedings of DISCRETE2010 Conference, 6-11 December 2010, Sapienza University, Roma, Italy in Journal of Physics, Conference Series.



## *4 – Theory and Phenomenology*



## FA51: Fisica Astroparticellare

D. Aristizabal Sierra (Ass.), E. Nardi (Resp.)

### 1 Activity

**i.** Flavour effects in soft leptogenesis were revisited in ref. [1], by relaxing the assumption of universality for the soft supersymmetry breaking terms. We have found that with respect to the case in which the heavy sneutrinos decay with equal rates and equal CP asymmetries for all lepton flavours, hierarchical flavour configurations can enhance the efficiency by more than two orders of magnitude. This translates in more than three order of magnitude with respect to the one-flavour approximation. We have thus shown that soft leptogenesis can be successful for previously excluded values of the relevant parameters, allowing for example for  $B \sim \mathcal{O}(\text{TeV})$ . This means that soft leptogenesis can successfully proceed with natural values for all supersymmetry soft breaking terms.

**ii.** A rigorous study of leptogenesis in the supersymmetric standard model plus the seesaw was carried out in ref. [2]. We have identified important qualitative differences that characterize supersymmetric leptogenesis with respect to the non-supersymmetric case. The lepton number asymmetries in fermions and scalars do not equilibrate, and are related via a non-vanishing gaugino chemical potential. Due to the presence of new anomalous symmetries, electroweak sphalerons couple to winos and higgsinos, and QCD sphalerons couple to gluinos, thus modifying the corresponding chemical equilibrium conditions. A new constraint on particles chemical potentials corresponding to an exactly conserved  $R$ -charge, that also involves the number density asymmetry of the heavy sneutrinos, appears. These new ingredients determine the  $3 \times 4$  matrices that mix up the density asymmetries of the lepton flavours and of the heavy sneutrinos. Our work establishes the correct theoretical framework for carrying out leptogenesis studies in the supersymmetric case.

**iii.** In ref. [3] we have developed that general concept of *effective theory* for studying particle physics processes in the early Universe. As an application of these ideas, we have discussed the case of soft leptogenesis when it occurs at temperatures  $T > 10^7 \text{ GeV}$ . We have shown that in this regime, the main source of the B-L asymmetry is the CP asymmetry of a new anomalous R-charge that couple to generalized anomalous electroweak processes. Baryogenesis thus occurs mainly through R-genesis, and with an efficiency that can be up to two orders of magnitude larger than in usual estimates. Contrary to common belief, we have shown that a sizeable baryon asymmetry is generated also when thermal corrections to the CP asymmetries in sneutrino decays are neglected which, in soft leptogenesis, implies vanishing lepton-flavour CP asymmetries. We have also worked out the general Boltzmann equations for leptogenesis valid for all temperature regimes.

**iv.** The importance of flavor effects in models in which leptogenesis proceeds via the decay of Majorana electroweak triplets were analyzed in ref [4]. We found that depending on the relative strengths of gauge and Yukawa reactions the  $B - L$  asymmetry can be sizably enhanced, exceeding in some cases one order of magnitude. We also discussed the impact that such effects can have for TeV-scale triplets, and we have shown that, as long as the  $B - L$  asymmetry is produced by the dynamics of the lightest of such triplets, they are negligible. However, open the possibility for scenarios in which the asymmetry is generated above the TeV scale by heavier states, possibly surviving the washouts related to the TeV triplets, remains open. We have investigated these possibilities and we have shown how they can be disentangled at the LHC by using collider observables specifically related to Majorana triplets. In the case of minimal type III see-saw models lepton flavor violation observables can also provide a useful discriminating tool.

## References

1. C. S. Fong, M. C. Gonzalez-Garcia, E. Nardi and J. Racker, JHEP **1007**, 001 (2010), [arXiv:1004.5125 [hep-ph]].
2. C. S. Fong, M. C. Gonzalez-Garcia, E. Nardi and J. Racker, JCAP **1012**, 013 (2010) [arXiv:1009.0003 [hep-ph]].
3. C. S. Fong, M. C. Gonzalez-Garcia and E. Nardi, JCAP **1102**, 032 (2011). [arXiv:1012.1597 [hep-ph]].
4. D. Aristizabal Sierra, J. F. Kamenik and M. Nemevsek, JHEP **1010**, 036 (2010), [arXiv:1007.1907 [hep-ph]].
5. D. Aristizabal Sierra, F. Bazzocchi, I. de Medeiros Varzielas, L. Merlo and S. Morisi, Nucl. Phys. B **827**, 34 (2010) [arXiv:0908.0907 [hep-ph]].
6. E. Nardi, Proc. of “NOW 2010” Neutrino Oscillation Workshop, Conca Specchiulla (Otranto, Lecce, Italy), September 4-11, 2010. To be published in Nucl Phys. B (Proc. Suppl.).

## Talks at Conferences

1. “*Leptogenesis.*”  
Enrico Nardi,  
Invited talk at INIFA 2010: “*Incontro Nazionale Iniziative di Fisica Astroparticellare.*”  
22-23 June 2010, INFN - Laboratori Nazionali di Frascati, Frascati, Rome.
2. “*Leptogenesis and Neutrino Masses*”  
Enrico Nardi,  
Plenary talk at NOW 2010: “*Neutrino Oscillation Workshop*”,  
4-11 September 2010, Conca Specchiulla (Otranto, Lecce, Italy)  
[<http://www.ba.infn.it/now/now2010/TALKS/sept.5/plenary/Nardi-NOW-2010.pdf>].
3. “*Leptogenesis and TeV-scale alternatives for baryogenesis.*”  
Enrico Nardi,  
Invited talk at  $\nu$ TheME 2010: *Neutrino Theory, Models, and Experimental perspectives*,  
13-22 September 2010; CERN, Geneva, Switzerland.
4. “*Some remarks on the fermion mass problem.*”  
Enrico Nardi,  
Invited talk at the III Prometeo Workshop: *LHC: Physics at the Limit*,  
2-5 and 15-19 November 2010; Universitat de Valencia, Valencia, Spain.

## Editorial Work

1. Proceedings of the 2<sup>nd</sup> Young Researchers Workshop “*Physics Challenges In The LHC Era,*”  
Frascati, Italy, May 10 & 13, 2010. E. Nardi, Editor.  
[<http://www.lnf.infn.it/sis/frascatiseries/Volume51/volume51.pdf>].

## LF21

### Phenomenology of Elementary Particle Interactions at Colliders

O. Cata (Bors.), V. Del Duca, G. Isidori (Resp.), J. Jones Perez, O. Shekhovtsova (Bors.)

#### 1 Summary of the project

The research topics investigated by this project can be divided into the following two main areas:

- flavour physics, precision tests and physics beyond the Standard Model (O. Catà, G. Isidori, J. Jones Perez);
- theoretical and phenomenological aspects of QCD and collider physics (V. Del Duca, O. Shekhovtsova).

In the following we shall briefly describe some of most significant projects undertaken by the above participants in 2010.

#### 2 Flavour physics, precision tests, and physics beyond the Standard Model

One of the strategies to obtain additional clues about the nature of New Physics (NP) is by means of precision tests of the Standard Model (SM) at low energies. These are particularly interesting in: i) electroweak processes calculable with high precision, where even tiny deviations from the SM can be detected; ii) processes which are not mediated by tree-level SM amplitudes, where the relative effect of NP contributions can be enhanced. Up to now there is no clear evidence for deviations from the SM in both type of processes, and this leads to significant constraints in building realistic extensions of the SM. For instance, realistic models must possess a highly non-generic flavour structure. These constraints are particularly severe for NP models with new degrees of freedom around the TeV scale, as required by a natural stabilisation of the  $SU(2)_L \times U(1)_Y \rightarrow U(1)_Q$  spontaneous symmetry breaking. The attempt to clarify this problem, both at the phenomenological level (with the help of precision data on rare decays) and at a more fundamental level (with the help of new symmetry principles), is one of the main activity of our group.

A closely related subject –which is also one of the primary research objectives of our group– is a better understanding of the SM itself, fixing its fundamental couplings (quark masses, CKM angles, non-perturbative condensates, ...) by means of precise calculations within the framework of effective field theories and Lattice QCD.

Within this general scenario, the highlights of the 2010 activity include:

*Higgs-mediated FCNCs: Natural Flavour Conservation vs. Minimal Flavour Violation.* <sup>1, 2)</sup>

We have compared the effectiveness of two hypotheses, Natural Flavour Conservation (NFC) and Minimal Flavour Violation (MFV), in suppressing the strength of flavour-changing neutral-currents (FCNCs) in models with more than one Higgs doublet. We have shown that the MFV hypothesis, in its general formulation, is more stable in suppressing FCNCs than the hypothesis of NFC alone when quantum corrections are taken into account. The phenomenological implications of the two scenarios have been discussed analysing meson-antimeson mixing observables and rare  $B$  decays. We have demonstrated that, introducing flavour-blind CP phases, two-Higgs doublet models respecting the MFV hypothesis can accommodate a large CP-violating phase in  $B_s$  mixing, as hinted by CDF and D0 data

and, without extra free parameters, soften significantly in a correlated manner the observed anomaly in the relation between  $\epsilon_K$  and  $S_{\psi K}$ .

*Quark flavour mixing with right-handed currents: an effective theory approach.* 3)

The impact of right-handed currents in both charged- and neutral-current flavour-violating processes has been analysed by means of an effective theory approach. More explicitly, we have analysed the structure of dimension-six operators assuming a left-right symmetric flavour group, commuting with an underlying  $SU(2)_L \times SU(2)_R \times U(1)_{B-L}$  global symmetry, broken only by two Yukawa couplings. The model contains a new unitary matrix controlling flavour-mixing in the right-handed sector. We have determined the structure of this matrix by charged-current data, where the tension between inclusive and exclusive determinations of  $|V_{ub}|$  can be solved. Having determined the size and the flavour structure of right-handed currents, we investigate how they would manifest themselves in neutral current processes, including particle-antiparticle mixing,  $Z \rightarrow b\bar{b}$ ,  $B_{s,d} \rightarrow \mu^+\mu^-$ ,  $B \rightarrow Xs, K, K^*\nu\bar{\nu}$ , and  $K \rightarrow \pi\nu\bar{\nu}$  decays. The possibility to explain a non-standard CP-violating phase in  $B_s$  mixing in this context, and the comparison with other predictive new-physics frameworks addressing the same problem, has also been discussed. While a large  $S_{\psi\phi}$  asymmetry can easily be accommodated, we have pointed out a tension in this framework between  $|V_{ub}|$  and  $S_{\psi K}$ .

*Precise tests of the Standard Model from world data on kaon decays.* 4, 5)

We have presented a global analysis of leptonic and semileptonic kaon decay data, including all recent results published by the BNL-E865, KLOE, KTeV, ISTRA+ and NA48 experiments. This analysis, in conjunction with precise lattice calculations of the hadronic matrix elements now available, leads to a very precise determination of  $|V_{us}|$  and has allowed us to perform several stringent tests of the Standard Model. We have also analysed the structure of long distance contributions to the CP-violating parameter  $\epsilon_{\text{CP}}$ , that generally affect both the absorptive and the dispersive parts of the  $K^0-\bar{K}^0$  mixing amplitude.

*Progress in holographic approaches to QCD.* 6, 7)

We have obtained a new determination of the hadronic light by light scattering contribution to the muon anomalous magnetic moment, focussing on the (dominant) pion exchange diagram. We have used as input the existing experimental low energy data on the anomalous electromagnetic pion form factor  $F_{\pi^0\gamma^*\gamma^*}$ , QCD short distance constraints and, additionally, predictions coming from holographic models of QCD. We have been able to quantify the theoretical uncertainty in  $(g-2)_\mu$  coming from experimental input, QCD short distances and model dependences.

### 3 Theoretical and phenomenological aspects of QCD and collider physics

*Scattering amplitudes in the maximally supersymmetric  $N = 4$  super-Yang-Mills theory.* 8, 9, 10, 11)

In the planar  $N = 4$  supersymmetric Yang-Mills theory, the conformal symmetry constrains multi-loop  $n$ -edged Wilson loops to be given in terms of the one-loop  $n$ -edged Wilson loop, augmented, for  $n$  greater than 6, by a function of conformally invariant cross ratios. That function is termed the remainder function. We have displayed the first analytic computation of the two-loop six-edged Wilson loop, and thus of the corresponding remainder function. Although the calculation was performed in the quasi-multi-Regge kinematics of a pair along the ladder, the Regge exactness of the six-edged Wilson loop in those kinematics entails that the result is the same as in general kinematics. We have shown in detail how the most difficult of the integrals is computed, which contribute to the six-edged Wilson loop. The remainder function is given as a function of uniform transcendent weight four in terms of Goncharov

polylogarithms. We have considered also some asymptotic values of the remainder function, and the value when all the cross ratios are equal.

*Precision in hadronic cross sections at low energy: Monte Carlo tools vs. experimental data.* 12, 13)

We have presented a general framework for the model-independent decomposition of the fully differential cross section of the reactions  $e^+e^- \rightarrow \pi^0\pi^0\gamma$  and  $e^+e^- \rightarrow \pi^0\eta\gamma$ , which can provide important information on the properties of scalar mesons:  $f_0(600)$ ,  $f_0(980)$  and  $a_0(980)$ . For the model-dependent ingredients in the differential cross section, an approach is developed, which relies on Resonance Chiral Theory with vector and scalar mesons. Numerical results are compared to data. The framework is convenient for development of a Monte Carlo generator.

#### 4 Main contributions to Conference Proceedings in 2010

1. G. Isidori, *The Challenges of Flavour Physics*, invited plenary talk at ICHEP 2010, Paris, July 2011, [arXiv:1012.1981 [hep-ph]].
2. O. Cata, *Two-forms in holographic QCD*, invited talk at Light Cone 2010, Valencia, June 2010 PoS **LC2010** (2010) 032.

#### References

1. A. J. Buras, M. V. Carlucci, S. Gori, G. Isidori, *Higgs-mediated FCNCs: Natural Flavour Conservation vs. Minimal Flavour Violation*, JHEP **1010** (2010) 009. [arXiv:1005.5310 [hep-ph]].
2. A. J. Buras, G. Isidori, P. Paradisi, *EDMs versus CPV in  $B_{s,d}$  mixing in two Higgs doublet models with MFV*, Phys. Lett. **B694** (2011) 402-409. [arXiv:1007.5291 [hep-ph]].
3. A. J. Buras, K. Gemmler, G. Isidori, *Quark flavour mixing with right-handed currents: an effective theory approach*, Nucl. Phys. **B843** (2011) 107-142. [arXiv:1007.1993 [hep-ph]].
4. M. Antonelli *et al.*, *An Evaluation of  $|V_{us}|$  and precise tests of the Standard Model from world data on leptonic and semileptonic kaon decays*, Eur. Phys. J. **C69** (2010) 399-424. [arXiv:1005.2323 [hep-ph]].
5. A. J. Buras, D. Guadagnoli, G. Isidori, *On  $\epsilon_K$  beyond lowest order in the Operator Product Expansion*, Phys. Lett. **B688** (2010) 309-313. [arXiv:1002.3612 [hep-ph]].
6. L. Cappiello, O. Cata, G. D'Ambrosio, *The hadronic light by light contribution to the  $(g-2)_\mu$  with holographic models of QCD*, to appear in Phys. Lett. B. [arXiv:1009.1161 [hep-ph]].
7. L. Cappiello, O. Cata, G. D'Ambrosio, *Antisymmetric tensors in holographic approaches to QCD*, Phys. Rev. **D82** (2010) 095008. [arXiv:1004.2497 [hep-ph]].
8. V. Del Duca, C. Duhr, V. A. Smirnov, *A Two-Loop Octagon Wilson Loop in  $N = 4$  SYM*, JHEP **1009** (2010) 015. [arXiv:1006.4127 [hep-th]].
9. V. Del Duca, C. Duhr, V. A. Smirnov, *The Two-Loop Hexagon Wilson Loop in  $N = 4$  SYM*, JHEP **1005** (2010) 084. [arXiv:1003.1702 [hep-th]].

10. V. Del Duca, C. Duhr, V. A. Smirnov, *An Analytic Result for the Two-Loop Hexagon Wilson Loop in  $N = 4$  SYM*, JHEP **1003** (2010) 099. [arXiv:0911.5332 [hep-ph]].
11. V. Del Duca, C. Duhr, E. W. Nigel Glover, V. A. Smirnov, *The One-loop pentagon to higher orders in epsilon*, JHEP **1001** (2010) 042. [arXiv:0905.0097 [hep-th]].
12. S. Eidelman, S. Ivashyn, A. Korchin, G. Pancheri, O. Shekhovtsova,  *$e^+e^-$  annihilation to  $\pi^0\pi^0\gamma$  and  $\pi^0\eta\gamma$  as a source of information on scalar and vector mesons*, Eur. Phys. J. **C69** (2010) 103-118. [arXiv:1003.2141 [hep-ph]].
13. S. Actis *et al.*, *Quest for precision in hadronic cross sections at low energy: Monte Carlo tools vs. experimental data*, Eur. Phys. J. **C66** (2010) 585-686. [arXiv:0912.0749 [hep-ph]].

## LF61

### Low-dimensional strongly correlated electron systems, spin-Hall effect and nanoscale science and technology

S. Bellucci (Resp. Naz.), M. Benfatto, M. Cini (Ass.), L. Coderoni (Art. 2222),  
K. Hatada (Borsista PD), K. Hayakawa (Borsista PD), G. Iovane (Ass.), F. Micciulla (Art. 2222),  
C. Natoli (Ass.), P. Onorato (Borsista PD), F. Palumbo (Ass.), N. Pugno (Ass.),  
I. Sacco (Bors.), G. Stefanucci (Ass.)

#### 1 External collaborating Institutions:

1. IHEP-Protvino, Russia
2. Univ. Pavia, Italy
3. Belarus State Univ. Minsk,
4. Department of Physics, Yerevan State University, A. Manoogian 1, Yerevan 0025, Armenia
5. Department of Physics, Univ. Roma Tor Vergata, Italy
6. Dipartimento di Ingegneria dell'Informazione, Seconda Università di Napoli, 81031 Aversa (CE), Italy
7. Institute of Solid State Physics, University of Latvia, Kengaraga Str. 8, 1063 Riga, Latvia
8. Instituto de Ciencia de Materiales de Aragon, CSIC-Universidad de Zaragoza, 50009 Zaragoza, Spain.
9. ICB, UMR 5209 Université de Bourgogne - CNRS, BP 47870, F-21078 Dijon, France
10. Institut de Physique de Rennes, UMR UR1-CNRS 6251, Campus de Beaulieu, Université de Rennes1, 35042 Rennes-cedex, France

#### 2 Research Activity

We investigated the comparative field emission from vertically aligned few-layer graphene and carbon nanotubes. In collaboration with Yerevan State Univ., we studied the fermionic condensate in a conical space with a circular boundary and magnetic flux, quantum ring models and action-angle variables, as well as the external field influence on semiflexible macromolecules: geometric coupling. In collaboration with IHEP Protvino we studied the uses of crystals in connection to accelerator physics.

We carried out a study of nanojunctions as logic operators for the spintronics, of spin filtering effects in a one dimensional artificial lattice with ring geometry subject to Rashba coupling, of single spin-qubit rotators based on nanojunctions using a semiclassical path integral approach interaction. Also spin phases and currents in ring shaped one-dimensional quantum dot arrays, was investigated, as well as the role of quantum wires as logic operators, in connection to the XNOR and NOR gate response in a ballistic interferometer. Landau levels and edge states in a cylindrical two-dimensional electron gas in a semiclassical approach were studied.

A modal analysis of piezoelectric bodies with voids was also the object of our research.

We have continued our work on a rigorous derivation of a real space full-potential multiple-scattering theory (FP-MST), valid both for continuum and bound states, for the calculation of core-level synchrotron radiation spectroscopy as applied to many interdisciplinary problems in condensed matter physics. We have been able to show that, contrary to the common belief in the literature, multiple scattering theory converges absolutely, so that the angular momentum truncation procedure is well founded. In this way we have solved a problem that had been staying around for almost thirty years.

We have started the implementation of codes, based on our Full Potential MST, to calculate in real space properties of the ground state of molecules and in general clusters of atoms in a self-consistent way, in order to obtain self-consistent charge densities, the position of the Fermi level, the equilibrium atomic positions and other useful quantities both for ground state and continuum spectroscopies.

In collaboration with the ICMA Institute in Zaragoza (Spain), a resonant x-ray scattering study at the Mn K-edge and Tb L3-edge of TbMnO<sub>3</sub> was performed to investigate the local distortions responsible for the ferroelectricity. TbMnO<sub>3</sub> perovskite is indeed an interesting representative of those materials, of great technological importance, where antiferromagnetism (AFM) and ferroelectricity coexist at low temperatures.

In collaboration with the Univ. of Bourgogne-Dijon we have extended the multichannel MS program developed by P. Kruger in Dijon to complex algebra, in order to implement contour integration for the multichannel Green's Function and describe electronic correlation not only in the excited state but also in the ground states of molecules and clusters of atoms. It is hoped that this approach will cure the deficiencies of the current Density Functional Theory (DFT) programs and go beyond the Dynamical Field Theory Approach (DMFT) in treating electronic correlations in solids.

Particle-particle response function as a probe for electronic correlations in the p-d Hubbard model, time-dependent transport in graphene nanoribbons, magnetic moments in biased quantum circuits, were also important topics of interest for our investigations, along with the dynamical Coulomb Blockade and the derivative discontinuity of time-dependent Density Functional Theory. Lastly, we assessed the accuracy of Kohn-Sham conductances using the Friedel sum rule.

We organized, so far, ten Schools and Workshops on nanoscale science and technology, aiming to assess the current state of the art and stimulate research networking, held under the patronage of INFN and other institutions from both the public and private sectors. The most recent edition was Nanoscience & Nanotechnology 2010, Laboratori Nazionali di Frascati - 20-23 September 2010, <http://www.lnf.infn.it/conference/nn2008/>.

18 september 2010 Prof. Gerardo Iovane, associated INFN LNF within the LF61 project, was the recipient of the Leonardo Award for Scientific Research, owing to the results he obtained in research, innovation and technology transfer.

### 3 Conference Talks

1. P. Onorato, "Quantum wires as logical gates for nanoelectronics". Presented at the XCVI Congresso Nazionale SIF Bologna, 20-24 September 2010.
2. P. Onorato, "Quantum interferometers patterned in Quantum Wires: Logic gate responses". Presented at Nanoscience & Nanotechnology 2010 Laboratori Nazionali di Frascati 20-23 September 2010.
3. L. Coderoni, "Mechanical and electrical characterization of nanocomposites coatings for electronic circuits", Presented at Nanoscience & Nanotechnology 2010 Laboratori Nazionali di Frascati 20-23 September 2010.

4. S. Bellucci, “Carbon nanotube based composites: Microwave probing towards electromagnetic shielding”, Con. NANOSEA, Cassis, July 2, 2010.
5. S. Bellucci, “Effectiveness of microwave electromagnetic shielding in carbon based epoxy nanocomposites”, Con. IRMMW-THz 2010, Rome, September 7, 2010.

## References

1. S. Bellucci, E.R. Bezerra de Mello, A.A. Saharian, “Fermionic condensate in a conical space with a circular boundary and magnetic flux”, Phys. Rev. D (in press), e-print: arXiv:1101.4130 [hep-th].
2. S. Bellucci *et al.*, “Comparative field emission from vertically aligned few-layer graphene and carbon nanotubes”, Nanoscience and Nanotechnology Letters (NNL) 2011.
3. A.G. Afonin *et al.*, “Crystal-Assisted Beam Extraction and Collimation at the U-70, Circular Accelerator”, IHEP-PREPRINT-2010-12, published in Instr. Exp. Tech. 54:1-7,2011. e-print: arXiv:1102.2711 [physics.acc-ph].
4. S. Bellucci, Y. Mamasakhlisov, A. Nersessian, “External field influence on semiflexible macromolecules: geometric coupling”, e-print: arXiv:1011.0644 [cond-mat.soft].
5. S. Bellucci, B.N. Tiwari, “Thermodynamic Geometry: Evolution, Correlation and Phase Transition”, e-print: arXiv:1010.5148 [cond-mat.stat-mech].
6. S. Bellucci, A. Nersessian, A. Saghatelian, V. Yeghikyan, Quantum ring models and action-angle variables”, Journal of Computational and Theoretical Nanoscience, Vol. 8, N. 4, 769 (2011), e-print: arXiv:1008.3865, [cond-mat.mtrl-sci].
7. S. Bellucci, P. Onorato, The European Physical Journal B **73**, 563 (2010).
8. S. Bellucci, P. Onorato, The European Physical Journal **B 73**, 215 (2010).
9. S. Bellucci and P. Onorato, Physica E Low-dimensional Systems and Nanostructures **42**, 1571 (2010).
10. S. Bellucci, P. Onorato, Journal of Applied Physics **107**, 073703 (2010).
11. S. Bellucci and P. Onorato, Phys. Rev. B **81**, 165427 (2010).
12. S. Bellucci and P. Onorato, Journal of Nanophotonics **4**, 043508 (2010).
13. Quantum Hall Fabry-Perot interferometer: Logic gate responses, S.Bellucci, P. Onorato Journal of Applied Physics **108**, 033710 (2010).
14. Landau levels and edge states in a cylindrical two-dimensional electron gas: A semiclassical approach S. Bellucci and P. Onorato Phys. Rev. B **82**, 205305 (2010).
15. K- Hatada, K- Hayakawa, M. Benfatto *et al.*, Full-potential multiple scattering theory with space-filling cells for bound and continuum states, Journal of Physics-Condensed Matter Vol. **22** Issue: 18 Article Number: 185501 (2010).

16. Structural Characterization of a High Affinity Mononuclear Site in the Copper(II)-alpha-Synuclein Complex, Bortolus M, Bisaglia M, Zoleo A, et al., *Journal of the American Chemical Society* Vol. **32**, Issue: 51,18057 (2010).
17. Modal analysis of piezoelectric bodies with voids. II. Finite element simulation, Iovane G, Nasedkin AV, *APPLIED MATHEMATICAL MODELLING* Volume: 34 Issue: 1 Pages: 47-59 Published: JAN 2010
18. Modal analysis of piezoelectric bodies with voids. I. Mathematical approaches, Iovane G, Nasedkin AV, *APPLIED MATHEMATICAL MODELLING* Volume: 34 Issue: 1 Pages: 60-71 Published: JAN 2010
19. Scissors Modes in crystals with cubic symmetry, Hatada K, Hayakawa K, Palumbo F, *EUROPEAN PHYSICAL JOURNAL B* Volume: 77 Issue: 1 Pages: 41-45 Published: SEP 2010
20. Correlation-Induced Memory Effects in Transport Properties of Low-Dimensional Systems, Perfetto E, Stefanucci G, Cini M, *PHYSICAL REVIEW LETTERS* Volume: 105 Issue: 15 Article Number: 156802 Published: OCT 5 2010
21. Particle-particle response function as a probe for electronic correlations in the p-d Hubbard model, Ugenti S, Cini M, Seibold G, et al., *PHYSICAL REVIEW B* Volume: 82 Issue: 7 Article Number: 075137 Published: AUG 27 2010
22. Time-dependent transport in graphene nanoribbons, Perfetto E, Stefanucci G, Cini M, *PHYSICAL REVIEW B* Volume: 82 Issue: 3 Article Number: 035446 Published: JUL 30 2010
23. Magnetic moments in biased quantum circuits, Cini M, Perfetto E, Stefanucci G, *PHYSICAL REVIEW B* Volume: 81 Issue: 16 Article Number: 165202 Published: APR 15 2010
24. Dynamical Coulomb Blockade and the Derivative Discontinuity of Time-Dependent Density Functional Theory, Kurth S, Stefanucci G, Khosravi E, et al., *PHYSICAL REVIEW LETTERS* Volume: 104 Issue: 23 Article Number: 236801 Published: JUN 7 2010
25. Assessing the accuracy of Kohn-Sham conductances using the Friedel sum rule, Mera H, Kaasbjerg K, Niquet YM, Stefanucci G, *PHYSICAL REVIEW B* Volume: 81 Issue: 3 Article Number: 035110 Published: JAN 2010

## MI12: Gauge and String Theories

S. Bellucci (Resp.), S. Ferrara (Ass.), E. Latini (Dott.), S. Krivonos (Osp.),  
A. Marrani (Bors. PD), V. Ohanyan (Osp.), A. Shcherbakov (Bors. PD),  
A. Saharian (Osp.), A. Sutulin (Osp.), B.N. Tiwari (Bors. PD), A. Yeranyan (art. 23)

### 1 Research Activity

The topics covered in 2010 are related to current issues in the theory of elementary particle interactions and of the theory of the gravitational force and interrelations among them. The main research activities in this period focused along different directions, within the broad field of High-Energy Theoretical Physics: study of the intriguing, recently established black-hole/qubit correspondence; study of algebraic and group-theoretical aspects of the Attractor Mechanism, with particular emphasis on the multi-center solutions and their split flow dynamics and marginal stability phenomena; study of general, group-theoretical and mathematical issues in the (extended) supersymmetric theories of supergravity; study of the embedding of inflationary cosmological dynamics into  $N=1$  supergravity, with special emphasis on the recently proposed Higgs inflation within the NMSSM. We studied black hole entropy, flat directions and higher derivatives, as well as Quantum Special Kaehler Geometry. We studied also  $N=4$  supersymmetric mechanics in multi dimensions.

Most of the ongoing research deals with supersymmetric field theories and supergravity, the latter as a low energy approximation of quantum gravity (superstrings or M theory). Emerging aspects in the physics of extremal black holes are flow equations for scalar fields in single-center and double-center solutions and relative attractor and split attractor flows. Stability and decays of BH composites depend on wall crossing through walls of marginal stability. These issues are studied extending the marginal stability formulae to  $N=8$  supergravity. A generalized mirror symmetry for seven-manifolds has been introduced. Self-mirror theories correspond to theories with vanishing on shell trace anomalies and enjoy milder quantum corrections. Different aspects in the classifications of classical and quantum (discrete) charge orbits for extremal black holes (in 4 and 5 dimensions) have been studied, together with the description of the fake superpotential for small black holes. General fake superpotentials connecting 4D spherical to 5D spinning BH have been investigated. Inflationary cosmological supergravity models with Higgs generated inflation have been also studied. In these models, an important role is played by superconformal symmetry.

Furthermore, we studied thermodynamic geometric methods and State-space Manifold to describe rotating black holes, Black Strings, Black Rings and Hawking radiation. We discussed further the properties of Black Branes in string theory and M-Theory, and thereby took an account of the microscopic viewpoint and statistical correlations for the spherical and non-spherical horizon configurations in  $D=5$ . We studied statistical correlations, quark number susceptibilities for the hot Quantum chromodynamics and extended our examinations for the stability of quarkonium bound states. The former investigation was communicated to the Conference on Quark confinement and the hadron spectrum QCHS IX, Madrid last summer, whereas the latter one has been accepted as an oral presentation which was given at The Symposium on Prospects in the Physics of Discrete Symmetries organized by the Physics Department of "Sapienza" University of Rome, and by INFN (Istituto Nazionale di Fisica Nucleare) in December 2010. Apart from the latter work in the High Energy Physics, our contribution in 2010 has been extended towards the low energy scientific applications of Riemannian geometry.

In the past year we have also studied a class of supersymmetric spinning particle models derived from the radial quantization of stationary, spherically symmetric black holes of four dimensional  $N=2$  supergravities. These spinning particles move in quaternionic Kahler manifolds and the quantized models are gauge invariant field theories with fields equaling sections of special

quaternionic vector bundles. Moreover we have also proposed a new approach to study four dimensional gravity recasting it in terms of six dimensional quantum mechanics by melding the two times and "tractor" approaches. In the past year we have also computed the transition amplitude for a relativistic  $O(N)$  extended fermionic particle in curved space, and we computed the counterterm by using different renormalization schemes.

In the future we intend to extend the results obtained in the past year in many directions. First of all, noting that a quaternionic Kahler space can be thought as the base manifold on a hyper Kahler cone, we would like to reinterpret ghost coordinates of the quaternionic Kähler spinning particles as the extra coordinates one needs to uplift the model from the 4d dimensional base to the  $4(d+1)$  dimensional cone; we intend also to analyze the reduction from the hyper Kähler cone to the  $4d+2$  dimensional twistor space. Another interesting project we are developing, is related to the well known AdS/CFT correspondence. We are trying, in fact, to use tractor technique to calculate holographic anomalies as well as partially massless higher spin fields in ADS manifold.

In 2011, particular attention will be devoted to the cross-fertilizing nature of the black-hole/qubit correspondence, at the edge between supergravity Physics and Quantum Information Theory, and the many unsolved issues within the multi-center black p-brane dynamics. The physics of 4D- multicenter black holes is planned to be further studied with special emphasis to a combined horizontal-duality symmetry, introduced recently, which is expected to classify these more general BH solutions with split-attractor flow. Supergravity flux compactifications and supersymmetry breaking in particle physics will be further investigated.

For 2011, we also wish to continue research application of the Riemannian geometry in the directions including (1) black holes in string theory, M-theory and F-theory; (2) hot QCD, quantum field theories, (3) electrical engineering, (4) condensed matter physics and (5) stability properties of topological black holes in arbitrary Yang-Mills theories. At this juncture, we have communicated two papers on black holes physics for their publication and one conference proceeding is to be published in a special volume of Journal of Physics: Conference Series. During the forthcoming period, we shall continue state-space geometry, black hole physics, non-perturbative properties of QCD, non-linear sigma models, gauge theories, moduli space manifolds and their update applications.

Active collaborations include: JINR-Dubna Russia, Imperial College London, Leuven, Annecy, UCLA, UC Berkeley, Stanford University, Univ. Hannover Germany, Turin Polytechnic Italy, CERN, Switzerland Annecy, LAPTH France, Valencia Univ. Spain.

We also organized, between 2005 and 2009, four Schools on topics within MI12, with the participation of fair amount of MI12 collaborators, both as lecturers and as students. We published in 2010 the fourth volume containing the lecture notes of the recently held School on Attractor Mechanism SAM2007, 18 - 22 June 2007 - INFN-Laboratori Nazionali di Frascati, <http://www.lnf.infn.it/conference/sam2007>, with the title: The Attractor Mechanism, Proceedings of the INFN-Laboratori Nazionali di Frascati School 2007 Series: Springer Proceedings in Physics, Vol. 134, Bellucci, Stefano (Ed.) 2010, X, 346 p., ISBN 978-3-642-10735-1 (print), 978-3-642-10736-8.

## 2 List of Conference Talks

1. S. Ferrara, invited speaker at the UCLA conference on "Supersymmetry in Mathematics and Physics" (Feb. 2010) delivering a talk on "Black Holes and first order flow in Supergravity".
2. S. Ferrara, invited speaker in the 2010 Erice School for Subnuclear Physics, 48th course (August 2010), lecturing on "Perturbative and non-perturbative aspects of N=8 Supergravity" (contribution to the proceedings by S. Ferrara and A. Marrani in preparation) and at the Singapore Conference (Feb. 2010) in honour of Murray Gell-Mann's 80th birthday with a

speech on "Black Holes and Attractors in Supergravity" arXiv:1009.4175 A. Ceresole and S. Ferrara contribution to the Proceedings.

3. S. Ferrara, invited lecturer at the LACES school (GGI Florence, Dec. 2010), lectures on "Introduction to Black Holes Physics".
4. S. Ferrara, invited speaker at the Abdus Salam Center for Theoretical Physics at the Conference for ICTP's Dirac Medal of 25th Anniversary (November 2010).
5. B.N. Tiwari, Statistical Fluctuation and Black Holes in Strings and M-Theory, INFN, Laboratori Nazionali di Frascati, Roma, Italy (26/10/2010).
6. B.N. Tiwari, Statistical Fluctuation and Black Holes in String Theory, String Theory Group, INFN & Physics Department, University of Rome Tor Vergata, Roma, Italy (11/10/2010).
7. B.N. Tiwari, Correlations, Stabilities and Black Holes in String Theory and M-Theory, Department of Physics, Indian Institute of Technology Kanpur, India (18/05/2010).

## References

1. S. Ferrara, A. Marrani, E. Orazi, Nucl. Phys. B **846** 541, (2011), e-print: arXiv:1010.2280 [hep-th].
2. S. Ferrara, A. Marrani, JHEP **1012**, 038 (2010), e-print: arXiv:1009.3251 [hep-th].
3. S. Ferrara, R. Kallosh, A. Linde, A. Marrani, A. Van Proeyen, Phys. Rev. D **83** 025008, (2011), e-print: arXiv:1008.2942 [hep-th].
4. B. L. Cerchiai, S. Ferrara, A. Marrani, B. Zumino, Phys. Rev. D **82** 085010, (2010), e-print: arXiv:1006.3101 [hep-th].
5. S. Ferrara, A. Marrani, Phys. Lett. B **693** 366 (2010), e-print: arXiv:1006.2007 [hep-th].
6. L. Borsten, D. Dahanayake, M.J. Duff, A. Marrani, W. Rubens. Published in Phys. Rev. Lett. **05**, 100507 (2010), e-print: arXiv:1005.4915 [hep-th].
7. S. L. Cacciatori, B. L. Cerchiai, A. Marrani, Published in J. Math. Phys. **51**, 102502 (2010), e-print: arXiv:1005.2231 [hep-th].
8. S. Ferrara, R. Kallosh, A. Linde, A. Marrani, A. Van Proeyen, Phys. Rev. D **82**, 045003 (2010), e-print: arXiv:1004.0712 [hep-th].
9. L. Borsten, D. Dahanayake, M.J. Duff, S. Ferrara, A. Marrani, W. Rubens, Class. Quant. Grav. *27*,185003 (2010), e-print: arXiv:1002.4223 [hep-th].
10. State-space Manifold and Rotating Black Holes, Stefano Bellucci, Bhupendra Nath Tiwari, [JHEP 1101:118, 2011]. e-print: arXiv:1010.1427 [hep-th].
11. S. Bellucci, B. N. Tiwari, JHEP **1011** 030, (2010). e-print: arXiv:1009.0633 [hep-th].
12. S. Bellucci, B. N. Tiwari, JHEP **1005**, 023 (2010), e-print: arXiv:0910.5314 [hep-th].
13. S. Bellucci, B. N. Tiwari, Entropy **12**, 2097 (2010), e-print: arXiv:0808.3921v1 [hep-th].
14. S. Bellucci, V. Chandra, B. N. Tiwari, Int. J. Mod. Phys. A **26**,43, (2011), e-print: arXiv:0812.3792v2 [hep-th].

15. S. Bellucci, B. N. Tiwari, Phys. Rev. D **82**, 084008 (2010), e-print:arXiv:0910.5309 [hep-th].
16. S. Bellucci, B. N. Tiwari, *Thermodynamic Geometry: Evolution, Correlation and Phase Transition*, [doi:10.1016/j.physa.2010.12.043], e-print: arXiv:1010.5148.
17. R. Bonezzi, E. Latini, A. Waldron, Phys. Rev. D **82**, 064037 (2010).
18. M.J. Duff, S. Ferrara, Phys. Rev. D **83**, 046007 (2011), e-print: arXiv:1010.3173 [hep-th].
19. M.J. Duff, S. Ferrara, Class. Quant. Grav. **28**, 065005 (2011), e-print: arXiv:1009.4439 [hep-th].
20. L. Andrianopoli, R. D'Auria, S. Ferrara, M. Trigiante, JHEP **1008**, 126 (2010), e-print: arXiv:1002.4340 [hep-th].
21. A. Ceresole, G. Dall'Agata, S. Ferrara, A.Yeranyan, Nucl. Phys. B **832**, 358 (2010), e-print: arXiv:0910.2697 [hep-th].
22. A. Ceresole, G. Dall'Agata, S. Ferrara, A. Yeranyan, Nucl. Phys. B **824**, 239 (2010), e-print:arXiv:0908.1110 [hep-th].
23. S. Bellucci, S. Krivonos, A. Sutulin, Three dimensional N=4 supersymmetric mechanics with Wu-Yang monopole. Phys. Rev. D **81**,105026, (2010), e-print: arXiv:0911.3257 [hep-th].
24. S. Bellucci, A. Marrani, R. Roychowdhury, On Quantum Special Kaehler Geometry, Int. J. Mod. Phys. A **25**, 1891 (2010), e-print: arXiv:0910.4249 [hep-th]
25. *The Attractor Mechanism*, Proc. of the INFN-Laboratori Nazionali di Frascati School 2007 Series: Springer Proc. in Physics, Vol. **134**, Bellucci, S. (Ed.) 2010, X, 346 p., ISBN 978-3-642-10735-1 (print), 978-3-642-10736-8.
26. S. Bellucci, V. Chandra, B. N. Tiwari, *A geometric approach to correlations and quark number susceptibilities*, Contributed to the Conference on Quark confinement and the hadron spectrum QCHS IX, Madrid, Spain, 30 August 2010 - 03 September 2010. Proc. will be published by the American Institute of Physics]. e-print: arXiv:1010.4405 [hep-th].

## PG21: TOTAL CROSS-SECTIONS AT COLLIDERS

G. Pancheri (Senior Ass.)

### 1 Total cross-sections at LHC <sup>1, 2)</sup>

During the year 2010, we have investigated total cross-sections at LHC. Our research has focused on understanding the phenomenological implications of the large distance behaviour of QCD through the study of hadronic cross-sections. This work is done in collaboration with Y. Srivastava from University of Perugia, A. Grau and O. Shekhovtsova from Spain and Rohini Godbole from India. We have focused on the two following problems:

- pions and protons total cross-section at LHC as a way to study if there is an universal slope for all total cross-sections
- the inelastic and total cross-sections for pp at LHC at current  $\sqrt{s} = 7 \text{ TeV}$ .

The second problem is in progress and its results will be published in the year 2011. The first problem has been studied in details <sup>2)</sup> and has been presented in a number of Workshops and conferences (see list). In <sup>2)</sup> we have examined the total cross-sections for pion interactions at LHC which has been proposed to be measured through forward neutron detection with Zero Degree Calorimeters. We show the process of interest in the left panel in Fig. 1 and the result from our model in the right panel. This figure shows that our model for pion total cross-sections is in agreement with the Additive Quark Parton Model at low CM energies,  $\sqrt{s} = 5 - 10 \text{ GeV}$ , and satisfies factorization at high energies <sup>2)</sup>.

### 2 Other activities

I have also collaborated to studies of the low energy hadronic cross-section <sup>3)</sup> and meson production at DAPHNE <sup>4)</sup>. In addition, a Workshop on Linear Collider Physics was organized in Frascati, 1-3 December 2010, held together with the Bruno Touschek Memorial Lectures, on December 1st,

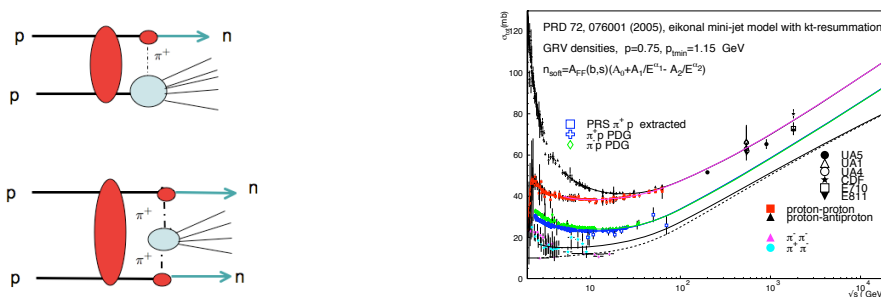


Figure 1: At left, the processes proposed to measure pion cross-sections at LHC. At right, predictions for the total cross-sections for pp,  $\pi p$ , and  $\pi\pi$  using our eikonal minijet model <sup>2)</sup>.

focused on LHC and on the future of Linear Colliders. These activities will continue in 2011, with LC11, Linear Collider Workshop 2011, to be held in Trento at the ECT\*, with coordination from PG21 and LNF1.

### 3 Conference Proceedings

1. G. Pancheri *et al.*, “Total Cross-sections at very high energies: from protons to photons”, in Proceedings of Non Perturbative QCD 2009, Paris, France e-Print: arXiv:1001.4749 [hep-ph].
2. G. Pancheri, “Large distance and ultra-soft gluon effects in total cross-sections in  $pp$ ,  $\gamma p$  and  $\gamma\gamma$ ”, presented at Diffractive and Electromagnetic processes at LHC, ECT\*, January 2010
3. Y. Srivastava, A. Grau, G. Pancheri, O. Shekhovtsova, “Modeling Pion and Nucleon Total Cross-sections”, Diffraction 2010, Marseille, France, September 2010
4. G. Pancheri, “Soft gluon kt-resummation and total cross-sections in the asymptotic limit”, presented at SCET 2010, April 2010, Ringerg, Gemany
5. G. Pancheri *et al.*, “Soft gluon resummation in the infrared region and the Froissart bound”, DIS 2010, Florence, April 2010, e-Print: arXiv:1007.0208 [hep-ph]
6. G. Pancheri *et al.*, “QCD mini-jets contribution to the total cross-section and expectations at LHC”, presented at Forward Physics at LHC, La Biodola, Isola d’Elba, May 2010, arXiv:1012.5169
7. G. Pancheri, “Soft gluon kt-resummation in the infrared region and energy behaviour of total total cross-sections”, presented at the Italian Theoretical Physics meeting in Cortona, May 2010
8. G. Pancheri *et al.*, “ Modeling large distance QCD via kt-resummation in total cross-sections”, presented in Telaviv, for 79th birthday of Eugeny Levin, October 2010
9. G. Pancheri “Modeling large distance QCD via kt-resummation in total cross-sections”, Seminar held in Orsay, France, December 9th, 2010

### References

1. A. Grau, R. M. Godbole, G. Pancheri and Y. N. Srivastava, *Soft Gluon kt-Resummation and the Froissart bound*, Phys. Lett. B **682** (2009) 55.
2. A. Grau, G. Pancheri, O. Shekhovtsova and Y. N. Srivastava, *Modeling pion and proton total cross-sections at LHC* Phys. Lett. B **693** (2010)456.
3. Working Group on Radiative Corrections and Monte Carlo Generators for Low Energies (S. Actis et al.), *Quest for precision in hadronic cross sections at low energy: Monte Carlo tools vs. experimental data*, Eur. Phys. J. **C66** (2010) 585, e-Print: arXiv:0912.0749 [hep-ph].
4. S. Eidelman, S. Ivashyn, A. Korchin, G. Pancheri, O. Shekhovtsova,  *$e+e-$  annihilation to  $(\pi^0\pi^0\gamma)$  and  $(\pi^0\eta\gamma)$  as a source of information on scalar and vector mesons*, Eur. Phys. J. **C69** (2010)103, e-Print: arXiv:1003.2141 [hep-ph].

## *5 – Technological and Interdisciplinary Research*



## ALTCRISS

M.A.Franceschi, G.Mazzenga (Tecn.), T. Napolitano, M.Ricci (Resp.), B.Spataro

Participant Institutions:

ITALY: INFN LNF and Roma 2-Tor Vergata; ASI (Italian Space Agency);

Mars Center Telespazio, Napoli

GERMANY: DLR German Space Agency

RUSSIA: MePhi, IBMP, Roscosmos

ESA-ESTEC European Space Agency

JAPAN: JAXA Japan Aerospace Exploration Agency

### 1 Introduction

The ALTCRISS experiment (Alteino Long Term monitoring of Cosmic Rays on the International Space Station) - previously named SI-RAD - is a continuation of the activities carried out for the experiments SIEYE1 and SIEYE2 on board the Russian Space Station MIR in the years 1995-2002 and for the experiment SIEYE3/ALTEINO on board the International Space Station (ISS), still running. <sup>1)</sup> <sup>2)</sup> <sup>3)</sup>.

The task of the ALTCRISS experiment (approved by ESA and ASI in Phase A) is to develop a detector to be placed on the external part of the ISS. The detector will be used to monitor cosmic rays and radiation environment in Low Earth Orbit. Long term (Solar modulation) and short term (coronal mass ejections, orbit dependence) effects on the particle flux will be monitored as well as the dose absorbed by the astronauts. In addition, data will be compared with measurements taken inside the ISS with ALTEA <sup>4)</sup>, ALTEINO and LAZIO/SIRAD <sup>5)</sup> detectors to validate radiation transport and dose estimation codes. At the same time, the investigation, with a more sophisticated instrument, of the "Light Flashes" phenomenon <sup>6)</sup>, will be conducted to improve and refine the results obtained with the previous SIEYE experiments.

The preparation of the next ALTCRISS extended mission is advancing towards the completion of the full flight instrument consisting of a 16-plane tower of double-sided silicon detectors (8x8 cm<sup>2</sup> area) equipped with trigger and anticoincidence counters. The total weight is about 15 kg and the total power consumption should not exceed 30 W. The hardware set-up is accomplished through three steps by the construction of a laboratory prototype model, an engineering model and the final flight, space qualified model.

The activity has been mainly focused on the development of the following systems of the engineering model:

- Trigger system.
- Development of Silicon Photomultiplier (SI-PM) technology for space applications and test of different SI-PM configurations.
- Completion and test of a highly integrated silicon board (16 cm x 16 cm).
- Production and test of a low-power, low-mass Digital Processing Unit (DPU).

For the year 2011, the planned activity includes the completion of the engineering unit and the set-up of the flight configuration equipped with autotrigger capabilities for heavy nuclei and a

trigger for crossing protons and nuclei. The interface with the ISS Space Station will be realized with an intermediate CPU to manage the telecommands from ground and the download of the data. Beam tests at the LNF-BTF, GSI/Darmstadt and other facilities are also planned together with the continuation of the R&D on the SI-PM technology.

## 2 Activity of the LNF group

The LNF group has taken the responsibility of the design, construction and test of the mechanical structures and interfaces of the three models of the detector also contributing to the integration of the mechanical support for the DAQ. This activity is carried out with the support and the participation of the LNF Service for Design and Mechanical Costructions (SPCM). The activity in 2010 has been mainly devoted to the completion of the mechanical support of the engineering model and to the interfaces of the front-end and DAQ with the detector, ready to be tested on beams. These systems are being developed for the final space-qualified flight configuration in the year 2011. The LNF group participates as well in the beam test activities at the above mentioned facilities having the responsibility of the beam trigger counters and of the general arrangement and set-up.

## 3 Selection of recent publications

1. V. Zaconte *et al.*, “The radiation environment in the ISS-USLab measured by ALTEA”, *Adv. Sp. Res.* **46**, 797 (2010).
2. C. La Tessa *et al.*, “Estimate Of The Space Station Shielding Thickness At A USLab Site Using ALTEA Measurements And Fragmentation Cross Sections”, *Nucl. Instr. Meth. Phys. Res.* **B267**, 3383 (2009)
3. M. Casolino *et al.*, “Investigation of radiation environment and Light Flash phenomenon on board manned space stations with silicon detector telescopes”, *Nuovo Cim.* **31C**, 77 (2008).
4. M. Casolino *et al.*, “The ALTCRISS project on board the International Space Station”, *Adv. Space Res.* **40**, 1746 (2007).

## References

1. V. Bidoli *et al.*, “In-flight performances of SilEye-2 Experiment and cosmic ray abundances inside space station MIR”; *Journal of Physics G: Nuclear and Particle Physics* **27**, 2051(2001).
2. M. Casolino *et al.*, “The Sileye/3-Alteino experiment on board the International Space Station”; *Nucl. Phys.* **113B**, 88 (2002).
3. V. Bidoli *et al.*, “Dual origin of light flashes in space”, *Nature* **422**, 680 (2003).
4. L. Narici *et al.*, “ALTEA: Anomalous long term effects in astronauts. A probe on the influence of cosmic radiation and microgravity on the central nervous system during long flights”, *Adv. Space Res.* **31**, 141 (2003).
5. F. Altamura *et al.*, “Preliminary results from the LAZIO-Sirad experiment on board the International Space Station”, *Proc. XXIX ICRC, Pune (2005)*, SH35 p.101.
6. G. Horneck, “Radiobiological experiments in space: a review”, *Nucl. Tracks Radiat. Meas.*, **20**, 185 (1992).

**FAST**  
**(FEMTOSECOND ACTIVE TIMING AND SYNCHRONIZATION)**

D. Alesini (Tecn.), M. Bellaveglia (Art. 23 - Tecn.), A. Drago (I Tecn.),  
A. Gallo (Resp. - I Tecn.), G. Gatti (art. 23 - Tecn.), A. Ghigo (Dir. Tecn.)  
A. Mostacci (Ass. - Ricercatore Roma1), M. Serio (Dir. Ricerca), A. Stella (Tecn.)

## 1 Introduction

The "Femtosecond Active Timing and Synchronization" (FAST) experiment supported by the INFN, V National Committee, is an R&D program to obtain general synchronization among laser pulses, RF fields and LINAC electron bunches in the femtosecond scale in the complex constituted by the SPARC FEL facility and the FLAME laser, both situated in the same experimental area of the LNF (LIFE laboratory).

Timing and Synchronization in the femtosecond scale is becoming a crucial item for a large variety of applications:

- Laser seeding of FEL process;
- Pump and probe measurements with different sources (FEL, LASER, e-bunches);
- Wakefield Laser-plasma Acceleration of externally injected electron bunches;
- Thomson scattering of counter-propagating short laser pulses and electron bunches.

The high brightness beams required to drive the FEL process are characterized by minimum transverse emittance ( $\epsilon \approx 1\mu m$ ) and short bunches ( $\sigma_z \approx 1mm$ ).

One necessary condition to minimize the transverse emittance is to precisely synchronize the laser pulse on the photocathode with the accelerating RF field in the RF gun. The required synchronization is  $< 1ps_{RMS}$  (SPARC working point).

A very efficient way to compress the bunch and reduce its length is to adopt the RF compression scheme described in <sup>1</sup>). Optimization of the compression factor requires  $< 500fs_{RMS}$  synchronization between bunch arrival time and RF field in the RF compressor (SPARC).

These specifications have been already achieved by the SPARC synchronization system, which is based on a distribution of electrical reference signals through a coaxial cable network.

However, in the near future more severe synchronization specifications need to be achieved in order to cope with the requests of a family of new experiments where the SPARC beam will interact with the FLAME laser. To fulfill the requests of these experiments, as discussed in section 2.3, one have to provide a time jitter between the two beams (electrons and photons) less than  $100fs_{RMS}$ .

## 2 Tasks and achieved results in the year 2010

The FAST collaboration is aimed at studying and implementing upgrades of the existing SPARC synchronization system to cope with the most demanding specifications of future experiments. During year 2010 the FAST work program for the LNF component of the collaboration consisted in the following points:

- Design and installation of a new RF pulse shaping system to feed the SPARC RF gun;

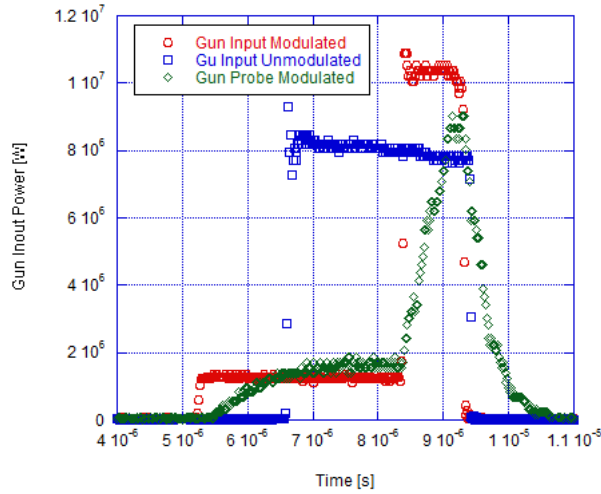


Figure 1: *RF pulse shaping to increase the RF gun accelerating gradient and preserving the phase noise performance.*

- Design and installation of a new timing scheme in the SPARC photoinjector;
- Design of synchronization solutions for the LIFE laboratory (SPARC-FLAME interaction).

## 2.1 RF pulse shaping for gun feeding

To obtain a larger accelerating gradient in the electron gun without damaging the RF structure, we reduced the pulse duration from  $2.5\mu s$  to  $1\mu s$ . The breakdown rate dramatically dropped. Unfortunately the PLL for the klystron phase stability (see <sup>4</sup>) needs  $\approx 2 \div 3\mu s$  to be effective. So we used an amplitude modulation technique to solve the problem. In particular, in a same RF pulse, we switch on the RF at a moderate power level and after the phase loop began to operate at its best, we switch to the operational RF level (about 10 times greater). The second level is held for  $1\mu s$  since the gun filling time is of  $\approx 700ns$ . The laser pulse for the generation of electrons arrives on the cathode just before the RF pulse falling edge so that higher accelerating gradients are reachable with same level of phase stability of the accelerating field respect to the former operating mode (see <sup>3</sup>) and <sup>4</sup>). In figure 1 the envelopes of the unmodulated and modulated RF pulses generated by the LLRF system are shown. The maximum forward RF power exciting the RF gun passed from  $\approx 9MW$  to  $\approx 10.5MW$ , while the measured phase noise of the gun RF field respect to the reference remained less than  $100fs$ , the standard specification of the system.

## 2.2 New timing scheme

A new timing scheme for the SPARC project has been designed and installed. This scheme provides a new way to produce and distribute the machine triggers and improves the charge stability of the accelerated e-bunch. Also the system physical cabling has been simplified to include all the laser systems (photo-cathode, seeding and FLAME). The new scheme (figure 2) essentially produce the machine  $1kHz$  and  $10Hz$  triggers starting from the photocathode laser oscillator repetition rate of  $79.33MHz$ . As reported in <sup>2</sup>), this means that the new timing scheme guarantees that the laser

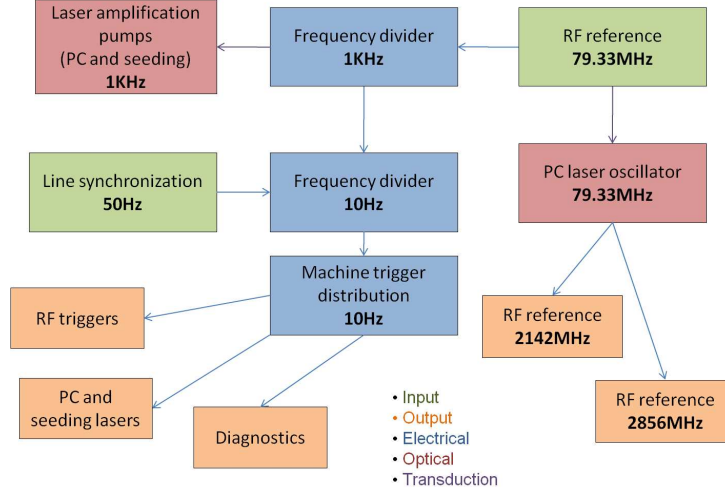


Figure 2: *The SPARC upgraded timing system layout.*

amplification gate occurs at the same time respect to the infrared seed arrival for each e-bunch trigger event. With the transition to the new layout, the relative jitter of the  $1kHz$  trigger respect to the IR laser pulse repetition rate is less than  $500ps_{pp}$ . The machine shot-to-shot stability is then increased. In fact the previous timing system layout foresaw an active re-synchronization of the  $1kHz$  laser pump trigger. From the  $79.33MHz$  pulse train, the system selected the one nearest to the front of the free running  $1kHz$  trigger. This brought to a  $\pm 12.6ns$  uncertainty of the UV pulse time arrival on the cathode respect to the RF trigger. Since we are injecting the laser UV pulse in the RF gun during the filling transient (see section 2.1), this brought to an instability in beam charge and energy. We can assert that with the new timing scheme we can also provide a charge stability of less than  $5\%_{RMS}$ .

### 2.3 LIFE synchronization

As mentioned in the introduction, the most demanding experiment in the near future is to perform a wakefield laser-plasma acceleration with the SPARC beam injected in a plasma wave generated by the FLAME laser colliding with a proper target. This technique requires a synchronization between the SPARC electron bunch and the plasma wave (synchronous with the FLAME laser) at  $< 100fs_{RMS}$  level. For a better overview of the problem you can see <sup>6)</sup>.

We designed two possible solutions reported in figure 3. The first one is to connect the two experimental areas of SPARC and FLAME with a bundle of coaxial cable to transport the synchronization and timing signals. This solution is very easy and can be operational in few weeks. To obtain the maximum performance by this kind of technology we are planning to use a temperature stabilized cable bundle. However the best performance we expect from this solution is a time jitter of hundreds of femtoseconds between the SPARC and FLAME beams. The second solution that we are designing foresee an optical fiber distribution for the synchronization signals. An optical master oscillator should be placed in the synchronization rack in the SPARC hall and should serve both the photo-cathode and the FLAME laser. Also the RF waveform to feed the accelerating

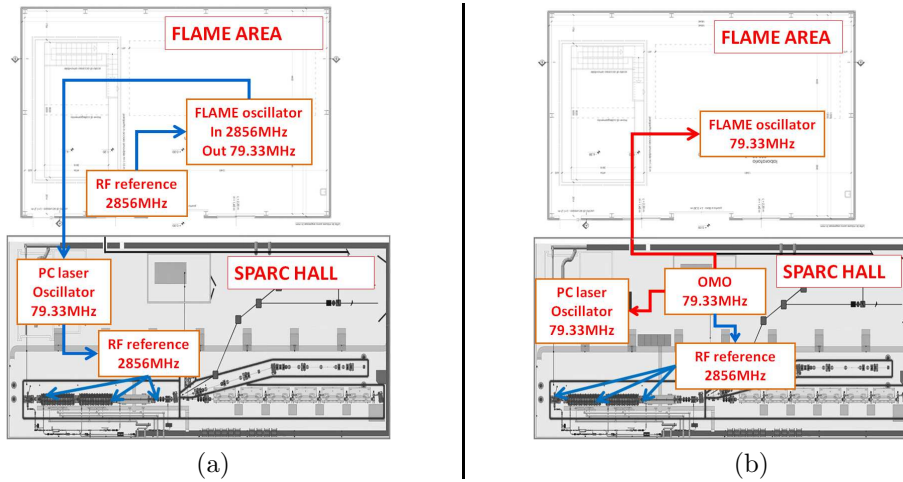


Figure 3: *LIFE* synchronization possible solutions: (a) coaxial reference distribution and (b) optical fiber reference distribution.

structures should be derived from the optical  $79.33\text{MHz}$  reference. This solution needs a more complicated system modification, has a higher cost, but new techniques for the synchronization like optical cross correlation and active stabilization for the fiber length could be used.

The performance of this kind of system has been yet tested in other large scale facilities in the world and the synchronization obtained was a two-beam time jitter well below  $100f_{SRMS}$ . A master oscillator for experimental tests has been yet acquired at LNF synchronization laboratory and a new phase detection technique based on cross correlation with a foreseen resolution of less than  $10f_{SRMS}$  is under study.

### 3 Conference Talks

1. M. Bellaveglia, Synchronization and LLRF control at SPARC and PLANS for SPARX, PSI SwissFEL meeting, 25th March 2010

### References

1. M. Ferrario *et al.*, Phys. Rev. Lett. **104**, 054801 (2010).
2. M. Bellaveglia *et al.*, “Laser timing and synchronization measurements”, INFN-LNF technical note LS-06/001
3. M. Bellaveglia *et al.*, “SPARC photo-injector synchronization system and time jitter measurements”, EuroFEL-Report-2006-DS3-027
4. M. Bellaveglia *et al.*, “SPARC photo-injector synchronization system and time jitter measurements”, EuroFEL-Report-2007-DS3-051
5. M. Bellaveglia *et al.*, “Measurement devices for the SPARC synchronization system”, Proc. of DIPAC09, Basel, Switzerland
6. M. Bellaveglia, “Timing and synchronization at SPARC”, 40th LNF Scientific Committee, <http://agenda.infn.it/materialDisplay.py?contribId=4&sessionId=0&materialId=slides&confId=2674>

## FLUKA2

M. Pelliccioni (Resp.)

### 1 Report year 2010

2010 main activities included the collaboration with three Working Groups (DOCAL, TG67, RC26) of the most important International Commissions (ICRP, ICRU) operating in the field of radiation protection. DOCAL is preparing a joint ICRP/ICRU Report for the revision of the ICRP Publication 74 and ICRU Report 57. The ICRP Task Group 67 is preparing the first ICRP Publication dedicated to Radiation Protection in Space. The ICRU Report Committee 26 is engaged in an update in matter of Operational Radiation Protection Quantities for External Radiation. The results of calculations performed in recent years with the FLUKA code are going to be included in the publications currently under development by the three Working Groups.

In 2010 the ICRU has published the Report 84 dedicated to the doses received by air crew, where the results of simulation performed by FLUKA are also mentioned. In this case, the collaboration has been provided as a consultant to Report Committee.

The results of calculations carried out by Fluka for the radiation protection problems of CNAO have been summarized in a presentation to the Eurados Meeting held in Frascati (4-5 February).

### 2 Publications

1. R. Bedogni, M. Pelliccioni, A. Esposito, Nucl. Inst & Meth. **A 615**, 78 (2010).
2. M. Pelliccioni, "Radiation Protection at Hadron Therapy Facilities", paper presented at the Eurados Meeting, Frascati 4-5 February 2010.
3. K. Parodi on behalf of the Fluka Coll., "The recent and future developments of the Fluka MC code for ion beam therapy", paper presented at MCNEG 2010, NPL, Teddington, UK.
4. W. Bolch *et al.*, "DOCAL External Dosimetry Subgroup", Status of the Revision of ICRU Report 57/ICRP Publication 74. Paper presented at the ICRP DOCAL2010 Meeting, Nara, Japan, 17-21 May, 2010.
5. S. Roesler on behalf of the Fluka Coll., The Application of the "Monte", Joint International Conference on Supercomputing in Nuclear Applications and Monte Carlo 2010 (SNA + MC2010), Hitotsubashi Memorial Hall, Tokyo, Japan, October 17-21, 2010.
6. V. Vlachoudis, on behalf of the Fluka Coll., "Applications of FLUKA Monte Carlo code for Nuclear and Accelerator Physics", paper presented at ECAART10.
7. G. Battistoni *et al.*, "Fluka capabilities and applications for radiation damage to electronics and high energy hadron accelerators", Joint International Conference on Supercomputing in Nuclear Applications and Monte Carlo 2010 (SNA + MC2010) Hitotsubashi Memorial Hall, Tokyo, Japan, October 17-21, 2010.
8. M. Pelliccioni (as Consultant to the Report Committee), "Reference data for the validation of doses from cosmic-radiation exposure of aircraft crew", ICRU Report 40.

## HCPAF

S. Bini (Art. 2222), P. Chimenti (Art.15), V. Chimenti (Ass.),  
R. Di Raddo (CTER), V. Lollo (CTER), B. Spataro (D.T.) (Resp.)

### 1 Aim of the experiment

The HCP-AF Group technological activity is dedicated to the construction of two 3 cells linear accelerating structures working at 11.424 GHz in the framework of the collaboration with SLAC (Stanford Linear Accelerator Center) and KEK (Kō Enerugī Kasokuki Kenkyū Kikō). Two sections made of copper and sintered molybdenum bulk operating at 11.424 GHz have been fabricated using the high temperature brazing technique. Here we describe the technological procedure used for fabricating the sections and the low level RF tests results.

### 2 Copper section construction and characterization

An intense technological activity is dedicated to set up X-band accelerating structures operating at 11.424 GHz using different materials and methods <sup>1, 2, 3, 4, 5, 6, 7</sup>).

The device under study is a 3-cell structure fed by the circular waveguide, as shown in Fig. 1. The central one is the cell under test at high gradient while the other ones are used to match the RF power from the input circular waveguide and to balance the electric field in order to have the maximum intensity in the central one. This scheme is that used at SLAC for the cell test <sup>8</sup>).

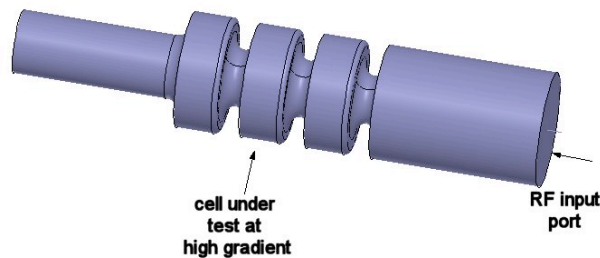


Figure 1: *Sketch of the cells structure to be tested at high power.*

The mode excited to test the structure is the  $\pi$ -mode. Its electric field profile on axis and the reflection coefficient obtained by HFSS simulations <sup>9</sup>) are reported in Fig. 2. They show the good matching at the nominal RF frequency of 11.424 GHz and the maximum field intensity in the central cell.

The relevant cell dimensions for the copper structure are reported in the mechanical drawing of Fig. 3. The section has been made of oxygen free Cu (OFHC) realized by mechanical machining with a numerical controlled lathe; the obtained precision is below  $1.5 \mu\text{m}$  while the roughness is not worst than 80 nm. The surface finishing was obtained directly by mechanical machining with custom cutting tools (diamond mono-crystal), avoiding any polishing technique. Each cell has been checked with a quality control test. A dedicated simple and cheap cleaning procedure after the machining has been adopted, too.

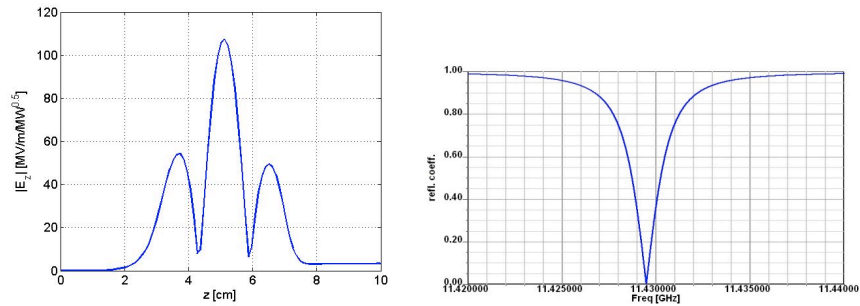


Figure 2: Electric field profile on axis and reflection coefficient at the RF input port for the  $\pi$ -mode (HFSS simulations).

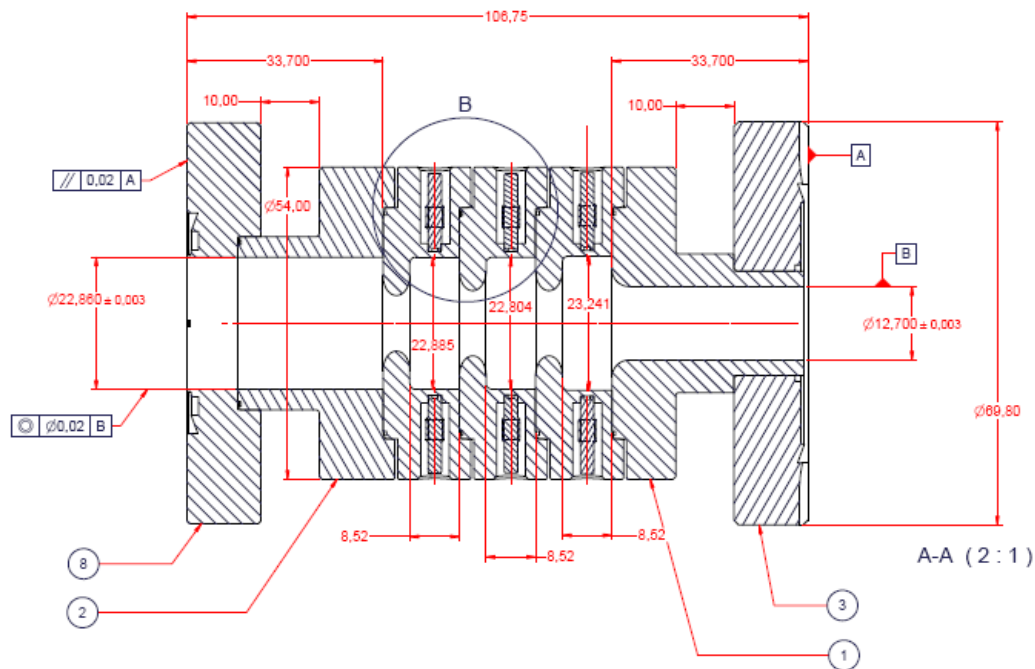


Figure 3: Mechanical drawing of copper structure with dimensions.

The brazing of the structure requires two different steps: the brazing of the copper-copper cells and the brazing of the stainless steel flanges on the copper beam pipe. Different composition of the PALCUSIL (Palladium-Copper-Silver) alloys with different melting points were used for the two different brazing procedures. In the subsequent brazing of the tuners one has to consider the effect of the gravitation; as shown in Fig. 3, they are placed in opposite sides of the structure and therefore they have been brazed in two different steps using the PALCUSIL alloy with decreasing melting temperature. After extensive tests, we have concluded that the better brazing with PALCUSIL was obtained when the structure was brazed in vertical position (due to the gravitation effects).

The tuners are designed for elastic wall deformation, i.e they are copper cylinders of 2.3 mm diameter acting on a copper surface 0.9 mm thick; the maximum allowed (measured) elastic deformation is of 0.6 mm height. Tuners are brazed in order to guarantee a bidirectional (i.e. push-pull) tuning able to recover 1.6 MHz each mm<sup>3</sup> of wall deformation.

To identify structures we use abbreviations derived from the names of the corresponding periodic structures including the manufacturers name and the serial number. As an example, the initials 1C-SW-A5.65-T4.6-Cu-Frascati-#2 refer to the high-gradient cell 1C with a 5.65 mm aperture radius (A5.65) a 4.6 mm thick iris (T4.6) manufactured by INFN at the LNF. Finally, #2 indicates that this is the second structure manufactured.

### 3 Low power RF measurements results for the copper structure

Fig. 4 shows the picture of the copper structure designed according to Fig. 3. The structure has been closed by two metallic plates and two small probes have been inserted to excite the field avoiding the coaxial-circular waveguide transitions used in the high power tests for practical reasons. With respect to the case of a circular mode launcher this configuration introduces a shift of the resonant frequencies and a perturbation of the electric field profile, but the perturbation on the  $\pi$ -mode is negligible. The multi-cell mode frequencies, quality factors and the related field profiles obtained by SUPERFISH<sup>10)</sup> are reported in Table 1 and Fig. 5. The fourth mode corresponds to the  $\pi$ -mode.

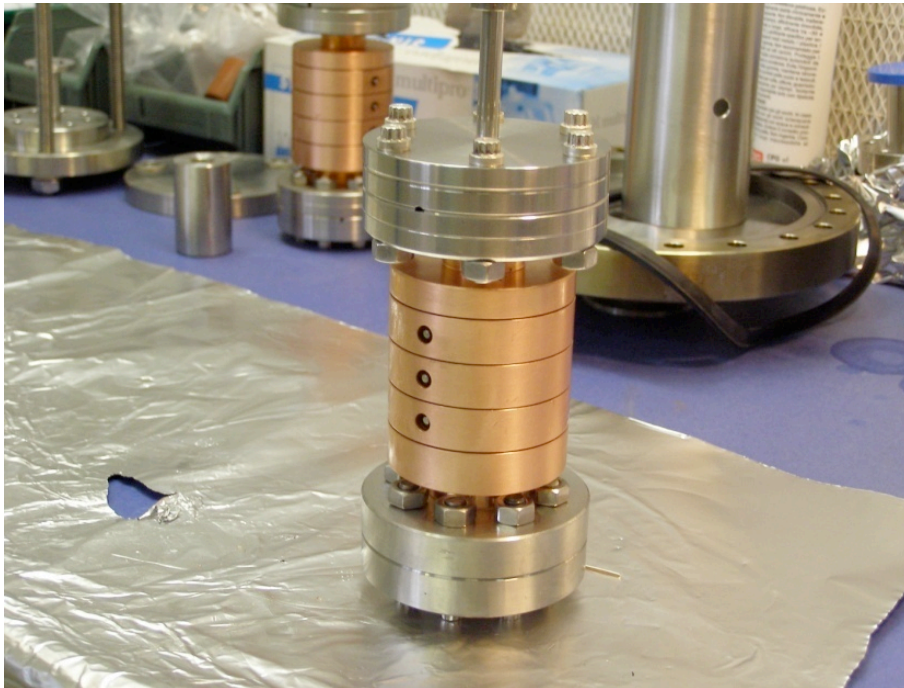


Figure 4: *Picture of the copper structure under test.*

The measured resonant frequencies and the quality factors of the structure simply assembled and before brazing are reported in Table 1 as well. As an example the measured field profiles of

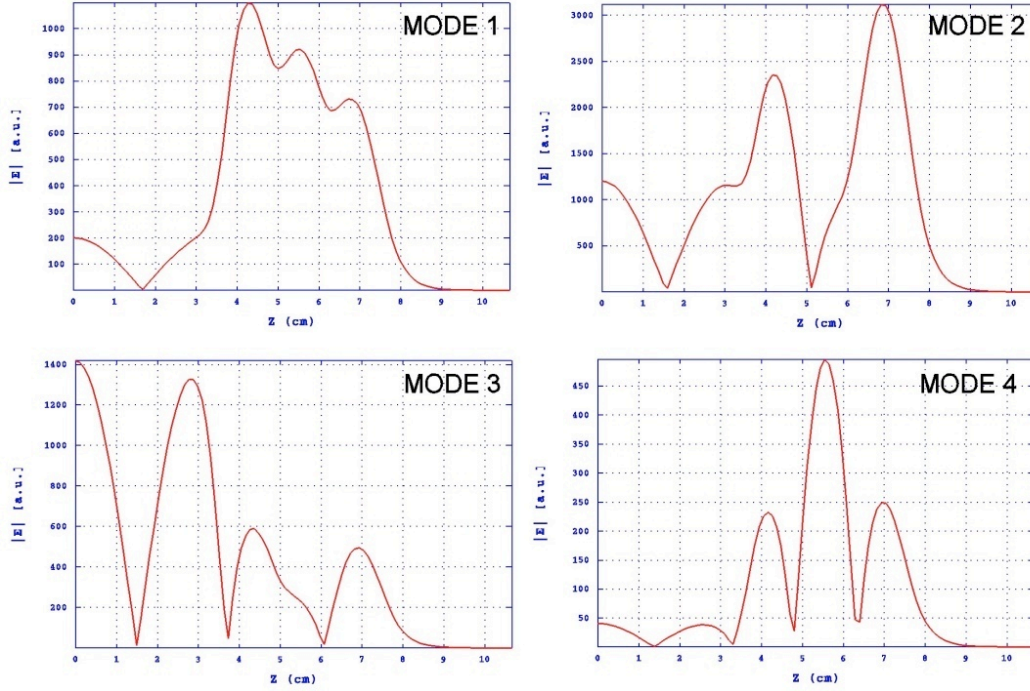


Figure 5: *Field profiles of the resonant modes (SUPERFISH results).*

Table 1: *Mode frequencies and quality factors (given by SUPERFISH) and measurements results of copper structure before brazing. We have to remind that after brazing the quality factors increase by  $\sim 5\%$ .*

MODE	Res. Freq. [MHz] (simul.)	Res. Freq. [MHz] (meas.)	Q (simul.)	Q (meas.)
1	10980	10983	8478	7700
2	11118	11127	8889	7600
3 <sup>1</sup>	11211	11209	12354	–
4	11433	11429	8380	7200

the  $\pi$ -mode and of the mode number 1 (0 multi-cell mode) are reported in Fig. 6. They have been obtained by standard bead-pull technique.

RF measurements after brazing have been performed as well, but no significant differences have been measured with respect to the case of the structure simply assembled.

<sup>1</sup>This mode is not a multi-cell mode but the mode of the circular waveguide. Its frequency is strongly depend on the circular waveguide length and strongly coupled with the probes used to characterize the other multi-cell modes.

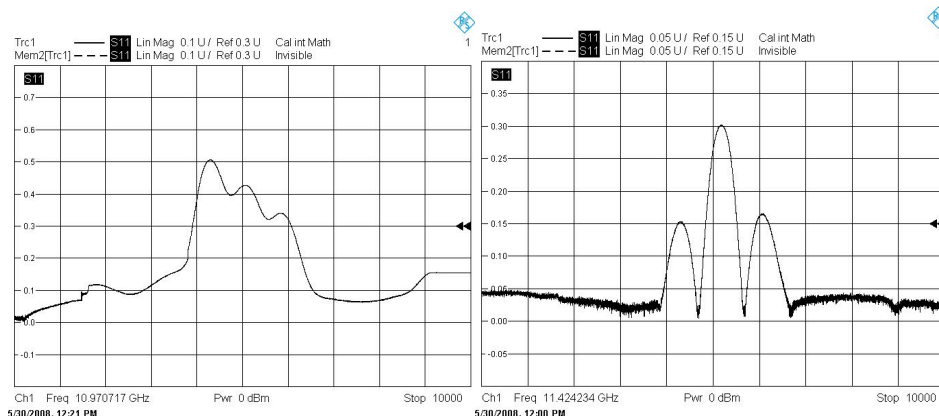


Figure 6: Measured  $\pi$ -mode and 0-mode field profiles (by bead-pull technique) corresponding to MODE 1 and MODE 4 of Fig. 5 respectively.

#### 4 Sintered molybdenum section

In the following we report on the construction issues and RF characterisation of a Molybdenum bulk section, since sintered Mo is seen as a possible novel material to build accelerating section with improved breakdown performances.

Stainless Steel and sintered molybdenum bulk are not wetted by the PALCUSIL. A simple way to overcome this difficulty is to create a thin layer with a few microns thickness of Copper or Nickel, electrolytically deposited. Then the eutectic Ag/Cu (Silver-Copper) alloy can be used without any difficulty because it wets very well both Cu and Ni.

A galvanoplastic process was adopted in order to obtain thin layers of Cu or Ni. That is based on the use of a graphite anode, wrapped up with a cotton pad which is soaked in a special electrolytic bath that contains ions of Cu or Ni. This method is simple and quick to use and makes easy to treat only the area interested in the process. The Cu layer gives the best results if it is fixed, both on Stainless Steel and Mo, through a vacuum thermal treatment at roughly 800 °C, before brazing, while for Ni this is not necessary.

A 3 cells standing wave section realized with the sintered Molybdenum bulk has been built and vacuum brazed following the above procedure (Fig. 7). The structure has dimensions slightly different with respect to the copper one to take into account the different surface conductivity<sup>9</sup>), as shown in the mechanical drawing of Fig. 8.

The structure has been machined with a numerical controlled lathe and the obtained precision is around at  $\pm 2.5 \mu\text{m}$  while the roughness is not worst than 300 nm. The surface finishing was obtained directly by mechanical machining with custom cutting tools tungsten carbide tools. The tuners are identical to the copper case discussed in sec. 2, except that the maximum measured allowed elastic deformation is of 0.3-0.4 mm height on a 0.8 mm thick surface.

RF measurements have been done before and after the brazing of the structure. The results after brazing are shown in Table 2. In the table we have compared the experimental results with simulations. The discrepancy between the resonant frequencies (simulated and measured) is given by the fact that we performed the measurements at a different temperature with respect to the working one. Field profiles measurements (by the bead pull technique) gave results similar to the case of copper structure.



Figure 7: *Picture of the molybdenum structure under test.*

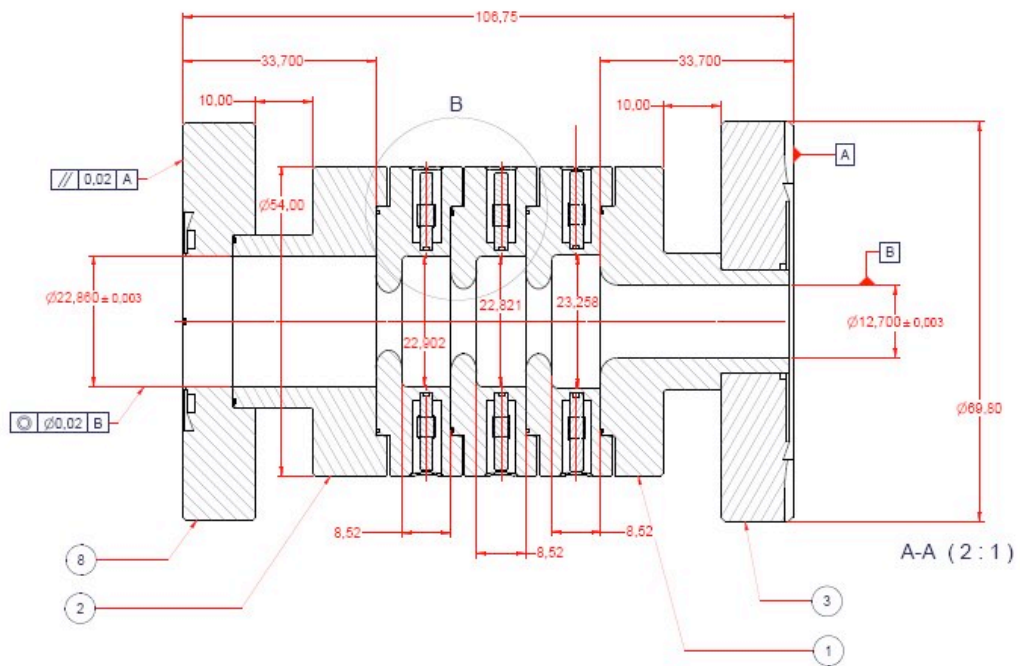


Figure 8: *Measured mechanical drawing of molybdenum structure with dimensions.*

Table 2: *Mode frequencies and quality factors (given by SUPERFISH) and measurements results of molybdenum structure after brazing.*

MODE	Res. Freq. [MHz] (simul.)	Res. Freq. [MHz] (meas.)	Q (simul.)	Q (meas.)
1	10985	10977	4850	4850
2	11120	11129	5150	5000
3	11430	11425	4850	4800

## 5 Conclusions and future activity

Copper and Molybdenum X-band RF structures have been constructed at LNF using two different high temperature brazing techniques, one for each structure. The brazed Cu and Mo structures as soon as possible will be tested at SLAC with a RF high power to study the breakdown rate behaviour. In the meantime additional investigations on the electroplating method for realizing linear accelerating sections operating at 11.424 GHz and the design of the triple-choke cavity are under study, too.

## References

1. V.A. Dolgashev *et al.*, “Status of High Power Tests of Normal Conducting Single-Cell Standing Wave Structures”, Proceeding of IPAC 2010, Kyoto, Japan, 2010, pp. 3810-3812 (and references therein);
2. P. Chimenti *et al.*, “An Investigation on Electrforming Procedures for R.F. 11 GHz Linear Accelerating Structures at Frascati Laboratory”, Frascati Report LNF-05/ 23 (IR), 2005.
3. S.Bini *et al.*, “Electroforming Procedures Applied to the Construction of 11.4 GHz Linear Accelerating Structures: Status Report on SALAF Activity”, RF-07/003, 29/05/2007;
4. S. Bini *et al.*, 2008 Status report on SALAF technical activity on X-band linear accelerating structures project at Frascati Laboratories, SPARC-RF-08/001, July 31, 2008.
5. S. Bini *et al.*, “Status report on SALAF technical activity during the first half of 2009”, SPARC-RF-09/002 April 30, 2009;
6. S. Bini *et al.*, SALAF Group technological activity , SPARC-RF-09/003 June 30, 2009;
7. S. Bini *et al.*, “Activities on the sputtered metals thin films for accelerating cavity applications”, RF-10/001 12/01/10;
8. V. Dolgashev, private communications and his seminar held at LNF.
9. www.ansoft.com.
10. J.H. Billen, L.M. Young, Part. Acceler. **7**, 213 (1976).

## IMCA (Innovative Materials and Coatings for Accelerator) - NTA

A. Balerna, R. Cimino (Resp.), M. Commisso, T. Demma, D. R. Grosso, R. Larciprete,  
S. Guiducci, R. Flammini, C. Milardi, V. Nistor, C. Vaccarezza, M. Zobov

In collaboration with:  
University of Calabria and INFN

IMCA experiment was started in 2010 in order to develop new materials and coatings with stable and low enough SEY (Secondary Electron Yield) to guarantee full operation of present and future accelerator machines. This item, in fact, is crucial in controlling Electron Cloud formation and in reducing its effects, that are well known to be a potential bottle-neck to the performances obtainable from present and future accelerators. Frascati has a longstanding experience in qualifying materials in terms of surface parameters of interest to e-cloud issues. We are routinely measuring SEY, its dependence from electron energy, temperature and scrubbing. We are about to be ready to study not only the Photo Electron Yield (PEY), but more importantly, we are setting up our Laboratory to be able to characterize in situ the surface chemical composition and eventual modifications occurring during electron or photon irradiation by using XPS with conventional X-ray source or synchrotron radiation beamlines in construction at DAΦNE (see this annual report). Our experimental measurements of the relevant parameters can be also confidently compared to simulations, performed by running the EC codes, in order to elucidate the final consequences on machine performances. Such a combined characterization effort is also suggesting ways to produce low SEY materials coatings. This issue is particularly important in view of the possible construction in Italy of a Super-B high luminosity collider <sup>1)</sup>, where e-cloud issues are foreseen to be a potential bottleneck to operational machine performances. The previous experimental and theoretical results obtained with the Nuvola experiment during the past years, are the scientific base of this project. Indeed during these years in the Surface Laboratory in Frascati, we measured SEY reduction (scrubbing) not only versus the dose (the number of impinging electrons per unit area on sample surfaces) of the impinging electrons, but also versus their energy, with special attention to low energy primary electrons (< 20 eV) which have been recently shown to have peculiar behavior in terms of reflectivity <sup>2)</sup>. Such studies, performed on Cu prototype of the beam screen adopted for the Large Hadron Collider (LHC), have shown that scrubbing efficiency depends not only on the dose but also on the energy of incident electron beams <sup>3, 4)</sup>. So, while now it is clear that scrubbing is one possible solution to obtain low SEY beam pipe accelerators, it seems very useful to study the actual chemical phenomena occurring at the real surfaces and causing the observed SEY reduction. In this context surface science techniques and synchrotron radiation spectroscopies are ideal tools to perform in situ characterization of the chemical composition of a relevant surface material and its eventual modifications occurring during electron or photon irradiation. Before having access to the XUV beamlines in construction at DAΦNE we also performed preliminary experiments at Elettra focussing on the relation between the SEY and the surface condition of representative LHC samples. We correlate the SEY reduction obtained by electron bombardment with the surface chemical composition by using photoemission spectroscopy, confirming that the electron bombardment results in the graphitization of the carbon impurities on the copper surface <sup>5)</sup>. Such characterizations have suggested also ways to produce low SEY materials and to develop IMCA project.

During 2010 we designed and optimized a dedicated experimental apparatus shown in Fig. 1. This apparatus will allow us to grow and characterize thin films by dissociation of hydrocarbons

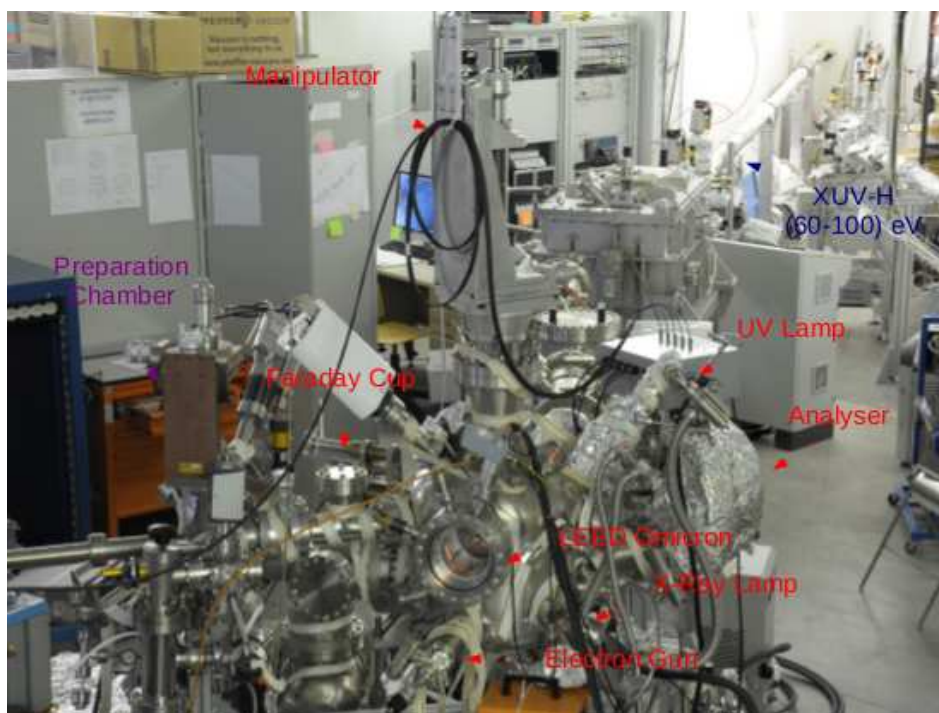


Figure 1: *Photo of the experimental apparatus designed for the IMCA experiment.*

by Chemical Vapor Deposition in UHV (Ultra High Vacuum). Samples will be grown in the preparation chamber equipped with a manipulator with a heater and a sputter gun. They will be transferred in the analysis chamber with a transfer system. The UHV  $\mu$ -metal chamber with less than 5 mGauss residual magnetic field at the sample position, was steadily in a vacuum better than  $2 \times 10^{-10}$  Torr after bake-out. This chamber is equipped with an Omicron LEED, an electron gun to measure the SEY of produced samples and a Faraday cup to characterize beam currents and the profile of beams. The chemistry of samples before and after irradiation will be investigated by photoemission studies performed by using the XUV DAΦNE beamline (60-1000 eV), and other two sources of irradiation: X-Ray and UV Lamps. Photoemission spectra will be acquired using an Omicron Analyser. An XPS spectrum, from which we can extract chemical information on the studied surface and, hopefully, on the electron bombarded low SEY one, is shown in Fig. 2, where the overview photoemission spectrum measured with our experimental set-up, on the LHC sample as received. In the photoemission spectrum we can notice the clear signature of Cu and its contaminants like oxygen and carbon. Subtle spectral changes may be expected to be observable at, for instance, a fully scrubbed surface, allowing us to detail the chemical changes occurring at the surface.

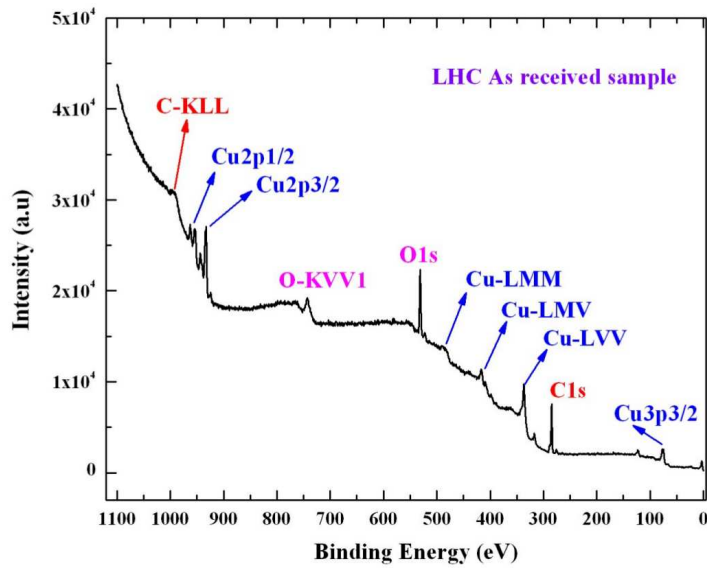


Figure 2: An overview photoemission spectrum measured with our experimental set-up on the LHC sample as received.

### Conference Talks

- R. Cimino, Realistic scrubbing scenario to reduce Secondary electron yield for LHC and new rings Low Emittance Ring Workshop LER2010. CERN, 13 January 2010.
- M. Commisso, Surface Studies for Improving the Performance of Accelerator, IFA 2010.
- R. Cimino, Experimental efforts at LNF to reduce Secondary Electron Yield in particle accelerators Ecloud10, Cornell 10-9-2010.
- R. Cimino, Summary talk on: Electron Cloud Build-Up Modeling session Ecloud10, Cornell 10-9-2010.

### References

1. M. E. Biagini, R. Boni, M. Boscolo *et. al.*, Proc. of European Particle Accelerator Conference (EPAC08), and references therein p. 2605.
2. R. Cimino *et. al.*, Phys. Rev. Lett. **93**, 14801 (2004).
3. R. Cimino *et al.*, to be published.
4. M. Commisso, Study of the SEY dependence on the electron beams dose and energy, in press on Il Nuovo Cimento C.
5. LNF Annual Report 2008 and 2009.
6. R. Cimino *et. al.*, Experimental efforts at Lnf to reduce secondary electron yield in particle accelerators, proceedings of ELOUD10, 2010.

## MoonLIGHT-ILN

G. Bellettini (Ass.), S. Berardi (Bors.), G. Bianco (Ass.), A. Boni (Dott.), C. Cantone (AR),  
S. Dell’Agnello, G.O. Delle Monache, M. Garattini (Dott.), C. Graziosi (Bors.),  
N. Intaglietta (Tecn.), C. Lops (Dott.), M. Maiello (Dott.), R. March (Ass.), M. Martini (Bors.),  
G. Patrizi (Bors.), L. Porcelli (Bors.), R. Tauraso (Ass.), M. Tibuzzi (Bors.)

### 1 Introduction

Lunar Laser Ranging (LLR) experiment, performed since 1969 with retro-reflector arrays deployed by Apollo 11, 14 and 15, is the only Apollo experiment, designed by a team led by C. O. Alley, D. Currie, P. Bender and Faller et al [1], still taking data today. In the past 40 years, laser ranging to these arrays has provided most of the definitive tests of the many parameters describing General Relativity [2, 3]. In addition, the analysis of the LLR data, has greatly enhanced our understanding of the interior structure of the Moon [4, 5]. Initially, the Apollo arrays contributed a negligible portion of the LLR error budget. Nowadays, the ranging accuracy of ground stations has improved by more than two orders of magnitude: the new APOLLO station at Apache Point, USA, is capable of mm-level range measurements [6]; MRLO, at the ASI Space Geodesy Center in Matera, Italy, has re-started LR operations. Now, because of lunar librations, the Apollo arrays dominate the LLR error budget, which is a few cm. The University of Maryland, Principal Investigator for the Apollo arrays, and INFN-LNF are proposing an innovative CCR array design that will reduce the error contribution of LLR payloads by more than two orders of magnitude, down to tens of microns. This is the goal of the MoonLIGHT-ILN (Moon Laser Instrumentation for General relativity High-Accuracy Tests for the ILN)[7, 8] a technological experiment of INFN and of the SCF, the CCR space test facility at LNF.

### 2 Science Objectives of MoonLIGHT-ILN

Lunar Laser Ranging (LLR) has for decades provided the very best tests of a wide variety of gravitational phenomena, probing the validity of Einstein’s theory of General Relativity. The lunar orbit is obviously influenced by the gravity fields of the Earth and Sun, but also is sensitive to the presence of many other solar system bodies. This makes the dynamics of the lunar orbit complex, but the system is relatively pure in that non-gravitational influences (solar radiation pressure, solar wind, drag) are negligible. This makes the Earth-Moon distance a useful tool for testing the nature of gravity, constraining potential deviations from general relativity[9, 10, 11]. LLR currently provides the best constraints on tab.1.

The equivalence principle states that any mass, independent of composition, will react (accelerate) in precisely the same way when placed in a gravitational field. This is the same as saying that the inertial mass and gravitational mass of any object are precisely the same. The equivalence principle is fundamental to GR, allowing gravity to be treated as an aspect of the geometry of spacetime. In general, scalar additions to general relativity – motivated by string theories or quantum gravity – produce a violation of the equivalence principle and also lead to secular changes in the fundamental constants. Scalar fields are also frequently invoked to account for the apparent acceleration of the expansion of the universe. Thus tests of the equivalence principle are a vital part of understanding the interface between gravity and quantum mechanics, and in probing our cosmological fate.

The equivalence principle comes in two flavors. The WEP relates to the composition of an object, in effect probing electromagnetic, strong nuclear, and weak nuclear energy contributions. The SEP extends to include gravity itself. The Earth-Moon system allows a test of the SEP in a way that laboratory tests cannot, in that the contribution of gravitational self-energy to the total

Table 1: *The expected improvements on the GR measurements with MoonLIGHT are shown in table, together with their measurement time scale.*

Phenomenon	Current limit	1 mm ranging	100 $\mu\text{m}$ ranging	Measur. timescale
Weak EP ( $\Delta a/a$ )	$10^{-13}$	$\sim 10^{-14}$	$\sim 10^{-14}$	2yr
Strong EP (Nordvedt param.)	$4 \times 10^{-4}$	$\sim 10^{-5}$	$\sim 10^{-6}$	2yr
$\dot{G}/G$	$10^{-12}$ per year	$\sim 10^{-13}/yr$	$\sim 10^{-14}/yr$	4yr
Geodetic Precession	$\sim 5 \times 10^{-3}$	$5 \times 10^{-4}$	$\sim 5 \times 10^{-5}$	6-10 yr
$1/r^2$ deviations	$10^{-10} \times \text{gravity}$	$\sim 10^{-11}$	$\sim 10^{-12}$	6-10yr

mass-energy budget is  $5 \times 10^{-10}$  for the earth, but only  $10 \times 10^{-27}$  for typical laboratory masses. LLR allows us to ask the questions: "Do the Earth and Moon fall at the same rate toward the sun? Does the gravitational self-energy of the Earth fall toward the Sun at the same rate as the less gravity-burdened Moon? Does gravity pull on gravity in the same way it pulls on ordinary matter?". The Earth-Moon system is currently the best laboratory for answering these questions. If the SEP were to utterly fail – that is, gravitational self-energy failed to gravitate – the Moon's orbit would be shifted by 13 meters. Current LLR constrains this shift to be less than 5 mm, constituting a  $4 \times 10^{-4}$  constraint on violation of the SEP.

LLR can also constrain new theoretical paradigms. An example is an idea to account for the apparent acceleration of the universe by allowing gravitons to leak off of our 4-dimensional spacetime "brane" into another bulk dimension, thus weakening gravity over cosmological scales [12]. Though small, such a process would have an impact on the lunar orbit, causing it to precess by effectively invalidating the  $1/r^2$  force law of gravity. LLR needs to see a factor of 15 improvement to reach this level of sensitivity to new physics.

Furthermore much of our knowledge of the interior of the Moon is the product of LLR [13], often in collaboration with other modalities of observation. These physical attributes of the lunar interior include Love number of the crust, the existence of a liquid core, the Q of the Moon, the physical and free librations of the Moon and other aspects of lunar science.

### 3 2nd Generation of Lunar Laser Ranging

The general concept of the second generation of LLR is to consider a number (notionally eight) large single Cube Corner Retroreflectors (CCRs). Each of these will have a return that, with a single photoelectron detection system such as current APOLLO system located at the Apache Point Observatory, can be used to determine the range to the limit determined by the librational effects of the current arrays and the laser pulse length. By using single CCRs, the return is unaffected by the libration. That is, there is no increased spread of the FWHM due to the CCR and the librational effects. We plan to use eight such single reflectors spread over tens of meters. The return from each of the CCRs will be registered separately and can be identified by comparison with the nominal lunar orbit and earth rotational parameters. This is shown schematically in Fig.1.

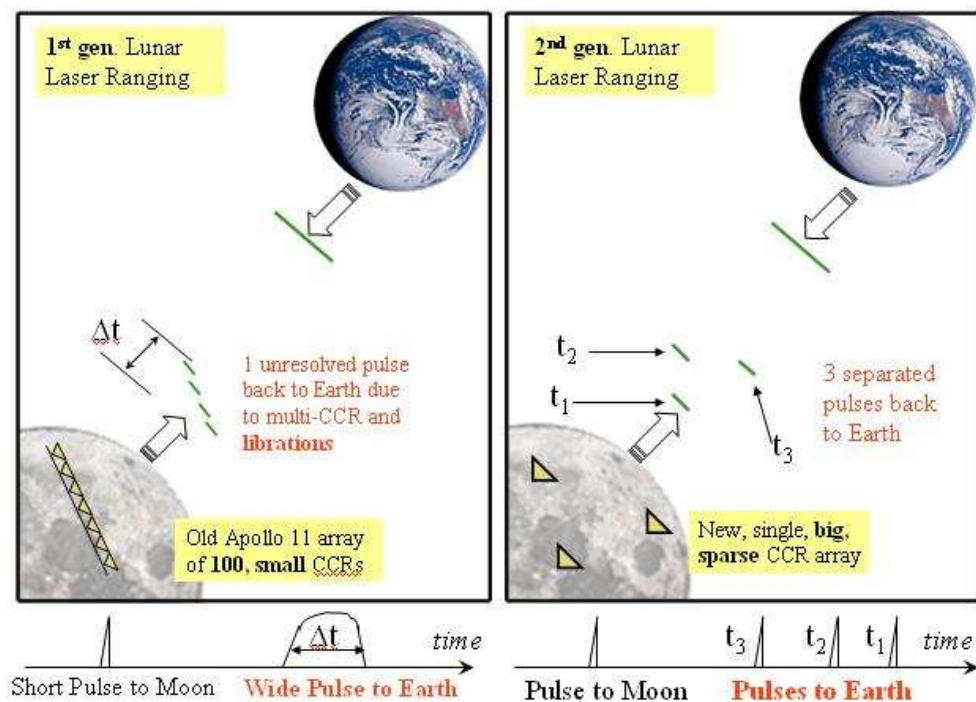


Figure 1: *Concept of the 2nd generation of Lunar Laser Ranging*

#### 4 The New Maryland/Frascati Payload

We currently envision the use of 100 mm CCRs composed of T19 SupraSil I. This is the same material used in LLRA 20<sup>th</sup> and both LAGEOS satellites. This will be mounted in an aluminum holder that is thermally shielded from the Moon surface, in order to maintain a relatively constant temperature through the lunar day and night. It is also isolated from the CCR, by two coaxial "gold cans", so the CCR receives relatively little thermal input due to the high temperature of the lunar day and the low temperature of the lunar night. The mounting of the CCR inside the housing is shown in Fig.2 [14, 15]. KEL-F could be used for this mounting (its used in LAGEOS) due to its good insulating, low out-gassing and non-hygroscopic properties.

#### 5 Technical challenges of the MoonLIGHT CCR

The primary technical objectives of the LLRRA-21 are to provide adequate laser return to Earth ground stations and to be stable over long term, decades, with respect to the center of mass of the Moon. The major technical/engineering challenges that follow from the technical objective are then:

- Fabricate a large CCR with adequate homogeneity and that meet the required tolerances, mentioned in the previous section.
- Thermal control to reduce thermal gradients inside the CCR to acceptable levels. Thermal gradients produce index of refraction gradients, which cause beam spread and low return.
- Emplacement goal of long-term stability of  $10\mu\text{m}$  with respect to the Center of Mass of the Moon.

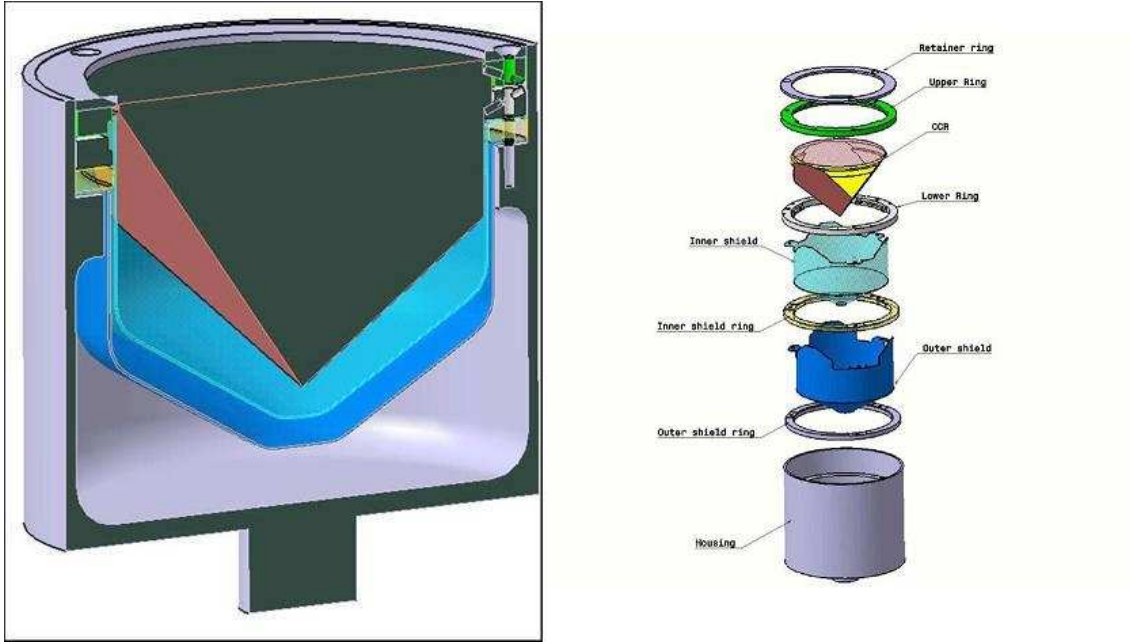


Figure 2: Section and exploded of the MoonLIGHT CCR housing with the two "gold cans" and Kel-F rings.

The large diameter of the CCR introduces a great challenge in its fabrication, the availability of such material of the required homogeneity, the fabrication and polishing procedures and the measurement methods. The angle between the three back reflecting faces, which govern the shape of the pattern, have a more challenging tolerance of  $\pm 0.2$  arcsec; this is more restrictive by a factor of 2.5 than the current state of the art for SLR CCR fabrication. The material choice is primarily driven by three requirements:

- extremely uniform index of refraction (very good homogeneity)
- resistance to darkening by cosmic radiation
- low solar radiation absorption

To satisfy these requirements, this CCR has been fabricated with SupraSil 1. For the next generation of CCRs, LLRRA-21, we plan to use SupraSil 311 which has even better homogeneity.

The optical performance of the CCR is determined by its Far Field Diffraction Pattern (FFDP), which represents the intensity of the laser beam reflected back to the ground by the CCR. Fig.3 is a simulation of the FFDP of the LLRRA-21 (performed with the software CodeV) according to its dimensions and angle specifications; at the correct velocity aberration the intensity (calculated in optical cross section) should have a value which guarantees that enough photons come back to the ground station. Optical cross section is an intrinsic characteristic of CCRs or LRAs, and its defined as follows:

$$\sigma_{CCR} = I_{CCR/MIRR}(\theta_x, \theta_y) 4\pi \left( \frac{A_{CCR}}{\lambda} \right)^2 \quad (1)$$

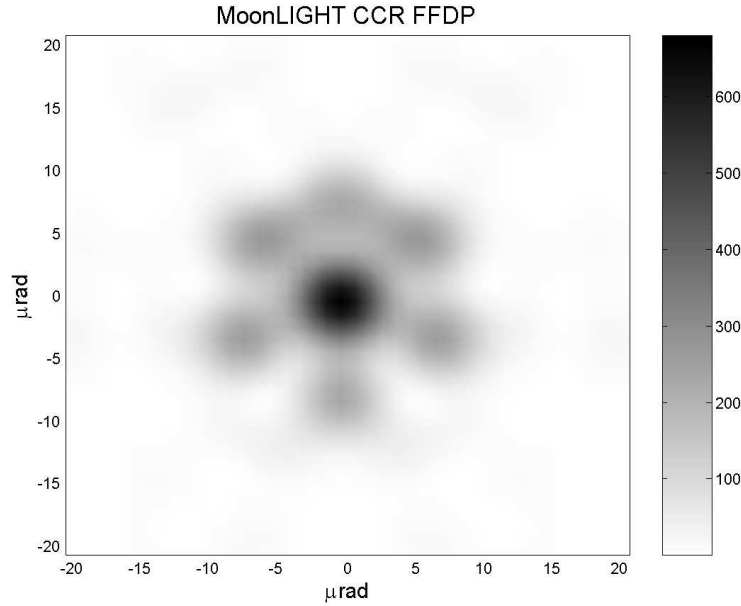


Figure 3: *FFDP of LLRRA-21 under its design specification of offset angles (0.0" 0.0" 0.0"). Grid is in angular dimensions ( $\mu\text{rad}$ )*

Where  $I_{CCR/MIRR}$  is the intensity of the FFDP of the CCR, at a certain point of the  $(\theta_x, \theta_y)$  plane, referred to a perfect mirror of the same aperture as the CCR,  $\lambda$  is the laser wavelength. One of the most critical challenges of this new model is the issue of the thermal gradient. Since the index of refraction of the fused silica depends upon temperature, a thermal gradient inside the CCR will cause the index of refraction to vary within the CCR and thus modifying the FFDP.

In Fig.4, is represented the average intensity over the velocity aberration for the LLRRA-21 at Standard Temperature and Pressure (STP). At the velocity aberration for the Moon,  $\sim 4\mu\text{rad}$ , we will test thermal perturbations and, if needed, develop an optimized design to control the drop of FFDP intensity to an acceptable level. For this reason we need to understand in detail how the external factors heat the CCR and in what magnitude, either on the Moon or on a satellite. This is accomplished using dedicated programs developed in parallel at LNF and UMD. To perform these simulations we use Thermal Desktop, a software package of C&R Technologies of Boulder CO. Then using IDL and CodeV we translate these thermal gradients into the effects on the FFDP of the CCR. There are three primary sources of heat that causes thermal gradients; here we briefly describe their effect:

- *Absorption of solar radiation within the CCR:* during a lunar day, the solar radiation enters the CCR and portions of this energy are absorbed by the fused silica. Since the different wavelengths in the solar radiation are absorbed with different intensity, according to fused silica absorptivity characteristic, the heat is deposited in different parts of the CCR.
- *Heat flux flowing through the mechanical mounting tabs:* if the CCR is at a temperature that is different than the housing temperature there will be a flux of heat passing into (or out of) the CCR through the holding tabs. Conductivity of the mounting rings should be reduced.

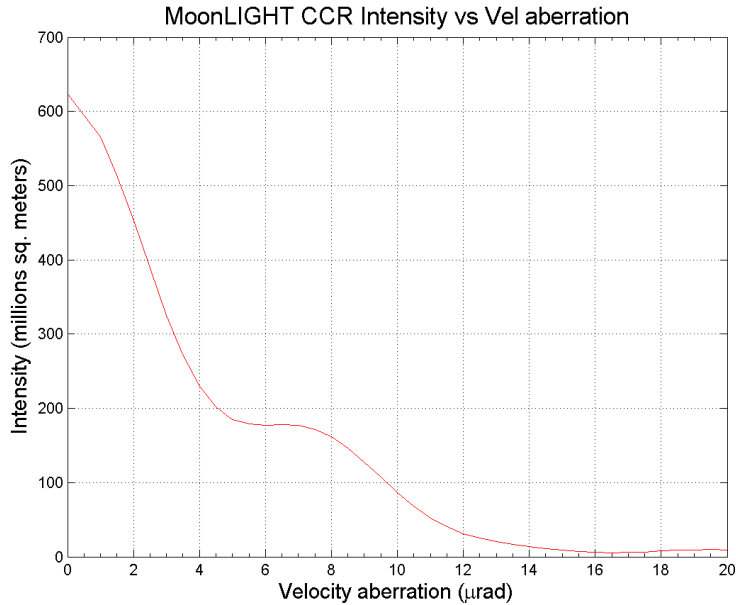


Figure 4: Average intensity over velocity aberration of an unperturbed MoonLIGHT CCR

- *Radiation exchange between the CCR and the surrounding pocket:* in the case of the Apollo LRAs, the back surfaces of the CCRs view the aluminum that makes up the housing, machined with a relative high emissivity/absorptivity. If the temperatures of the CCR and the aluminum are different there is a radiation exchange of thermal energy, which in turn causes a flux in the CCR as the heat exits out of the front face to cold space. In the Apollo array this is not been a serious issue, but the bigger dimensions of the LLRRA-21 complicate things, and we need to reduce this effect. Thus we enclose the CCR into two thermal shields, with a very low emissivity (2%), that should prevent this radiative heat flow.

Thermal simulations performed on the current configuration show that currently the variation of the  $\Delta T$  between the front face and the tip of the CCR is within 1K (Fig.5). We are still proceeding to optimize this further, both with optical design procedures and with thermal stabilization of the overall housing.

As mentioned earlier, to achieve the desired accuracy in the LLR, a long term stability is needed with respect the center of mass of the Moon; to attain this we must understand and simulate the temperature distribution in the regolith (and its motion), the effects of a thermal blanket that will be spread about the CCR and the effects of heat conduction in the INVAR supporting rod. A locking depth is chosen such that the thermal motion effects are small ( $\sim 1m$ ). The placement of the thermal blanket further reduces the thermal effects and also reduces the effects of conduction in the supporting rod. This simulation cycles through the lunation and annual cycles.

## 6 Thermal and Optical Tests in Frascati

### 6.1 SCF: the Satellite/lunar laser ranging Characterization Facility

SCF (Satellite/lunar laser ranging Characterization Facility), at LNF/INFN in Frascati, Italy, is a cryostat where we are able to reproduce the space environment: cold (77 K with Liquid Nitrogen),

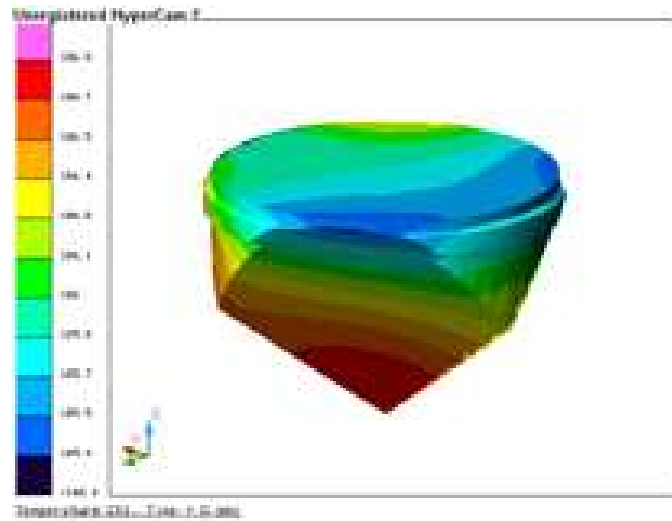


Figure 5: *Typical distribution of temperature inside the CCR for a given set of conditions.*

vacuum, and the Sun spectra. The SCF includes a Sun simulator ([www.ts-space.co.uk](http://www.ts-space.co.uk)), that provides a 40 cm diameter beam with close spectral match to the AM0 standard of 1 Sun in space ( $1366.1 \text{ W/m}^2$ ), with a uniformity better than  $\pm 5\%$  over an area of 35 cm diameter. Next to the cryostat we have an optical table, where we can reproduce the laser path from Earth to the Moon, and back, studying the Far Field Diffraction Pattern (FFDP) coming back from the CCR to the laser station, useful to understand how good is the optical behavior of the CCR (Fig.6).

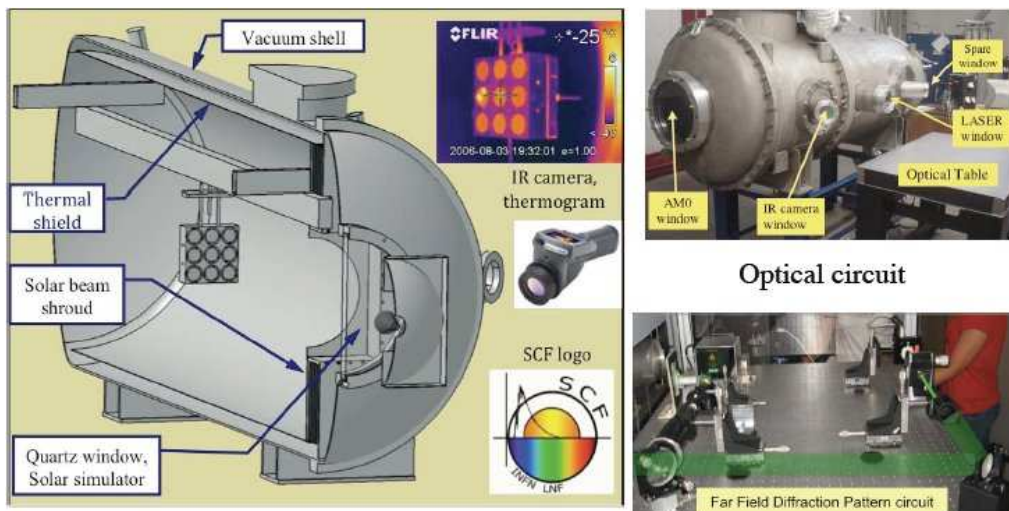


Figure 6: *SCF sketch (left side), SCF cryostat and optical table (right side)*

## 6.2 SCF-Test on the MoonLIGHT CCR

The SCF-Test[16] is a new test procedure to characterize and model the detailed thermal behavior and the optical performance of laser retroreflectors in space for industrial and scientific application,

never before been performed. We perform an SCF-Test on the MoonLIGHT CCR to evaluate the thermal and optical performance in space environment. About thermal measurements we use both an infrared (IR) camera and temperature probes, which give a real time measurements. The IR camera, through a Germanium window, can give thermograms of all the components of the CCR and its housing. Instead, to measure the thermal gradient on the CCR surface, we glued, three calibrated temperature sensors (silicon diode) along one of the back faces of the CCR, with a distance between every probes of 35 mm. The glue is Staycast 2850 + catalyst 9 (Fig. 7). Every probe is cabled with four wires of manganine RGW 36, tin soldered. This kind of solution ensures a better thermal isolation of the probe from the environment and a better accuracy of the measurement. We also measure the real time temperature of the two "gold cans" by two platinum resistors probes (PT111). In particular we look at the temperature difference from the front face to the tip, studying how the FFDP changes during the different thermal phases. This is the best representative of the thermal distortion of the return beam to the Earth. Various configurations and designs of the CCR and the housing have been and are being tested in the SCF Facility, with the solar simulator, the temperature data recording with the infrared camera and the measurement of the Far Field Diffraction Pattern (FFDP)(Fig. 7). Note that we have, up to now, only a very preliminary results indicating that the CCR and its assembly work well enough. During the 2011 we will start the analysis of the experimental data, and matching with the computer simulations. Other experimental measurements and simulations will follow, with the aim of improving and optimizing the performance of this second generation of lunar laser ranging retroreflectors.

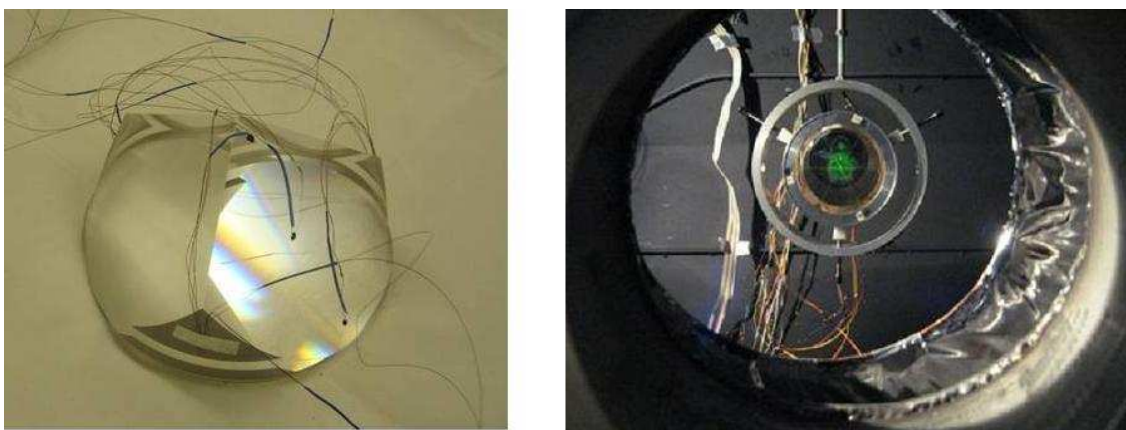


Figure 7: *Temperature sensors diodes glued on the back face of the MoonLIGHT CCR (left) and the CCR in its housing during measurements in SCF (right).*

## 7 Conclusions: Mission Opportunities

The initial approach of our program was to define a package that would allow a very significant improvement in the accuracy of lunar laser ranging in order to support the new vistas of lunar science, general relativity and cosmology. This initial effort was addressed to the next NASA Manned Lunar Landings and the research was supported by the Lunar Science Sortie Opportunities (LSSO) program out of NASA Headquarters.

However, since then several other opportunities have arisen. The International Lunar Network has been proposed by NASA, which consists of the launch of four "Anchor Nodes" in about 2015. This is a robotic mission. The initial specification of the payload will contain a 100 mm CCR for Lunar Laser Ranging.

## 8 Acknowledgements

We wish to acknowledge the support of INFN-Laboratori Nazionali di Frascati, and its Director, Prof. Mario Calvetti, during the last five years. We would like also to acknowledge, University of Maryland and all the LSSO (Lunar Science Sortie Opportunities) team funded by NASA. A special thank to Prof. Douglas Currie for his great support and the helpful discussions. Special thanks to the Italian Space Agency (ASI) for the support during the 2007 Lunar Study, the MAGIA Phase A study [17]. In particular we thank S. Espinasse, formerly at ASI, now at ESA, for encouraging the applications of our work for the ILN and ESAs first lunar lander.

## References

1. P.L. Bender *et al.*, Science, Volume **182**, Issue 4109, 229 (1973).
2. Williams J. G., Turyshv S. G., Boggs D. H., Ratcliff J. T., “Lunar Laser Ranging Science: Gravitational Physics and Lunar Interior and Geodesy”, 35th COSPAR Scientific Assembly, July 18-24, 2004.
3. Williams J. G., Turyshv S. G., Boggs D. H., “Lunar Laser Ranging Test of the Equivalence Principle with the Earth and Moon”, International Journal of Modern Physics D, Volume 18, 1129-1175, 2009.
4. Williams J. G., Boggs D. H., Ratcliff J. T., “A larger lunar core?”, 40th Lunar and Planetary Science Conference, March 23-27, 2009.
5. Rambaux N., Williams J. G., Boggs D. H., “A Dynamically Active Moon-Lunar Free Librations and Excitation Mechanisms”, 39th Lunar and Planetary Science Conference, March 10-14, 2008.
6. Murphy T., Battat J., *et al.*, “The Apache Point Observatory Lunar Laser-Ranging Operation (APOLLO): two years of Millimeter-Precision Measurements of the Earth-Moon Range”, PASP 121, 29 (2009).
7. D.G.Currie, S. Dell’Agnello, “A Lunar Laser Ranging Retroreflector Array for the 21st Century”, AMOS 2009.
8. Nordtvedt K., “Lunar Laser Ranging: a comprehensive probe of post-Newtonian gravity”, Gravitation: from the Hubble length to the Planck length, edited by Ciufolini I., Coccia E., Gorini V., Peron R., Vittorio N., ISBN 07503 0948, published by Institute of Physics Publishing, the Institute of Physics, London, 2005, p.97.
9. J.G.Williams, S.G.Turyshv, D.H.Boggs, “Progress in Lunar Laser Ranging Test of Relativistic Gravity”, Phys.Rev.Lett.93:261101,2004.
10. Murphy T. W., Adelberger E. G., Strasburg J. D., Stubbs C. W., Nordtvedt K., “Testing Gravity via Next Generation Lunar Laser-Ranging”, Nuclear Physics B Proceedings Supplements, Volume 134, 155-162.
11. Nordtvedt K., “Testing the Equivalence Principle with laser ranging to the Moon”, Adv. in Space Research, Volume 32, Issue 7, 1311-1320.
12. Dvali G., Gruzinov A., Zaldarriaga M., “The Accelerated Universe and the Moon”, Physical Review D, Vol. 68, Issue 2, id. 024012.

13. Williams J. G., Boggs D. H., Ratcliff J. T., “Lunar Tides, Fluid Core and Core/Mantle Boundary”, 39th Lunar and Planetary Science Conference, March 10-14, 2008.
14. F. Prete, “Contact structural analysis of the MoonLIGHT Laser Retro-reflector Assembly with ANSYS”, Bachelor thesis (unpublished), Dipartimento di Meccanica e Aeronautica, University of Rome “La Sapienza”.
15. A. Minghiglioni, “Modal analysis of the MoonLIGHT Laser Retro-reflector Assembly with ANSYS”, Bachelor thesis (unpublished), Dipartimento di Meccanica e Aeronautica, University of Rome “La Sapienza”.
16. S. Dell’Agnello, G.O. Delle Monache, D.G. Currie *et al.*, “Creation o the new industry-standard space test of laser retroreflectors for the GNSS, fundamental physics and space geodesy: the SCF-Test”, Galileo Issue in Journal of Advances in Space Research, Scientific application of Galileo Navigation Satellite System, March 2010, ASR-D-10-00101.
17. Currie D. G., *et al.*, “A Lunar Laser Ranging Retro-Reflector Array for NASA’s Manned Landings, the International Lunar Network, and the Proposed ASI Lunar Mission MAGIA”, 16th International Workshop on Laser Ranging Instrumentation, October 13-17, 2008.

## MUEXC

M. Cestelli Guidi (Art. 23), G. Della Ventura (Ass.), D. Di Gioacchino (Resp. Naz.),  
L. Gambicorti (Ass.), A. Marcelli, A. Mottana (Ass.), E. Pace (Ass.), P. Postorino (Ass.),  
A. Puri (Ass.), N. Saini (Ass.), F. Tabacchioni (Tech.), R. Sorchetti (Tech.)

### 1 *MUEXC* project

*MUEXC* is an experimental program based on the PRESS-MAG-O apparatus designed to make possible experiments under extreme conditions of pressure, magnetic field in a wide temperature range on materials for technological applications of the interest of the Institute. The project is based on a large collaboration between INFN personnel of the LNF, of the INFN section at the University of Florence, the 'High-pressure Raman group' and the 'Spectroscopy group' of the Department of Physics of the Sapienza University and the Department of Geological Science of the Roma Tre University.

In 2010 the main activities of the *MUEXC* collaboration on the PRESS-MAG-O apparatus have been: **a)** the commissioning of the PRESS-MAG-O instruments, in particular has been fixed the vacuum leak detected at low temperatures adopting a new sealing configuration with indium based o-rings inside the cryostat; **b)** have been manufactured and tested the optical system designed to focus the IR beam inside the diamond anvil cell (DAC) once installed in the cryostat; **c)** the commissioning of the sapphire sample-holder has been completed. The different breaks of the sample-holder, the excitation coil, DAC and PEEK supports to insert the slider of the pick-up coil of the micro-gradiometer have been now installed. The complete system is now available on the PRESS-MAG-O insert; **d)** proceeds the activity of the Research Doctorate of the XXIV Material Science cycle of the University 'La Sapienza' that joined project with the following research program: '*Study of highly correlated materials under extreme conditions*'. **e)** The work to set up the new **L**aboratory of **M**agnetism and **H**igh **P**ressure and **S**pectroscopy experiments (**LAMPS**), in the Legnaro building has been completed. In this area, waiting the installation of PRESS-MAG-O system, is now possible perform electronic transport and magnetic measurements vs. magnetic field, pressure and temperature with the available apparata. In particular, are operative two He liquid cryostats with a superconducting magnet for electrical transport and magnetic gradiometer measurements.

### 2 *PRESS-MAG-O* cryostat

To fix the cold leak in the PRESS-MAG-O cryostat, a new sealing configuration with indium o-rings that now connect the optical lines and vertical port of the split magnet with the stainless steel HV chamber of the cryostat have been realized. In the panels in Figure 1 is shown the procedure to seal with indium the internal flanges of the cryostat. The chamber and the shields of the PRESS-MAG-O cryostat have been again reassembled. Soldering of the superconducting magnet electrical connections and installations of thermometers and Allen-Bradley resistances to control the He liquid level in the internal magnet tank have been also done (see photographs in Figure 2).

### 3 Optical concentrator

The manufacture and some optical tests of the concentrator designed to focus the radiation inside the PRESS-MAG-O device have been performed by INO-CNR (Florence, Italy). A preliminary



Figure 1: *Photographs of the PRESS-MAG-O cryostat during the reassembling operations of the optical lines of the superconducting magnet.*



Figure 2: *Photographs taken during the soldering procedure of the superconducting cables and the installation of thermometers inside the cryostat.*

alignment and the evaluation of the main performances have been performed at the LNF. This Cassegrain optic has two elements: a primary concave mirror M1 and a secondary convex mirror M2 mounted on a spider structure that allows tilt in the three directions and a translation along the axis of the concentrator. These two gold coated mirrors have been optimized to work in the IR wavelength range. Their parameters are ( $M1 = \phi = 40mm, R = 600mm$ ) and ( $M2 = \phi=6mm, R = 100,9mm$ ). The mechanical structure allows to set distances and angles between the two mirrors in order to align the system and optimize the transmission (figure 3 A, B). The tests of the optical surfaces of the concentrators have been performed with a Zygo interferometer using a reference mirror. The concave reference mirror is placed at a distance  $R/2$  (mirror focal distance) from the concentrator focus, allowing the light to be back reflected from the concave mirror in the collector and to cross it with the same optical path of the interferometer. In figure 3 we show some components of the device during the assembly and tests and a photo of the focus spot obtained using a laser source.

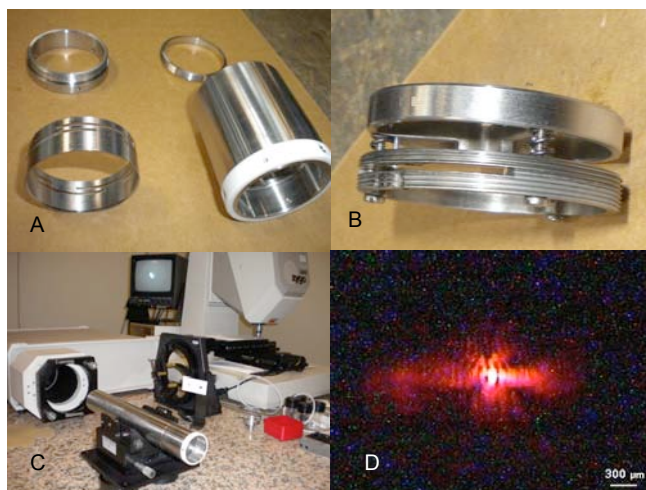


Figure 3: a) Mechanical components of the concentrator. (top left) the primary mirror ring stop and other components, b) photograph of the spider framework, c) PRESS-MAG-O concentrator and the optical system on the optical table, d) image of the spot during the tests

#### 4 DAC sample-holder

During 2010 have been also manufactured small components in PEEK, a unique plastic material with excellent low temperature properties, for the sapphire DAC-holder necessary to install the excitation coil and the slider for micro-gradiometer. The sample-holder has been then installed in the PRESS-MAG-O insert stages. (see figure 4 A-C). The final assembled configuration of the PRESS-MAG-O X-Y- $\Theta$  insert is showed in figure 4 (panels D, E).

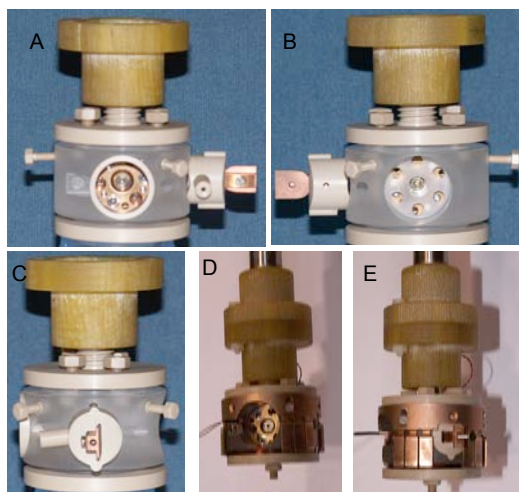


Figure 4: *Different photographs of the PEEK components assembled on the the sapphire DAC-holder, mounted in the internal part of the insert*

## 5 LAMPS laboratory

It has been completed the transfer from the old laboratory to the new area inside the LNF in the LEGNARO building (see Fig. 5). The new **L**aboratory of **M**agnetism and **H**igh **P**ressure end **S**pectroscopy (*LAMPS*) now hosts the PRESS-MAG-O system and other two cryostats: 1) one with a temperature control using a manual dip in a liquid He bath for resistive measurements. Moreover this cryostat will be used to check the start-up of the PRESS-MAG-O insert, 2) a second with a temperature control via a cold helium flux vapor. In this second system is available electric transport and ac magnetic multi-harmonic susceptibility inserts. For this cryostat is also available a superconducting magnets up to 8 T.

## 6 Experimental activity on highly correlated materials

In addition to the commissioning of the PRESS-MAG-O instruments whose status has been presented in an oral contribution at the *48th EHPRG International Conference* in Uppsala (25-29 July 2010) during the 2010 we continued the experiments of ac susceptibility on new iron based high  $T_c$  superconductors. In particular, we compared  $\text{NdFeAsO}_{0.86}\text{F}_{0.14}$  ( $T_c=49\text{K}$ ) and  $\text{FeSe}_{0.88}$  superconductors ( $T_c=7\text{K}$ ). These systems have similar structures but only the  $\text{NdFeAsO}_{0.86}\text{F}_{0.14}$  system includes a stack of layers along the c-axis direction. Actually, it is composed by alternating FeAs and NdO layers which act like spacers, while the  $\text{FeSe}_{0.88}$  is composed by only FeSe layers. We characterized the flux dynamics of these materials by performing ac multi-harmonic magnetic susceptibility measurements and showed that the  $\chi_3$  third harmonic component modulus of the magnetic susceptibility is larger in the  $\text{NdFeAsO}_{0.86}\text{F}_{0.14}$  sample with respect to the  $\text{FeSe}_{0.88}$ . Moreover,  $\text{FeSe}_{0.88}$  measurements show that the harmonic component is for this system more sensitive to both amplitude and frequency of the applied  $H_{ac}$  field respect to  $\text{NdFeAsO}_{0.86}\text{F}_{0.14}$ . In the  $\text{FeSe}_{0.88}$  sample this component of the magnetic susceptibility is strongly reduced with the appli-



Figure 5: Photographs of the LAMPS laboratory

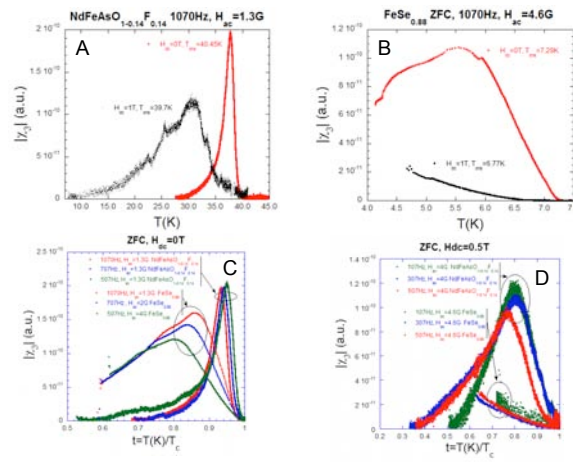


Figure 6: The third harmonic  $\chi_3$  modulus of the magnetic susceptibility in  $\text{NdFeAsO}_{0.86}\text{F}_{0.14}$  and  $\text{FeSe}_{0.88}$  samples respect to DC magnetic field (A,B) and frequencies (C,D)

cation of a  $H_{dc}$  field. Some data shown in figure 6 clearly show that the  $\text{NdFeAsO}_{0.86}\text{F}_{0.14}$  system could be characterized by a strong pinning strength even with a larger thermal fluctuations. A final consideration has to be devoted to the pinning processes in the case of the  $\text{NdFeAsO}_{0.86}\text{F}_{0.14}$ . This mechanism is typically associated to F doping and a similar pinning contributions observed in  $\text{FeSe}_{0.88}$  has been correlated to Se vacancies. To clarify the presence of a strong pinning in the  $\text{NdFeAsO}_{0.86}\text{F}_{0.14}$  respect to the  $\text{FeSe}_{0.88}$  we hypothesizes that in addition to doping, the Nd magnetic moment ( $\mu \sim 3.6 \mu_b$ ) in the REO plane and the stack of layers along the  $c$ -axis direction both strongly contributes to the pinning mechanism.

## 7 Acknowledgements

We thank the technical staff of the DA $\phi$ NE-Light laboratory for their continuous and invaluable technical support.

## References

1. D. Di Gioacchino *et al.*, “Status of PRESS-MAG-O: the experimental apparatus to probe material and phenomena under extreme conditions”, *J. Phys. Chem. Solid* **71**, 1042 (2010).
2. D. Di Gioacchino, A. Marcelli, A. Puri, A. Bianconi, “The a.c. susceptibility third harmonic component of  $\text{NdO}_{1-0.14}\text{F}_{0.14}\text{FeAs}$ ”, *J. Phys. Chem. Solid* (2010) **71**, 1046 (2010).
3. W. Xu, A. Marcelli *et al.*, “Oxygen disorder and its effects on the local structure of  $\text{REOFeAsO}$  Experiments and multiple scattering calculations”, *J. Phys. Cond. Matter* **22**, 125701 (2010).
4. W. Xu *et al.*, “Arsenic K-edge XANES study of  $\text{REFeAsO}$  oxypnictides”, *Europhys. Lett.* 90 57001 (2010).
5. D. Di Gioacchino *et al.*, “PRESS-MAG-O: a unique instrument to probe materials and phenomena under extreme conditions at Frascati”, *High Pressure Research* (2010) in press DOI: 10.1080/08957959.2010.525511

## The n@BTF project

B. Buonomo, R. Bedogni (Art. 23), A. Esposito, G. Mazzitelli (Resp.), L. Quintieri (Art.23)

The n@BTF technical Staff:  
M. De Giorgi, M. Chiti, A. Gentile

### 1 Description of the project

At the Beam Test Facility of the DAΦNE collider, we have designed and realized a photo-neutron source, by exposing an heavy nuclei target to a high energy electron beam. The n@BTF project arrived at its end, the main tasks of the experiment being successfully achieved as planned. This experiment has been funded by the CSN5 of INFN for 3 years.

In what follows the main results of n@BTF will be presented and discussed.

#### 1.1 Physics background: the photo-neutron production

The photonuclear physic is well known in accelerator field, mainly because related to shielding issues for neutrons, that are produced as a consequence of electron and photon interaction with matter (especially in dumps and shields). The most effective way to shield electromagnetic radiation is to use high atomic number ( $Z$ ) materials (Lead, Tungsten and so on). On the other side, high  $Z$  nuclei exhibit higher cross sections for photonuclear reactions than medium and low  $Z$  materials, that means a related production of neutrons and protons that has to be properly taken into account for dose calculation and so far in the shielding design.

In this way, what is normally an issue from the radioprotection point of view, has been successfully exploited as main source for our task.

More than 80% of electrons, passing through the target, loose energy by bremsstrahlung: the ensuing photon shower interacts with the nuclei exciting them (essentially on the base of Giant Dipole Resonance mechanism for photon energy lower than 30 MeV and on the base of Quasi Deuteron Mechanism for higher photon energy). In going back to the fundamental state, the excited nuclei boil-off a nucleon, typically a neutron (in fact, the emission of protons, that is a possible channel, is strongly repressed in heavy nuclei due to the high Colombian barrier). These neutrons are emitted almost isotropically all over the space, with a continuous energy spectrum that is peaked around the equilibrium nuclear temperature characteristic of the target material.

To estimate the neutron rates and energy spectra, all around the target, we used both FLUKA (20083d release) <sup>1)</sup> and MCNPX <sup>2)</sup> (MCNPX2.5.0) codes. The detailed description of the feasibility study and the related Monte Carlo simulations can be found in the previous edition of the LNF annual report <sup>3)</sup> and in ref <sup>4)</sup>, <sup>5)</sup>, <sup>6)</sup>.

### 2 Final experimental set-up: the feasibility test

The photo-neutron source has been located in the BTF experimental hall, at the end of the transfer line and since it is not allowed that the produced neutrons could be scattered everywhere, it was necessary to shield closely the whole solid angle around the target, with the exception of well defined extraction lines, along which we should be able to properly collect neutrons.

The shield is a multilayered structure made of lead and polyethylene. Boron Carbide sheets are also foreseen to be used in next future. These are already available as inventory of the new neutron facility.

In Fig. 1 the experimental set-up, installed in April 2010, is shown, while Fig. 2 shows the Tungsten target placed inside the shielding apparatus.

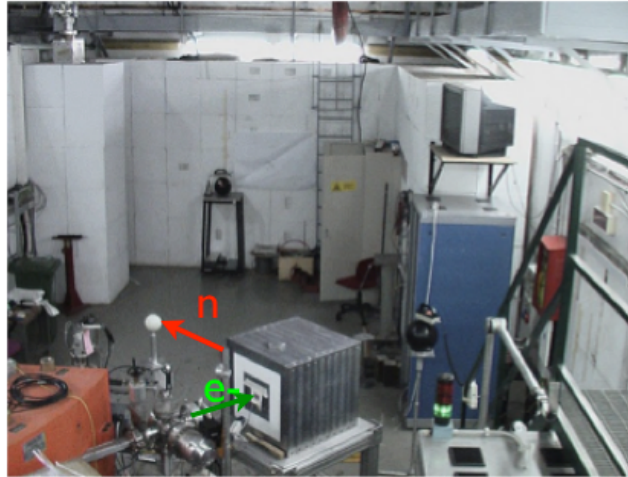


Figure 1: *Experimental set-up (for feasibility test).*



Figure 2: *Target located inside the shielding apparatus.*

The measurement campaign took about 15 days (up to 7th of May) and has been done in collaboration with the LNF-FISMEL group, using the Bonner Spheres <sup>7)</sup> neutron detectors.

The set of Bonner Spheres (LNF-ERBSS) used for the BTF measurements included:

- 7 polyethylene spheres (density 0.95 g/cm<sup>3</sup>). The following spheres were exposed: 2", 3", 5", 7", 8", 10", 12" diameter spheres.
- Dysprosium activation foils (12 mm diameter and 0.1 mm thickness). These are detector of thermal neutrons located at the centre of each sphere. The exploited isotope is <sup>164</sup>Dy (28.2% abundance in natural Dysprosium)<sup>1</sup>.

---

<sup>1</sup><sup>165</sup>Dy is a  $\gamma$ - $\beta$  emitter with  $E_{max} = 1.3$  MeV and  $T_{1/2} = 2.334$  h.

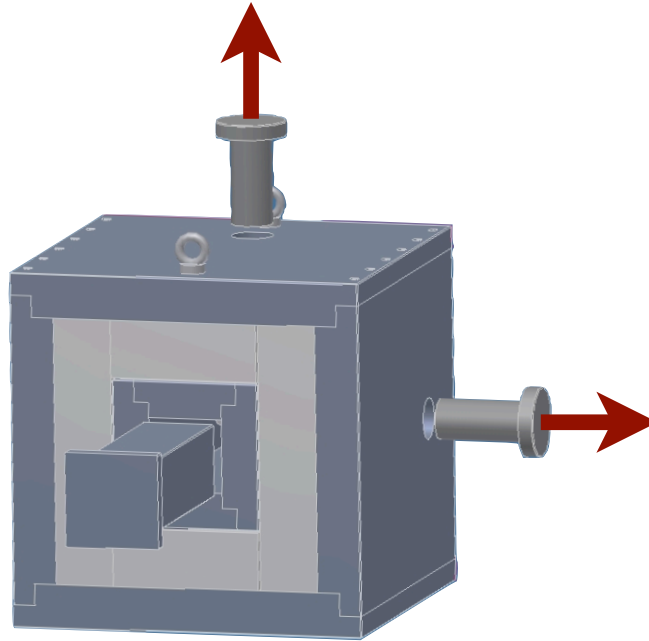


Figure 3: *Extraction lines (with lead caps) are designed in the plane perpendicular respect to the impinging electron direction. The beam dump is also visible (the larger lead cap in the middle of the shield).*

For our feasibility test we used a Dysprosium activation foil since it appears to be more suitable for working in a high photon background.

The Dy-BSS response matrix was calculated with MCNPX on the basis of a 68-groups energy equi-lethargy structure from  $1.5\text{E-}9$  MeV to  $1.16\text{E}+3$  MeV<sup>8)</sup>.

A validation experiment performed in the ENEA-Bologna  $^{252}\text{Cf}$  reference field, allowed estimating the response matrix overall uncertainty in  $\pm 2.3\%$ . This figure refers to the energy interval covered by the  $^{252}\text{Cf}$  spectrum, i.e. from 0.1 to 15 MeV.

The spheres with Dy activation foils in their centre were sequentially exposed for an irradiation time of around 0.5 h for each sphere in a well defined reference point: 149 cm from the target centre along the 90 direction at 124 cm from the floor.

The foils were counted in a portable beta counter, their specific activity was corrected for the discrete activation function, the decay from the exposure and the counting, the decay during counting, and finally normalized to the number of 510 MeV electrons delivered to the target. These values were unfolded using the FRUIT code<sup>9)</sup>.

The energy distribution of the incident electrons was measured by a spectrometer consisting of a pulsed magnet, which deviates the beam from the transfer line, and a 60 bending magnet, which focuses the beam on a system of secondary emission metallic strips<sup>10)</sup>. The FWHM of this distribution is lower than 1%.

The delivered charge per pulse was about 50 pC. To measure the charge and transverse profile of the beam delivered on the tungsten target, a Bergoz ICT (high sensitivity, beam charge to output charge ratio 5:1) and two fluorescent screens (beryllium oxide and YAG:CE) were mounted at the exit of the BTF line. The Integrating Current Transformer (ICT) is composed of a capacitively shorted transformer and a fast read out transformer with a common magnetic circuit designed to measure the charge in a very short pulse with high accuracy.

Variations in the neutron fields due to small instabilities in the electron beam were minimized

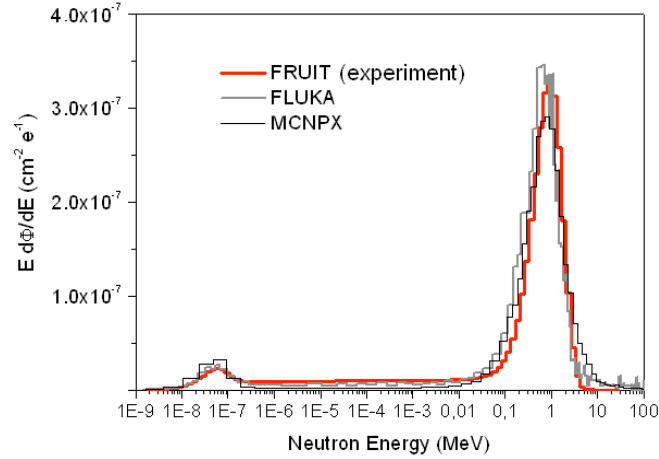


Figure 4: *Experimental and MC computed neutron spectra, 149 cm apart from the target at 90° wr to the impinging electron beam.*

by keeping the beam position and beam spot dimensions as constant as possible. These parameters can be easily checked and controlled using wall current monitors and fluorescent targets suitably located along the BTF transfer line <sup>11</sup>).

Taking into account that the optimized target is a cylindrical bulk (R=35mm and L=60 mm), since the maximum electron beam spot size on the target is enclosed in a circle of 1cm radius and the accuracy by which we can set the transversal beam size and its centre is much better than few mm, we can be confident that, even in the most disadvantageous case, all the energy of the primary electrons will be deposited in the target. Because the photo-neutron yield depends essentially on the value of the deposited energy, the estimated neutron yield sensitivity with respect to the beam geometrical parameters (beam spot size and radial location of the beam center) is actually negligible (less than 3%).

### 3 Final test: Comparison between Monte Carlo Predictions and Experimental data

In Fig. 4 the lethargic ( $E d\Phi/dE$ ) spectra, normalized to the total neutron flux, estimated by Monte Carlo codes are shown together with the normalized lethargic spectrum, obtained with Bonner Spheres.

As we can see, there is a good agreement between measurements and simulation results concerning the shape of the neutron spectrum. Moreover statistical tests have been performed in order to quantify properly the accordance of Monte Carlo predictions with experimental values. In particular we used the  $\chi^2$  Goodness of Fit test in order to asses quantitatively the Monte Carlo accuracy around the Giant Dipole Resonance. The p-values that we found, respectively for MCNPX and FLUKA, are 0.996 and 0.967. This allows to conclude that MCNPX and FLUKA provide an accurate reconstruction of the experimental resonance, both in energy position and amplitude.

As predicted for, the majority of produced neutrons belongs to the energy range from 10 KeV to 20 MeV: the calculated neutron spectrum has a Maxwellian shape with average around 0.7 MeV.

The experimental and calculated neutron fluxes, collected over a sphere of 10 cm, whose center is 1.49 m far away from the target along one of the two extraction lines, are reported in Table 1, confirming again the good agreement between experimental and predicted values.

Table 1: *Total neutron flux per primary: comparison between experimental measurements and predictions.*

Measurements [BSS]	MCNPX	Fluka
1/[cm <sup>2</sup> /pr]	1/[cm <sup>2</sup> /pr]	1/[cm <sup>2</sup> /pr]
8.04E-7±3%.	8.06E-7± 4%	8.12E-7±5%

We can conclude that at present, because we are authorized to deposit only a small fraction of the total Linac power (40-50 W), we are able to have, at about 1.5 m from the target, a maximum neutron rate of 4E+5 n/cm<sup>2</sup>/s, that ( $\geq 80\%$ ) is mainly composed of neutrons with energy around 1 MeV, as correctly predicted by Monte Carlo simulations.

#### 4 Conclusion and future plan

A photo-neutron source has been successfully realized in BTF, concluding the n@BTF project as scheduled.

In fact the feasibility test was successfully carried out in May 2010, demonstrating definitively the BTF ability of providing not only electrons, positrons and tagged photons, but also neutron beam of well defined and reconstructed energy spectrum and fluences.

The measured neutron rate and spectrum were in good agreement with the simulations, taken into account the limitations due to the modest energy resolution of the used BS spectrometer. Further investigations are foreseen, in the direction of developing a photon-insensitive high-energy spectrometer to measure with much higher accuracy also the high-energy component of the neutron spectrum (10 MeV and above).

The BTF neutron source will be made available to the whole international scientific community for its scopes.

The complete characterization of the new neutron facility is still in progress. In fact other measurements of both neutron and photon field in several points of the BTF experimental hall have to be done, but they have been already scheduled in short time and their results will be soon available. Moreover a new project “NESCOFI” has started as direct spinoff of the neutron feasibility study in BTF: one of the main goals of this project is to develop neutron diagnostic instrumentations for the BTF neutron facility.

In spite of this, we have already received requests for running BTF with neutrons by several groups of University of Roma area, involved in studying inelastic scattering of neutrons and development and characterization of neutron detectors.

#### 5 Conference Talks

1. L. Quintieri *et al.*, “N@BTF: Feasibility study of a photo neutron source at the DAΦNE Beam Test Facility”, Invited Seminar 25 Febbraio 2010, INFN Trieste, Area di Ricerca di Padriciano.
2. G. Mazzitelli *et al.*, “Neutron Source at the DAΦNE Beam Test Facility (BTF)”, Poster Session, IPAC, Kyoto, 24 May 2010.

3. G. Mazzitelli *et al.*, “New Neutron Source at the Beam Test Facility (BTF) of Frascati: design and first experimental results”, Invited Seminar at Channeling 2010, Ferrara 3-8 October 2010.
4. L. Quintieri *et al.*, “Photo-Neutron Source by High Energy Electrons on Target: Comparison Between Monte Carlo Predictions and Experimental Measurements”, Oral Presentation (N31-6) at NSS-IEEE, Scientific Simulation and Computation: Simulation R&D, Knoxville, 3 November 2010.

## 6 Publications

- G. Mazzitelli, *et al.*, “Neutron Source at the DAΦNE Beam Test facility”, Proceedings of IPAC-2010 (MOPEB063), 23-28 Maggio 2010, Kyoto, Japan
- L. Quintieri *et al.*, “Photo-Neutron Source by High Energy Electrons on Target: Comparison Between Monte Carlo Predictions and Experimental Measurements”, Submitted article for IEEE-NSS 2010 proceedings, publication in progress

## References

1. A. Fasso *et al.*, “A multi-particle transport code”, CERN-2005-10 (2005), INFN/TC-05/11.
2. D. B. Pelowitz (Ed.), MCNPX Users Manual Version 2.6. Report LA-CP-07-1473 (2008).
3. Annual Report 2009, LNF - 10 / 15(IR).
4. L. Quintieri *et al.*, “Feasibility Study of a neutron source at the DAΦNE Beam test Facility”, using Monte Carlo codes”. 2009 IEEE Nuclear Science Symposium Conference Record (N33-6).
5. G. Mazzitelli, *et al.*, “Neutron Source at the DAΦNE Beam Test facility”, Proceedings of IPAC-2010 (MOPEB063), 23-28 Maggio 2010, Kyoto, Japan.
6. L. Quintieri, *et al.*, “Photo-Neutron Source by High Energy Electrons on Target: Comparison between Monte Carlo Predictions and Experimental Measurements”, 2010 IEEE Nuclear Science Symposium Conference Record (N31-6), October 30 to November 6, 2010, Knoxville, Tennessee.
7. R. Bedogni, *et al.*, “Comparing active and passive Bonner Sphere Spectrometers in the 2.5 MeV quasi mono-energetic neutron field of the ENEA Frascati Neutron Generator (FNG)”. Radiat. Meas., submitted manuscript.
8. A. Esposito *et al.*, Nucl. Instr. & Meth. A **580**, 1301 (2007).
9. R. Bedogni, C. Domingo, A. Esposito, F. Fernandez, Nucl. Instr. and Meth. A **580** (2007) 1301.
10. R. Boni, *et al.*, “DAΦNE Linac Operational Performances”, Proceed. European Particle Accelerator Conference, Stockholm (Sweden), 22-26/6/1998, p. 764; LNF-98/023(P), 27/07/1998.
11. B. Buonomo, *et al.*, “Beam Diagnostic for a wide Range Beam Test Facility”, Proceedings of Beam Instrumentation Workshop-08 (THPC143) Lake Tahoe, California.

## **ODRI** **(Optical Diffraction Radiation Interferometry)**

M. Castellano (Resp.), L. Cacciotti (Tecn.), E. Chiadroni (Art. 23), R. Sorchetti (Tecn.)

Participant Institutions:

Italy: INFN LNF, Roma 2-Tor Vergata; University of Roma Tor Vergata.

Germany: DESY (Hamburg)

### **1 Introduction**

The successful development of both FEL in the X-ray range and linear colliders requires the characterization of high charge density, high energy electron beams, for which standard, intercepting diagnostics might not be suitable. Diffraction radiation (DR) diagnostic is based on the observation of the DR angular distribution emitted by an electron beam passing through an aperture in a metallic foil. DR is produced by the interaction of the electromagnetic field of an electron beam with the screen surface. Since the beam passes through the aperture, DR based diagnostics is suitable for measuring the properties of such beams in a parasitic way.

### **2 ODRI experiment**

The aim of the experiment, set up at FLASH (DESY), is studying the angular distribution of incoherent optical DR (ODR) which gives information on both transverse beam size and angular divergence, to allow a single shot emittance measurement provided the beam has its waist on the DR screen. Some limitations of ODR diagnostic <sup>1)</sup>, can be overcome by ODRI, i.e. Optical Diffraction Radiation Interferometry, produced by the interference between forward ODR emitted on the shielding mask and backward ODR from the DR target <sup>2)</sup>. Since the two slits have different apertures, the amplitudes of the two sources are different both in intensity and in angular distribution, resulting in an advantageous interference effect. The main benefits are given by the reduction of synchrotron radiation background, the increase of the sensitivity of the angular distribution on the beam size, and the possibility to distinguish effects caused by beam size and offset <sup>3)</sup> within the slit.

### **3 Achievements in 2010**

The activity in 2010 was focused on the design and production of the new DR experimental setup, consisting of both target and optical system, and on the improvement of the online data analysis and fitting procedure. The ODRI setup is shown in fig.1. Both the DR screen and the shielding mask are mounted on two actuators and can be moved separately for a better alignment of the two slits. In particular the positioning of the shielding mask has been improved with micrometer precision. The optical system consists of a 45° mirror to reflect radiation parallel to the beam pipe through the optics down to the CCD camera, a vertical bellow which allows to select either the custom apochromat lens for angular distribution or the achromatic one for 2f geometry; two wheels for holding interference filters from 450 nm to 800 nm to select the emission wavelength, and both horizontal and vertical polarizers to study the contribution of each polarization one by one.

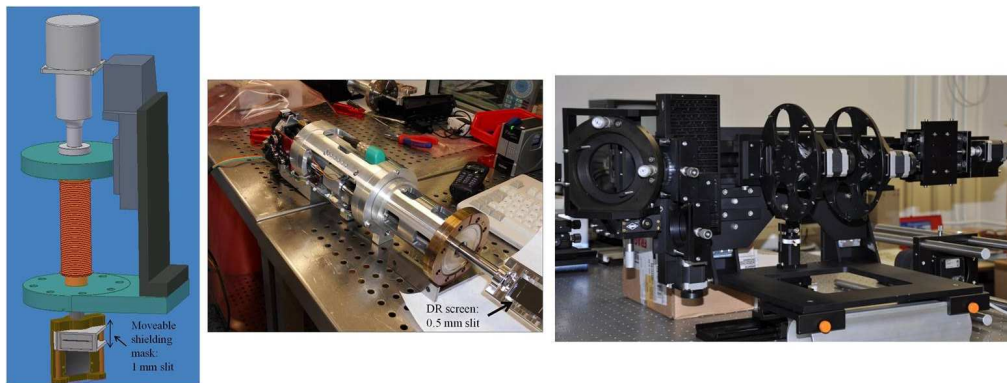


Figure 1: *Technical drawing (left) and picture (center) of the renewed DR target holder and shielding mask and light optics system (right).*

#### 4 Outlook for 2011 Activity

Beam time at FLASH is foreseen in 2011 to fully understand the physics of the emission in the two-slits configuration and to develop a real diagnostic tool to be used as standard non-intercepting diagnostic device. At this regard, it is of great importance to test the ODRI beam size monitor with electron beams with different transverse aspect ratios, e.g. round beam (for linac driven FEL radiation) and flat beam (for colliders) to clearly understand the influence of the horizontal beam angular spread. A detailed study of the vertical polarization of ODRI angular distribution is also planned at different wavelengths to retrieve from a fitting procedure the vertical beam size. In addition, the horizontal polarization, so far neglected, might reveal interesting information which needs to be further investigated. We expect to operate at 1.2 GeV electron beam energy, up to 30 bunches in the bunch train (up to 1nC per bunch). Next beam time studies will allow to test both, the new ODRI setup and the totally renewed optical system, with the final purpose of finding confirmations on the possibility of using this system as standard diagnostics for such beams.

#### 5 Publications

- M. Castellano, E. Chiadroni, A. Cianchi, “Phase Control Effects in Optical Diffraction Radiation from a Slit”, Nucl. Inst. & Meth. A **614**, 163 - 168 (2010).
- A. Cianchi *et al.*, “Optical diffraction radiation interferometry”, submitted to PRST-AB.
- E. Chiadroni, M. Castellano, A. Cianchi, K. Honkavaara, G. Kube, “Effects of Transverse Electron Beam Size on OTR Angular Distribution”, in preparation.

#### 6 Acknowledgment

Authors wish to thank colleagues collaborating from participant institutions: L. Catani, A. Cianchi (INFN Roma 2-Tor Vergata) and K. Honkavaara, G. Kube (DESY).

#### References

1. E. Chiadroni *et al.*, Nucl. Instr. & Meth. B **266**, 37893796 (2008).
2. E. Chiadroni, M. Castellano, A. Cianchi, K. Honkavaara, G. Kube, TUOA02, in: Proc. of DIPAC 2009, Basel, Switzerland.
3. A. Cianchi *et al.*, “Optical diffraction radiation interferometry”, submitted to PRST-AB.

## TERASPARC: THE TERAHERTZ RADIATION SOURCE AT SPARC

F. Anelli (Tecn.), M. Boscolo, P. Calvani (Resp., Ass.), M. Castellano,  
M. Cestelli Guidi (Art. 23), E. Chiadroni (Art. 23), G. Di Pirro, M. Ferrario,  
S. Fioravanti (Tecn.), E. Pace, R. Sorchetti (Tecn.), C. Vaccarezza

Participant Institutions:

INFN LNF, Roma 1-La Sapienza, Roma 2-Tor Vergata; University of Roma Tor Vergata.

### 1 Introduction

The interest for Terahertz (THz) radiation is rapidly growing, both as it is a powerful tool for investigating the behavior of matter at low energy, and as it allows for a number of possible applications spanning from medical science to security.

During the last decade, great efforts have been devoted to fill the so-called “THz gap” which resulted in a great technological improvement.

Unlike conventional THz sources for time-resolved spectroscopy, a linac-driven THz source can deliver broadband THz pulses with femtosecond shaping, and with the possibility to store much more energy in a single pulse. In addition, taking advantage from electron beam manipulation techniques, high power, narrow-band THz radiation can be also generated. This provides a unique chance to realize THz-pump/THz-probe spectroscopy, a technique practically unexplored up to now.

Beyond the applications described above, coherent THz radiation is a valid tool for electron beam diagnostics to fully reconstruct the beam longitudinal charge distribution.

### 2 The THz source at SPARC

The TERASPARC project, which aims at the development and characterization of THz radiation at SPARC <sup>1)</sup>, is the result of a collaboration between LNF, INFN-Roma1 and University of Roma Tor Vergata and INFN-Roma2.

THz radiation is produced as pulsed coherent transition radiation (CTR) from a silicon aluminated screen placed in the vacuum pipe at 45 deg with respect to the beam direction. By means of short electron beams, sub-ps long, a broad band radiation source is produced whose cut-off and cut-on frequency are estimated to be 150 GHz and 5 THz, due to screen finite size, optics acceptance, etc. and vacuum window transmission. In order to achieve sub-ps electron beams, RF compression is applied by means of the velocity bunching technique <sup>2)</sup>. SPARC can also produce narrow band THz radiation by means of a longitudinally modulated beam, the so-called comb beam <sup>3)</sup>.

### 3 Achievements in 2010: First characterization of the THz source

The backward CTR radiation, reflected normally to the beam direction, is extracted from the vacuum pipe through a z-cut quartz window and collected by means of two 90° off-axis parabolic mirrors in order to be focused onto the THz detector (see Fig. 1). Either pyroelectric or Golay cell detectors have been used, in an operating spectral range of 0.1 - 3 THz and 0.04 up to 10 THz, respectively.

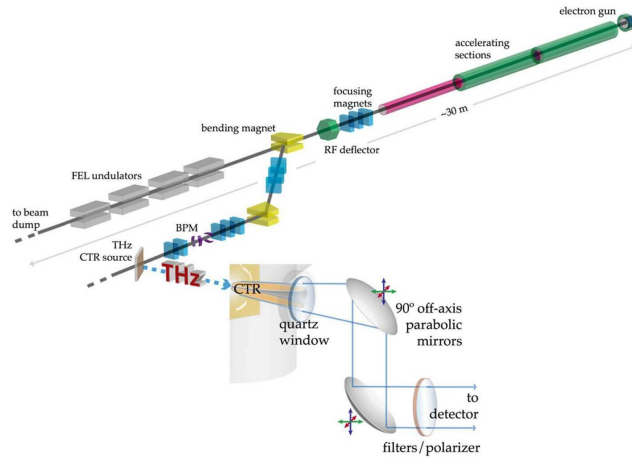


Figure 1: *Cartoon of the SPARC accelerator layout with a zoom of the THz source set-up.*

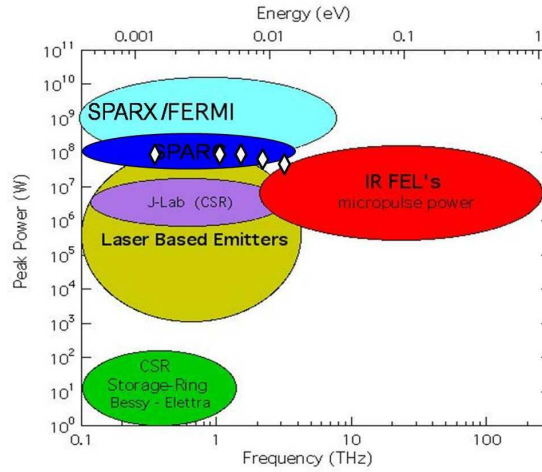


Figure 2: *Figure of merit for existing THz sources compared to simulation and data (white diamonds) measured at SPARC.*

In order to fully characterize the THz spectrum several band-pass filters with characteristic frequency of 0.38 - 1.5 - 2.5 - 3.4 - 4.3 - 4.8 THz<sup>4)</sup>, can be inserted between the THz source and the detector. In addition a wire grid polarizer can be also used to select the polarization.

The pulse intensity has been studied as function of bunch charge, compression factors and laser pulse shapes, in order to exploit a wider range of coherent emission regimes, thus revealing the characteristics of coherence of the THz radiation. These data are represented in the cartoons of Fig. 2 (white diamonds) superimposed to the expected values from simulations, and compared to both existing THz sources and expected performances for the future light sources. First measurements dedicated to the production and optimization of electron pulse trains for THz radiation generation have been performed. We have been operating with two Gaussian longitudinal profiles, 0.18 ps rms long and separated by 4.3 ps. The total extracted charge was 180 pC. In order to select the CTR emission at the THz frequency and enhance its intensity, the pulse inter-distance has been reduced down to 0.7 ps and the pulse profile shrunk by means of RF compression. Since the two pulses are not clearly separated, the corresponding form factor shows a slight modulation centered

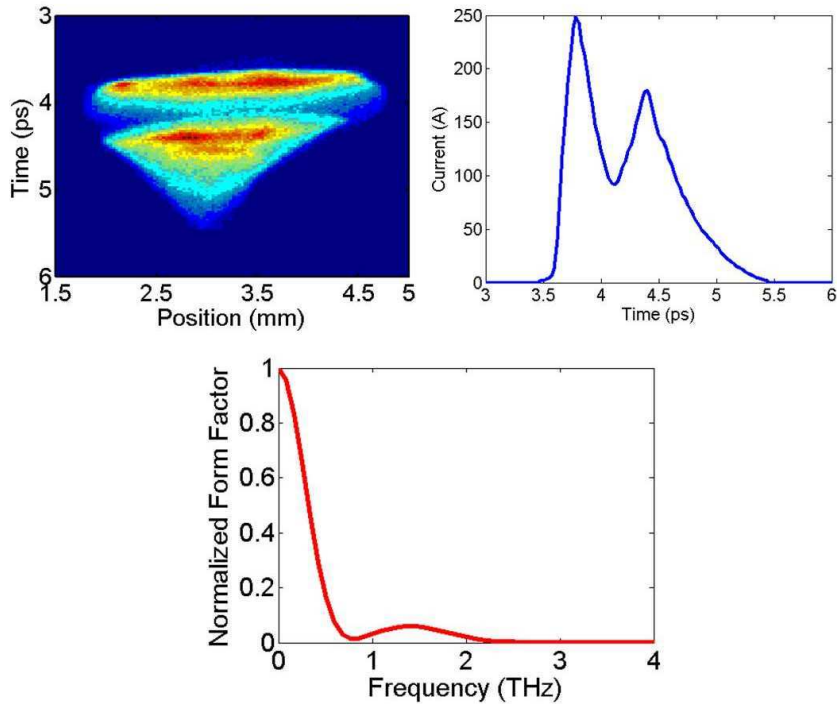


Figure 3: *Top: Measured comb image and temporal profile; bottom: comb form factor.*

at the comb frequency, i.e. 1.5 THz (see Fig. 3).

#### 4 Outlook for 2011 Activity

The activity in 2011 will be dedicated to the spectral characterization of the THz source by means of both bandpass filters and interferometers with calibrated detectors, in particular Golay cell and pyroelectric ones. Furthermore this work will allow to set a valid and permanent tool for the reconstruction of the electron beam longitudinal profile.

A detailed campaign of measurements on electron beam parameters and linac settings is mandatory to optimize the THz source in terms of peak power and frequency extension. Both schemes of THz radiation production, standard, e.g. through the generation of ultra-short high brightness electron beams, and novel ones, e.g. laser comb technique, will be used to produce high power, broadband or narrow band and tunable THz radiation.

An upgrade of the experimental layout, i.e. diamond viewport in place of the z-cut quartz one, optical components for pump and probe experiments,  $N_2$  flushing, etc., is also planned.

Finally, first THz-pump/THz-probe experiments are foreseen to measure the lifetime of an excited level in quantum wells Ge/Si-Ge.

#### 5 Conference Talks

1. E. Chiadroni, Characterization of the THz source at SPARC, Invited seminar at Karlsruhe Institut of Technology - ANKA (2010), Karlsruhe, Germany
2. E. Chiadroni, Characterization of the THz source at SPARC, International Particle Accelerators Conference IPAC'10, Kyoto, Japan

## 6 Publications

- E. Chiadroni *et al.*, “Characterization of the THz radiation source at SPARC”, in: Proc. of IPAC’10 Conference, Kyoto, Japan (2010).
- E. Chiadroni *et al.*, “Production of high power terahertz radiation through the SPARC Free-Electron Laser”, in: Proc. of the 35th International Conference on Infrared Millimeter and Terahertz Waves (IRMMW-THz), Rome (2010).

## 7 Acknowledgment

Authors wish to thank colleagues collaborating from participant institutions:

- INFN Roma 1-La Sapienza: O. Limaj, S. Lupi, M. Mattioli, D. Nicoletti, A. Nucara, M. Serluca.
- University of Rome La Sapienza, SBAI: L. Palumbo.
- INFN Roma 2-Tor Vergata: L. Catani, A. Cianchi, B. Marchetti.

## References

1. D. Alesini *et al.*, Nucl. Inst. & Meth. A **507**, 345 (2003).
2. M. Ferrario *et al.*, Phys. Rev. Lett. **104**, 054801 (2010).
3. M. Ferrario *et al.*, Nucl. Inst. & Meth. A (2010), doi:10.1016/j.nima.2010.02.018.
4. N. I. Landy, 1-4244-1449-0/07/\$25.00 c 2007 IEEE (2007); P. Carelli *et al.*, unpublished (arXiv:0907.3620v2).

## TPS

M. Anelli (Tecn.), E. Iarocci, A. Paoloni, V. Patera (Resp.),  
L. Piersanti (Dott.), A. Sciubba, A. Sarti

### 1 The INFN Treatment Planning System for Hadrontherapy

Clinical results obtained with hadrontherapy have been positive for various tumours, with percentages of local control and survival higher than those gathered with conventional radiotherapy. So far, almost 50000 patients all over the world have been treated with charged hadrons. Most clinical data obtained with these particles are related to protontherapy (more than 49000 patients at the end of 2006) but the implementation of carbon ion therapy has demonstrated to be of great interest in the last decade (more than 3300 patients at the end of 2006).

These results, together with the progress in accelerator technology and calculation systems of the delivered dose, have caused over the past years an increased interest for the development of hadrontherapy, with the construction of new centers provided with equipments dedicated to clinical applications.

Two different beam delivery techniques have been worldwide implemented: active scanning and passive modulation. With the active system thousands of elementary pencil beams are aimed at an equivalent number of virtual voxels in which the tumor has been divided. Indeed it is possible to obtain both excellent conformation to the tumor and reduction in fluences of unwanted secondary particles even at large distance from the target.

At present INFN is deeply involved in the construction of the synchrotron for protons and  $^{12}\text{C}$  ions at CNAO, the new Italian center for hadrontherapy in Pavia, based on active beam scanning technology. Taking into account the various multidisciplinary expertise grown within the INFN research groups, a further contribute to the developments in the field of hadrontherapy could concern the design of new and advanced Treatment Planning Systems (TPS). In short the TPS is a set of tools that allow the translation of the dose prescription into a set of beam energies, positions and intensities needed for the treatment. Innovative contribution in this field is particularly needed in case of the use of ions. Several INFN research groups, active in different scientific areas, such as experimental and theoretical and phenomenological nuclear physics, Monte Carlo calculations and techniques for numerical analysis, Radiobiology and Hardware/Software development for dose monitoring purposes, propose to cooperate in order to develop an improved TPS for ion therapy with active scanning.

### 2 LNF activity: $^{12}\text{C}$ fragmentation measurement at therapeutical energies

Reliable Monte Carlo transport codes like FLUKA and GEANT4 require total and partial fragmentation cross sections as critical inputs. The limited experimental data available make up the highest uncertainty in these codes and in their medical application. A number of measurements of fragmentation cross sections in the (Z; E) range (4-56; 200-1000 MeV/A) have been performed in the past using both silicon telescopes or passive detectors (for bibliography see <sup>1</sup>).

There are still several energy, beam and target settings of primary importance for hadrontherapy applications that need to be studied. Even more important is the fact that the measurements performed so far do not include all the information that is required for our purposes like, for instance, the angular distribution and the multiplicity of the different types of fragments and particles. No further information in this respect is available from the measurements with nuclear track

solid state detectors ( 2).

The interest for differential cross section measurements of high energy projectile on thin target is due to the fact that only by measuring those cross sections, we can have a suitable perspectives to develop and validate nuclear interaction models to be implemented in Monte Carlo codes. These codes are the unique tool we can use to calculate in any real conditions (materials, primary beams, energy) the whole particles spectra in terms of fluence, energy and angular distributions also as function of the depth and material types. Then it will be possible to have a significant improvement in Treatment Planning System radioprotection.

To overcome the lack of data at intermediate energies of  $^{12}\text{C}$ ,  $^{16}\text{O}$  and  $^{56}\text{Fe}$  fragmentation on different targets (C, Ni, Au), the fragmentation of  $^{12}\text{C}$  beam accelerated by the Superconducting Cyclotron at 32 MeV/A, 62 MeV/A on  $^{197}\text{Au}$ ,  $^{207}\text{Pb}$  and  $^{12}\text{C}$  targets has been studied at the INFN Laboratori Nazionali del Sud. While preliminary results show that for higher energy angular distributions are mostly forward peaked and data suggest an energy dependence in the fragment production mechanism, the scenario is not completely understood.

Theoretical double differential cross sections for proton and alpha particles computed with two different hadronic physical models, Binary light Ion Cascade (BIC) and Quantum Molecular Dynamic (QMD), differ by an order of magnitude. This result confirms the weakness of the modelization also due to the lack of validation programs based on experimental data. The fragmentation task of the TPS experiment will produce the data sets needed by the simulation codes. The energies of hadrontherapy interest are higher than those achievable at the LNS Cyclotron, so this task will be performed at GSI with 200-300 MeV/A beams within an international collaboration made of Saclay-CEA, ESA and GSI physicists. The experiment label at GSI is S371, while the collaboration name is FIRST (Fragmentation of Ions Relevant for Space and Therapy).

To perform efficiently such program we need to upgrade the detector already existing and available at GSI. The upgrade of this set-up, made of the Aladin magnet, the Music Time Projection Chamber (TPC), the Time of Flight (ToF) system, the LAND neutron detector (see details in 3)) will be done mainly in the interaction region. The LNF group is involved in this upgrade, needed to achieve the required time and momentum resolution. This resolution is crucial to discriminate between the different charges and to measure the energy of all the produced fragments.

Following the beam path, the improved set-up will have a ToF start counter, a beam tracker drift chamber, the target, a "vertex" detector and a calorimeter. The insertion of two tracking devices has the aim to provide precise information of the beam impact point in the target and to have a first measurement of the produced fragment tracks nearby the target, before the Aladin magnet. This information will help the several meters back tracing of the fragments from the MUSIC detector through the magnetic field, as well as the fragment emission angle determination at the target. Such a design fits particularly for the light beam, where the start counter must have enough thickness to achieve a resolution of the order of 300 ps. In this case the beam track chamber should be able to detect (and veto) secondary products of eventual interactions of the beam in the start counter. Common design requirements for both tracking detectors are the reduced size, the low material budget (interaction probability at the % level) and a good spatial hit resolution (order of 0.2 mm). Furthermore the vertex detector must also have good track separation capability. The beam monitor and start counter prototypes that have been built in 2009 and 2010 are described in section 3, where we also review their performances.

### 3 The beam monitor and the start counter prototypes

#### 3.1 Beam Monitor

For the beam monitoring and tracking, a drift chamber technology has been chosen. A first prototype, with an active area of  $4\times 4\times 10\text{ cm}^3$ , equipped with hexagonal cells (radius equal to

0.5 cm), was designed and built in 2009 (see Figure 1, right). The chamber had four layer for each x-y view, each layer made of four cells. The sense wires had a  $30\ \mu\text{m}$  diameter and were made of tungsten, gold plated. The chamber was operated and tested at the LNS  $^{12}\text{C}$  beam at 62 MeV/nucleon in 2010. The spatial resolution obtained with a 20-80% Ar- $\text{CO}_2$  gas mixture, and high voltage at 1.9 kV, was  $\sim 100\ \mu\text{m}$ , comparable with the resolution on the wire positioning in the chamber. The chamber efficiency as a function of the HV and gas mixture has been measured. Results are shown in Figure 1, showing that the chamber is properly working and can be safely operated in a 2.0–2.3 kV range.

A second prototype, with a slightly different layout, has been designed and built in 2010, in the LNF, in order to improve the tracking efficiency and resolution of the monitor. Two wire planes on each view have been added, and the wire spacing has been enlarged, reducing from four to three the number of sense wires for each plane. The new cells are rectangular with a  $1 \times 1.6\ \text{cm}^2$  area, in order to widen the free space around the wires and reduce the probability of a  $^{12}\text{C}$  interaction with the detector.

This second prototype has been partially built in 2010 (only 4 out of 6 wire planes were wired in 2010) and has been tested on the LNS carbon beam showing improved performances with respect to the first prototype in terms of spatial resolution. The same sense wires, gas mixture and operational voltages are foreseen, and will be thoroughly tested in a dedicated test beam at the LNF Beam Test Facility in 2011.

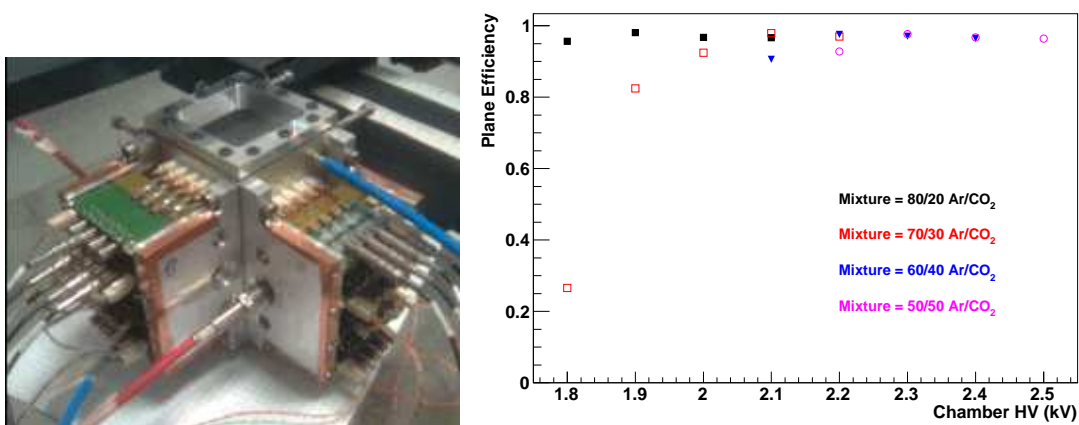


Figure 1: *Left: Beam monitor drift chamber first prototype. Right: Chamber plane efficiency as a function of the applied HV and of the gas mixture, measured on 62 MeV/A carbon beam in LNS in 2010.*

### 3.2 Start Counter

Three different start counter prototypes have designed and built in 2009-2010. While the three detectors active area is identical in shape and active material ( $100\ \mu\text{m}$  thick, square shaped, plastic scintillator), the implemented readout layout show several differences. The first prototype, shown in Figure 2 left, was built in 2009 and was read out by light fibers glued on two opposite sides. In the second prototype an attempt was made in order to maximize the light output and minimize the light loss due to coupling of scintillator with the light guide. The scintillator material was thus cut and bent in order to couple it directly to the photomultiplier. The third prototype (still under

construction) has a readout implemented with scintillating fibers that are glued on all the 4 sides of the active areas and read by Hamamatsu 10721-210 photomultipliers.

The first and second prototypes, developed before 2010, were tested on the LNS carbon beam: a time resolution  $\sim 300$  ps was obtained (see Figure 2 right) for the first prototype, while the second prototype showed some operational problems that have been tracked down afterwards, to cracks appeared in the bent scintillating material.

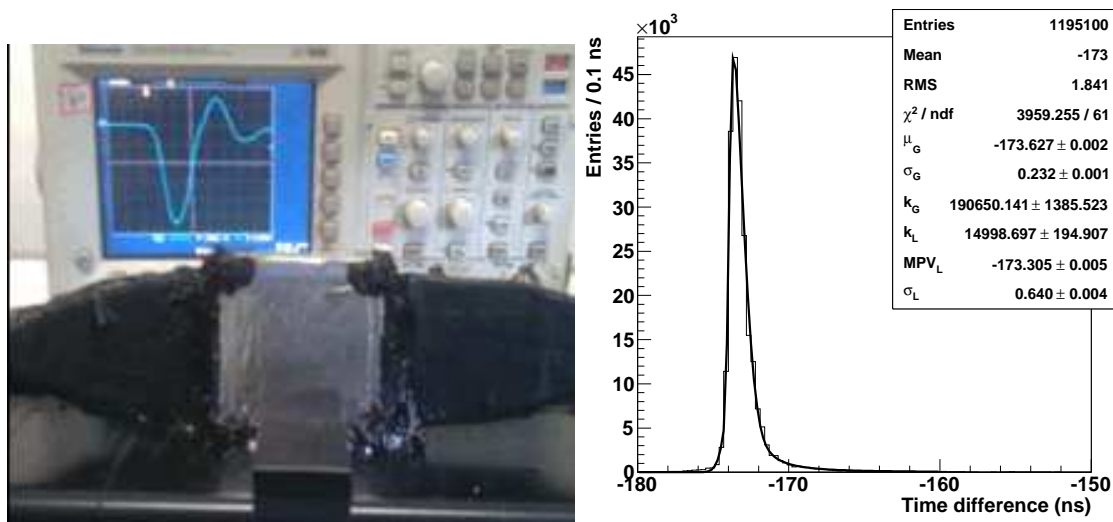


Figure 2: *Left: Start counter scintillator, first prototype. Right: Time resolution of the FIRST start counter prototype measured at the LNS carbon beam of 62 MeV/A energy. A  $\sigma$  of  $\sim 232\mu\text{m}$  is obtained.*

#### 4 Conference Talks

1. V. Patera, “Status Report on FIRST at GSI”, Catania, 18 Novembre 2010, [http://totlxl.to.infn.it/presentations/LNS2010/FIRST\\_GSI\\_Patera.pdf](http://totlxl.to.infn.it/presentations/LNS2010/FIRST_GSI_Patera.pdf)
2. A. Sarti, “L’esperienza FIRST nell’ambito del progetto TPS dell’INFN”, Firenze, 8 marzo 2010, <http://agenda.infn.it/conferenceDisplay.py?confId=2461>

#### References

1. C. Zeitlin *et al.*, “Shielding experiments with high energy heavy ions for spaceflight applications”, *New J. Phys.* **10** 075007 (2008).
2. S. Cecchini *et al.*, “Fragmentation cross sections of Fe26+, Si14+ and C6+ ions of 0.3-10 AGeV on polyethylene, CR39 and aluminum targets”, *Nucl. Phys. A* **807**, 206 (2008).
3. T. Aumann, “Giant Resonances in Exotic Nuclei. Experimental Status and Perspectives”, *Nucl. Phys. A* **805**, 198c-209c (2008).

**CATHERINE**  
**(Carbon nAnotube Technology for High-speed nExt-geneRation nano-InterconNEcts)**

S. Bellucci (Resp. Naz.), R. Baldini (Tecn.), S. Bini (Art. 2222),  
L. Coderoni (Art. 2222), G. Giannini (Art. 2222), F. Micciulla (Art. 2222)  
P. Onorato (Art. 2222), I. Sacco (Bors.)

**1 External collaborating Institutions:**

Univ. Roma La Sapienza and Consorzio Sapienza Innovazione, Technische Universiteit Delft and Philips Electronics Nederland B.V. The Netherlands, Université Paul Sabatier Toulouse France, Univ. Salerno, IMT Bucharest Romania, Latvijas Universitates Cietvielu Fizikas Instituts, Swedish Defence Research Agency and Smoltek AB Sweden).

We participate as a partner (the INFN unit) to the EU FP7 Project CATHERINE, Carbon nAnotube Technology for High-speed nExt-geneRation nano-InterconNEcts, Grant Agreement number: 216215, Funding Scheme: Collaborative Project - Small or medium-scale focused research project (STREP). CATHERINE has a duration of 36 months and started its activities on 1st January 2008. The consortium binds together five Universities, three Research Organizations, one Large Industry, one SMEs and one Service Company. The partners are located in 6 EU Member States (Italy, The Netherlands, Sweden, France, Romania, Latvia).

**2 Project objectives:**

The aim of CATHERINE was to develop an innovative cost-effective and reliable technological solution for high-performance next-generation nano-interconnects beyond the limit of current technology. This new approach, which exploits the carbon nano-tube (CNT) technology, has permitted to realize interconnects with high-transmission speed, high current density, exceptional mechanical and thermal properties, optimum signal and power integrity. CATHERINE was focused on delivering cost-effective solution to the ITRS roadmap for late CMOS and post-CMOS systems, requiring continuous miniaturization of electrical and electronic devices (down to 22 nm node in 2011), high integration level, increasing working frequency and power density, reduction of global interconnection delay.

**3 Relevant results achieved:**

The results achieved by CATHERINE are summarized as follows: R1) Definition of all causal relations within the design-chain microstructure characteristics fabrication process functional properties; R2) Development of multiscale multiphysics simulation models for the prediction of the multifunctional performance of the interconnect and for the EMC analysis; R3) Development of electromagnetic and multifunctional test procedures and experimental characterization methods; R4) Manufacturing and testing of proof-of-concept samples of nano-interconnects at laboratory level. The final CATHERINE products were: P1) Integrated data-base for nano-interconnect design; P2) Proof-of-concept nano-interconnect.

CATHERINE has been finalized to develop innovative cost-effective and reliable technological solutions for high-performance next-generation nanointerconnects beyond the limit of current technology. The new approaches developed in CATHERINE have exploited the carbon nanotube (CNT) technology, with the scope of delivering a cost-effective solution for high frequency applications (up to 40 GHz). The new bottom-up approach proposed in CATHERINE project consisted in

realizing CNT-based nano-interconnects for integrated circuit exploiting two different techniques: 1. A template-based CVD technique that allows high control of the growth of perfect aligned arrays of CNTs. The CNTs are synthesized within the pores of properly designed alumina membrane. CNTs wall number is controlled by the reaction time, the CNT length by the thickness of alumina membrane, the CNT external tube diameter by the membrane pore size. 2. CVD growth carbon nanofibers (CNFs) on substrate patterned with nano-imprint lithography. Both techniques do not require electron beam lithography (EBL) for CNTs growth or substrate preparation. The resulting process is cost-effective and can be easily implemented at industrial scale.

CNT-to-metal contacts characterized by low impedance have been also realized in order to optimize interconnect performances. A multiscale design tool of the new nano-interconnect, implementing advanced multifunctional simulation models at different scale, has been developed and experimentally validated. The electromagnetic compatibility (EMC) aspects related to the integration of the nanointerconnect in complex systems have been analysed in the frequency range up to 100 GHz in order to demonstrate the feasibility and concrete advantages of the new technology. A multiscale simulation has been also implemented to predict the mechanical/thermal properties of the nanointerconnect. MD (Molecular Dynamics) simulation of the CNTs have been first implemented to obtain the homogeneous properties of the nanostructure, and these have been imported into the macro-scaled finite element (FE) model. Then, the global thermal/mechanical loadings have been applied onto the FE model, and the stress/strain distribution around the interconnections was obtained. Finally, the mechanical information obtained from the FE model has been imported to the MD model as the loading conditions.

The project was organized in six workpackages and in two phases. The first phase of the project, having duration of two years, was dedicated to the development of: the simulation tools for both the electrical, electromagnetic and mechanical/thermal properties; the basic technology for CNT/CNF growth and nanointerconnect fabrication and bonding to metal contacts; the techniques for the characterization of the functional properties of the interconnects. All developed models have been integrated in a data-base and made available on CATHERINE web site. The second phase of the project, developed during the third year, was finalized to the optimization of the simulation models for the design of proof-of-concept nanointerconnects and to their fabrication, characterization and testing for technology validation and assessment.

Two different technologies have been selected and optimized to produce two different test fixtures including proof-of-concept nanointerconnects. The first approach is based on the growth of CNTs with controlled morphology inside the pores of an alumina membrane, at temperature around 850 centigrades. The CNT-alumina composite is integrated in a the test device by developing an hybrid approach which is compatible with standard microelectronics technology. This is a real advantage of the proposed technology which can be directly transferred for industrial application. It is demonstrated that the proof-of-concept device is suitable for electromagnetic testing in the range up to 40 GHz. The second approach is based on the growth of CNFs by CVD at the temperature of 440 centigrades, which is compatible with CMOS processes, starting from an array of nickel nanodots obtained by nano-imprint lithography or also EBL. This method has the advantage that the growth of the CNFs can be done in line, due to the low temperature.

In conclusion CATHERINE has achieved the final objectives of: 1) Developing a cost-effective and reliable technological process for realization of high-performance next-generation interconnects for radio-frequency applications (up to 40 GHz); 2) Developing a multi-scale simulation tool for the prediction of the multifunctional performance of the interconnect and for the electromagnetic-compatibility analysis up to 40 GHz; 3) Developing a test procedures and experimental methods to characterize the electrical, electromagnetic, mechanical and thermal properties of nano-interconnects made of carbon nano-tubes or carbon nano-fibres; 4) Manufacturing and testing proof-of-concept nano-interconnects at laboratory level and analysis of the signal propagation prop-

erties at radio-frequency up to 40 GHz.

Within the Conf. Nanoscience and Nanotechnology - N&N2010, held at INFN Frascati (20-23 September 2010), we organized a special session Electronic Structures of Nano-Materials, open to all N&N2010 participants and devoted also to review some of the CATHERINE progresses. During the session, which was attended by 99 persons, the following presentations were given: 1. Low voltage scanning electron microscopy in nanotechnology, A. Dinescu, R. Miller (IMT); 2. Synthesis and Characterization of Carbon Nano tubes grown by CVD inside pores of Alumina membrane for high speed inter connections, F. Micciulla (INFN); 3. Argon glow discharge for surface cleaning of alumina membrane with Carbon Nano tubes, S. Bini (INFN); 4. Mechanical and electrical characterization of nano composites coatings for electronic circuits, L. Coderoni (INFN); 5. Radial effects on physical Models for Multiwall Carbon Nano tube Interconnects, S. Bellucci (INFN); 6. Ab initio simulations on electric properties for junctions between carbon nano tubes and metal electrodes, Y. Shunin, Y. Zhukovskii, V. Gopejenko, N. Burlutskaya, S. Bellucci (LU CFI and INFN).

#### 4 Publications

1. Y. Shunin, Y. Zhukovskii, N. Burlutskaya, S. Bellucci, Central European Journal of Physics, **9**, 519 (2011), DOI: 10.2478/s11534-010-0086-9;
2. Y. Zhukovskii, S. Piskunov, E. Kotomin, S. Bellucci, Central European Journal of Physics, **9**, 530 (2011) DOI: 10.2478/s11534-010-0079-8.
3. S. Bellucci, P. Onorato, Journal of Applied Physics, **108**, 073704 (2010), DOI:10.1063/1.3491028.
4. S. Bellucci, P. Onorato, Y. Shunin, Y. Zhukovskii, N. Burlutskaya, Multiwall Carbon-nano-tube Interconnects: radial effects on physical models and resistance calculations for various metal substrates, IEEE Publication Title: The 33rd Semiconductor Conference (CAS 2010), Sinaia, Romania, 11-13 October 2010.
5. S.Piskunov, G. Zvejnieks, Y. Zhukovskii, S. Bellucci, (LU CFI and INFN), Atomic and electronic structure of both perfect and nano structured Ni(111) surfaces: first-principles calculations, Thin Solid Films, (2011).
6. Y. Zhukovskii, S. Piskunov, E. Kotomin, S. Bellucci, "Atomic carbon adsorption on flat and nano-structured Ni catalyst with further CNT growth: predictions from first principles calculations", Physica E, (2011).
7. Y. Shunin, Y. Zhukovskii, N. Burlutskaya, S. Bellucci, CNT-metal interconnects: Electronic structure calculations and resistivity simulations, Journal of Nano-electronic and Optoelectronic, (2011).
8. S. Piskunov, V. Kashcheyevs, Y. Zhukovskii, S. Bellucci, "Theoretical simulations on the inter-shell interactions in double-wall CNTs of different morphology", Computational and Theoretical Chemistry, (2011).
9. S. Bellucci and P. Onorato, "Transport Properties in Carbon Nanotubes, in Physical Properties of Ceramic and Carbon Nanoscale Structures", Lecture Notes in Nanoscale Science and Technology Volume 11: Physical Properties of Ceramic and Carbon Nanoscale Structures: The INFN Lectures - Vol II, p 45, Ed. S. Bellucci, (2011).
10. Y. Shunin, Y. Zhukovskii, V. Gopejenko, N. Burlutskaya, S. Bellucci, "Ab initio simulations on electric properties for junctions between carbon nano tubes and metal electrodes", Nanoscience and Nanotechnology Letters (NNL) 2011.

## 5 List of Conference Talks

1. Y. Zhukovskii, S. Piskunov, E. Kotomin, S. Bellucci, "Growth mechanism for CNT bundle upon both flat and nano structured Ni catalyst: ab initio simulations", Inter. Conf. Functional materials and nanotechnologies, FM&NT-2010, Riga, Latvia, March, 2010.
2. Y. Shunin, Y. Zhukovskii, S. Bellucci, N. Burlutskaya, "Resistance simulations for junctions of SW and MW carbon nano tubes with various metal substrates", Inter. Conf. Functional materials and nanotechnologies, FM&NT-2010, Riga, Latvia, March, 2010.
3. Y. Shunin, Y. Zhukovskii, S. Bellucci, N. Burlutskaya, "Nano-sized systems modeling: carbon-based electronic structure calculations and CNT interfaces simulations", the 8th Inter. Conference Information Technologies and Management, IT&M'2010, Riga, Latvia, April, 2010.
4. Y. Shunin, Y. Zhukovskii, S. Bellucci, N. Burlutskaya, "Nano-sized systems modeling: CNT electronic structure calculations and CNT-metal interconnect simulations", GENNESYS Inter. Congress on Nanotechnology and Research Infrastructures, Barcelona, Spain, May 2010;
5. S. Piskunov, Y. Zhukovskii, E. Kotomin, S. Bellucci, "Atomic carbon adsorption on nano-structured Ni catalyst and further CNT growth: predictions from first principles calculations", Spring European Materials Research Society (E-MRS) Meeting, Strasbourg, France, June, 2010;
6. Y. Shunin, Y. Zhukovskii, S. Bellucci, N. Burlutskaya, "CNT-metal interconnect electronic structure calculations and resistivity simulations", Inter. Workshop on Nano-carbon Photonics and Optoelectronics, NPO-2010, Koli, Finland, August, 2010;
7. S. Bellucci, E. Kotomin, S. Piskunov, Y. Shunin, Y. Zhukovskii, "Ab initio model of carbon nano-tubes growth on nano-structured Ni catalyst in a nano porous Al<sub>2</sub>O<sub>3</sub> membrane and resistance calculations for their junctions with various metal substrates", European, Microwave Week, Focused session on Nano interconnects for Advanced RF Packaging, CNIT, Paris, 30 September 2010;
8. Y. Shunin, Y. Zhukovskii, N. Burlutskaya, T. Lobanova, S. Bellucci, "Novel nano electronic devices based on carbon nano tubes and graphene, 4th Inter. Conf. on Innovative Information Technologies, IIT-2010, Vilnius, Lithuania, November, 2010.
9. S. Bellucci, P. Onorato, Y. Shunin, Y. Zhukovskii, N. Burlutskaya, "Multiwall Carbon-nano-tube Interconnects: radial effects on physical models and resistance calculations for various metal substrates", Invited talk at the 33rd Semiconductor Conference (CAS 2010), Sinaia, Romania, 11-13 October 2010.
10. F. Micciulla, "Synthesis and Characterization of Carbon Nano tubes grown by CVD inside pores of Alumina membrane for high speed inter connections".
11. S. Bini "Argon glow discharge for surface cleaning of alumina membrane with Carbon Nano tubes".
12. L. Coderoni, Mechanical and electrical characterization of nano composites coatings for electronic circuits".
13. S. Bellucci, "Radial effects on physical Models for Multiwall Carbon Nano tube Interconnects".

## INNOVATIVE METHODOLOGIES FOR RISK ASSESSMENT IN THE OCCUPATIONAL EXPOSURE TO NANOMATERIALS

S. Bellucci (Resp. Naz.), R. Baldini (Tecn.), S. Bini (Art. 2222),  
L. Coderoni (Art. 2222), G. Giannini (Art. 2222), F. Micciulla (Art. 2222),  
P. Onorato (Art. 2222), I. Sacco (Bors.)

### 1 External collaborating Institutions

Università Roma La Sapienza, Policlinico Umberto I University Hospital Roma; ISPEL Monte Porzio Catone, Italy; Univ. Roma Tor Vergata, Italy; Univ. Parma, Italy; Fondazione Salvatore Maugeri Pavia, Italy; Agenzia Regionale Prevenzione e Ambiente Regione Puglia, Italy; CNR-Institute for Electromagnetic Sensing of Environment, Naples, Italy

We participate as a partner (the INFN unit) since 1 January 2008 to the project financed by the Italian Ministry of Health, "Innovative Methodologies for risk assessment in the occupational exposure to nanomaterials", coordinated by the Italian Institute for Occupational Health and Prevention (ISPEL). The project will run until 2011.

Aim: We investigate the effect of four different types of sterilization procedures on the structural properties and morphological features of single-wall carbon nanotube samples approachable by micro-Raman spectroscopy. Sterilization procedures (treatment in humid heat autoclave or ethylene oxide and irradiation with g.rays or UV light) are necessary in view of the use of carbon nanotube sterile samples in in vivo toxicity tests on laboratory rats. Micro-Raman spectroscopy allows us to estimate several details about the morphology of the single-wall carbon nanotube mixture (mainly the presence of disorder and diameter distribution) before and after the sterilization treatment. Results: The best of these treatments, in other words, the one that least affected the morphology and structural properties of carbon nanotubes, was found to be UV irradiation and has thus been selected for future in vivo tests on rats.

### 2 List of Conference Talks

1. S. Bellucci, "Nanotechnology in Occupational Medicine", Postgraduate Course on Occupational Health and Safety in the Workplace, International Training Centre of the International Labour Organization (ILO), Torino (Italy), 17 March 2010.
2. S. Bellucci *et al.*, "Buckypaper in Vitro and in Vivo Effects in Toxicology and in Biology", Invited talk given at BITs 1st Annual World Congress of Nanomedicine 2010 Beijing, China, 23–25 October 2010.
3. S. Bellucci *et al.*, "Il Buckypaper inibisce la crescita cellulare dei Linfociti umani del sangue periferico", Istituto Superiore di Sanità NANODRUG2010, Roma, 12 Maggio 2010.
4. O. Zeni *et al.*, "Cytotoxicity of multiwalled carbon nanotube buckypaper in human lymphocytes", poster presented at Sensors and Microsystems: AISEM 2010, Messina February 8-10 2010.
5. S. Bellucci *et al.*, "Carbon Nanotubes in Vitro and in Vivo Biological Effects", Conference CIMTEC 2010 Montecatini Terme, Italy, 14 June 2010.

## References

1. D. Cavallo *et al.*, "MWCNTs induce cytotoxicity and genotoxicity in human lung epithelial cells", submitted to Toxicology.
2. S. Bellucci *et al.*, *Nanomedicine* **5** (2), 209 (2010).
3. S. Bellucci, Toxicology, Diagnostics, and Therapy Functions of Nanomaterials, *Handbook of Nanophysics: Nanomedicine and Nanorobotics*, Ed. K.D. Sattler, CRC Press, Taylor and Francis Group, 2010, ISBN: 9781420075465.
4. S. Bellucci, Carbon Nanotubes In Vitro and In Vivo Biological Effects, *Advances in Science and Technology* **76**, 229 (2010).
5. O. Zeni *et al.*, Cytotoxicity of Multiwalled Carbon Nanotube Buckypaper on Human Lymphocytes, *Sensors and Microsystems: AISEM 2010 Proceedings (Lecture Notes in Electrical Engineering)* [Hardcover] Giovanni Neri (Editor), Nicola Donato (Editor), Arnaldo d'Amico (Editor), Corrado Di Natale (Ed.), # Springer, ISBN-10: 9400713231.



## *6 – Accelerator Physics*



## DAΦNE

### The DAΦNE Team

D. Alesini, M.E. Biagini, S. Bini, C. Biscari, R. Boni, M. Boscolo, F. Bossi, B. Buonomo, A. Clozza, G. Delle Monache, T. Demma, E. Di Pasquale, G. Di Pirro, A. Drago, M. Esposito, L. Foggetta, A. Gallo, A. Ghigo, S. Guiducci, C. Ligi, S. Liuzzo, F. Marcellini, C. Marchetti, G. Mazzitelli, C. Milardi, F. Murtas, L. Pellegrino, M. Preger, L. Quintieri, P. Raimondi (*Head of Acc. Div.*), R. Ricci, U. Rotundo, C. Sanelli, M. Serio, F. Sgamma, B. Spataro, A. Stecchi, A. Stella, S. Tomassini, C. Vaccarezza, P. Valente, M. Zobov

### The DAΦNE Technical Staff

G. Baldini, P. Baldini, A. Battisti, A. Beatrici, M. Belli, B. Bolli, L. Cacciotti, G. Ceccarelli, R. Ceccarelli, A. Cecchinelli, S. Ceravolo, P. Chimenti, P. Ciuffetti, R. Clementi, O. Coiro, S. De Biase, M. De Giorgi, R. Di Raddo, M. Di Virgilio, A. Donkerlo, G. Ermini, M.R. Ferrazza, G. Fontana, U. Frasacco, C. Fusco, F. Galletti, E. Gaspari, M. Giabbai, O. Giacinti, E. Grossi, F. Iungo, V. Lollo, M. Marchetti, C. Marini, M. Martinelli, A. Mazzenga, C. Mencarelli, M. Monteduro, M. Paris, E. Passarelli, V. Pavan, S. Pella, D. Pellegrini, G. Piermarini, S. Quaglia, F. Ronci, M. Rondinelli, L.A. Rossi, F. Rubeo, M. Sardone, M. Scampati, G. Sensolini, R. Sorchetti, A. Sorgi, M. Sperati, A. Spreccacenero, S. Strabioli, R. Tonus, T. Tranquilli, M. Troiani, V. Valtriani, R. Zarlenga, A. Zolla

DAΦNE is an electron-positron  $\Phi$  meson factory operating at Frascati since 1997. Factories are storage ring colliders designed to work at the energies of the meson resonances, where the production cross section peaks, to deliver a high rate of events to high resolution experiments.

The factory luminosity (the number of events per unit time produced by the reaction under investigation divided by its cross section weighted by the acceptance of the detector) is very high, about two orders of magnitude larger than that obtained at the same energy in colliders of the previous generation. One of the key-points to get a substantial luminosity increase is the use of separated vacuum chambers for the two beams merging only in the interaction regions (IRs). When sharing the same ring the two  $N$ -bunch trains cross in  $2N$  points and the maximum luminosity is limited by the electromagnetic beam-beam interaction. The unwanted effects of this interaction can be reduced with a very strong focussing (called "low- $\beta$ ") at the interaction point (IP), obtained by means of quadrupole doublets or triplets. However these magnetic structures take up much space and excite chromatic aberrations which must be corrected elsewhere in the ring.

This limitation does not hold for the double ring option, consisting in two separate rings crossing at two low- $\beta$  points. The number of bunches that can be stored in such a collider is limited only by the geometry of the IR's.

DAΦNE is an accelerator complex consisting of a double-ring collider, a linear accelerator (LINAC), an intermediate damping ring to make injection easier and faster and 180 m of transfer lines connecting these machines. The beam accelerated by the Linac can also be switched into a laboratory called "Beam Test Facility (BTF)", for dedicated experiments and calibration of detectors. Three synchrotron radiation lines, two from bending dipoles and the other from the wiggler are routinely operated by the DAΦNE-LIGHT group in a parasitic mode, providing photons from the infrared to soft x-rays.

## 1 Injection System

In a low energy electron-positron collider, such as DAΦNE, the lifetime of the stored current is mainly limited by the Touschek effect, namely the particle loss due to the scattering of the particles inside the bunches. In the present typical operating conditions the Touschek lifetime is below 1000 s. It is therefore necessary to have a powerful injection system, capable of refilling the beam without dumping the already stored one. In addition, flexibility of operation requires that any bunch pattern can be stored among the 120 available buckets. The injection system of DAΦNE is therefore designed to deliver a large rate of particles in a single bunch at the working energy of the collider. It consists of a linear accelerator with a total accelerating voltage of 800 MV. In the positron mode, electrons are accelerated to  $\approx 250$  MeV before hitting a tungsten target (called positron converter) where positrons are generated by bremsstrahlung and pair production with an efficiency of  $\approx 1\%$ . The positrons exit from the target with an energy of few MeV and are then accelerated by the second section of the LINAC to their final energy of  $\approx 0.51$  GeV. The positrons are then driven along a transfer line and injected into a small storage ring, called Accumulator, at frequency of 50 Hz. Up to 15 positron pulses are stacked into a single bucket of the Accumulator, then injection stops and the bunch damps down to its equilibrium beam size and energy spread, which are much smaller than the LINAC ones. Damping takes  $\approx 0.1$  s and then the beam is extracted from the Accumulator and injected into the positron main ring at an overall repetition rate of 2 Hz. A powerful and flexible timing system allows the storage of any desired bunch pattern in the collider. In the electron mode, a magnetic chicane deviates the particle trajectory around the positron converter and electrons are directly accelerated to 0.51 GeV and injected into the Accumulator in the opposite direction with respect to positron operation. They are then extracted like in the positron case and injected into the electron main ring through the second transfer line.

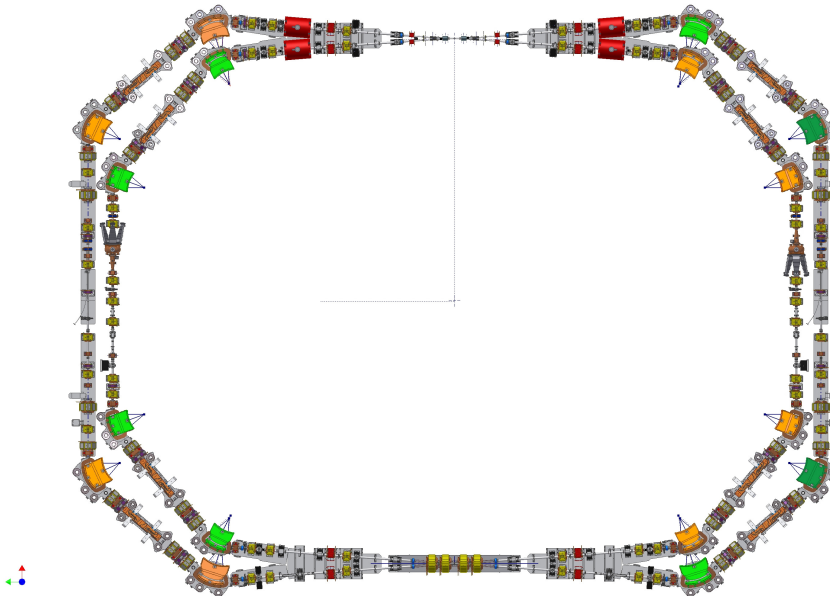


Figure 1: *The DAΦNE Main Rings.*

The Accumulator ring has been introduced in the accelerator complex to increase the injection efficiency, especially for the positrons that are produced by the LINAC at 50 Hz rate in 10 ns pulses with a charge of  $\approx 0.5$  nC. Since the design charge of the main ring at the maximum

luminosity is  $\approx 1.5 \mu\text{C}$  and the longitudinal acceptance of the main rings is only 2 ns, the number of 50 Hz pulses necessary to fill the ring is of the order of  $10^4$ . In order to avoid saturation it is therefore necessary that at each injection pulse a fraction smaller than  $10^{-4}$  of the already stored beam is lost, and this is not easy to achieve. The Accumulator instead works with a lower frequency RF cavity and therefore with a larger longitudinal acceptance. In this way the full charge coming from the LINAC can be stored in a single RF bucket. In a complete injection cycle, that has a duration of 500 ms, up to 15 LINAC pulses can be stored in a single Accumulator RF bucket, and after being damped to the ring equilibrium emittances and energy spread, the whole stacked charge can be stored into a single RF bucket of the main ring. In this way the nominal single bunch charge can be stored with only one pulse from the Accumulator, reducing to 120 the number of injection pulses (at 2 Hz) into each main ring. As an additional benefit, the transverse beam size and energy spread of the beam coming from the Accumulator are at least one order of magnitude smaller than those of the LINAC beam, and this strongly reduces the aperture requirements of the main ring and, as a consequence, the overall cost of the collider.

## 2 Main Rings

In the DAΦNE collider the two beam trajectories cross at the interaction point (IP) with an horizontal angle that has been recently increased from  $\approx 25$  mrad to  $\approx 50$  mrad. A positron bunch leaving the IP after crossing an electron one will reach the following electron bunch at a distance of half the longitudinal separation between bunches from the IP.

Due to the horizontal angle between the trajectories of the two beams, the distance in the horizontal direction between the two bunches is equal to the horizontal angle times half the longitudinal distance between the bunches in each beam. The beam-beam interaction can be harmful to the beam stability even if the distance in the horizontal direction between bunches of opposite charge is of the order of few bunch widths at points where the  $\beta$  function is high and this sets a lower limit on the bunch longitudinal separation and therefore on the number of bunches which can be stored in the collider. However, the so called *crab waist collision scheme* (CW) recently implemented in the machine alleviates this problem, as it will be exhaustively explained in the following of this report.

By design the minimum bunch separation at DAΦNE has been set to  $\approx 80$  cm, and the maximum number of bunches that can be stored in each ring is 120. This number determines the frequency of the radiofrequency cavity which restore at each turn the energy lost in synchrotron radiation, which must be 120 times the ring revolution frequency. The luminosity of the collider can therefore be up to 120 times larger than that obtainable in a single ring with the same size and optical functions. Crossing at an angle could in principle be a limitation to the maximum single bunch luminosity. In order to make the beam-beam interaction less sensitive to this parameter and similar to the case of single ring colliders where the bunches cross head-on, the shape of the bunches at the IP is made very flat (typical ranges of r.m.s. sizes are  $15 \div 30$  mm in the longitudinal direction,  $0.2 \div 1.5$  mm in the horizontal and  $2.5 \div 10 \mu\text{m}$  in the vertical one). The double ring scheme with many bunches has also some relevant challenges: the total current in the ring reaches extremely high values (5 A in the DAΦNE design,  $\approx 1.4$  A in the DAΦNE operation so far) and the high power emitted as synchrotron radiation needs to be absorbed by a complicated structure of vacuum chambers and pumping systems in order to reach the very low residual gas pressure levels necessary to avoid beam loss. In addition, the number of possible oscillation modes of the beam increases with the number of bunches, calling for sophisticated bunch-to-bunch feedback systems.

The double annular structure of the DAΦNE collider as it is now after the recent modifications

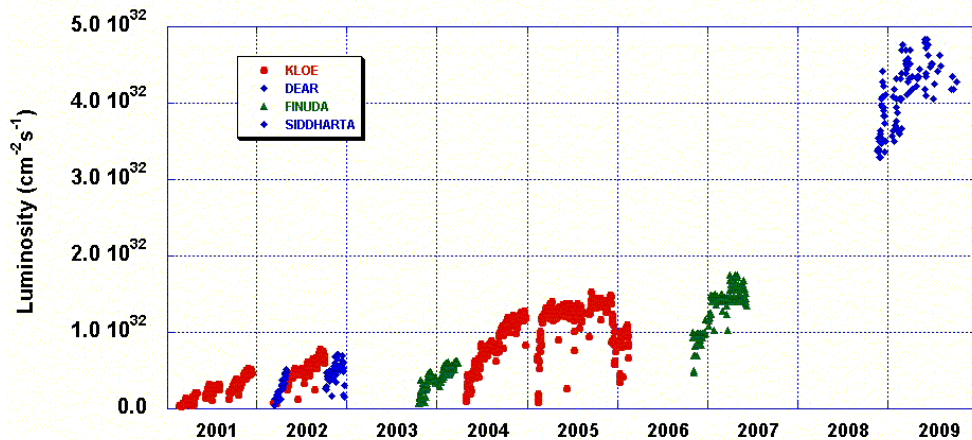


Figure 2: *Peak luminosity at DAΦNE.*

to implement the crab waist scheme is shown schematically in Fig. 1. Both rings lay in the same horizontal plane and each one consists of a long external arc and a short internal one. Starting from the IP the two beams share the same vacuum chamber while traveling in a common permanent magnet defocusing quadrupole (QD) which, due to the beam off-axis trajectory increases the deflection of the two beam trajectories to  $\approx 75$  mrad. Shortly after the QD, at a distance of  $\approx 82$  cm from the IP, the common vacuum chamber splits in two separated ones connected to the vacuum chambers of the long and short arcs. Two individual permanent magnet quadrupoles (QFs) are placed just after the chamber separation. Together with the previous QD they constitute the low- $\beta$  doublets focusing the beams in the IP. The long and short arcs consist of two "almost achromatic" sections (deflecting the beam by  $\approx 85.4$  degrees in the short arc and  $\approx 94.6$  degrees in the long one) similar to those frequently used in synchrotron radiation sources, with a long straight section in between. Each section includes two dipoles, three quadrupoles, two sextupoles and a wiggler. This structure is used for the first time in an electron-positron collider and it has been designed to let DAΦNE deal with high current beams.

The amount of synchrotron radiation power emitted in the wigglers is the same as in the bending magnets and the wigglers can be used to change the transverse size of the beams. The increase of emitted power doubles the damping rates for betatron and synchrotron oscillations, thus making the beam dynamics more stable, while the possibility of changing the beam sizes makes the beam-beam interaction parameters more flexible.

The straight section in the long arc houses the kickers used to store into the rings the bunches coming from the injection system, while in the short straight arc there are the radiofrequency cavity and the equipment for the feedback systems which are used to damp longitudinal and transverse instabilities. The vacuum chambers of the arcs have been designed to stand the nominal level of radiation power emitted by the beams (up to 50 KW per ring). They consist of 10 m long aluminum structures built in a single piece: its cross section exhibits a central region around the beam and two external ones, called the antechambers, connected to the central one by means of a narrow slot. In this way the synchrotron radiation hits the vacuum chamber walls far from the beam and the desorbed gas particles can be easily pumped away. The chambers contain water cooled copper absorbers placed where the radiation flux is maximum: each absorber has a sputter ion pump below and a titanium sublimation pump above. The Main Rings have undergone many readjustments during the years to optimize the collider performances while operating for different

detectors.

In principle the rings could host two experiments in parallel, but only one at a time has been installed so far. Three detectors, KLOE, DEAR and FINUDA, have taken data until 2007 and logged a total integrated luminosity of  $\approx 4.4 \text{ fb}^{-1}$  with a peak luminosity of  $\approx 1.6 \cdot 10^{32} \text{ cm}^{-2} \text{ s}^{-1}$  and a maximum daily integrated luminosity of  $\approx 10 \text{ pb}^{-1}$ .

KLOE has been in place on the first IP from 1999 to 2006, while DEAR and FINUDA have alternatively run on the second one. The detectors of KLOE and FINUDA are surrounded by large superconducting solenoid magnets for the momentum analysis of the decay particles and their magnetic fields represent a strong perturbation on the beam dynamics. This perturbation tends to induce an effect called "beam coupling", consisting in the transfer of the betatron oscillations from the horizontal plane to the vertical one. If the coupling is not properly corrected, it would give a significant increase of the vertical beam size and a corresponding reduction of luminosity. For this reason two superconducting anti-solenoid magnets are placed on both sides of the detector with half its field integral and opposite sign, in this way the overall field integral in the IR vanishes.

The rotation of the beam transverse plane is compensated by rotating the quadrupoles in the low- $\beta$  section. In the case of KLOE the low- $\beta$  at the IP was originally designed with two quadrupole triplets built with permanent magnets, to provide high field quality and to left room to the detector. The structure of the FINUDA IR is quite similar to the KLOE one. Since its superconducting solenoid magnet has half the length (but twice the field) of the KLOE one, the low- $\beta$  focusing at the IP was obtained by means of two permanent magnet quadrupole doublets inside the detector and completed with two other conventional doublets outside.

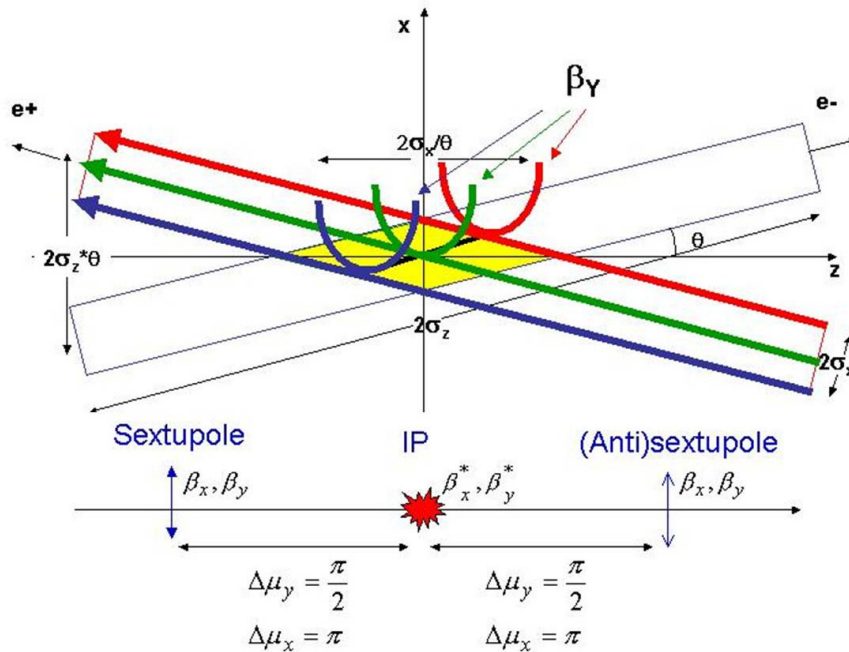


Figure 3: Crab waist scheme

The DEAR experiment, which was installed on the IR opposite to KLOE, took data during the years 2002-2003. It does not need magnetic field and therefore only conventional quadrupoles were used for the low- $\beta$ . FINUDA rolled-in at DEAR's place in the second half of 2003 and took data until spring 2004. It was then removed from IP2 in order to run the KLOE experiment with

only one low- $\beta$  section at IP1, and rolled-in back in 2006 for a second data taking run ended in June 2007. After that the detector has been rolled-out again, and presently there are no detectors installed in IR2. The two chambers are vertically separated so that the two beams do not suffer from parasitic interactions in the whole IR2. A summary of the peak luminosity during these runs is shown in Fig. 2.

### 3 The large Piwinski angle and crab waist collision scheme at DAΦNE

In standard high luminosity colliders the key requirements to increase the luminosity are: very small vertical beta function  $\beta_y$  at the IP, high beam intensity  $I$ , the small vertical emittance  $\epsilon_y$  and large horizontal beam size  $\sigma_x$  and horizontal emittance  $\epsilon_x$  required to minimize beam-beam effects. The minimum value of  $\beta_y$  is set by the bunch length to avoid the detrimental effect on the luminosity caused by the hour-glass effect. It is very difficult to shorten the bunch in a high current ring without exciting instabilities. Moreover, high current implies high beam power losses, beam instabilities and a remarkable enhancement of the wall-plug power. In the CW scheme of beam-beam collisions a substantial luminosity increase can be achieved without bunch length reduction and with moderate beam currents. For collisions under a crossing angle  $\theta$  the luminosity  $L$  and the horizontal  $\xi_x$  and vertical  $\xi_y$  tune shifts scale as:

$$L \propto \frac{N\xi_y}{\beta_y} \propto \frac{1}{\sqrt{\beta_y}} \quad (1)$$

$$\xi_y \propto \frac{N\sqrt{\beta_y}}{\sigma_z\theta}; \quad (2)$$

$$\xi_x \propto \frac{N}{(\sigma_z\theta)^2} \quad (3)$$

The Piwinski angle  $\phi$  is a collision parameter defined as:

$$\phi = \frac{\sigma_z}{\sigma_x} \tan\left(\frac{\theta}{2}\right) \approx \frac{\sigma_z}{\sigma_x} \frac{\theta}{2} \quad (4)$$

with  $N$  being the number of particles per bunch. Here we consider the case of flat beams, small horizontal crossing angle  $\theta \ll 1$  and large Piwinski angle  $\phi \gg 1$ . In the large Piwinski angle and Crab Waist scheme described here, the Piwinski angle is increased by decreasing the horizontal beam size and increasing the crossing angle. In such a case, if it were possible to increase  $N$  proportionally to  $\sigma_z\theta$ , the vertical tune shift  $\xi_y$  would remain constant, while the luminosity would grow proportionally to  $\sigma_z\theta$ . Moreover, the horizontal tune shift  $\xi_x$  would drop like  $1/\sigma_z\theta$ . However, the most important effect is that the overlap area of the colliding bunches is reduced, as it is proportional to  $\sigma_x/\theta$  (see Fig. 3). Then, the vertical beta function  $\beta_y$  can be made comparable to the overlap area size (i.e. much smaller than the bunch length):

$$\beta_y \approx \sigma_x/\theta \ll \sigma_z \quad (5)$$

We get several advantages in this case:

- Small spot size at the IP, i.e. higher luminosity  $L$ .
- Reduction of the vertical tune shift  $\xi_y$  with synchrotron oscillation amplitude.
- Suppression of synchrotron resonances.

Table 1: *DAΦNE Beam parameters for KLOE (2006) and SIDDHARTA (2008-2009).*

PARAMETERS	KLOE Run	SIDDHARTA Run
$L$ [ $\text{cm}^{-2}\text{s}^{-1}$ ]	$1.5 \cdot 10^{32}$	$4.5 \cdot 10^{32}$
$N_{part}/\text{bunch}$	$2.65 \cdot 10^{10}$	$2.65 \cdot 10^{10}$
$I_{bunch}$ [mA]	13	13
$\epsilon_x$ [ $10^{-9}$ m · rad]	340	260
$\epsilon_y$ [ $10^{-9}$ m · rad]	1.5	1
$\sigma_x$ [ $\mu\text{m}$ ]	760	200
$\sigma_y$ [ $\mu\text{m}$ ]	5.4	3.5
$\sigma_z$ [mm]	25	17
$\beta_x^*$ [m]	1.7	0.25
$\beta_y^*$ [mm]	17	9
$\theta$ [mrad]	$2 \times 12.5$	$2 \times 25$

There are also additional advantages in such a collision scheme: there is no need to decrease the bunch length to increase the luminosity as proposed in standard upgrade plans for B- and  $\Phi$ -factories. This will certainly help solving the problems of HOM heating, coherent synchrotron radiation of short bunches, excessive power consumption etc. Moreover, parasitic collisions (PC) become negligible since with higher crossing angle and smaller horizontal beam size the beam separation at the PC is large in terms of  $\sigma_x$ .

However, large Piwinski angle itself introduces new beam-beam resonances which may strongly limit the maximum achievable tune shifts. At this point the crab waist transformation enters the game boosting the luminosity, mainly because of the suppression of betatron (and synchro-betatron) resonances arising (in collisions without CW) through the vertical motion modulation by the horizontal oscillations. The CW vertical beta function rotation is provided by sextupole magnets placed on both sides of the IP in phase with the IP in the horizontal plane and at  $\pi/2$  in the vertical one (see Fig. 3).

For comparison, the parameters used during the last DAΦNE run with the KLOE detector (2005-2006) are shown in Table 1. As discussed above, in order to realize the CW scheme in DAΦNE, the Piwinski angle  $\phi$  should be increased and the beam collision area reduced: this is achieved by increasing the crossing angle  $\theta$  by a factor 2 and reducing the horizontal beam size  $\sigma_x$ . In this scheme the horizontal emittance  $\epsilon_x$  is reduced by a factor 1.5, and the horizontal beta function  $\beta_x$  lowered from 1.5 to 0.2 m. Since the beam collision length decreases proportionally to  $\sigma_x/\theta$ , the vertical beta function  $\beta_y$  can be also reduced by a factor 3, from 1.8 cm to 0.6 cm. All other parameters are similar to those already achieved at DAΦNE.

#### 4 Hardware upgrades for the Crab Waist test at DAΦNE

DAΦNE has been upgraded to allow the CW collision scheme test with the SIDDHARTA run during the summer shutdown of 2007.

The major upgrades on the machine are summarized as:

- new IR1 geometry for the CW test;
- new IR2 geometry with two completely separated vacuum chambers with half moon profile;
- new shielded bellows;

- the four  $e^+ e^-$  transverse feedbacks have been upgraded;
- solenoid windings in the two long IRs sections of the  $e^+$  ring;
- new calorimeter for luminosity measurement and tuning;
- new longitudinal position of the two IRs horizontal collimators;
- new injection kickers.

The need of a new IR geometry is essentially due to have a very small  $\beta_y$  (9 mm) and a large crossing angle (25 mrad per beam). Splitter magnets installed in the original design have been removed thanks to the large crossing angle in the CW scheme. Defocusing and focusing quadrupoles (QD, QF) on both sides of the IP have been placed to obtain the required low- $\beta$  structure. Further trajectory separation is provided by two small dipole correctors upstream and downstream the quadrupole doublets, while other three quadrupoles are used to match the betatron functions in the arcs.

The low- $\beta$  section quadrupoles near the IP are of permanent magnet (PM) type. The QDs are located near the IP where the beams share a common vacuum chamber, while the QFs are positioned where the chambers are splitted and each one acts on a single beam. Therefore a total of two QDs and four QFs is required to get the two doublets around IP1. Four corrector dipoles provide a deflection of 9.5 mrad to match the inlet and outlet arc chamber flanges.

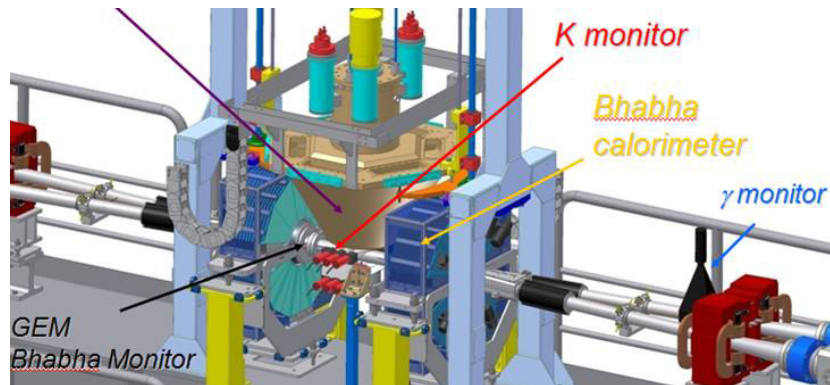


Figure 4: Overview of the upgraded DAΦNE IR1 showing the various luminosity detectors.

CW sextupoles are placed at  $\sim 9.3$  m far from the IP1. Bending dipoles facing the IRs have been rotated and their field adjusted according to requirements. They have been powered with independent supplies to match these requirements.

For the SIDDHARTA experiment a new aluminium alloy (AL6082T6) chamber with two thin windows (0.3 mm 0.02 thickness) in the top and bottom sides has been designed and built.

Electromagnetic simulations have shown the presence of trapped modes which add resonant contributions to the beam coupling impedance in the Y-chamber junctions, the regions where the two separate ring pipes merge in the common vacuum chamber near the IP. In the worst possible scenario, that occurs when a beam spectrum line at a frequency equal to a multiple to the bunch repetition rate is in full coupling, the joule loss does not exceed 200 W. To keep this effect under control the Y-chambers have been equipped with cooling pipes.

This additional cooling circuit allows to remove the beam induced HOM heating and, if necessary, to reduce it by detuning the mode frequencies with respect to the dangerous beam spectrum lines.

A new design of the central IR2 beam pipe has been implemented, the two vacuum chambers are completely separated and their cross section has an half moon profile.

In order to ensure a fast, accurate and absolute measurement of the luminosity and to fully understand the background conditions, the new interaction region has been equipped with three different luminosity monitors (Fig. 4): a Bhabha calorimeter, a Bhabha GEM tracker and a gamma Bremsstrahlung proportional counter. Different processes are used to measure luminosity:

- the Bhabha elastic scattering  $e^+e^- \rightarrow e^+e^-$ : it has a very clean signature (two back-to-back tracks); the available angle is limited due to the presence of the low- $\beta$  quadrupoles, however, in the actual polar angle range covered by our calorimeters, 18 deg  $\div$  27 deg, the expected rate ( $\sim 440$  Hz at a luminosity of  $10^{32}$  cm $^{-2}$ s $^{-1}$ ) is high enough and the backgrounds low enough to allow an online clean measurement;
- the very high rate of the radiative Bhabha process  $e^+e^- \rightarrow e^+e^-\gamma$ : it has the advantage that 95% of the signal is contained in a cone of 1.7 mrad aperture, but it suffers heavily from beam losses due to interactions with the residual gas in the beam-pipe, Touschek effect, and particles at low angles generated close to IR;
- the resonant decay  $e^+e^- \rightarrow \Phi \rightarrow K^+K^-$ : a rate of about 25 Hz at  $10^{32}$  is expected in the SIDDHARTA experiment monitor at  $\approx 90$  degrees.

The main Bhabha monitor consists of a 4-modules sandwich calorimeter, made of lead and scintillator. Four modules of calorimeters surround the final permanent quadrupole magnets, located at a distance of 32.5 cm on both sides of the IR, as shown in Fig. 4. They cover an acceptance of 18  $\div$  27 degrees in polar angle, and are segmented in azimuthal angle in five sectors, 30 degrees wide.

Two gamma monitor detectors are located 170 cm away from the IR, collecting the photons radiated by electron or positron beam. The detectors are now made of four PbW04 crystals (squared section of 30  $\times$  30 mm $^2$  and 110 mm high) assembled together along  $z$ , in order to have a 30 mm face towards the photon beam, and a total depth of 120 mm corresponding to about 13  $X_0$ . Thanks to the high rate, those detectors are mainly used as a fast feedback for the optimization of machine luminosity versus background, since the relative contribution of background is changing with the machine conditions. A total systematic uncertainty on the luminosity measurement of 11% can be estimated.

## 5 Luminosity achievements during the SIDDHARTA run

The commissioning of the upgraded machine started in November 2007. At the end of the year the ring vacuum was almost recovered, the beams were stored in the upgraded rings, all the sub-systems went quickly to regime operation.

The first collisions in the CW scheme have been obtained in February 2008, with the first experimental confirmation of the potentiality of the new configuration in terms of specific luminosity growth and reduction of the beam-beam detrimental effects.

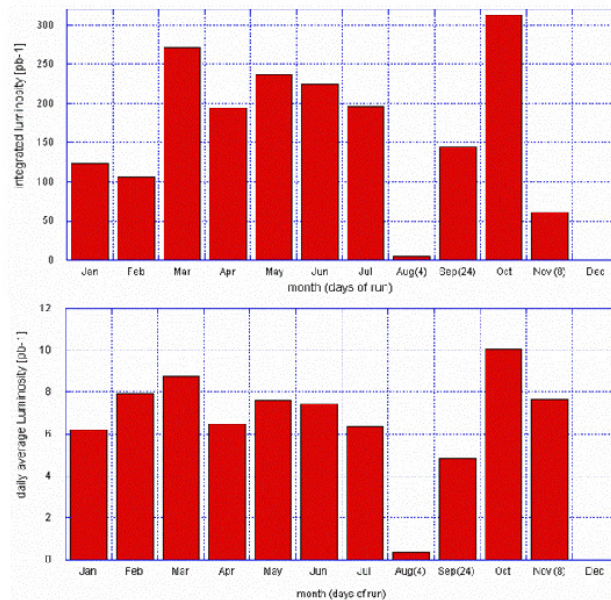


Figure 5: *SIDDHARTA Integrated Luminosity.*

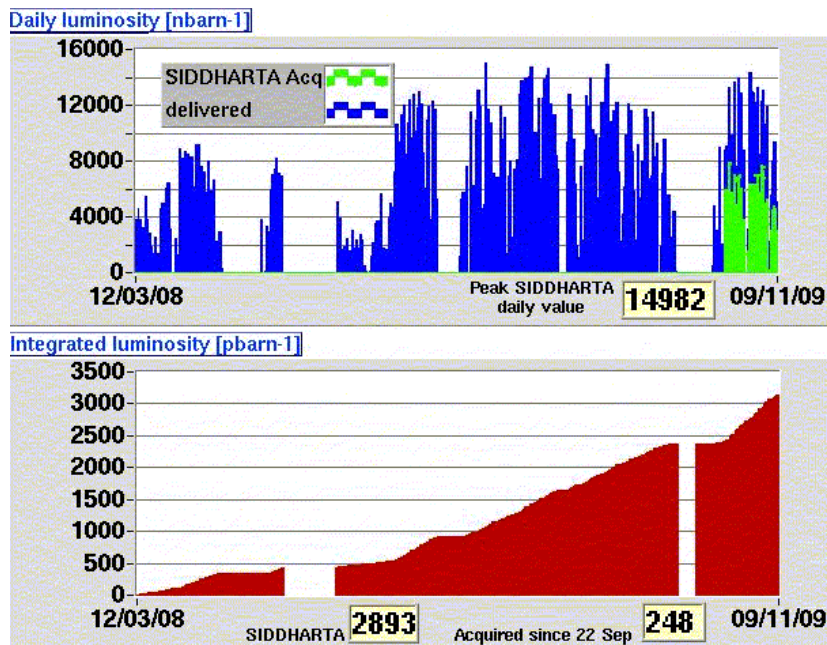


Figure 6: *SIDDHARTA Integrated Luminosity.*

Table 2: Present DAΦNE luminosity performances with the CW scheme and low- $\beta$  parameters compared to the KLOE and FUNUDA runs. SIDDHARTA data taking does not profit of the fast injection rate system, that would increase  $L_{\int \text{logged}}$ .

	SIDDHARTA March 08 ÷ Nov 09	KLOE May 04 ÷ Nov 05	FINUDA Nov 06 ÷ Jun 07
$L_{peak}$ [ $\text{cm}^{-2}\text{s}^{-1}$ ]	4.5	1.5	1.6
$L_{\int \text{day}}^{MAX}$ [ $\text{pb}^{-1}$ ]	15.24	9.8	9.4
$L_{\int \text{hour}}^{MAX}$ [ $\text{pb}^{-1}$ ]	1.033	0.44	0.5
$I_{coll}^{- MAX}$ [A]	1.4	1.4	1.5
$I_{coll}^{+ MAX}$ [A]	1	1.2	1.1
$n_{bunches}$	105	111	106
$L_{\int \text{logged}}$ [ $\text{fb}^{-1}$ ]	2.9	2.0	0.966
$\beta_x^*$ [m]	0.25	1.5	2.0
$\beta_y^*$ [m]	0.009	0.018	0.019
$\epsilon_x$ [ $10^{-6}$ m·rad]	0.25	0.34	0.34
$\xi_y$	0.0443	0.025	0.029

Fig. 5 reports the integrated luminosity for each month during 2009 (top) and the averaged daily integrated luminosity in the same year (bottom). Fig. 6 summarizes daily integrated luminosity (top) and integrated luminosity (bottom) during the SIDDHARTA data taking, which ended at the beginning of November 2009.

The integrated luminosity profited from implementing a new software procedure to switch the injection system from electrons to positrons and the other way round. The switch time has been reduced by a factor three and now it is less than one minute.

A continuous injection regime provides  $L \approx 1 \text{ pb}^{-1}$  hourly integrated luminosity, which is not compatible with the SIDDHARTA experiment data taking since the acquisition is vetoed during injection due the higher background level. However this result opens significant perspectives for the KLOE experiment, which is much less sensitive to background. The best integrated luminosity obtained in a moderate injection regime compatible with the SIDDHARTA operation with a  $\approx 50\%$  duty cycle is  $L \approx 0.79 \text{ pb}^{-1}$  hourly averaged over two hours.

DAΦNE luminosity as a function of the colliding bunches compared to past runs is reported in Fig. 7. Blue and red dots refer to the two KLOE runs, with the initial triplet low- $\beta$  IR quadrupoles and with the new IR doublet, respectively. Yellow dots refer to the FINUDA run; in green is the luminosity with the CW scheme. The gain provided by the new IR gets higher with the products of the currents and the difference with respect to collisions with the crab sextupoles off can reach 50%. During 2009 the peak luminosity has been progressively improved by tuning the collider and increasing the beam currents; the maximum value achieved is  $\approx 4.5 \cdot 10^{32} \text{ cm}^{-2}\text{s}^{-1}$  measured in several runs with good luminosity to background ratio. The present peak luminosity is close to the nominal one predicted by numerical simulations. The highest single bunch luminosity achieved is  $\approx 5 \cdot 10^{30} \text{ cm}^{-2}\text{s}^{-1}$  measured with 20 bunches in collisions instead of the usual 105. The single bunch specific luminosity, defined as the single bunch luminosity divided by the product of the single bunch currents, at low currents exceed by 4 times the best value measured during the past DAΦNE runs (present values are red and blue dots in Fig. 8). It gradually decreases with colliding beam currents, as can be seen in Fig. 8. This reduction can be only partially explained by the growing beam size blow up due to the beam-beam interaction. Another factor comes from the fact

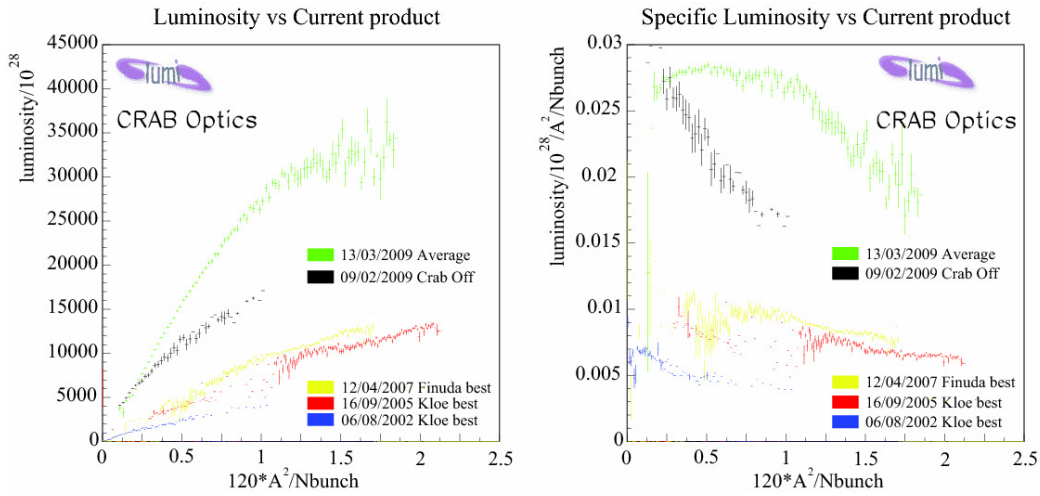


Figure 7: Comparison of the upgraded DAΦNE performance (green) with respect to the results during previous KLOE (blue, red) and FINUDA runs (yellow).

that in the large Piwinski angle regime the luminosity decreases with the bunch length, which in turn is affected by the ring coupling impedance. The impact of the Crab-Waist sextupoles can be recognized comparing runs taken with CW sextupoles on and off (Fig. 8). At low current the luminosity is the same in the two cases and higher than the one measured with the original collision scheme. As the product of the stored currents exceed 0.3 A, the luminosity with CW sextupoles off becomes lower and a corresponding transverse beam size blow up and beam lifetime reduction are observed as a consequence of the uncompensated beam-beam resonances. The convolved vertical beam size at the IP in collision has been measured by means of a beam-beam scan technique. The measured  $\Sigma_y$  of  $5.6 \mu\text{m}$  is compatible with the value obtained by using the coupling value ( $k = 0.7\%$ ) as measured at the Synchrotron Light Monitor (SLM), being the single vertical beam size at the IP1 of the order of  $4 \mu\text{m}$ .

Fig. 9 reports another proof of the crab sextupoles effectiveness, where the positrons transverse beam profile measured at the synchrotron light monitor with crab sextupoles OFF (left plot) and with crab sextupoles ON (right plot) is shown. The measurement refers to collision in a strong-weak regime (1 A electrons beam current against 0.1 A of positrons beam current): it is evident that the transverse beam size is smaller and its shape remains Gaussian during collision with the sextupoles ON.

The crab waist sextupoles proved to be of great importance for the collider luminosity increase, since much lower luminosity is achieved with crab sextupoles off, with a larger blow up and a sharp lifetime reduction is observed for single bunch currents greater than 8-10 mA. This is in agreement with beam-beam simulations taking into account the DAΦNE nonlinear lattice. The results achieved at DAΦNE have pushed several accelerator teams to study and consider the implementation of this scheme on their machines. Besides, the physics and the accelerator communities are discussing a new project of a Super B-factory with luminosity as high as  $10^{36} \text{ cm}^{-2}\text{s}^{-1}$ , i.e. by about two orders of magnitude higher with respect to that achieved at the existing B-factories at SLAC and KEK.

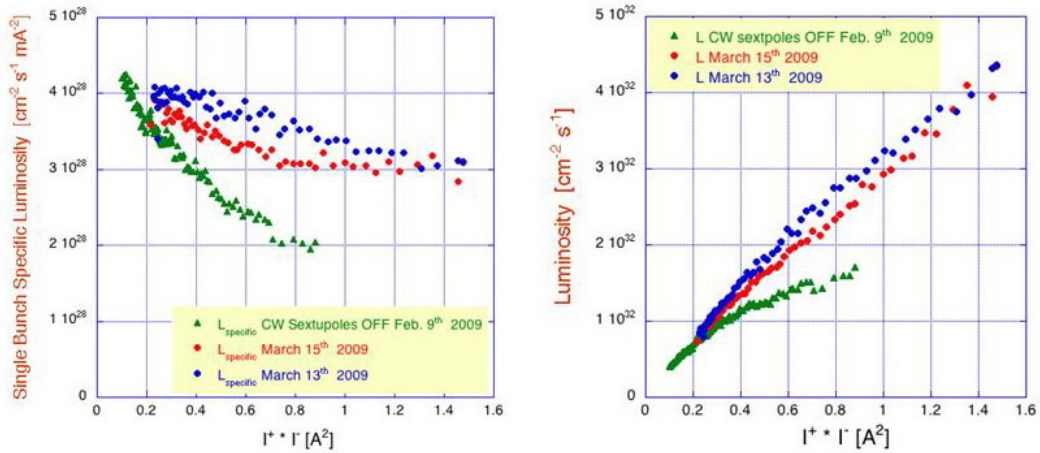


Figure 8: Single bunch specific luminosity (left) and luminosity (right) versus the product of the colliding currents for two of the best run and for the crab waist sextupoles off.

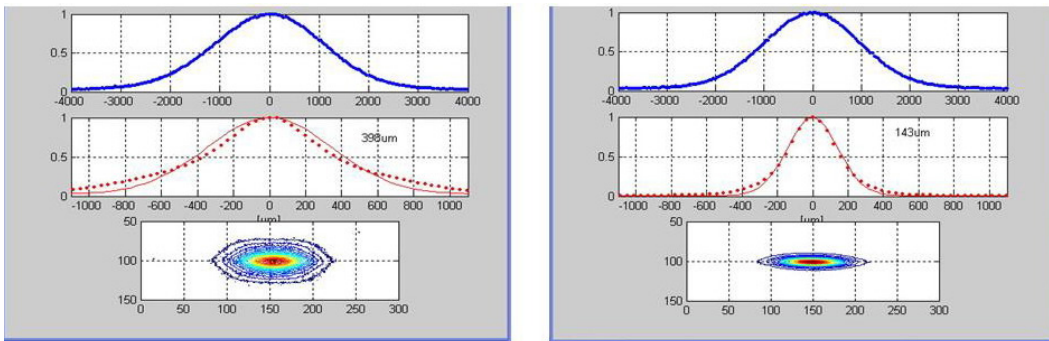


Figure 9: Transverse positron beam profile as measured at SLM with crab sextupoles off (left) and crab sextupoles on (right) for beams in collisions (103 bunches).

## 6 Hardware modifications for the KLOE run

During 2009 the new interaction region design for KLOE has been completed and several components of the new hardware have been acquired. In beginning 2010 the KLOE detector has been rolled in on IR1.

The new IR magnetic layout, sketched in Fig. 10, has been designed in order to maximize the beam stay clear letting the beam trajectory pass as much as possible through the center of the magnetic elements. The field integral introduced by the solenoidal detector is almost cancelled by means of two anti-solenoids, installed symmetrically with respect to the IP in each ring, which provide compensation also for off-energy particles. Due to the larger crossing angle, the vertical displacement of the beam in the IR is about an order of magnitude larger than in the last KLOE run. To keep the beam vertical trajectory within reasonable values, two permanent magnet dipoles (PMD) have been added just after the first permanent magnet horizontally focusing quadrupole, inside the detector magnetic field, in each one of the four IR branches (see Fig. 10). The PMDs are based on a modular design in view of a possible KLOE-2 run at a lower solenoidal field. Since

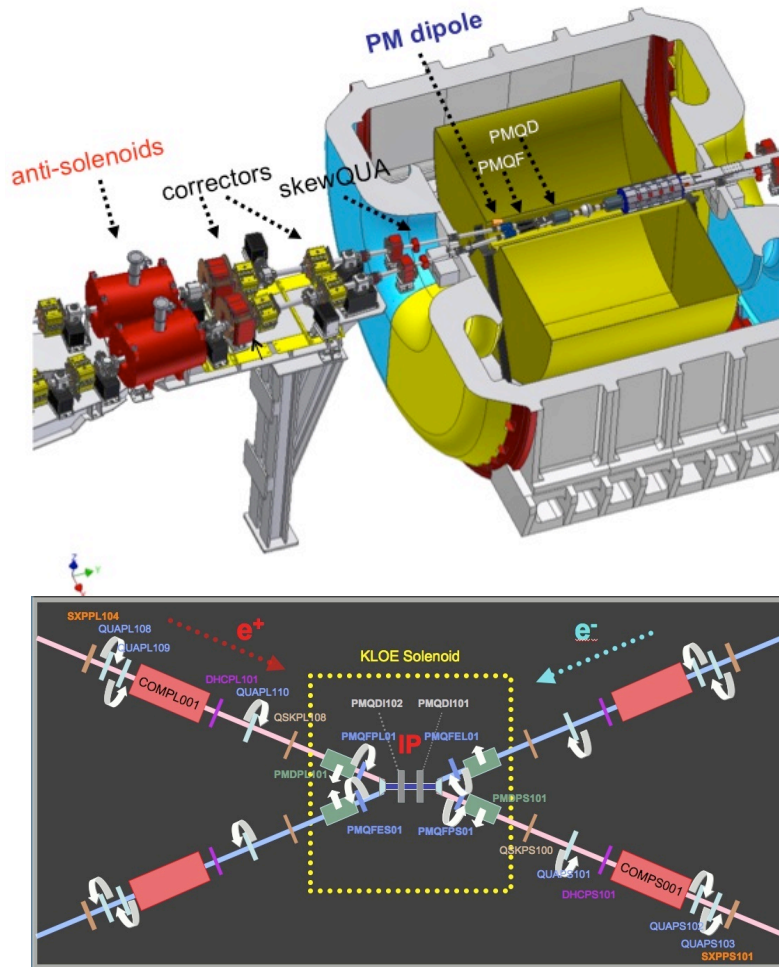


Figure 10: (Top) The KLOE-2 detector and the new DAΦNE Interaction Region 1. (Bottom) Schematic drawing of the DAΦNE Interaction Region 1 magnetic layout.

the two beams are vertically deflected in opposite directions by the KLOE solenoid, they provide a horizontal magnetic field directed towards the center of the ring in the positron ring and towards the outside in the electron one. Four new skew quadrupoles have been added on the IR, just outside the KLOE magnet, to provide fine tuning for the coupling compensation.

The shimmed plates added on the wiggler poles in 2004 have been removed and the poles displaced alternately in the horizontal direction by  $\pm 8$  mm with respect to the wiggler axis in order to keep the beam trajectory as much as possible centered with respect to the pole axes. Due to the reduction of the gap and of the overall length of the magnetic circuit, this new configuration allows to reach, at a current of 450 A, a magnetic field still higher than that achieved at 550 A in the previous configuration with shimmed plates inserted. A further improvement has been obtained by powering in series all the 7 poles of the wigglers, while before each couple of terminal poles was powered independently. This has been obtained by short-circuiting one out of the five windings in the terminal poles coils and correcting the field integral in each wiggler below 1 Gm by tuning the end pole clamps aperture. In this way eight power supplies are no more necessary and the cycling

procedure at startup is much more reliable. All the DAΦNE wigglers have been removed, modified and measured.

New stripline electrodes have been designed and inserted in the wiggler and dipole vacuum chambers of the positron ring. These electrodes, powered by DC voltages, counteract the parasitic electron cloud formation, which helps in increasing the positron beam current threshold.

The exhausted LINAC gun cathode has been replaced with a new one.

The modifications on the machine for the KLOE-2 run have been completed at the beginning of May. At the end of June the KLOE magnet has been partially warmed-up to allow the installation of the anti-solenoids cryogenic transfer lines. Since then, and up to mid November, several problems at the cryogenic plant and its ancillary systems occurred, preventing the KLOE solenoid energization. In September a magnetic setup without the KLOE magnet, but using the anti-solenoids, has been found to allow the DAΦNE beam conditioning. Up to about 1 A of positrons has been stored in the main ring with this optics, while the electron current was limited to  $\approx 0.1$  A due to ion trapping. On November 16th, the KLOE magnet was cooled and energized and beam conditioning in the nominal configuration was started with currents around 0.8 A stored at the same time in both rings, with half circumference filled in each one to avoid beam-beam interactions.

In November all the six DAΦNE bunch-by-bunch feedback systems have been upgraded to new software and hardware versions. The two (electron and positron) longitudinal feedbacks have been completely replaced with new ones, with the goal to have more compact systems with updated hardware components and new software programs compatible with the currently used operating system. These efforts are motivated also by reaching lower noise in detecting and better performance in damping the beam longitudinal oscillations. The vertical feedback systems have been equipped with 12-bit AD and DA converters in place of the 8-bit old units to reduce the quantization noise impact in the system gain. The positron ring horizontal feedback power has been doubled (1 kW now) providing about 40% increase in the kick strength. Furthermore, the horizontal feedback kicker has been replaced with a device with a double length stripline and reduced plate separation, providing larger shunt impedance at the low frequency typical of the positron horizontal unstable modes. The kicker has been also moved in a position with a higher horizontal  $\beta$  value.

## 7 Publications

1. M. Zobov *et al.*, "Test of Crab-Waist collisions at the DAΦNE Φ Factory", Phys. Rev. Lett. **104**, 174801 (2010).
2. D. Alesini, S. Guiducci, F. Marcellini, P. Raimondi, "Design, test and operation of new tapered stripline injection kickers for the  $e^+e^-$  collider DAΦNE", Phys. Rev. Special Topics – Accelerators and Beams **13**, 111002 (2010).
3. P. Valente *et al.* "Detectors for absolute luminosity measurement at DAΦNE", Nucl. Instrum. and Meth. A **617**, 453 (2010).
4. M. Boscolo *et al.* "Luminosity and background measurement at the  $e^+e^-$  DAΦNE collider upgraded with the crab waist scheme", Nucl. Instr. & Meth. A **621**, 121 (2010).
5. M. Boscolo *et al.* "Description and performances of luminosity and background detectors at the upgraded  $e^+e^-$  DAΦNE collider", Nucl. Instrum. and Meth. A **621**, 157:170 (2010).
6. S. Bettoni *et al.* "Multipoles Minimization in the DAΦNE Wigglers", Proc. of IPAC10, Kyoto, Japan (2010).
7. C. Milardi *et al.* "DAΦNE Developments for the KLOE-2 Experimental Run", Proc. of IPAC10, Kyoto, Japan (2010).
8. C. Milardi, M. Preger, P. Raimondi, G. Sensolini, F. Sgamma "High Luminosity Interaction Region Design for Collisions with Detector Solenoid", Proc. of IPAC10, Kyoto, Japan (2010).
9. D. Alesini *et al.* "Design and Test of the Clearing Electrodes for  $e^-$  cloud Mitigation in the  $e^+$  DAΦNE Ring", Proc. of IPAC10, Kyoto, Japan (2010).
10. A. Drago, P. Raimondi, M. Zobov, D. Shatilov, "Synchrotron Oscillation Damping due to Beam-beam Collisions", Proc. of IPAC10, Kyoto, Japan (2010).
11. M. Zobov, "Beam-beam Interaction in Novel, Very High Luminosity Parameter Regimes", Proc. of IPAC10, Kyoto, Japan (2010).
12. M. Zobov *et al.*, "Crab waist approach: from DAΦNE to SuperB", Proc. of RUPAC-2010, Protvino, Russia (2010).

### The DAΦNE Beam Test Facility (BTF)

The BTF Staff: B. Buonomo, L. Foggetta (T.d.), G. Mazzitelli (Resp.),  
L. Quintieri (Art.23), P. Valente (Osp.)

#### The DAΦNE Operation Staff:

G. Baldini, A. Battisti, A. Beatrice, M. Belli, B. Bolli, G. Ceccarelli,  
R. Ceccarelli, A. Cecchinelli, O. Coiro, S. De Biase,  
M. De Giorgi, G. Ermini, G. Fontana, C. Fusco, O. Giacinti, E. Grossi,  
F. Iungo, C. Marini, M. Martinelli, C. Mencarelli, E. Passarelli, V. Pavan, D. Pellegrini,  
G. Piermarini, S. Quaglia, M. Sardone, G. Sensolini, A. Sorgi,  
M. Sperati, A. Spreccacenero, R. Tonus, T. Tranquilli, M. Troiani, R. Zarlenga

#### The LNF Technical Staff:

P. Ciuffetti, V. Lollo, M.R. Ferrazza, R. U. Frascaco, A. Mazzenga, F. Galletti

#### BTF Committee

P. Di Nezza, INFN-LNF; F. Gatti, INFN Genova, C. Matteuzzi (Chairperson), INFN Milano;  
G. Mazzitelli (Resp.), INFN-LNF; A. Passeri, INFN, Roma III; P. Valente, INFN Roma I

## 1 Description of the DAΦNE BTF 2010 Activities

During 2010 the DAΦNE Beam Test Facility provided effectively electron, positron and neutron beams to about 22 different experiments of important scientific collaborations, mainly from Italian Institutes but also coming from the rest of Europe (France, Germany, etc), covering a total of 230 days<sup>1</sup>. It is important to stress that during September and October 2010, the BTF stopped to work, as required from the LNF director in order to make fully available all the technical operators for the DAΦNE engineering run.

The majority of the hosted experiment during 2010 requested to run with multiplicity from 1 to  $1E+3$  particles per bunch, while only very few of them asked for high multiplicity run (up to  $1E+7$  particles per bunch).

As important task successfully accomplished in 2010, the photo-neutron source has been mounted and made operative at BTF. Details about the feasibility study and design of the photo-neutron source have been reported in chapter §(n@BTF). First measurement campaign ended in May 2010: the experimental data are in optimum agreement with Monte Carlo predictions, showing the real possibility to make available neutrons for experiments in BTF.

A continuous activity of upgrading and maintenance of diagnostic and instrumentation systems has been also accurately performed, in order to offer the best support to the BTF users.

## 2 2010 User Experiences

The complete list of collaborations that were hosted at the BTF during 2010, to perform measurement for their experimental activities, is the following one: RICCE, n@BTF, c-SPEED, PLAS-MAG, VIPIX, NA62, Siddharta/Amadeus, TPC-GEM, TPG, C-SHAPE, QCALT, UA9, SuperB-LYSO, K2HET, LENA, CU, PANDA, NRD, CMS-UP, BES-III, MAMBO, TPS. All these users were able to take data according the scheduled time and to profitably use them for their scientific tasks. In what follows some of the hosted experimental activities will be briefly described, putting

in evidence the different operative conditions the BTF had to fulfill in order to satisfy the user requirements

## 2.1 RICCE

This is an experiment proposed by a group of researchers of the Institute of Nuclear Physics in Lyon (CNRS/IN2P3). The main goal of their research is the observation of an internal clock in an electron channeling (“Zitterbewegung” theory).

The starting idea refers to the beginning of Quantum Mechanics. A particle at rest has a self energy  $E_0 = m_0c^2$ , which could also be equal to  $h\nu_0$ , if it has a self internal frequency  $\nu = m_0c^2/h$ , in accordance with the relation  $E = h\nu$  valid for photons. This internal frequency must be divided in the laboratory frame by the factor  $\gamma$  due to relativistic delay clock. This could lead to some resonance effects if a beam of charge particles (electrons for available energies) is directed along the major crystallographic axis of a crystal and if the beam energy is tuned so that the frequency of the successive collisions of the projectile with the target atoms matches this internal frequency. The most interesting feature with crystal is that this effect can be seen only inside a small momentum window ( $\simeq 1\%$ ) but smoothed and therefore not visible outside it, as it is expected from several phenomenological models. This property makes it more easily distinguishable from other more conventional effects if any.

The experiment in BTF used 80 and 160 MeV/c electrons, since some phenomenological models and the Zitterbewegung theory predict momentum resonance for these values of energy. The beam made available in BTF for this experiment had the following characteristics:

- A well collimated electron beam:  $\delta p/p \simeq 10^{-3}$
- Momentum adjustable by small steps:  $\delta p/p \simeq 10^{-3}$
- Intensity of  $10^4 - 10^5$  particles/s- depending on the duty cycle.

The set-up for the measurements in BTF was made of:

- a set of collimators: diameter of 1 mm; about 1 m apart one from the other
- an analyzing magnet to provide the necessary momentum resolution
- a second set of collimators: diameter of 1 mm; about 1 m apart one from the other
- a thin silicon crystal mounted on a goniometer, located after the last collimator
- a 2D location detector at 1 m downstream respect to the crystal, just after the vacuum window

Everything has been kept under vacuum, except the detector.

The Channeling of 160 MeV electrons in a thin germanium crystal has been successfully achieved at the Beam Test Facility at the end of the run. A beam of about  $10^2$  electrons per second with a selected emittance and a narrow momentum spread was sent onto a 0.9 m thick Ge crystal aligned along the  $\langle 110 \rangle$  axial direction. By means of additional collimation slits, in complement to the existing ones, the beam angular divergence was set at 0.3 mrad (full envelope) in the horizontal and vertical directions, and the beam spot size on the crystal was 1.5 mm FWHM vertically and 2 mm horizontally. The larger horizontal size was due to the momentum spread (the target is located behind a dipole magnet). Spatial distributions of transmitted electrons were measured by means of two stripped silicon detectors, located four meters downstream the target, enabling the simultaneous measurement of the horizontal and vertical distributions. The evidence

of the crystal channelling effect was proved comparing the vertical spatial beam distributions with a random oriented crystal target.

The variations observed when scanning the incident beam energy around 160 MeV by  $10^{-3}$  dp/p steps were dominated by the LINAC beam instabilities. Beside necessary improvements of the beam quality toward the observation of the internal electron clock, these first results already open the way to experiments dedicated to many application of electron and positron channeling, such as channeling radiation and other coherent effects.

## 2.2 UA9

The UA9 experiment is funded by the CNS1 of INFN. It has as main goal to show the feasibility of hadron collimation by crystal channeling. The instrumentation used for the measurements in BTF consists mainly of Medipix and TPC-GEM detectors. The Medipix detectors have been used on SPS at CERN to monitoring the halo of the channeled beam. The test in BTF has been carried out to have a calibration of the Medipix charge measurement. The pulsed beam delivered in BTF has been very useful since it allowed to supply in few ns a selected number of particles distributed on a spot of size equal to that of a chip. Furthermore in BTF has been possible to test the Medipix by using an external trigger and to check effectively the time coincidence between two chips. In addition, TPG-GEM detectors have been used in order to study ion channeling at CERN. As a consequence, testing simultaneously the Medipix and TPC-GEM integrated signals at the BTF has been an important step to guarantee the success of the next test beam at CERN.

## 2.3 TPC-GEM

GEM chambers are developed and studied for monitoring the beam position and beam width with very high spacial resolution: a telescope for beam tracking has been built on the base of GEM technology at LNF and tested in BTF at the beginning of May 2010. The designed spacial resolution of this telescope is lower than  $100\mu\text{m}$ . In figure 2, the measured X-Y beam profile has been reported: the Y resolution is better than  $50\mu\text{m}$  (limited by drift time), instead the X resolution is about 1 mm (limited by pad pitch).

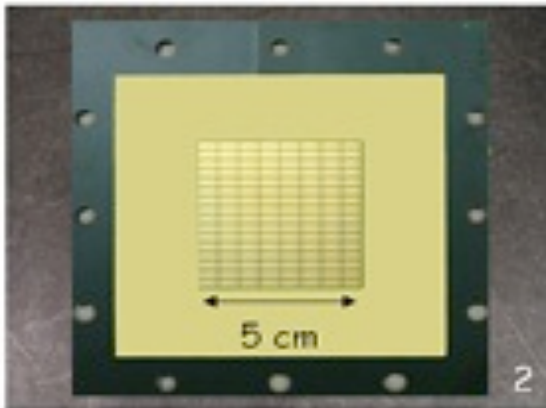


Figure 1: *TPC-gem detector.*

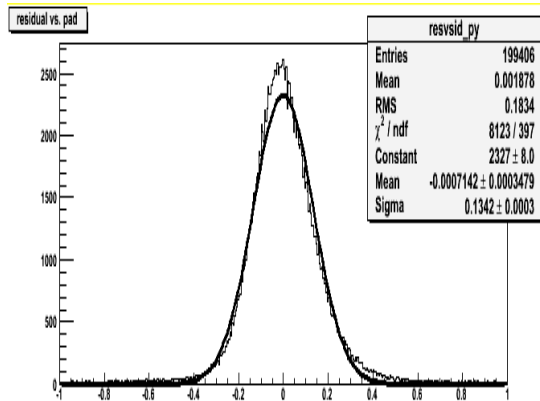


Figure 2: *Spacial resolution of tested TPG-gem.*

## 2.4 SuperB-LYSO

LYSO calorimeter has been prepared as a SuperB prototype to provide a map of beam energy in various beam operations parameter. The main goal of the LYSO tests in BTF was to study the dependence of the detector resolution on the beam operating parameters. In figure 3 the prototype of the calorimeter tested in BTF at the end of June 2010 has been shown: it consisted of 6 crystals, inserted in the mechanical support, two different readouts (PiN and APD) and a complete FE electronic system.

The results of the measurements performed in BTF are summarized in plot 4. This plot shows the measured energy resolution of the tested detector: the measured resolution is, respectively, of 6.620.07% for 1 electron at 297 MeV (4.640.17% for 2 electrons), while it has to be stressed that the expected resolution at 1 GeV for the complete 5x5 crystal matrix should be 2%.

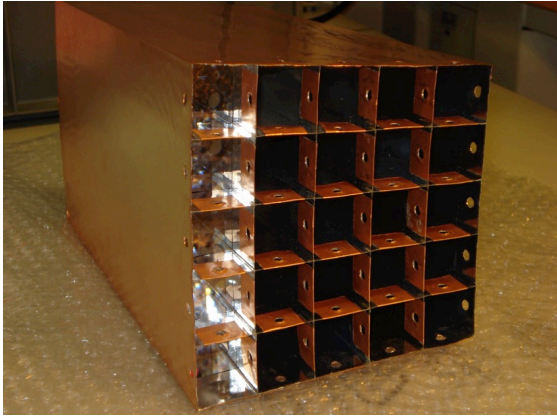


Figure 3: *LYSO calorimeter prototype.*

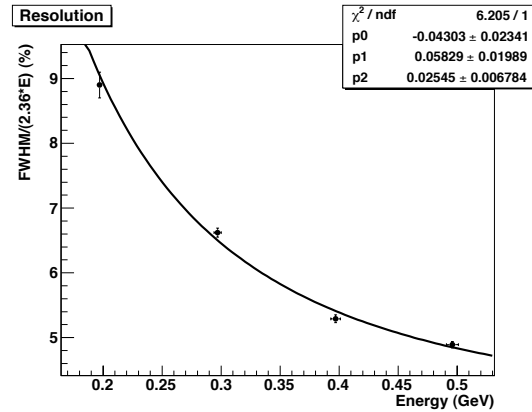


Figure 4: *Measured Resolution of the tested prototype in BTF.*

## 3 The n@BTF experiment

One of the most important scientific activities developed at the BTF during 2010 has been the feasibility test of the photo-neutron source. Neutrons have been produced in BTF, by sending high energy electrons against an optimized high Z target <sup>2)</sup>, <sup>3)</sup>, <sup>4)</sup>. Neutron fluences have been measured along the extraction lines, showing an excellent agreement with the Monte Carlo previsions (obtained by FLUKA and MCNPX code, respectively).

In figure 5, the experimental set-up of the final feasibility test is shown. The maximum rate of neutron that, at the present, could be obtained along one of the 2 extraction lines, at 1.5 m from the center of the target, is  $4 \cdot 10^5 [\text{n}/\text{cm}^2/\text{s}]$ <sup>1</sup>. The neutron spectrum has been measured over more than 9 decades in the energy range (from tenths of eV up to several hundreds MeV), showing that the majority of neutrons (more than 80%) are produced around 1 MeV (this means that we have a fast neutron source).

A more accurate description of the n@BTF experiment can be found in the dedicated chapter §(n@BTF).

<sup>1</sup>This value corresponds to a beam power deposited on the target of about 40 W



Figure 5: *Experimental set-up of n@BTF experiment.*

#### 4 Conclusion and future plan

One of the most important results of the 2010 scientific activities in BTF has been the realization of a neutron source by photo-production.

The feasibility test was successfully carried out in May 2010, demonstrating definitively the ability of BTF to provide neutron beam with a well reconstructed spectrum. This source will be made available to the whole scientific community for its scopes. This means that, even if the n@BTF project can be considered successfully concluded, the BTF staff, together with the LNF's FISMEL service, will continue in characterizing more in details the neutron and photon field around the target and will supply with the diagnostics and instrumentations, necessary to properly arrange a complete neutron facility.

In this frame, the BTF staff is working to improve the efficiency of the facility in order to be able to host different user communities: from high-energy physics to accelerator physics, from nuclear to solid state physics.

A continuous work of integration and upgrade of the diagnostic system is also carried out, in order to obtain an ever better characterization of the beam quality (spot size, position, multiplicity) delivered in BTF.

#### 5 Conference Talks

1. L. Quintieri *et al.*, "N@BTF: Feasibility study of a photo neutron source at the DAΦNE Beam Test Facility", Invited Seminar 25 Febbraio 2010, INFN Trieste, Area di Ricerca di Padriciano.
2. G. Mazzitelli *et al.*, "Neutron Source at the DAΦNE Beam Test Facility (BTF)", Poster Session, IPAC, Kyoto, 24 May 2010.

3. G. Mazzitelli *et al.*, “New Neutron Source at the Beam Test Facility (BTF) of Frascati: design and first experimental results”, Invited Seminar at Channeling 2010, Ferrara 3-8 October 2010.
4. L. Quintieri *et al.*, “Photo-Neutron Source by High Energy Electrons on Target: Comparison Between Monte Carlo Predictions and Experimental Measurements”, Oral Presentation (N31-6) at NSS-IEEE, Scientific Simulation and Computation: Simulation R&D, Knoxville, 3 November 2010.

## 6 Publications

- G. Mazzitelli, *et al.*, Neutron Source at the Da?ne Beam Test facility, Proceedings of IPAC-2010 (MOPEB063), 23-28 Maggio 2010, Kyoto, Japan.
- L. Quintieri *et al.*, “ Photo-Neutron Source by High Energy Electrons on Target: Comparison Between Monte Carlo Predictions and Experimental Measurements”, Submitted article for IEEE-NSS 2010 proceedings, publication in progress.

## References

1. <http://www.lnf.infn.it/acceleratori/btf/php/schedule.php?year=2010&acc=1>
2. L. Quintieri *et al.*, “Feasibility Study of a neutron source at the DAΦNE Beam Test Facility, using Monte Carlo codes”. 2009 IEEE Nuclear Science Symposium Conference Record (N33-6), October 25-31, Orlando, USA.
3. G. Mazzitelli, *et al.*, “Neutron Source at the DAΦNE Beam Test facility”, Proceedings of IPAC-2010 (MOPEB063), 23-28 Maggio 2010, Kyoto, Japan.
4. L. Quintieri, *et al.*, “Photo-Neutron Source by High Energy Electrons on Target: Comparison between Monte Carlo Predictions and Experimental Measurements”, 2010 IEEE Nuclear Science Symposium Conference Record (N31-6), October 30 to November 6, 2010, Knoxville, Tennessee.

## DAΦNE-Light Laboratory and Activity

A. Balerna (Resp.), P. Calvani (Ass.), M. Cestelli Guidi (Art. 23), R. Cimino,  
M. Commisso (Ass. Ric.), A. De Sio (Osp.), L. Gambicorti (Osp.), A. Grilli (Tecn.),  
R. Flammini (Ass.), D. R. Grosso (Bors.), R. Larciprete (Ass.), C. Mirri (Osp.),  
A. Nucara (Ass.), V. Nistor (Osp.), E. Pace (Ass.), M. Pietropaoli (Tecn.), A. Raco (Tecn.),  
V. Sciarra (Tecn.), V. Tullio (Tecn.), G. Viviani (Tecn.)

### 1 Summary

The experimental activity on the synchrotron beamlines was performed, in 2010, only at the SINBAD-IR beamline with conventional sources, due to the DAΦNE upgrade operation that prevented the use of synchrotron radiation. The experimental teams that got access to the IR beamline were from Italian Universities and Research Institutions, and from EU countries within the INFN-FAI framework.

During this year the new EU FP7-I3 initiative E.L.I.S.A. (European Light Source Activities) for research cooperation involving the world largest network of synchrotron and FEL facilities in Europe was not attended due to the DAΦNE shutdown. The program will start in 2011 in parallel with the KLOE runs and will give access to EU users, in order to complete the approved experiments within the end of the contract (August 2011).

The experimental activities, performed in 2010, were also dedicated to the organization and improvement of the existing soft X-ray beamline, to the upgrade of the IR beamline with new instrumentations and the design of a clean-room laboratory for biological sample preparation, to the reorganization of the UV beamline and also the construction of the two new XUV beamlines that going to be commissioned in 2011.

### 2 Activity

#### 2.1 SINBAD - IR beamline

SINBAD is the Synchrotron Infrared Beamline At DAΦNE, facility that gives access to users for IR spectroscopy experiments since 2002. The beamline is equipped with two experimental stations which can be used both with synchrotron radiation and conventional sources. Biomedical, chemical and material science research activities can be performed in different conditions of temperature and pressure. High resolution (diffraction limited at  $\sim 5 \mu\text{m}$ ) IR imaging of biological tissues and cells can be taken with an Infrared microscope equipped with a 64 x 64-element focal plane array (FPA) detector.

The experimental activity on the SINBAD IR beamline mainly concerns the study of biological samples at micrometric spatial resolution, owing to the imaging capabilities of the IR microscope coupled to the synchrotron source. This activity has been carried out in the past by many experimental teams, within the framework of EU projects and INFN-FAI collaborations.

Concerning the upgrade of the IR beamline, a clean-room laboratory to support the sample preparation and conservation has been designed in 2010 and dedicated instruments like a cryo-microtome to allow thin tissue preparation (down to 1 micron sections), a  $-85^\circ\text{C}$  freezer for cryo-conservation, and other instruments (thermal bath, centrifuge, inverted microscope, laminar flow hood) have been purchased for this purpose. The clean-room will be installed in 2011 and will be available for users right after. The imaging capabilities of the beamline will be improved by the construction of a system to image live biological cells. This system development, which has been co-funded by the V Commission of INFN, consists of an Attenuated Total Reflection (ATR) microscope objective modified to allow cell growth and immersion in their culture medium. The

system is completed by a dedicated IR spectrometer Vertex70v with unprecedented performance for vacuum microspectroscopy, and a dedicated optical coupling with the synchrotron beamline. All the system will be placed on an optical table to be isolated from vibrations. The complete setup will be installed at the end of 2011 and will be operational in 2012 for users to perform the first live cell experiments.

The 2010 the experimental activity on the beamline was dedicated to experiments with conventional IR sources due to the DAΦNE shut-down. Experimental groups from Italian and European Universities and Research Institutions carried out their research activity at the SINBAD beamline. We had a total of 8 experimental groups coming for several weeks during the whole year. The main results were obtained in the field of FTIR (Fourier Transform Infrared Spectroscopy) imaging and its applications to life science and earth science, archeometry and solid state physics. Some of the experimental results achieved are here presented:

1. *Chemical analysis of brain tumor vasculature using inorganic nanoparticles as contrast agents - University of Bordeaux*

The very first results achieved using the conventional IR source show that FTIR imaging can be used as a functional histopathology tool potentially interesting for further clinical applications (Fig. 1). In 2010 FTIR imaging has been performed on glioma (because malignant gliomas are the most common primary tumors of brain and spinal cord) vasculature using inorganic nanoparticles (NP) as contrast agents.

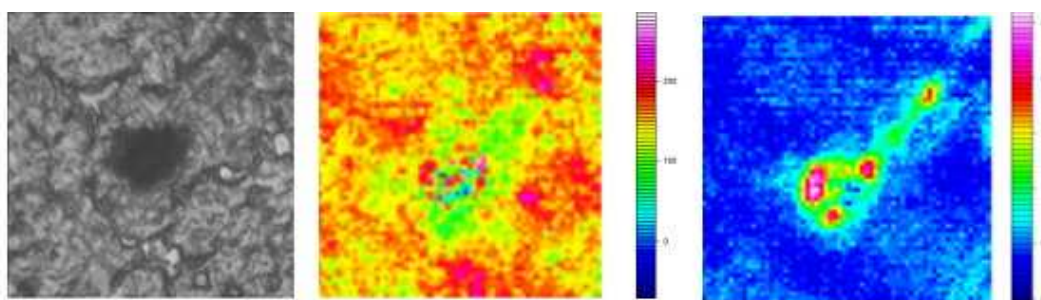


Figure 1: *FTIR imaging of solid tumor perfused with PBS (Phosphate Buffered Solution) and Au-NP. Left: mice brain tumor tissue section (20  $\mu\text{m}$ ) with a large coopted blood vessel. Center: 2D-FTIR image of blood vessel (4000-900  $\text{cm}^{-1}$  spectral interval). Right: 2D-FTIR image with highest absorption contrast for Au-NP vs. tissue using the 1150-950  $\text{cm}^{-1}$  spectral interval.*

2. *Influence of hydrostatic pressure on the spin transition in the spin crossover system - University of Zaragoza and University Sapienza Rome*

In the present experiment the influence of hydrostatic pressure (up to 1.2 GPa) on the spin transition in the spin crossover system  $[\text{Fe}(\text{Butrz})_3](\text{BF}_4)_2 \cdot 2\text{H}_2\text{O}$  has been investigated. The reversible change between low-spin (LS) and high-spin (HS) states driven by a variation of temperature and/or pressure is one of the most attractive examples of molecular bistability. Indeed, in the area of functional materials research such classes of compounds are promising particularly for applications in memory and display devices as well as molecular switches. Pressure effect studies are very helpful in elucidating the mechanism of cooperative dynamic electronic structure phenomena accompanied by significant volume changes. Application of hydrostatic pressure serves as a tool for modifying the ligand field strength in a controlled manner (Fig. 2).

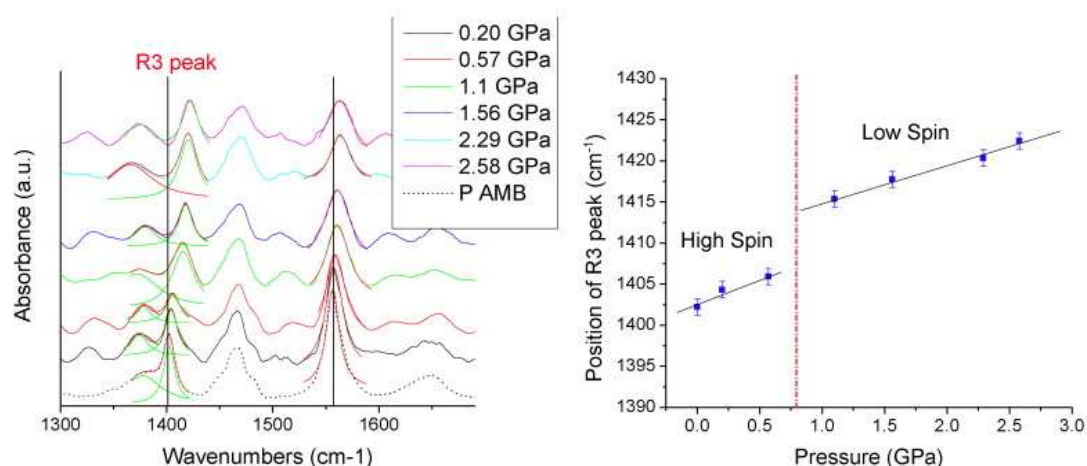


Figure 2: The spin crossover HS to LS transition occurring at 0.7 GPa and its pressure behavior in the FT-IR transmission spectra.

3. FTIR imaging as a tool for studying cell-asbestos fibers interaction - University of Bordeaux

A series of measurements were performed for determining the effect of asbestos fibers on human lung cells in culture. Again, this study has proved that FTIR imaging is able to determine both organic and inorganic contents of complex biosamples, thus now enlarging the usual applications of the technique to cytopathology studies (Fig. 3).

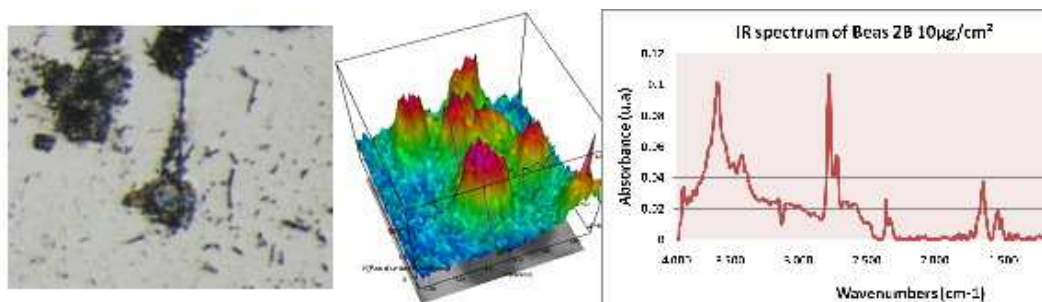


Figure 3: FTIR imaging of human lung cells (36x magnification, 1x1 μm resolution, 256 scans, 8 cm⁻¹ spectral resolution).

4. Tunability of structural, electronic and optical properties of eumelanin films by electro spray deposition have been investigated by FTIR spectroscopy - University of Camerino

Electrospray deposition (ESD) technique was used to grow thin synthetic melanin films with good morphological properties, proved to be an important additional tool to tailor the bio-material for possible implementation of functional devices, but also to disclose intrinsic still to assess properties of the same material due to a better local supramolecular organization. To this aim infrared spectroscopy plays a key role to identify promptly the modifications by

spreading light on refinements in the structure which can be obtained when moving from the solution to a realistic high quality thin film.

5. *FTIR characterization of zoning and speciation of H and C in a variety of geological materials - University Roma Tre*

FTIR spectroscopy was used to characterize the zoning and speciation of H and C in a variety of geological materials, including microporous minerals, nominally anhydrous volcanic minerals (NAMs), and crystal inclusions (Fig. 4). These investigations show that use of the modern techniques of FTIR imaging enables detection of the zoning of volatile species across the studied samples, and possible configuration changes of structurally-bound carbon molecular species (e.g.,  $\text{CO}_2$  vs  $\text{CO}_3$ ) during crystal growth. Such features, which are not accessible with other micro-analytical techniques, may provide information about the physicochemical properties which act as constraints in the genesis of the samples, and important information about the evolution of the geological system. Tests performed with focal-plane-array detectors (FPA) show that resolution close to the diffraction limit can be achieved if the amounts of the target molecules in the sample are substantially different. The possibility of using FTIR imaging for investigations under non-ambient conditions was also pointed out.

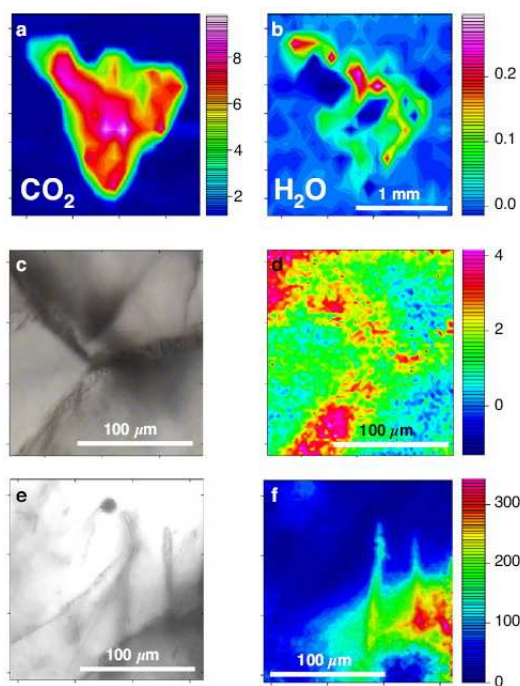


Figure 4: *FTIR mapping of  $\text{CO}_2$  (a) and  $\text{H}_2\text{O}$  (b) on a (010) oriented crystal section of cordierite HO33, thickness  $140\ \mu\text{m}$ . (c) to (f) FTIR FPA images of the  $\text{H}_2\text{O}$  distribution in the same section as shown in (a); the optical image is on the left side, the corresponding FTIR image is on the right side. The image in (d) shows how the water content of this sample is associated with fractures and is probably related to alteration products, whereas the image in (f) shows that water is also associated with sillimanite needles included in the host cordierite matrix.*

## 2.2 DXR1 - Soft X-ray Beamline

The DAΦNE soft X-ray beamline, DXR-1, is mainly dedicated to soft X-ray absorption spectroscopy. The X-ray source of this beamline is one of the 6-poles equivalent planar wiggler devices installed on the DAΦNE electron ring (0.51 GeV) for the vertical beam compaction. The 6 wiggler poles and the high storage ring current (higher than 1 Ampere) give a useful X-ray flux for measurements well beyond ten times the critical energy. The useful soft X-ray energy range is 900 eV - 3000eV where the lower limit is given by the Beryl crystals used in the double-crystal monochromator and the higher limit is given by the wiggler working conditions.

During 2010 some tests were performed on the double wire beam monitor and a small change including an horizontal slit was realized and mounted. A new system to control, set and include in the experimental files the values of the pressures of the ionization chambers has been installed and tested and only small changes in the acquisition program were performed. Some of the experimental results published in 2010 are here summarized:

### 1. *Crystal-quasicrystal transition in the AlCuFe system: analysis of the local atomic structure*

Quasicrystals (quasiperiodic crystals) are attracting intense interest due to their unique properties being non-typical for their crystalline and amorphous phase analogues. Changes of the local structure around Al, Cu, Fe atoms from the quasicrystalline to the crystalline phase transition have been studied. Investigation of the local atomic structure of the  $\text{Al}_{65}\text{Cu}_{22}\text{Fe}_{13}$  quasicrystal and its crystal analogue has been performed on the basis of the (XANES) X-ray absorption near edge structure analysis. Analysis of experimental XANES spectra permits to determine the 3D local atomic structure of the given materials. Theoretical analysis of the experimental data has been carried out on the basis of a self-consistent, real space multiple scattering method (FEFF8.4 code) and a finite difference method (FDMNES2009 code) (Fig. 5).

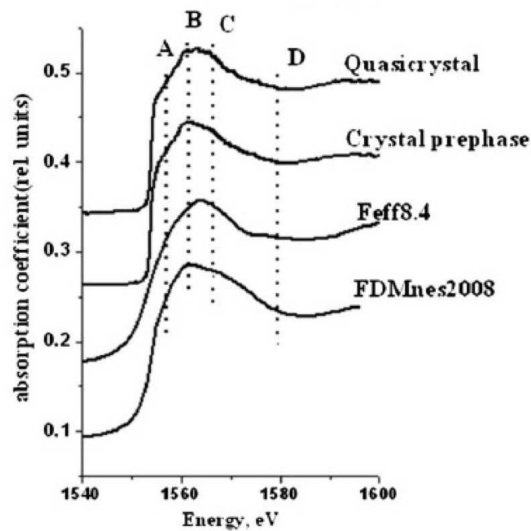


Figure 5: Comparison of the experimental Al K-XANES of the quasicrystal and the crystal prephase with the theoretical one calculated on the basis of the FMS method (FEFF8.4 code) and the FDM theory (FDMNES2009 code).

2. *Surfactant-assisted synthesis of  $Cd_{1-x}Co_xS$  nanocluster alloys and their structural, optical and magnetic properties.*

The study concerns the synthesis of Co-doped CdS nanoclusters ( $Cd_{1-x}Co_xS$ ) for different doping concentrations ( $x = 0.10, 0.20$  and  $0.30$ ) and characterization of their structural, optical, and magnetic properties. The structural properties studied by X-ray diffraction revealed hexagonal-greenockite structure and a decrease of the lattice parameters ( $a$  and  $c$ ) with doping, showing incorporation of Co in the lattice. The morphology of the nanoclusters was studied by scanning electron microscopy. The optical absorption studies, using diffused reflectance spectroscopy, revealed that Co doping modifies the absorption band edge. Ferromagnetic phase was observed in the magnetization measurements at room-temperature due to high carrier concentration. X-ray absorption near edge fine structure measurements at the sulfur (S) K-edge performed at the DAΦNE soft X-ray beamline of the Co-doped samples revealed that the valence remains divalent and that there are some changes with Co doping in the spectral intensity.

Results achieved by W. Kwiatek and co-workers (Institute of Nuclear Physics PAN - Krakow, Poland) on *First approach to studies of sulphur electron DOS in prostate cancer cell lines and tissues studied by XANES* were presented at the ISSRNS (International School and Symposium on Synchrotron Radiation in Natural Sciences) 2010 conference held in Szklarska Poreba (Poland) in June.

### 2.3 DXR2 -UV branch Line

The synchrotron radiation (SR) photon beam from a wiggler installed on the DAFNE storage ring is split by a grazing incidence Au-coated mirror ( $\theta_i = 40$  mrad, cut-off energy about 800 eV), in order to provide the X-ray and UV beamlines. The reflected UV radiation travels through the UV beamline and ends in a 38 mm diameter sapphire window. The experimental apparatus installed at the exit window of the branch line is partially refurbishing and partially under construction; commissioning would be completed at the beginning of 2011 after restarting the DAΦNE storage ring.

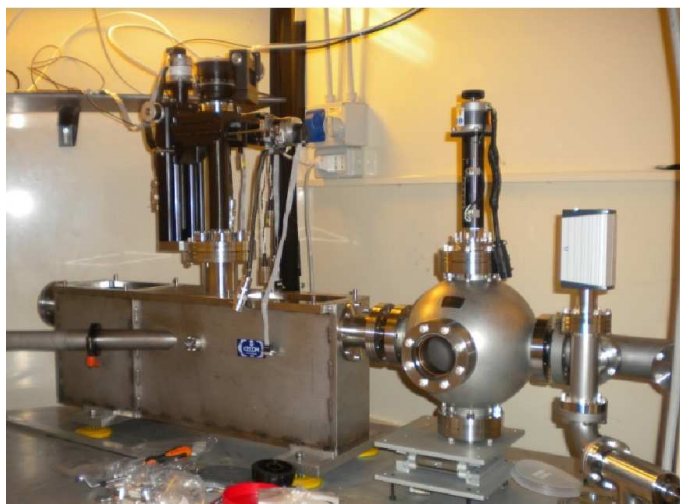


Figure 6: *DXR2 beamline optical vacuum chambers.*

As the Synchrotron Radiation (SR) beam was not available for the most part of time for upgrading the DAΦNE storage ring, the activity on the DXR-2 facility during 2010 was strongly focussed on completing the instrumentation setup of the 3 light channels in order to be ready to get the first light as soon as the SR beam will be available. In addition, fully independent radiation paths have been developed based on high-power lamp sources. This is in order to have radiation sources always available for users and experiments and to cover 100% experimental time. Firstly, the optical layout of the DXR-2 facility has been fixed after some variations in the optical scheme due to improving the optical matching of the monochromator apertures with the exiting SR.

The final optical layout provides a monochromatic visible channel (200-650 nm) and UV channel (120-400) nm both placed in the clean room area and fed by the SR along with a wide band channel (180-650 nm). In parallel, monochromatic VIS and UV channels are also available fed by lamp sources (500 W D<sub>2</sub> lamp, 1000 W Hg-Xe lamp and 2000 W solar lamp). The SR and lamp-fed UV channels can be operated in parallel.

During 2010, the optical elements have been designed, produced and characterised; presently, they are mounted and aligned inside the optical vacuum chamber (OVC) that is the second chamber after the beamline exit (Fig. 6), and sends collimated radiation to the main clean room by means of two mirrors: the first is a spherical concave mirror, while the second is a spherical convex mirror. The OVC has been mounted after a pre-camera mounting a moveable folding mirror that will be used for the polarimetric channel that will be arranged in parallel to the main beam once the current facility will be completed.

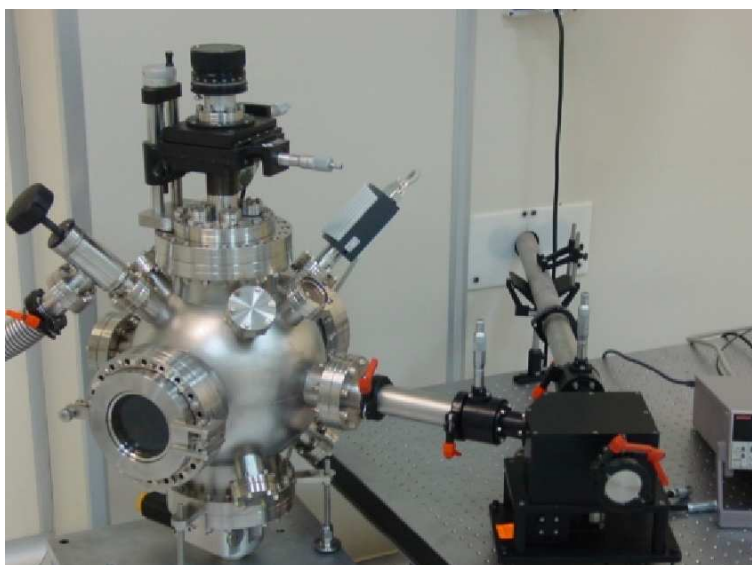


Figure 7: *Vacuum UV monochromator and sample chamber.*

Large efforts have been spent to setup lamp-based radiation channel that finally will be definitely separated from the SR beams, just sharing the monochromator used for the visible channel. On the other hand, the UV D<sub>2</sub> lamp will be coupled to a dedicated monochromator (Fig. 7) that is different from the one used on the SR UV channel. The lamp-based channel have been set up and aligned in order to optimise and calibrate the exiting radiation. Presently, these two lamp-based channels are already available for the final assembly before opening them to users for experiments.

## 2.4 New XUV beamlines

In 2010, the new XUV laboratory has continued its construction, based both on the detailed plans approved by the SRL Committee and on available resources. Aim of this laboratory is to host two bending magnet beamlines covering the photon energy range from 30 eV to 1000 eV. One beamline will cover the low energy part of this interval (30-200 eV) and is called LEB (Low Energy Beamline), the other will cover the energy range from 60 eV to 1000 eV and is called HEB (High Energy Beamline). The laboratory as it stands at the end of the year is shown in fig. 8.



Figure 8: *Overview of the XUV DAΦNE-L laboratory. On the right side: the LEB beamline and (in front) its experimental chamber. On the left side: the HEB beamline under construction with the recently mounted PGM monochromator, and the experimental set-up.*

The LEB beamline is all in UHV, all safety protocol and control systems are ready and tested and is ready to start commissioning with light as soon as it becomes available. A newly designed photo diagnostic chamber is ready to observe the light by a fluorescence screen, measure light as passing through a metallic mesh and measure photon fluxes with a photodiode. After these tests a *state of the art* spectroscopic chamber, is ready to be connected to the beamline in order to perform angle resolved photoemission experiments, also at low temperature.

All the optical elements and UHV vacuum chambers needed for the construction of the HEB beamline have been delivered and are about to be mounted. The PGM (plane grating) monochromator has been mounted, all the optical elements (mirrors and gratings) have been inserted and carefully aligned, and we are ready to operate and commission it with SR light coming from the DAΦNE bending magnet as soon as it becomes available. A picture of this PGM monochromator is shown in fig. 9.

Also for this beamline we designed and assembled an experimental set-up to be able to perform SR photoemission and absorption spectroscopy in UHV condition. The setup is ready to be installed on line and is under detailed tests with commercial X-ray and VUV sources. Such tests are also used to perform experiments on SEY (Secondary Electron Yield) reduction versus electron bombardment, surface conditions and carbon deposition, which are the objectives of IMCA-NTA



Figure 9: *The HEB beamline under construction with the recently mounted PGM monochromator on the left side.*

project (see this annual report) and are done in collaboration with R. Larciprete (ISC-CNR) and R. Flammini (IMIP-CNR) associated to the project.

#### References

1. A. Balerna *et al.*, “DAΦNE-Light INFN-LNF Synchrotron Radiation Facility”, AIP **1234**, 285 (2010) doi:10.1063/1.3463191
2. G. Della Ventura *et al.*, “Application of micro-FTIR imaging in the Earth sciences”, Anal Bioanal Chem **397**, 2039 (2010).
3. C. Petibois, M. Cestelli-Guidi, M. Piccinini, M. Moenner , A. Marcelli, “Synchrotron radiation FTIR imaging in minutes: a first step towards real-time cell imaging”, Anal Bioanal Chem. **397**, 2123 (2010).
4. C. Petibois, M. Piccinini, M. Cestelli Guidi, A. Marcelli , “Facing the challenge of biosample imaging by FTIR with a synchrotron radiation source”, J. Synch. Rad. **17**,1 (2010).
5. M.A Evsyukova *et al.*, “Crystal-quasicrystal transition in the Al-Cu-Fe system: Analysis of the local atomic structure”, Physica B **405**, 2122 (2010).
6. R. Sathyamoorthy *et al.*, “Surfactant-assisted synthesis of Cd(1-x)Co(x)S nanocluster alloys and their structural, optical and magnetic properties”, J. of Alloys and Compounds **493**, 240 (2010).

## **GILDA - GENERAL PURPOSE ITALIAN BEAMLINE FOR DIFFRACTION AND ABSORPTION - AT ESRF**

A. Balerna, A. Grilli (Tecn.), S. Mobilio (Resp.), A. Raco (Tecn.),  
V. Sciarra (Tecn.), V. Tullio (Tecn.)

### **1 Introduction**

GILDA (General Purpose Italian BeamLine for Diffraction and Absorption), is the Italian CRG beamline, built to provide the Italian scientific community with an easy access to the European Synchrotron Radiation Facility to perform experiments with a high energy and brilliance X-ray photon beam. GILDA was proposed, designed, constructed and commissioned by a collaboration between LNF and a large number of University groups; it is operative since autumn 1994. Today GILDA is funded by the Italian public research Institutes: Consiglio Nazionale delle Ricerche (CNR) and Istituto Nazionale di Fisica Nucleare (INFN). Experimental stations for X-ray Absorption Spectroscopy, Anomalous X-ray Scattering and X-ray Diffraction (XRD) are present on the GILDA beamline.

The LNF group is involved in the technical maintenance and update of the beamline, with particular emphasis to the electronic and software controls of all the instrumentation and to the apparatus for X-ray diffraction.

### **2 Technical activity on the GILDA beamline during 2010**

During 2010 the main implementations on the instrumentation were:

1. the restart of the diffraction hutch after a long shutdown due to the failure of the image plate detector; an image plate detector of ESRF was used at this purpose. This solution is not ideal due to the very long reading time required. A much better solution is under development;
2. the implementation of a new motor control system of the REFLEXAFS experimental chamber, based on the ICEPAP hardware and the SPEC software ESRF standards; this implementation is a further step towards the complete migration of the hardware and software in use at the beamline toward the standards of the ESRF;
3. the test of a fluorescence spectrometer based on a curved focussing crystal; an energy resolution of roughly 80 eV was achieved. The spectrometer will allow to increase the signal to noise ratio of absorption spectra recorded in fluorescence mode for moderately concentrated samples (up to few percent).

### **3 Beamtime use during 2010 and scientific outcomes**

During 2010 ESRF delivered beam for about 5000 hours; about 4000 hours were used for user's experiments, the remaining for in-house research, beamline improvements, maintenance and alignment. Totally 35 experiments were performed, 21 of Italian users and 14 of European users. All the experiments were approved by the ESRF experiment review panels for the public beamtime and by the Italian GILDA scientific committee for the Italian beamtime.

During 2010 42 papers were published in international journals with referees, the main topics being material science, catalysis, nanoparticles and cultural heritage. The following studies are to be mentioned:

1. *Dopants and defects: Local structure and dynamics in barium cerates and zirconates.*  
An overview of state-of-the-art EXAFS measurements and data analysis on Ba, Ce, Zr, Y, In and Gd local environments in Y:BaCeO<sub>3</sub>, In:BaCeO<sub>3</sub>, Gd:BaCeO<sub>3</sub>, Y:BaZrO<sub>3</sub>, and In:BaZrO<sub>3</sub>, at different temperatures, hydration degrees and doping levels allowed to reach unprecedented insights on the peculiar role of the dopant, and its interactions with the other lattice defects. In particular, each different dopant shows unique behavior, depending mainly on its electronic structure; it was demonstrated that the usual criterion of ionic radius matching is not useful to outline an effective doping strategy of proton conducting perovskites. As what concerns the structure-property relationships, the high dopant solubility, the high symmetry around the doped site, and the low local disorder, are detrimental for proton conductivity.
2. *High Yield Synthesis of Pure Alkanethiolate-Capped Silver Nanoparticles.*  
One-phase, one-pot synthesis of Ag<sup>0</sup> nanoparticles capped with alkanethiolate molecules has been optimized to easily achieve a pure product in quantitative yield. An extensive chemophysical, structural, and morphologic characterization of dodecanethiolate-capped silver nanoparticles performed by way of UV-vis, <sup>1</sup>H NMR, and X-ray photoelectron (XPS) spectroscopies, X-ray powder diffraction (XRD) and X-ray absorption fine structure analysis (XAFS), electron diffraction and high-resolution transmission electron microscopy (HR-TEM), and scanning and transmission electron microscopy (SEM and TEM) showed that depending on the molar ratio of the reagents (dodecylthiosulphate/ Ag<sup>+</sup>), the mean Ag<sup>0</sup> particle size DXRD is tuned from 4 to 3 nm with a narrow size distribution. The particles are highly soluble, very stable in organic solvents (hexane, toluene, dichloromethane, etc.), and resistant to oxidation; the hexane solution after one year at room temperature does not show any precipitation or formation of oxidation byproducts.
3. *Microstructure and magnetic properties of colloidal cobalt nano-clusters.*  
The correlation between structural properties and magnetic response of nanometer-sized Co nano-particles (NP) prepared using reverse micelle solutions was investigated. The use of complementary structural and morphological probes (like transmission electron microscopy, high resolution electron microscopy, X-ray absorption spectroscopy) allowed to relate the magnetic properties to the size, morphology, composition and atomic structure of the nanoparticles. All data agree on the presence of a core-shell structure of NPs made of a metallic Co core surrounded by a thin Co-oxide layer. The core-shell microstructure of NPs affects its magnetic response mainly by raising the anisotropy constant.
4. *Structural origin of perpendicular magnetic anisotropy in epitaxial CoPt<sub>3</sub> nanostructures grown on WSe<sub>2</sub>(0001).*  
A detailed analysis of the local ordering in CoPt<sub>3</sub> nanostructures epitaxially grown on WSe<sub>2</sub>(0001) and NaCl(001) low-energy surfaces was performed. Polarized extended x-ray absorption fine-structure measurements at the Co K-edge show a local structural anisotropy in fcc CoPt<sub>3</sub> nanostructures grown at 300 K on WSe<sub>2</sub>. It is characterized by preferential Co-Co bonding along the in-plane direction balanced with preferential heteroatomic bonding along the out-of-plane direction and explains the unexpected perpendicular magnetic anisotropy. Such anisotropy almost vanishes in partially L12-ordered nanostructures grown at 700 K. In contrast, the short-range order is isotropic in CoPt<sub>3</sub> nanostructures grown on NaCl(001) at 370 K. These different behaviors emphasize the favorable role of Se segregated

atoms of WSe<sub>2</sub> in the dynamic segregation of Pt atoms at the advancing surface during codeposition, which governs the local structural anisotropy. In the absence of Se, as previously observed in epitaxial CoPt<sub>3</sub> films grown on Ru buffer layers, the development of similar structural anisotropy requires higher growth temperatures (550–720 K).

5. *XAS and GIXRD Study of Co Sites in CoAl<sub>2</sub>O<sub>4</sub> Layers Grown by MOCVD.*

The chemical environment of Co sites in CoAl<sub>2</sub>O<sub>4</sub> layers grown by metal-organic chemical vapor deposition has been investigated by X-ray absorption spectroscopy (XAS) and X-ray diffraction (XRD). It is shown that the air- or [O<sub>2</sub> + H<sub>2</sub>O]-annealing at 500 C of the layers deposited at low temperature induce a partial crystallization with the formation of (Co<sub>1-2 $\eta$</sub>  Al<sub>2 $\eta$</sub> )(Co<sub>2 $\eta$</sub> Al<sub>2(1- $\eta$ )</sub>)O<sub>4</sub> spinel ( $\eta=0.2-0.27$ ). Nevertheless, slightly more than half of Co remains in an amorphous phase, and XAS data are consistent with the formation of a medium-range ordered Co<sub>3</sub>O<sub>4</sub> phase, especially upon air-annealing. Layers grown at higher temperatures (600-650 C) exhibit a similar but more complex structure, since the presence of an additional medium-range ordered phase (likely, CoAl<sub>2</sub>O<sub>4</sub>) is also revealed. The air-annealing at high temperature (800 C) generates blue, almost completely crystalline, CoAl<sub>2</sub>O<sub>4</sub> layers. Optical properties of deposited layers are discussed by referring to the outcomes of structural results. In particular, the optical absorption spectrum results negligibly affected by the presence of the amorphous phase, while absorptions present in the 300-500 nm range, responsible for the green layer color and evident in samples annealed in an oxidizing atmosphere or grown at high temperature, are likely caused by the octahedrally coordinated Co ions of the partially inverted spinel (Co<sub>1-2 $\eta$</sub>  Al<sub>2 $\eta$</sub> )(Co<sub>2 $\eta$</sub> Al<sub>2(1- $\eta$ )</sub>)O<sub>4</sub> phase. Despite the XRD analysis that ultimately demonstrates the presence of octahedrally coordinated Co ions, whose oxidation state in the spinel phase is in majority Co(II), the occurrence of Co(III) species with an octahedral environment cannot be ruled out.

#### 4 Beamline Memorandum of understanding

The memorandum of understanding between the ESRF and the Italian Institutions INFN and CNR which regulates the beamline activity has been renewed for five years (2010-2014).

#### 5 2011 - GILDA Forseen Activity

During 2011:

1. the user facility operation will continue and roughly 4000 hours of beamtime will be allocated to external users through the experiment review panels;
2. a new fluorescence Ge(hp) multi-detector recently purchased by DESY will be installed and commissioned in the absorption hutch. This detector, used together with the exiting one, will allow to increase the solid angle of detection with a significant increase of the signal to noise ratio;
3. a new 2-dimensional detector will be installed in the diffraction hutch. This detector, readable on line, will allow faster acquisition of time resolved powder diffraction patterns;
4. a software for the remote control of the beamline will be installed and commissioned, thus allowing to perform absorption experiments remotely. This will favor the operations of external users that may in principle perform the experiment at home only sending the samples and without coming to Grenoble;

5. a further step towards the complete standardization of the beamline hardware and software will be performed.

## 6 Publications

1. F. Giannici, A. Longo, K.-D. Kreuer, A. Balerna, A. Martorana, "Dopants and defects: Local structure and dynamics in barium cerates and zirconates", *Solid State Ionics* **181**, 122 (2010).
2. F. Liscio *et al.*, "Structural origin of perpendicular magnetic anisotropy in epitaxial CoPt<sub>3</sub> nanostructures grown on WSe<sub>2</sub>(0001)", *Physical Review B* **81**, 125417 (2010).
3. R. Torchio *et al.*, "Microstructure and magnetic properties of colloidal cobalt nano-clusters", *Journal of Magnetism and Magnetic Materials* **322**, 3565 (2010).
4. R. Torchio *et al.*, "Magnetic properties of colloidal cobalt nanoclusters", *Journal of Physics: Conference Series* **200**, 72100 (2010).
5. A. Mari *et al.*, "High Yield Synthesis of Pure Alkanethiolate-Capped Silver Nanoparticles", *Langmuir* **26**, 15561 (2010).

## NTA.CLIC

D. Alesini, C. Biscari, B. Buonomo, A. Ghigo (Resp.),  
F. Marcellini, M. Serio, A. Stella

### 1 Introduction

The next high energy lepton collider will be a Linear Collider. The Compact Linear Collider (CLIC) is an electron-positron collider, with a c.m. energy up to 3 TeV, based on high acceleration gradient using high frequency RF cavities in the two-beam acceleration scheme.

Aim of the CLIC Test Facility (CTF3), realized at CERN by an international collaboration, is the feasibility demonstration of the acceleration gradient of 100 MeV/m, provided by high power radiofrequency. The 12 GHz RF power is generated decelerating a high intensity electron drive beam in power extraction structure: the power is transferred to the 12 GHz cavities in which the main beam is accelerated.

The INFN Frascati Laboratory (LNF) designed the two rings of the drive beam recombination system in the framework of this international collaboration. The first ring, named Delay Loop, was realized under LNF full responsibility and commissioned in 2006.

INFN was in charge of the construction of the RF deflectors, the vacuum chambers, the wiggler and diagnostics of the second ring (Combiner Ring). In 2009 we completed the commissioning of the ring and the recombination at full current was proved with the multiplication of factor 8 of the linac current, achieving the project value of 28 A at 12 GHz pulse frequency.

The electron beam is extracted and delivered to the CLIC experimental area in which the 12 GHz RF power production has been demonstrated and used to accelerate a probe beam with a gradient of more than 100 MeV/m in a short accelerating section.

### 2 LNF Group Contribution in year 2010

During 2010 LNF group contributed with different items to the CLIC scientific program.

Deep theoretical study of the beam dynamics in the Combiner Ring with RF deflectors has been performed. A special computer code has been developed and the simulation results have been compared with the beam measurements before and after the change of the RF deflector (cfr.: CLIC- activity report 2009).

A phase monitor that permits the test of the synchronization of the CLIC drive beam with the main beam has been studied. This special diagnostics is an RF pick-up perfectly tuned on the beam frequency and strongly insulated from the RF noise coming from the beam pipe through special notch filters. The expected resolution of the phase measurement will be of the order of 10 fs. The electromagnetic and the mechanical design have been completed and the prototype is now in preparation.

The CLIC group is participating to the CLIC Conceptual Design with the design of the Combiner Rings system; in particular the first version of the optics design has been developed.

### 3 Foreseen activity of the LNF group during year 2011

In 2011 the foreseen activities include:

The realization of the phase monitor with RF test in lab; the installation of the monitor in the chicane zone, at the end of the linac; test of the acquisition system on the electron beam.

The study and realization of the feedback kickers that permits the test of the synchronization of the CLIC drive beam with the main beam. The low coupling impedance kickers will be installed in the transfer line from the combiner to the experimental area in order to change the beam path length. A second monitor will be placed after the correction to monitor the effectiveness of the feedback system.

The completion of the CLIC Conceptual Design and involvement to the CLIC scientific program.

#### References

1. F. Marcellini *et al.*, “The Clic Drive Beam Phase Monitor”, in: Proc. International Particle Accelerator Conference, Kyoto (Japan), 2010.
2. D. Alesini *et al.*, “Studies on Beam Loading in the CLIC RF Deflectors”, in: Proc. International Particle Accelerator Conference, Kyoto (Japan), 2010.
3. C. Biscari *et al.*, “Progress towards the CLIC Feasibility Demonstration in CTF3 ”, in: Proc. International Particle Accelerator Conference, Kyoto (Japan), 2010.

## NTA ILC

D. Alesini, M. E. Biagini, S. Bini, R. Boni, R. Cimino, A. Clozza, A. Ghigo,  
S. Guiducci (Resp.), F. Marcellini, P. Raimondi, A. Stecchi

### 1 Introduction

The INFN has contributed to the GDE (Global Design Effort) for the International Linear Collider (ILC) since the beginning in 2005 with a qualified participation to the project design and R&D. The LNF activity is focused on damping rings and consists of studies and simulations and on the realization of prototypes of some critical elements. The possibility of making experimental observations at DAΦNE offers a great opportunity to test simulation studies and prototypes. This activity is fully integrated at the international level: within the GDE LNF has the responsibility of the Damping Rings (DR) area system.

### 2 Year 2010 Activities

In the present phase one of the GDE main objectives is the choice of the ILC new baseline configuration to be used for the Technical Design Report. The baseline choice requires studies on the various accelerator systems and their integration: a dedicated workshop, BAW2, at SLAC in January will finalize the recommendation. In 2010 LNF has been actively involved in the preparation of BAW2 coordinating the DR design activity. In particular work has been done on lattice design for the 3.2 km long damping ring required for the new configuration and on the comparison between this lattice and the previous one, 6.4 km long, with respect to the electron cloud effects. To increase the luminosity at c.m. energies below 250 GeV it has been proposed to operate the accelerator with a different configuration and a higher repetition frequency with respect to the one used for the nominal 500 GeV energy. A solution to operate the DR in this configuration has been found including modifications of the lattice, wiggler and radio frequency systems.

An important step in preparation for the TDR, with active involvement of LNF, was the recommendation for mitigations of the electron cloud effect. A working group has been set up to evaluate the electron cloud effect and instability and recommend mitigation solutions for the electron cloud formation. The working group met at Cornell University on October 13, 2010, as a satellite meeting to the E-CLOUD10 Workshop held on October 8-12. The workshop was devoted to hearing the results of detailed studies of a range of mitigation options, which form the basis for the recommendations. The working group meeting was dedicated to the preparation of the recommendations for the baseline and alternate solutions for the electron cloud mitigation in various regions of the ILC positron damping ring.

The effect of wiggler magnets on beam dynamics is a relevant issue for the ILC DRs, which need a wiggler section nearly 200 m long to increase the radiation damping and achieve the nominal damping time. Studies and experiments on wiggler beam dynamics have been performed at DAΦNE. During the 2010 shutdown the poles of the DAΦNE wigglers have been modified to reduce the nonlinear components of the magnetic field on the beam trajectory and to improve the dynamic aperture of the main rings. Tune shift measurements as a function of the beam orbit position inside the wigglers have shown a good linearity, as it was foreseen from simulations.

Electron clearing electrodes have been installed in DAΦNE in order to reduce by more than one order of magnitude the e-cloud density in the dipole and wiggler vacuum chambers. At present

they show a good performance but to make systematic tests of their effect on e-cloud density and beam impedance it is necessary to wait for the conclusion of the machine commissioning phase.

Another activity aimed at developing e-cloud mitigation techniques is the realization of a sputtering system for thin film deposition on vacuum chamber samples in order to reduce the Secondary Emission Yield (SEY). A set-up for coating small aluminium objects using a RF magnetron operating at 13.56 MHz has been realized. The device allows varying the parameters of the coating process, in particular, the relative pressure of the ionization gas and reactive gas can be controlled. A few samples coated with TiN have been produced. They show a good uniformity and the characteristic golden colour and are ready for the chemical characterization and the SEY measurement.

### 3 Plans for Year 2011

LNF will continue to coordinate the Damping Rings (DR) working group within the GDE, with the responsibility of the DR area system for the preparation of the Technical Design Report, due end of 2012. The technical and research activity will be focussed in particular on e-cloud studies. The comparison between simulations and experimental tests at DAFNE will continue in order to improve the comprehension and mitigate the electron cloud instability.

In 2011 the activities on thin film coatings will continue with two main objectives. The first one is magnetron sputtering deposition of thin films of different materials (TiN, NEG, C) on small samples. This will be done with the present set-up in order to optimize the process and measure the characteristics of the coated samples (secondary emission yield, chemical and surface properties). The second objective is to realize a dedicated set-up and perform thin films deposition on DAΦNE vacuum chamber prototypes.

### 4 Publications and Talks

1. S. Guiducci, M. Biagini, “3.2 km SuperB-type Lattice”, LCWS 2010, International Linear Collider Workshop 2010, Beijing, 26-30 March 2010.
2. S. Guiducci M.E. Biagini, “A Low Emittance Lattice for the ILC 3 km Damping Ring”, p. 3545, Proc. of IPAC10, Kyoto, Japan, (2010).
3. M.T.F. Pivi et al., “Recommendation for the Feasibility of More Compact LC Damping Rings”, p. 3578, Proc. of IPAC10, Kyoto, Japan, (2010).
4. S. Guiducci, “Design Progress for the ILC Damping Rings”, IWLC2010 International Workshop on Linear Colliders 2010, CERN 18-22 October.
5. S. Guiducci et al., “Accelerator WG2 summary (Damping rings, ATF and Cesr-TA)”, IWLC2010 International Workshop on Linear Colliders 2010, CERN 18-22 October 2010.
6. T. Demma, “Electron Cloud Build-up and Instability in DAΦNE”, ELOUD10, 49th ICFA ABD Workshop on ELOUD physics, Cornell University, USA 8-12 October 2010.
7. R. Cimino, “Experimental Efforts at LNF to Reduce Secondary Electron Yield in Particle Accelerators”, ELOUD10, 49th ICFA ABD Workshop on ELOUD physics, Cornell University, USA 8-12 October 2010.
8. S. Bettoni et al., “Multipoles Minimization in the DAΦNE Wigglers”, p. 4665, Proc. of IPAC10, Kyoto, Japan, (2010).
9. D. Alesini et al., “Design and Test of the Clearing Electrodes for e- cloud Mitigation in the e+ DAΦNE Ring”, p. 1515, Proc. of IPAC10, Kyoto, Japan, (2010).
10. S. Bini, “Synthesis of nitride titanium film by RF Sputtering”, ILC-LNF Technical Note, ILC-LNF-004, January 8, 2011.

## NTA-PLASMONX

S. Bellucci, S. Bini, M. Castellano, A. Clozza, G. Di Pirro, A. Drago,  
M. Esposito, M. Ferrario, A. Gallo, G. Gatti, P. Gaudio, A. Ghigo,  
G. Giannini, T. Levato\*, F. Micciulla, M. Migliorati, D. Nanni,  
E. Pace, L. Palumbo, A. Petrucci, C. Sanelli, A. Tenore,  
F. Terra, S. Tomassini, C. Vaccarezza (Resp.)

In collaboration with:

Sezione INFN Bologna, Sezione INFN Milano, Sezione INFN Milano Bicocca,  
Intense Laser Irradiation Laboratory, INO-CNR and Sezione INFN Pisa,  
Università La Sapienza, Roma

\* also at ILIL, INO-CNR, Pisa, Italy

### 1 Introduction

In the 2010 the NTA-PLASMONX project has seen the completion of FLAME-laboratory that was officially opened in December. The commissioning activity has been carried on through all the year and also the Self Injection Test Experiment has completed its first phase. The MultiGev spectrometer has seen the completion of the prototype tests and the detector has been constructed and assembled, its commissioning also started. The electron beam transfer lines for the Thomson Scattering and Plasma Acceleration experiments are going to be installed in the mid of 2011, being the procurement of all components finalized for that date. The Thomson source interaction setup will also be installed together with the setup of the BEATS2 experiment. The description of this activity is given in the following.

### 2 FLAME and SITE

During 2010 the main part of the FLAME laboratory was completed including the laser area, the target area, the beam transport and most of the radiation protection shielding. This activity culminated in the Official opening which took place during the LIFE meeting at LNF on Dec. 17th. In section 2.1 of this report we describe in details the commissioning activity and the series of tests carried out including sub-system tests and full system test with laser power up to 50 TW in the target chamber. In Section 2.2 we describe the outcome of the preliminary phase of the Self Injection Test Experiment (SITE) [1]. Here a list of the main data concerning the entire Laboratory with some specification on the first test on instrumentations including the auxiliary (probe) and main laser beams.

#### 2.1 FLAME LASER OPERATION

During 2010 all subsystems of the laser, namely the front-end, the 10 pumping units of the main cryo amplifier, the beam transport, the optical compressor vacuum chamber and the compressor optics were commissioned and successfully tested. In particular, during specific test runs a full beam compression test was carried out in March 2010 in which a pulse duration of 26 fs was demonstrated for the main beam and 23 fs for the aux beam (see Fig. 1). In addition, in April 2010, the contrast of the laser pulse at a TW power level was measured, demonstrating the expected contrast ratio of better than 109 as shown by the plot of Fig. 2.

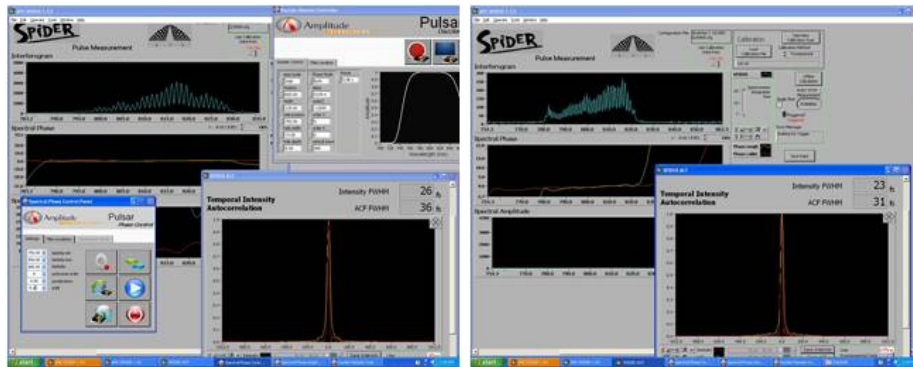


Figure 1: User interface of the Dazzler-Mazzler control showing optimized pulse duration of 26 fs for the main pulse (left) and 23 fs for the the auxiliary (probe) pulse (right).

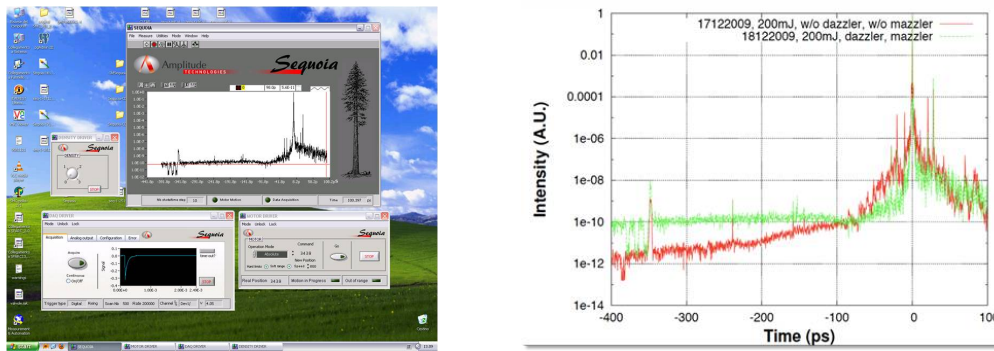


Figure 2: (Left) User interface of the Sequoia cross-correlator during contrast measurements at FLAME. (Right) Plot of the cross-correlation curve with and without pulse duration optimization showing an optimum contrast of better than  $10^{10}$ .

### 2.1.1 FLAME Target Area shielding

During May 2010, the vertical radiation shield was completed to enable full shielding of the target vacuum chamber. The shielding consists of concrete blocks of 50 cm thickness held together by a state-of-the-art steel frame. During the following month, the horizontal shielding, consisting of 50 cm thick, "T" shaped, concrete beams was also commissioned. These shielding structures, together with the additional labyrinth vertical shielding planned in 2011 (see general FLAME plan on 2009 report [2]) will provides full protection against ionizing radiation generated in laser-plasma acceleration interaction conditions [3] as from SITE design [4] (Fig.3).

### 2.1.2 Beam transport and pointing stability test

During June 2010, full commissioning took place of the beam transport line from the laser clean room (laser output) to the target chamber, via the in-vacuum optical compressor and turning mirrors. This also included the installation of the 1m focal length off-axis parabolic mirror (OAP) for beam focusing at the target vacuum chamber center. Beam pointing stability tests were carried out to evaluate overall pointing performance including intrinsic laser pointing stability and transport line mechanical stability. The final result is shown in Fig.4 where the focal spot image taken



Figure 3: Vertical (left) and horizontal (right) concrete shielding for the underground FLAME target area were the test esperiment of laser-plasma acceleration with self-injection takes place.

with a 20x microscope objective is shown along with the statistical distribution of the centroid of the focal spot in the X and y directions. According to these measurements an excellent pointing stability of better than  $2\mu\text{rad}$  is found, which is a small fraction of the focal spot itself.

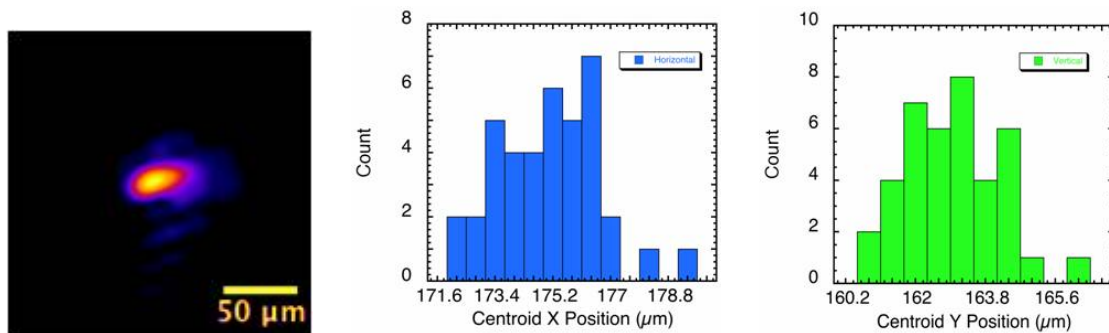


Figure 4: Beam pointing stability at target chamber center. Left image shows the focal spot image taken with a 20x microscope objective. Centre and right images show the statistical distribution of the centroid of the focal spot in the X and y directions.

For the optimization of the off-axis parabola, in addition to standard alignment procedures, an additional alignment procedure previously used and tested at ILIL, was established at FLAME. The procedure is based upon the optimization of the forward scattered radiation from laser interaction in air at relatively low laser power. Due to interaction of the laser pulse with the air gases, a self-phase modulation occurs along with harmonic generation. A symmetric image (see figure 5) is indicative of a well optimized focal spot, with a minimum astigmatism.

### 2.1.3 Gas-jet installation and tests

During July 2010 the gas-jet system including the nozzle and the valve, the high pressure gas system and the XYZ micrometric target motion mechanism were fully commissioned and tested. The pictures of Fig. 6 show the entire system (left) and a detail of the nozzle (right) during propagation of the laser pulse in the gas-jet. The latter image was obtained from the Thomson scattering imaging channel which is looking at the target from the top, in the direction perpendicular to the plane of oscillation of the electric field of the laser e.m. wave.

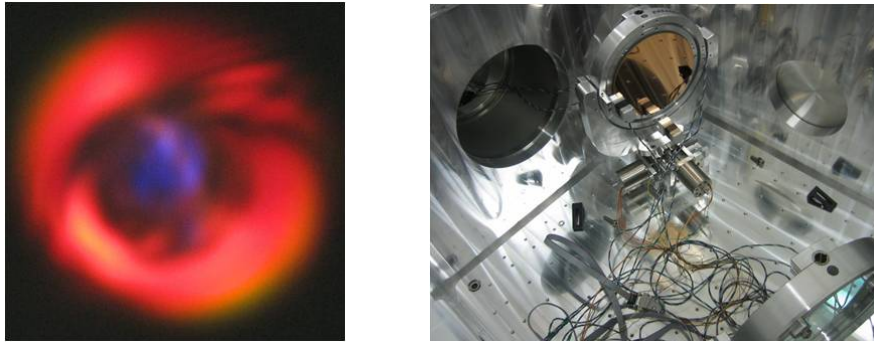


Figure 5: *Beam pointing stability at target chamber center. Left image shows the focal spot image taken with a 20x microscope objective. Center and right images show the statistical distribution of the centroid of the focal spot in the X and y directions.*

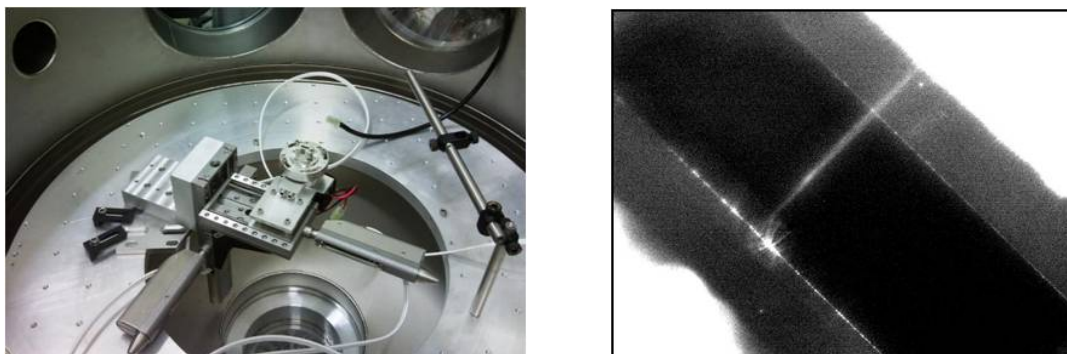


Figure 6: *(Left) Panoramic view of the target motion assembly with XYZ micro metric translation stages. (Right) Magnified top-view of the gas-jet nozzle (gas ejected normal to the image) showing the passage of the laser pulse focused at the center the slit through the gas at low laser power. The width of the nozzle is 1.2 mm.*

#### 2.1.4 Laser on gas-jet target: first plasma

Starting from August 2010, a series of tests were carried out to optimize the entire optical system and establish alignment procedures to be used during the SITE experimental phase. These tests culminated with the generation of the first plasma from gas-jet interaction with a 300 mJ level. During this phase a great effort was dedicated to the control of the pulse duration via optimization of the FLAME Dazzler-Mazzler devices for optimization of the bandwidth. These tests enabled the experimental team to gain full control of the procedure and knowledge of the critical parts of the system enabling them to successfully reproduce optimum laser-pulse duration during experimental runs.

#### 2.1.5 First laser accelerated electron bunches from self-injection

Starting in September 2010 an intense experimental activity was initiated aimed at finding the conditions for achievement of laser-plasma acceleration with self injection. During this phase, due to safety constraints, the main power amplifier was turned off (no pumping) and the laser output was limited to a few TW. A detailed description of the experimental set up of this phase is given elsewhere ([4]) and a more detailed description of the results is given below in the next session. In Fig. 7 we show an example of the first electron bunch obtained on October 6th, as detected from the LANEX screen placed along the path of the accelerated electrons in the direction of propagation of the laser pulse. This result demonstrated that the experimental set up, including main laser and experimental such as pulse compression and beam focusing and target system synchronization, were successfully controlled and that performance of the entire system at this relatively low laser power were within specifications required for laser-plasma acceleration.

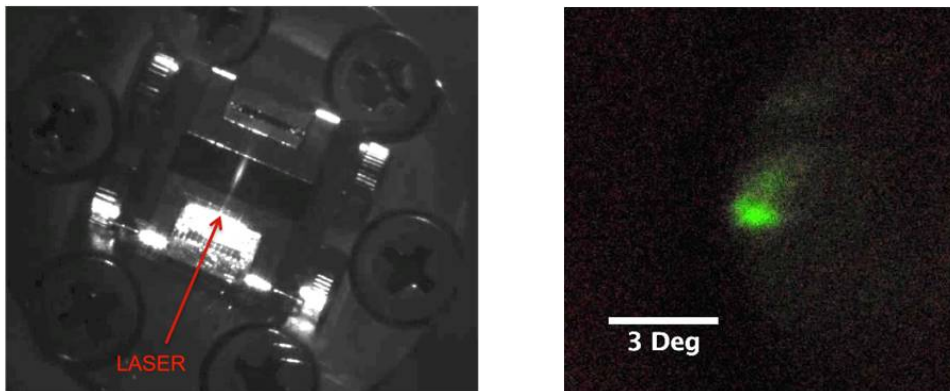


Figure 7: Left) Top-view of the gas-jet nozzle showing Thomson scattering from the laser-plasma interaction region along the path of the laser pulse at relatively higher power than in the similar image of Fig. 6. Right) First electron bunch obtained with FLAME on October 6<sup>th</sup>, as detected from the LANEX screen placed along the path of the accelerated electrons in the direction of propagation of the laser pulse.

#### 2.1.6 Starting up the main power amplifier

Immediately after the first successful generation of laser-accelerated electron bunches with self injection, tests began on the optimization of the last power amplifier which culminated with systematic tests of the full energy stability. The plots of Fig 8 (left) show the stability tests of the

energy over a relatively large number of shots. After the entire optimization process, the full laser energy before compression was found to be 7.3 J (Fig. 8 right).

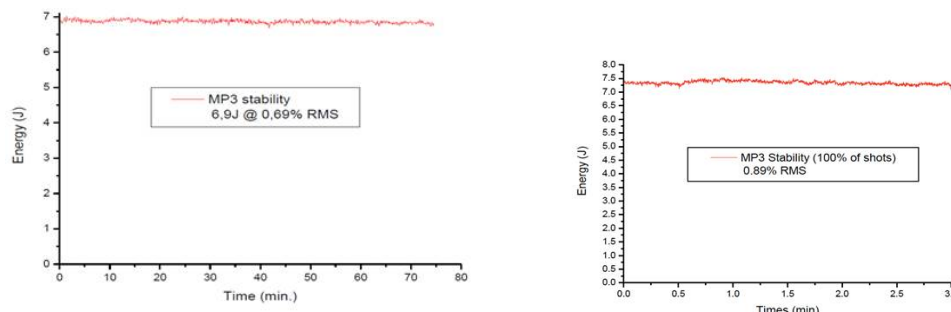


Figure 8: (Left) Full output energy stability of the laser over a 80 min period showing RMS stability of better than 1 at 6.9 J. This level of energy was further increased to 7.3 J after additional optimization.

### 2.1.7 Starting up the main power amplifier

As a final step for laser characterization during 2010, wavefront measurement were carried out in view of the planned installation of the adaptive optics planned for 2011. These measurements were carried out before and after the main power amplifier. Measurements before the main amplifier (top of Fig. 9) show a high quality wave front before the main amplifier, with only minor distortions on the edges of the beam and a Strehl ratio of better than 0.9.

The same measurements carried out after the main amplifier (Fig.9 bottom) show a significant increase in the distortions introduced by the main amplifier. In fact, a close look at the expected intensity in the far field (focal spot) shows the presence of a secondary focal spots, containing a significant fraction of the energy with remaining energy filling up the area around these two spots. Further investigation of these issues was carried out by the laser manufacturer and an upgrade of the main amplifier is foreseen during 2011 to mitigate these issues. An almost complete correction of the phase distortion will eventually be carried out using the full aperture adaptive mirror.

### 2.1.8 Summary of laser performance as end of 2010

Following the results of all the tests carried out on the laser system during 2010 and also taking into account the measurements performed at the target chamber center, the performance of the laser at this stage can be summarized by the table 1.

As compared with the expected performance and in view of the forthcoming planned experimental activity, at this stage we can conclude that, following the installation of the adaptive optics, all laser parameters are expected to be well within required specifications. Currently, the uncorrected wave-front distortion limits the intensity in the focal spot in the present configuration (SITE) to the mid  $10^{18} W/cm^2$ .

## 2.2 THE SELF-INJECTION TEST EXPERIMENT(SITE) - Phase 1

As originally planned, the first phase of SITE took place in parallel with the laser optimization to enable assessment of the laser performance and establishment of all procedures, including safety

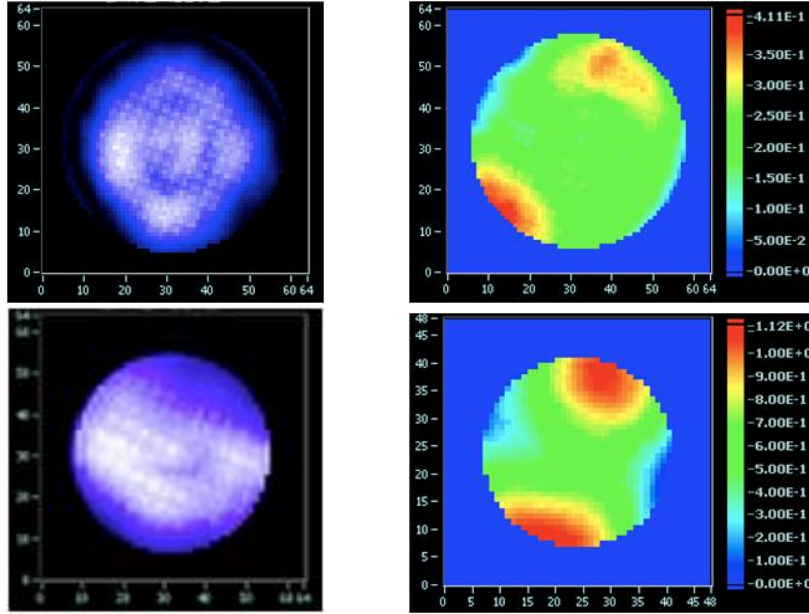


Figure 9: Wave-front measurements of the FLAME laser pulse showing the intensity (left) and the phase (right) of the beam before (top) and after the main power amplifier (bottom). Analysis of these wave fronts yields a Strehl ratio of 0.9 before the main amplifier.

Table 1: Summary of FLAME performance.

Energy before compression	7.3J
Vacuum compressor transmission	> 70%
Pulse duration down to	23fs
ASE Contrast ratio: better than)	$1 > 2 \times 10^9$
Prepulse contrast: better than	$10^8$
RMS Pulse Stability	< 0.8%
Pointing Stability (incl.path)	< 2 $\mu$ rad
Phase front correction needed:	adaptive optics
Full power vacuum compression:	to be performed

procedures. SITE - Phase 1 also served for a preliminary assessment of radiation protection measures and, in fact, measurements were carried under the supervision of LNF radiation protection authority.

### 2.2.1 SITE experimental arrangement

A minimum set of experimental diagnostics was set up to establish key physical parameters, including laser propagation and focusing, target reliability, electron beam production and energy. For these studies we used a nitrogen gas-jet with backing pressure ranging from 5 to 60 Bars. The gas-jet nozzle could be moved with micrometric resolution along the three Cartesian axes. Here we recall the basic experimental set-up schematically shown in the image of Fig. 10 where the gas-jet nozzle is shown with the laser pulse focused close to the edge.

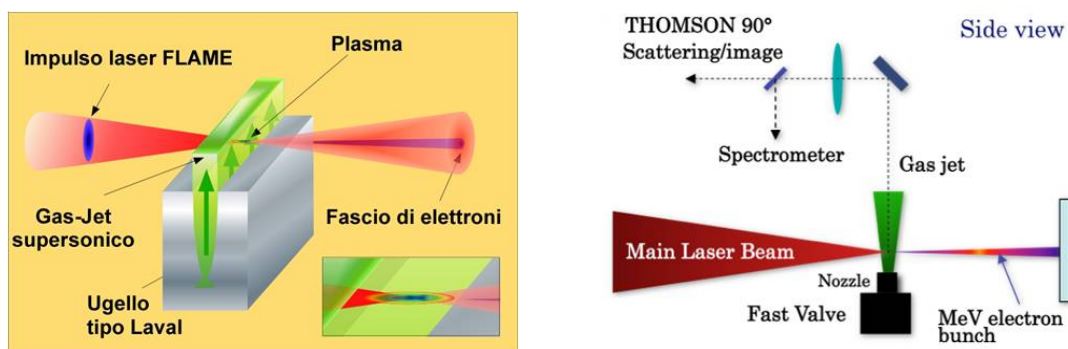


Figure 10: *Schematic experimental set-up for the self-injection test experiment showing the focusing configuration relative to the gas jet nozzle and the main diagnostics for laser, plasma and electron bunch characterization.*

Following the initial successful shots with production of accelerated electron bunches, a more systematic study was carried out aimed at identifying optimum conditions for production of collimated electron bunches of the highest energy for the given laser power. Using available diagnostics, a position scan was carried of the laser focal spot position relative to the gas-jet input wall. For a given longitudinal gas-jet position, a transverse (horizontal and vertical) scanning was also carried out to look for the best injection conditions which, as discussed elsewhere [4], are sensitive to the gas density gradient as well as to the gas absolute density. The latter parameter was scanned by changing the backing pressure of the gas.

### 2.2.2 Electron bunch collimation study

Initially we looked for the minimum laser energy requirements for electron acceleration, and we found it near the 500 mJ laser output level. In this condition we investigated the forward transmitted optical radiation during gas-jet longitudinal positioning and gas pressure. During this study we found condition in which self-focusing was most likely taking place enabling an acceleration regime similar to the one already explored at ILIL in a previous experimental campaign [5]. The effect of self-focusing was clearly shown by the dramatic change in the spectrum and divergence of the transmitted radiation. This also had a direct effect on the production of energetic electron bunches. In fact, it was possible to identify three different interaction condition for which accelerated electrons were characterized by no collimation, medium (around 30 mrad) and high collimation (around 5 mrad).

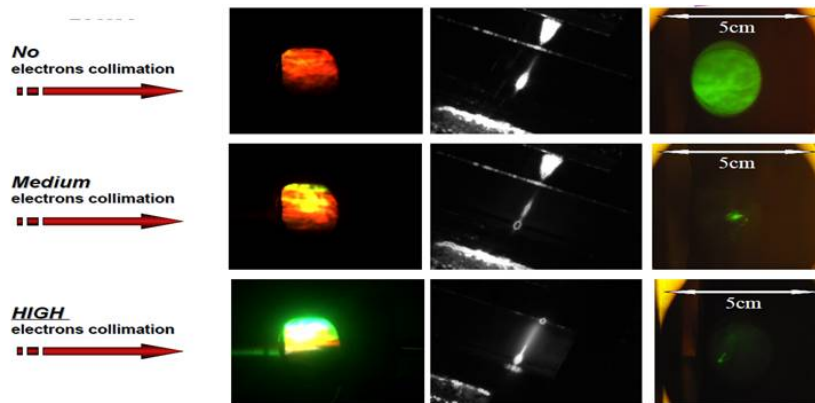


Figure 11: *Raw data from the initial measurements for the SITE Phase 1. The three columns of images show (from the left) the beam after propagation in the plasma, the Thomson scattering image and the electron bunch on the LANEX screen. The upper row shows the interaction regime in which no collimation was found. Middle and bottom show similar results for medium and high degree of electron bunch collimation.*

These three different collimation regimes were observed to be also related to the different spectrum in the transmitted laser radiation as shown in Fig. 11. According to these images, collimation of electrons is reasonably correlated with a longer interaction length in the gas, as shown by the Thomson scattering image. In addition, the transmitted light appears to be strongly blue-shifted when collimation occurs. This is most likely due to the sustained propagation and increased effect of ionization induced blue-shift in the gas.

### 2.2.3 Collimated bunches: pointing and quality

Following the collimation study presented above, a stable regime of production of collimated bunches could be established at 1 J laser energy. The sequence of LANEX images of Fig. 12 shows a sample of the data in which electron bunches in the range between 5 and 30 mrad were systematically accelerated. In this interaction regime, a first investigation was also carried out on the role of the front-phase distortion and consequent spot size energy distribution with related effect on accelerated electron bunch.

Once this condition was established, data were also taken at higher laser energy, up to the maximum of 2.5 J before compression. These additional measurements enabled us to identify the role of phase front distortions in the quality of accelerated electron bunches. In fact, further increasing the laser energy to the multi-Joule level (less than 2.5 J) showed the effect of the secondary focal spot in the interaction region, as discussed above in Section 2.1.8. Fig. 13 presents the LANEX data (top) which clearly show the production of a double electron bunch structure. The corresponding Thomson scattering images (bottom row of Fig. 13) consistently show a double propagation channel. Indeed, these results seem to confirm the presence of a double focal spot in the interaction region as obtained from the wave-front analysis discussed above. This effect only appears at a relatively high energy level when the secondary focal spot contains a sufficient level of energy resulting, in some case, in a second accelerated bunch. A detailed analysis of this effect is in progress [6].

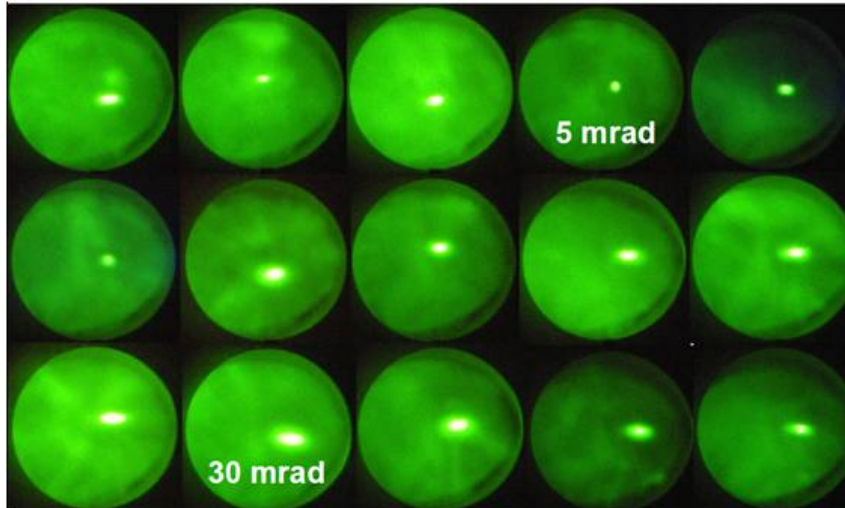


Figure 12: *Raw LANEX data showing the production of collimated electron bunches in the range of 5 to 30 mrad.*

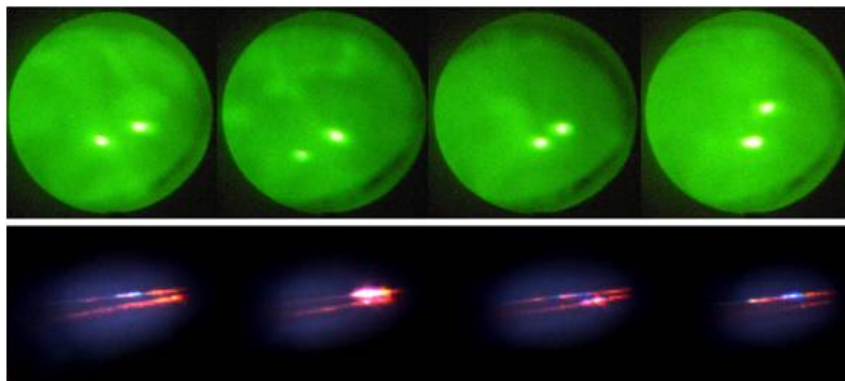


Figure 13: *Raw LANEX data (top) showing the production of a double electron bunch structure. The corresponding Thomson scattering images (bottom) consistently show a double propagation channel.*

### 2.2.4 Collimated bunches: electron energy

As discussed in the dedicated section below, a high resolution magnetic electron spectrometer was undergoing commissioning during 2010. During this preliminary SITE - Phase 1 measurements, the activity of the magnetic spectrometer was devoted mainly to calibration and noise reduction. In spite of this, a successful preliminary energy measurement was also obtained and described in the spectrometer section below. Here we report on the results obtained initially with a stack of radiochromic films as described in [7], see Fig. 14. Preliminary analysis of SHEEBA measurements confirmed that the energy of electron accelerated at 1J level laser energy were already in the 50 MeV level. Following these preliminary encouraging measurements, we also used a low resolution magnetic spectrometer built using a 1T permanent magnets and a LANEX screen as shown schematically in Fig. 15.

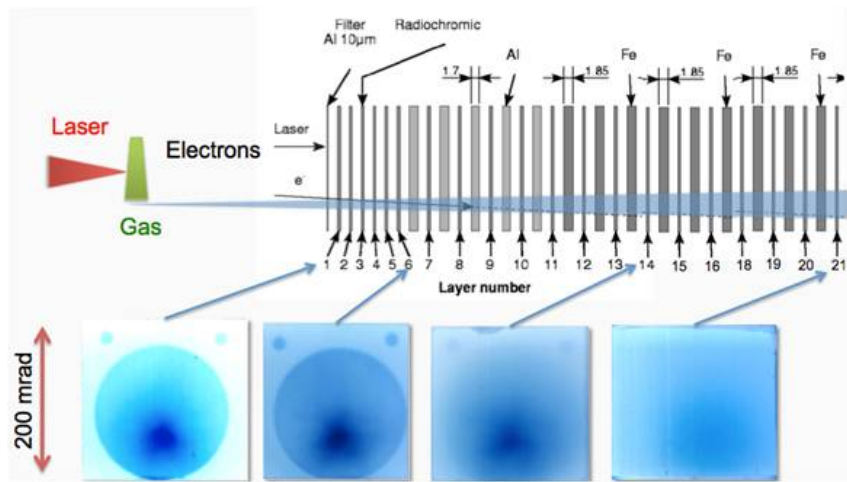


Figure 14: Raw data from preliminary energy measurements of the accelerated electron bunches obtained using a stack of radiochromic films configured according to [7]. Data were obtained after integration over 31 shots.

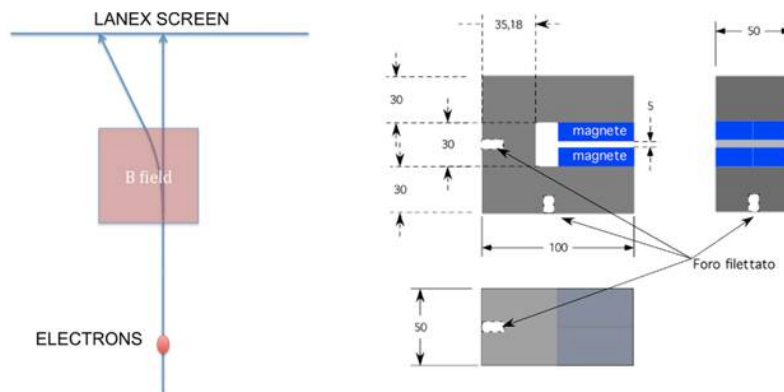


Figure 15: Schematic of the low-resolution permanent magnet electron spectrometer.

In this way it was possible to observe the main feature of the accelerated electrons increasing

the laser energy at fixed pulse duration and focal spot. Preliminary analysis of the low resolution spectra show clearly that high collimated and high energetic electron bunches (around 5 mrad and over 200 MeV level) was accelerated. Although more accurate measurements are still needed to confirm these preliminary, we can conclude that SITE-Phase 1 measurements fully succeeded in demonstrating activation of high energy laser-plasma electron acceleration with self-injection at FLAME in the multi-hundred MeV range. This is extremely encouraging in view of the ultimate goal of the SITE which, as described in details [4], aims at delivering stable production of 1 GeV class electron bunches with moderate-to-small energy spread.

### 3 The Multi-GeV Electron Spectrometer

As far as the electron spectrometer [8] is concerned, during the year 2010 three main activities have taken place: the studies on the prototype have been finalized, the detector has been constructed and assembled and the commissioning of the detector on the final environment has started. The prototype is made of 64 1mm fibers coupled with the same readout chain as the detector 16. It has been tested on the SPARC THz line and at BTF. The major problem that had to be faced was a saturation effect induced by the extremely large number of photons produced in the fibers. To avoid saturation of the electronics readout the HV supplied to the photomultipliers (PMT) was reduced down to typically 500V from the 900V nominal value. A trickier saturation effect was although observed in the tests on beam: the signal shape resembled the beam profile, but the integral of the observed signal was independent of the total impinging charge (see figure 17). This was due to a saturation of the anodic current and was cured by attenuating the light on the photocathode with optical filters.



Figure 16: *Prototype of the fiber detector of the electron spectrometer of SITE.*

After fixing this problem we could calibrate the detector response in charge utilizing the variable charge of the BTF beam. There is still a saturation effect but it starts when more than a hundred of nC impacts a set of 64 fibers, condition that should not occur in the final experimental setup (Fig. 18).

During 2010 the construction of the detector was completed, with the realization of the vacuum chamber equipped with fibers, the assembly of the photomultipliers and the electronics. The final detector is shown in figure 19.

To complete the assembly of the detector, each PMT mask was aligned at the sub-millimeter level to reduce the effect of cross talk.

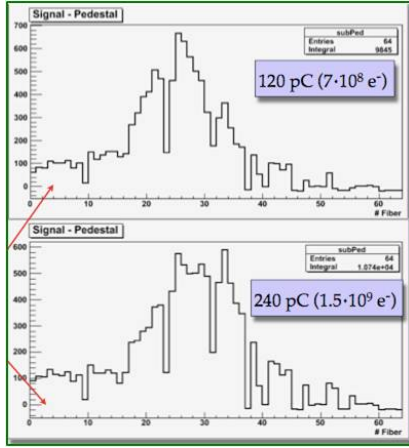


Figure 17: Saturation effect: measured spectra of the BTF beam. Note missing variation with increasing charge.

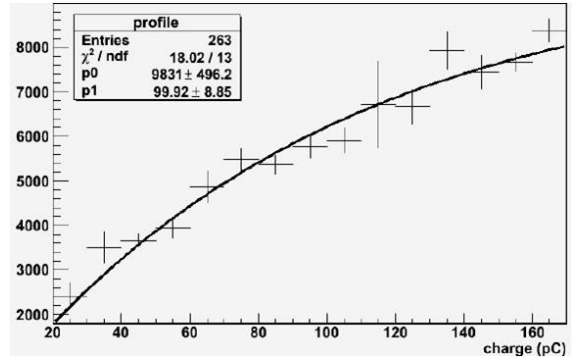


Figure 18: Calibration curve of the fiber detector of the electron spectrometer of SITE.



Figure 19: The Magnetic Spectrometer of SITE.

Finally in november 2010 two days of shots of FLAME with the target where devoted to the commissioning of the spectrometer. The first tests showed a huge electromagnetic noise induced by the interaction of the laser with the plasma. It was found to have contributions from several sources: it was picked up both by the PMT and by the cables and could be screened by moivng the detector behind the wall. While prolongations of the fibers are being built a temporary solution to the problem was found by reading the PMTs with cameras. After running the resulting images through the standard reconstruction algorithms, the spectra in Fig. 20 (taken under different conditions than the ones previously shown) were observed, thous demonstrating that the rest of the measurement chain works.

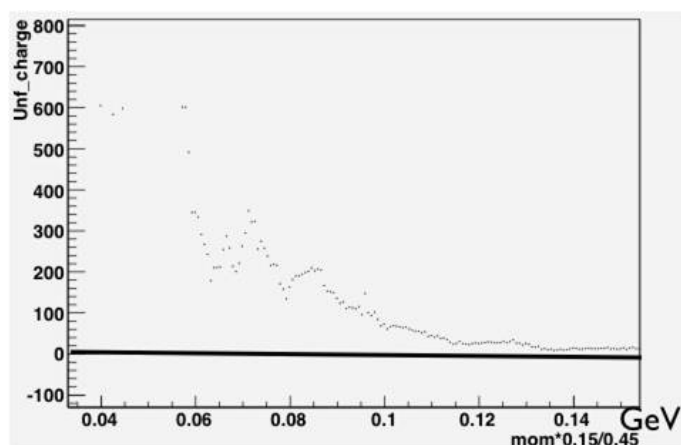


Figure 20: *First electron spectrum from Laser-Plasma acceleration coming from the magnetic spectrometer of SITE.*

#### 4 The Thomson Source

In this facility several experiments are foreseen such as high gradient plasma acceleration and the production of monochromatic ultra-fast X-ray pulses by Thomson back-scattering(TS). The TS X-ray source [9] will be the first one to be installed and its main features are flexibility and potential compactness with respect to conventional synchrotron sources. A TS source driven by high-quality electron beams can work in different operating modes, e.g.: the high-flux- moderate-monochromaticity-mode(HFM2) suitable for medical imaging when high-flux sources are needed; the moderate-flux- monochromatic-mode(MFM) suitable to improve the detection/ dose performance [10]; short-and-monochromatic-mode(SM) useful for pump-and-probe experiments e.g. in physical-chemistry when tens of femtosecond long monochromatic pulses are needed.

##### 4.1 Electron beamlines

The electron beamlines design has been completed in 2009, with the capability to transport electron beams with energies ranging from 28 MeV up to 150 MeV in two separate interaction points (IP's). The goal of the electron beam transport is to preserve the high brightness coming from the linac and to ensuring a very tight focusing for the whole energy span. The final features that the electron beam will show at the two interaction points, are reported in Table 2. The general layout has been revised in the last months of 2010 in order to accomplish the conventional safety requirements: basically the two interaction points have been switched in order to provide a suitable high energy

diagnostic line for the plasma accelerated electron beam while keeping a proper free way out from the SPARC hall in the two ways as required from the conventional safety system. The new all view of the PLASMONX beam lines within the SPARC hall is showed in Fig. 21.

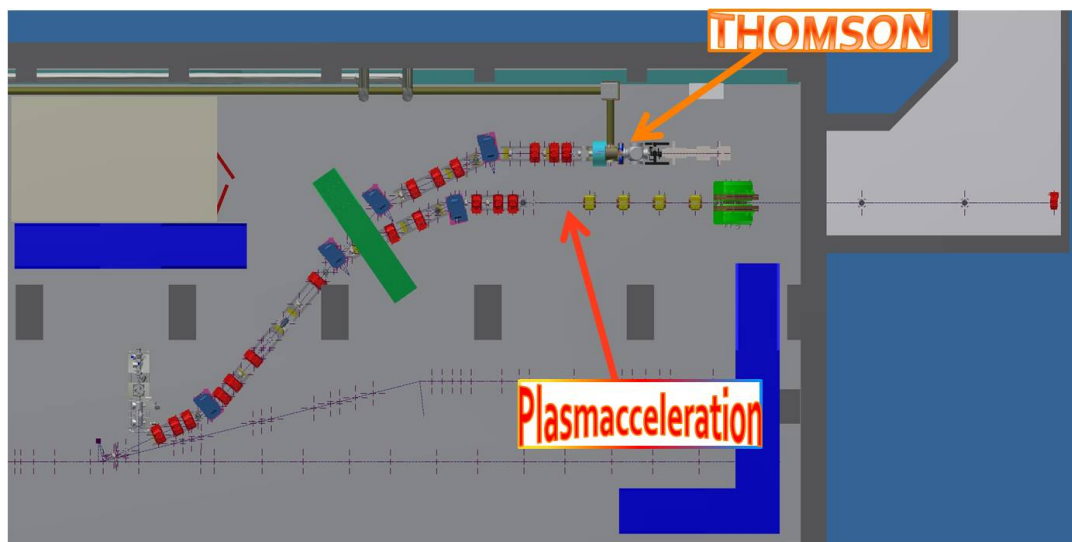


Figure 21: Updated lay-out of the dog-leg like electron beamline for the PlasmonX experimental area.

In detail the electron beamline consists in a 30 m double dogleg starting downstream the SPARC photoinjector; it ends in a two branch beam delivery line that provides two separate interaction regions with the possibility to host two different experiments at the same time. The total beam deflection is about six meters from the SPARC photoinjector and undulator axes. A total of six 25 degrees dipoles and 20 quadrupoles are needed to drive the electron beam up to the two IPs, their procurement has been finalized in July 2009 and the complete delivery is expected by summer 2011, together with the related Power Supplies for a total of 26 units. The installation will begin in July and is foreseen to end in September 2011. The commissioning will follow right after.

After the layout update the beam dynamics for the electron beam has been checked to ensure the all the required parameters reported in Table 2 are still valid. Three main cases have been addressed in term of electron beam transverse dimensions at the IP's, emittance dilution due to Coherent Synchrotron Radiation, final energy spread and longitudinal dimension:

- a) 30-150 MeV beam for Thomson scattering experiment
- b): 150 MeV for Plasma Acceleration experiment

As an example for the Thomson scattering experiment the main challenge regarding the electron beam generation is related to the capability to focus down a high-charge beam (1-2 nC) to focal spot sizes in the order of  $10\mu\text{m}$  in the collision point, which in turns implies to accurately take under control emittance and energy spread of the beam itself [11]. The emittance growth is controlled by the emittance compensation method, which is one of the main challenges addressed to the SPARC project. The low energy spread values will be obtained by a proper setting of the injection phases into the accelerating structures, which compensates the linear correlation of the longitudinal phase-space, while, in a second step, the use of an X-band short length RF structure [12]

will allow to reach an rms energy spread smaller than  $5 \times 10^{-4}$ . A normal conducting large solenoid provides the final focusing element at the IP that will see the first experiment to be set up. The solenoid will ensure a high field on axis (0.9T), its technical specifications have been finalized in 2009, and the delivery is expected by the summer of 2011.

In Fig. 22 the transverse beam rms size evolution is reported for the Thomson scattering setup starting from the photoinjector down to the IP as obtained from the simulations performed with the Tstep code tracking 15 kparticles, for a beam energy of 30 meV (BEATS2 experiment), i.e. where the space charge effects are still important. The same is provided in Fig. 23 where the beam energy instead is around 150 MeV and the simulations performed with the Elegant code and about 120kparticles.

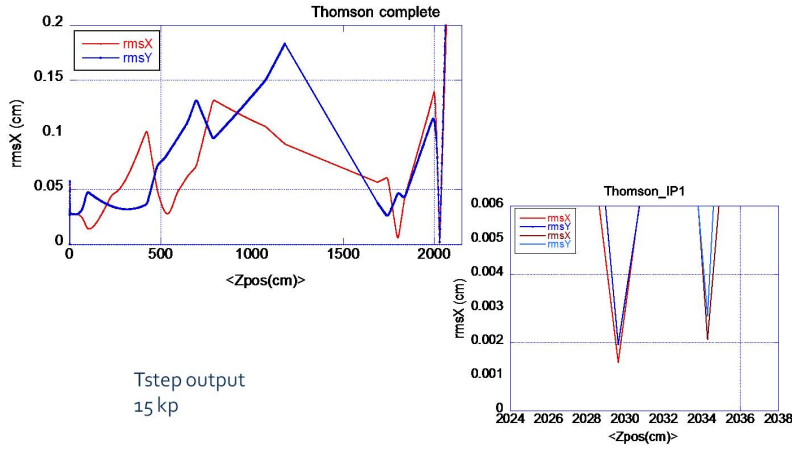


Figure 22: Rms beam sizes evolution along the transfer line (left), and detail of longitudinal "tunability" of the beam waist at the interaction point.

In Fig. 24 the 3D drawing of the whole interaction chamber is shown as embedded in the solenoid and dumping dipole field, together with the parabolic mirror that focuses the laser beam coming from Flame on the interaction point. The interaction chamber layout has been designed in order to fit all the necessary devices (magnetic elements, optical elements, vacuum vessels, diagnostics, etc.) in agreement with the beams transport constraints, its delivery is foreseen in summer 2011.

The electron beam alignment will be monitored using BPMs and high resolution imaging systems. The time overlapping between laser pulse and electron beam (in the interaction chamber) will be adjusted using an optical delay line, while jitter/delay readout will be made through a picosecond streak-camera, by monitoring laser and some kind of electron beam induced radiation

Table 2: Electron beam parameters at the two interaction points.

Parameter	Thomson Scattering Exp.	Plasma Acceleration Exp.
Bunch charge(nC)	1 ÷ 2	0.020
Energy (MeV)	28 ÷ 150	150
Length (ps)	15 ÷ 20	0.010
$\epsilon_{n,x,y}$ (mm-mrad)	1 ÷ 5	1 ÷ 0.5
Energy spread(%)	0.05 <sup>1</sup> ÷ 0.2	0.01
Spot size at interaction point rms (mm)	5 ÷ 10	5 ÷ 10

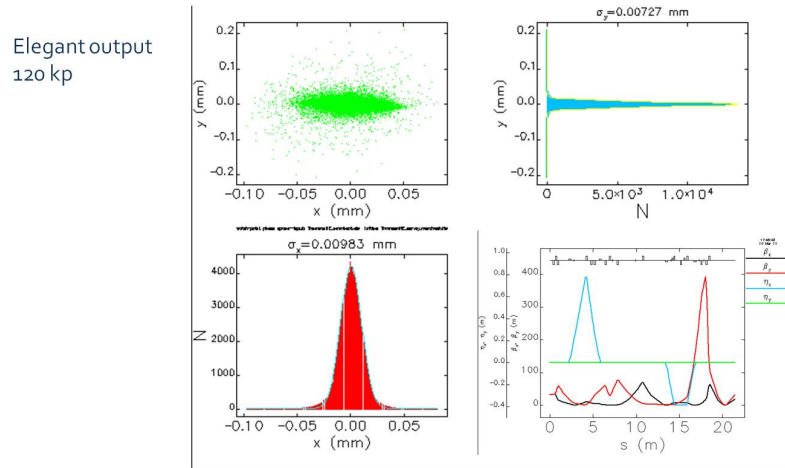


Figure 23: *Rms beam sizes of the 150 MeV beam at the interaction point, together with the twiss parameters for the transfer line (down right).*

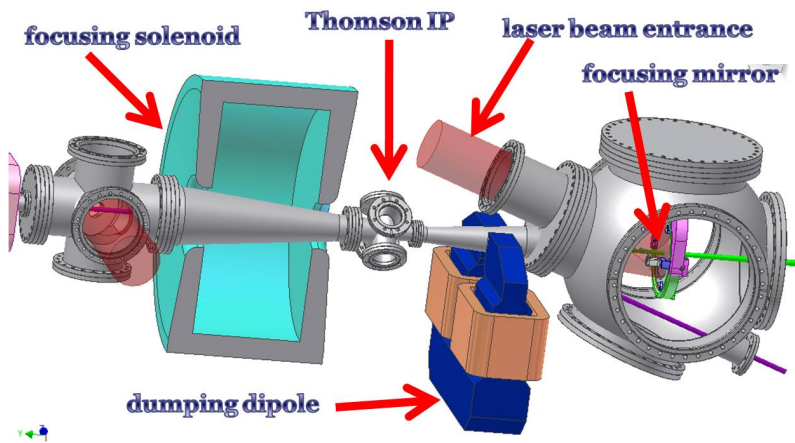


Figure 24: *3-D schematic layout of the Thomson scattering interaction chamber.*

(e.g. Cherenkov, transition radiation).

For the experiment of plasma acceleration the electron beam transport tracking has been also performed with Elegant checking the feasibility of the parameter list reported in Table 2, the results are shown in Fig. 25 and 26.

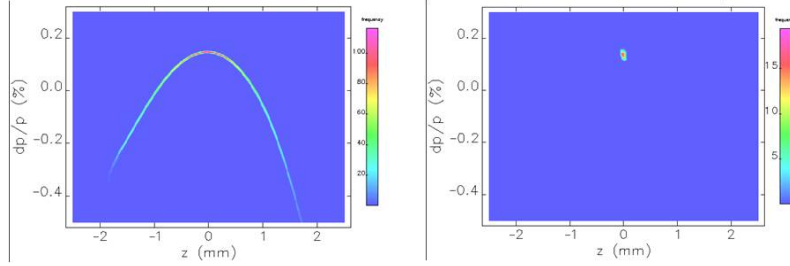


Figure 25: Longitudinal distribution of the electron beam at the exit of the photoinjector (left), and at the plasma acceleration interaction point.

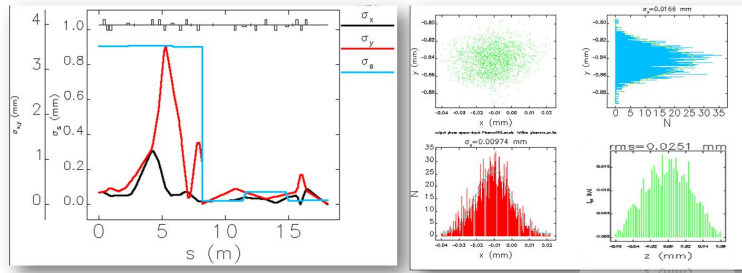


Figure 26: Evolution of the rms electron beam sizes along the transfer line (left) and at the interaction point (right).

#### 4.2 The laser beam transferline

The laser beam transfer line to the interaction region is composed by a series of high reflectivity mirrors installed in a vacuum pipe 50 m long. The mirrors, 8 inches diameter, will be supported by motorized gimbal mounts in order to assure the alignment to the off-axis parabola that focus the laser pulse on the electron beam. The design of the line has been performed with ZEMAX optical code to simulate the effect of the misalignment of the mirrors on the final spot. The coating of the individual mirror has been chosen with the best reflectivity at the work polarization that change because of the beam trajectory. All the components of the lines: mirrors, gimbal mounts, vacuum chambers, pumps etc. have been ordered.

Table 3: *List of expected laser beam parameters.*

Parameter	Value
Wavelength(nm)	800
Compressed pulse energy(J)	5
Pulse duration/bandwidth (ps/nm)	$3 \div 12(80)$
Rep.Rate(Hz)	10
Prepulses contrast	$> 10^6$
Contrast ratio at 1 ns before (ASE)	$> 10^8$
Contrast ratio at 1100 ps before	$> 10^6$
Contrast ratio of replica	$> 10^5$
Beam quality $M^2$	$\leq 1.5$
Energy stability	10%
Pointing stability ( $\mu\text{m}$ )	$< 2$
Synchronization with SPARC clock	$< 1$ ps

## References

1. L. A. Gizzi *et al.*, Il Nuovo Cimento C, **32**, 433 (2009).
2. S. Bellucci *et al.*, NTA PlasmonX, on "Annual Activity Report 2009", (2010).
3. L. A. Gizzi, E. Clark, D. Neely, L. Roso, and M. Tolley, "High repetition rate laser systems: targets, diagnostics and radiation protection" AIP Conf. Proc. The 2nd International Conference on UltraIntense Laser Interaction Science, Vol. 1209, pp. 134-143, February 2, 2010 doi:10.1063/1.3326308
4. F. Anelli *et al.*, "Design of the Test Experiment for the Sub-Petawatt Flame Laser System at LNF-Frascati: Electron Acceleration with Self-Injection (SITE)", Unpublished, October 2009.
5. L. A. Gizzi *et al.*, "Laser-Plasma Acceleration: First Experimental Results from the Plasmon-X Project", Proceedings of the 51st Workshop of the CHANNELING 2008 Conference on "Charged and Neutral Particles Channeling Phenomena", World Scientific Publishing, The Science and Culture Series - Physics, pp. 495-501, (2010), ISBN:978-981-4307-00-0.
6. L.A. Gizzi *et al.*, Abstract, Plasma Physics Conference, European Physical Society, 2011.
7. M. Galimberti, A. Giuliotti, D. Giuliotti, L.A. Gizzi, Rev. Sci. Instrum. **76**, 053303 (2005).
8. R. Faccini *et al.*, Nucl. Instr. & Meth. A **623**, 704 (2010).
9. P. Oliva *et al.*, Nucl. Instr. & Meth. A **615**, 93, (2010).
10. U. Bottigli, *et al.*, Il Nuovo Cimento **29C**, N.2, Marzo Aprile 2006.
11. W.J. Brown *et al.*, Phys. Rev. STAB **7** (2004) 060702
12. D. Alesini *et al.*, Nucl. Instr. & Meth. A **586** (2008) 133.

## THE SPARC FEL EXPERIMENTS

M. Ferrario (Resp. Naz.), D. Alesini, F. Anelli (Art. 15), A. Bacci (Art. 23), M. Bellaveglia (Art. 23), M. Benfatto, R. Boni, M. Boscolo, L. Cacciotti (Tecn.), M. Castellano, E. Chiadroni (Art. 23), P. Chimenti (Art. 15), L. Cultrera (Art. 23), G. Di Pirro, A. Drago, A. Esposito, M. Esposito (Art. 15), L. Ficcadenti (Art.23), D. Filippetto,(Art. 23), S. Fioravanti (Art.1 5), A. Gallo, G. Gatti (Art. 23), A. Ghigo, V. Lollo (Tecn.), A. Marcelli, C. Marrelli (Dott.), M. Migliorati (Ass), A. Mostacci (Ass.), E. Pace, L. Palumbo (Ass.), L.A. Rossi (Art. 15), A.R. Rossi (Art.23), M. Serluca (Dott.), R. Sorchetti (Tecn.), B. Spataro, S. Strabioli (Art. 15), S. Tomassini, C. Vaccarezza, M. Vescovi, C. Vicario (Art. 23)

### 1 Abstract

The SPARC is a collaboration between different institution, the main is ENEA, INFN, University Tor Vergata and CNR; the project foresees the realization of a free electron laser operating at 500 nm driven by a high brightness photo-injector at a beam energy of 150-200 MeV. We report hereafter the recent results obtained at SPARC, which has successfully been operated both in SASE and in seeded mode. Full SASE has been achieved by combining the velocity bunching compression technique, to increase the peak current, with an undulator tapering, to compensate the chirp in the longitudinal phase space <sup>1)</sup>. The seeded mode operation has been accomplished, both as a single amplifier and as a single stage cascade doubling the frequency of the input seed at 400 nm.

### 2 Introduction

Commissioning of the SPARC FEL initiated in autumn 2008 with the following main goals:

1. transport the beam through the vacuum chamber up to the beam dump consistently with the matching condition in the undulators;
2. characterization of the spontaneous and stimulated radiation in the undulators;
3. demonstration of velocity bunching technique in the linac with emittance compensation.

All these steps were carried out during winter 2009, with the first SASE FEL spectra obtained on February 17th <sup>7)</sup> and beam compression via velocity bunching with emittance compensation demonstrated in April 2009 <sup>8)</sup>. The study of FEL dynamics in seeded and cascaded configurations and the FEL operation with exotic beams has been the main goal in the scientific program of SPARC <sup>2, 3)</sup> during the year 2010.

In the framework of the DS4 EUROFEL collaboration, a research work plan aiming at the investigation of seeded and cascaded FEL configurations was implemented <sup>3)</sup>. The main goal was to study and test the amplification and the FEL harmonic generation process of an input seed signal such as higher order harmonics generated both in crystals and in gases. The SPARC FEL can be configured to test several seeded and cascaded FEL configurations.

In the next sections we report on the first seeding experiments exploited at SPARC and on the chirped pulse operation in SASE mode. In the Sec. 3 we analyze the FEL operation in seeded mode with the SPARC undulator arranged as a single long amplifier. In Sec. 4 we analyze the results obtained operating the FEL with a single stage HGHG cascaded configuration, with one section tuned at the seed wavelength and five undulators tuned at its second harmonic.

Furthermore the FEL has been recently operated in fully saturated conditions by combining the technique of velocity bunching for increasing the peak current <sup>4)</sup>, with the idea originally proposed in ref. <sup>1)</sup>, consisting in tapering the undulator gaps to mitigate the effect of the residual chirp and correlated energy spread resulting from the compression process. Future experiments are foreseen in the so called laser comb regime, preliminary results obtained so far will be reported in the last section.

### 3 Single Pass Seeded Amplifier

The SPARC FEL is driven by a high brightness accelerator providing a high quality beam at energies between 150 and 200 MeV. The undulator beam line is composed of six, variable gap, undulator sections (See Fig. 1).

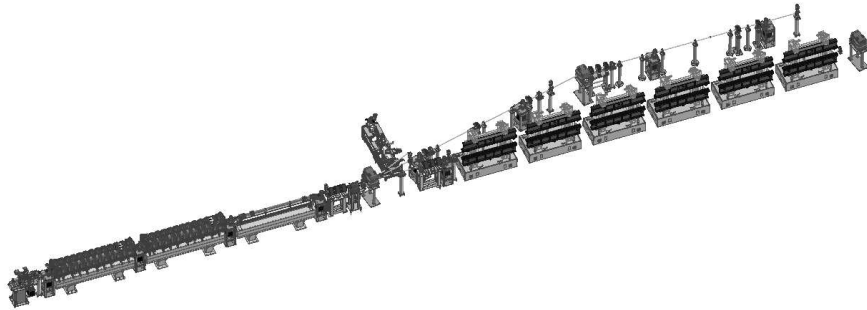


Figure 1: *Layout of the SPARC FEL test facility.*

A detailed description of the SPARC layout is given in <sup>2, 3, 4, 5, 6)</sup>. The SPARC undulators are variable gap modules of 75 periods each, with a period length of 2.8 cm and a maximum  $K=2.2$ .

The beam transport is obtained with a FODO lattice where quadrupoles in the undulator intersections provide the horizontal focusing and the undulator field provides the vertical focusing. In this condition the matching Twiss  $\beta$  parameter depends on the resonant frequency which sets the undulator field strength. The mean beam energy measured with a magnetic spectrometer installed on the transfer line leading the beam to the undulator is 177.2 MeV. A RF deflector cavity installed on the transfer line before the magnetic spectrometer allows the measure of the beam parameters as a function of the longitudinal coordinate <sup>7)</sup>. The seed used in this experiment is the second harmonics of the Ti:Sa laser, i.e.  $\lambda=401$  nm, 120 fs FWHM. The seed energy may be increased up to 150  $\mu$ J but energies below 10  $\mu$ J were sufficient for the experiments described hereafter. With the undulators tuned at the seed wavelength we match the orbit minimizing the transverse beam size and imposing that the transverse average Twiss  $\beta$  coefficients are the same in the two ( $\langle \beta_x \rangle = \langle \beta_y \rangle$ ). With these conditions we have  $\langle \beta_x \rangle = \langle \beta_y \rangle @ 1.5$  m. The analysis of the images acquired with the combined use of the deflector cavity and the spectrometer magnet allows the determination of mean energy, energy spread (slice and projected), energy chirp, bunch length and, knowing the bunch charge, measured independently, the longitudinal profile of the bunch current. A list of these parameters is presented in Tab. 1.

An in vacuum spectrometer designed and built by the LUXOR laboratory in Padova is the

Table 1: *Summary of the main beam parameters.*

Beam energy (MeV)	177.2
Energy spread (proj. %)	0.13
Energy spread (slice, %)	0.05
Length (ps - rms)	2.64
Peak current (A)	54
Emittance X (mm mrad)	2.9
Emittance Y (mm mrad)	2.5

main radiation diagnostic. The spectrometer gratings and the CCD detector have been calibrated in efficiency and yield to allow the simultaneous determination of spectral properties of the observed radiation and of the single shot pulse energy <sup>9</sup>). The spectra shown in Fig. 2 were acquired with all the undulators tuned at 400 nm, after ensuring temporal and spatial superposition between the seed and the electron beam. The vertical axis on the image represents the vertical position on the input

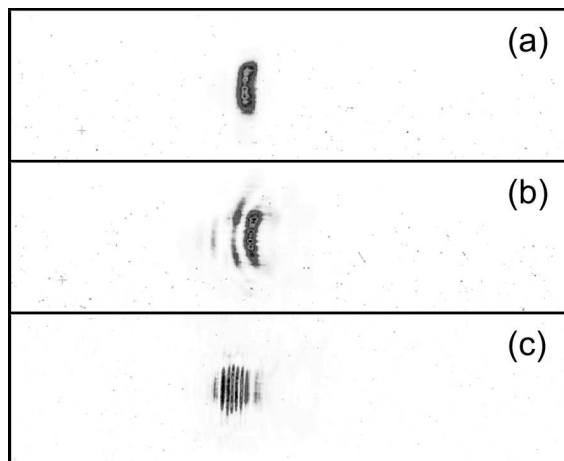


Figure 2: *Spectrum of the seeded amplifier. The horizontal axis represents the wavelength, the window range is 45 nm and the central wavelength is 400 nm. The vertical axis indicates the position on the (vertical) entrance slit of the spectrometer. The images with labels (a), (b) and (c) have been obtained with different seed energy: (a)  $E_1 0.5 \mu\text{J}$ , (b)  $E 3 \mu\text{J}$ , (c)  $E 9 \mu\text{J}$ .*

spectrometer slit, while the horizontal axis represents the wavelength. The window is centered at 400 nm and the represented wavelength range is about 45 nm. The figures Fig. 2a to Fig. 2c represent spectra obtained at different seed energy as indicated in the figure caption. The multi-peak structure, corresponding to the presence of various spectral lines, slightly red-shifted compared to the unseeded and HHG is about a factor two larger than the expected SASE bandwidth. The Pierce <sup>9</sup>) parameter should be , corresponding to a bandwidth of the order of 1.3 nm, while the spectrum in Fig. 2c is larger than 2 nm. The observed pattern, appearing at high seed energy, is completely different both in shape and in intensity from the typical SASE spiking where the number of peaks and their position change from shot to shot. The sidebands structure which appears in the spectrum at high seed energy only, is a saturation effect. This structure may be interpreted as the effect of a saturated pulse slipping forward along the electron pulse, with the radiation

emitted by fresh electrons in the pulse front, interfering with radiation out of phase produced by overbunched electrons in the rear part of the pulse. Numerical simulations have been carried out with the GENESIS 1.3 <sup>10, 11)</sup>, implemented with harmonics and with PERSEO Time Dependent code <sup>12)</sup> (PTD), taking into account the spectral overlap and three-dimensional effects, such as the transverse mismatch. An amplification of the seed in the exponential regime in the first two sections of the undulator, and superradiance in the other four ones is observed in the simulations. In order to compare the spectra with the simulations the field data generated by GENESIS have been post processed through a numerical procedure resembling the slit/grating/CCD of the spectra detection system.

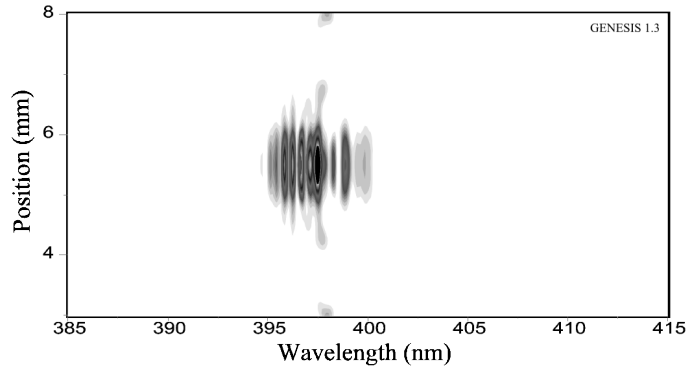


Figure 3: *GENESIS 1.3* data, obtained with the following data:  $I=65$  A ,  $\epsilon_x=2.9$  mm mrad,  $\epsilon_y=2.5$  mm mrad (norm.).

One of the results obtained is shown in Fig. 3 where the spectrum has been deduced from GENESIS 1.3, obtained with the following simulation data:  $I=65$  A ,  $\epsilon_x=2.9$  mm mrad,  $\epsilon_y=2.5$  mm mrad (normalized). The energy per pulse is  $E=50$  mJ, to be compared with the energy observed in the experiment  $E=20$  mJ with a standard deviation of 6 mJ.

Harmonics of the fundamental frequency  $l_n = l/n$  have been observed up to  $n=11$ . The spectral emission on the harmonics presents regular Gaussian shape pulse to pulse. In Fig. 4 the spectrum from 32 up to 115 nm is shown with the presence of eight harmonics from 11<sup>th</sup> up to 4<sup>th</sup> from left (in sequence: 36.18 nm, 39.8nm, 44.2 nm, 49.75 nm, 58.6 nm, 66.3 nm, 79.6 nm, 99.5 nm). Both even and odd harmonics are visible, with the odd ones slightly more intense. In Fig. 5 the spectral band from 115 up to 205.85 is shown with the presence of the second and the third harmonics (132.66 nm and 199 nm). The spatial shape seems to be similar to the unseeded emission.

The process of coherent higher order harmonics generation in this regime of operation, i.e. with a seed pulse shorter than the e-bunch length was studied in <sup>13)</sup>. The regime was originally analyzed in ref. <sup>14, 15, 16)</sup> and explored in a single pass FEL amplification experiment in <sup>17)</sup>. It is characterized by a self similar pulse amplified while it propagates through the undulator. The main reason of the expected intense harmonics emission can be found in the structure of the front side of the pulse and in the interaction with the co-propagating electron beam.

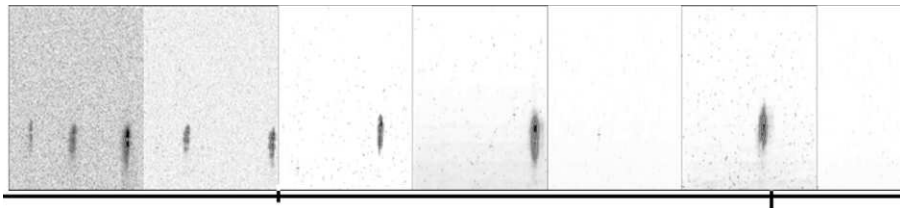


Figure 4: Spectrum from 32 up to 115 nm is shown with the presence of eight harmonics from 11<sup>th</sup> up to 4<sup>th</sup> from left (in sequence: 36.18 nm, 39.8nm, 44.2 nm, 49.75 nm, 58.6 nm, 66.3 nm, 79.6 nm, 99.5 nm).

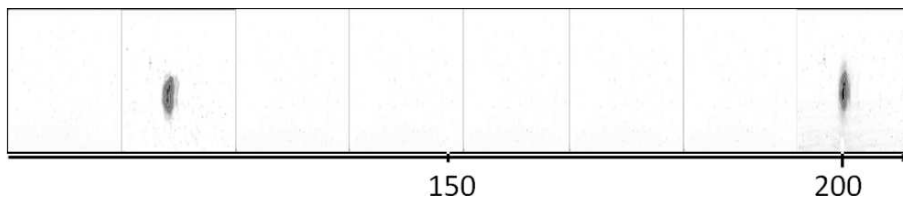


Figure 5: Spectral range from 115 up to 205.85 nm is shown with the presence of the second and the third harmonics (132.66 nm and 199 nm).

#### 4 Superradiant Cascade

Intense short seed pulses allow to test the super-radiant cascade concept <sup>13)</sup> where the seed laser power is sufficient to bring the radiation pulse close to saturation in the modulator. The pulse generated in these conditions propagates with the typical signature of superradiance in the next radiators. The six SPARC undulators may be configured in order to set up a single stage cascaded FEL based on a modulator-radiator configuration, similar to the one originally tested at BNL <sup>18)</sup>.

The number of sections playing the role of modulator and radiator may be adjusted to the intensity of the available seed. In conditions similar to the one analyzed in the previous section, we have tested the configuration composed by a single undulator tuned at 400 nm and playing the role of modulator and five undulators tuned at 200 nm as radiators

The spectrum at resonance corresponding to the shot characterized by the maximum energy is displayed in Fig. 6. The spectrum shows a structure qualitatively similar to the one shown in Fig. reffig2 suggesting that saturation is reached at this wavelength as well. As in the previous case a significant harmonic emission is expected. The spectrum of the third harmonic of the radiator is shown in Fig. 7. Several shots show energy at the 0.1  $\mu$ J level. The large fluctuation of the observed energy is associated to the beam energy jitter which affected the beam during the shift.

#### 5 SASE with a chirped beam

The SPARC layout, shown in Fig. 1, does not include a magnetic compressor. When the linac is operated in velocity bunching mode, the first linac section is tuned off crest, close to the zero crossing phase. The result is a strong chirp in the longitudinal phase space which leads to an increase of the peak current. This condition has been extensively studied at SPARC <sup>4)</sup>. Compression factors up to 17 and compensation of the emittance growth with the superposition of a magnetic field

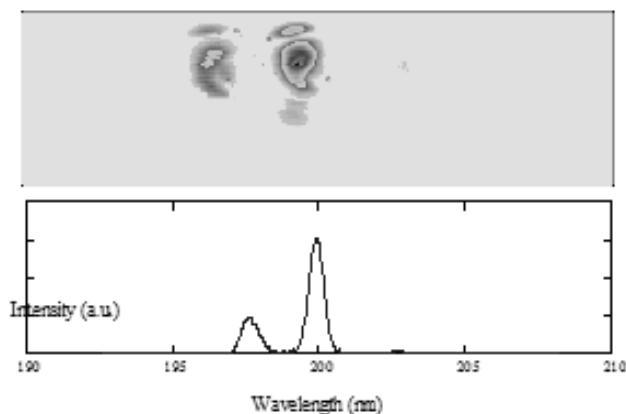


Figure 6: *Spectrum of the radiation emitted by the radiator tuned at 200 nm.*

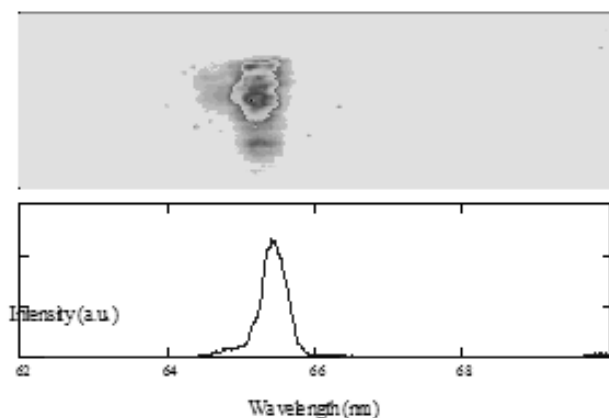


Figure 7: *Spectrum of the third harmonic of the radiator.*

on the first linac section have been demonstrated. The correlated energy spread associated to the chirp would be mitigated in a long linac by longitudinal wakes and by acceleration itself. In the SPARC case the linac is composed of three SLAC type sections only, allowing a maximum energy of about 180 MeV. In compression mode, the first section operated out of phase is not optimized for acceleration and the final energy is about 120 MeV. The linac structure, typical of an injector, is not sufficient for compensating the correlated energy spread. The phase space at the linac exit still contains a strong residual chirp and despite the high peak current which can be obtained, the detrimental effect of the chirp on the gain prevents the FEL from reaching full saturation.

The effect of the chirp on the gain can be compensated by tapering the undulator. When the beam propagates through the undulator, the slippage process leads the spike out of resonance. When the chirp is combined with an appropriate undulator taper the resonance condition can be preserved.

We have tested the effect of the tapered undulator with the SPARC FEL operating in velocity bunching mode. The central wavelength used in the experiment is 540 nm and the corresponding  $\beta$

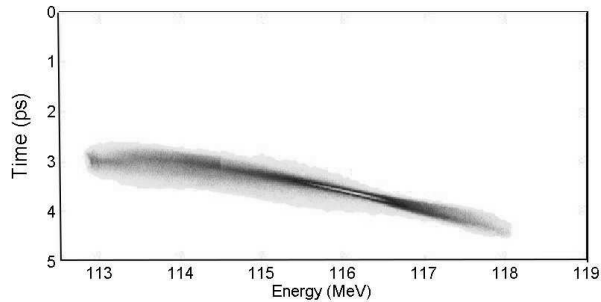


Figure 8: *Longitudinal phase space reconstruction at the exit of the linear accelerator.*

Twiss coefficient is about 1.5 m. The mean beam energy measured with the magnetic spectrometer is 116 MeV and the emittances measured with the quadrupole scan technique in the transfer line between the linac and the undulator beamline are 2.7/3.0 mm-mrad (x/y). The longitudinal phase space measured with the RF deflector cavity used in combination with the dipole spectrometer is shown in Fig. 8.

A list of the beam parameters measured before the injection of the beam in the undulator is presented in Tab. 2. The operation in compression mode, i.e. with the first linac section at a phase close to zero crossing, is very sensitive to phase drift and jitter. This is the main reason in the large uncertainty factor in the chirp figure.

Table 2: *Summary of the main beam parameters.*

Beam energy (MeV)	115.2
Energy spread (proj. %)	1.15
Energy spread (slice, %)	0.6
Chirp (keV/ $\mu\text{m}$ )	$6 \pm 1.5$
Length (ps - rms)	2.64
Peak current (A)	54

The radiation diagnostic was the same used in the experiments presented in the previous sections and it is based on the in vacuum spectrometer. In Fig. 9 it is shown a typical spectrum collected with three undulator gaps set to the resonant wavelength of 540 nm (at the mean beam energy).

The vertical structure in the spectrum image is due to the radiation diffraction caused by the vacuum pipe. With the first three undulator set at resonance and the last three undulators opened, the radiation has to propagate through about 8 m of vacuum pipe without gain guiding. The structure disappears in Fig. 10, obtained with six sections tuned at the resonance of 540 nm (un-tapered undulator).

The strong chirp in the electron bunch shows up as a broadband spectrum filling up the wavelength acceptance window of the spectrometer.

The average pulse energy obtained in these conditions is  $7.8 \mu\text{J}$ . The r.m.s. of the distribution is comparable to the mean value ( $8 \mu\text{J}$ ).

The technique used to compensate the chirp with the taper was that of progressively closing the gaps one module at the time, starting from the first one while observing the emitted spectrum. For each module we found the gap minimizing the spectral width.

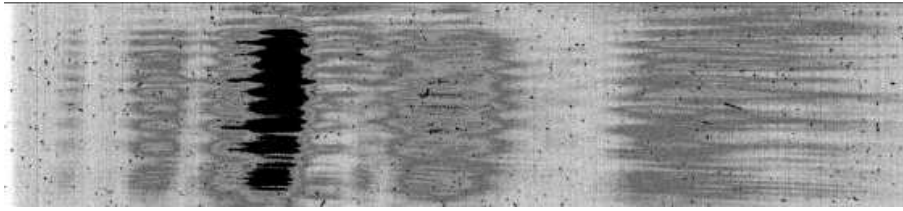


Figure 9: *Single shot spectrum acquired with three undulator closed. The vertical axis represents the vertical position at the spectrometer entrance slit. The window is centered at 540 nm and the window width is 45 nm.*

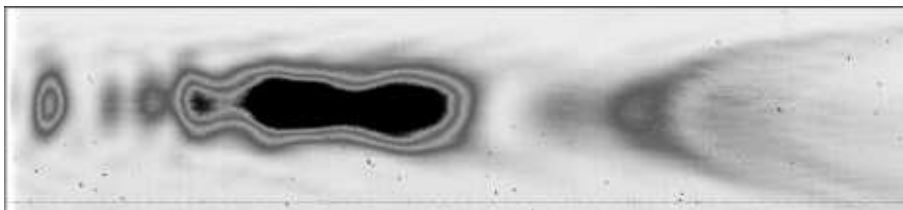


Figure 10: *As in Fig. 9, single shot spectrum acquired with six undulators set at the resonance of 540 nm.*

After the procedure, we have obtained a substantial increase of the pulse energy which reached  $140 \mu\text{J}$  with a standard deviation of about  $100 \mu\text{J}$  and a reduction of the average linewidth which was  $8 \times 10^{-3}$  averaged over 100 pulses. Several spectra in the acquired set were characterized by a spectral pattern similar to the one shown in Fig. 11, constituted by a single coherence region (no SASE spikes).

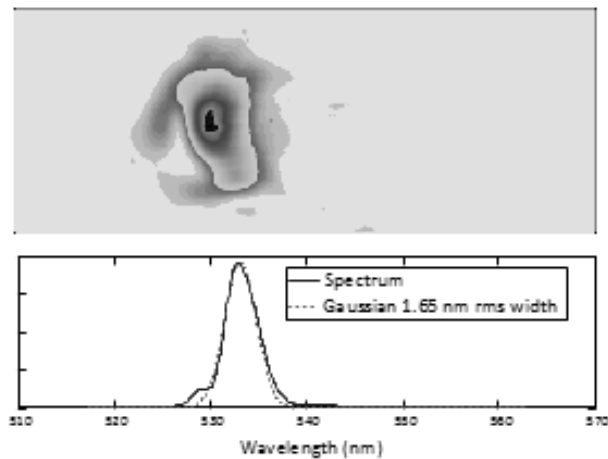


Figure 11: *Typical spectrum showing a single coherence region (single spike).*

## 6 Conclusion

The SPARC scientific activity encompasses FEL physics and beam dynamics experiments. In this report we have summarized three of the main recent achievements consisting in the observation of high harmonics emission from a single pass FEL amplifier seeded at saturation levels with an external laser, in the realization of a cascaded FEL operating above saturation with the observation of the third harmonic in the radiator and finally in the operation in SASE mode with a chirped beam compensated by the undulator taper. This is a promising way to obtain short Fourier limited radiation pulses and we have confirmed for the first time the observation of spectra without any typical SASE spiking structure.

## 7 Acknowledgments

L. Giannessi, A. Petralia, G. Dattoli, F. Ciocci, M. Del Franco, M. Quattromini, C. Ronsivalle, E. Sabia, I. Spassovsky, V. Surrenti ENEA C.R. Frascati, IT.

L. Poletto, F. Frassetto CNR-IFN, IT. J.V. Rau, V. Rossi Albertini ISM-CNR, IT.

G. Marcus, P. Musumeci, J. Rosenzweig, UCLA, CA, USA. S. Spampinati, ST, IT and University of Nova Gorica, Nova Gorica, M. Labat, F. Briquez, M. E. Couprie, SOLEIL, FR. B. Carr, M. Bougeard, D. Garzella CEA Saclay, DSM/DRECAM, FR. G. Lambert LOA, FR.

## 8 Publications

1. L. Giannessi *et al.*, “FEL Experiments at SPARC”, invited talk at the Free Electron Laser Conference, Malmoe, Sweden, 2010.
2. E. Chiadroni *et al.*, “Characterization of the THz Source at SPARC”, oral contribution, International Particle Accelerator Conference, Kyoto, Japan, 2010.
3. V. Petrillo *et al.*, “Momentum Modulations Produced by Laser-Beam Interaction at a Photocathode”, Free Electron Laser Conference, Malmoe, Sweden, 2010.
4. V. Petrillo *et al.*, “One-Dimensional FEL Equations Without the Slowly Varying Envelope Approximation”, Free Electron Laser Conference, Malmoe, Sweden, 2010.
5. L. Palumbo *et al.*, “The SPARX-FEL Project”, International Particle Accelerator Conference, Kyoto, Japan, 2010.
6. M. Migliorati *et al.*, “Microbunching and RF Compression”, International Particle Accelerator Conference, Kyoto, Japan, 2010.
7. C. Vaccarezza *et al.*, “Microbunching Instability Effect Studies and Laser Heater Optimization for the SPARX FEL Accelerator”, International Particle Accelerator Conference, Kyoto, Japan, 2010.
8. G. Gatti *et al.*, “Electron Beam Conditioning with IR/UV Laser on the Cathode”, International Particle Accelerator Conference, Kyoto, Japan, 2010.
9. M. Ferrario *et al.*, “Advanced Beam Dynamics Experiments with the SPARC High Brightness Photoinjector”, International Particle Accelerator Conference, Kyoto, Japan, 2010.
10. R. Boni *et al.*, “Beam Energy Upgrade of the Frascati FEL LINAC with a C-band RF System”, International Particle Accelerator Conference, Kyoto, Japan, 2010.

11. J.B. Rosenzweig *et al.*, “Breaking the Attosecond, Angstrom and TV/m Field Barriers with Ultra-fast Electron Beams”, International Particle Accelerator Conference, Kyoto, Japan, 2010.
12. L. Faillace *et al.*, “Experimental Characterization of the RF Gun Prototype for the SPARC-FEL Project”, International Particle Accelerator Conference, Kyoto, Japan, 2010.

Published papers are 4) and 19, 20, 21, 22)

## References

1. E.L. Saldin, E.A. Schneidmiller, and M.V. Yurkov, PRST-AB **9**, 050702 (2006).
2. M. Ferrario *et al.*, Proc. of 2009 FEL Conf, Liverpool, Jacow.
3. L. Giannessi *et al.*, Nuc. Inst. & Meth. Phys. Res. A **593**, 132-136 (2008).
4. M. Ferrario *et al.*, ”Experimental Demonstration of Emittance Compensation with Velocity Bunching“, Phys. Rev. Lett. **104**, 054801 (2010).
5. M. Quattromini *et al.*, Proceedings of EPAC08, Genoa, Italy (2008).
6. M. Quattromini *et al.*, [http : //www.frascati.enea.it/SPARC/SPARC.FEL\\_09\\_005.pdf](http://www.frascati.enea.it/SPARC/SPARC.FEL_09_005.pdf)
7. L. Ficcadenti *et al.*, Proceedings of PAC07, Albuquerque, New Mexico, USA (2007).
8. L. Giannessi *et al.*, Proc. Of 2010 FEL Conf, Malmoe.
9. J.R. Pierce, Traveling-Wave Tubes. New York: Van Nostrand, (1950).
10. S. Reiche, Nuc. Inst. & Meth. Phys. Res. A **429**, 2438 (1999).
11. L. Giannessi, P. Musumeci, New J. Phys. **8**, (2006).
12. L. Giannessi, Procs. of the 2006 FEL conference (JACOW), 91-94.
13. L. Giannessi, P. Musumeci, S. Spampinati, J. Appl. Phys. **98**, 043110 (2005).
14. R. Bonifacio, B.W.J. McNeil, P. Pierini, Phys. Rev. A **40**, 4467 (1989).
15. R. Bonifacio, N. Piovela and B.W.J. McNeil, Phys. Rev. A **44**, 3441 (1991)
16. R. Bonifacio *et al.*, Rivista del nuovo cimento **18**, 1-69 (1990).
17. T. Watanabe *et al.*, Phys. Rev. Lett. **98**, 034802 (2007)
18. L.H. Yu *et al.*, Science **289**, 932-934 (2000).
19. P. Musumeci *et al.*, “Multiphoton photoemission from a copper cathode illuminated by ultra-short laser pulses in an rf photoinjector”, Phys. Rev. Lett. **104**, 084801 (2010).
20. M. Ferrario *et al.*, ”Laser comb with velocity bunching: Preliminary results at SPARC“, Nuc. Inst. & Meth. Phys. Res. A, in press (2010).
21. M. Venturini *et al.*, “Dynamics of longitudinal phase-space modulations in an rf compressor for electron beams”, Phys. Rev. ST Accel. Beams **13**, 080703 (2010).
22. V. Petrillo *et al.*, “Analysis of single-spike FEL visible radiation from three-dimensional and realistic beams”, Nuc. Inst. & Meth. Phys. Res. A **621**, Issues 1-3, pp. 1-14 (2010).

## THE SUPERB ACCELERATOR PROJECT

M.E. Biagini (resp.), R. Boni, M. Boscolo, T. Demma, A. Drago,  
M. Esposito, S. Guiducci, G. Mazzitelli, M. Preger, P. Raimondi,  
C. Sanelli, M. Serio, A. Stella, S. Tommasini, M. Zobov

### 1 Introduction

*SuperB* is an asymmetric (6.7 GeV HER, 4.2 GeV LER)  $e^+e^-$  collider at the center of mass B pairs production energy (10.58 GeV), to be built in Italy, with a design peak luminosity of  $10^{36}$   $\text{cm}^2 \text{s}^{-1}$ . A collider like *SuperB* will open a unique window on this physics because it allows a high statistics study of the current hints of new aggregations of quarks and gluons. Besides the physics one can study in running at the  $\Upsilon(4S)$  resonance, the following alternative energies are of interest:  $\Upsilon(3S)$  (at least  $0.3 \text{ ab}^{-1}$ ) and a high luminosity scan between 4-5 GeV (5 MeV steps of  $0.2 \text{ fb}^{-1}$  each would require a total of  $40 \text{ fb}^{-1}$ ). While this is not huge statistics, this scan is only feasible with *SuperB*. The only possible competitor, BES-III, is not planning to scan above 4 GeV, since their data sample would, in any case, be lower than that of the B Factories alone. Finally, the search for exotic particles among the decay products of the "bottomonia" can probe regions of the parameters space of non-minimal supersymmetric models that cannot be otherwise explored directly, for instance at LHC.

The superiority of *SuperB* with respect to the planned upgrade of KEKB lies both in the ten times higher statistics, which broadens the range of cross sections the experiment is sensitive to, but also in the flexibility to change center of mass energy, and the possibility to collide with a polarized electron beam. Moreover the *SuperB* design will also allow for running at the  $\tau$ /charm threshold with an expected luminosity of  $10^{35} \text{ cm}^2 \text{ s}^{-1}$ .

In December 2010 the *SuperB* project, included by the Minister of Education and Research in the list of the Italian "Flagship Projects", has been funded with a preliminary 19 Meuro allocation. Fundings for as much as 50 Meuro/year in the next 5 years have been also foreseen.

In the following section the work performed at LNF on the design of the accelerator will be briefly described. LNF contribution is essential for the design and construction of *SuperB*. This activity at LNF has been funded by the INFN NTA commission, and has received by INFN a special funding in 2010.

### 2 Design strategy

The construction and operation of modern multi-bunch  $e^+e^-$  colliders have brought about many advances in accelerator physics in the area of high currents, complex interaction regions, high beam-beam tune shifts, high power RF systems, controlled beam instabilities, rapid injection rates, and reliable uptimes. The *SuperB* design is based on a novel collision scheme, the so called "large Piwinski angle and crab waist" [1, 2], which will allow to reach unprecedented luminosity with low beam currents and reduced background at affordable operating costs. A polarized electron beam will allow for producing polarized leptons, opening an entirely new realm of exploration in lepton flavor physics. The principle of operation of this scheme has been tested in 2008-2009 at the upgraded DAΦNE  $\Phi$ -Factory in Frascati with very successful results [3].

A first Conceptual Design Report (CDR) [4] was issued in May 2007, with about 200 pages dedicated to the accelerator design. A second version [5], with a more updated design, has been

published in September 2010. This report discusses site requirements, crab waist compensation scheme, parameters optimization in order to save power, IP quadrupole design, ring lattice design, Touschek backgrounds, spin rotator scheme, injection and other hardware systems, as well as project costs. The ring lattices have been designed to produce very small horizontal (a few nm-rad) and vertical emittances (a few pm-rad). The crab waist scheme, with a couple of sextupoles per ring in a dispersive section near the Interaction Region (IR), and appropriate betatron phase with respect to the IP, will create a longitudinal waist shift over the width of the beam, so allowing for a vertical beta function which is much smaller than the bunch lengths and providing suppression of betatron and synchro-betatron resonances arising from the crossing angle geometry.

*SuperB* consists of two rings of different energy (positrons in HER, 6.7 GeV, electrons in LER, 4.2 GeV) colliding in one IR at a large (60 mrad total) horizontal angle. Spin rotator sections in the LER will provide helicity of a polarized electron beam. With respect to the past years design an important change is to have polarized electrons in the LER instead of the HER. This was chosen for easier insertion of Spin Rotator (SR) sections in LER lattice. Also the beam energies have been changed in order to avoid spin resonances, with a consequent small reduction of the center-of-mass boost.

The two rings lay in the horizontal plane, each has two arcs and two long straight sections. The Final Focus (FF) in one straight is combined with the two ARCs in two half-rings (one inner, one outer) and a straight section on the opposite side. The straight section comes naturally to close the ring and readily accommodate the RF system and other necessities (e.g. injection). In this utility region crossing without collisions for the two rings will be provided.

Two sites have been considered for the construction of *SuperB* up to now: the University of Tor Vergata campus and the Frascati National Laboratories. The latter presents advantages from the point of view of the infrastructures, with the drawback of the lack of available space to allocate the whole complex inside the laboratory. A possible solution is to build *SuperB* underground both the ENEA and LNF laboratories, for this reason a shorter machine design has also been carried out. The site choice is however still an open issue, which will be solved in the first half of 2011.

### 3 Year 2010 activity

During 2010 the activity has been focused to address the most crucial aspects of the project, such as lattice design, beam dynamics studies, parameters choice, site issues. The results have been summarized in the new Progress Report [5], published in September 2010.

The lattice has been optimized to fit also the smaller LNF site, the IR re-designed to get better performances in terms of IP quadrupoles gradients, betas and aperture, and the overall optics design has been improved in terms of nonlinear behaviour. Since the very small beam coupling is one of the main design parameters of *SuperB*, work on the compensation scheme of the detector solenoidal field, main source of coupling, has also been performed. Besides the design of the IR with solenoidal magnets used for the cancelation of the detector solenoid field outside the IR, a scheme of coupling compensation at the IP with correctors and skew quadrupoles has also been studied.

Simulations of intensity related effects, such as beam-beam, electron cloud and fast ion instabilities, Intra Beam Scattering (IBS), have been updated for the new parameters and design. A new beam-beam scan of the tunes region with the *SuperB* updated parameters has shown that the resonances free region is very wide, allowing for a smooth machine operation. In particular, the reduction of the design beam-beam tune shift parameter from 0.17 to 0.1 has reduced the dangerous resonances number and pattern. In Figure 1 a comparison of the beam-beam scan for the CDR parameters (left) and the new ones (right) is shown. The red area corresponds to a peak luminosity of  $10^{36} \text{ cm}^2 \text{ s}^{-1}$ .

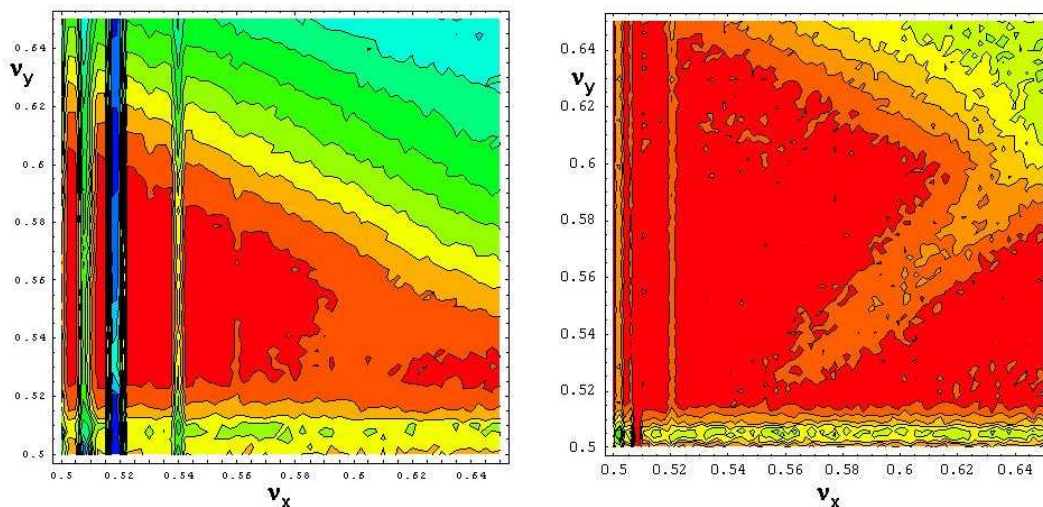


Figure 1: *Beam-beam scan. Left: old parameters [4], right: new parameters [5].*

Work on the machine magnetic lattice has continued for all 2010. The optimization of the lattice is a crucial point, since the machine performances will heavily depend on it. The LER and HER lattices are very similar, and based on the reuse of most PEP-II (SLAC) hardware. Their main difference is that the LER arc dipoles are shorter (bend radius about 3 times smaller) than in the HER in order to match the ring emittances at asymmetric beam energies. The two horizontal crossings (main and parasitic) result in each ring having one inner and one outer arc. Both the inner and outer arcs provide the same bending angle but the outer arc is made longer by increasing the drift space around the dipole magnets in order to provide the same azimuth location with the inner arc. In order to have a more compact rings design the arc cells have been further modified, keeping emittances and damping times constant. The layout has been optimized in order to fit in the LNF site, but its properties would be optimal for any site.

The ultra low vertical emittances in *SuperB*, 7 pm in the LER and 4 pm in the HER, need a careful study of the misalignment errors effects on the machine performances. Low Emittance Tuning procedures were applied to *SuperB* HER. To correct the orbit due to misalignments and tilts, Dispersion, Coupling and  $\beta$ -beating Free Steering techniques are applied, improving significantly the correction obtained using only Orbit Steering, as done in standard procedures. The aim of this work is to build a Table of tolerances for the ring magnets displacements, tilts and beam position monitor offsets, that will set the requirements for the installation of the magnetic elements and diagnostics. A new tool which combines Matlab and MADX, very fast and flexible, has been developed for the analysis of imperfections, allowing for both correction and tuning. In Figure 2 an example of the vertical emittance computed for 50 simulations with misalignment and tilts in the HER magnets, before and after the correction, is shown. The rms vertical emittance after the correction is reduced by more than 300 times (note the different horizontal scale in the two plots).

*SuperB* can be also used as a synchrotron light (SL) source with very good properties. Preliminary studies have assumed undulators characteristics as those of the NSLS-II, in construction at the Brookhaven Labs (US). A comparison of brightness and flux from bending magnets and

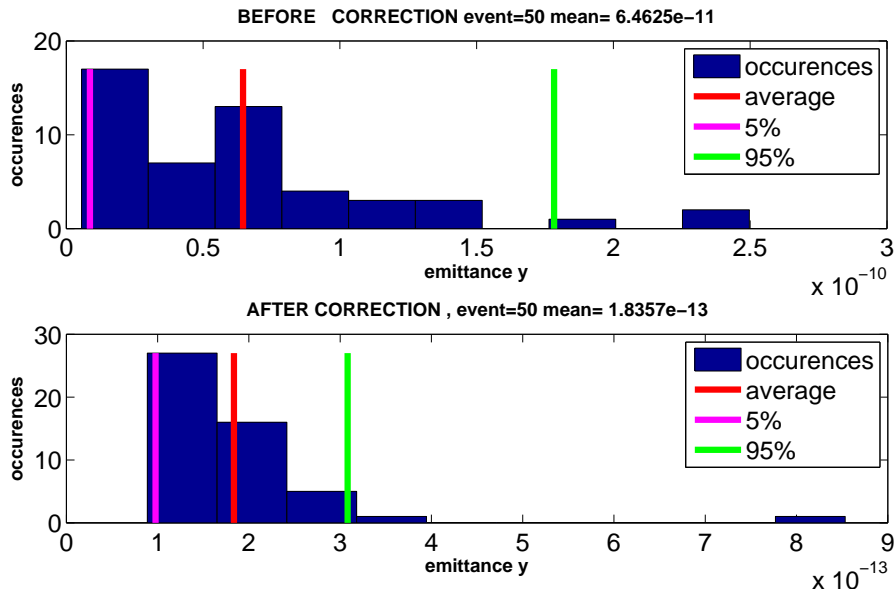


Figure 2: Vertical emittance for 50 simulations with misalignment and tilts. Top: before correction, bottom: after correction. Please note the different scale.

undulators for different energies dedicated SL sources and the *SuperBHER* and LER rings has shown that:

- synchrotron radiation generated with both HER and LER compete very well with state of the art dedicated SL in operation, construction and design;
- light properties from undulators are still better than most SL, slightly worst than PEP-X (latest generation project at SLAC, not yet funded);
- the lattices are already well optimized with respect to source point parameters;
- layout work has advanced to a point for specific choices of beam lines and site related considerations.

In Figure 3 a comparison of spectral brilliance and flux for several existing and proposed SL sources and *SuperB* is shown.

The design of the first IP SuperConducting quadrupole doublets has continued in Pisa, with the collaboration of INFN Genova experts. The design has been finalized and procurement of material has started. During 2011 two prototypes of the first quadrupole, QD0, will be built and then measured at CERN.

The injection system for *SuperB* will be capable of injecting electrons and positrons into their respective rings at full energies. At full luminosity and beam currents, up to 4 A, the HER and LER have expected beam lifetimes as low as 5 minutes. Thus, the injection process must be continuous, called top-up injection, to keep nearly constant beam current and luminosity. Multiple bunches will be injected on each linac pulse into one or the other of the two rings. Positron bunches are generated by striking a high charge electron bunch onto a positron converter target and collecting

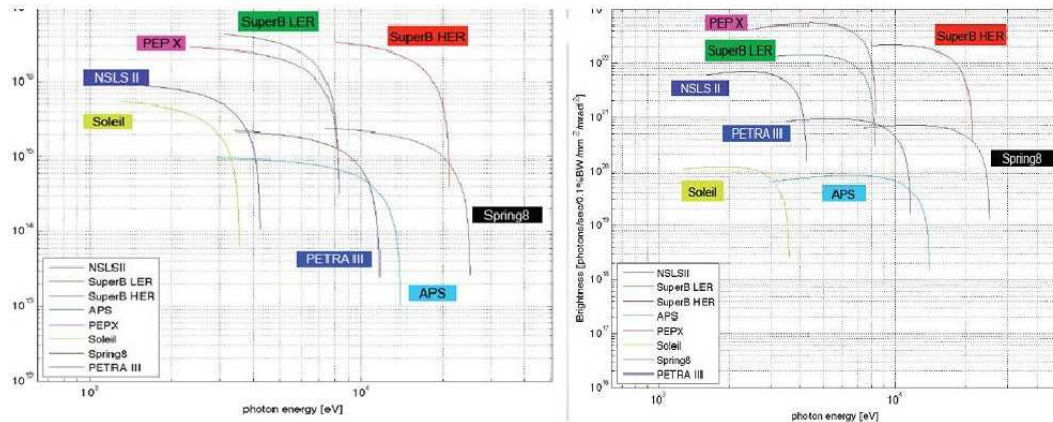


Figure 3: Comparison of spectral brilliance (right) and flux (left) for several existing and proposed SL sources and SuperB.

the emergent positrons. The transverse and longitudinal emittances of the electron bunches and, especially, of the generated positron bunches are larger than the LER and HER acceptances and must be pre-damped. A specially designed Damping Ring at 1 GeV, shared between the two particle types to reduce costs, is used to reduce the injected beam emittances. Electrons from the gun source are longitudinally polarized. The particle spins are rotated to the vertical plane in a special transport section downstream of the gun. The spins remain vertical for the rest of the injection system and injected in this vertical state into the LER. A bunch compressor system between the DR and the accelerating sections has also been designed, as well as the complete Transfer Lines for electrons at 4.2 GeV and positrons at 6.7 GeV for injection into the rings.

Work on the RF system has shown that good performances and design luminosity can be achieved, if needed, even in a "high" beam current (4 A) regime. High Order Modes in all vacuum chamber components have been simulated, with particular attention to the IP region. R&D on the bunch-by-bunch feedback system has continued, with special tests on the DAΦNE rings. The system will have better performances than the one used up to now.

Studies have started on the control of the vibrations in the FF elements, in particular in the IP quadrupole doublets. The movement of these elements would result in reduced machine performances in terms of luminosity. An IP beam feedback has been proposed, and a budget for motion of the cryostat and quadrupoles has been set in order to keep the luminosity loss less than 1 %.

A new campaign of ground motion measurements at different locations on the LNF site have been performed by the Annecy-LAPP group who has worked for the Virgo facility. All the results clearly show that the noise coming from various vibrations sources (such as traffic, air cooling, railway track...) is well attenuated in depth. These measurements will be of course repeated in case the site selected will be different from LNF.

For the site choice a "site requirements" document was prepared and an "International Site Review Committee" has been appointed. Recommendation are expected within few months and

the INFN decision will immediately follow.

Four general *SuperB* meetings have been organized in 2010: in March at LAPP (France), in June at Elba (Italy), in September at LNF (Italy) and in December at Caltech (US). A complete description of the work done is available from the meetings slides at:

<http://agenda.infn.it/categoryDisplay.py?categId=109>.

#### 4 Year 2011 activity

During 2011 the activity will be focused on the choice of the site, the project of the infrastructures needed (depending on site), and the start of the procurement phase. Theoretical work will of course continue to optimize the machine design. There will be contacts with the SLAC Laboratory for the selection of the PEP-II elements that will be reused in *SuperB*, such as the RF cavities for example. Two prototypes of the first IP quadrupole will be built, following a very original design made in Pisa, and measured at CERN.

The collaboration for the accelerator studies, formed up to now by Italy (LNF, Pisa), US (SLAC), France (CNRS), Russia (BINP), will expand with the contribution of collaborators from UK and Spain.

In the following is a list of the publications the Accelerator Division *SuperB* group has issued in the framework of the *SuperB* collaboration.

#### 5 Publications in 2010

1. M.E. Biagini, P. Raimondi *et al.*, “*SuperB* Lattice Studies”, Proc. of International Particle Accelerator Conference (IPAC10), Kyoto, Japan, 23-28 May 2010.
2. M.E. Biagini *et al.*, “Status of the *SuperB* accelerator project”, Proc. of International Particle Accelerator Conference (IPAC10), Kyoto, Japan, 23-28 May 2010.
3. T. Demma, M. Pivi, “Collective Effects in the *SuperB* Collider ”, Proc. of International Particle Accelerator Conference (IPAC10), Kyoto, Japan, 23-28 May 2010.
4. M. E. Biagini *et al.*, “Polarization in *SuperB*”, Proc. of International Particle Accelerator Conference (IPAC10), Kyoto, Japan, 23-28 May 2010.
5. M. Biagini, S. Liuzzo *et al.*, “Low Emittance Tuning Studies for *SuperB*”, Proc. of International Particle Accelerator Conference (IPAC10), Kyoto, Japan, 23-28 May 2010.
6. A. Drago *et al.*, “ *SuperB* bunch-by-bunch feedback R&D”, Proc. of International Particle Accelerator Conference (IPAC10), Kyoto, Japan, 23-28 May 2010.
7. S. Tomassini *et al.*, “Preliminary Ground Motion Measurements at LNF Site for the *SuperB* Project”, Proc. of International Particle Accelerator Conference (IPAC10), Kyoto, Japan, 23-28 May 2010.
8. *SuperB* Coll., “*SuperB* Progress Report - Accelerator”, arXiv:1009.7178v2 [physics.acc-ph] Sep. 2010.
9. M. Zobov for the *SuperB* and DAΦNE collaborations, “Crab waist approach: from DAΦNE to *SuperB*”, Proc. of RUPAC-2010-TUXHX03, Protvino, Russia, 27 Sep - 1 Oct 2010.

## 6 References

- 1 P. Raimondi, “*SuperB* design directions”, Proc. of Particle Accelerators Conference, Albuquerque, June 2007.
- 2 P. Raimondi, D. Shatilov, M. Zobov, “Beam-beam issues for colliding schemes with large Piwinski angle and crabbed waist”, LNF-07/003 (IR), January 2007.
- 3 P. Raimondi et al, “DAΦNE crab waist beam tests”, Proc. of 11th European Particle Accelerator Conference (EPAC 08), Genova, Italy, June 2008.
- 4 “*SuperB* Conceptual Design Report”, INFN/AE-07/2, SLACR-856, LAL 07-15, arXiv:0709.0451 [hep-ex] March 2007.
- 5 “*SuperB* Progress Report - Accelerator”, arXiv:1009.7178v2 [physics.acc-ph] Sep. 2010.



## *General Information*



## COMMUNICATION and OUTREACH

R. Centioni (Resp.), V. Ferretti (Art.15), L. Sabatini, S. Vannucci (Resp.)  
Scientific Information and Documentation Service

From many years, the LNF has been interested in and active in communication in the area of scientific education. Throughout the year they provide basic education in physics by means of a vast outreach program for the general public, teachers and students.

The aims of the program are various: “open the laboratories” inviting general public to be part of INFN “scientific world”; to “stimulate” the curiosity on scientific issues; to offer a more complete view of the scientific institutions operating in the area; to transfer scientific knowledge, methodology and technologies of the research; to inform people about the latest developments in physics; to enable people to acquire the knowledge and understanding of INFN research activities.

Most of the activities are organized inside LNF, such as Visits, Scientific Week, Open Days, Physics Lessons, Meetings with authors of scientific books, Concerts.

Special events are dedicated to schools:

- Incontri di Fisica course for high school teachers
- Stages for high school students

Other activities are organized outside LNF such as Seminars at school or at the public Libraries, European Researchers Night.

These activities are made possible by the enthusiastic involvement of INFN-LNF people: graduate students, postdocs, researchers, engineers and technicians.

1. **Visits** [http : //www.lnf.infn.it/edu/visite/](http://www.lnf.infn.it/edu/visite/) to LNF are a well established tradition. They consist of a brief historical presentation of the Laboratories and their activities on site and abroad and of a guided tour to the “en plein air museum” and to the experimental areas. The visits are organized for high school students (age: 17-19) and for primary and secondary schools (age: 10-14). In this last case a special program is foreseen that includes a first meeting with the students at their school to introduce the world of research and some basic concepts of modern physics followed by the visit to the LNF in small groups. The visits are requested not only by Italian schools, but also by other countries: Denmark, Austria, Czech Republic, Belgium, Germany, France, Greece, Japan, India, Taiwan, USA. Each year about 4000 people visit the LNF. It is interesting to remark that about 35% of schools that visit come back two or more times during the years, a sign of a good performance of LNF dissemination effort.
2. **Scientific week and Open Days** [http : //www.lnf.infn.it/edu/settimana/](http://www.lnf.infn.it/edu/settimana/) are organized at LNF in collaboration with the other Research Centres located in the Frascati area, Public Institutions, Cultural Associations, International non-government organizations. This type of event provides guided tours, conferences, public lectures, scientific videos. Most of the LNF employees are in action to present their research centre, answer questions and care for their guests.

LNF April 19, 2010.



Figure 1: *SPARC, Open Day 2010. (INFN-LNF Photo).*

3. **Lessons of Physics** <http://www.lnf.infn.it/edu/media/> (Care of M. Calvetti, O. Ciaffoni, G. Di Giovanni and SIDS-Communication and Outreach) are held by world leading scientists in various field of the science. Students and teachers are invited to attend the lessons which are video-registered. Slides and videos are available on the LNF website to be utilized even for lessons at school.

2010 Lessons: “I Neutrini”, Alessandro Paoloni and “La Relatività in due pillole”, Mario Calvetti.

4. **Christmas' Concert** <http://www.lnf.infn.it/edu/eventi/> is organized since 2002 in the week preceding Christmas. In the Bruno Touschek Auditorium, general public is invited to discover the laboratories in a particular evening of solidarity with local charity associations. 2010 Concert: “Teatro in Musica”, Evento artistico del CRAL INFN di Frascati, LNF December 16, 2010.



Figure 2: *Christmas' Concert 2010 (INFN-LNF Photo).*

5. **Seminars** <http://www.lnf.infn.it/edu/seminaridivulgativi/> Upon request, LNF researchers give lessons to high school students and general public. A special program is performed to-

gether with public Libraries, especially with Frascati town Library. The arguments deal with science and society or they take inspirations from scientific or fiction books and theater.

- Raggi cosmici, February 2010, LNF;
- Appunti di fisica moderna. La fisica delle particelle elementari, February 2010, Lic. Sc. Farnesina, Roma;
- La Meccanica Quantistica e i suoi misteri, March 2010, Lic. Sc. S. Cannizzaro, Roma;
- Da Galileo alla Fisica Moderna: un viaggio oltre il “senso comune”, March 2010, Lic. Sc. F. d’Assisi, Roma;
- La Fisica e l’Arte: due modi complementari per esprimere la creatività, April 2010, Lic. Sc. A. Landi, Velletri (RM);
- Il metodo scientifico e l’indagine statistica, April 2010, Lic. Sc. Calzecchi-Onesti, Fermo (MC);
- LHC: una nuova era, April 2010, Lic. Sc. P. Levi, Roma;
- Introduzione agli acceleratori di particelle e loro possibili applicazioni, April 2010, IIS Tor Marancia, Roma;
- La Meccanica Quantistica e i suoi misteri, April-May 2010, Lic. Sc. V. Volterra, Ciampino (RM);

6. **Incontro con l’Autore** [http : //www.lnf.infn.it/edu/ica/](http://www.lnf.infn.it/edu/ica/) LNF organize meeting with authors who present their scientific book to the general public, students, teachers.

“La Fisica del Tacco 12”, Monica Marelli, LNF October 8, 2010.

7. **European Researchers’ Night** [http : //www.lnf.infn.it/nottedellaricerca/](http://www.lnf.infn.it/nottedellaricerca/) is organized since 2006. The Laboratories are involved in this project organizing guided tours at LNF. This event is performed also in other european cities to promote the activities of the main research centres at international level. During all day and night are organized: experiments held by the researchers, games for children, visits to major Italian and European research laboratories, science shows, science coffees, and so on. These initiatives enable dialogue with researchers and help people to discover science through entertainment. LNF September 24, 2010.

Among the activities organized inside LNF two particular events are performed in the education program: Incontri di Fisica and Stages.

8. **Incontri di Fisica** [http : //www.lnf.infn.it/edu/idf/](http://www.lnf.infn.it/edu/idf/) is organized since 2001. It is a three-days course for high school teachers and people involved in scientific research dissemination. About 160 teachers coming from all over Italy attend each year this event. The goal is to stimulate teachers’ professional training and provide an occasion for interactive and hands-on contact with the latest developments in physics. The program consists of plenary lessons, presentation of INFN-LNF activities, visit to LNF experimental area and discussion. The peculiarity of this course is the second day entirely dedicated to the special participation in working groups (8 hours laboratory). The working groups concern arguments on INFN research (nuclear and subnuclear physics, astroparticle physics and technology). They are conducted by INFN researchers, engineers and technicians and they are held in the various experimental laboratories of LNF. Each working group consists of a theoretical lesson, hands-on activity or data analysis of a real experiment. In this way, teachers have a direct contact with researchers and they can use typical experimental instrumentation of frontier physics.

The lessons are given by speakers from INFN or from other Institutions such as Universities or other Laboratories like CERN. They concern arguments on physics or other scientific matters, application of physics and more general topics. If we only think that each teacher is in contact with about 120-130 students and their families, Incontri di Fisica represents an important occasion of dissemination of physics. Moreover, by informing them on frontier science, it is possible to introduce modern and contemporary physics in school programs. Teachers can stay in contact with INFN researchers also after the course. The evaluation of the course is performed by a questionnaire. The analysis is very useful for the study of future programs. Teachers, authorized by the Minister of Education, receive a certificate of participation. All the programs are published on LNF web site (lessons, video, photo).

LNF October 6-8, 2010. (*Organizing Committee: P. Di Nezza (Chair), M. Calvetti, P. Campana, R. Centioni, C. Curceanu, M. Dreucci, V. Ferretti, S. Miozzi, L. Sabatini, S. Vannucci, G. Venanzoni*)

9. **Stages for students** <http://www.lnf.infn.it/edu/stagelnf/> are organized since 2000 for high school students (age 18-19). Students are selected by their teachers on the basis of their curriculum but especially on the basis of their interest and motivation.

Tutors are INFN staff: researchers, engineers and technicians. They prepare the program with the following goals: to offer a special experience in an important research Institute; to transfer scientific knowledge, methodology and high level research technology; to present INFN-LNF experimental activities; to promote the teaching of modern and contemporary physics; to contact schools from all over Italy and abroad; for student orientation (university or career).

In a direct contact with their tutors (1 tutor / 2 students), students are involved in theoretical lessons and practical operations. They acquire knowledge and understanding of INFN research activities in an interactive modality. Curiosity, investigation, hands-on learning, working in *équipe* are the key words of this experience. During their stay at LNF, students are like staff members, working from 8 a.m. to 4 p.m. and they participate in the social events (e.g. lunch at the LNF canteen). At their arrival students receive educational material and general information about INFN-LNF and they visit the experimental area. Various types of stages in different periods of the year are organized.

- The Winter stages have a duration of 9 days. Students come at LNF once a week from 8 a.m. to 4 p.m. Theoretical lessons and working groups are scheduled. Winter Stages 2010 - LNF February 1-May 19, 2010 (Scientific Coordinator: C. Curceanu)
- The Stage Masterclass is organized on behalf of EPPOG Masterclasses European Project. It has a duration of 4 full days, usually during the month of February. Students, in a unique group of 40, follow lessons on modern physics and analyze data from an experiment at CERN. Stage Masterclass 2010 - LNF February 1-4, 2010 (Scientific Coordinator: F. Bossi)
- The Summer Stages are organized in June, at the end of the school year, and have a duration of 10 full days. Summer Stages - LNF June 15-26, 2010 (Scientific Coordinator: C. Bloise)

The theoretical plenary lessons are scheduled during the morning. Then, divided in small groups, students participate in various experimental activities.

At the end of the stages, students make a report of their experience. This report is presented in the LNF main auditorium during a ceremony at the presence of families, teachers and other

students. Each student receive a certificate of participation and evaluate the experience of stages by filling a questionnaire.

Tutors consider the experience of Stage very positively. They think it can be replicated also in other INFN laboratories or Research Centres.

The project phase of the stage program is very important. Tutors take into account that students belong to various schools of different italian regions so their school preparation may not be the same. They give particular importance to the use of a scientific/technical language appropriate to the educational preparation of students. Being the scientific language very peculiar, tutors recommend the explanation of the concepts not included in school programs.

Surely, it is extremely important to keep in contact with school teachers, so to better understand the preparation of students. Moreover tutors take particular care of the experimental activities which represent the real different pedagogical approach to the scientific studies

For the students the Stages are a very special occasion. They can work and study in a big research Centre and meet students from other schools. Particularly fascinating is the use of sophisticated instrumentation that is not surely available in school laboratories.

The stages offer the opportunity to know about physics but also computing and electronics and to be oriented for the university choice or career.

The interaction with the scientists is very stimulating as well as the knowledge of their work and their life. Meeting researchers of different ages, nationalities and experience, the students can understand better the role of the researcher, too often simply considered only as a person who works into a laboratory, far from the real world. Students are curious to make questions about scientists ' experiences and their reasons to become a physicist, their hobbies and passions.

Teachers note that at the end of the stage students are well oriented in a working experience different from a school one, having had the opportunity to integrate their knowledge on scientific matters. They say that students learn how the research is an enthusiastic adventure made by passion and study realized working in *équipe* on the solution of problems. Concerning science and scientists students appreciate: the importance of the scientific collaboration, to being passionate and tenacious for achieving the goals, the effort needed in the study, curiosity, and the importance of doing sacrifices.

Each school, participating in the LNF Stage program, includes it into their own Annual Training Project. This also means that schools often organize an event during which students make a report on the stage experience to their classmates and parents.

From this point of view Stages become a special initiative of diffusion of the scientific culture with a big impact on the territory: families, other students, teachers.

Regarding the university choice students who participate in the LNF stages are oriented to scientific studies in particular Engineering and Physics.

The participation in the stage program increased during these last 10 years: since 2000, 1235 students attended the stages. In the year 2000 LNF hosted 12 students from only one local school while in the year 2010, 166 students of 60 different schools all over Italy came to Frascati.

The LNF monitor the success of the various initiatives proposed mostly through questionnaires (each one specific of the event type) and also keep track of the history using dedicated databases by which it is possible to perform simple statistical analysis. The questionnaires are a valid instrument to know students' evaluation of the stages: general organization, lessons contents and exposition by the tutors, working groups, their personal considerations about

Table 1: *10 years of Stages.*

<b>Year</b>	<b>Students All over Italy</b>	<b>Schools All over Italy</b>	<b>INFN Tutors</b>
<b>2000</b>	12 (F=1; M=11)	1	7
<b>2001</b>	14 (F=3; M=11)	1	14
<b>2002</b>	57 (F=15; M=42)	8	50
<b>2003</b>	56 (F=11; M=45)	14	22
<b>2004</b>	114 (F=34; M=80)	21	25
<b>2005</b>	154 (F=42; M=112)	29	56
<b>2006</b>	161 (F=48; M=113)	46	58
<b>2007</b>	163 (F=45; M=118)	51	55
<b>2008</b>	161 (F=47; M=114)	51	63
<b>2009</b>	177 (F=40; M=137)	54	67
<b>2010</b>	166 (F=36; M=130)	60	60

the modality and the opportunity of the stages and their idea concerning university or career choice.

- Web Page** <http://www.lnf.infn.it/>In 2010 the project “LNF Web Portal for General Public” in Italian and English language, was completed. The website is a starting point, a gateway for “non expert” users to know about modern and contemporary physics so to bridge the gap from science and society. People interested in physics can follow the developments and the results of INFN-LNF experiments and international collaborations. Students, teachers and general public may have access to useful information on educational programs and scientific cultural events (tutor lessons, videos, photos, student reports, information and educational material).

Table 2: *Number of participants to LNF events during 2010.*

<b>EVENTS 2010</b>	<b>PARTICIPANTS</b>
Visits	2273
Scientific Week an Open Days	582
Lessons of Physics	110
Christmas' Concert	180
Seminars (at LNF and outside)	1000
European Researchers' Night	220
Incontri di Fisica for high school teachers	149
Stages for high school students	166

### **Acknowledgments**

Thanks to LNF Director, Heads of Accelerator, Research and Technical Divisions. Special thanks to all INFN-LNF Tutors and Services staff.

## CONFERENCES, WORKSHOPS and MEETINGS

International conferences, workshops and meetings hosted and/or organized by LNF:

1. International Conference on *XXIV Rencontres de Physique de La Valle d'Aoste*, La Thuille, 28 February - 5 March, 2010.
2. Workshop on *Microbunching Instability III*, LNF 24 - 26 March, 2010.
3. Workshop on *LighTnet Dissemination*, LNF 29 March - 2 April, 2010.
4. Workshop on *Comunicare Fisica*, LNF 12 - 16 April, 2010.
5. LNF Spring School *Bruno Touschek*, LNF 10 - 14 May, 2010.
6. Workshop on *La fisica nella società italiana*, LNF 20 May, 2010.
7. Workshop on *Vulcano 2010 - Frontier Objects in Astrophysics and Particle Physics*, Vulcano 24 - 29 May, 2010.
8. *LNF Institute 2010-Spring Session*, LNF 24 May -10 June 2010.
9. International Symposium on *Lattice 2010*, Villasimius, 14 -19 June 2010.
10. *Iniziativa di Fisica Astroparticellare "INIFA 2010"* Meeting, LNF 22-23 June, 2010.
11. *ECFA2010* Meeting, LNF 1-2 July, 2010.
12. *Quark Matter Italia* Course, LNF 21 - 23 July, 2010.
13. *Nanoscience & Nanotechnology 2010*, LNF 20 - 23 September, 2010.
14. *XIV SuperB* General Meeting, LNF 27 September - 1 October, 2010.
15. International Conference *Channeling 2010*, Ferrara 3 - 8 October, 2010.
16. Workshop on *Heavy Quarks & Leptons*, LNF 11 - 15 October, 2010.
17. Workshop on *Probing Strangeness in Hard Processes*, LNF 18 - 21 October, 2010.
18. *Bruno Touschek Memorial Lectures*, LNF 30 November, 2010;
19. Workshop on *LC10 - New Physics: complementarities between direct and indirect searches*, LNF, 30 November - 3 December, 2010.

## FRASCATI PUBLICATIONS

Available at [www.lnf.infn.it](http://www.lnf.infn.it)

### 1 – Frascati Physics Series

#### Volume XLVIII

*First Young Researchers Workshop “Physics Challenges in the LHC Era” 2009*

Ed. E. Nardi

Frascati, May 11th and May 14th, 2009

ISBN 978-88-86409-57-5

#### Volume XLIX

Proceedings of the Workshop on Monte Carlo’s, Physics and Simulations at the LHC

Ed. P. Nason

Frascati, February 27-28, 2006

ISBN 978-88-86409-58-2

#### Volume L - Special Issue

*Les Rencontres de Physique de la Valle d’Aoste – Results and Perspectives in Particle Physics*

Ed. M. Greco

La Thuile, Aosta Valley, March 1-7, 2009

ISBN 978-88-7438-053-4

#### Volume LI

Second Young Researchers Workshop Physics Challenges in the LHC Era 2010

Ed. E. Nardi

Frascati, May 10th and May 13th, 2010

ISBN 978-88-86409-60-5

#### Volume LII– Special Issue

*Les Rencontres de Physique de la Vallée d’Aoste – Results and Perspectives in Particle Physics*

Ed.: M. Greco

La Thuile, Aosta Valley, February 28, March 6<sup>th</sup>, 2008

ISBN 978-88-7438-060-8

### 2 – LNF Frascati Reports

#### LNF - 10 / 1(P)

S. Bartalucci, V. Angelov

*Optimization of a Linac-Based Neutron Source for Time-of-Flight Measurements*

Submitted to Nucl. Inst. & Methods in Physics Research

#### LNF - 10 / 2(P)

M. Cordelli, R. Habel, A. Martini, L. Trasatti

*PORFIDO: Oceanographic Data for Neutrino Telescopes*

Submitted to Nuclear Inst. & Meth. A

**LNF - 10 / 3(P)**

KLOE-2 Collaboration: F. Archilli, D. Badoni, D. Babusci, G. Bencivenni, C. Bini, C. Bloise, V. Bocci, F. Bossi, P. Branchini, A. Budano, S. A. Bulychjev, P. Campana, G. Capon, F. Ceradini, P. Ciambrone, E. Czerwinski, E. Dan'è, E. De Lucia, G. De Robertis, A. De Santis, G. De Zorzi, A. Di Domenico, C. Di Donato, B. Di Micco, D. Domenici, M. Dreucci, O. Erriquez, G. Felici, S. Fiore, P. Franzini, P. Gauzzi, S. Giovannella, F. Gonnella, E. Graziani, F. Happacher, B. Hoistad, E. Iarocci, M. Jacewicz, T. Johansson, A. Kupsc, V. V. Kulikov, L. Kurdadze, J. Lee Franzini, F. Loddo, M. A. Martemianov, M. Martini, M. A. Matsyuk, D. Mchedlishvili, R. Messi, S. Miscetti, G. Morello, D. Moricciani, P. Moskal, F. Nguyen, V. Patera, A. Passeri, L. Quintieri, A. Ranieri, P. Santangelo, I. Sarra, M. Schioppa, B. Sciascia, A. Sciubba, M. Silarski, M. Tabidze, C. Taccini, L. Tortora, G. Venanzoni, R. Versaci, W. Wislicki, M. Wolke, J. Zdebik and A. Balla, S. Cerioni, M. Gatta, N. Lacalamita, S. Lauciani, R. Liuzzi, M. Mongelli, A. Pelosi, M. Pistilli, V. Valentino  
*Technical Design Report of the Inner Tracker for the KLOE-2 experiment*  
<http://arxiv1.library.cornell.edu/abs/1002.2572>

**LNF - 10 / 4(P)**

L. Benussi, S. Bianco, S. Colafranceschi, F.L. Fabbri, D. Piccolo, G. Saviano, A.K. Bhattacharyya, A. Sharma  
*A New Approach in Modeling the Response of RPC Detectors*  
Submitted to Journal of Instrumentation

**LNF - 10 / 5(IR)**

M. Benfatto, S. Bianco, F. Bossi, V. Chiarella, S. Dell'Agnello, R. de Sangro (WG Chair), P. Di Nezza, M. L. Ferrer, E. Pace, L. Pellegrino, R. Ricci, F. Ronchetti, F. Terranova, E. Vilucchi  
*Feasibility Study for the Realization of a Scientific Computing Service at the Laboratori Nazionali di Frascati of INFN – Report of the Scientific Computing Service Working Group*

**LNF - 10 / 6(IR)**

AA VV  
*SPARX-FEL – Technical Design Report (Version 2.00) Version 2.00*

**LNF - 10 / 7(P)**

E.N. Tsyganov (communicated by S.B. Dabagov)  
*DD Fusion in Crystals*  
Accepted for publication in Russian Journal Nuclear Physics , Yadernaya Fisika

**LNF - 10 / 8(P)**

A. Marcelli, Wei Xu, D. Hampai, L. Malfatti, P. Innocenzi, U. Schade, and Z. Wu  
*Infrared and X-ray Simultaneous Spectroscopy: A Novel Conceptual Beamline Design for Time Resolved Experiments*  
Submitted to Analytical and Bioanalytical Chemistry (2010)

**LNF - 10 / 9(IR)**

L. Marchitto, L. Allocca, D. Hampai, and S.B. Dabagov  
*X-Ray Refraction 3D-Simulation Software: First Approach*

**LNF - 10 / 10(P)**

L. Allocca, L. Marchitto, S. Alfuso, D. Hampai, G. Cappuccio, S. B. Dabagov

*Polycapillary X-Ray Imaging of a Gasoline Spray*

Presented at the ICXOM 20th, Karlsruhe, (2009). Accepted for AIP Proc. (in short version)

**LNF - 10 / 12(IR)**

B. Azadegan, and S.B. Dabagov

*Spectral Characteristics of Planar Channeling Radiation by 20-800 MeV Electrons in a Thin Silicon Carbide*

**LNF - 10 / 13(IR)**

L. Benussi, S. Bianco, A. Ceccarelli, P. Gianotti, L. Passamonti, D. Pierluigi, A. Russo, A. Tiburzi  
*Construction and Test of a Prototype of Segmented Straw*

**LNF - 10 / 14(P)**

KLOE-2 Collaboration: F. Archilli, D. Badoni, D. Babusci, G. Bencivenni, C. Bini, C. Bloise, V. Bocci, F. Bossi, P. Branchini, A. Budano, S. A. Bulychjev, P. Campana, G. Capon, F. Ceradini, P. Ciambrone, E. Czerwinski, E. Dan'è, E. De Lucia, G. De Robertis, A. De Santis, G. De Zorzi, A. Di Domenico, C. Di Donato, B. Di Micco, D. Domenici, M. Dreucci, O. Erriquez, G. Felici, S. Fiore, P. Franzini, P. Gauzzi, S. Giovannella, F. Gonnella, E. Graziani, F. Happacher, B. Hoistad, E. Iarocci, M. Jacewicz, T. Johansson, A. Kupsc, V. V. Kulikov, L. Kurdadze, J. Lee Franzini, F. Loddo, M. A. Martemianov, M. Martini, M. A. Matsyuk, D. Mchedlishvili, R. Messi, S. Miscetti, G. Morello, D. Moricciani, P. Moskal, F. Nguyen, V. Patera, A. Passeri, L. Quintieri, A. Ranieri, P. Santangelo, I. Sarra, M. Schioppa, B. Sciascia, A. Sciubba, M. Silarski, M. Tabidze, C. Taccini, L. Tortora, G. Venanzoni, R. Versaci, W. Wislicki, M. Wolke, J. Zdebik and A. Balla, S. Cerioni, M. Gatta, N. Lacalamita, S. Lauciani, R. Liuzzi, M. Mongelli, A. Pelosi, M. Pistilli, V. Valentino

*Technical Design Report of the gamma gamma Taggers for the KLOE-2 Experiment*

**LNF - 10 / 15(IR)**

AA VV

*Annual Report 2009*

**LNF - 10 / 17(P)**

D. Babusci, C. Bini, F. Bossi, G. Isidori, D. Moricciani, F. Nguyen, P. Raimondi, G. Venanzoni, D. Alesini, F. Archilli, D. Badoni, R. Baldini-Ferroli, M. Bellaveglia, G. Bencivenni, M. Bertani, M. Biagini, C. Biscari, C. Bloise, V. Bocci, R. Boni, M. Boscolo, P. Branchini, A. Budano, S.A. Bulychjev, B. Buonomo, P. Campana, G. Capon, M. Castellano, F. Ceradini, E. Chiadroni, P. Ciambrone, L. Cultrera, E. Czerwinski, E. Dane', G. Delle Monache, E. De Lucia, T. Demma, G. De Robertis, A. De Santis, G. De Zorzi, A. Di Domenico, C. Di Donato, B. Di Micco, E. Di Pasquale, G. Di Pirro, R. Di Salvo, D. Domenici, A. Drago, M. Esposito, O. Erriquez, G. Felici, M. Ferrario, L. Ficcadenti, D. Filippetto, S. Fiore, P. Franzini, G. Franzini, A. Gallo, G. Gatti, P. Gauzzi, S. Giovannella, A. Ghigo, F. Gonnella, E. Graziani, S. Guiducci, F. Happacher, B. Hoistad, E. Iarocci, M. Jacewicz, T. Johansson, W. Kluge, V.V. Kulikov, A. Kupsc, J. Lee Franzini, C. Ligi, F. Loddo, P. Lukin, F. Marcellini, C. Marchetti, M.A. Martemianov, M. Martini, M.A. Matsyuk, G. Mazzitelli, R. Messi, C. Milardi, M. Mirazzita, S. Miscetti, G. Morello, P. Moskal, S. Meller, S. Pacetti, G. Pancheri, E. Pasqualucci, A. Passeri, M. Passera, V. Patera, A.D. Polosa, M. Preger, L. Quintieri, A. Ranieri, P. Rossi, C. Sanelli, P. Santangelo, I. Sarra, M. Schioppa, B. Sciascia, M. Serio, F. Sgamma, M. Silarski, B. Spataro, A. Stecchi, A. Stella, S. Stucci, C. Taccini,

S. Tomassini, L. Tortora, C. Vaccarezza, R. Versaci, W. Wislicki, M. Wolke, J. Zdebik, M. Zobov  
*Proposal for taking data with the KLOE-2 detector at the DAPHNE collider upgraded in energy*

**LNF - 10 / 18(IR)**

S. Bartalucci

*Potenzialit di una Sorgente di Neutroni per Misure di Tempo di Volo da Installare su Spar-X*

**LNF - 10 / 19(P)**

D. Babusci, G. Dattoli, E. Sabia *Operational Methods and Lorentz-Type Equations of Motion*  
<http://arxiv.org/abs/1009.3818>

**LNF - 10 / 20(IR)**

G. Baffone

*CMS Trapezoidal GEM Foils Structural Analysis*

**LNF - 10 / 22(IR)**

O.V. Bogdanov, and S.B. Dabagov

*On Moderate Energy Electron Dechanneling in Thick Si Crystals*

**LNF - 10 / 23(IR)**

G. Franzini, D. Pellegrini, A. Stella, M. Pezzetta, M. Pallia

*Caratterizzazione preliminare del sistema di misura di campo magnetico del B-TRAIN di CNAO*

**LNF - 10 / 24(NT)**

detail S. Bianco, S. Colafranceschi, F. Felli, T. Greci, L. Passamonti, D. Pierluigi, C. Pucci, A. Russo, G. Saviano

*Material Studies for the RPC Muon Detector of CMS*

**LNF - 10 / 25(IR)**

G. Venanzoni, D. Babusci, M. Bertani, C. Bloise, F. Bossi, A. Clozza, A. Drago, A. Gallo, G. Isidori, C. Milardi, M. Mirazita, D. Moricciani, A. Passeri, M. Preger, P. Raimondi, C. Sanelli, B. Spataro, S. Tomassini, M. Zobov, *et. al.* (the total list of autors is reported in the last page of the document)

*A High-Luminosity  $e^+ e^-$  Collider for Precision Experiments at the GeV scale*

### 3 – INFN Reports

#### INFN / AE– / 10 / 1

R. Bertoni, A. Blondel, M. Bonesini, G. Cecchet, A. de Bari, J.S. Graulich, Y. Kharadzov, M. Rayner, I. Rusinov, R. Tsenov, S. Terzo, V. Verguilov  
*The Design and Commissioning of the MICE Upstream Time-of-Flight System*  
Submitted to Nuclear Instr & Meth. A

#### INFN / TC–10 / 1

H. Riahi, F. Vella  
*Installation and Configuration of dCache Storage System with INFN GRID Profile for gLite Middleware*

#### INFN / TC–0 / 2

L. Mauro, Bonardi, F. Groppi, S. Manenti, E. Rizzio, E. Sabbioni  
*Nuclear Chemistry, Radiochemistry, Radiation Chemistry, Health Physics and Sustainable Nuclear Energy Production*

#### INFN / TC–10 / 3

M. Bonari, F. Groppi  
*Production of Nuclear Hydrogen Nu2 or Hydricity by High Temperature Nuclear Reactor*

#### INFN / TC–10 / 4

M. Bonardi F. Groppi  
*Presente e Futuro nell'utilizzo delle Risorse Energetiche Nucleari con una Valutazione di Rischi e Benefici: L'Anomalia del Caso Italiano*

#### INFN / TC–0 / 5

F. Odorici, M. Cuffiani, L. Malferrari, R. Rizzoli, G. P. Veronese, S. Gammino, L. Celona, D. Mascali, N. Gambino, R. Miracoli, G. Castro, F. P. Romano, T. Serafino, F. Di Bartolo, V. Guglielmotti, S. Orlanducci, V. Sessa, M. L. Terranova  
*The Cantos Experiment: a Carbon Nanotubes Based Electron Gun to Improve the Performances of the Electron Cyclotron Resonance Ion Sources*  
Presented at the 12th Topical Seminar on Innovative Particle and Radiation Detectors (IPRD10), 7 - 10 June 2010, Siena, Italy

#### IINFN / TC–10 / 6

V. Scanziani, M. L. Bonardi, F. Groppi, S. Manenti, P. Pierini  
*La Trasmutazione delle Scorie Nucleari per la Chiusura del Ciclo dell'Energia Nucleare*  
da: Relazione dal Corso di Radiochimica di UNIMI, 2009

#### INFN / CCR–09 / 1

S. Parlati, P. Spinnato  
*Indagine sui Servizi Offerti dai Servizi Calcolo dell'INFN*

#### INFN / CCR–09 / 2

A. Ciampa, E. Vicari  
*rogetto Cluster GRID CSN4: La Proposta di PISA*

**INFN / CCR-09 / 3**

A. Crescente, M. Michelotto  
*HEP-SPEC06 - Guida All'uso*

**INFN / CCR-09 / 4**

A. Brunengo, A. De Salvo, D. Di Bari, G. Donvito, R. Gomezel, P. Lo Re, G. Maron, E. Mazzoni,  
A. Spanu, S. Zani  
*Valutazione di Apparati di Aggregazione e di Edge Routing per i TIER2 INFN*

**INFN / CCR-09 / 5**

A. Brunengo, A. De Salvo, D. Di Bari, G. Donvito, R. Gomezel, P. Lo Re, G. Maron, E. Mazzoni,  
M. Morandin, A. Spanu, S. Zani  
*Valutazione di Apparati di Aggregazione e di Edge Routing per i TIER2 INFN*

**INFN / CCR-09 / 6**

A. Ciampa, S. Arezzini, D. Fabiani, E. Mazzoli  
*Alcune Tecniche per Grid e Dintorni*

## SEMINARS

Giancarlo Piredda 19-01-2010	INFN Roma <i>First results from the MEG experiment</i>
Alfredo Dupasquier 20-01-2010	Politecnico Milano <i>New Physics with intense positron beams</i>
Hypolito J. Kalinowsky 26-01-2010	UTFPR Curitiba, Brazil <i>The 2009 Nobel Prize on Fiber Optics and its Origins</i>
Eugenio Coccia 10-02-2010	Tor Vergata University <i>Gravitational wave detection: state of the art</i>
Andreas Nyffeler 11-02-2010	Harish-Chandra Research Institute, Allamabad, India <i>Theory of the muon g-2: some recent developments</i>
S.H. Lau 22-02-2010	Xradia Inc. California, USA <i>Advances in Laboratory based computed tomography for multiscale imaging, with resolution from mm to the nm domain</i>
Roberto Coisson 26-02-2010	Parma University <i>Radiazione di Sincrotrone nell'infrarosso lontano</i>
Avetis Abel Sadoyan 31-03-2010	Erevan State University, Armenia <i>Gravitational waves from isolated compact objects</i>
Philip Schuster 14-04-2010	SLAC National Accelerator Laboratory, USA <i>Collider and fixed target experiments in search for a light vector boson</i>
Aliaksandr Pranko 20-04-2010	Fermi National Accelerator Laboratory, USA <i>New and old Physics with Diphotons</i>
Alexander Chao 4-05-2010	SLAC National Accelerator Laboratory, USA <i>Gravitational Instability of a Nonrotating Galaxy</i>
Nelson M. Carreira 18-05-2010	Instituto Superior Tecnico Portugal, Portugal <i>A plasma source for laser-plasma accelerators</i>
Livia Ludhova 20-5-2010	INFN Milano <i>Observation of geo-neutrinos with Borexino</i>
Marco Galimberti 27-05-2010	Central Laser Facility Science Tech., United Kingdom <i>High power laser systems at the central laser facility</i>
David Edward Jaffe 1-06-2010	BNL, USA <i>Measurement of <math>K^+ \rightarrow \pi^+ \nu, \bar{\nu}</math> at Fermilab</i>
Zisis Papandreou 30-06-2010	University of Regina, Canada <i>The GlueX experiment: Construction is underway</i>
Andrei Afanasev 15-07-2010	Hampton University-Jefferson Laboratory, USA <i>Electromagnetic form Factors of the nucleon and two-photon Exchange Effects</i>

- Jianming Bian  
20-07-2010  
IHEP, Beijing, China  
*Recent results of BESIII experiment*
- Giacomo M. D'Ariano  
9-9-2010  
University Pavia  
*Special relativity from quantum theory: simulation of quantum fields by a Quantum Computer as a new type of QFT*
- C. Christian Poll  
14-09-2010  
Fermi National Accelerator Laboratory, USA  
*Precision precession: how the history of  $g-2$  wound its way to Fermilab*
- Jozef Piotrowski  
21-09-2010  
VIGO System S.A., Ozarow Mazowiecki, Poland  
*Fast and sensitive long wavelength photodetectors operating without crycooling*
- V.V. Sagaradze  
27-09-2010  
Russian Academy of Sciences, Russian Federation  
*What is in the Earth's core? An experimental and thermodynamic study*
- Aram Kotzinian  
21-10-2010  
Torino University  
*Preasymptotic effects in extraction of strange quark polarization*
- Franz Schafers  
11-11-2010  
HZB - Berlin, Germany  
*Multilayer-based soft-X-ray polarimetry*
- Carlo Gustavino  
24.11.2010  
LNGS, L'Aquila  
*The LUNA experiment at LNGS*
- Beatrix Hiesmayr  
2-12-2010  
Wien University, Austria  
*Testing Bertlmann socks and other quantum features at KLOE2*
- Kiyoshi Hayasaka  
14-12-2010  
Nagoya University, Japan  
*Recent results for  $\tau$  LFV decays from Belle*
- Peter A. Lukin  
13-12-2010  
BINP, Novosibirsk, Russian Federation  
*Measurement of  $\phi(1020)$  meson leptonic width with CMD-2 detector at VEPP-2M collider*

**BRUNO TOUSCHEK MEMORIAL LECTURES 2010**

Mario Graco 30/11/2010	Roma Tre University <i>Nicola Cabibbo and Frascati</i>
Giorgio Bellettini 30/11/2010	Pisa University <i>CDF Physics at the Fermilab collider</i>
Lyndon Evans 30/11/2010	CERN, Geneva, Switzerland <i>The Large Hadron Collider</i>
Jonathan R. Ellis 30/11/2010	CERN, Geneva, Switzerland <i>Perspectives for new physics at the LHC and beyond</i>
Jean Pierre Delahaye 30/11/2010	CERN, Geneva, Switzerland <i>Review of New Accelerator Projects for the future of High Energy Physics</i>
Francois Richard 30/11/2010	LAL, Orsay, France <i>A global project for the future linear collider</i>

## THE GENERAL SERVICES AND TECHNICAL DIVISION

M. Arpaia, G. Bernardi, G. Bisogni, F. Bocale, M. Campoli, P. Caponera,  
B. Casagrande, A. Cassarà (Art. 15), G. Catitti, A. Ceccarelli, P. Celli, O. Cerafogli,  
A. Chiarucci, A. Clozza, V. Crisanti, A. De Paolis, A. Donkerlo, G. Ferretti,  
M.A. Franceschi, C. Fusco, M. Giorgi, E. Iacuesa, L. Iannotti, M. Marchetti, U. Martini,  
M. Meli, S. Monacelli, A. Giovanni, M. Monteduro, T. Napolitano (Art. 23), A. Olivieri,  
P. Panattoni, E. Passarelli, L. Pellegrino, R. Ricci, A. Riondino, M. Rondinelli,  
M. Rossi, U. Rotundo (Art. 23), M. Ruggeri, C. Sanelli (Head, Tech. Div.),  
F. Sanelli, A. Saputi, A. Sorgi, A. Tacchi, A. Tiburzi, R. Tonus, R. Valtriani

### 1 Introduction

The General Services and Technical Division was created in February 2009 and started to operate in April 2009. The year 2010 has been the first fully operational year of the Division.

The Division has collected some Departments from other LNF Divisions. More in detail, the Mechanical Design and Construction Department from the Research Division, the Electrical Installation Department and Heating, Ventilation and Air Conditioning Department from the Accelerator Division. In addition, the following departments, which in the past reported directly to the LNF Director, were collected in this new Division: the Building Management Department, the Central Stores and Purchasing Department and the General Services Department. A Secretariat was also created to take care of the many and various requests and activities relating to the General Services and Technical Division. The main task of the Division is the facility management of the Frascati Laboratories, but at the same time the Division must guarantee all the needed support to research activities, mainly in the field of mechanics, electrical systems and HVAC systems. However, the Division can also give support in the fields of vacuum and diagnostics systems, magnets and power electronics for accelerating machines.

During 2010, about 1/3 in terms of the Division's budget has been dedicated to activities strictly related to scientific activities, e.g. for DAΦNE, KLOE-2, SPARC, FLAME, PLASMON-X, OPERA, Super-B, CUORE, AMADEUS, ETRUSCO and many other projects and Physics experiments. A special mention must be given to the CNAO project, the hadron-therapy centre based on a synchrotron accelerator, in Pave, which is now under commissioning following the years of design and construction, and which will start the first phase of experimentation with the irradiation of the first sample of patients very soon. The other 2/3 of the Division budget was dedicated to the facility management of the LNF infrastructures, including some general activities of particular interest for the personnel, like the nursery, the bar and canteen, buses, etc.. A more detailed description of the activities of each Division Department follows.

### 2 General Services

The General Services Dept. of LNF deals with the organization and management of the general operation activities of LNF and Central Administration of INFN, such as:

1. ENEA Canteen + Bar/Canteen LNF.
2. Cleaning Service.
3. Guards Service.
4. Gardening Service.
5. Porterage.

6. Purchasing of new and recycling of old furniture.
7. Nursery.
8. Buses.
9. Coffee breaks and lunches
10. Deratization and pest control.
11. Purchasing of Hygienic materials and rental of no-dust carpet.
12. Purchase and laundry of working clothes.
13. Rental of drinking water dispensers.
14. Microbiological analysis on food and equipment of the LNF bar.
15. Lease, insurances, maintenance and documentation of LNF vehicles.
16. Identification badges for staff & guests.
17. Liaisoning with the City of Frascati for licenses, authorizations and taxes.
18. Liaisoning with the ENEA Frascati Center.

In addition to routine activities, in 2010 the Service has dealt with several bid procedures, such as:

- Management of the bar and the canteen of LNF.
- Guards Service of LNF.
- Cleaning Service of LNF.
- Adjustment works and purchasing of equipment and furniture for the new Canteen of LNF.

Porterage activities have been particularly intense, due to several staff relocations as well as lab changes (e.g. dismantling of the Clean Room of the Cap. Gran Sasso, relocation of several Technical Division Depts.)

Collaboration with the Research Groups to organize meetings and conferences (Comunicare Fisica, Spring School, Microbouncing Instability, Lightnet Dissemination, ECFA, SuperB, Incontri di Fisica, LC10 etc).

Installation of a turnstile for the secondary entrance of the LNF, including the update of badge production software due to new equipment installed on the turnstile.

### **3 Central Stores And Purchasing Department**

During the past year, the Central Stores and Purchasing Dept. has supervised the purchasing and stocking of goods of the Central Stores as well as those of the Metal Stores, and of all the goods entering and leaving the Central Stores of the Laboratories; development and extension of the stocked articles.

Moreover, the Dept. has carried out market research upon request of the users to update the collection of stocked goods, and has maintained standards of stocked articles. Maintenance and updating of web pages, including the General Catalog for the general users.

Budget for 2010: € 263.000,00 of which

- € 70.000,00 on Cap. 130110 (*consumo standard*),
- € 160.000,00 on Cap. 130120 (*consumo ricerca*),
- € 33.000,00 on Cap. 520110 (*inventario - implementazione pool di elettronica*).

#### 4 Building Management Department

In the course of 2010, the construction of the window shielding in reinforced concrete of the Daφne building was started; so far 15 of a total of 36 windows have been provided with a shield.

The bid procedures for the contract regarding fencing and landscaping works of the area around the new LNF Service Centre have been concluded.

The final project for the hooking up of the internal LNF sewage system onto the communal sewage system on Via Fermi has been concluded and forwarded to the local authorities, together with a request for authorization to connect to the communal entrance.

During the year normal and extraordinary building maintenance activities have been performed with an eye to the preservation of the building assets of the LNF; modifications, adaptations and improvements have been implemented as required by the experimental groups of the LNF.



Figure 1: *JEM-EUSO: PDM and focal surface mechanics (partial full scale prototype).*

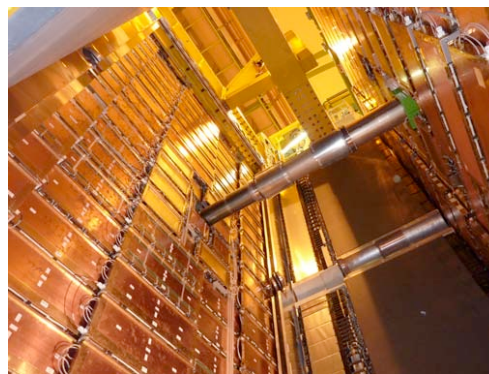


Figure 2: *LHCb: muon system (installed at CERN).*

#### 5 Mechanical Design and Constructon Department

Five different Units compose the Mechanics Design and Construction Department (SPCM): Mechanical Design, Carpentry and Soldering, Machine Tools, Metrology and Alignment, Material Store.

The SPCM performs the following tasks:

- mechanical design of experimental apparatus and detectors, using CAD/CAE software and FEM analysis;
- construction of prototypes and structures with the support of various soldering techniques and numeric control machine tools;
- production of high precision mechanical components, relying on manual and numeric control machine tools equipped with CAM control;
- high precision dimensional check, material strength test, large structures and apparatus optical alignment;
- acquisition and storing of mechanical components, tooling, metallic and plastic materials of workshop common use.

During 2010, the SPCM supported some experimental activities, playing a role of direct responsibility in the design, production, construction or installation: LHCb at CERN (muon system mechanical structures), CUORE at LNGS (engineering coordination and integration of the whole experimental apparatus), JEM-EUSO to be installed aboard the International Space Station (photo detector module and focal surface mechanics).

Many other activities were supported as well, though with no direct involvement in terms of responsibility: ALTCRISS, DAΦNE, ETRUSCO2, KAONNIS, KLOE2, MOONLIGHT, NA62, NEMO, PANDA, PSUPERB, ROG, TPS, VIP2 were supported in terms of mechanical design, construction, or dimensional checks and functional tests.

Finally, more than 40 short-term actions were taken by the SPCM personnel to support experimental activities, due to unplanned interventions or urgent repairs.

## **6 Heating, Ventilation, Air Conditioning Department**

The group is in charge of the operation and the maintenance of water cooling plants, water treatment facilities, compressed air and other gases production and distribution systems, air conditioning plants for accelerators and experiments and clean rooms.

In this framework, the group attends to the spare parts procurement and takes care of the procedures for the bids. It deals with the design of new installations and upgrades too.

In 2010 the group has supported DAΦNE, KLOE, BTF, SPARC, FLAME, DAΦNE-LUCE and the LNF Data Center.

During the year, some work has been done on special components, i.e. the cooling circuits of several DAΦNE magnets and of some power electronic cabinets. The upgrade for the Frascati Data Center has been defined and the detailed design has been assigned, and some work has been done to prepare the upgrade of SPARC.

## **7 Electrical Installation Department**

The group manages the LNF electrical installation from the high voltage power supply to end users and lighting. The 150 kV substation and the 8 cabins are operated by staff, that also cover emergency calls and fault fixing, while routine activities of safety and functional maintenance are usually performed by external operators under our supervision. Maintenance involves several skilled scheduled activities on switchboards, transformers, medium voltage devices, safety lighting, UPS, emergency generating sets and the electrical devices of the Dafne cooling system, but also small repairs or changes.

During 2010, some electromagnetic compatibility activities have been performed on the electrical installations of DAΦNE accelerator. Low frequencies electromagnetic interferences have been detected on the Dafne electronic system which caused beam instability. Stray current measurements permitted to identify a few power cable trays as source of the irradiation due to non optimized layout. The reshuffling of these power cables largely reduced the noise induced at 50 Hz. Moreover an even harmonic order noise induced by the RF modulator power supply was detected on the RF feedback, and it was reduced using an appropriate bonding system.

In this year, the safety inspection performed by ARPA (the Regional Environment Protection Agency) has been positively concluded. Outdoor lighting has been partially upgraded, replacing about one half of lighting devices. New, more efficient lamps, contribute to energy saving too.

The Kloe computing room UPS and the distribution system have been upgraded and the design of the main data center upgrade has been completed and the job started up.

In the electrical substation the main 20 kV switchboard and switchgear general overhaul has been executed.



Figure 3: *MV switchboards internal maintenance.*

## 8 Other Activities

### CNAO:

During 2010, the support activity to CNAO has been concentrated on the installation of vacuum components located in treatment rooms: thin wall carbon fiber exit windows and fiber glass loaded epoxy scanning magnet vacuum chambers. Now the whole treatment room vacuum system is under vacuum and fully operating. These items complete the vacuum system installation. A further

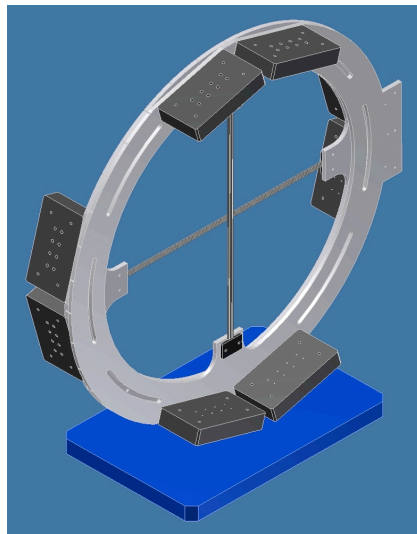


Figure 4: *AMADEUS Experiment: scintillating fibre system under test.*

activity has been carried out on the optimization of the gas mixing and controlling system for the ion sources, with the aim to obtain a stable and well reproducible gas mixture. The system has been tested with good results, and will be implemented on the sources.

### E-CLOUD:

In the last year an activity has been started on the deposition of thin film on the inner side of the vacuum chambers. The aim of this work is to obtain a coating of TiN that could be effective

for the reduction of secondary electron yield coefficient, in order to cope with e-cloud build up in positron storage rings. A system for thin film deposition is presently under realization.

**AMADEUS:**

Some work has been done on mechanical setup of the AMADEUS detector, more precisely the arrangement of the gas target around the KLOE interaction region. Another work in the frame of the AMADEUS experiment has been realized: a test setup to investigate the behavior of scintillating fibers coupled to silicon photo multipliers (SiPM), this is a prototype of a detector that will be used for the AMADEUS trigger system. This test setup consists essentially of two aluminum frames, one fixed and the other rotating; each frame holds 16 scintillating fibers and relative SiPM, with front-end electronics. This device has been successfully tested with dedicated runs on BTF at LNF and on a pion beam at PSI, Zurich.

**9 Some Statistics**

In December 2009 a general purpose form was put online in order to help users formulate their requests and enable fast & efficient processing. During 2010, a total number of 468 job requests reached the Division through this form. These requests were for four of the six Division Departments (the General Stores & Purchasing Dept. and the Mechanical Design and Construction Dept. are not included); the HVAC & Telephone services are handled by the Electrical Systems Unit. In Fig. 5 the weight of these requests on the various departments & unit is represented, whereas in Fig. 6 the origin of the requests is shown.

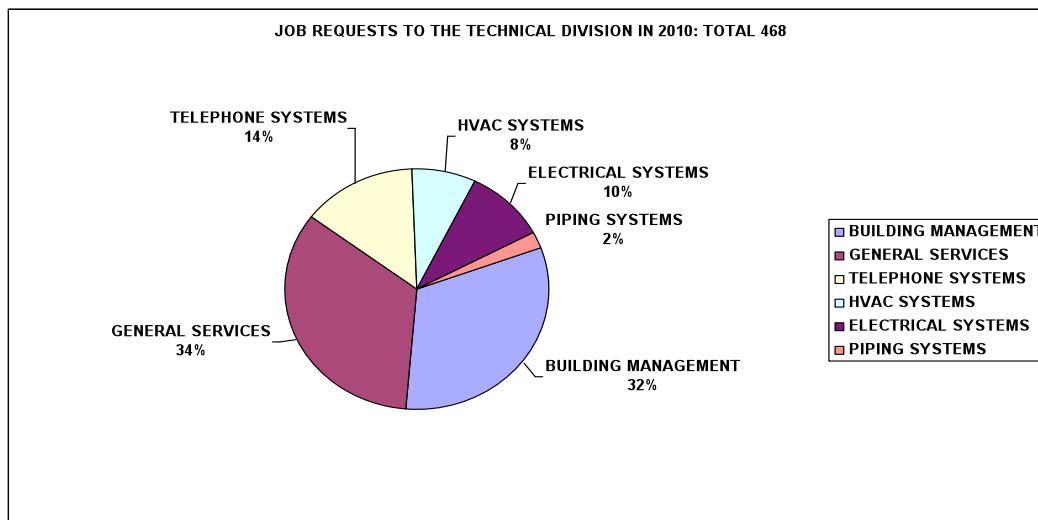


Figure 5: Job requests to the Technical Division in 2010: total 468.

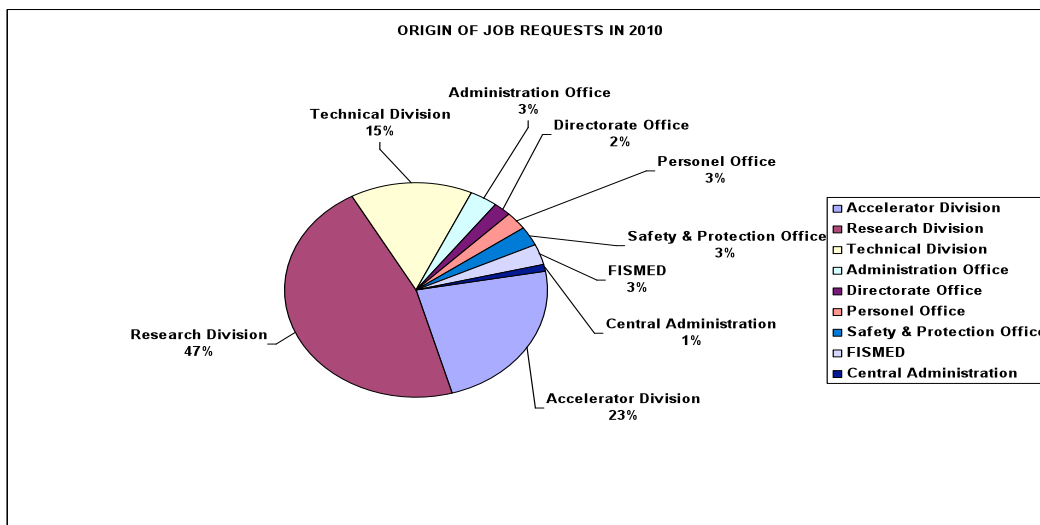


Figure 6: *Origin of job requests in 2010.*

A separate online procedure has been set up for the small jobs requests to the Mechanical Design and Construction Department, which was used 34 times during 2010. These data are not included in the above diagrams.

In order to enable users to identify people & tasks within the TD, web pages:

<http://www.lnf.infn.it/dtecnica/>

were set up which allow navigation through the organizational structure of the Division, as well as providing useful information on opening hours, users services and procedures. The pages are available in English and Italian.

## Glossary

These are the acronyms used in each status report to describe personnel qualifications other than Staff Physicist:

Art 15	Term Contract (Technician)
Art. 2222	Collaboration Contract
Art. 23	Term Contract (Scientist)
Ass.	Associated Scientist
Ass. Ric.	Research Associate
Bors.	Fellowship holder
Bors. PD	PostDoc Fellow
Bors. UE	European Community Fellow
Dott.	Graduate Student
Laur.	Undergraduate Student
Loc. Coord.	Local Coordinator
Osp.	Guest Scientist
Perfez.	PostLaurea Student
Resp.	Local Spokesperson
Resp. Naz.	National Spokesperson
Specializ.	PostLaurea Student
Tecn.	Technician